THE UNIVERSITY of ADELAIDE

2020

School of Biological Sciences
Molecular and Biomedical Science

Bacteriophage 186

Investigating the role of transcriptional regulators CI, Apl, CII and Tum at the lytic/lysogenic switch during 186 prophage induction

Thesis submitted in fulfillment of the requirements for the degree of Doctor of Philosophy

Alejandra Isabel

7th August 2020

Declaration

I certify that this work contains no material accepted for the award of any other degree or diploma in my name, in any university or other tertiary institution. To the best of my knowledge and belief, this document contains no material previously published or written by another person, except where due reference has been made in the text. Furthermore, I certify no part of this work will, in the future, be used in a submission in my name, for any other degree or diploma in any university or other tertiary institution without the prior approval of the University of Adelaide and where applicable, any partner institution responsible for the joint-award of this degree.

I acknowledge that copyright of published works contained within this thesis resides with the copyright holder(s) of those works. I give consent for the digital version of my thesis to be made available on the web, via the University of Adelaide's Digital Research Repository, the Library Search, the Australasian Digital Thesis Program (ADTP) and through web search engines, unless permission has been granted by the University of Adelaide to restrict access for a period of time. I acknowledge the support I have received for my research through the provision of an Australian Government Research Training Program Scholarship.

Alejandra Isabel 7th August 2020

Acknowledgements

This thesis has become a reality with the kind support and help of many individuals and I would like to express my heartfelt thankfulness to all of them. My sincere gratitude goes to my supervisors, Dr. Keith Shearwin and Dr. Ian Dodd for imparting their knowledge and expertise and providing an endless stream of support and encouragement as I worked through this study. I wish to thank all the members of the Egan/Dodd/Shearwin laboratory for their help and encouragement throughout my PhD. It has been a pleasure to work with such a kind, knowledgeable and experienced team and I wish everyone the best of luck for the future.

A special mention goes to my mentor and dear friend, Mrs. Lynn Rogers (Biochemistry Lecturer, Department of Molecular and Biomedical Science). I am extremely grateful and indebted to her for the expertise, support and encouragement she has extended to me throughout my undergraduate and postgraduate studies. She is by far, the best teacher I have ever had and I am grateful for all she has taught me and most importantly, to never give up.

I must also express my upmost gratitude to the two most important people in my life, my parents, Mrs. Mieke and Dr. Luis Isabel. Words cannot express the gratitude I feel for all their support, encouragement, influence, patience and love. I wish to dedicate this thesis to them in gratitude for all they have done and for the successes they have empowered me to achieve.

Finally, I would like to document that from all I have learnt during my studies, I wholeheartedly appreciate that *'the role of the infinitely small in nature is infinitely great'* (Louis Pasteur) and that *'no amount of experimentation can ever prove me right; a single experiment can prove me wrong'* (Albert Einstein).

Abstract

I am not a living entity, but I am very much alive. I am of tiny proportions and yet endowed with immense power. I am constantly waging war across the prokaryotic kingdom and have proven to be an aggressive, formidable and exceptionally deadly enemy of bacteria and archaea.

Who am I?

I am bacteriophage.

Coliphage 186 is a UV-inducible, non-lambdoid temperate phage of the family *Myoviridae* (genus *P2-likevirus*). As a temperate phage, 186 has the ability to undergo two alternative modes of development - lytic development is the active, developmental default state and lysogeny is the alternate, dormant state, where the phage DNA integrates into its host's genome. The lysogenic state is reversible and thus the lytic pathway can be resumed upon activation of the host SOS response, a phenomenon termed prophage induction. To control the entry into, and the transition between these states, 186 employs both a lytic/lysogenic transcriptional switch and an SOS inducible operon, each existing as independent modules in the 186 genome. Whilst extensive studies of 186 have provided significant insights into how the lytic and lysogenic cycles are regulated and into the process of prophage induction, there are a number of unique aspects for which our understanding remained incomplete. To progress our understanding of 186 prophage induction and how this phage makes its developmental decisions, four separate studies we undertaken to investigate the role(s) of four key transcriptional regulatory proteins (CI, Apl, CII and Tum) at the 186 switch. This knowledge was then used to re-wire the 186 modules to design and build a simple bistable memory circuit, capable of switching between alternate states in response to a chemical signal.

In Chapter 2, to investigate the role of the CI immunity repressor in prophage induction, we asked, does disruption of CI negative autoregulation reduce prophage induction efficiency? Using the *goa8* mutation (a 5bp deletion between the two promoters CI regulates, *pR* and *pL*) we demonstrated that when CI negative autoregulation is disrupted, this has a negative impact on prophage induction efficiency. This outcome underlined the importance of 186 being able to establish the correct lysogenic level of CI, so as to not only maintain stable lysogeny, but to remain optimally primed for prophage induction. To investigate the role of the Apl protein, we asked, why does Apl act as a weak transcriptional repressor at *pR* and *pL* during prophage induction? A series of hypothesises were framed on the idea that Apl binding at *pR.pL* is required to control *cII, cI* and/or *int* gene expression during prophage induction. With the experimental outcomes resulting in the rejection of all hypotheses however, this investigation contributed only to our understanding of what Apl *does not* do at the 186 switch.

In the context of 186 prophage induction, the role of the Tum antirepressor and the host SOS response were investigated in Chapter 3. Using a series of minimal 186-like UV- and chemically-inducible, chromosomally-integrated reporter systems and a cumic acid-inducible 186 phage, we confirmed that Tum is essential and sufficient in single-copy for stable 186 lysogenic to lytic switching and that the fundamental role of host SOS activation is to induce expression of the *tum* gene.

In Chapter 4, we asked, what is the significance of having a short-lived/protease sensitive CII protein? By replacing the short-lived, wildtype CII with a stabilised variant (CII145), we demonstrated that not only was there a significant bias towards lysogeny, but also that prophage induction efficiency was very strongly inhibited. The outcomes of this study suggested that the key purpose of having a highly active, and rapidly degraded CII is to quickly equilibrate CI levels in a lysogen to ensure the lysogen is established and ready for induction as soon after infection as possible.

Lastly, in Chapter 5 we used the data collected throughout this thesis, combined with existing knowledge on 186 to engineer a bacterial whole-cell biosensor that can establish impressively stable cellular memory, with two distinct alternate, stable states. Specific features of the 186 lytic/lysogenic switch and SOS operon were isolated, remodelled and progressively optimised to engineer such a system. We are confident that with the appropriate modifications this system could potentially serve as an environmental sensor or one that can detect and diagnose disease (e.g. cancer) with high sensitivity and specificity.

Table of Contents

Glossary

Term	Definition
°C	Degrees Celsius
186^{+}	Wildtype bacteriophage 186
$186^{p.cym}$	Cumic acid inducible bacteriophage 186
Amp	Ampicillin
attB	Attachment site on the bacterial chromosome
attL	Attachment site to the left of a lysogen/integrant
attP	Attachment site on a phage chromosome or an integrating plasmid (e.g. pIT3/4)
attR	Attachment site to the right of a lysogen/integrant
bp	Base pair
Chlor	Chloramphenicol
$chlor^{R}$	Chloramphenicol resistance gene
CA	Cumic acid (i.e. cumate)
DNA	Deoxyribonucleic acid
dNTPs	Deoxyribonucleoside triphosphates
F	Forward DNA primer
g	Gram
hr	Hour
HTH	Helix-turn-helix
Kan	Kanamycin
Kan^{R}	Kanamycin resistance gene
kb	Kilobases
kDa	KiloDalton
L	Litre
LacZ	β-galactosidase
LB	Luria Bertani broth
L-plates	1.5% agar Luria Bertani broth culture plate
M	Molar
M9MM	M9 minimal media without glucose
M9MM-1	M9 minimal media with 1mM glucose
M9MM-2	M9 minimal media with 2mM glucose
M9MM-20	M9 minimal media with 20mM glucose
min	Minute
ms	Milliseconds
MQ H_2O	MilliQ water
nt	Nucleotides
O/N	Overnight
OD_{600}	Optical density as measured at 600nm
ONPG	O-nitrophenyl-β-D-galactopyranoside
ORF	Open reading frame
ori	Origin of replication
orits	Temperature sensitive origin of replication
p95	Promoter of the 186 SOS operon
PCR	Polymerase chain reaction
pE	Lysogeny establishment promoter of 186
pL	Leftward lysogenic promoter of 186
pR	Rightward lytic promoter of 186
rcf	Relative centrifugal force (i.e. G-force)
s	Second
SA	Salicylic acid (i.e. Sodium salicylate)
S/N	Supernatant
Spec	Spectinomycin
VA	Vanillic acid
X-gal	5-bromo-4-chloro-3-indolyl-β-D-galactopyranoside

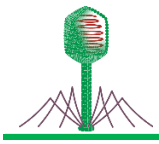

Chapter 1

Introduction

1.0 Bacteriophage

1.0.1 Background

Bacteriophage (phage) are obligate intracellular parasites (viruses) that only infect bacteria and archaea. The name bacteriophage - derived from 'bacteria' and the Greek word φαγεῖν (phagein) - means 'to devour', a suitable title given that (in most cases) phage cause complete lysis of their host cell. They have existed alongside bacteria for billions of years and are considered the most abundant entities on Earth, with the planet estimated to harbour 10^{31} phage particles (Keen, 2015). Phage are extremely host specific, with every strain of bacteria thought susceptible to at least one type of phage. To identify their host(s), phage use their receptor binding proteins to recognise and interact with certain host cell surface moieties such as outer membrane-bound receptors, glycolipids, flagella proteins, teichoic acids and lipopolysaccharides (Stone et al., 2019).

Phage have many means different means of reproduction, including virulent and temperate lifecycles. Virulent phage are strictly lytic developers; as soon as they encounter their host, they degrade the cell wall and inject their genetic material into the host's cytoplasm. Immediately after infection, the bacterium's biological machinery is hijacked to replicate the phage genome, synthesise all proteins required to build and assemble new phage particles and produce the lytic factors required for host cell lysis (De Paepe et al., 2014). Depending on the phage, lytic cycles can exhibit latent times (the time it takes to reproduce inside an infected host cell) that last a few minutes or extend for hours. Coliphage T4 and λ exhibit short latent periods of ≥20 and ≥50mins respectively (De Paepe et al., 2014), whilst a 9 to 17hr period of latency has been observed for *cyanophage S-BBS1* infecting *Synechococcus BBCI* (Suttle and Chan, 1993).

Rather than undergo lytic development, temperate phage can undergo an alternate cycle called lysogeny (Bertani, 2004; Dodd and Egan, 1999). In this cycle, the phage DNA either circularises to form a stable plasmid (like coliphage P1) or (in most cases) integrates into the host's genome and exists (as a prophage) in a state of dormancy (like coliphage λ and 186). Under spontaneous or induced conditions, temperate phage can undergo prophage induction, where the prophage excises from the host's genome and switches back to lytic development (De Paepe et al., 2014). Given this ability, prophage can be regarded as 'dangerous molecular time bombs' capable of bursting their hosts in response to environmental triggers.

1.0.2 The dawn of bacteriophage

Phage made their existence known in the early 20th century, but it took a number of chance encounters before their discovery was formally recognised. In 1896, British bacteriologist Ernest Hanbury Hankin sampled the rivers in India and found something with antibacterial properties against *Vibrio cholerae* (Hankin, 1896), but he did not pursue his finding. Almost two decades later (1915), the British bacteriologist Frederick Twort was working on a vaccine for smallpox and was trying to propagate the vaccinia virus in bacteria. What appeared on his culture plates was contaminating bacteria and a scattering of mysterious transparent spots. The spots turned out to be zones of dead bacteria, lysed by infecting virulent phage (Keen, 2015). Twort published his findings (Twort, 1915), but his work was interrupted by the First World War and from a lack of funding. In France 1917, French-Canadian microbiologist Felix d'Herelle formally discovered phage at the Pasteur Institute. He observed that dysentery bacteria disappear when inoculated with a bacteria-free filtrate prepared from sewage. d'Herelle was immediately convinced he had discovered a new type of virus, one that only infected bacteria (Orlova, 2012; Keen, 2015) . He published his findings (d'Herelle, 1917), captivating the scientific community and kick-starting the study of phage. Over the next century, phage would prove to be extremely useful biological entities, playing leading roles in the discovery of many central elements fundamental to our understanding of bacterial genetics and evolution and making advances in molecular biology, synthetic biology and biotechnology.

1.0.3 Bacteriophage classification and morphology

The current taxonomic system for bacteriophage - developed by the Bacterial Virus Subcommittee of the International Committee on Taxonomy of Viruses (ICTV) - comprises of a single order (*Caudovirales*), 13 families and 34 genera. Host preference, virion morphology, nucleic acid properties and lifecycle are just some of the 40+ criteria used to differentiate each phage into their correct order, family, genera and species (Novik et al., 2017). Studies of phage biodiversity have revealed a vast range of morphological properties, where they seem to exist in an endless range of shapes, sizes and complexity. Despite this diversity, all phage are composed of a proteinaceous capsid that encapsulates a nucleic acid genome that is either linear, circular or segmented ss/dsDNA or ssRNA (never both). Phage genomes range in size from 4kb to 500kb and can encode as little as four genes to as many as hundreds of genes (Keen, 2015). Figure 1.1 presents the classical morphological structure of phage, however, for added complexity, phage can feature a long or short, contractile or non-contractile tail and a baseplate adorned with tail fibres and spikes.

The most numerous and widely distributed group are that of the tailed phage, encompassing more than 95% of the phage described in the literature (Ackermann, 2005; Kutter, 2001). The ICTV classes these phage within the order *Caudovirales,* where they are assigned to one of three families; *Myoviridae* (viruses with contractile tails; e.g. coliphage T4), *Siphoviridae* (viruses with long, non-contractile tails; e.g. coliphage λ) and *Podoviridae* (viruses with short non-contractile tails; e.g. coliphage T7) (Kutter, 2001; Maniloff and Ackermann, 1998). The remaining families are far less extensive and encompass the highly morphologically diverse tailless phage, that can have spherical, rod-shaped (even lemon-shaped) or filamentous, enveloped or non-enveloped capsids and ss/dsDNA or ssRNA genomes that are linear, circular or segmented (ICTV, 2019; Kutter, 2001; Novik et al., 2017). For example, phage of the *Microviridae* family (e.g. coliphage φX174) have a circular ssDNA genome encased within a polyhedral capsid, whilst phage of the *Inoviridae* family (e.g. coliphage M13) have a circular ssDNA genome encased within a rod-shaped or filamentous body that exhibits helical symmetry (Maniloff and Ackermann, 1998).

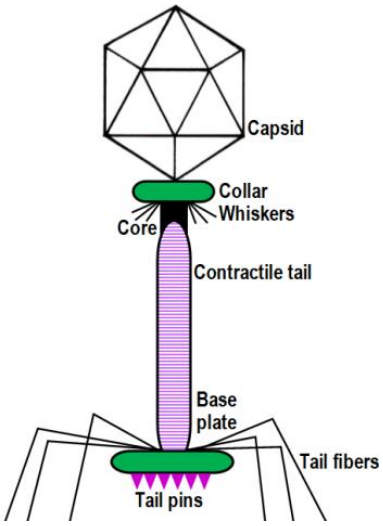

Figure 1.1: The classical morphological properties of phage. Lytic coliphage T4 and temperate coliphage 186 of the *Myoviridae* family have the classical phage structure, which features a linear dsDNA genome encased within an icosahedron capsid. Connected to the capsid is a contractile tail composed of an inner hollow tube (core) and sheath. The tail is ornamented with a whiskered collar and a base plate with pins and long tail fibers Image adapted from Maniloff and Ackermann (1998) and Novik et al. (2017).

1.0.4 Why study bacteriophage?

For more than a century, phage have served as model organisms for probing the basic chemistry of life. They have enabled scientists to make some of the most important discoveries in biological sciences and have equipped us with a molecular tool kit that enables researchers to modify and manipulate DNA with tremendous ease. The ability of phage to manipulate the DNA of their host(s) also makes them significant modellers of bacterial genomes, thereby driving the adaptive evolution of these microorganisms. With the emergence of antibiotic-resistant bacteria, phage therapy (PT) is also undergoing renewed interest in the West, with research being undertaken to develop a 'new age' of diagnostic agents, therapeutic agents and detective tools to prevent bacterial contamination and combat bacterial infection (Nelson, 2004). Sequencing of phage DNA also provides new insights into the unknown, as their genomes are highly mosaic, with each type encompassing a combination of sophisticated gene modules shuffled and remodelled repeatedly over evolutionary time (Harada et al., 2018).

Many discovered phage-encoded proteins now act as tools for genomic editing and cloning and have been used to develop food safety diagnostics, biosensor technologies and antimicrobial therapies (Citorik et al., 2014a; Harada et al., 2018). What was initially considered by the West to be a form of Soviet pseudoscience, phage biology in the 21st century is proving to be an exciting time, with the opportunity to make many new and exciting discoveries a reality.

1.0.4.1 Using bacteriophage to understand bacterial genetics and pathogenesis

Analysis of bacterial genomes has shown that a considerable amount of microbial DNA consists of prophage sequences and prophage-like elements (Orlova, 2012), proving they are prolific drivers of bacterial evolution. Two key processes that give phage the ability to shape bacterial genetics is transduction and lysogenic conversion. Transduction is the transfer of genes from one bacterial strain to another via a viral vector and can be of a generalised or specialised nature. *Generalised transduction* occurs during lytic development, when random pieces of the host genome (due to disintegration of the bacterium) are accidentally packaged into the capsids of new daughter phage (often replacing phage genomic DNA). Should the new phage inject this DNA into a new neighbouring host, it may integrate into the bacterium's chromosome, altering its genome and that of its daughter cells (Kasmna and Porter, 2019). *Specialised transduction* occurs through incorrect excision of an inducing prophage, where a hybrid genome of phage DNA and bacterial DNA is packaged into the capsids of new phage. If subsequent infection of a new host results in lysogeny, the host will harbour a hybrid genome that may deliver a new/altered phenotype (Chiang et al., 2019).

Unfortunately, the ability of phage to shape bacterial genetics is not entirely beneficial to humanity, with many phage genomes encoding antibiotic resistance genes, highly pathogenic bacterial toxins, adhesins, invasions and other virulence factors. When a bacterium horizontally acquires foreign DNA that encodes one or more virulence genes, this mobile element is referred to as a pathogenicity island (PAI). PAIs are known to play a pivotal role in the virulence of bacterial pathogens and can be acquired through a number of horizontal gene flux mechanisms such as conjugation, transposition and (not surprisingly) phage (Schmidt and Hensel, 2004). As discussed, transduction is one mechanism where a bacterium can acquire a new capability when delivered (via phage) a genetic cargo that encodes foreign gene(s). Phenotypic modification (i.e. pathogenicity) can also be acquired through *lysogenic conversion*, a process in which a bacterium is lysogenised with a toxin-encoding temperate phage (Keen, 2015). The M13-like filamentous phage CTXφ for example, encodes the structural genes for the cholera toxin. When establishing lysogeny within its naturally harmless host (*Vibrio chloerae*) it can convert the bacterium into the cholera-causing pathogenic strain (Kim et al., 2017; Waldor and Mekalanos, 1996). Other examples include the corynebacteriophage that encode the diphtheria toxin and introduce toxicity into strains of *Corynebacterium diphtheria* (Holmes, 2000) and the

pathogenic Shiga toxin (Stx)-producing *E. coli* lysogenised with a lambdoid phage encoding the *stx* genes (O'Brien et al., 1984). The exact reason(s) as to why phage encode virulence factors remains largely unknown, but we presume that imparting a pathogenic phenotype somehow enhances the bacterium's survival fitness, meaning it can serve as a more robust and reliable host for the prophage. Despite this unknown, knowledge of this phenomenon has proven useful in our understanding of the evolution of bacterial pathogenesis and has directly influenced how we design and develop new bacterial vaccines.

1.0.4.2 Bacteriophage in molecular biology

Phage have played an inordinate role in our understanding of how life works at the molecular level. Their simplicity and compactness makes them natural choices in the lab as they serve as ideal model organisms to study prokaryotic transcription, gene regulatory networks and biological decision making (i.e. genetic switches). Studies of phage have also enabled scientists to prove DNA is the genetic material that encodes life (Crick et al., 1961) and that messenger RNA (mRNA) is the information intermediate between DNA and protein (Brenner et al., 1961). Furthermore, phage have made significant contributions to our molecular toolbox, providing techniques like phage display and tools like DNA and RNA polymerases, DNA ligases (enzymes that connect DNA strands by catalysing the formation of a phosphodiester bond) and recombinases (enzymes that catalyse site-specific recombination events within DNA causing deletions, insertions, translocations or inversions) (Citorik et al., 2014a). These phage components allow scientists to easily manipulate, modify and recombine DNA, RNA and protein to adapt or create new compounds, cellular pathways, genetic circuits and even entire organisms that outperform their wildtype counterparts (IOM, 2011; Salmond and Fineran, 2015). Table 1.1 lists some of the major events and discoveries where phage have played a significant role in the advancement of genetics, molecular biology, synthetic biology and biotechnology.

Table 1.1: A 100-year timeline of phage history. This table lists just some (of the many) events where phage have been central in revealing key scientific concepts and providing new molecular tools, crucial to the advancement of genetics, molecular biology, synthetic biology and biotechnology.

Year	Event
1917 Discovery of bacteriophage	♦ Phage are discovered (or rediscovered) by French-Canadian microbiologist Félix d'Hérelle (d'Herelle, 1917).
1943 The nature of mutation	♦ Using T1 phage, Luria and Delbrück (1943) designed the fluctuation test, to demonstrate that (in bacteria) the nature of mutation is spontaneous and random.
1952 The genetic material of life	♦ Hershey and Chase (1952) confirmed DNA (not protein) is the hereditary material of life. Using radioactively labelled T2 phage, they proved that upon infection only phage DNA enters the host cell whilst capsid proteins that encapsulate the DNA remain extracellular.
1952 Transduction	♦ Studies by Zinder and Lederberg (1952) on P22 phage infection of *Salmonella* found some phage can mobilise bacterial genes and transduce them from one bacterium to another.
1958 The nature of genes	♦ Central insights into the linear molecular nature of genes was revealed by American physicist Seymour Benzer through his studies of the *rII* gene region of the T4 phage (Benzer, 1959).
1961 DNA recombination	♦ The molecular basis of DNA recombination was determined by Meselson and Weigle (1961) and their studies on coliphage λ. They revealed recombinant DNA molecules are produced by the breaking and re-joining of parental DNA.

Year	Event
1961 The nature of gene regulation	♦ Jacob and Monod (1961) provided insight into the nature of gene regulation through their extensive studies of the *E. coli lac* operon and λ coliphage.
1961 The triplet code	♦ Crick et al. (1961) demonstrated (via the Crick-Brenner experiment) that DNA is a triplet code. The experiment assayed T4 phage rIIB protein activity following proflavin-induced mutations of the *rIIB* gene. The test proved a triplet of nucleotides encodes a single amino acid, with a string of triplets encoding a sequence of amino acids for a particular protein.
1961 Messenger RNA	♦ The Brenner et al. (1961) experiments on phage-infected *E. coli* confirmed DNA and protein are collinear and mRNA is the intermediate information carrier. mRNAs are transcribed from DNA and then translated by ribosomes to produce proteins.
1967 Creating life *in vitro*	♦ Leading in the age of synthetic biology, American biochemist, Arthur Kornberg used phage φX174 as a model to first prove DNA synthesised in a test tube by purified enzymes can produce all the features of a natural virus (NIH, 1959).
1967 DNA ligase	♦ The *E. coli* and T4 phage DNA ligases were independently discovered by five different laboratories (Cozzarelli et al., 1967; Gefter et al., 1967; Gellert, 1967; Olivera and Lehman, 1967; Weiss and Richardson, 1967). These enzymes are considered guardians of genomic integrity and are commonly used in standard molecular cloning procedures.
1969 Restriction enzymes	♦ A new toolset was added to the molecular toolbox when Arber and Linn (1969) discovered restriction endonucleases. Found in phage-resistant bacteria, these enzymatic proteins degrade foreign DNA (e.g. phage DNA) by cutting it into pieces.
1977 First phage genome sequenced	♦ The phage φX174 ssDNA genome was sequenced by British biochemist Fred Sanger and co. (Sanger et al., 1977).
1985 Phage display	♦ American biologist George Pearson Smith developed phage display (Smith, 1985). The technique usually uses filamentous phage (e.g. M13) as carriers of peptide libraries displayed on their surface, but T4, T7 and λ phage have also been used (Pande et al., 2010). Phage display is used in antibody development and to study protein-protein/peptide/DNA interactions.
1987 The Cre-Lox system	♦ The phage P1-derived Cre-Lox system developed by Dr. Brian Sauer (Sauer, 1987) is a modern day synthetic biology tool used for carrying out site-specific recombination.
1996 Lysogenic conversion	♦ The phenomenon of lysogenic conversion in *Virbrio cholerae* (Waldor and Mekalanos, 1996) proved temperate phage can impart pathogenicity to a naturally harmless host.
2007 The CRISPR-Cas system	♦ The CRISPR-Cas prokaryotic immune system was discovered by Barrangou et al. (2007). The system confers resistance to foreign genetic elements (e.g. phage DNA) providing bacteria with a form of acquired immunity. The system was later repurposed by scientists to act as the powerful CRISPR-Cas9 genome editing tool (Deltcheva et al., 2011; Jinek et al., 2012).
2009 Gibson Isothermal Assembly®	♦ Dr. Daniel G. Gibson at the J. Craig Venter Institute developed Gibson Assembly®; a DNA assembly methodology used to construct large, complex DNAs by joining multiple DNA oligonucleotides. To generate single-stranded complementary overhangs between each assembly fragment, the reaction employs the T5 exonuclease, naturally encoded by the T5 coliphage *D15* gene (Gibson et al., 2009).
2012 The Cas9 RNA-guided nuclease	♦ Jinek et al. (2012) developed the programmable Cas9 RNA-guided nuclease for genome editing.

1.0.4.3 Bacteriophage therapy

Since their discovery, the therapeutic use of phage for the prevention and treatment of bacterial disease (i.e. phage therapy; PT) has been under continuous debate. With mounting concerns over the emergence and spread of multidrug resistant bacteria and a decreasing number of newly licensed drugs entering the market, the West has finally revived its studies of phage. It is with hope that scientists will be able to engineer and program these highly specified viruses to act as a new age of 'intelligent' antibiotics, thereby establishing a new antimicrobial program.

PT is by no means new. In the early decades of the 20th century, the Soviet Union used phage to treat a wide variety of infections such as cholera, typhoid and the bubonic plaque (Harper et al., 2015). At present, PT continues to be extensively researched and readily practiced in Eastern Europe, with Russia, Poland and Georgia dominating the field of phage research and expertise. In Tbilisi, Georgia, the George Eliava Institute of Bacteriophage, Microbiology and Virology (GEI; founded 1923) and the Phage Therapy Centre (PTC; founded 2003) serve as pioneers of phage research. With almost 100 years of history, the GEI has made immense contributions to PT, having developed treatments that can combat major bacterial and viral diseases such as anthrax, tuberculosis, dysentery and brucellosis. The GEI is also renowned for having the World's most extensive collection of bacterial and phage strains (Eliava Institute, 2018). The newly established PTC specialises in the development of PTs to treat acute and chronic infections (e.g. acne, bronchitis and colitis), infections where circulation is poor (e.g. bedsores and diabetic foot) and infections caused by antibiotic resistant bacteria (strains include *E. coli, Staphylococcus spp, Streptococcus spp.* and *Klebsiella* spp.) (Phage Therapy Center, 2018).

Regrettably, the West abandoned the use of phage in medicine when Alexander Fleming discovered penicillin in 1928 (Fleming, 1929), which revolutionised the treatment of bacterial infection with antibiotics. The therapeutic potential of phage was overlooked because antibiotics offered an affordable, clean, versatile, easy and efficient solution to combatting bacterial infection. In contrast, large-scale production of phage tends to be more complex because they have a habit of being more sensitive to manufacturing and handling conditions. Moreover, inconsistencies in experimental protocol and trial design resulted in clinical trials on early PTs generating unreliable and varying results, with some studies reporting successful therapeutic outcomes whilst others only achieving marginal reductions in bacterial growth (Barbu et al., 2016). From a past, present and future perspective, the most significant deterrent of PT is cost. In the West, the manufacture of drugs and other therapeutic products must comply with current Good Manufacturing Practice (cGMP) regulations, where cGMP systems are designed to assure the identity, strength, quality and purity of drug products are not compromised during manufacturing operations. To develop a broad-spectrum PT - a cocktail of multiple independent phage types - that complies with cGMP quality control processes, each independent phage would need to be produced and purified independently, which would multiply production costs to exorbitant levels (Barbu et al., 2016). So, with a generally poor understanding of phage biology, a lack of standardised techniques and protocols in clinical trials, strict regulatory controls and associated manufacturing costs and quality control issues encountered with the preparation of stable therapeutic stocks (Haq et al., 2012), the West's interest in phage dwindled and PT was displaced by antibiotics.

Unfortunately, excessive and careless use of antibiotics is driving the modern world into an 'antibiotic apocalypse'. With the rising emergence of bacteria immune to even the most potent antibiotics, gone will be the days of modern medicine. Routine surgeries, joint replacements, caesarean sections, chemotherapy and organ transplants will become impossible. The simplest of bacterial infections will be untreatable and something as minor as a paper cut or a graze could pose serious threat to life. With the antibiotic resistance crisis only worsening, it is clear something else is needed and perhaps that need can be satisfied with phage. There are a number of unique benefits to using phage to treat bacterial infection. First is their host-specificity; phage only target one or a few specific strains of bacteria. This specificity may (at first) be considered a disadvantage because the disease-causing bacterium must be identified before PT can be administered, but phage-host selectivity permits PT to be directed at specific bacterial populations. This prevents the emergence of secondary infections because non-target/healthy bacteria remain unaffected (Phage Therapy Center, 2018). Second, since phage reproduction is dependent on the presence of their host, they can be delivered right to the site of infection and act exactly where they are needed. Moreover, if their host is absent then they will not persist in the body for long. In comparison, antibiotics have broad-spectrum effects, killing both harmful and healthy microflora. These agents can significantly disrupt a host's microbiome and cause serious health implications such as increased susceptibility to secondary infection, the emergence of food allergies, digestive/metabolic complications (e.g. vomiting and diarrhea) and in severe cases cause liver damage and even death (Lin et al., 2017; Phage Therapy Center, 2018). Antibiotics also do not necessary concentrate at the site of infection, especially for infections with poor circulation (Phage Therapy Center, 2018).

Another attractive advantage of PT is that the resistance hurdle may be easier to overcome with phage than that of antibiotics. Phage-bacterium coevolution is the phenomenon where a bacterium and its native phage evolve in tandem by exerting selection pressures on each other (De Sordi et al., 2018; Koskella and Brockhurst, 2014). Bacteria commonly develop phage resistance through spontaneous mutation(s) that enable them to inhibit phage adsorption by downregulating, phenotypically altering or hiding cell surface moieties recognised by native phage (Barbu et al., 2016). Bacteria have also acquired resistance by developing defence mechanisms like the restriction-modification system that degrades incoming phage DNA and the CRISPR-Cas system that imparts adaptive immunological memory to reinfecting phage (Barbu et al., 2016). Phage however, have immortalised the phage-bacterium war by developing a plethora of genetically encoded bacterial counter-resistance mechanisms. For example, mutations in the gene encoding the receptor-binding protein allows coliphage λ to recognise a new cell surface receptor on its *E. coli* host (Meyer et al., 2012), whilst coliphage φX174 and T7 can adsorb to a modified LPS structure (Michel et al., 2010; Pepin et al., 2008).

Coliphage T3 and T7 can evade restriction enzyme digestion by encoding the ocr protein, which mimics B-form DNA thereby blocking DNA binding by type I DNA restriction enzymes (Krüger and Bickle, 1983; Walkinshaw et al., 2002). Furthermore, Streptococcus *thermophilus* phage can evade the CRISPR-Cas system by acquiring mutations or deletions in the protospacer or PAM sequence (Deveau et al., 2008), whilst other phage have genes that encode anti-CRISPR proteins that interfere with the system (Bondy-Denomy et al., 2013). It is thought that the ability of phage to develop such counter-resistance mechanisms means bacteria acquiring resistance to PTs may be harder to achieve than that of antibiotics.

Overall, it is unlikely the West will use PT as the primary antibacterial therapy; instead, it will serve as a complementary therapy to antibiotics. The West's use of PT is a slow and arduous process and is currently only legally dispensed to people on a compassionate basis (Haq et al., 2012). The outlook is promising with the US Food and Drug Administration (FDA) approving the first accelerated antibiotic-susceptibility test, the KeyPath™ MRSA/MSSA Blood Culture Test-BT in 2011. This *in vitro* diagnostic tool uses a phage cocktail to detect *Staphylococcus aureus (S. aureus)* and directly determine methicillin susceptibility or resistance from positive blood cultures (Smith, 2012). In early 2019, the FDA also approved the first US clinical trial of an intravenously administered PT designed to treat participants suffering from *S. aureus* infections in ventricular assist devices with an experimental phage, AB-SA01 (Voelker, 2019).

It is important to note that whilst phage can be of a virulent or temperate nature, it is the virulent phage that have been exploited for PT. Temperate phage have been avoided largely due to their inherent ability to modify bacterial genomes and mediate the horizontal transfer of genes between bacteria. Furthermore, should a temperate phage divert to lysogeny, this would not only delay the desired antibacterial effect (Monteiro et al., 2019), but the patient may need to be exposed to a secondary agent to induce prophage induction. Despite these concerns, there is a role for temperate phage in PT with researchers now working to use them as vessels to deliver synthetic gene circuits that lethally interrupt vital bacterial intracellular processes or revert resistant bacteria back to antibiotic susceptible strains (Monteiro et al., 2019). For example, antimicrobial sensitivity to streptomycin and gentamicin was established in *E. coli* when lysogenised with a mutant λ phage engineered to deliver a CRISPR-Cas system targeting beta-lactamase genes (Yosef et al., 2015).

1.0.4.4 Bacteriophage as biocontrols

Apart from using phage to treat bacterial infections, phage biocontrol (PB) is becoming an increasingly attractive means to target specific foodborne bacteria, largely because, despite the many advances in food sanitation techniques and pathogen surveillance, foodborne illnesses remain a major cause of hospitalisation and death worldwide (Moye et al., 2018).

PBs have proven to be highly effective, natural and green alternatives to traditional methods (e.g. pasteurisation, high pressure processing, irradiation and chemical disinfectants), which are expensive to establish and maintain, often have deleterious impacts on the organoleptic qualities and nutritional value of foods and indiscriminately harm/kill good and bad bacteria (Moye et al., 2018; Sulakvelidze, 2013). PBs are considered clean and green, because almost all currently available commercial PBs contain cocktails of natural phage isolated from the environment (not genetically modified in the laboratory) suspended in a water-based low-salt solution that contains no additives or preservatives (Sulakvelidze, 2013). Many products are also certified Kosher and Halal and are available for use on organic foods (Moye et al., 2018). For example, Micreos Food Safety - a Netherlands-based phage and endolysin technology development company - have developed several FDA and US Department of Agriculture (USDA) approved PBs to act against dangerous bacteria in the food chain. In 2006, PhageGuard Listex™ (against *Listeria*) and PhageGuard S™ (against *Salmonella*) were approved and are now marketed in many countries worldwide. These PBs can be easily applied via spray, mist or dip to food contact surfaces and a wide range of raw and cooked food products (e.g. meat, poultry, fish, dairy, fresh fruits and vegetables, ready-to-eat meals and smallgoods) without affecting product taste, colour, texture and odour (Micreos, 2019). Micreos is also the biotechnology behind the skincare brand Gladskin, products of which are used to treat inflammatory skin conditions (e.g. acne, eczema and rosacea) aggravated by *S. aureus.* All Gladskin products contain the *S. aureus* specific endolysin, Staphefekt™, which kills the bacterium by breaking down the cell wall. Furthermore, with its target specificity, the commensal bacteria essential for healthy skin remain intact (Gladskin, 2019). It appears that PBs not only offer an elegant, natural and organic way to safeguard food products during processing, but they may mark as a new era in the treatment of skin conditions. The hope is that by demonstrating the effectiveness of PBs this will encourage the use of phage in a clinical setting.

Another promising application of phage is their use in the prevention and elimination of biolfilms. These surface-attached heterogeneous clusters of bacterial cells are bound together within a self-synthesised protective extracellular polysaccharide substance (EPS) - a gooey-like network of sugars, proteins and nucleic acids (Lopez et al., 2010). Biofilm formation is a protective mode of growth that allow bacteria to survive in hostile environments. They are prolific in nature and found on essentially any biotic or abiotic surface where moisture is present (IOM, 2011). Indwelling medical devices (e.g. urinary catheters, endotracheal tubes, prosthetic joints, pacemaker leads and enteral feeding tubes) are important cost-effective devices used to assist in the recovery from major surgery, restore normal physiological function and/or facilitate the regeneration of tissue (Barbu et al., 2016). Unfortunately, the use of these devices is significantly compromised by their susceptibility to serve as abiotic supports for biofilm formation, leading to medical device-associated infections.

Biofilms also cause many persistent and chronic infections where surgery is often required to remove these microbial masses and they readily form on foods, making them a dangerous source of food contamination (IOM, 2011). To overcome this complication, scientists are working to develop cocktails of lytic phage to eliminate established biofilms and/or prevent their formation. For example, a reduction in *Staphylococcus epidermidis* biofilm formation was achieved when hydrogel-coated catheters were pre-treated with phage (Curtin and Donlan, 2006) and Sillankorva et al. (2004) showed anti-*Pseudomonas fluorescens* phage eliminated biofilms in the early stages of development. A major issue associated with biofilm treatment is achieving sufficient penetration of the microbial mass. Biofilms are often resistant to numerous antibiotics because these agents cannot overcome the protection provided by the EPS. Scientists however, are looking to engineer phage that synthesise and release specific enzymes that can digest the bacterial cell wall (e.g. endolysins) and/or degrade the biofilm matrix (e.g. EPS depolymerases) (Salmond and Fineran, 2015). Lu and Collins (2007) for example, explored the potential to use engineered phage to target and disaggregate established biofilms. They engineered a Dispersin B hydrolase (DsPB)-expressing T7 phage, where upon initial infection of an *E. coli* biofilm there is rapid multiplication of phage and expression of DsPB. Upon host cell lysis, both phage and DsPB are released, leading to subsequent infection and degradation of the EPS component.

Review of the literature leaves no doubt that there is an immense number of benefits phage can offer humanity, with the above examples only providing a snapshot of the possible applications of phage as biocontrols and medical therapeutics. Whilst acceptance by the FDA and USDA is encouraging, to achieve full acceptance of PT in the West, more *in vivo* research is necessary and more investment in clinical trials is required. PT primarily focuses on the development of therapies using virulent/lytic phage, but there is a role for temperate phage and work is in progress to include these phage in our antibacterial arsenal. Despite the slow progress, perhaps one day (soon) the potential benefits of PT will be realised and we will all be able to say, "*some phage a day will keep the bugs at bay*".

1.0.5 Bacteriophage development

All phage can be divided into two groups according to their type of infection. Virulent phage, such as the T-phage (T1-7) are characterised by their exclusive use of lytic development. Temperate phage like Mu, P2, λ and 186 can undergo lytic or lysogenic development, where the decision to go lytic or to establish lysogeny is made shortly after infection (Fig. 1.2). Lytic development is exclusive to virulent phage and is the default developmental cycle for temperate phage. It is a highly effective reproductive strategy as only a few cycles of lytic infection can allow phage to spread like wildfire through a bacterial population.

The lytic cycle begins when a phage recognises and binds to a specific moiety expressed on the surface of a susceptible host (Salmond and Fineran, 2015). Coliphage λ for example, recognises and binds *E. coli* via its J protein (located in the tail tip), which interacts with the host's maltose outer membrane porin (Werts et al., 1994). Following host recognition, the phage genome is injected into the host's cytoplasm with the empty phage capsid remaining extracellular. To establish the lytic cycle, early transcription immediately occurs from early lytic promoters, which then proceeds to middle lytic gene expression to produce the phage DNA replication proteins required for replication of the phage genome. During late lytic development, morphological proteins and proteins required for the assembly of new phage are expressed. For the majority of phage, the late stage also expresses holin and endolysin proteins required for host cell lysis, where upon lysis of the bacterium a burst of new phage are released into the extracellular environment where they will infect other neighbouring susceptible hosts (B Guttman et al., 2004; Sturino and Klaenhammer, 2006). An exception to this outcome are the filamentous phage (e.g. coliphage M13), which do not lyse their *E. coli* host but rather 'secrete' new phage through the outer membrane, thereby manifesting a chronic infection that significantly slows the growth of the bacterium (Salmond and Fineran, 2015).

Lysogenic development is an alternative mode of development utilised only by temperate phage. The cycle begins as per the lytic cycle (recognition, attachment and injection), but if the phage is exposed to a specific signal(s), rather than hijacking the host's biological machinery the phage genome typically integrates into the host's chromosome as seen with coliphage λ and 186 (Bertani, 2004). In some cases, like coliphage P1, the genome is maintained as a low copy number plasmid (Lobocka et al., 2004). Lysogeny establishes a symbiotic-like relationship in which the lysogen (bacterium) continues to live and reproduce normally and the prophage (phage genome) is transmitted to daughter cells at each subsequent division. During this cycle, there is no reproduction of new phage, only passive replication of the phage genome. This is because a phage encoded immunity repressor inhibits the lytic promoters, preventing expression of genes required for lytic development. If the inhibitory action of the immunity repressor is interrupted, repression of the lytic genes is relieved (i.e. derepression) and the prophage can excise from the host chromosome and resume lytic development. This process is called prophage induction and in many temperate phage is initiated when a stressor activates the host SOS system in response to DNA damage. Such stressors include changes in nutrients, pH or temperature, exposure to H_2O_2, antibiotics or DNA damaging agents like UV and mitomycin C (Casjens and Hendrix, 2015; Howard-Varona et al., 2017; Sturino and Klaenhammer, 2006). Not all temperate phage are SOS-inducible however, coliphage Mu and P2 for example, exhibit spontaneous induction that is independent of SOS activation (Christie and Dokland, 2012; Liu et al., 1997; Ljungquist and Bukhari, 1977; Rozanov et al., 1998).

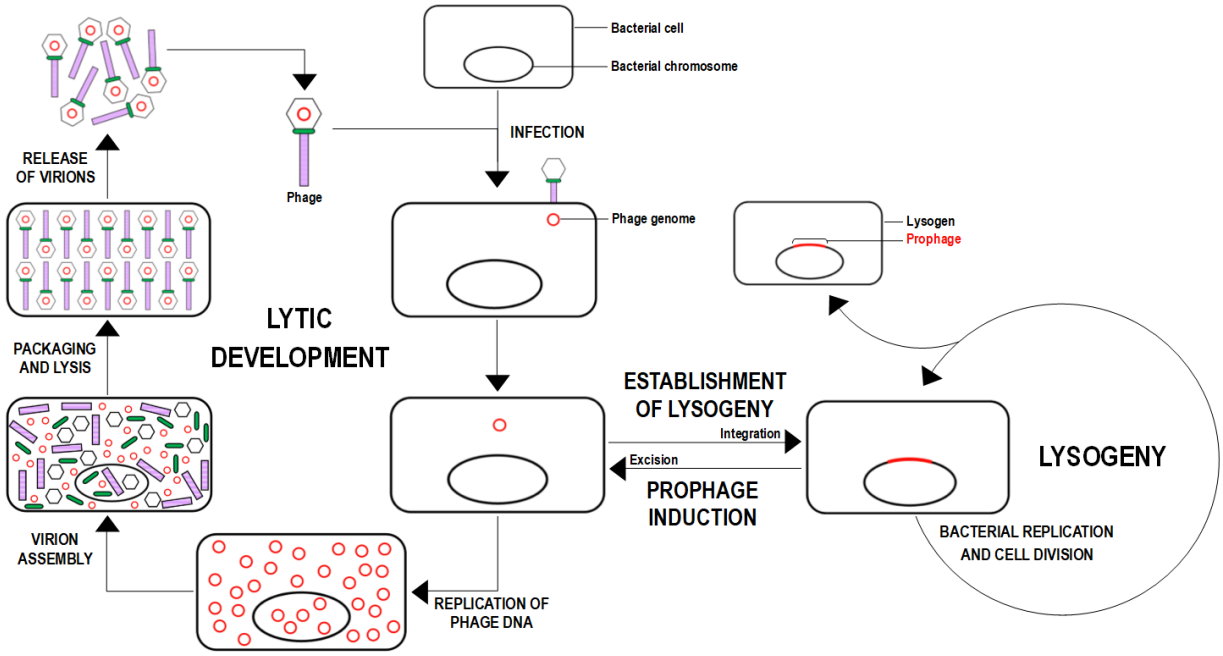

Figure 1.2: The lytic and lysogenic lifecycles of phage. Infection begins with the recognition and binding of phage to a bacterial surface moiety. The phage genome is injected into the host's cytoplasm and circularises via cohesive ends. *The lytic cycle* begins with expression of early lytic genes, which sets off the lytic cascade, resulting in replication of phage DNA and synthesis of late phage proteins required for virion assembly, DNA packaging and host cell lysis. *The lysogenic cycle* results in the phage genome integrating into the bacterial chromosome and enters a dormant/repressed reproductive state; passively transferred to daughter cells during bacterial replication. The lysogenic state is very stable; a phage will remain a prophage until it encounters a specific stressor. *Prophage induction* is typically activated when a DNA damaging event activates the host SOS response, which initiates prophage excision and the continuation of lytic development. Image adapted from Reed (1994).

The decision to lyse or not to lyse is controlled by a number of factors such as the presence or stabilisation of pro-lysogenic factors, low temperature, cell malnourishment and/or a high multiplicity of infection (MOI; the number of virus particles infecting a single cell) (Howard-Varona et al., 2017). Lysogeny offers the prophage a safe refuge when there is a shortage of host cells and conditions are unfavourable for their rapid reproduction. Establishing lysogeny in response to a high MOI is a strategy thought to prevent phage from wiping out their bacterial host(s). This essentially protects the phage and the host because the phage-encoded immunity repressor expressed to maintain lysogeny inhibits similar infecting phage from undertaking lytic development. Furthermore, expression of some phage-encoded genes during lysogeny can alter the cell surface phenotype of the host, making them invisible to compatible phage. In coliphage λ, the *rex* region of the phage genome encodes *rexA* and *rexB* genes, where coordinate expression of these genes is responsible for the Rex phenotype, a characteristic that provides the lysogen with the ability to exclude a wide variety of superinfecting phage (Landsmann et al., 1982). Furthermore, whilst nested within the host chromosome, a prophage can achieve accurate replication of its DNA and should it sustain any damage, utilise the host's DNA repair machinery, thereby protecting the integrity of its genome. Establishing lysogeny also protects the prophage from host defence mechanisms such as proteases, restriction enzymes and the CRISPR-Cas system (Paul, 2008).

1.0.5.1 Lytic and lysogenic development in bacteriophage λ

At a genetic/molecular level, temperate phage have developed numerous strategies to control their decision-making endeavours. A common strategy is the use of a specifically designed, highly evolved lytic/lysogenic transcriptional switch, encompassing two mutually exclusive operons (lytic or lysogenic). In this strategy, the establishment and stable maintenance of gene expression from one or the other operon is dependent on the host cellular conditions encountered by the phage early after infection. Coliphage λ and 186 are model examples of temperate phage that use such systems, where extensive studies on their regulatory genetic frameworks have contributed immensely to our understanding of the universal principles associated with prokaryotic transcription and gene regulation.

In the λ system, the *cI*-P_{RM}-O_R-P_R-*cro*-P_{RE}-*cII* lytic/lysogenic switch (Fig. 1.3) directs the decision to go lytic or lysogenic. Action at this switch entails an integrated set of protein-protein and protein-DNA interactions facilitated by short- and long-range cooperativity. The switch encompasses a central rightward regulatory region (O_R) arranged with three operator sites (O_R1, O_R2 and O_R3). O_R is an essential component for the regulation of lytic and lysogenic genes and overlaps promoters, P_R and P_{RM}. These promoters have a back-to-back orientation (separated by 82bp), where P_R controls transcription of genes from the lytic operon and P_{RM} controls transcription of genes from the lysogenic operon (Ptashne, 2006). Other elements important in influencing λ's developmental decisions are the *cII* gene expressed from P_R, the leftward regulatory region (O_L) located ~2.3kb upstream of the O_R region (Anderson and Yang, 2008) and the *cIII* gene expressed from P_L.

Lytic development starts with constitutive expression of early lytic genes from P_L, P_R and $P_{R'}$ promoters ($P_{R'}$ is the secondary rightward promoter, located downstream of P_R). Most importantly, the P_R transcript encodes *cro*, which gives rise to λCro, a repressor protein that prevents expression of *cI*. The product of *cI* is the immunity repressor (λCI), which is responsible for maintaining lysogeny. At low concentrations, λCro inhibits *cI* expression by binding with high affinity to the O_R3 site and blocking the recruitment of RNA polymerases (RNAP) to P_{RM} (Meyer et al., 1980; Ptashne, 2006; Takeda et al., 1989). At high concentrations, λCro binds to the weaker O_R2 site followed by binding to the O_R1 site to weakly repress transcription of P_R (Svenningsen et al., 2005). It has been proposed that the purpose of this regulation is to control *cII* expression, which encodes λCII, the lysogenic establishment factor that activates transcription of *cI* from the establishment promoter, P_{RE} (Ptashne, 2006). During lytic development, λCro inhibition of *cI* expression (from P_{RM} and P_{RE}) allows for the expression of all early, middle and late lytic genes required for the synthesis of the phage genome, assembly of new phage particles and the production of holin and endolysin proteins required for host cell lysis.

Lysogenic development is controlled by λCI. It represses *cro* expression by binding (as a dimer) to the O_R1 and O_R2 sites, thereby blocking recruitment of RNAP to P_R (Ptashne, 2006; Svenningsen et al., 2005). λCI's action at the O_R and O_L regions allows it to positively and negatively autoregulate the transcription of its own gene, which is essential for maintaining the repressor at a steady state that is sufficient to maintain lysogeny (Anderson and Yang, 2008). λCI's interaction with the O_R1 and O_R2 sites is a model example of cooperativity, because binding of a λCI dimer to O_R1 enhances the binding of a second λCI dimer to O_R2. Cooperativity at these sites not only represses *cro* expression, but also positively regulates the expression of *cI* from P_{RM}, such that when a λCI dimer is bound at O_R2, P_{RM} is activated ~10-fold by a direct protein-protein interaction with RNAP (Li et al., 1994; Meyer et al., 1980). Interestingly, the cooperativity observed between the O_R1 and O_R2 sites does not enhance λCI's affinity for the O_R3 site, which is occupied only when repressor levels are high. For λCI to bind at O_R3 (at physiological concentrations), the O_L regulatory region is required (Dodd et al. 2001, Dodd et al. 2004, Anderson and Yang, 2008).

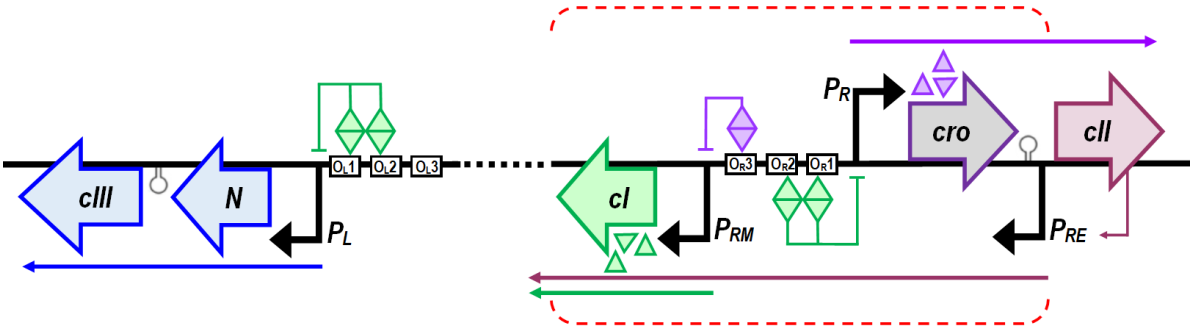

Figure 1.3: A genetic map of the λ lytic/lysogenic switch together with other genes and regulatory elements known to influence developmental decision-making. The central domain of the λ switch is the *cI-*P_{RM}*-*O_R*-*P_R*-cro-*P_{RE}*-cII* region (enclosed within red dotted brackets). During *lytic development,* Cro binds with high affinity to the O_R3 site to inhibit expression of *cI* from P_{RM}. To *establish lysogeny* high levels of CIII stabilise CII by protecting it from host proteolysis. CII activates expression of *cI* from P_{RE} to establish the initial pool of CI. During *lysogeny,* CI dominates the switch and represses expression of lytic genes from P_R and P_L by forming a tetramer at $O_R1/2$ and at $O_L1/2$ respectively. The *N* gene encodes the N antitermination protein, required for RNAPs to read over terminators located at the end of the early lytic genes. Genes are shaded left-and-right facing arrows. Promoters are solid black right-angled arrows and terminators are stem-loops. Coloured arrows indicate transcriptional output from each promoter. O_R and O_L regions feature as three black unshaded rectangles. CI and Cro monomers and dimers are green and purple triangles and diamonds respectively. CI tetramers appear as two horizontally linked diamonds (each triangular segment represents a single CI monomer). Image adapted from Anderson and Yang (2008); Lewis et al. (2011); Schubert et al. (2007) and Svenningsen et al. (2005).

λ (like other temperate phage) has evolved the ability to fine-tune the expression of its lysogenic immunity repressor such that the protein is equilibrated to a level that maintains lysogeny with remarkable stability - in the absence of an inducing agent, lysogeny is stable for countless generations - but keeps the prophage primed for induction. Finding this balance is crucial because being 'slow-off-the-block' when it comes to prophage induction could compromise phage survival, especially since host cell survival can be disturbed by numerous factors like, exposure to extreme temperatures, unfavourable pH conditions, antibiotics, antibacterials or conditions with low/no oxygenation, water and/or nutrients.

Whilst λCI's ability to positively control its own expression allows for the maintenance of lysogeny, it is thought that its negative autoregulation is important to ensure the repressor is maintained at a steady state that is not too high that it would compromise prophage induction. λCI negative autoregulation is carried out via a phenomenon called long-range cooperativity (Fig. 1.4A), where at high repressor concentrations, λCI dimers bind to operators O_L1 and O_L2 (in the O_L region). When these dimers are bound to O_L1, O_L2, O_R1, and O_R2 a 2.3kb loop is induced in the DNA, allowing these dimers to bind together to form an octamer (Anderson and Yang, 2008; Dodd et al., 2001; Oppenheim et al., 2005). Upon formation of the octamer, more λCI dimers may cooperatively bind to O_L3 and O_R3, blocking P_{RM} to repress transcription of *cI* (Fig. 1.4B). Hence, a lysogenic stable state of λCI is established and sustained by balancing the continual lodging and dislodging of λCI dimers from the O_L region, rendering P_{RM} in a closed or open state respectively.

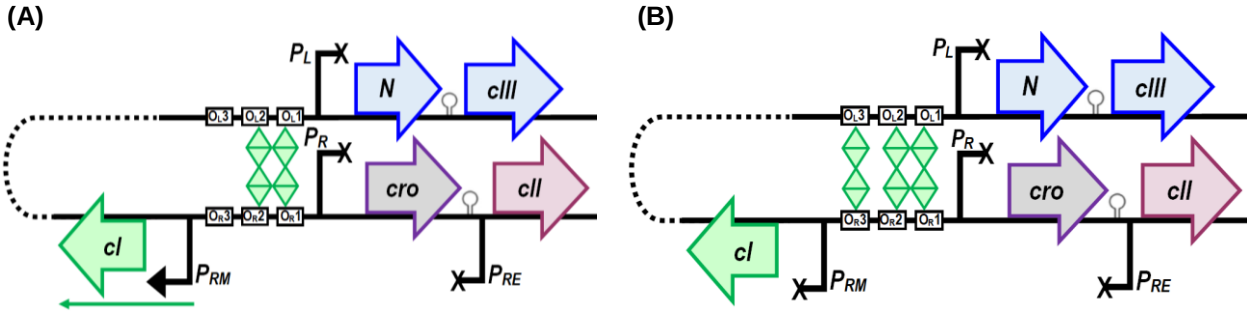

Figure 1.4: Genetic representation of λCI positive and negative autoregulation. For positive and negative autoregulation, DNA looping is observed between the O_L and O_R regions, facilitated by long-range cooperativity between CI tetramers bound at O_L and O_R operator sites. **(A)** *Positive autoregulation* is achieved when CI dimers at O_R1 and O_R 2 interact with CI dimers at O_L1 and O_R2 to form an octamer complex. The octamer represses the expression of all genes from P_R and P_L, but leaves P_{RM} open for transcription of *cI* by RNAPs. **(B)** *Negative autoregulation* is required when CI levels become too high. Cooperative recruitment of CI dimers to the weak O_R3 and O_L3 operators forms a repressive tetramer complex that blocks expression of *cI* from P_{RM}. Symbolism defined in Fig. 1.3. Image adapted from Lewis et al. (2011); Oppenheim et al. (2005) and Svenningsen et al. (2005).

If lytic development is the default cycle in temperate phage, then how does λ establish lysogeny? The lysogenic decision is largely dependent on the concentration of λCII, a pro-lysogenic factor expressed from P_R (second gene after *cro*). λCII establishes the initial pool of λCI, by acting as a potent transcriptional activator of *cI* expression from the establishment promoter, P_{RE} (Fig. 1.3) (Ptashne, 2006). λCII also activates transcription of the *int* gene from P_I (immediately downstream of *cIII* gene), the product of which is Integrase, a site-specific recombinase required for integration of the λ genome into the *E. coli* chromosome (Ptashne, 2006). To prevent unnecessary activation of P_{RE}, λCII has a protease sensitive C-terminal domain; making it highly vulnerable to host proteases such as the ATP-dependent protease, FstH (Kobiler et al., 2007). Expressing a protease-sensitive lysogenic establishment factor is an evolutionally adaptation that ensures λ does not enter lysogeny inappropriately.

If host proteases rapidly degrade λCII then how does λ elevate the level of this protein such that it can sufficiently activate P_{RE}? The λCIII protein, expressed from P_L, protects λCII from host proteases by acting as a competitive inhibitor of FstH, such that upon binding to the protease, λCIII induces a conformational change within the active site, inhibiting FstH binding and consequent degradation of the λCII substrate (Kobiler et al., 2007). Hence, high λCIII levels will allow for the stabilisation of λCII resulting in activation of *cI* expression from an activated P_{RE}, thereby facilitating the establishment of lysogeny. To maintain lysogeny, λCI will positively and negatively autoregulate its transcription from P_{RM} as the expression of all genes from early lytic promoters (including *cII* and *cIII*) become inhibited by λCI (Ptashne, 2006).

After having established lysogeny, λ's ability to switch back to lytic development (i.e. prophage induction) is an event inherently linked to the host SOS response. In response to a DNA damaging event (e.g. exposure to UV) the host encoded DNA repair protein, RecA stimulates the cleavage and consequent inactivation of λCI, whilst expression of *cI* from P_{RM} is repressed by λCro (*cro* now expressed from a derepressed P_R) (Oppenheim et al., 2005; Schubert et al., 2007; Svenningsen et al., 2005). Inactivation of λCI derepresses the early lytic promoters, thereby enabling the expression of *xis* gene from P_I, the product of which is the excisionase - the protein factor required to remove the λ prophage from the host chromosome - and all the necessary lytic factors required for lytic reproduction.

It is important to address the fact that within the realm of temperate phage, λ is only one member and demonstrates just one of many developmental switch systems. Other phage have evolved their own regulatory frameworks that inherently solve the same question but in a different way. As mentioned previously, the temperate coliphage 186 also uses a bistable lytic/lysogenic switch to make developmental decisions. Despite their being a number of overlapping similarities between λ and 186, studies have revealed the 186 switch has a number of unique aspects. These unique characteristics also make 186 an ideal model system for the study of molecular mechanisms involved in the regulation of prokaryotic gene expression. The following section provides an in-depth explanation of 186 biology and development and the underlying molecular mechanisms this phage has evolved to regulate its reproduction.

1.1 Bacteriophage 186

Coliphage 186 is a UV-inducible, non-lambdoid temperate phage of the family *Myoviridae* (genus *P2-likevirus*) (Nilsson and Haggård-Ljungquist, 2005). It has the standard tailed morphological phage structure (see Fig. 1.1) and a small linear dsDNA genome (30.6kb). The ability of 186 to undergo two interchangeable modes of development (lytic or lysogeny) is regulated by the *int-cI-pR-pL-apl-pE-cII* lytic/lysogenic switch (Fig. 1.5 - red dotted brackets). Like the λ system, action at the switch entails numerous protein-protein and protein-DNA interactions assisted by short- and long-range cooperativity.

Located to the left of the switch is the *pB* promoter that drives expression of the *B* gene. *B* encodes the B protein required for activation of late lytic gene expression (Portelli et al., 1998). The 186 switch encompasses two key promoters, *pL* and *pR*, which have a face-to-face orientation, separated by 62bp. *pR* controls transcription of genes from the lytic operon and *pL* controls transcription of genes from the lysogenic operon. The *int* gene encodes Integrase, a site-specific recombinase that binds the phage attachment site (*attP*) and catalyses the insertion of the phage genome into one of two *E. coli* attachment sites (*attB1/2*) (Neufing et al., 2001; Reed et al., 1997).

Like λ, the *cI* gene encodes the CI immunity repressor, which is essential for the maintenance of lysogeny. To maintain lysogeny, CI represses the expression of lytic genes by binding to high affinity operator sites at *pR* and *pB* (Reed, 1994) and positively and negatively regulates the expression of its own gene by cooperative binding to weaker operator sites within the switch region (found at *pL, FR* and *FL*) (Dodd and Egan, 2002, 1996). The *apl* gene encodes the Apl excisionase, a recombination directionality factor (RDF) that (during prophage induction) controls excision of the prophage from the host chromosome. Apl also weakly represses *pR* and *pL* during prophage induction (Reed, 1994), the purpose of which is poorly understood. The *cII* gene encodes the CII establishment of lysogeny factor and as the name suggests, is required for the establishment of lysogeny (Murchland et al., 2014). Whilst not studied in this thesis, the *A* gene encodes the A replicase, which is required for replication of the 186 genome (Sivaprasad et al., 1990).

Like all temperate phage, 186 can undergo prophage induction, which (like λ) is naturally linked to the host SOS response. In the λ system, prophage induction occurs when RecA stimulates autoproteolysis of λCI (Svenningsen et al., 2005). Lamont et al. (1989) discovered that in the 186 system, RecA is not directly involved in the inactivation of CI due to the absence of a RecA protease cleavage site in the repressor's amino acid sequence. Instead, prophage induction occurs when the antirepressor protein, Tum is expressed from the 186 SOS operon and inactivates CI by reversibly sequestering it into a non-DNA binding form (Shearwin et al., 1998).

This brief comparison of the λ and 186 lytic/lysogenic switch shows that despite achieving the same outcome, the mode in which these phage make their developmental decisions differs, with each system having different promoter arrangements and alternative modes of regulation. The use of these systems to achieve a common goal via uncommon means demonstrates why λ and 186 serve as model systems to investigate the natural evolution of alternative prokaryotic gene regulatory circuits.

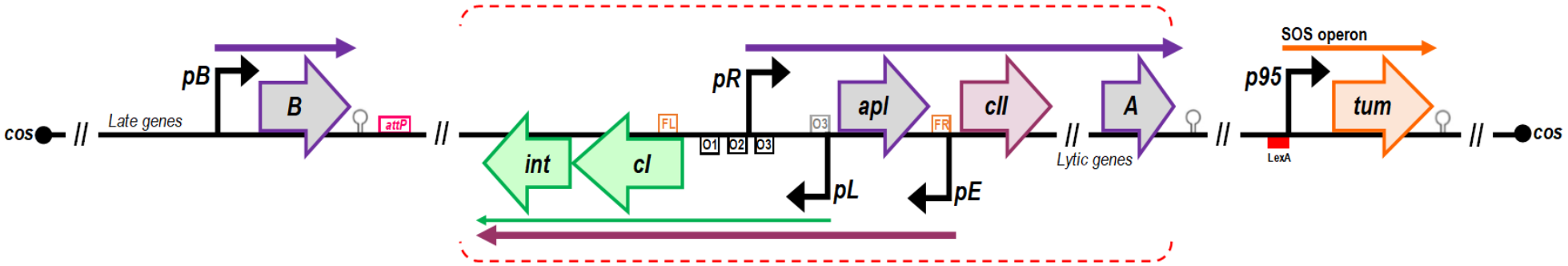

Figure 1.5: A genetic map of the 186 lytic/lysogenic switch together with other genes and regulatory elements known to influence developmental decision-making. The central domain of the 186 switch is the *int-cI-pR-pL-apl-pE-cII* region (enclosed within red dotted brackets). During *lytic development*, *pR* and *pB* are active and express the early lytic genes required to initiate the lytic cascade. Late stage lytic development is dependent on expression of the *B* gene from *pB*. During *lysogeny*, CI (expressed from *pL*) dominates the switch and represses *pR* and *pB* to inhibit lytic development, whilst weakly repressing *pL* to autoregulate the expression of its own gene. *Prophage induction* is dependent on the expression of *tum* from the SOS operon, which is naturally repressed by the host encoded LexA repressor. Genes are shaded left-and-right facing arrows. Promoters are solid black right-angled arrows and terminators are stem-loops. Coloured arrows indicate transcriptional output from each promoter, with thickness indicating approximate promoter strength. *pR* operators are black-bordered rectangles, the *pL* operator a grey-bordered rectangle and *FL* and *FR* sites are orange-bordered rectangles. The red rectangle under *p95* is the LexA operator site and the pink-bordered rectangle is the phage attachment site (*attP*). (*B*) encodes Activator B, (*int*) encodes Integrate, the 186 site-specific recombinase, (*cI*) encodes the CI immunity repressor, (*apl*) encodes Apl, the 186 excisionase and CI transcriptional repressor, (*cII*) encodes the CII establishment of lysogeny factor, (*A*) encodes Replicase A and (*tum*) encodes Tum, the CI anti-repressor. Image adapted from Dodd et al. (1993); Dodd and Egan (1996); Reed (1994) and Shearwin et al. (2002).

1.1.1 Lytic and lysogenic development in bacteriophage 186

The 186 temperate lifecycle encompasses lytic and lysogenic development, with the decision to enter either cycle made shortly after infection. The spontaneous and SOS-inducible properties of 186 allow it to switch back from lysogenic to lytic development via a process termed prophage induction. Extensive research of 186 over the last four decades has provided the scientific community with a reasonably coherent picture of what regulatory proteins are involved in the lytic and lysogenic cycles of 186.

1.1.1.1 186 lytic development

Lytic development is the default developmental state and occurs shortly after injection of the linear 186 genome into the host cell and its circularisation via *cos* sites (12-base GC-rich cohesive 'sticky' ends) (Christie and Calendar, 2016; Ziermann and Calendar, 1990). Lytic development begins with rightward transcription of early lytic genes from promoter, *pR* and *pB.* In contrast to λ, to undergo lytic development 186 does not employ a Cro-like factor, rather, the naturally weak *pL* promoter for *cI* and *int* is inhibited some 10-fold by convergent transcription from the naturally strong *pR* promoter (Fig. 1.6). This phenomenon is termed transcriptional interference (TI), defined by Shearwin et al. (2005) as *'the suppressive influence of one transcriptional process, directly and in cis, on a second transcriptional process'*.

Transcription from *pR* results in expression of early lytic genes. The first two genes, *apl* and *cII* encode helix-turn-helix (HTH) DNA binding regulatory proteins, Apl and CII. Apl is the 186 RDF (i.e. excisionase), but it also weakly represses transcription of lysogenic genes from *pL* and weakly represses *pR* to autoregulate its own expression (Reed et al., 1997). CII is the pro-lysogenic factor required for establishing lysogeny. It is a potent transcriptional activator of the establishment promoter, *pE*, which when activated transcribes *cI* to establish the initial pool of CI required for setting the 186 switch to the lysogenic state (Murchland et al., 2014). The *A* gene is the final gene of the *pR* operon and encodes the A replicase, which is the only phage-encoded factor required for replication of the 186 genome (Sivaprasad et al., 1990). Late stage lytic development is dependent on expression of the *B* gene from the *pB* promoter. The B protein is a critical activator of late lytic promoters, which drive expression of some 20+ genes encoding structural, assembly, DNA processing, DNA packaging and host cell lysis proteins (Portelli et al., 1998). With continual expression of *A* and *B*, late stage lytic development results in extensive replication of phage DNA, the assembly of new virus particles and their release into the extracellular environment via lysis of the host cell.

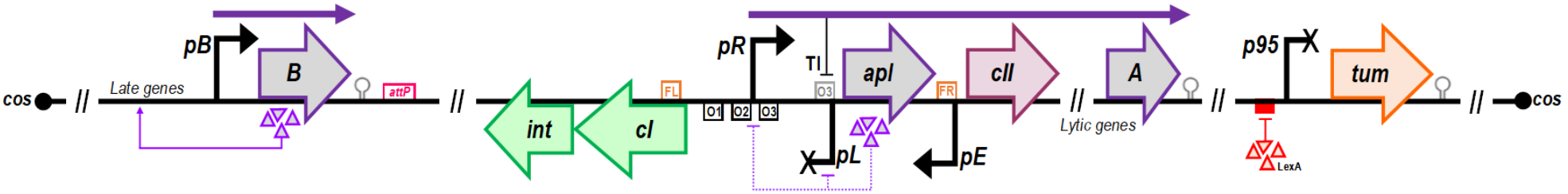

Figure 1.6: Action at the 186 lytic/lysogenic switch during lytic development. Lytic development begins with transcription of early lytic genes from *pR* and *pB*. Expression of lysogenic genes (from *pL*) is inhibited by *pR* transcriptional interference (TI). Apl also weakly represses transcription of *cI* and *int* from *pL* and weakly represses *pR* to autoregulate its own expression. The A replicase is required for replicating the phage genome and the B protein is required for activating the expression of the late lytic genes. The SOS operon remains dormant due to LexA repression of *p95*. Symbolism as defined in Fig. 1.5. Image adapted from Reed (1994).

1.1.1.2 Maintenance of lysogeny

During lysogeny, the *E. coli* host and 186 exist as a lysogen and prophage respectively, with replication of the phage genome occurring passively with host cell DNA replication. The *pL* promoter becomes the predominant phage promoter active in the lysogen and expresses *cI* and *int* genes (Fig. 1.7). In the presence of CI, *pR* and *pB* are repressed; inhibiting transcription of all lytic genes and *pL* is indirectly activated with the removal of *pR* TI by CI (Dodd and Egan, 2002). Like λCI, 186CI also positively and negatively regulates the expression of its own gene from *pL,* which establishes a lysogenic steady state of CI that is sufficient to maintain lysogeny (Dodd et al., 2001).

Since the 186 switch lacks the O_R and O_L regions of the λ system, 186CI maintains lysogeny by cooperatively binding to specific operator sites (of varying affinities) within the switch region. To repress *pR,* CI binds three high affinity operator sites (at *pR*), whilst the presence of a weak putative operator at *pL* allows CI to repress *pL* when at high concentrations, which is important for negative autoregulation. The presence of two distal operator sites, *FL* and *FR* assist with CI *pR* repression to maintain lysogeny and *pL* derepression to facilitate positive autoregulation of *cI* from *pL* (Dodd and Egan, 2002, 1996).

Furthermore, to maintain lysogeny, the Apl and Tum proteins must be repressed. Transcription of *apl* is inhibited by CI *pR* repression, which stabilises the integration status of the prophage as the Apl-Int interaction would form the excision complex. To prevent unnecessary induction, expression of the *tum* gene from the SOS operon is inhibited by LexA repression of *p95.* LexA also represses various *E. coli* genes involved in the response to DNA damage; forming part of the host SOS regulon (Voloshin et al., 2001).

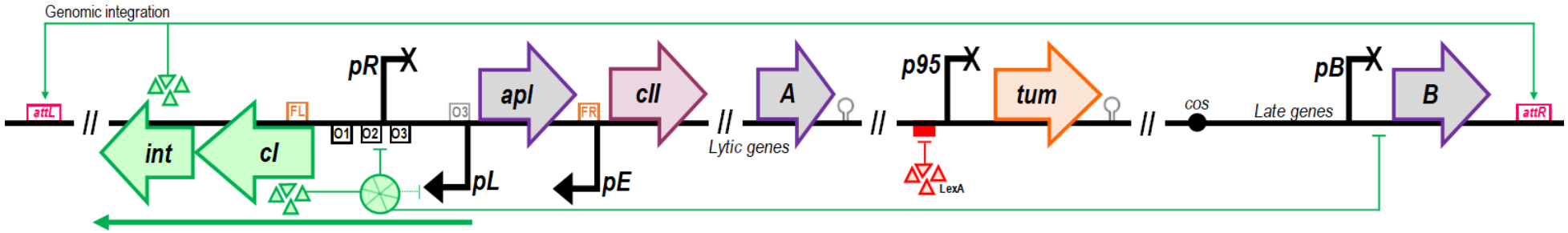

Figure 1.7: Action at the 186 lytic/lysogenic switch during lysogeny. Entry into lysogeny requires a brief period of CII mediated *pE* activation to establish the initial pool of CI and Int. Once *pE* initiated CI represses *pR*, Apl and CII expression is inhibited and the *pL cI* transcript is employed to maintain CI at its lysogenic steady state. sDuring lysogeny, CI inhibits lytic development by repressing transcription of the early lytic genes from *pR* and *pB*. To regulate the transcription of its own gene, when CI levels become high, CI represses *pL* thereby establishing an autoregulatory negative feedback loop. For 186 to maintain its prophage status, *apl* expression must be inhibited (achieved by CI repression of *pR*) to prevent formation of the Apl-Int excisionase complex. The SOS operon must also remain dormant, which is achieved by LexA repressing *p95.tum* expression, the product of which would inactivate CI and thus trigger prophage induction. Symbolism as defined in Fig. 1.5. Image adapted from Reed (1994).

1.1.1.3 The Immunity Repressor, CI

The CI immunity repressor - encoded from the *cI* gene of the *pL* lysogenic operon - is the regulatory factor essential for the maintenance of lysogeny. CI takes repressive action at the 186 switch in the form of a multimeric wheel where it intricately wraps onto DNA using designated operator sites (Fig. 1.8A/B). *In vitro* binding studies with purified CI have identified CI binding sites at *pR.pL, pB, FL* and *FR. FL* and *FR* sites are located -327 and +352bp from *pR* respectively and are important in CI *pR* and *pL* regulation (Dodd and Egan, 2002, 1996). The DNA sequence determinants of CI binding however are not well defined. Genetic studies indicate three operators at *pR* and a consensus operator sequence has been obtained for sites at *pB, FL, FR* and *pR-O2,* but these are not matched by the *pR-O1* and *pR-O3* sites (Dodd and Egan, 1996).

Dodd and Egan (2002) extensively studied CI *pR* and *pL* regulation using *pR* and *pL* LacZ reporters with CI expressed from IPTG-inducible plasmids. In Figure 8C, the *pR(pL$^+$)* LacZ reporter shows CI strongly represses *pR* and repression is enhanced in the presence of *FL* and *FR* sites. *pL* is a naturally weak promoter and in the absence of CI, is weakened further by *pR* TI (promoter activity ~6-fold greater when *pR* is mutated or deleted) (Fig. 1.8C *pL(pR$^-$)* and *pL(pR$^+$)* LacZ reporter data). CI at low concentrations activates *pL* by the exclusive removal of *pR* TI, as CI does not activate *pL* when *pR* is mutated. At high CI concentrations, CI represses *pL,* but repression is lost if the three *pR* operators are removed or if 5bp insertions or deletions are made in the DNA between *pR* and *pL*. This suggests cooperative binding occurs between the *pR* sites and a putative/weak operator at *pL* (Dodd and Egan, 2002, 1996).

Structural information about CI has provided the basis for a model of how CI regulates *pR* and *pL.* The CI N-terminal domain (NTD) contains a HTH DNA binding motif and the C-terminal domain (CTD) is responsible for self-association (Shearwin et al., 2002; Shearwin and Egan, 1996). X-ray structures of crystals of the CI CTD and a full-length CI dimer led to a model where 14 CI dimers arrange in a wheel-like structure, with the CTDs forming the interior of the wheel and the NTDs locating to the exterior/rim of the wheel (Pinkett et al., 2006). Such a structure was proposed to allow DNA to wrap around the outside of the wheel (Fig. 1.8B), with evidence of this wrapping obtained by atomic force microscopy (AFM) (Wang et al., 2013). Recent X-ray crystallography data for a protein-DNA complex organised by the CI-CTD confirms this wheel-like structure. These studies however, indicate the original 14-mer CI structure is likely to be a crystal artifact and rather a 12-mer CI wheel exists as the primary structure in solution (Jia Truong, personal communication). According to the regulatory model, CI repression of *pR* is achieved by strong binding of the three *pR* operators to a single CI wheel (Fig. 1.8D Species 1).

The DNA adjacent to these operators can also wrap onto the wheel with DNase footprinting and AFM measurements indicating a preference for the DNA on the *pL* side (Fig. 1.8D Species 2) (Pinkett et al., 2006; Wang et al., 2013). The *FL* and *FR* sites are envisaged to assist CI repression of *pR* by binding to the same wheel and provide cooperative stabilisation of the CI-*pR* complex (Fig. 1.8D Species 3). CI repression of *pL* is thought to occur when the *pL* DNA wraps onto the *pR*-bound wheel (Fig. 1.8D Species 2).

Strong CI activation of *pL* requires the presence of *FL* and *FR* sites. The ability of *FL* and *FR* to enhance *pL* activity is thought to result from competition for limited sites on the CI wheel, where at most a single CI wheel can accommodate *pR* plus one of three possible operators to give CI-*pR.pL,* CI-*pR.FL* or CI-*pR.FR* looped configurations (Dodd et al., 2007). RNAP accessibility to *pL*, requires *pL* operators to be unoccupied by CI and this is achieved when CI binds *FL* or *FR* sites because it prevents *pL* DNA from wrapping onto the CI wheel (Fig. 1.8D Species 3). In the presence of *FL* and *FR, pL* is active because it can remain unbound while *pR* is repressed by CI and its TI relieved. At higher CI concentrations however, *FL* and *FR* sites become occupied by independent CI wheels and can no longer outcompete *pL* off the CI wheel at *pR*, leading to repression of *pL* (Fig. 1.8D Species 4).

Repression of *pL* by CI at higher concentrations is expected to provide negative autoregulation of *cI*, which should limit the concentration of CI produced in a 186 lysogen. For comparison, in Figure 8C, the *pL(pR$^+$)* LacZ reporter in the presence of *FL* and *FR* produces approximately the same amount of CI as a 186 lysogen when supplied ~40uM IPTG (Dodd and Egan, 2002). In a study by Dodd et al. (2001) the analogous λCI protein was shown to negatively regulate its own transcription at higher concentrations via a mechanism that reduces the lysogenic CI concentration ~2.5-fold. In the same study, when this negative autoregulation was eliminated, there was a significant decrease in the efficiency of λ prophage induction by UV, presumably because higher CI levels make it more difficult to derepress the lytic promoters. Hence, studies of λ phage have revealed positive and negative autoregulation of the immunity repressor is important for the maintenance of lysogeny and for keeping the prophage primed for induction. As part of our studies of CI, we decided to investigate whether the same principle applies to 186; asking the question, is 186CI negative feedback autoregulation important for optimisation of 186 prophage induction efficiency?

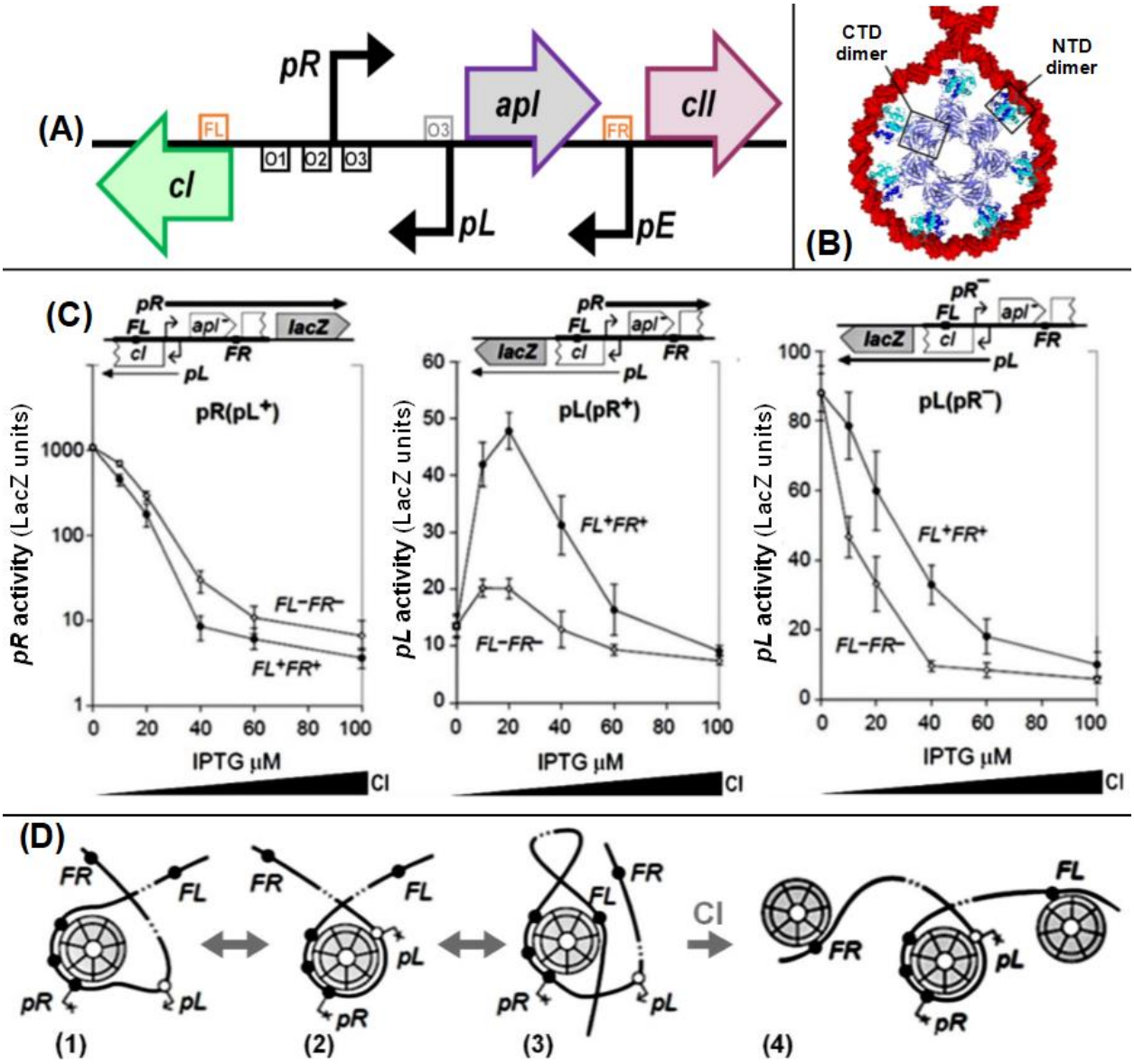

Figure 1.8: The 186CI immunity repressor. **(A)** A simplified genetic map of the 186 switch showing key CI operator sites (not to scale). Boxes denote CI binding sites based on footprinting data and sequence analysis. Black boxes represent strong, well defined binding sites, grey boxes represent more weakly protected regions at *pL* and *FL* and *FR* sites are shown as orange boxes. **(B)** A hypothetical structural model of the CI wheel based on crystal structures of the CI-CTD 14-mer and an intact dimer (Dodd et al., 2007). **(C)** To study *pR* and *pL* CI regulation Dodd and Egan (2002) measured *pL* and *pR* activity in response to various concentrations of CI supplied from IPTG-inducible plasmids. The reporter constructs are shown, with *pL(pR+)* and *pL(pR–)* presenting *pL* LacZ activity as a function of CI concentration in the presence and absence of *pR* TI respectively. Both plots show the presence of *FL* and *FR* sites to be important in *pL* derepression. *pR(pL+)* presents *pR* LacZ activity as a function of CI concentration, where repression increases in response to increasing CI and is enhanced in the presence of *FL* and *FR* sites. **(D)** Examples of CI-DNA predicted binding configurations (Dodd et al., 2007). The HTH domains of three adjacent CI homodimers can bind three major grooves of adjacent *pR* operators (Species 1). CI binding to the weaker *pL* operator can produce a wrapping configuration that facilitates negative autoregulation (Species 2). Species 3 illustrates how *FL* and *FR* sites conserve *pR* repression but relieve CI repression of *pL*. At high CI concentrations, the presence of *FL* and *FR* becomes redundant as *pR* and *pL* are repressed when multiple CI wheels are bound to DNA (Species 4).

1.1.1.4 Establishment of lysogeny

In approximately 10% of infections, 186 establishes lysogeny (Bertani, 2004; Dodd and Egan, 1999). Figure 1.9 illustrates that access to lysogenic development requires transcription of *cII* from *pR* and *cI* and *int* from *pE.* CI is required to inhibit lytic development by repressing the expression of the early lytic genes from *pR* and *pB.* Integrase (Int), the 186 site-specific recombinase is required to catalyse the insertion of the phage genome into one of two *E. coli* attachment sites (*attB1/2*). To establish lysogeny, both coliphage λ and 186 express a CII pro-lysogenic factor from the lytic transcript. This factor acts as a potent transcriptional activator of the establishment promoter (P_{RE} in λ and *pE* in 186), where when activated can achieve sufficient production of the immunity repressor (Murchland et al., 2014; Neufing et al., 2001).

In the 186 system, a CII-activated *pE* is required for lysogeny because early after infection TI from an active *pR* exerts a strong repressive effect on *pL* (Dodd and Egan, 2002). In the absence of CII, *pR* also exerts ~2-fold TI effect on *pE* (Hao et al., 2019; Neufing et al., 2001), but when *pE* is activated by CII it becomes a very strong promoter such that it can overpower any convergent transcription from *pR* and thus achieve adequate expression of *cI* and *int* early after infection. The need for a CII-activated *pE* to establish lysogeny was clearly demonstrated by Shearwin and Egan (2000) where they developed and characterised a series of 186 phage mutants defective for activation of *pE*. As expected, these mutants exhibited significant impairment in establishing lysogenic development, with <1% of infections resulting in lysogeny.

Initiating expression of the *pE-cI* transcript early after infection leads to repression of *pR*, which is important for preventing the expression of *apI,* the product of which would form the Apl-Int excisionase complex. Furthermore, with *pR* inactivated, the TI it exerts on *pE* and *pL* is relieved - Dodd and Egan (2002) showed in the absence of *pR* TI, *pL* activity increases ~7.5-fold. This allows for a transitory period of *cI* (and *int)* expression from both promoters, where the output from each promoter has an additive effect and so confirms the decision to go lysogenic (Neufing et al., 2001). After establishing lysogeny, CII and *pE* are not required for the maintenance of lysogeny (*pR.cII* expression becomes inhibited by CI). Instead, the weak *pL* promoter that is no longer repressed by *pR* TI is employed to maintain CI levels, with the lysogenic CI steady state controlled by positive and negative autoregulation.

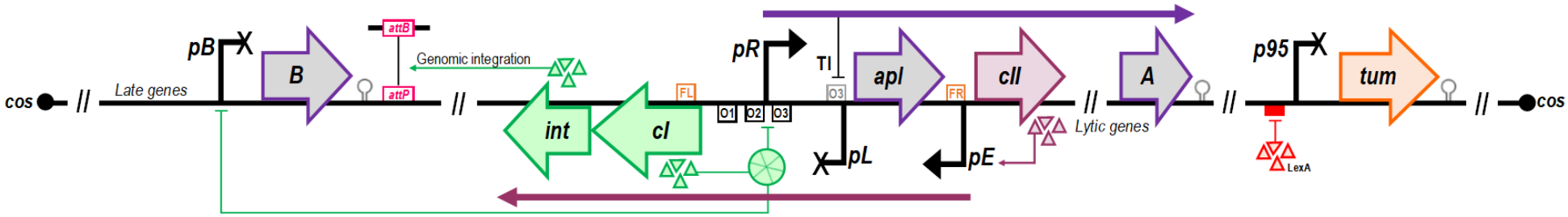

Figure 1.9: Action at the 186 lytic/lysogenic switch during the establishment of lysogeny. Lysogeny is established by activation of the *pE-cI* transcript by the establishment of lysogeny factor, CII. CI is required to inhibit lytic development by repressing expression of the early lytic genes from *pR* and *pB*, whilst Integrase binds the 186 attachment site (*attP*) and catalyses the insertion of the phage genome into one of two *E. coli* attachment sites (*attB*). Whilst the naturally weak *pL* promoter is inhibited by *pR* TI, a CII-activated *pE* is strong enough to overcome any convergent transcription from *pR* and so achieves adequate expression of *cI* and *int* to establish lysogeny. During this stage of development, the SOS operon is repressed by LexA so to not compromise the decision to go lysogenic. The 12-mer CI wheel is represented as a green-segmented circle, with each segment representing a single CI dimer (12 monomers in total). Remaining symbolism as defined in Fig. 1.5. Image adapted from Reed (1994).

1.1.1.5 The Establishment of Lysogeny Factor, CII

The *cII* gene of the 186 *pR* lytic operon encodes CII, an 18.7kDa pro-lysogenic factor that acts as a potent transcriptional activator of the establishment promoter, *pE.* CII has a NTD with a predicted HTH motif and a CTD that is highly sensitive to host proteolysis. Active CII exists as a pre-formed tetramer, where the NTD-HTH motif is responsible for binding the protein to two inverted 7-mer half-sites (ATGTTTG) at *pE*, which significantly amplifies promoter activity (up to ~400-fold activation) by facilitating the direct recruitment of RNAPs (Murchland et al., 2014). For coliphage λ and 186 there is an apparent paradox in expressing a pro-lysogenic factor from the lytic promoter, which is, would the activity of CII not introduce a bias towards lysogeny? In the λ system, this paradox is resolved by the fact that λCII is rapidly degraded by the host protease FtsH and so in only a small fraction of infections does λCII accumulate to the level necessary for the establishment of lysogeny (Hoyt et al., 1982; St-Pierre and Endy, 2008). As part of our investigation of 186CII, we also wished to determine whether its susceptibility to proteolysis serves a similar role such that it prevents CII levels from becoming elevated early after infection to prevent the phage from developing a bias towards lysogeny.

1.1.1.6 Prophage induction

Prophage induction is the process in which 186 switches from lysogenic to lytic development. It encompasses two key steps, (1) the inhibition of active CI and repression of *cI* gene expression from *pL* and (2) excision of the prophage from the host chromosome (Fig. 1.10). Spontaneous switching occurs at a low rate in 186, but in contrast to its close relation P2 (a non-inducible coliphage), 186 is surprisingly SOS-inducible; meaning DNA damaging agents that activate the host SOS response (e.g. UV irradiation or mitomycin C) are strong inducers of 186 prophage induction (Lamont et al., 1989).

SOS-induction of 186 is dependent on the *tum* gene, which is not transcribed during lysogeny due to repression of the *p95* promoter by LexA. DNA damage that results in single-stranded DNA (an SOS-inducing condition) activates the *E. coli* DNA repair protein, RecA, which stimulates autoproteolysis of LexA. This results in derepression of host SOS genes and 186 *tum*. Tum is an antirepressor protein that reversibly sequesters active CI into a non-DNA binding form (Shearwin et al., 1998). Removal of CI activity derepresses *pR* and *pB* and restarts lytic development. With *pR* active, two things occur, (1) *pL.cI* expression is inhibited as *pL* is inactivated by *pR* TI and (2) Apl expressed from an active *pR* binds to the pre-existing Int to form the Apl-Int excision complex, which is required to remove the prophage from the host chromosome. Rapid replication of phage DNA and the expression of the late lytic genes results in full lytic development and subsequent lysis of the host cell for the release of new daughter phage into the extracellular environment.

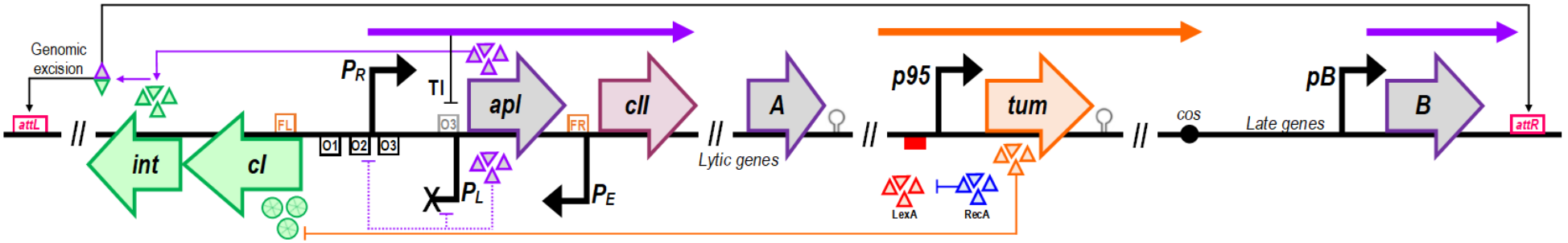

Figure 1.10: Action at the 186 lytic/lysogenic switch during prophage induction. Prophage induction begins with activation of the host SOS system (via DNA damage). The DNA repair protein RecA, catalyses the autoproteolysis of LexA, resulting in *p95* depression and *tum* expression. Tum inactivation of CI results in the derepression of *pR* and *pB,* thereby initiating lytic gene expression. Excision of the prophage from the host chromosome occurs when Apl (expressed from a derepressed *pR*) binds Int to form the Apl-Int excision complex. The excised phage then proceeds with DNA replication, the assembly and packaging of new daughter phage and their release into the extracellular environment via host cell lysis. Symbolism as defined in Fig. 1.5 and Fig. 1.9. Image adapted from Reed (1994).

1.1.1.7 The Antirepressor, Tum

Prophage induction is the ability of temperate phage to switch from lysogenic to lytic development. For λ and 186, prophage induction is triggered when RecA catalyses the autoproteolysis of λCI or LexA respectively. For 186, inactivation of LexA allows for the expression of the *p95.tum* transcript, resulting in the production of Tum. The full-length *tum* gene (also termed *orf95.1*) encodes a 146-amino acid (27.5kDa) *trans*-acting antirepressor that binds and reversibly antagonises CI into an inactive state. This prevents CI from binding to its operator sites and thus relieves repression of lytic promoters, *pR* and *pB* (Shearwin et al., 1998).

Interestingly, previous studies have identified five additional potential in-frame translation start sites within the *orf95.1* sequence, referred to as *orf95.2* to *orf95.6*. Whilst *orf95.2*, *orf95.4* and *orf95.5* are actively expressed only the full-length product has antirepressor activity (Brumby et al., 1996). Functional analysis of Tum protein structure suggests the antirepressor activity resides within the NTD. The CTD and the shorter Orf95.4 and 5 proteins are thought to play an inhibitory role in 186 SOS-induction because they exhibit homology to the *E. coli* DinI protein, a factor thought to act as a physiological down-regulator of the SOS response (Voloshin et al., 2001). This inhibitory role was reinforced when *tum* mutants lacking the CTD or the ability to express the nested Orf95.4 and 5 proteins were observed by Brumby et al. (1996) and in our Tum study to exhibit enhanced prophage induction. Whilst we have some understanding of DinI, its role in the SOS response remains unclear and the exact function of the short Tum proteins and the DinI-like CTD of full-length Tum is yet to be determined.

1.1.1.8 The Excisionase, Apl

Encoded from the *apl* gene of the 186 *pR* lytic operon is Apl, a small 87-amino acid protein that acts as the 186 recombination directionality factor (RDF) (i.e. excisionase) and a weak transcriptional repressor at *pR* and *pL* during early lytic development and prophage induction (Dodd et al., 1990). Apl's role as the excisionase is well characterised, but its role as a transcriptional repressor at *pR* and *pL* remains unclear. DNase footprinting studies revealed Apl binds to the *attP* region and between *pR.pL,* where five and seven copies (respectively) of a 6bp consensus sequence (TGGCAA) are arranged as direct repeats spaced 10-11bp apart (Fig. 1.11) (Dodd et al., 1993). Apl is a monomeric HTH DNA binding protein that requires three consecutive operators for efficient binding and binds with high cooperativity to the *attP* and *pR.pL* sites (Shearwin and Egan, 1996). In a study by Dodd et al. (1993), Apl's excisionase behaviour was described to be analogous to that of λXis, where during prophage induction, Apl (in complex with Int) binds its *attP* direct DNA repeats and modulates the reversal of the site-specific recombination reaction catalysed by Int during the establishment of lysogeny.

In the same study, 186 *apl*$^{-}$ phage were observed to be strongly defective in prophage induction, which is consistent with the need for Apl for excision of the prophage. This mutant phage however, remained competent for lytic development after infection and for the establishment of lysogeny, indicating Apl binding at *pR.pL* is not required for lytic development, nor does it impose any restraint on the decision to enter lytic or lysogenic development after infection.

A revised hypothesis for Apl's transcriptional repression at *pR.pL* is that it plays a role in prophage induction. Reed et al. (1997) proposed Apl may aid in the efficiency of prophage induction by repressing *cI* expression from *pL.* This activity is analogous to λCro, where repression of P_{RM} by Cro is needed to prevent synthesis of new CI that would otherwise impede lytic development (Schubert et al., 2007). A similar role for Apl *pL* repression in 186 prophage induction is supported by studies of phage mutants defective in Apl binding at *pR.pL.* It has been observed that lytic development of infecting 186 phage is blocked in cells over-expressing Apl, presumably due to repression of *pR.* A family of 16 spontaneous Apl-resistant operator 186 phage-mutants called the grow-on-*apl (goa)* mutants are able to overcome this block because they carry mutations in the *pR.pL* Apl binding sites (Reed et al., 1997). The class A *goa2* mutant (Fig. 1.11) was found partially defective in Apl *pR* repression but retained Apl *pL* repression and was competent for prophage induction. The class B *goa8* mutant (Fig. 1.11) was defective in Apl repression of both *pR* and *pL* and defective in prophage induction. The difference between these mutants supports the idea that Apl *pL* repression is important for prophage induction.

The *goa8* mutation does complicate the situation however, because it is a 5bp deletion centred between *pR.pL*. The mutation strongly reduces Apl binding to the whole *pR.pL* region (Keith Shearwin, personal communication) but it also disrupts the spacing between the *pR* and *pL* CI operator sites, which in consequence may affect the ability of CI to cooperatively bind at *pR* and *pL* due to the incorrect alignment of these operators with a CI-HTH motif. Previous reporter studies by Dodd and Egan (2002) showed altering the *pR.pL* spacing by 5bp insertions or deletions prevented CI repression of *pL*. An alternative explanation is that disruption of the spacing between *pR* and *pL* operator sites by *goa8* leads to the loss of negative CI autoregulation. This would explain the defective prophage induction of the *goa8* mutant because if CI concentration within the host cell exceeds the optimal lysogenic CI level a strong bias towards lysogeny and its maintenance would be established. As part of this thesis, we decided to investigate the nature in which the *goa8* mutation impairs 186 prophage induction, either by disrupting CI negative autoregulation or by impeding Apl repression of the *pL.cI* transcript.

An alternative way Apl binding at *pR.pL* might aid prophage induction is by affecting the expression of CII. During prophage induction, expression of CII from *pR* may lead to the production of CI from a CII-activated *pE,* which could counteract lytic development. A 186 phage made to express a stabilised CII protein (CII145) is strongly defective in prophage induction presumably due to excessive activation of *pE-cI* expression following derepression of *pR* during prophage induction (Murchland et al., unpublished results). It is possible that partial repression of *pR* by Apl is needed to assist in limiting CII levels to avoid the reversal of lytic development. Apl repression at *pL* is thought to be a means to inhibit *cI* expression during prophage induction and to facilitate efficient excision of the prophage by preventing *int* expression. To continue our study of Apl, these hypothesises were also investigated.

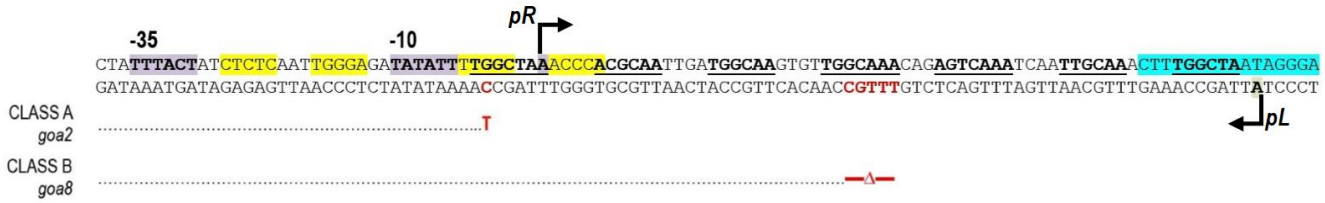

Figure 1.11: Apl operator sites at *pR.pL* and the nature of the *goa2* and *goa8* mutations. Bold, underlined text denotes the seven predicted Apl recognition sequences arranged as direct repeats spaced 10-11bp apart. The DNA sequences for *goa2* and *goa8* are shown with their mutations coloured red. Blue highlighted text represents the putative *pL* CI operator binding site. Yellow highlighted text represents *pR-O1* and *pR-O3* CI binding sites. Adapted from Dodd et al. (1993), Dodd and Egan (1996) and Reed et al. (1997).

1.2 Synthetic biology and biosensor design

1.2.1 Applications of bacteriophage in synthetic biology

1.2.1.1 What is synthetic biology?

Synthetic biology (SynBio) is an innovative interdisciplinary area of science that draws on the expertise of numerous scientific and engineering disciplines to design new/novel biological systems (Fig. 1.12A). The central core of SynBio is to apply the methods used by computational scientists and engineers to design and construct novel synthetic biological systems by taking naturally occurring systems and breaking them down into their individual components (Fig. 1.13) (Khalil and Collins, 2010). These parts are then characterised, standardised and redesigned into novel biological systems that impart an improved or new function. Scientists expect this style of genetic engineering will allow for the development of genetically-modified organisms (GMOs) that can facilitate the production of cheaper drugs, make biofuels from renewable sources, sense the presence of toxins in water, foods and other compounds and detect, diagnose and combat infection and disease (Fig. 1.12B).

The modification of naturally occurring biological systems is not a new phenomenon. Food producers, plant cultivators and animal breeders have been mixing and matching genetic material for thousands of years to create novel organisms with desirable traits. The term 'synthetic biology' can be traced back to the early 20th century (Leduc, 1912), but over the last 20 years scientists have intensified their efforts to advance this engineering inspired discipline to better understand the intricate workings of biology and to refashion the old and original into new and improved systems. These efforts are now being realised largely due to advances in SynBio technology. Traditional breeding, cloning and propagation techniques have been surpassed by the discovery of new biological parts (e.g. promoters, ribosome binding sites and terminator sequences), DNA modification tools (e.g. restriction enzymes, polymerases, integrases and DNA ligases) and genome editing technologies (e.g. the Cre-Lox recombination system and the CRISPR-Cas9 genome editing tool). These editing tools are wonderfully simple yet sophisticated systems that are versatile and precise in their methods of genetic editing/manipulation. They enable scientists to knock-down, knock-out and knock-in genes by introducing rational or random site-specific mutations, deletions and/or insertions or by rearranging the genomic architecture through the translocation or inversion of DNA.

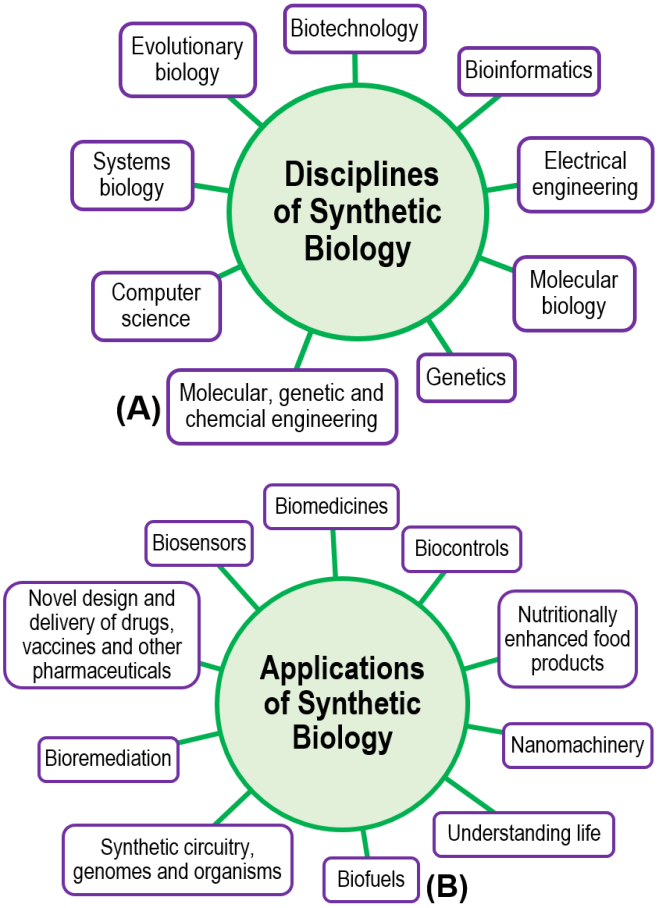

Figure 1.12: The disciplines and potential real-life applications of synthetic biology. **(A)** Synthetic biologists integrate and draw expertise from various disciplines of science and engineering to study, characterise, design and build novel biological systems. **(B)** SynBio has many potential real-life applications. Aspects of this field could advance our understanding of the molecular complexities that drive and sustain life or improve the quality of life through the development of novel treatments and diagnostic tools. By developing biocontrols to detect toxic compounds and microorganisms that can synthesise biofuels from cheap renewable resources, SynBio has the potential to contribute to the development of a world that employs more environmentally sustainable practices (Gui et al., 2017).

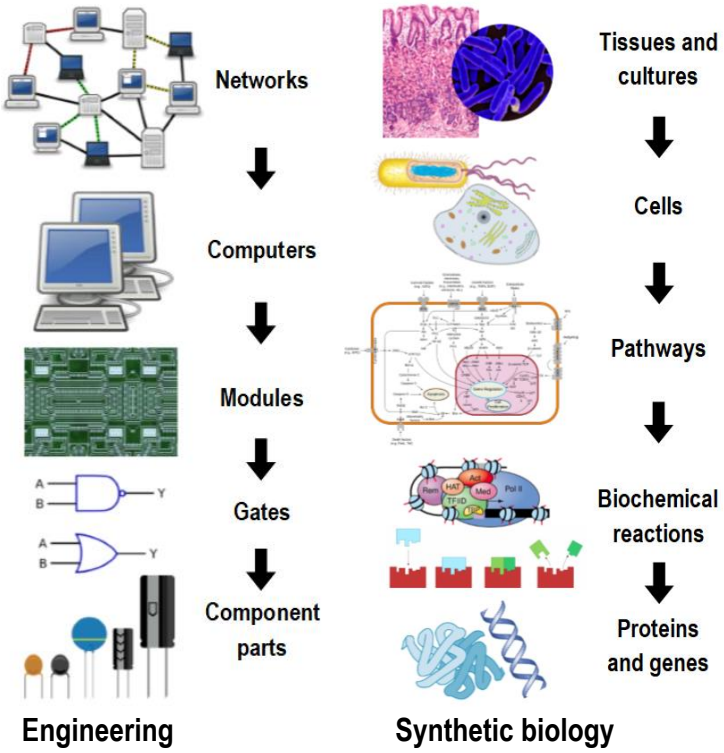

Figure 1.13: A conceptual hierarchy for synthetic biology. In parallel with mechanical, electrical and civil engineering disciplines, SynBio relies on a hierarchal abstraction of complexity and modularity. This approach assumes biological systems can be broken down into sets of standardised component parts and then rebuilt into new and improved systems. The conceptual hierarchy for SynBio views tissues and cultures analogous to a complex computerised network, which can be broken down into individual cells (the functional platform), complex pathways (for information transfer), biological reactions (for data generation) and at the basic level; proteins, genes and regulatory DNA elements (the physical biological parts). Image adapted from Andrianantoandro et al. (2006).

1.2.1.2 Synthetic biology versus Systems biology

It is important not to confuse SynBio with Systems Biology (SysBio). Whilst the distinction between these two areas is often blurred, they are two distinct areas of science. In SysBio, biologists adopt a 'big picture' approach, where high-throughput, genome-wide tools (e.g. microarrays) are used to gather large quantities of data on the simultaneous activity of thousands of genes and proteins to obtain a quantitative understanding of an existing biological system (IOM, 2011). In contrast, synthetic biologists reduce the very same systems down to their simplest unique component parts and in using these 'parts' focus on the rational engineering of a biological system that has an enhanced performance or can perform an entirely new task. SynBio and SysBio are however, complementary scientific domains, where advances in SynBio are highly dependent and interactive with advances made in SysBio and vice versa. For instance, to assemble a biological system that operates as desired, in a manner that is sensitive, specific, stable and predictable a synthetic biologist must have a thorough understanding of the complexity instilled by the interactions existing between each individual component. In other words, how does each biological component interact and function in the context of the entire system? Do the components interact with DNA, RNA or protein? Where does each component act in the system? How does it function and how is it regulated? Without a quantitative understanding of a system's functionality and underlying complexity, it would be impossible to fine-tune the system and optimise its performance parameters (IOM, 2011).

1.2.1.3 Applying engineering principles in synthetic biology

The link between SynBio and engineering is that many of the basic systems used in engineering are also observed in biology, with many of the earliest synthetic systems modelled from biological toggle switches, latches and oscillators. Two renowned early examples of synthetic circuitry is the Toggle Switch developed by Gardner et al. (2000) (Fig. 1.14A) and the Repressilator developed by Elowitz and Leibler (2000) (Fig. 1.14B). Both successfully reassembled basic transcriptional regulatory elements into the biological equivalents of electronic memory storage and timekeeping respectively. Gardner et al. (2000) engineered a genetic toggle switch that operates analogously to a reset-set latch; one of the most basic elements used for storing memory. These devices are bistable, meaning they can exist in two mutually exclusive states that can be 'toggled' with the delivery of specified outputs (IOM, 2011). The Toggle Switch entails two promoters, each of which are repressed by the gene product of the other. The investigators demonstrated this system could be toggled in one direction with the addition of the chemical inducer isopropyl-ß-d thiogalactopyranoside (IPTG) or in the other direction with a transient increase in temperature.

Timing is another aspect of engineering that features ubiquitously throughout nature. From an electrical engineering perspective, timekeeping can be achieved with the basic LC circuit, whilst in biology, keeping time has been achieved with circadian clocks and other oscillatory networks (IOM, 2011). Elowitz and Leibler (2000) engineered the Repressilator, an oscillatory system that periodically induces production of a green fluorescent protein (GFP) in *E. coli.* Oscillatory output in gene expression was achieved by engineering a cyclic negative feedback loop composed of three promoter-gene pairs, where promoter *A* drives expression of the repressor for promoter *B*, which drives expression of the repressor for promoter *C*, which drives expression of repressor for promoter *A*. These early studies demonstrated engineering-based methodology can be used to build sophisticated, computing-like behaviour into biological systems and has been applied to construct many more genetic switches, oscillators, memory elements, pulse generators, digital logic gates, filters and messaging modules (IOM, 2011).

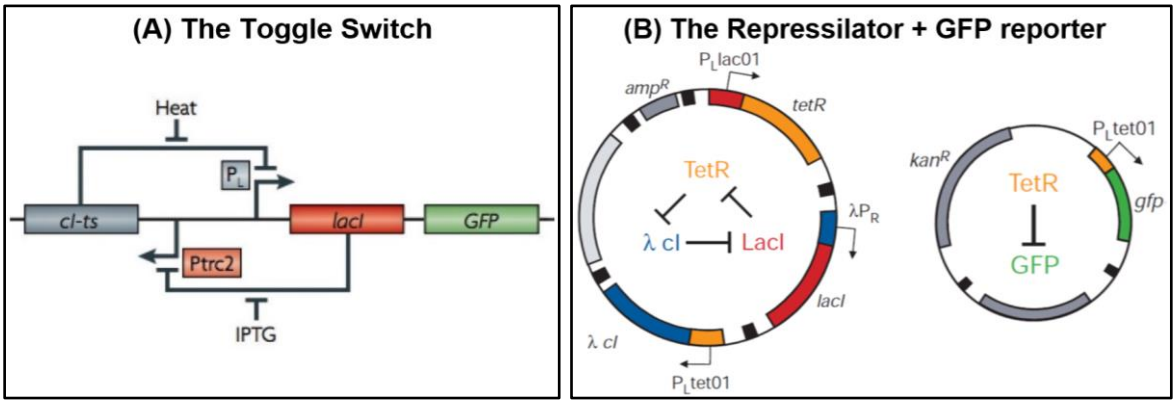

Figure 1.14: Early synthetic switches - the Toggle Switch and the Repressilator. **(A)** The Toggle Switch operates analogously to a reset-set latch, where it can exist in two mutually exclusive states and 'toggled' with the delivery of IPTG or with a transient increase in temperature. The switch employs two promoters, each repressed by the gene product of the other. Module 1 features the *lacI* gene (encodes LacI repressor) driven by λP_L and module 2 features the λ*cIts* gene (encodes temperature sensitive λCIts repressor) driven by *Ptrc2* (a variant of the native *lac* promoter). In the presence of LacI, expression of the *Ptrc2.λcIts* transcript is inhibited. In the presence of IPTG, LacI is inactivated and λ*cIts* expressed. In the presence of λCIts, expression of the λP_L*.lacI* transcript is inhibited. When cells are grown at high temperature, λCIts is inactivated and *lacI* expressed. Activity of the circuit is monitored through the expression of the Green Fluorescent Protein (GFP; encoded by *gfp* gene), where cells fluoresce green when λCIts is inactivated. Image reproduced from Khalil and Collins (2010). **(B)** The Repressilator periodically induces production of GFP in *E. coli* and consists of three promoter-gene modules cloned onto a low-copy plasmid. Module 1 (P_L*lacO1.tetR*) encodes the Tet repressor, module 2 (λP_R*.lacI*) encodes the LacI repressor and module 3 (P_L*tetO1.λcI*) encodes λCI repressor. LacI represses module 1, λCI represses module 2 and TetR represses module 3. Using another higher-copy plasmid, circuit activity was monitored through expression of GFP from P_L*tetO1.gfp*, also repressed by TetR. Image reproduced from Elowitz and Leibler (2000).

1.2.1.4 The future of synthetic biology - standardised interchangeable parts

Early projects in SynBio were mostly limited to building small genetic circuits consisting of only a few parts, but with significant advances being made in SynBio scientists are now able to design more highly advanced complex synthetic systems and even build complete bacterial genomes from scratch (Gibson et al., 2010, 2008). These advancements can be accredited to the development of powerful DNA synthesis and assembly technologies, undertaking research to increase our understanding of gene regulation and molecular circuitry and establishing The Registry of Standard Biological Parts (http://partsregistry.org).

The Registry was established in 2003 at the Massachusetts Institute of Technology (MIT) with the intent to make 'biology easier to engineer' by making available a repository of standardised interchangeable parts, devices and modular construction methods. The Registry itself resides at MIT and is managed by The International Genetically Engineered Machine (iGEM) Foundation. As of 2018, it contained more than 20,000 parts, making it the largest collection of publically available parts for synthetic biologists (iGEM, 2019). The Registry website is a publically accessible domain that provides information about each part, and its partial design as a 'wiki' means users can edit its content directly. Recipients of The Registry include academic labs, scientists and undergraduates participating in the annual iGEM SynBio competition (iGEM, 2019). The types of biological parts offered by The Registry include DNA, plasmids, plasmid backbones, primers, promoters, protein coding sequences, protein domains, ribosomal binding sites, terminators, translational units and riboregualtors. It also includes devices such as protein generators, reporters, inverters, receptors, senders and measurement devices (iGEM, 2019).

All parts and devices within The Registry adhere to a strict BioBrick™ restriction-enzyme assembly standard. This standard was pioneered by American synthetic biologist, Tom Knight and provides a more reliable approach for combining parts to form larger systems, thereby removing much of the irregularity and unpredictability encountered during the assembly of genetic components into larger (more complex) systems (Knight, 2003). As stated in IOM (2011) *'the goal of this effort is to one day be able to select these 'parts' from a catalogue and use them to create completely synthetic 'novel' self-replicating life forms that are purpose-built rather than derived from a pre-existing organism'.* The core advantage of having these standardised interchangeable parts is that they are composable, meaning scientists would have access to an endless repertoire of possible combinations to form new/novel complex systems. Furthermore, assuming each part/device is 'standardised' means independent groups of synthetic biologists located in different parts of the world should be able to reuse a BioBrick™ part without having to going through the whole cycle of design and manipulation.

Whilst this all sounds wonderful, creating a repository of standardised interchangeable parts is by no means a modest endeavour. Despite each part/device having to adhere to Knight's BioBrick™ assembly standard, standardising these parts from a functional and quantitative standpoint - as achieved with components used to fashion electronic devices (e.g. resistors, transistors, capacitors, inductors and diodes connected by conductive wires or traces) - remains an imminent challenge. As presented in Table 1.2, some of the key challenges associated with the design, assembly, characterisation and application of synthetic systems include poor standardisation, unpredictable circuitry, unknown biology, system complexity and chassis incompatibility.

Traditionally, the approach to the study of genetic circuitry was to isolate and characterise each individual component to determine what role each part plays in the system and how this role is carried out. The key assumption to this approach is that each component operates in isolation, where functionality is not influenced by the actions of other operating components. Whilst this may be true for components used in engineering, as our understanding of prokaryotic and eukaryotic biology has advanced over time, it is clear this assumption is invalid. We know cells are highly complex computational systems that dynamically detect and respond to their environment (IOM, 2011). Their biology is intricately regulated at various levels (e.g. signal-transduction, transcription, translation and post-translation) and this regulation can take place in the form of short- and/or long-range cooperativity, DNA looping, DNA wrapping, oligermisation of regulatory factors into complex mutlimers and the establishment of negative and positive feedback regulatory loops. Cells are inherently installed with biological systems, switches and circuits that operate via establishing a complex interplay between all components, where the functionality of each part is readily influenced by the actions of other parts, which may conflict (repress) and/or encourage (activate) action. So, whilst the functionality of a 'part' may be relatively easy to define, standardising performance quantitatively is significantly more challenging as its behaviour in isolation (uncoupled) can be significantly different to that observed when integrated (coupled) into a biological system. Understanding system complexity is ultimately key to successful construction of biological circuitry.

In addition to complexity, a synthetic biologist must also ensure the chosen biology is compatible with the engineered system. For instance, a genetic circuit made from eukaryotic components would need to be installed within a eukaryotic chassis (e.g. yeast), as a prokaryotic organism (e.g. bacteria) would likely lack the host factors and protein modification machinery required to correctly assemble these higher-order regulatory factors into their functional constituents. The performance of biological systems can also vary significantly between biological platforms within the same kingdom. Hence, while *E. coli* may be the standard biotechnological workhorse, many other strains have been utilised like, *P. fluorescens, P. putida, S. aureus* and *B. subtilis* because they enable improved performance of a synthetic circuit (Chang et al., 2017; IOM, 2011). The performance variability ensued by the nature of the biological chassis also makes the challenge of standardising the functionality of a biological building block more complex. Overall, it is clear that to successfully engineer completely new biological systems from scratch synthetic biologists need to move away from the traditional reductionist approach to understanding gene regulation and rather embrace a systems approach to understanding biological interactions. It is important to understand that the ease at which engineers have at making predictable electronic circuits is largely due to the fact they are not encumbered by the underlying/background biology that occurs within a cell; a lot of which will have direct and indirect repercussions on the performance of a synthetic system.

Table 1.2: The challenging realities of synthetic biology. A long-standing goal of SynBio is to employ engineering design principles to build novel biological circuits from simpler cellular devices and building blocks. Unlike engineers, synthetic biologists are faced with the complexity and unpredictability of living systems; hence, it is of no surprise that engineering new/novel biological systems is accompanied with a unique set of challenges (Kwok, 2010; Porcar et al., 2011; Schyfter et al., 2013).

Challenge		Description
Poor standardisation and quantification	♦	Working with standardised biological parts should help compartmentalise design problems, simplify assembly and enable rapid production of systems with higher-level functions. The BioBrick™ assembly standard (Knight, 2003) aims to remove the irregularity and unpredictability encountered when 'wiring' component parts to make complete systems. This standard however, does not guarantee the quality and performance of each part when integrated within a complex system. From a quantitative perspective, individual components remain largely undefined, meaning system performance is uncalculated and unpredictable and the performance of a biological part is not replicable by another person in a different laboratory.
Unpredictable circuitry	♦	Biological parts often operate unexpectedly when installed within a complex system because these parts do not operate in isolation. Studies have consistently demonstrated component parts are influenced (directly and indirectly) by other parts of the system and by central biological processes (e.g. cell reproduction, genome replication and metabolism). Since it is near impossible to tame the biological climate of a cell, getting a synthetic circuit to behave in a consistent and predictable manner is a significant challenge. Synthetic biologists are often caught in a laborious process of trial-and-error when trying to fine-tune system performance.
Misunderstanding of system biology and complexity	♦	Biological systems are highly complex genetic and cellular networks linked together by dynamic feedback interactions. It is inevitable that the more parts a system has the more complex it becomes and the more optimisation it will require. Optimisation may involve the need to use a different regulatory protein or a variant of the original version, the tinkering of regulatory components such as promoter and RBS strength and/or the re-organisation of genes and DNA elements. Optimisation requires time, labour and resources and without an understanding of the system's natural complexity, such efforts often fail to improve the system.
Incompatibility with biological chassis	♦	The functionality of a part, device or system within different biological platforms can be remarkably different. If a particular component disrupts the expression of genes required for essential life sustaining processes then what works in one host type may fail to work in another. Furthermore, the chassis needs to be robust. If its intended use is to generate a biofuel then it will need to be able to metabolise simple carbon sources (e.g. biofuel feedstocks - wheat, corn and sugarcane). If the system is to play a role in bioremediation then it will need to be tolerant of complex samples that contain toxic compounds (e.g. heavy metals, biocides, oils and grease). Choosing the right chassis is a challenge, especially when having to ensure the synthetic system is compatible with the host's natural biology and the chosen host is 'fit' for the intended real-life application of the envisioned system.
Variability and system stability	♦	Calibrating variability in system performance is a significant challenge and (if unregulated) will ultimately crash the entire system. Variability arises by innate random fluctuations in molecular activities (i.e. biological noise), changes in growth conditions and (over time) the acquisition of random mutations. Mutations often arise when the synthetic system imposes a 'metabolic tax' on the host, such that it 'steals/depletes' resources needed for life sustaining processes.
	♦	Many synthetic biologists adopt a plasmid-based approach when expressing their synthetic constructs. Plasmids can be a significant source of variability as high- and low-copy plasmids often exist at different copies in individual cells. Hence, the more or less copies a cell has of the system the more or less gene output the cell will generate, which will reflect on the system's overall performance. When Elowitz and Leibler (2000) engineered *E. coli* with their plasmid-based Repressilator variability in cell behaviour was observed, where some cells fluoresced brighter, blinked faster and in some cases, skipped cycles altogether.
	♦	Plasmid-based systems are also unstable and inherently lost from the host because they are taxing, non-essential entities. To retain a plasmid-based system, it must encode a selective marker, which often imposes an additional 'tax' to the cell, thereby reducing its fitness further. To mitigate this problem, scientists are now integrating their synthetic circuitry directly into the host's genome, which not only improves system stability but also reduces 'noise' as the copy-number of the synthetic construct remains the same within all cells.

1.2.1.5 The contribution of phage to synthetic biology

The modern age of SynBio aims to make biology 'easier to engineer' so to create novel organisms that can produce useful molecules (e.g. biofuels) or perform specific functions (e.g. detect toxins in drinking water) (Schyfter et al., 2013). The ability to reprogram or create a new biological system does depend upon the availability of functionally standardised parts, devices and assembly tools. Due to the mosaic nature of phage genomes, these viruses serve as a great place to start when searching for new biological parts, genes that encode novel proteins and regulatory circuits that employ unique control strategies. From the phage already discovered, they have contributed immensely to the SynBio toolbox enabling scientists to manipulate and alter DNA with high precision and ease. Moreover, due to the lack of functional redundancy of phage genomes, many elements can be isolated and fashioned together to make new gene circuits and networks that successfully program whole-cells (i.e. bacteria) to perform specific tasks that can be applied in medicine, food, agriculture, environmental monitoring and bioremediation.

As previously discussed, some of the key biological parts provided by phage include promoter elements, ribosomal binding sites, terminators and feedback loops. Moreover, there is pervasive use of phage-derived enzymes in common laboratory protocols such as PCR, Gibson isothermal assembly, DNA ligation and genomic integration. The DNA-dependent RNA polymerase of T7 phage for example, can specifically drive high-level *in vitro* and *in vivo* transcription from the T7 promoter and has been used to build a number of genetic switches and oscillators (Citorik et al., 2014a; Shis and Bennett, 2013). The extensively studied λCI immunity repressor has been incorporated into the design of many synthetic modules including the Repressilator by Elowitz and Leibler (2000), a mammalian memory device by Kotula et al. (2014), a kill switch by Stirling et al. (2017) and a pulse-detecting circuit by Noman et al. (2016). Phage Cre, Bxb1 and PhiC31 recombinases have also been used to construct a variety of circuits such as counters (Friedland et al., 2009) and Boolean logic gates (Siuti et al., 2013). These recombinases not only allow precise editing of genomic material but they also let synthetic biologists integrate their gene circuits and switches into the genome of their chosen chassis, thereby moving away from plasmid-based systems that are inherently 'noisy' and less stable than that of integrated systems.

One potential application of phage is their use as nanosynriges. When using lytic phage in PT, a concern is that side effects may ensue with the sudden release of bacterial endotoxins upon lysis of the host. To overcome this issue, scientists have been working to engineer non-replicative phage that deliver and inject a specifically designed drug or a novel gene circuit that expresses a toxin once established within the cell.

The filamentous M13 phage and its relatives are commonly used as transducing vectors to deliver DNA payloads (i.e. phagemids) to bacteria. An example of leveraging M13's DNA delivery capabilities is to deliver CRISPR/Cas nuclease constructs to specifically remove antibiotic resistance markers or virulence genes from microbiomes (Citorik et al., 2014b). The payload however, does not necessarily need to be harmful. Non-lethal genetic circuits could also be delivered to bacteria to reprogram their behaviour, so they can sense the presence of a specific toxin in drinking water for example, or catch the early development of a disease by detecting a disease-specific compound.

1.2.2 Whole-cell biosensors

Imagine having the ability to transform bacteria into tiny programmable computers. Well, imagine no longer! Modern-day synthetic biologists are now working to program microorganisms to perform simple computations, where they detect and report on the presence of a particular substance or environmental condition. These microbial 'computers' are known as whole-cell biosensors (WCBs) and are developed as novel methods for the detection of pathogens, disease, toxins, pollutants and various other biological entities and compounds. Due to the cross-disciplinary nature of their construction, research on the development of this technology has been published in the fields of biology, chemistry, physics and information science. Biosensor technology is gaining popularity because our progress in DNA sequencing, assembly and manipulation technologies has made it remarkably easier for scientists to design and construct gene circuits and switches that can program microorganisms to perform unique behaviours that would otherwise never be observed in nature.

A standard biosensor is defined as *'an analytical device that converts a biological response into a detectable signal'* (Mehrotra, 2016). These devices generally consist of a biological sensory component (the bioreceptor) that can detect the presence of a particular analyte (or condition) within a complex sample (e.g. water, foods, tissues, blood, urine, saliva and faeces). Upon detection of the target analyte, the stimulus released from the interaction of the analyte and the bioreceptor is identified by the transducer/detector, which then transforms the signal into a detectable electrochemical, optical, thermal or piezoelectric readout (Fig. 1.15) (Patel et al., 2016). Examples of classical biosensors that rely on electrochemistry - the conversion of the concentration of a molecule into a digital display - are the oxygen sensor and the glucometer (Patel et al., 2016). The former is an electronic device fitted into the exhaust pipe of automobiles to monitor how much unburned oxygen is in the exhaust fumes. The objective is to improve engine efficiency and reduce the production of carbon emissions (Bosch, 2019). The glucometer is a glucose-oxidase-based medical biosensor used for determining the approximate concentration of glucose in the blood.

To produce a reading, a blood sample is applied to the test strip (from a skin prick) and the capillary in the strip sucks the blood up into the meter. When the blood sample reaches an enzyme electrode, an electrical current is produced. The charge passing through the electrode is proportional to the amount of glucose in the blood sample and is numerically shown on the screen of the meter (Yoo and Lee, 2010).

As presented in Figure 1.16, biosensor design is not without its challenges. A 'good' biosensor must adhere to specific performance parameters, with high sensitivity and specificity being key statistical measures of performance. Selectivity refers to the biosensor's ability to differentiate and detect a specific analyte within a complex sample; whilst sensitivity refers to the minimum amount of analyte the biosensor can detect (Patel et al., 2016). When developing biosensors for disease diagnostic purposes, these two parameters are vital to ensure the technology can consistently differentiate and report with high accuracy between diseased and healthy individuals (Herman, 2006). Another desirable performance parameter is bistability, which refers to the system's ability to exist in one of two mutually exclusive states with stochastic switching between these stable states being rare. The ability to achieve bistability - by converting a transient signal or stimulus into a sustained response - is termed cellular memory (Burrill and Silver, 2010). There is a plethora of biological phenomena that possess this ability, with each having evolved their own natural memory circuits. Examples include the transcriptional switches of coliphage λ and 186 that control lytic and lysogenic development (Dodd et al., 1990; Ptashne, 2006; Shearwin and Egan, 2000), the *E. coli lac* operon required for lactose transport and metabolism (Muller-Hill, 1996) and the positive-feedback bistable networks for the control of *Xenopus* oocyte maturation (Novak and Tyson, 1993; Thron, 1996).

In SynBio, the design and construction of synthetic memory circuits has been achieved by using a diverse array of these natural mechanisms such as DNA recombination (e.g. excision and inversion), transcriptional positive and negative feedback loops, chromatin epigenetics (e.g. methylation of DNA and histones) and chemical modification of signalling proteins (e.g. phosphorylation) (Burrill and Silver, 2010; Inniss and Silver, 2013). Memory is useful in biosensor technology as it allows for delayed interpretation, meaning the ability to 'detect' and 'remember' informs the operator/technician/physician that a certain stimulus or condition did occur, even if it is no longer present. From a medical perspective, these systems could be potentially engineered for the precise delivery of a therapeutic, where upon exposure to a disease-specific stimulus cells are induced to start producing a therapeutic that is sustainability delivered (over time) at a prescribed/controlled amount. Once the patient has recovered, exposure to a secondary stimulus would then instruct cells to stop delivering the therapeutic and thus prevent the continuation of unnecessary treatment (Inniss and Silver, 2013).

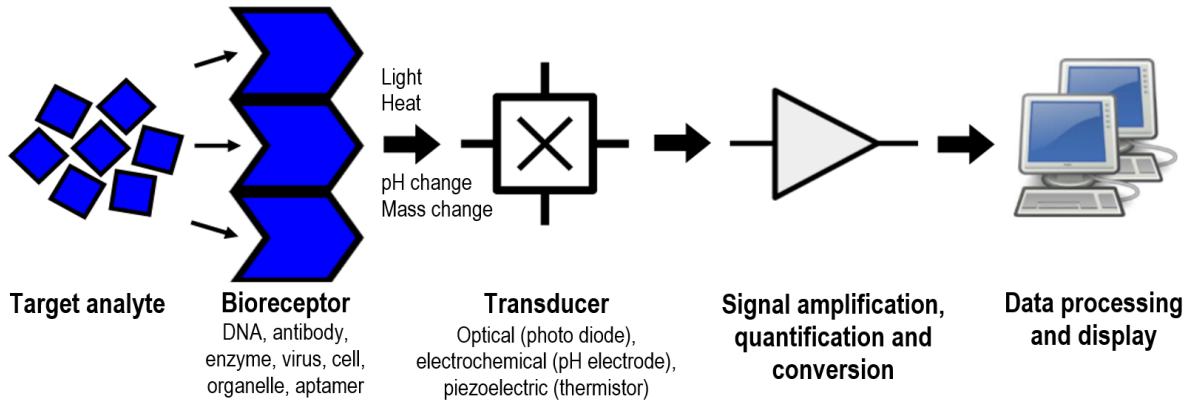

Figure 1.15: A schematic of a conventional biosensor. A biosensor is a self-contained analytical device that combines a biological element with a physicochemical component to generate a measurable signal for detection of a target analyte. The bioreceptor (biological component) exhibits high specificity for the target analyte, where upon detection the analyte-bioreceptor interaction will generate a stimulus (e.g. light or heat) identified by the transducer. The transducer converts the biorecognition event into a measurable optical, electrical or piezoelectric signal. The electronics system will amplify and process the signal into a quantitative readout (e.g. numerical or graphical) that appears on the display unit of the biosensor (e.g. a computer screen or printed onto paper). Adapted from Bhalla et al. (2016).

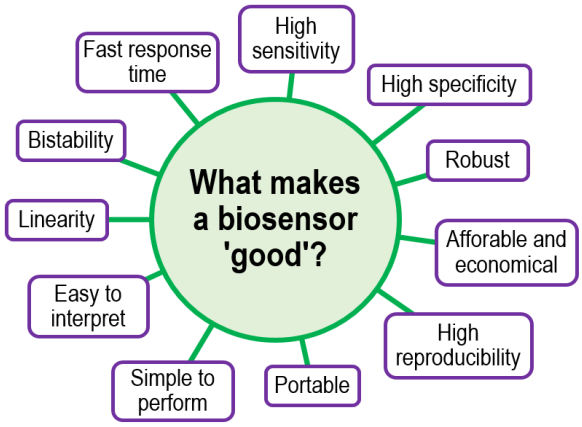

Figure 1.16: What makes a biosensor 'good'? A 'good' biosensor should serve as a reliable decision support tool, where the output is quick and easy to interpret and assists the user in making the appropriate decision. *High specificity* refers to the ability of the bioreceptor to detect a specific analyte within a complex/crude sample (e.g. cell culture, tissue biopsy, urine, water or food). *High sensitivity* refers to the minimum amount of analyte detectable by the biosensor. The lower the analyte concentration the more sensitive (and better) the biosensor. A 'good' biosensor needs to be *robust* to tolerate internal and external ambient disturbances, all of which can affect the precision and accuracy of the output.

A robust biosensor needs a stable bioreceptor (not readily degraded) that exhibits high affinity for the target analyte (stronger affinity means greater stability). *Long-term bistability* means the system can establish 'cellular memory' of a transient signal. *High reproducibility* means the biosensor generates identical responses for a duplicated experimental protocol. It is a reflection of the precision and accuracy of the transducer and electronics system. High precision means similar results are achieved every time a sample is measured, whilst high accuracy indicates the capacity to provide a mean value close to the true value when a sample is measured repeatedly. *Linearity* refers to linear range, defined as the range of analyte concentrations for which the biosensor's response changes linearly. It is generally associated with resolution, which needs to be high because most real-life applications require analyte detection and quantification over a wide concentration range. For regular widespread use, *affordability* is crucial. A biosensor should have a low requirement for reagents, labour, technical expertise, complex equipment/machinery and time. *Ease-of-use, speed* and *portability* (operable outside of a laboratory) are important attributes, especially if the biosensor is needed in developing countries where infrastructure, resources and expertise are poor (Bhalla et al., 2016; Herman, 2006; Maxim et al., 2014; Patel et al., 2016).

Molecular-based biosensors (MBBs) use biologically active substances such as enzymes, DNA, antigens, antibodies, viruses, aptamers and biofilms as the reporter elements (Gui et al., 2017). According to the type of biological recognition molecule used, MBBs can be of a catalytic or affinity type. The former are kinetic devices that use a biocatalyst (e.g. enzymes, organelles and microbes) to carry out a biocatalytic reaction to produce a transducer-detectable product. The latter are sensory devices that use receptor molecules (e.g. antibodies, DNA and protein receptors) to cause a physiochemical change upon binding that is detected by the transducer (Patel et al., 2016). For a comprehensive list of recently developed MBBs, see Patel et al. (2016) Table 1. Ahmed et al. (2014) also provides many examples of optical, mechanical and electrochemical biosensors used for whole-cell bacterial detection (Tables 4-6).

Whole-cell biosensors (WCBs) are engineered microorganisms designed to produce a detectable signal in response to exposure to a specific compound or a change in an environmental condition. All WCBs work to detect a particular analyte/condition (with high sensitivity and specificity) and convert the detection of this analyte/condition into a clear and detectable signal. In comparison to MBBs, WCBs entail a number of advantages. First, they are more economical as there is no need to replenish the biocatalyst or receptor as the microorganism would continue to synthesise new component parts, thus keeping the system in working order. Second, WCBs are more dynamic and adaptable because living cells are capable of metabolising complex compounds, which naturally results in the production of various molecules that can be monitored by different transducers. Third, WCBs make ideal environmental biocontrols because many have the ability to tolerate, sense and respond to a wide range of compounds (e.g. nucleic acids, hormones, toxins, heavy metals and chemicals) and environmental conditions (e.g. pH, UV, salinity and temperature) (Gui et al., 2017; Patel et al., 2016).

Most WCBs are of a transcriptional nature, meaning a microorganism is genetically modified with a gene circuit that consists of a reporter gene driven by an inducible promoter, where upon induction, will produce a colorimetric, luminometric or fluorimetric output (Fig. 1.17). The inducible promoter is often regulated by a transcriptional repressor or activator, where upon interaction with the target analyte results in derepression or activation of the promoter respectively. For example, Anderson et al. (2007) devised a transcriptional AND gate to integrate multiple environmental signals into a single genetic circuit. Using two environmentally inducible promoters, the system was designed to only give an optical output when arabinose AND salicylic acid are present. The first promoter (P_{BAD}, activated by arabinose) controls transcription of a T7 RNA polymerase (RNAP) gene, but its translation is blocked by the presence of two internal amber stop codons. The second promoter (P_{sal}, activated by salicylic acid) controls expression of the amber suppressor tRNA *supD.*

Only when arabinose and salicylic acid are present are both components expressed and the T7 RNAP faithfully transcribed. The active T7 RNAP then activates expression of a *gfp* reporter gene linked to the T7 promoter. WCBs can also be of a translational nature which are typically built by linking RNA aptamer domains to RNA regulatory domains (Bayer and Smolke, 2005; Winkler et al., 2004). Post-translational WCBs consist of membrane-bound protein receptors that trigger signal transduction cascades (Bashor et al., 2008; Looger et al., 2003) and those of a hybrid nature combine synthetic transcriptional, translational and post-translational circuits (Tabor et al., 2009).

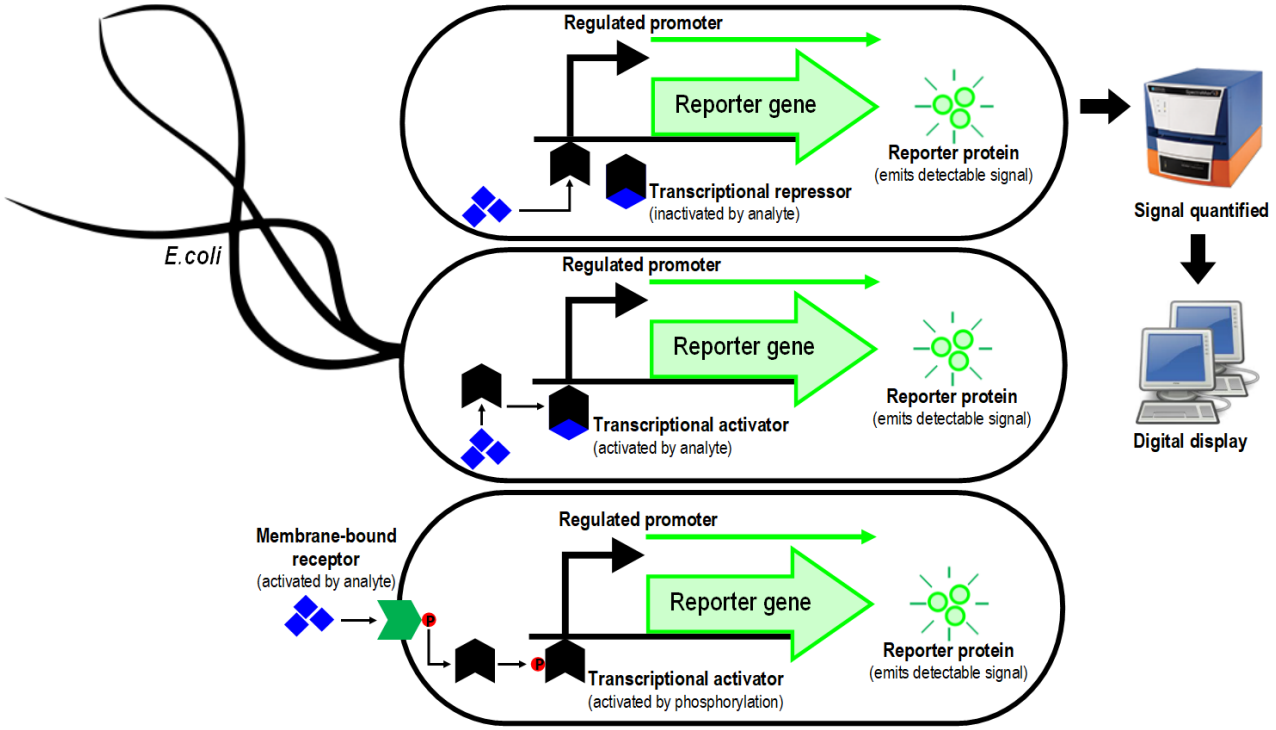

Figure 1.17: A schematic of some typical transcriptional whole-cell biosensors. WCBs are engineered microorganisms designed to detect a particular analyte and then amplify and convert the detection of this analyte into a clear and detectable signal. In a typical transcriptional WCB, the organism senses the presence of the target analyte, either internally or externally. Internal sensing occurs when the analyte is small enough to permeate the cell wall and enter the cytoplasm, where it binds the transcriptional regulator. The analyte may inactivate the regulator (top model), resulting in derepression of the regulated promoter or the analyte may activate the regulator (middle model), allowing for activation of the regulated promoter. External sensing occurs when a membrane-bound receptor senses the analyte (bottom model), which initiates a signal cascade when the transcriptional regulator is activated by chemical modification (e.g. phosphorylation). Induction of the regulated promoter results in expression of a reporter gene, which in this case produces a fluorescent protein. The fluorescence emitted can be visualised and photographed using special fluorescent imaging technology or quantified using a fluorospectrometer, from which the data is processed by a computer and visualised on the monitor.

According to Gui et al. (2017) the performance of WCBs is highly dependent on three key parameters, (1) the reporter gene chosen, (2) the selectivity and sensitivity of the molecular recognition between the target analyte and the regulatory protein (that controls the promoter for reporter gene expression) and (3) the biological chassis chosen to operate the system.

Synthetic biologists exploit a variety of different reporter systems that process an inductive response into a luminescent, fluorescent or chromogenic output, with commonly used reporter genes being *lux* (bacterial lucberase), *luc* (firefly luciferase), *gfp* (green fluorescent protein derived from *Aequoera victoria* jellyfish), *mCherry* (red fluorescent protein derived from *Discosoma* sea anemones) and *lacZ* (beta-galactosidase) (Gui et al., 2017). As presented in Figure 1 of the Gui et al. (2017) review, choosing the right reporter gene is difficult because not only are there a great number to choose from, but each type has its own set of advantages and disadvantages.

Engineering a WCB with high sensitivity and selectivity requires careful consideration of the regulatory protein chosen to detect the analyte of interest. In many cases, the wildtype version does not perform to the desired standard and so a variant with an enhanced phenotype needs to be sourced/created. For example, two inducible promoters commonly used in the design of synthetic circuits are the IPTG-inducible *lac* promoter (P_{lac}) and the arabinose-inducible *araBAD* promoter (P_{BAD}). These promoters however, are largely incompatible for use within the same synthetic system because IPTG induces P_{lac} but also inhibits P_{BAD}. This phenomenon is referred to as 'crosstalk' and can be detrimental to controlling gene expression. For instance, it would be difficult to use both promoters in a transcriptional AND module because the crosstalk would interfere with the simultaneous induction of each promoter (with IPTG AND arabinose), where the gene product(s) from P_{lac} AND P_{BAD} would be required to activate expression of a reporter gene. To overcome this crosstalk, Lee et al. (2007) used error-prone PCR to evolve the arabinose-binding repressor protein (AraC) to have improved sensitivity to arabinose and insensitivity to IPTG. Directed evolution of AraC enabled the investigators to construct a P_{BAD} system that was 10x more sensitive to arabinose and tolerated IPTG significantly better than wildtype, thereby improving its compatibility with their P_{lac} system.

Lastly, WCB performance is significantly influenced by the type of host cell used to drive the biological circuitry. Synthetic biologists need to consider two things; first, will any of the components within the synthetic system impede on any of the host's life sustaining processes? Second, is the host suitable for its envisioned real-life application? In other words, if the WCB is designed to detect a toxic compound within a crude/complex sample then the host organism will need to have the ability to tolerate a wide range of environmental conditions. Espinosa-Urgel et al. (2015) for example, found that when they installed their biosensor into *Alcanivorax borkumensis* SK2 it had a lower tolerance towards pollutants but a higher tolerance towards salinity; proving excellent at detecting pollutants at low concentrations in seawater samples. When the biosensor was engineered into *Pseudomonas putida* DOT-T1E it was found to be superior in heavily contaminated environments due to its high solvent tolerance.

1.2.3 Potential applications of whole-cell biosensors in medicine

It is widely accepted that effective prevention and treatment of infection and disease requires early diagnosis. The standard practice for detecting infectious agents is culture isolation, which requires knowledge, technical training and time. Amplification of pathogenic DNA is not adapted for low-cost, point-of-care testing in low-resource settings and enzyme-linked immunosorbent assays (ELISA) are expensive and not suited to use outside of a laboratory. Many of the current 'gold standard' tests for disease diagnosis (e.g. endoscopies, biopsies, X-rays and physical examinations) are invasive, unpleasant, too late to be relevant and/or too expensive to be practically applied in a wide setting (Herman, 2006). It is clear that there is a need to develop more reliable and accurate detective and diagnostic tools that can reduce the frequency at which these tests and procedures are performed.

Significant effort has been dedicated to the development of medical surveillance/screening tools that aim to be so easy to perform an individual can collect their own sample (e.g. saliva, faecal or urine) in the comfort of their own home and send it off for analysis by a laboratory technician. These screening tools are widely used to assess the likelihood that members of a defined asymptomatic population have a particular disease (Bauman, 1990; Maxim et al., 2014). It is important to note, current screening tests do not diagnose illness. Subjects who test positive will require further investigation by performing subsequent 'gold standard' tests and procedures that should verify a diagnosis with 100% confidence. For example, the National Prostate Cancer Screening Program encourages males ≥50 years to get a yearly Prostate-Specific Antigen (PSA) Test. This blood test measures PSA levels in blood samples, which are often elevated in males with prostate cancer. For positive recipients, further investigation usually involves a digital rectal exam (DRE) (performed by an urologist to feel the prostate) and a biopsy (the surgical extraction of sample cells or tissue for examination) (AGDH, 2019; Cancer Council Australia, 2019a). The National Cervical Cancer Screening Program recommends women aged ≥25 years to have a cervical screen every five years. This screen detects for the presence of the human papillomavirus (HPV), a virus that causes nearly all cervical cancers. Women who test positive for HPV will often require a colposcopy (an endoscopic examination of the cervix) and a biopsy (Cancer Council Australia, 2019b; National Cervical Screening Program, 2019). Lastly, the National Bowel Cancer Screening Program encourages men and women aged ≥50 years to undertake (every two years) a Faecal Occult Blood Test (FOBT). With frequent bleeding being a common characteristic of most colon cancers, the test works by detecting traces of blood in faecal samples. A positive result will require further investigation via a colonoscopy (an endoscopic examination of the colon) and a biopsy (Cancer Council Australia, 2019c; National Bowel Cancer Screening Program, 2019).

Regrettably, the majority of screening tests typically fall short and exhibit undesirable rates of false positive and false negative outcomes. In medical diagnosis, test sensitivity and specificity is the ability of a test to correctly identify those with the disease and correctly clear (with confidence) those without the disease. A false positive outcome incorrectly identifies a person as having the disease and is a reflection of poor specificity. A false negative outcome incorrectly identifies a person as not having the disease and is a reflection of poor sensitivity. The FOBT for example, is notorious for generating false positive outcomes because a faecal sample contaminated with blood can be due to a number of non-cancerous issues such as polyps, haemorrhoids or inflammation of the bowel (Cancer Council Australia, 2019c). This means many colonoscopy and biopsy procedures are performed unnecessarily, subjecting individuals to tests that are invasive, uncomfortable, encumbering and expensive. Furthermore, not all colon cancers bleed, so a percentage of recipients will also go undetected, perhaps for as long as two years, which is ample time for a benign mass to manifest into a malignant cancer.

The overall rationale for the implementation of medical surveillance programs is driven by the idea that earlier detection always has a better outcome for the patient, such that the disease can be cured or the chances of survival and quality of life (during treatment, recovery and remission) are improved. The detectable preclinical stage is the interval in which the disease is detectable by screening but the patient remains asymptomatic. It is at this stage that detection is critical and intervention is significantly more effective than if the disease were detected during the clinical phase (patient is symptomatic) (Herman, 2006). With current screening methods having the significant drawback of poor sensitivity and specificity, more affordable, reliable and conclusive screening methods are required if disease is to be detected (with confidence) at the preclinical control point.

Whilst the literature is abundant with studies of WCBs developed for environmental monitoring and bioremediation, WCBs also present great potential in disease detection and diagnostics. They act as ideal candidates because they are natural problem-solving biological molecularities that can respond to a vast range of biological and environmental signals with ultra-sensitivity and specificity. Furthermore, with the many recent advances in SynBio and the ease at which these autonomous, self-organising and robust organisms can be genetically manipulated means we are now able take advantage of what 'biology does best'. Many synthetic biologists are currently working to program synthetic circuits into these 'molecular workhorses' to have them detect, process and report on the presence of specific pathogens, cancerous cells or on the occurrence of specific molecular events. For example, Danino et al. (2015) designed a WCB with a transcriptional AND gate module to detect liver cancer in the urine of diseased mice. Through oral administration, mice were delivered a dose of the tumour colonising probiotic *E. coli* Nissle 1917 (EcN) engineered to constitutively express the LacZ enzyme.

EcN were given 24 hours to either colonise a liver tumour or (in healthy mice) be cleared from the system. Mice were then systemically injected with the LacZ substrate LuGal, which when cleaved by LacZ produces luciferin, a luminescent compound excreted into the urine. The luminescent signal detected in the urine, by simple oral delivery of EcN and systemic injection of LuGal is an encouraging example of how WCBs can serve as tools to detect and identify cancer. A similar concept was demonstrated by Piñero-Lambea et al. (2015), who successfully programmed the controlled adhesion of *E. coli* to target the surface of tumour cells using synthetic adhesins (SAs). They showed engineered *E. coli* expressing specific SAs could colonise solid tumours that expressed the antigen recognised by the SA.

Another interesting example is that of Kotula et al. (2014), who designed a WCB to act as a 'living diagnostic' by reporting on specific environmental signals in the gut of mice. In this case, *E. coli* were engineered with a synthetic memory circuit that consisted of a trigger element and a memory-reporter element. The memory element consisted of the simplified λ *cI-*P_{RM}*-*P_R*-cro* bistable switch with *lacZ* cloned immediately downstream of *cro*. The trigger element encoded a second copy of *cro* controlled by a tetracycline-inducible promoter (P_{TET}), repressed by the Tn10 tetracycline repressor (TetR). TetR was found to be highly sensitive to anhydrotetracycline (ATC), with doses as low as 100ng/mL achieving full derepression of P_{TET}. The system worked by detecting the presence of LacZ in the faecal samples of mice, where when exposed to ATC, TetR is inactivated and *cro* is expressed from the trigger element. Cro acts on the memory element by repressing P_{RM}; toggling the switch to the lytic state, where more *cro* and *lacZ* are expressed, thereby creating a cellular form of memory. This study clearly demonstrated *E. coli* can be easily engineered to act as 'memory' diagnostics that are capable of living within the mammalian gut (in a non-destructive/invasive manner) and selectively probe, remember and continuously report on the current state of the system.

As discussed in detail, many of the current medical surveillance programs employ screening methods that lack specificity and selectivity, resulting in a high proportion of recipients diagnosed as false positive or negative. Furthermore, their complementary 'gold standard' tests and procedures are often invasive, arduous and expensive making them largely inappropriate for regular widespread use. To advance our ability to diagnose and detect infection and disease at the preclinical control point, it is clear more sophisticated and accurate technology is required. WCBs are a promising avenue as they have the potential to detect molecular signals with high sensitivity and specificity in a manner that is non-invasive, affordable and easy to apply. In this thesis, to potentially contribute to the development of such technology, we also endeavoured to develop a WCB using discrete genetic components from the genome of coliphage 186, the results of which are presented in Chapter 5.

1.3 The scope of this thesis

With scientists having dedicated decades of research into 186, we now have a relatively comprehensive understanding of the molecular workings that characterise this coliphage as temperate. There are however, areas of 186 development where our knowledge remains incomplete. To improve our understanding, this thesis set out to answer a number of questions related to the action of CI, Apl, CII and Tum at the 186 switch during prophage induction. The scope of this thesis and the investigative approach taken to address the aims of each project are as follows.

The results of our investigation into the role of CI and Apl at the 186 switch during prophage induction are presented in Chapter 2. Extensive studies of CI from a functional and structural perspective (Dodd and Egan, 1996; Dodd and Egan, 2002; Pinkett et al., 2006; Shearwin et al., 2002; Shearwin and Egan, 1996; Wang et al., 2013) have provided great insight into CI's action at the 186 switch during lysogeny. These studies provided the basis for a model where a 12-mer CI wheel cooperatively interacts with specific operator sites found at the 186 switch. The presence of these operator sites in their defined number, affinity and position is crucial for the correct cooperative alignment of DNA onto a CI wheel, thereby enabling the repressor to inhibit expression of early lytic genes from *pR* whilst simultaneously autoregulating (positively and negatively) the expression of its own gene from *pL.*

Whilst Dodd and Egan (2002) provided a clear picture of CI *pR* and *pL* regulation a significant drawback in this study was the use of *pR* and *pL* LacZ reporters coupled to an IPTG-inducible CI expression plasmid. Plasmid-based systems can be inherently 'noisy' due a phenomenon termed plasmid copy-number variation, where within a bacterial population different copies of a plasmid exist within individual cells. This variation makes it difficult to achieve uniform/stable gene expression; hence, the LacZ output from a reporter module can be over- or under-represented. In similar studies of λCI regulation, Dodd et al. (2001) found fixed expression of λCI from chromosomal inserts was a preferable approach to that of induced IPTG-controlled CI expression. In this thesis, we decided to further test the model of CI regulation at *pR* and *pL* and determine if and to what extent a 5bp deletion between *pR.pL* (i.e. the *goa8* mutation) disrupts CI negative autoregulation and what implication this may have on 186 prophage induction efficiency. This investigation was conducted in three stages. To determine if the *goa8* mutation disrupts CI *pR* and/or *pL* regulation we first devised an *E. coli* chromosomally-integrated single-copy system of wildtype and *goa8 pL* and *pR* LacZ reporters coupled to a series of fixed CI expression modules. Second, a quantitative Western blot analysis of *E. coli* C600(186^{+}) and C600(186^{goa8}) lysogens previously prepared by Reed et al. (1997) was carried out to determine if (and to what extent) the *goa8* mutation increases CI levels in a lysogen. Lastly, a synthetic UV-inducible minimal prophage induction module was used to investigate what effect the *goa8* mutation has on *pR* derepression following UV induction. Overall, the use of the *goa8* mutation provided strong evidence that CI negative autoregulation is important in facilitating high inductive efficiency, thereby ensuring a 186 prophage can rapidly escape its host when conditions become unfavourable.

Early studies of Apl showed that during prophage induction Apl represses transcription from *pR* and *pL*, a function analogous to λCro (Dodd et al., 1990). Further studies by Dodd et al. (1993) using *apl*$^{-}$ phage demonstrated Apl is not essential for lytic development, but is required (as the excisionase) during prophage induction to excise the prophage from the host chromosome. The major unknown concerning Apl is why it acts as a weak transcriptional repressor at *pR.pL* during prophage induction. In the Reed et al. (1997) study, their interpretation of the class B *goa8* phage mutant led to the conclusion that Apl plays a key role in prophage induction as a repressor of *pL.cI* transcription during lytic derepression. With the *goa8* mutation now thought to impede prophage induction efficiency by disrupting CI regulation at *pL* (Dodd and Egan, 2002), a renewed investigation into Apl's role as a transcriptional repressor was required. To explain why Apl represses *pR.pL* during prophage induction, we decided to investigate three key hypothesises that focused on the idea that Apl is needed to control *cII, cI* and *int* gene expression during prophage induction to ultimately assist Tum in the inactivation/removal of CI and to facilitate prophage excision. To test these hypothesises, a series of chromosomally-integrated UV-inducible minimal prophage induction modules were made and characterised by assaying *pR* and *pL/pE* activity in the presence and/or absence of Apl and CII.

Chapter 3 presents the draft manuscript of the Tum study. In this study, work was carried out to (1) characterise the inductive efficiency of full-length Tum, (2) examine the significance of full-length Tum having a DinI-like CTD and (3) determine whether activation of the SOS response may contribute to 186 prophage induction in ways other than by inducing *tum* expression. Previous studies by Brumby et al. (1996), Lamont et al. (1989) and Shearwin et al. (1998) demonstrated Tum is necessary and sufficient for SOS-induced prophage induction of 186, but the key limitation of these studies was the use of high-copy plasmids for *tum* expression. The consequent high Tum levels left open the possibility that SOS activation may in some way aid in the action of Tum in its natural single-copy state in the prophage. To conduct our Tum study, specific components of the 186 prophage induction system were isolated and constructed into UV- and chemically-inducible chromosomally-integrated single-copy minimal reporter systems. To complement the outcomes of these minimal reporter systems (from a whole-phage perspective) a cumic acid-inducible 186$^{p.cym}$ phage was engineered. Both systems proved sufficient in expanding our knowledge of Tum's role in 186 prophage induction and in answering the question - is prophage induction enhanced by SOS activation or is the fundamental role of the SOS response to activate *tum* expression?

Chapter 4 presents the draft manuscript of the CII study, which investigated CII's role at the 186 switch during the establishment of lysogeny and prophage induction. In particular, this study addressed the apparent paradox of how 186 can encode a pro-lysogenic factor from the lytic promoter and yet avoid introducing a bias towards lysogeny. Studies of λ have revealed this phage has overcome the same issue by expressing a CII protein that is rapidly degraded by the host protease, FtsH (Hoyt et al., 1982; St-Pierre and Endy, 2008). We then speculated 186 might have adopted the same solution since it also encodes a protease sensitive lysogenic establishment factor. To investigate this theory, research was first performed by others to determine what specific *E. coli* proteases degrade 186CII. I later contributed to this study by investigating what repercussions the stabilisation of 186CII has on 186 prophage induction, reproduction and survival.

As a synthetic biology project, we used the information gathered in this study and from previous work on 186 to isolate and optimise specific components of the 186 switch and SOS operon to develop a 'living' bacterial biosensor that can establish impressive cellular memory of two distinct alternate states. Chapter 5 presents an in depth recount of this project, which details the numerous approaches we undertook to drive the development and optimisation of our biosensor system. Chapter 6 concludes this thesis with a summary of our findings and a discussion on the future of phage and the potential benefits these viruses can offer humanity.

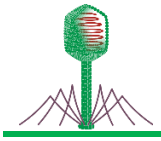

Chapter 2

Investigating CI and the *goa8* mutation and the role of Apl transcriptional repression at the lytic/lysogenic switch during 186 prophage induction

2.0 Introduction

Prophage induction is a phenomenon unique to temperate phage, defined as the event when a prophage exits lysogeny by excising from the host chromosome and resuming lytic development. In 186, prophage induction is linked to the host SOS response, such that when the host sustains DNA damage, activation of the bacterium's DNA repair pathway induces 186 to switch back to lytic development. For 186 to undergo prophage induction, two things must happen. First, the lytic/lysogenic switch must be set to lytic development, which requires derepression of the early lytic promoters (*pR* and *pB*) by inactivation of CI (Shearwin et al., 1998). Second, the prophage must be excised from the host chromosome. There are a number of important regulatory proteins involved in this event, two of which are the CI immunity repressor and the Apl protein, which has a dual role as the excisionase and weak transcriptional repressor at *pR* and *pL* (Dodd et al., 1990; Reed et al., 1997). This chapter presents the results of our investigation into the roles of CI and Apl at the 186 switch during prophage induction.

As discussed in Chapter 1, Apl is the 186 excisionase, or recombination directionality factor (RDF). Dodd et al. (1993) described Apl's excisionase behaviour to be analogous to λXis, where during prophage induction, Apl (in complex with Int) binds to the *att* region and facilitates the reversal of the site-specific recombination reaction initially catalysed by Int (during the establishment of lysogeny) to achieve excision of the prophage from the host chromosome. In the Dodd et al. (1993) study, 186 *apl*$^{-}$ phage were found to be strongly defective in prophage induction, which is consistent with the need for Apl for excision of the prophage. In an earlier study, Dodd et al. (1990) had found Apl to also act as a weak transcriptional repressor at *pR* and *pL*. It was later suggested Apl's action at *pR.pL* may serve to aid prophage induction because, despite the 186 *apl*$^{-}$ phage characterised by Dodd et al. (1993) being defective in prophage induction, they did remain competent for lytic development after infection and for the establishment of lysogeny. This indicated Apl binding at *pR.pL* is not required for lytic development and imposes no restraint on the decision to enter lytic or lysogenic development after infection.

The dual role of Apl as a λXis-like excisionase and a λCro-like transcriptional repressor was later investigated by Reed et al. (1997), the outcomes of which inspired our need to study Apl further. Using an *in vivo* plasmid-based assay for 186 site-specific recombination Reed *et al.* demonstrated Apl is functionally equivalent to λXis, such that it is directly required for prophage excision; ruling out the excision process as a mere consequence of Apl repression at *pR.pL*. To investigate the role of Apl as a transcriptional repressor, it was proposed Apl may aid the efficiency of prophage induction by repressing *cI* expression from *pL.* This activity is analogous to λCro, where λCro repression of P_{RM} is thought to assist in reducing λCI levels during prophage induction (Schubert et al., 2007). A similar role for Apl-mediated *pL* repression in 186 prophage induction was supported by Reed *et al.'s* characterisation of 16 spontaneous phage 186 Apl$^-$ resistant operator mutants (i.e. the grow-on-*apl (goa)* mutants), which are defective in Apl binding at *pR.pL.* It is assumed, that due to repression of *pR,* lytic development of infecting 186 phage is blocked in cells over-expressing Apl. Reed *et al.'s goa* mutants are able to overcome this block because they carry mutations in the *pR.pL* Apl binding sites. The class A *goa2* mutant and class B *goa8* mutant (see Fig. 1.11) provided preliminary supporting evidence that Apl-mediated *pL* repression is important for prophage induction. This is because *goa2* was found partially defective in Apl *pR* repression but retained Apl *pL* repression and was competent for prophage induction, whilst *goa8* was defective in Apl repression of both *pR* and *pL* and prophage induction.

Reed *et al.'s* interpretation of the class B *goa8* mutant led to the conclusion that Apl plays a key role in prophage induction as a repressor of *pL*-derived-*cI* transcription during lytic derepression. This conclusion came under question when a later study by Dodd and Egan (2002) showed insertions or deletions of 5bp between *pR* and *pL* abolished CI repression of *pL*, presumably because displacing *pL* by half a helical turn prevents the wrapping of *pL* CI binding sites onto the *pR*-bound CI wheel. Reed *et al.'s* interpretation of the *goa8* mutant was then somewhat confounded because the *goa8* mutation is a 5bp deletion centered between *pR* and *pL.* This means, the observed reduction in prophage induction efficiency could be attributed to the loss of CI *pL* repression rather than loss of Apl-mediated *pL* and *pR* repression. This would explain the defective prophage induction of the *goa8* mutant because if CI concentration within the host cell exceeded the optimal lysogenic CI level, a strong bias towards lysogeny and its maintenance would be established.

As part of this thesis, we decided to investigate the nature by which the *goa8* mutation impairs 186 prophage induction. Specifically, we wanted to determine if (and to what extent) the *goa8* mutation disrupts CI negative autoregulation. To do this, we developed an *E. coli* chromosomally-integrated system of wildtype and *goa8 pL* and *pR* LacZ reporters coupled to a series of fixed CI expression modules to analyse what happens at the 186 switch when CI *pL* repression is disrupted. We then extended our investigation to determine whether the *goa8* mutation increases CI levels in a lysogen by conducting a quantitative Western blot analysis of *E. coli* C600(186$^+$) and C600(186^{goa8}) lysogens.

Lastly, using a synthetic UV-inducible minimal prophage induction module, we wished to determine what (if any) degree of impairment the *goa8* mutation has on *pR* derepression following UV induction of this system. We anticipated *E. coli* harbouring the *goa8* version of the module would exhibit an impaired *pR* induction profile in comparison to *E. coli* harbouring the wildtype system. This result would be consistent with the Reed et al. (1997) study, as their C600(186^{goa8}) lysogen revealed significant impairment in prophage induction efficiency, such that in this mutant the latent period of the lytic cycle was extended by 15 minutes and an ~80% reduction in phage yield was observed following UV induction.

To investigate whether Apl transcriptional repression of *pR* and *pL* plays a role in prophage induction efficiency, several hypotheses were proposed. First, given CI inactivation and repression of *cI* gene expression is required for prophage induction, it was proposed Apl at *pL* may serve to repress *cI* expression. This would aid *pR* derepression by assisting Tum to reduce CI during prophage induction. We also hypothesised that Apl at *pR* plays a role in controlling *cII* expression during prophage induction to prevent over activation of *cI* expression from *pE.* A final hypothesis for why Apl represses *pR* and *pL* is to control Integrase (Int) expression. Another key requirement for prophage induction is the formation of the excisionase complex, where Apl assists Int, converting Int from an integrase into an excisionase. To facilitate efficient excision of the prophage from the host chromosome we propose Apl at *pR* and *pL* may serve as a 'self-assistance' mechanism by limiting *int* expression from *pL* and/or *pE*. We investigated these theories from a *pR, pL* and *pE* perspective by engineering a series of synthetic UV-inducible minimal prophage induction modules where induction profiles were obtained for *pR* and *pL/pE* in the presence and/or absence of Apl and CII.

2.1 The 186 CI immunity repressor and the *goa8* mutation

2.1.1 Testing the effect of the *goa8* mutation on CI regulation of *pR* and *pL*

2.1.1.1 The design of an improved CI expression-LacZ reporter system to study CI regulation of *pR* and *pL*

Dodd and Egan (2002) showed insertions or deletions of 5bp between *pR* and *pL* abolished CI repression of *pL*, presumably because displacing *pL* by half a helical turn prevents the wrapping of *pL* CI binding sites onto the *pR*-bound CI wheel. Since the *goa8* mutation is a 5bp deletion it is likely to have a similar effect, but this has not been tested. The effect of these changes have also not been tested in the presence of the flanking *FL* and *FR* CI binding sites (Dodd and Egan, 2002). As previously mentioned, a drawback of the Dodd and Egan (2002) study on CI regulation, was the use of an IPTG-inducible plasmid to supply induced levels of CI to their LacZ reporters. To avoid the cell-to-cell variability in expression levels associated with plasmid-based systems, we developed an *E. coli* chromosomally-integrated CI expression-LacZ reporter system.

We anticipated this system would allow for a better analysis of CI regulation of the *pL* and *pR* promoters, as it is a more stable system that achieves consistent expression of CI across individual cells, and does not require antibiotic selection. The system consists of a series of LacZ reporters (Fig. 2.1) supplied *in trans* with a fixed range of CI levels from a set of CI expression modules, each designed to supply their own fixed level of CI. To minimise cell-to-cell variability, the LacZ reporters and the CI expression modules were integrated (at single-copy) into the *E. coli* chromosome at independent attachment (*att*) sites. The integrated LacZ reporters measure *pL* or *pR* activity in the presence or absence of the *goa8* mutation. To reduce background activity from the reporter modules, translational fusions of *lacZ* with *cII* and *int* were used to assay *pR* and *pL* activity.

To supply fixed (rather than induced) levels of CI to each reporter module, we modelled the architecture of the CI expression module from the 186 switch, thereby retaining the natural ability of CI to establish negative autoregulation of its own gene from *pL*. This negative feedback control should further reduce cell-to-cell variation in CI levels. To provide different fixed levels of CI, we mutated *pL* to increase or decrease its natural activity. To assay the activity of our *pL* promoter variants each CI expression module was initially engineered with an *int::lacZ* translational fusion reporter (Fig. 2.2), which was later removed, leaving behind a small non-functional remnant of the fusion reporter gene (described in detail in Section 2.1.1.1.2).

2.1.1.1.1 The chromosomally integrated *pL and pR goa8*$^{+/-}$ *lacZ* reporters

To re-examine CI *pR* and *pL* regulation and determine what effect the *goa8* mutation has on CI negative feedback autoregulation, six LacZ reporters (Fig. 2.1) were designed and assembled into the pIT3-KT-*lacZ*trimfuse plasmid and the reporters chromosomally integrated into *E. coli* using the CRIM system (Haldimann and Wanner, 2001). The ***pR***$^{+}$(*pL*$^{+}$) reporter measures *pR* activity in the presence of *pL*. The ***pL***$^{+}$(*pR*$^{+}$) reporter measures *pL* activity in the presence of *pR* and a third reporter ***pL***$^{+}$(*pR*$^{-}$) measures *pL* activity in the absence of *pR* activity (no *pR* transcriptional interference). In this reporter, *pR* has inactivating mutations that do not affect CI binding (Dodd and Egan, 2002). Each reporter is either wildtype or harbours the *goa8* mutation, and all carry the *FL* and *FR* CI operator sites. The *cI* gene was inactivated in the reporters by a helix-turn-helix (HTH) mutation to remove its DNA-binding activity and a large deletion at the 103rd residue removed the majority of the CTD to prevent the repressor (expressed from the reporter) from multimerising with the CI supplied *in trans*. To prevent Apl from occupying the CI binding sites, the *apl* gene was inactivated by two HTH mutations.

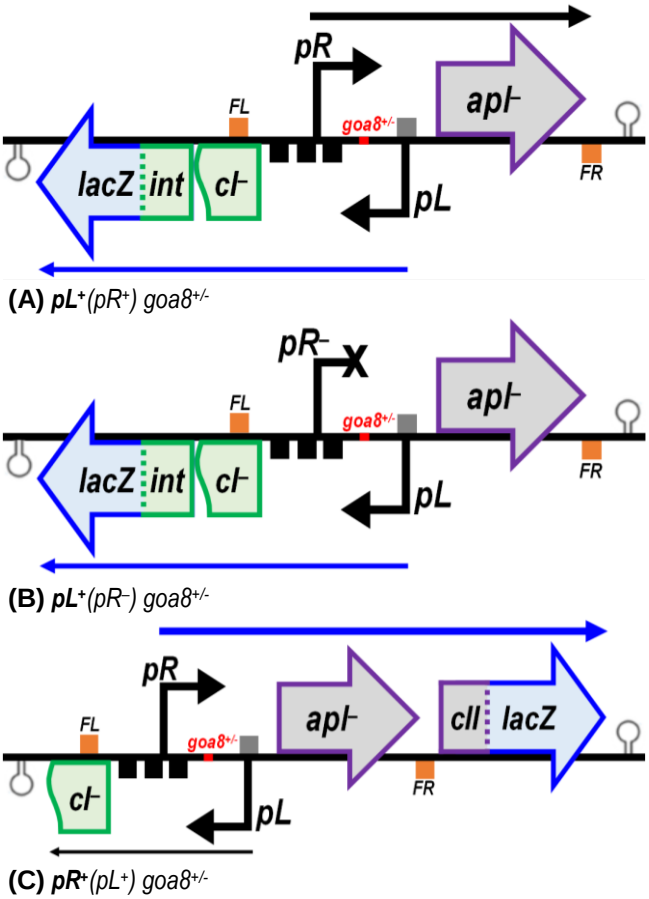

Figure 2.1: The *pL* and *pR goa8*$^{+/-}$ LacZ reporter modules. A series of four *pL* reporters (**A** and **B**) and two *pR* reporters **(C)**, harbouring a wildtype or *goa8* *pR.pL* region were made. Constructs were cloned into the pIT3-KT-*lacZ*trimfuse plasmid vector and chromosomally integrated at the φ21 *attB* site of E4643. Lytic and lysogenic genes are shown as purple and green left-and-right facing arrows respectively. Inactive and active promoters are solid black X or right-angled arrows, respectively. *pR*$^{-}$ was inactivated by changing the -35 hexamer from TTTACT to CTCGAG. Coloured arrows indicate transcriptional output from each promoter, with thickness indicating approximate promoter strength. *pR* operators are black rectangles, the *pL* operator a grey rectangle, *FL* and *FR* sites are orange rectangles and terminators are stem-loops. *(int::lacZ)* encodes Int::LacZ fusion reporter protein; the Int RBS and first nine amino acids of Int are fused to the ninth codon of LacZ. *(cII::lacZ)* encodes a CII::LacZ fusion reporter protein; the CII RBS and first codon of CII are linked to the ninth codon of LacZ. *(cI*$^{-}$*)* encodes a CI^{-} mutant deficient in DNA binding and oligomerisation. *cI* gene inactivated by a HTH mutation (site changed from CGTCCAGCTC to CGCGCGAGTC) and truncated to the 103rd residue to remove most of the CTD. *(apl*$^{-}$*)* encodes an Apl^{-} mutant defective in prophage excision and *cI* repression. *apl* gene inactivated by two HTH mutations (site changed from TGAACGCACCGCCTA to CGCGAAACCGCCTACCA G).

2.1.1.1.2 The design and characterisation of the chromosomally integrated CI expression modules

To achieve stable/consistent *in trans* supply of CI to each LacZ reporter, we used different chromosomally integrated modules expressing different fixed levels of CI. CI was expressed from *pL*, as the natural negative autoregulation should provide more stable CI levels. To provide different CI levels, *pL* was mutated at the -10 or -35 site to increase or decrease its natural activity. This section describes the process in which these modules were designed and characterised to generate a set of six CI expression modules, each made to establish their own CI steady state. The first stage was the design stage, where a preliminary series of CI expression *pL* LacZ reporter modules were made and *pL* promoter activity assayed via β-galactosidase (i.e. LacZ) activity. The outcome of these experiments identified which modules would make a suitable set of expression modules such that they covered a low-to-high range of fixed CI expression. In the second stage, the *lacZ* gene was removed (via restriction enzyme digestion and DNA ligation) to convert each selected *pL* variant into the appropriate CI expression module. A quantitative Western Blot analysis of CI for each expression module was carried out to make the final selection.

Stage 1A: Creating the pL promoter variants to vary CI expression levels

To establish a suitable series of modules, a preliminary series of CI expression *pL* LacZ reporter modules (Fig. 2.2) were designed and assembled into the pIT3-CL-*lacZ*trimfuse plasmid and then chromosomally integrated at the λ *attB* site of E4643 using the CRIM system (Haldimann and Wanner, 2001). To generate a series of modules that express CI at different stable states, the *pL* -10 or -35 site was mutated by performing high-fidelity PCR with primers designed to introduce specific changes. Presented in Table 2.1 are the eight variants made at the *pL* -10 sequence, all retain the final AT of the putative CI operator at *pL*. The M1 mutation was originally intended to be a perfect match to the -10 consensus (TATAAT) but an alternative sequence with a 1bp deletion was obtained, which retained the *pL* operator site and a close match to the -10 consensus. Three mutants that altered the *pL* -35 site towards or away from the -35 consensus (TTGACA) were also made.

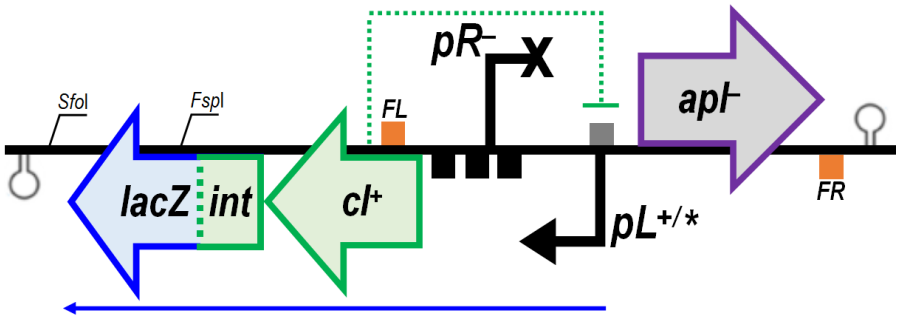

Figure 2.2: The CI expression *pL* LacZ reporter module. Each module generates a *pL* LacZ readout proportional to the level of CI expressed from *pL*, where the -10 and -35 sites were subject to site-specific mutagenesis to generate a library that expresses CI at different stable levels. The *Sfo*I and *Fsp*I restriction enzyme sites were later used to remove *lacZ* after preliminary screening of *pL* mutants. *(cI+)* encodes the wildtype CI immunity repressor, remaining symbolism defined in Fig. 2.1.

Table 2.1: The preliminary library of wildtype and mutant CI expression modules and their *pL* -10 or -35 mutations. Sequences are written from the bottom strand in standard 5' to 3' orientation. Bold blue bases of *pL* -10 site represent sequence overlap with the CI *pL* operator site. Dot (·) represents a nucleotide match to wildtype sequence, a letter (A, T, G, C) represents a mutation and a (–) represents a deletion. The final library was reduced to WT, M1, M2, M7, M8, and M9 through LacZ analysis and Western blotting.

***pL* variant**	***pL* -35**						***pL* -10**				**pL operator**					
Wildtype	T	T	G	C	G	A	**C**	**A**	**T**	**G**	**A**	**T**	T	C	C	C
M1	·	·	·	·	·	·	T	·	·	—	·	·	·	·	·	·
M2	·	·	·	·	·	·	T	·	·	C	·	·	·	·	·	·
M3	·	·	·	·	·	·	·	T	A	A	·	·	·	·	·	·
M4	·	·	·	·	·	·	G	G	·	C	·	·	·	·	·	·
M5	·	·	·	·	·	·	G	T	·	A	·	·	·	·	·	·
M6	·	·	·	·	·	·	G	C	C	C	·	·	·	·	·	·
M7	·	·	·	·	·	·	A	·	·	A	·	·	·	·	·	·
M8	·	·	·	·	·	·	G	T	A	C	·	·	·	·	·	·
M9	·	·	·	A	C	·	·	·	·	·	·	·	·	·	·	·
M10	A	·	·	T	C	·	·	·	·	·	·	·	·	·	·	·
M11	G	G	A	·	·	T	·	·	·	·	·	·	·	·	·	·

Stage 1B: Charactering the pL promoter variants to determine the range of CI expression levels

The *pL* activity of the wildtype and eleven mutants was compared by LacZ assays in microtitre plate format (Fig. 2.3). Wildtype plus seven mutants were selected as the preliminary set of CI expression modules (WT, M1, M2, M3, M7, M8, M9 and M11). Mutants M1, M2 and M9 generate LacZ values up to 10-fold higher than the wildtype reporter (9.4 LacZ units). M9 was expected to generate higher LacZ activity than wildtype *pL,* given its -35 consensus sequence (58.7 LacZ units), but it was not as active as M2, which returned 99.2 LacZ units. M2 is a *pL* -10 mutant, exhibiting only partial improvement towards consensus, consistent with the known stronger impact of the -10 sequence on promoter strength than the -35 site. Mutants M7, M3, M8 and M11 were selected for their lower than wildtype *pL* LacZ levels, exhibiting 77, 35, 24 and 4% of wildtype LacZ activity, respectively.

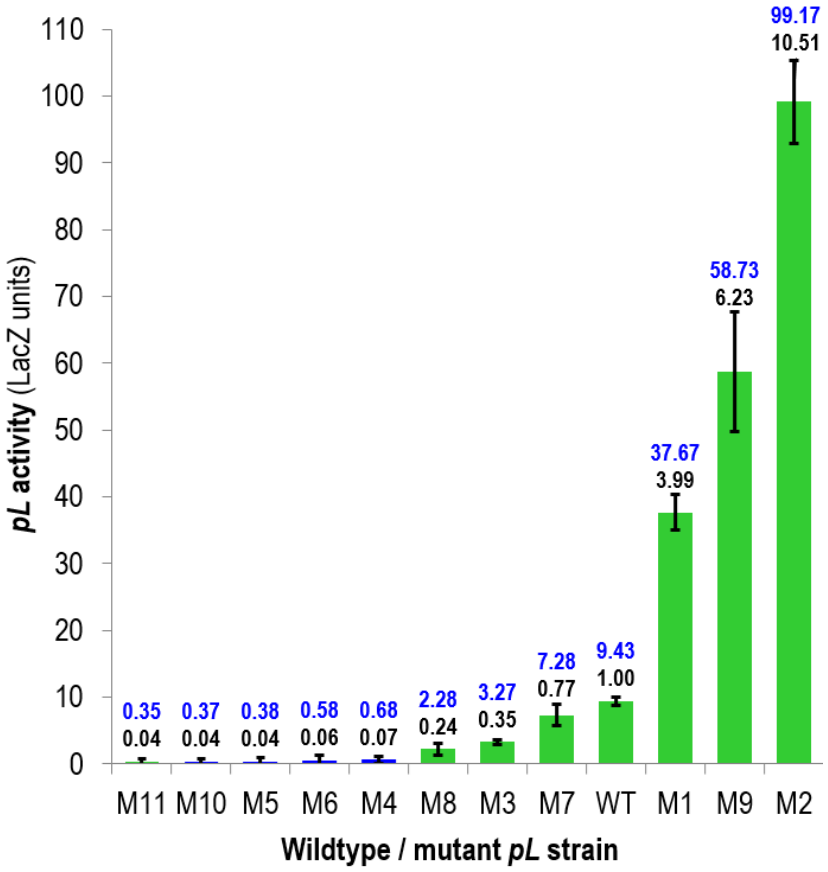

Figure 2.3: Activity of the *pL* promoter variants. LacZ assays screened for suitable CI expression modules harbouring site-specific mutations at the *pL* -10 or -35 site. CI expression levels were indirectly measured by expression of *int::lacZ;* a fusion of the *lacZ* gene with the RBS and first nine amino acids of the *int* gene. Constructs were integrated at the λ *attB* site of the E4643 chromosome. Strains shaded green were selected for further characterisation. Each data point represents an average of six independent assays, 95% confidence interval error bars are shown. For each *pL* variant strain, absolute and relative-to-wildtype LacZ values are coloured blue and black respectively.

Stage 2A: Conversion to the final CI expression modules

Following LacZ analysis of the CI expression *pL* LacZ reporters, the wildtype, five *pL* -10 mutants (M1, M2, M3, M7 and M8) and two *pL* -35 mutants (M9 and M11) were selected as they appeared to give an adequate range of CI levels. The removal of the *lacZ* gene *(*and shifting the *lacZ* terminators to reside a short distance downstream of the *int* ATG) was required to convert each reporter into the appropriate expression module (Fig. 2.4).

To make this modification, the selected reporters were *Fsp*I and *Sfo*I digested and then re-circularised via 'self' DNA ligation, which left a small remnant of the *int::lacZ* reporter gene that encodes the first 54-amino acids of the full-length 1026-amino acid protein, the product of which is non-functional. Each expression module was integrated into the λ *attB* site of E4643, which was already integrated with a *pR* or *pL goa8*$^{+/-}$ LacZ reporter (see Fig. 2.1). Preliminary LacZ analysis of these expression modules coupled to the six LacZ reporters (data not shown) led to the omission of the M3 mutant as it behaved unexpectedly, presumably due to the acquisition of mutation(s) within the CI expression module and/or LacZ reporter. This strain was rejected (rather than repaired) as we believed the WT, M1, M2, M7, M8, M9 and M11 modules would provide adequate low-to-high coverage of CI.

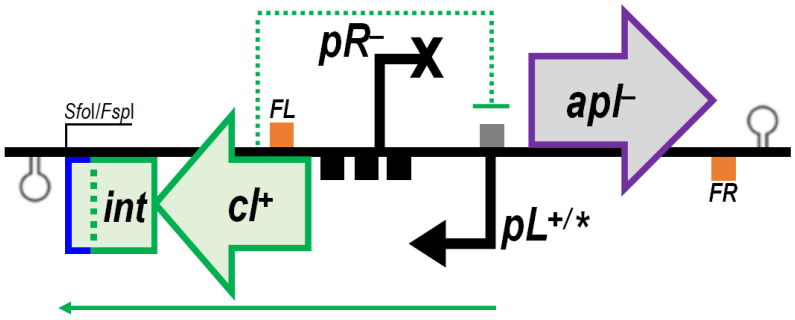

Figure 2.4: The CI expression module. The single-copy λ integrated CI expression module designed to express CI at a low, wildtype or high steady state from *pL*$^{+/*}$ derived by deletion of most of the *lacZ* gene (*Sfo*I-*Fsp*I restriction) from the constructs presented in Fig. 2.3. The *Sfo*I/*Fsp*I restriction enzyme ligation site is located 160bp downstream of *int* ATG. (*int*) encodes the first nine amino acids of Integrase fused to a short section of the LacZ NTD (~45 amino acids), the product of which is non-functional. Remaining symbolism defined in Fig. 2.1

Stage 2B: Direct measurement of CI expression levels

To gain a more direct measure of CI expression for each of the selected CI expression modules, fluorescent Western blotting was performed for whole-cell extracts using a primary rabbit polyclonal antibody raised against CI and a Cy5-labelled donkey-anti-rabbit secondary antibody. CI concentration [CI] was measured in lysogenic units, where 0 lysogenic units represents no CI and 1 lysogenic unit represents the [CI] observed in a wildtype 186 lysogen. Dodd and Egan (2002) quantified [CI] in a 186^{+} lysogen to be 1100 ±200nM. The control strain expressing no CI (AI19) contained the empty pIT3-CL plasmid vector integrated at the λ *attB* site while the positive control strain expressing a lysogenic level of CI (AI25) contained the empty pIT3-CL vector (at λ *attB*) and a 186^{+} prophage at the primary 186 *attB1* site (*E. coli* harbours two 186 *attB* sites). As presented in Table 2.2 and Figure 2.5, [CI] for each CI expression strain was quantified using a lysogenic CI standard curve; generated by adding various volumes of the AI25 (lysogenic) whole-cell extract to the AI19 (no CI) whole-cell extract.

To accurately interpolate [CI] for the high CI expression modules (M1, M2 and M9), these whole-cell extracts were diluted to ensure their signal fell within the range of the standard curve. As expected, the M11 module generated a very low (almost undetectable) level of CI. It was expected AI25 (the 186^{+} lysogen) and AI31 (the CI^{WT} expression strain) would reveal similar [CI] values, but AI31 generates a slightly higher [CI] (1.64). This difference could be due to CI being expressed from different integration sites, where CI is expressed from the 186 *attB1* site in AI25 and from the λ *attB* site in AI31. It is also possible that enhanced translation of the *cI* mRNA in AI31 may occur due to the module having the *pR* -35 mutation and/or because it produces a shorter *pL* transcript (terminates after transcribing the first nine amino acids of *int)* than the 186 prophage (produces the full-length *pL* transcript*)*. Another discrepancy (to note) is that while a general match exists between the relative-to-wildtype LacZ values and the Western blot derived [CI] values for AI31, AI55, AI37, AI67 and AI43, the AI61 strain (M8 module) has a much lower [CI] (0.05) than its relative-to-wildtype LacZ value (0.24). Whilst we do not understand this discrepancy we decided to use the Western [CI] when plotting the CI expression-LacZ reporter data.

Table 2.2: The final library of wildtype and mutant CI expression modules. Each module is listed with its *pL* -35 or *pL* -10 mutations and relative-to-lysogen CI expression level.

CI module	CI level[A]	95% CI	*pL* -35[B]						*pL* -10[B]						*pL* operator			
AI19 (pIT3-CL)	0.00	—																
AI25 (186^{+})	1.00	—	T	T	G	C	G	A	**C**	**A**	**T**	**G**	**A**	**T**	T	C	C	C
AI31 (WT)	1.64	*(1.38-1.94)*	·	·	·	·	·	·	·	·	·	·	·	·	·	·	·	·
AI61 (M8)	0.05	*(0.02-0.12)*	·	·	·	·	·	·	G	T	A	C	·	·	·	·	·	·
AI55 (M7)	1.31	*(1.00-1.72)*	·	·	·	·	·	·	A	·	·	A	·	·	·	·	·	·
AI37 (M1)	8.41	*(7.01-10.10)*	·	·	·	·	·	·	T	·	·	—	·	·	·	·	·	·
AI67 (M9)	16.39	*(14.52-18.50)*	·	·	·	A	C	·	·	·	·	·	·	·	·	·	·	·
AI43 (M2)	22.86	*(19.19-27.23)*	·	·	·	·	·	·	T	·	·	C	·	·	·	·	·	·

A. To quantify [CI] for each CI expression module, fluorescent Western blotting was performed for whole-cell extracts using a primary rabbit polyclonal antibody raised against CI and a Cy5-labelled donkey-anti-rabbit secondary antibody. CI levels are listed in lysogenic units, where 0 lysogenic units represents no CI and 1 lysogenic unit represents the CI level observed in a 186^{+} lysogen. Each CI value is the average of six independent measurements, with 95% confidence intervals shown for each CI expression module. CI M11 levels undetectable.

B. Blue bold bases of *pL* -10 site represent sequence overlap with the CI *pL* operator site. Dot (·) represents a nucleotide match to wildtype sequence, a letter (A, T, G, C) represents a nucleotide mutation and a (–) represents a deletion.

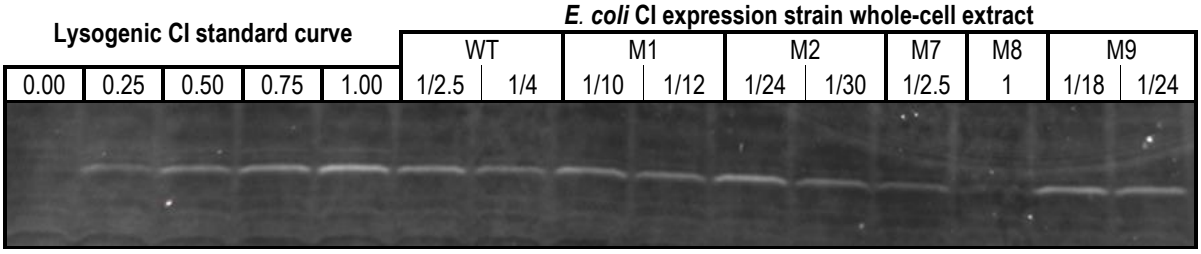

Figure 2.5: Fluorescent Western blotting of whole-cell extracts of the selected *E. coli* CI expression strains. Western blot performed with a primary rabbit polyclonal antibody raised against CI and a Cy5-labelled donkey-anti-rabbit secondary antibody. The lysogenic CI standard curve was prepared using whole-cell extracts of the AI19 no-CI strain and the AI25 186^{+} lysogen. The CI expression strain whole-cell extracts were diluted to ensure their signal fell within range of the standard curve. Dried membranes imaged on the Western blot Cy5 channel (Red Epi illumination with 695/55 filter) linked to the ChemiDoc™ MP Imaging System (BioRad). Western blot images analysed using the BioRad Image Lab software (Version 5.2.1 build 11, 2014).

2.1.1.2 The *goa8* mutation causes defective negative autoregulation of *pL* by CI

Integration of the six CI expression modules (wildtype + five mutants) into each of the six reporter strains, gave a total of 36 strains. As negative controls, the empty CI expression plasmid (pIT3-CL) was integrated into each reporter strain. To make positive controls, these no-CI strains were further lysogenised with 186^+ to provide CI at the natural lysogenic level. Colony PCR verified all six strains to be single lysogens harbouring a 186^+ prophage at the 186 *attB1* site, increasing the total number of strains to 48 (where six CI expression modules, plus the no-CI control and the 186^+ lysogen gives eight multiplied by six *pR* and *pL goa8*$^{+/-}$ *lacZ* reporters gives 48).

The LacZ data for the ***pR*$^+$*(pL*$^+$*)* reporters (Fig. 2.6A ● data) shows strong repression of *pR* at CI levels ≥1 lysogenic unit while at low CI levels (0.05 lysogenic units), *pR* is largely unrepressed (~72 LacZ units). When CI is absent, *pR* activity is ~82 LacZ units. The LacZ data for the ***pR*$^+$*(pL*$^+$*) goa8* reporters (Fig. 2.6A ▲ data) shows the *goa8* mutation appears to cause an ~32.5% decline in basal *pR* promoter activity. In the presence of CI (and the *FL* and *FR* sites) *pR* was repressed very effectively. Reed et al. (1997) also observed a reduction in basal *pR* activity in the presence of the *goa8* mutation, but promoter activity was only observed to be reduced by ~13.2%. With the *goa8* mutation located at the +27 position of *pR* it seems unlikely it would directly affect promoter activity (making it a *pR*-down mutation). We speculate the reduction in basal *pR* activity in the presence of the *goa8* mutation could be due to (1) partial termination of transcription, (2) an effect on Apl translation (as *goa8* lies 34bp upstream of the Apl translation initiation site) or (3) by changes in the stability of the ***pR*$^+$*.apl*$^-$*.cII::lacZ* mRNA.

The wildtype ***pL*$^+$*(pR*$^-$*)* (Fig. 2.6B ● data) and ***pL*$^+$*(pR*$^+$*)* (Fig. 2.6C ● data) reporter data are similar to previous results observed by Dodd and Egan (2002). First, under no-CI or low-CI conditions, the activity of the ***pL*$^+$*(pR*$^+$*)* reporter is ~9-fold lower than observed for the ***pL*$^+$*(pR*$^-$*)* reporter. This difference represents the decrease in *pL* activity due to the presence of *pR* transcriptional interference. Second, the wildtype ***pL*$^+$*(pR*$^+$*)* reporter is activated by intermediate CI levels, including the lysogenic level, but becomes repressed at higher CI levels. Third, the wildtype ***pL*$^+$*(pR*$^-$*)* reporter is repressed by increasing CI levels, since there is no *pR* transcriptional interference to be relieved.

The LacZ data for the ***pL*$^+$*(pR*$^-$*) goa8* reporter (Fig. 2.6B ▲ data) provides clear evidence of a defect in CI repression of *pL*. In the wildtype ***pL*$^+$*(pR*$^-$*)* reporter, when supplied CI at a lysogenic level *pL* activity declines by ~74% and greater levels of CI increase repression further (up to 92% decrease in *pL* activity). For the ***pL*$^+$*(pR*$^-$*) goa8* reporter, CI at the lysogenic level reduces *pL* activity by only ~20% and the highest CI expression levels reduce *pL* activity by ~34%. The defect in CI repression of *pL* is also seen in the ***pL*$^+$*(pR*$^+$*) goa8* reporter (Fig. 2.6C ▲).

In the wildtype ***pL*⁺*(pR⁺)*** reporter, CI levels reduce *pL* activity ~4.5-fold from their maximal level, while an ~1.2-fold reduction is seen for the *goa8* version. *pL* activity is also always higher in the presence of the *goa8* mutation. At lysogenic CI levels, *goa8* increases *pL* activity over 2-fold, while the activity of *pL* at high CI expression levels is ~8-fold higher in *goa8* compared to wildtype. No substantial effect of *goa8* on *pL* activity was seen in the absence of CI, an outcome consistent with that of Reed et al. (1997).

We reason impaired repression of *pL* by CI in the presence of the *goa8* mutation is due to the loss of the CI-*pR.pL* repressive complex (Fig. 2.7A), where *goa8* disrupts the precise spacing predicted for the *pL* operator site to correctly align/wrap onto the CI-*pR* wheel (Fig. 2.7E). The lack of effect of *goa8* on CI *pR* repression suggests *pL* wrapping does not substantially aid CI occupation of *pR* (at least in the presence of the *FL* and *FR* sites). We infer CI repression of *pR* is retained in the presence of the *goa8* mutation because (1) the three consecutive strong CI operators at *pR* are retained and (2) loss of the CI-*pR.pL* repressive complex is rescued by the formation of CI-*pR.FL* and CI-*pR.FR* wheels, which can still adequately shut down *pR* activity but do not assist in CI *pL* regulation (Fig. 2.7C).

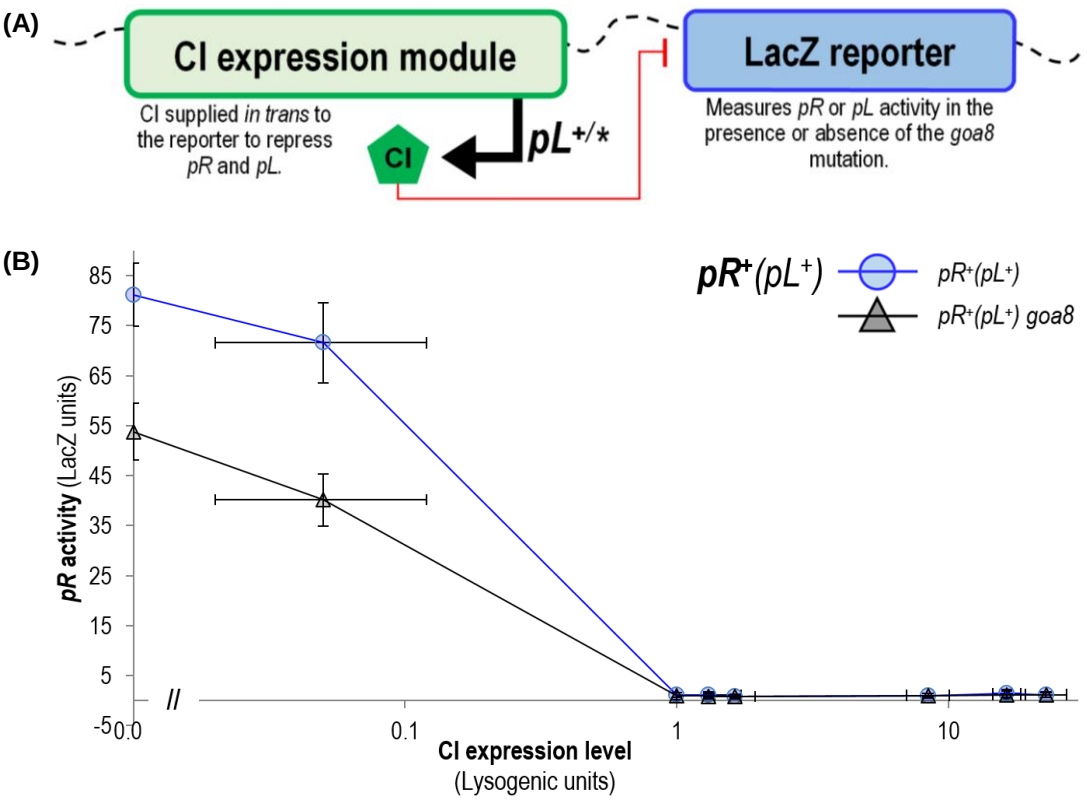

Continued to next page.

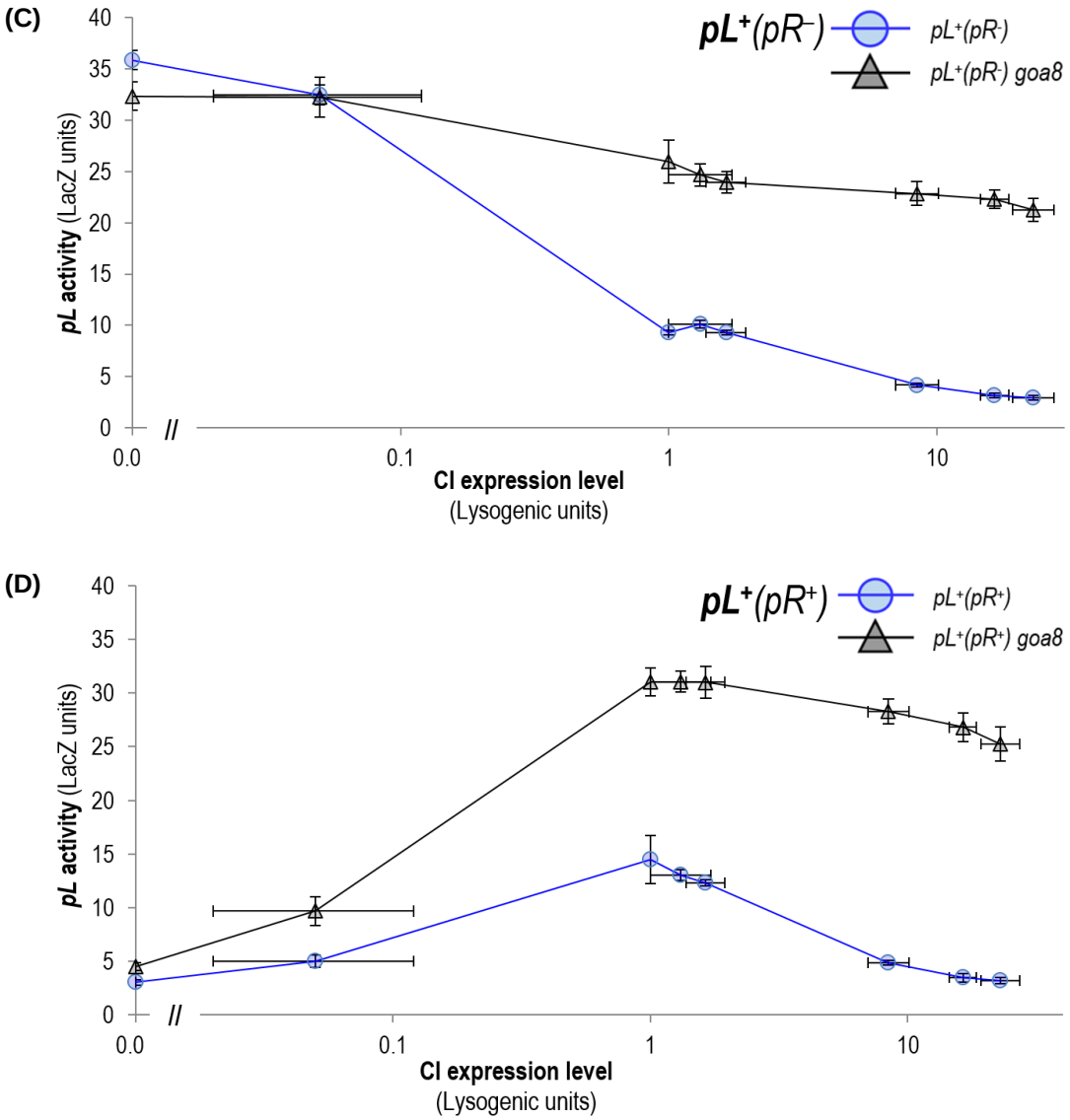

Figure 2.6: Observed *pR* and *pL goa8*$^{+/-}$ LacZ activity for the *E. coli* CI expression-LacZ reporter strains. **(A)** A schematic of the integrated CI expression-LacZ reporter system. A paired series of single-copy integrated CI expression modules designed to express CI at a fixed low, wildtype or high level coupled to one of six single-copy integrated *pL* and *pR goa8*$^{+/-}$ LacZ reporters. CI supplied from the expression construct not only regulates its own expression from *pL* but also acts upon the LacZ reporter to generate a LacZ readout in response to [CI] in the presence or absence of the *goa8* mutation. **(B)** The ***pR*$^{+}$***(pL*$^{+}$*) goa8*$^{+/-}$ reporters present *pR* activity as a function of different CI expression levels. **(C)** The ***pL*$^{+}$***(pR*$^{–}$*) goa8*$^{+/-}$ reporters present *pL* activity as a function of different CI expression levels in the absence of *pR* transcriptional interference. **(D)** The ***pL*$^{+}$***(pR*$^{+}$*) goa8*$^{+/-}$ reporters present *pL* activity as a function of different CI expression levels in the presence of *pR* transcriptional interference. Blue dots represent LacZ reporter activity for CI expression strains harbouring single-copy wildtype reporters. Black triangles represent LacZ reporter activity for CI expression strains harbouring single-copy *goa8* reporters. The X-axis displays (on a log scale) the [CI] produced by the six selected CI expression strains (plus controls) in order of low to high CI supply. Each data point represents ten to twelve independent assays, 95% confidence interval error bars for both CI levels and LacZ activity are shown.

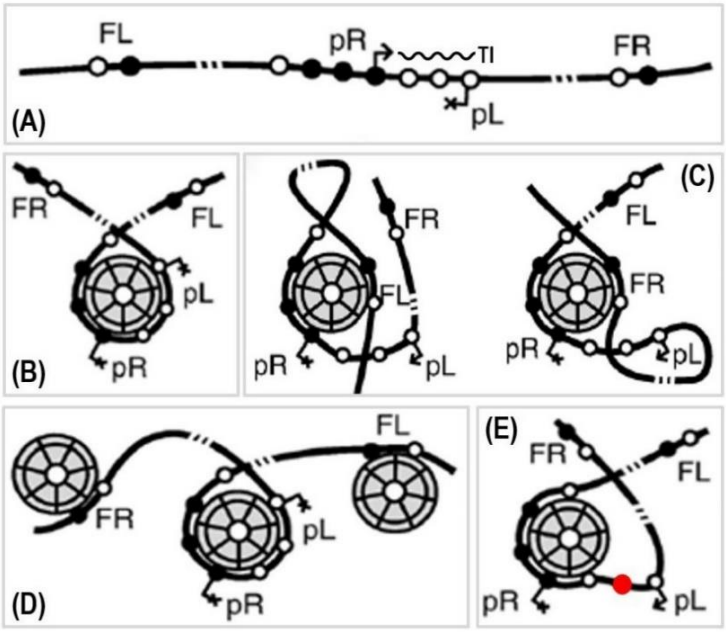

Figure 2.7: Examples of predicted 186 CI-DNA binding configurations. Filled and unfilled circles represent strong and weak defined DNA binding sites at the 186 switch region respectively. In the absence of CI **(A)**, *pR* is active and *pL* is repressed by *pR* transcriptional interference. The HTH domains of three adjacent CI homodimers on the CI wheel bind three adjacent *pR* operators. Binding to weaker operator sites at *pL, FR* and *FL* produce different wrapping configurations. The CI-*pR.pL* complex **(B)** naturally achieves tight repression of *pR* and *pL*. The CI-*pR.FR* and CI-*pR.FL* complexes **(C)** conserve *pR* repression but enhance *pL* activity by outcompeting the putative weak *pL* operator for limited sites on the CI wheel (Dodd et al., 2007). When CI levels exceed the lysogenic level, multiple CI wheels (at the switch) **(D)** results in repression of *pR* and *pL*. The *goa8* mutation (●) is thought to disrupt formation of the CI-*pR.pL* complex, resulting in loss of repression of *pL* by CI. **(E)** *pR* repression remains unaffected because the CI-*pR.FL* and CI-*pR.FR* complexes are thought to rescue the loss of the CI-*pR.pL* complex. Adapted from Dodd et al. (2007).

2.1.1.3 The *goa8* mutation increases CI levels in the lysogen

The results of the *pR* and *pL goa8*$^{+/-}$ LacZ reporter experiments (Fig. 2.6) clearly show the *goa8* mutation results in reduced CI repression of *pL*. Reed et al. (1997) also showed that an *E. coli* C600(186^{goa8}) lysogen had a lower prophage induction efficiency than an *E. coli* C600(186^{+}) lysogen, where it was inferred poor induction may be due to the loss of Apl repression of *cI* from *pL*. An alternative explanation is that since the *goa8* mutation disrupts CI negative autoregulation, this may result in an increased [CI] in a 186^{goa8} lysogen, with the level elevated to the extent that it could potentially make it more difficult for Tum to inactivate CI during prophage induction. To investigate this theory, quantification of [CI] for C600(186^{+}) (E0573) and C600(186^{goa8}) (E2564) lysogens was done via fluorescent Western blotting of whole-cell extracts using a primary rabbit polyclonal antibody raised against CI and a Cy5-labelled donkey-anti-rabbit secondary antibody. Prior to this analysis, the sequence of the switch regions of E0573 and E2564 were verified by Sanger sequencing and a PCR screen was performed to verify that E0573 and E2564 harbour only single prophages at the 186 *attB1* site. [CI] was quantified by comparing the E0573 and E2564 whole-cell extracts against a *goa8*-CI standard curve, generated by adding various volumes of the E2564 whole-cell extract to a C600 (no-CI) whole-cell extract. Western blotting and image analysis (Fig. 2.8) determined on average, the E2564-*goa8* lysogen generates 1.65-fold (95% confidence interval 1.48-1.83, *n*=8 independent extracts) more CI than the E0573-wildtype lysogen. Therefore, as hypothesised, the *goa8* mutation does increase the CI lysogenic level in a lysogen, but what is interesting is how such a relatively small difference in [CI] can cause an ~4.5-fold defect in prophage induction efficiency, as observed by Reed et al. (1997).

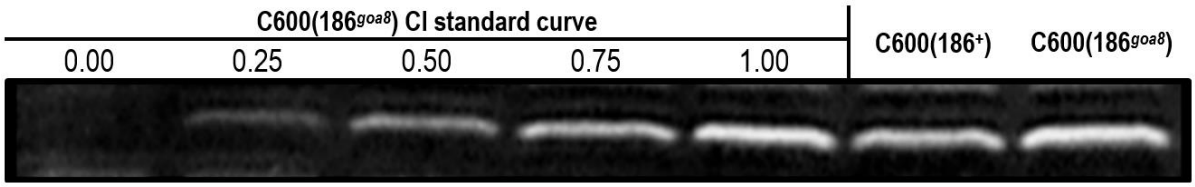

Figure 2.8: Fluorescent Western blotting of C600(186^{+}) and C600(186^{goa8}) whole-cell extracts. Western blot performed with a primary rabbit polyclonal antibody raised against CI and a Cy5-labelled donkey-anti-rabbit secondary antibody. Lanes 1-5 feature C600(186^{goa8}) standard curve and lanes 6-7 represent undiluted C600(186^{+}) and C600(186^{goa8}) whole-cell extract respectively. Dried membranes imaged on the Western blot Cy5 channel (Red Epi illumination with 695/55 filter) linked to the ChemiDoc™ MP Imaging System (BioRad). Western blot images analysed using the BioRad Image Lab software (Version 5.2.1, build 11, 2014).

2.1.1.4 In the minimal prophage induction module, the *goa8* mutation inhibits *pR* derepression following UV induction

So far, our investigation into the *goa8* mutation has demonstrated this mutation impairs CI's ability to negatively autoregulate its expression from *pL,* which results in a modest increase in the CI lysogenic level in a lysogen. The mutation also somewhat impairs the activity of an unrepressed *pR*. To evaluate the degree to which the *goa8* mutation affects *pR* derepression after UV induction; a minimal prophage induction system was used (see Chapter 4). The chromosomally-integrated minimal induction system consists of a *cI*$^{+}$.***pR***$^{+}$.*pL*$^{+}$.*apI*$^{+}$.*cII*$^{+}$.*fil::lacZ* reporter, coupled to a UV-inducible *p95.tum*$^{+}$ induction module (Fig. 2.9A). The reporter features the *pE* promoter and the face-to-face *pR* and *pL* promoters, flanked by intact *FL* and *FR* sites. The *cI, apI* and *cII* genes encode full-length wildtype proteins and to reduce the background from each reporter, a translational fusion of *lacZ* with *fil* reports on *pR* activity. The induction module features the LexA repressed *p95* promoter that drives *tum* expression, which encodes the full-length wildtype antirepressor, Tum. Thus, when UV is absent, the LacZ reporter exists in a stable pseudo-lysogenic state, where CI expressed from *pL* represses *pR,* and the host LexA inhibits expression of *tum* from *p95* (Fig. 2.9A, Lysogenic state). When the *E. coli* are exposed to UV, *p95* is derepressed and *tum* is expressed. Tum binds and inactivates CI resulting in *pR* derepression and the expression of *apI, cII* and *fil::lacZ* (Fig. 2.9A, Lytic state).

To assay whether the *goa8* mutation causes a defect in *pR* repression, a *goa8* version of the reporter was made. This reporter was integrated into E4643 already harbouring the UV induction module to give strain, AI116. To determine the optimal UV dose, an initial series of UV dose-response assays were conducted on E4643 integrated with a *cI*$^{+}$.***pR***$^{+}$.*pL*$^{+}$.*apI*$^{+}$.*cII*$^{-}$.*fil::lacZ* reporter, using an X-gal plate assay for the initial readout. Using this reporter allowed us to rapidly determine the exposure time required to achieve optimal induction/switching without compromising cell survival. The assay was carried out by exposing log phase cultures to 0 to 60s of UV, which were plated on L-plates supplemented with X-gal and the proportion of blue colonies scored the next day. The outcome indicated a 40s dose of UV (~5.2 J/m^{2}) was sufficient to achieve maximal switching without causing excess cell death (results not shown).

Log phase cultures of AI116 and AI85 were then UV irradiated for 40s (~5.2 J/m^2) and LacZ production tracked for 3hrs. Figure 2.9B presents the results of the UV induction LacZ timecourse experiments, where as expected, AI116 (*goa8*) exhibited a significantly impaired *pR* induction profile (Fig. 2.9B, ● data) in comparison to AI85 (Fig. 2.9B, ● data). The data shows that in the absence of the *goa8* mutation (AI85), *pR* activity follows a typical rise-and-fall induction profile, where prior to UV induction, *pR* activity is very low due to repression by CI. Upon UV exposure, CI is inactivated by Tum resulting in *pR* derepression and expression of *apl, cII* and *fil::lacZ.* It is important to note, due to the stable nature of the LacZ protein, the slope of the curve (i.e. the rate of change) is what gives the best indication of *pR* activity. Hence, whilst LacZ units peak at ~73 at the 150min mark, *pR* activity is actually at its greatest 30 to 90mins after UV induction and is then progressively re-repressed thereafter. We assume repression of *pR* by CI is gradually restored as LexA levels recover - due to the repair of DNA and shut-off of the SOS system - and repression at *p95.tum* is re-established. In the absence of Tum, CI repression resumes and gradually recovers back to its lysogenic equilibrium, where *pR* is re-repressed and expression of *apl, cII* and *fil::lacZ* is inhibited. Any decrease in the level of LacZ after 140mins is likely due to dilution of existing LacZ, due to cell growth.

Referring back to Section 2.1.1.2, LacZ analysis of the CI expression-*pR* LacZ reporter strains (Fig. 2.6B) revealed the *goa8* mutation reduces basal *pR* activity by ~32.5%, suggesting *goa8* acts as a *pR*-down mutation. Analysis of the AI116 (*goa8*) module *pR* reporter data (Fig. 2.9B), shows an almost parallel induction curve (in comparison to AI85), but LacZ units only peak at ~36 at the 150min mark, which represents a ~51% reduction in *pR* activity. This outcome raised a key question, is this ~51% decline in *pR* solely due to the *pR*-down effect of the *goa8* mutation or is this increased reduction in *pR* activity due to the *goa8* mutation also disrupting CI negative autoregulation? To answer this question, the wildtype LacZ data (AI85) was adjusted (reduced by 32.5%) and statistically compared to the *goa8* LacZ data (AI116) by conducting unpaired, one-tailed *t*-tests. The outcome of this analysis confirmed the ~51% defect in *pR* activity after induction of the *goa8* reporter cannot be explained solely by the *pR*-down effect of the *goa8* mutation. Shown in the inset of Figure 2.9B are the six adjusted wildtype values (● data) plotted with the six corresponding *goa8* values (unadjusted). The inset plot shows the *goa8* mutation causes a consistent induction defect (of at least 25%) beyond the *pR*-down effect. The differences between the six adjusted wildtype values and the six *goa8* values at each time point (from 30mins) are all statistically significant at the 0.05 level with *p*-values ranging from 0.008 to 0.034 (*t*-tests: unpaired, one-tailed, unequal variances, *n*=6). This supports the idea that the raised CI levels in the *goa8* lysogen contribute to defective *pR* induction.

From this data analysis, we conclude the marginal increase in [CI] in the *goa8* module (AI116) likely exceeds the sequestering capability of Tum. For AI116, the inability of Tum to inactivate all of the CI in the cell would leave *pR* vulnerable to partial repression by CI, which would explain why there is suboptimal expression of *apl, cII* and *fil::lacZ* from *pR* following UV induction.

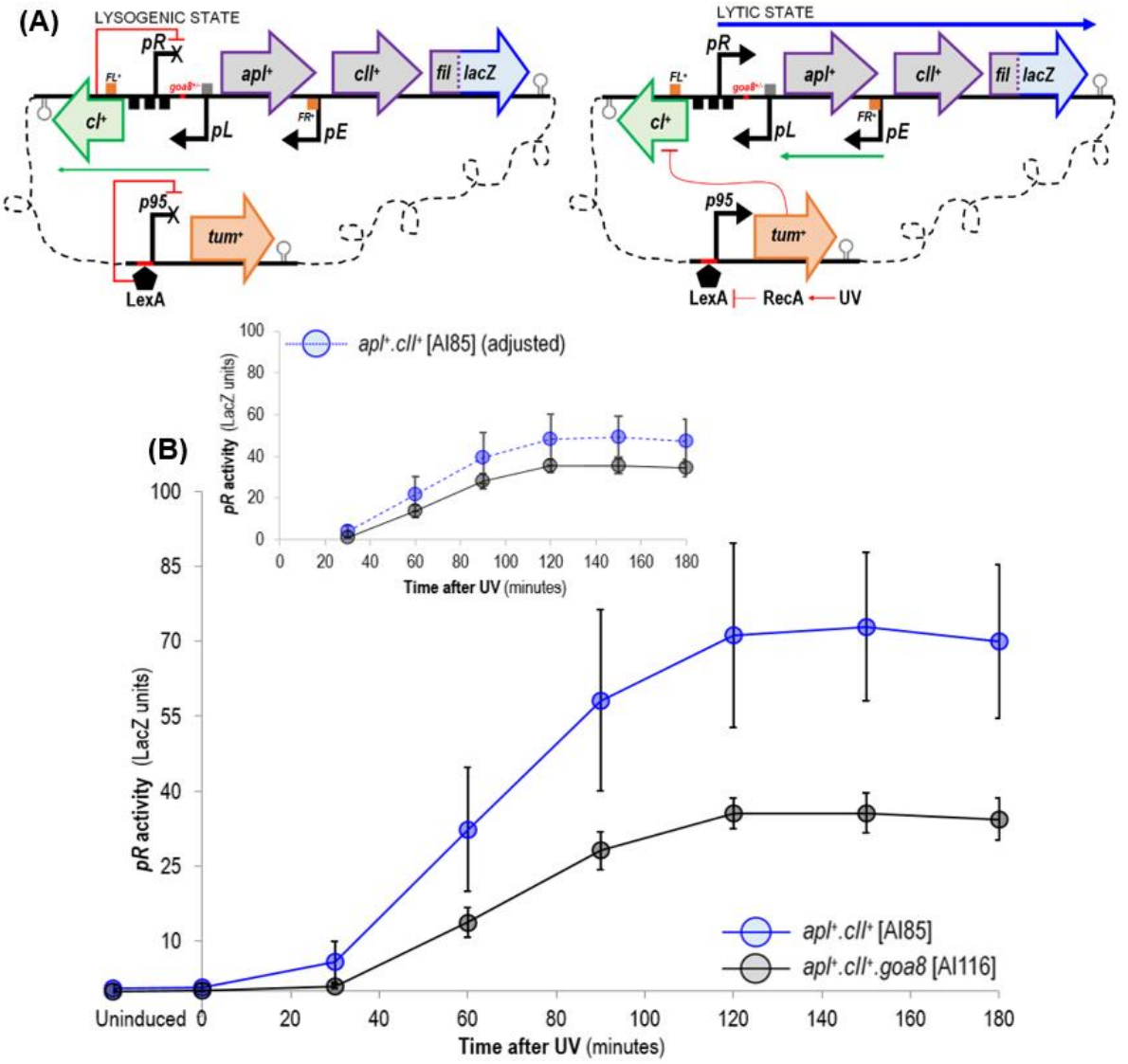

Figure 2.9: Observed *pR* activity for the *E. coli goa8*$^{+/-}$ minimal prophage induction modules. (A) Schematics of the lysogenic and lytic states of AI85 and AI116 strains harbouring a λ integrated wildtype or *goa8* ***pR***.*apl*$^{+}$.*cII*$^{+}$ reporter and a 186 *attB1* integrated *p95.tum*$^{+}$ induction module. In the lysogenic state, LexA represses expression of the *p95.tum*$^{+}$ transcript and CI represses expression of the *pR.apl*$^{+}$.*cII*$^{+}$.*fil::lacZ* transcript. In the lytic state, LexA is degraded and the *p95.tum*$^{+}$ transcript expressed. Tum inactivates CI, resulting in *pR* derepression and expression of the *pR.apl*$^{+}$.*cII*$^{+}$.*fil::lacZ* transcript. *(fil::lacZ)* encodes FiI::LacZ fusion reporter protein; the RBS and first three amino acids of Fil are linked to the ninth codon of LacZ. Remaining symbolism defined in Fig. 2.1. **(B)** Observed *pR* LacZ activity following UV induction of AI85 and AI116. AI116 (*goa8*) exhibits poor *pR* derepression with maximal promoter activity ~51% less than AI85 (wildtype). The adjusted *pR* LacZ activity for AI85 (inset plot, ● data reduced by 32.5%) shows the lower level of *pR* activity in the *goa8* mutant is more than can be explained by the ~32.5% *pR*-down effect g*oa8* has on basal *pR* activity. *pR* induction profiles were obtained by inducing log phase cultures with 40s UV and tracking LacZ production for 3hrs. To prepare for induction, O/N cultures were grown in M9MM-1, diluted to OD_{600} 0.15 in M9MM-20 and incubated at 37°C with aeration until cells reached OD_{600} 0.30. For UV induction, 5mL of culture (+1µL 10% TWEEN-20) was irradiated for 40s in a Petri dish. Cultures were incubated in tubes with aeration at 37ºC and samples taken and stored on ice every 30mins. Cultures were diluted periodically with pre-warmed M9MM-20 to maintain log phase growth and ensure a sample OD_{600} ~0.40. The LacZ assay was performed as per the M9MM induction LacZ assay protocol (see Chapter 7, Section 7.0.6.2). The uninduced time point represents samples taken immediately prior to induction. Each data point represents an average of six independent assays, 95% confidence interval error bars are shown.

2.2 The 186 Apl excisionase and transcriptional repressor

2.2.1 Investigating the role of Apl as a transcriptional repressor during 186 prophage induction

The 186 Apl-resistant operator mutants isolated by Reed et al. (1997) provided preliminary evidence of a role for Apl repression of *pL* in 186 prophage induction efficiency. Their interpretation is somewhat confounded however, since reduced prophage induction efficiency observed for the 186-*goa8* mutant is likely attributed to the loss of CI-mediated *pL* repression as well as reduced *pR* expression. As previously discussed, our study of Apl was directed at explaining why this protein acts as a transcriptional repressor at *pR* and *pL,* where after much discussion, three key hypotheses (listed in Table 2.3) were formulated.

Table 2.3: The Apl hypotheses. Three key hypothesises were framed and tested to determine the role of Apl as a transcriptional repressor at the 186 switch during prophage induction. Each hypothesis was tested by assaying *E. coli* strains integrated with a UV-inducible *pR* or *pL/pE* minimal prophage induction module.

A	♦	During 186 prophage induction, Apl aids *pR* derepression by assisting Tum in eliminating CI activity by repressing *cI* expression from *pL*.
B	♦	During 186 prophage induction, to prevent over activation of *cI* and/or *int* expression from an CII-activated *pE,* Apl reduces *cII* expression by repressing *pR*.
C	♦	To facilitate efficient excision of the prophage from the host chromosome during 186 prophage induction, Apl represses *pL* to control *int* levels.

To test these theories we expanded the minimal prophage induction/reporter system as described in Section 2.1.1.4 (Fig. 2.9A), to assay *pR* and *pL/pE* activity in the presence and/or absence of Apl and CII. Each of the new strains has a similar architecture, such that each contains a λ integrated *pR* or *pL/pE* LacZ reporter module and a 186 *attB1* integrated UV-inducible *p95.tum*$^{+}$ module (Fig. 2.10A and Fig. 2.11A). Each of the reporter modules features, *pE* and the face-to-face *pR* and *pL* promoters, flanked by intact *FL* and *FR* sites. *apl* and *cII* genes encode either wildtype or a HTH mutant that render Apl and CII deficient in DNA binding (hence Apl is also deficient in excision). To reduce the background LacZ activity from each reporter, translational fusions of *lacZ* with *fil* or *int* were used to assay *pR* or *pL/pE* activity.

In the *pR* module (Fig. 2.9A), there are eight strains, each harbouring one of eight *cI*$^{+}$.***pR***$^{+}$.*goa8*$^{+/-}$*pL*$^{+}$.*apl*$^{+/-}$.*cII*$^{+/-}$.*fil::lacZ* reporters (AI85, AI86, AI87, AI88, AI116, AI117, AI118 and AI119). A *goa8* version of each reporter was made to further investigate what effect this 5bp deletion has on prophage induction efficiency in the presence and/or absence of Apl and/or CII. In the *pL/pE* module (Fig. 2.9D), there are six strains, each harbouring one of six *cI*$^{+}$.*pR*$^{+}$.***pL***$^{+}$.*apl*$^{+/-}$.***pE***$^{+}$.*cII*$^{+/-/145}$.*int::lacZ* reporters (AI184, AI185, AI186, AI187, AI224 and AI225), with the *cII*^{145} reporters acting as positive controls. The *cII*^{145} gene encodes a stabilised, active CII145 mutant, truncated to its first 145 residues. This renders the protein absent of its protease sensitive CTD, thereby making it immune to host proteolysis (see Chapter 4).

CII145 is capable of achieving prolonged activation of the ***pE***.*cI*$^{+}$.*int::lacZ* transcript, hence in the absence of Apl we expect it will impede prophage induction efficiency. Each system operates exactly as described in Section 2.1.1.4, however, when the *pL/pE* module is in the lysogenic state, CI strongly represses expression of the *pR.apl.cII* transcript and weakly represses the *pL.cI.int::lacZ* transcript, resulting in a moderate *pL* LacZ readout. Following UV induction, Tum inactivates CI and *pR* is derepressed allowing for the expression of *apl* and *cII,* where Apl will weakly repress *pR* and *pL* and CII will transiently activate *pE,* hence both Apl and CII will influence expression of the *int::lacZ* reporter from *pL* and *pE.*

To assay each module, log phase cultures were UV irradiated for 40s (~5.2 J/m^2) and LacZ activity tracked for 3hrs. Hypothesis A was tested by assaying two *pR.lacZ* strains, AI86 (*apl*$^{+}$.*cII*$^{-}$) and AI88 (*apl*$^{-}$.*cII*$^{-}$). The LacZ data (Fig. 2.10B, ● and ● data) shows expression of *apl* does not aid in *pR* derepression. Rather, we observe greater levels of *pR* activity (~1.1-fold increase) in the absence of Apl, presumably due to the lack of direct Apl repression of *pR*. This indicates Apl is not assisting Tum in the removal of CI, or at least if it is, this effect does not outweigh the direct repression of *pR* by Apl. With this observation, hypothesis A was rejected and we moved onto testing hypothesis B (Table 2.3).

As previously discussed (Chapter 1), CII is required for the establishment of lysogeny, but due to the presence of a protease sensitive CTD, this protein is rapidly degraded by host proteases (Murchland et al., 2014). The strength of CII-mediated *pE* activation means when CII activity is high it can enforce the lysogenic pathway by producing a burst of CI, and thus inhibit lytic development. In Chapter 4, the effect of a mutation stabilising CII (i.e. CII145) was tested for the establishment of lysogeny and prophage induction. A 100% frequency of lysogeny was observed for 186(*cII*^{145}) phage compared to ~10% for 186(*cII*$^{+}$). Phage production after UV induction of a 186(*cII*^{145}) lysogen was also severely defective, recording a phage yield ~200-fold less than that observed for a UV-induced wildtype lysogen. From these observations, it was proposed high CII levels result in high production of CI from *pE*, which exceeds Tum's ability to inactivate CI.

Hypothesis B was tested by assaying all *pR* module strains. The wildtype *pR* module strains, AI85 (*apl*$^{+}$.*cII*$^{+}$) and AI86 (*apl*$^{+}$.*cII*$^{-}$) (Fig. 2.10B, ● and ● data) returned the expected induction profiles, where *pR* LacZ levels gradually increased following UV exposure, due to *pR* being derepressed by Tum's inhibition of CI activity. *pR* activity however, did not exceed 77.3 LacZ units (compared to the ~90 LacZ units observed for the *apl*$^{-}$ strains) presumably due to Apl weakly repressing *pR.* Towards the end of the timecourse, LacZ levels begin to taper as LexA re-establishes repression of *p95.tum*$^{+}$.

The wildtype *pR* module strains, AI87 (*apl*$^{-}$*.cII*$^{+}$) and AI88 (*apl*$^{-}$*.cII*$^{-}$) (Fig. 2.10B, ● and ● data) also returned similar *pR* derepression profiles, where *pR* activity is higher presumably due to the lack of Apl repression of *pR*. If Apl repression of *cII* expression were important in prophage induction, the AI87 strain (*apl*$^{-}$*.cII*$^{+}$) would be expected to show decreased *pR* derepression. Instead, we observed the opposite outcome (increased *pR* derepression); suggesting Apl repression at *pR.pL* does not provide an additional means of control of CII expression during prophage induction.

The LacZ data is complemented by the blue/white switch plate data of the wildtype *pR* module strains (Fig. 2.10C), where induction efficiency was visualised phenotypically for each system by plating cultures irradiated with 40s UV on L-plates supplemented with X-gal, and assaying for blue/white colonies the next day. The presence of a blue colony indicates that cells have been UV-induced to express *lacZ* from *pR* - which will cleave the X-gal substrate to give a blue coloured precipitate - and are able to remain in the 'lytic' state for sufficient generations to give rise to a blue-coloured colony. Cells that remain in the 'lysogenic' state grow as white colonies because CI repression of *pR* inhibits *lacZ* gene expression. If hypothesis B were correct, both the AI85 (*apl*$^{+}$*.cII*$^{+}$) and AI86 (*apl*$^{+}$*.cII*$^{-}$) strains would be expected to grow as a mix of blue and white colonies because after UV, Apl would negate the lysogeny-favouring activity of CII. However, blue/white switching was only observed for one of the four strains - AI86 (*apl*$^{+}$*.cII*$^{-}$). While the blue colonies observed for AI86 confirm that Apl does somehow influence switching after UV, the outcomes of the wildtype *pR* module LacZ and switch plate assays do not support hypothesis B, where it appears Apl repression at *pR.pL* does not serve to control CII activation of *pE* during prophage induction.

Returning back to the *goa8* mutation, the *goa8 pR* module LacZ reporter data (Fig. 2.10B, ▲ data) clearly shows this mutation significantly impairs lysogenic to lytic switching. All reporters returned similar suboptimal *pR* induction profiles, where from 60mins after UV induction, a ≥2-fold reduction in *pR* activity was observed for each reporter (taking note that ~32.5% of this reduction is likely due to the *pR*-down effect *goa8* has on basal *pR* activity, see Fig. 2.6B). To visualise induction efficiency, blue/white switch plate assays were also conducted and none of the *goa8 pR* reporter strains exhibited blue/white switching (data not shown). These outcomes demonstrate that the CI negative feedback autoregulatory loop is important for efficient prophage induction.

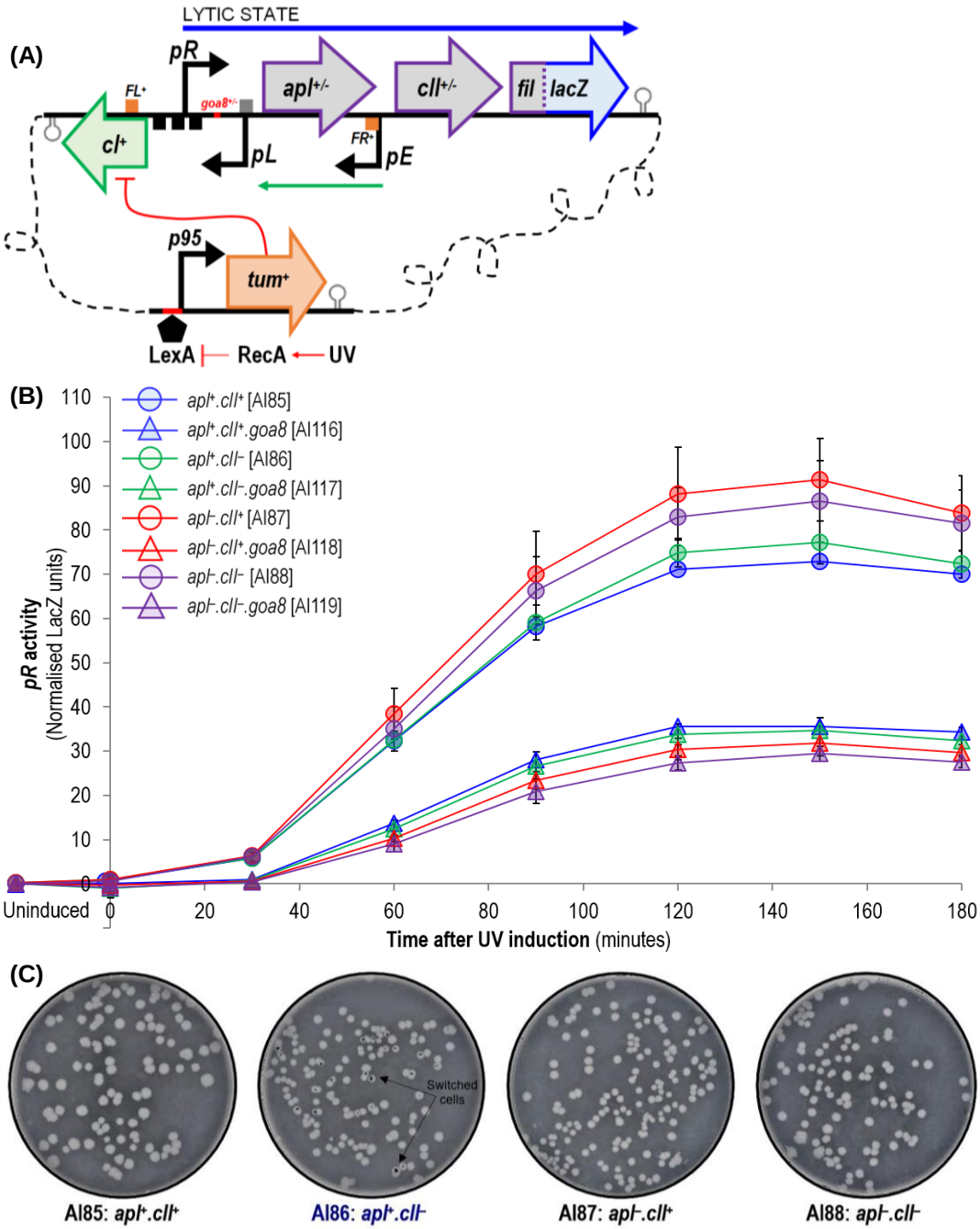

Figure 2.10: Observed *pR* activity for *E. coli* integrated with a *pR* minimal prophage induction module. **(A)** A schematic of the minimal prophage induction *pR* module in the lytic state. After exposure to UV, *pR* activity is expected to increase as Tum (expressed from a derepressed *p95*) inactivates CI. Symbolism defined in Fig. 2.1 and Fig. 2.9. **(B)** Observed LacZ activity for the minimal prophage induction *pR* modules. To reduce the day-to-day variation observed with these assays, the wildtype and *goa8* reporter data was normalised to the AI85 (*apl*$^{+}$*.cII*$^{+}$) data and AI116 (*apl*$^{+}$*.cII*$^{+}$*.goa8*) data respectively, obtained on the same day. *pR* induction profiles were obtained as per the protocol described in Fig. 2.9. The uninduced time point represents samples taken immediately prior to induction. Each data point represents an average of six independent assays, 95% confidence interval error bars are shown. **(C)** Blue/white switching for the wildtype *pR* module strains was only observed for the AI86 (*apl*$^{+}$*.cII*$^{-}$) strain. Switching was assayed by diluting O/N M9MM-1 cultures to OD_{600} 0.15 in M9MM-20 and incubating at 37°C with aeration to OD_{600} 0.30. 5mL of each culture was irradiated with 40s UV, diluted 10^{-4} and 10µL plated on L-plates containing X-gal (40µg/mL) and the growth of blue colonies scored the next day.

With Apl repression of *pR* during prophage induction providing no additional control of CI expression from a CII-activated *pE,* a third possible role for Apl is addressed by hypothesis C (Table 2.3). Is Apl *pL* repression required to control Int levels? To investigate Apl's effect on *pL* during prophage induction, the *pL/pE* module strains were assayed (Fig. 2.11B). If hypothesis C were correct, we expected to observe elevated LacZ levels for AI186 (*apl⁻.cII⁺*) (Fig. 2.11B, ● data), since in the absence of Apl, elevated expression of *cII* would enhance expression of *cI* and *int::lacZ* from *pE.* On the contrary, the results show the *pL/pE* module strains AI184 (*apl⁺.cII⁺*), AI185 (*apl⁺.cII⁻*), AI186 (*apl⁻.cII⁺*) and AI187 (*apl⁻.cII⁻*) have very similar induction profiles. The decision to reject hypothesis C (and B) was further endorsed by the positive control *pL/pE* module strains, AI224 (*apl⁺.cII¹⁴⁵*) and AI225 (*apl⁻.cII¹⁴⁵*) having near identical *pL/pE* LacZ induction profiles (Fig. 2.11E, ● and ● data). It is clear that the presence of the stabilised CII145 leads to a large (5-fold) increase in leftward transcription. However, if Apl at *pR.pL* were important for controlling *cII, cI* and *int* expression, then elevated LacZ expression should have only been observed for AI225 (*apl⁻.cII¹⁴⁵*).

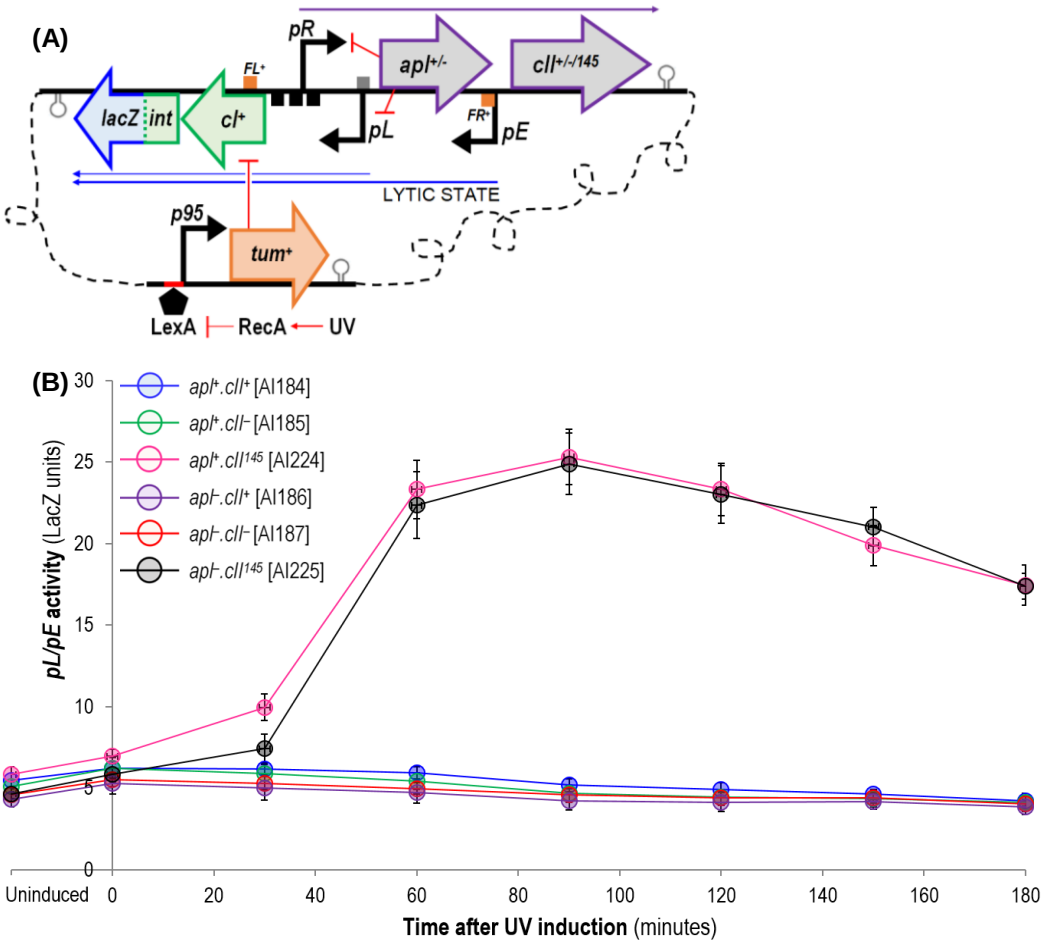

Figure 2.11: Observed *pL/pE* activity for *E. coli* integrated with a *pL/pE* minimal prophage induction module. (A) A schematic of the minimal prophage induction *pL/pE* module in the lytic state. (*cII¹⁴⁵*) encodes a stabilised CII145 mutant, truncated to its first 145 residues. Remaining symbolism defined in Fig. 2.1 and Fig. 2.9. **(B)** Observed LacZ activity for the minimal prophage induction *pL/pE* module strains. *pL/pE* induction profiles were obtained as per the protocol described in Fig. 2.9. The uninduced time point represents samples taken immediately prior to induction. Each data point represents an average of six independent assays, 95% confidence interval error bars are shown. The *apl⁺* reporter data has been reproduced from Fig. 4.5 in Chapter 4.

Overall, the outcomes of the *pL/pE* module complement the outcomes of the *pR* module, thereby augmenting our rejection of all three hypotheses. From this study, we conclude that while Apl has the ability to repress *pR* and *pL,* this repression has no role in (1) assisting Tum in the removal of CI, (2) reducing *cII* expression from *pR* to dampen CII-activation of *pE* or (3) controlling *cI* and *int* expression from *pL.* Therefore, whilst we have broadened our understanding of what Apl *does not* do at the 186 switch, we have yet to successfully determine what significance Apl *pR.pL* repression has on 186 development.

2.3 Conclusions

As discussed in the *introduction* of this chapter, the purpose of this study was to determine two things. First, explain why a C600(186^{goa8}) lysogen exhibits impaired prophage induction efficiency as observed by Reed et al. (1997) and second, determine the role of Apl as a transcriptional repressor at *pR.pL* and whether this repression is important for 186 prophage induction efficiency. To investigate the *goa8* mutation, we wanted to determine the nature in which this 5bp deletion impairs 186 prophage induction efficiency. The initial interpretation made by Reed et al. (1997) was that *goa8* disrupts Apl's ability to repress *cI* expression from *pL,* resulting in elevated CI levels that conflict *pR* derepression during prophage induction. This led to the conclusion that Apl repression of *pL* is required for efficient prophage induction. In a later study by Dodd and Egan (2002) it was shown insertions or deletions of 5bp between *pR* and *pL* abolish CI repression of *pL*. Since the *goa8* mutation is a 5bp deletion located between *pR.pL* we suspected Reed *et al.'s* C600(186^{goa8}) lysogen exhibited poor prophage induction because CI negative autoregulation is disrupted.

With Reed *et al.'s* interpretation under question, research was carried out to answer the question: does the *goa8* mutation disrupt CI negative autoregulation, such that this results in an elevated lysogenic level of CI, which impedes *pR* derepression during prophage induction? To do this, we first developed a CI expression-LacZ reporter system to assay the extent to which the *goa8* mutation effects CI repression at *pR* and *pL.* Using this module, we showed *goa8* not only acts as a *pR*-down mutation (reduces basal activity ~32.5%) but has a significant effect on the ability of CI to repress *pL,* with *pL* activity significantly higher in all *goa8* modules (Fig. 2.6). Western blot analysis of Reed *et al.'s* C600(186^{goa8}) lysogen confirmed that with CI-mediated *pL* repression disrupted, a 1.64-fold elevated level of CI is established in these cells (Fig. 2.8). Lastly, using a minimal prophage induction *pR* reporter module, we observed *pR* net activity to be reduced by ~51% in the presence of the *goa8* mutation and interpreted this outcome to be a consequence of cells having an overall increase in steady state [CI] such that this level of CI exceeds the sequestering capability of Tum. Our investigation into how the *goa8* mutation affects 186 prophage induction supports our theory that the CI negative feedback loop is likely important for 186 in achieving optimal prophage induction efficiency. Furthermore, the modest increase in CI levels in a C600(186^{goa8}) lysogen demonstrates how critical regulatory proteins must remain at their optimum steady states to allow for maximal induction efficiency.

With the *goa8* mutation being a rather complicated mutation - because it effects both Apl and CI regulation - to further investigate (in isolation) the repercussion(s) of disrupting CI negative autoregulation, the next logical step would be to create a CI *pL* operator mutant, which would allow us to directly observe the repercussions of no CI negative autoregulation on prophage induction. This could be done by creating site-specific mutations within the weak *pL* operator site, making sure however, to not affect Apl regulation of *pR.pL* or the strength of the *pL* promoter. As shown in Figure 2.12, this presents a challenge as most bases of the CI operator at *pL* also contribute to the *pL* -10 site, an Apl operator site and/or the *apl* RBS. We are optimistic though, that with careful planning, changing these bases could abolish or at least significantly reduce CI binding to *pL.*

Having determined the nature in which the *goa8* mutation affects 186 prophage induction, this led us back to Apl, as its role as a weak transcriptional repressor at *pR.pL* needed to be redefined. Three key hypothesises were devised and to test them we expanded our minimal prophage induction module to study *pR* and *pL/pE* activity during induction in the presence and absence of Apl and/or CII. The results revealed (1) Apl does not aid Tum in eliminating CI activity by repressing *cI* expression from *pL,* (2) Apl does not control *cII* expression by repressing *pR* to prevent over activation of *cI* and/or *int* expression from an CII-activated *pE* and (3) Apl repression of *pL* does not serve to control *int* expression to facilitate efficient prophage excision. Whilst the outcomes of our study led to the rejection of all hypotheses, we are confident that by progressively ruling out different theories, we will eventually determine why Apl represses *pR* and *pL* and where in the lifecycle of 186 this regulation is significant.

To further our study of Apl, it would also be ideal to design Apl operator mutants in which Apl *pR* and *pL* repression is lost but CI regulation remains unaffected. Since we know Apl requires three consecutive operators for efficient binding (Cutts et al., 2020) and binds with high cooperativity to the *attP* and *pR.pL* sites (Shearwin and Egan, 1996) we expect that introducing site-specific mutations within the third and fifth Apl operator sites (for example) we could disrupt Apl repression at *pR.pL* but keep CI regulation intact (Fig. 2.12).

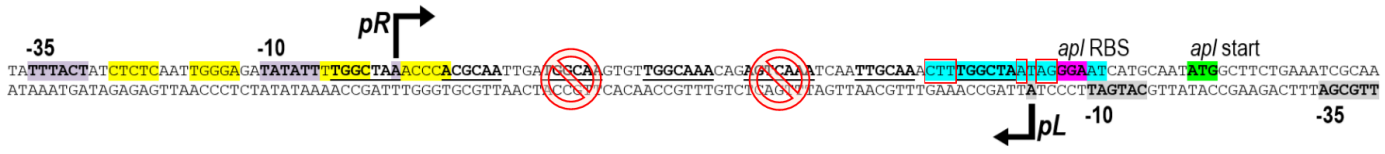

Figure 2.12: Potential mutation sites to generate a CI *pL* operator mutant and Apl operator mutants defective in *pR* and *pL* repression. There are six potential nucleotides (boxed red) within the weak *pL* operator site that could be mutated to generate a CI *pL* operator mutant without affecting other regulatory activities. Mutating both the third and fifth Apl operator sites (red stop-circles) could potentially generate an Apl binding mutant. If weak Apl binding remained, the central Apl site could also be mutated. Bold, underlined text are the seven predicted Apl recognition sequences arranged as direct repeats spaced 10-11bp apart. Blue highlighted text represents the putative *pL* CI operator binding site. Yellow highlighted text represents *pR-O1* and *pR-O3* CI binding sites. Grey highlighted bold text represent the *pR* and *pL* +1, -10 and -35 sites. Adapted from Dodd et al. (1993); Dodd and Egan (1996) and Reed et al. (1997).

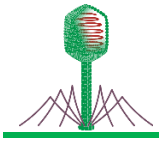

Chapter 3

Investigating the role of Tum and SOS activation in the process of 186 prophage induction

The following chapter presents a draft manuscript of our investigation into the role of Tum and activation of the host SOS response in the process of 186 prophage induction. This draft was written with the intent to submit to the Journal of Molecular Biology. I contributed to this study by engineering and characterising the cumic acid-inducible $186^{p.cym}$ phage, undertaking data analysis, preparing the results for publication, constructing the explanatory figures and diagrams and writing the manuscript. With some final experimentation still required, the draft manuscript has not yet been submitted.

Statement of Authorship

Title of Paper	Tum-dependent prophage induction of bacteriophage 186 is not enhanced by SOS activation.
Publication Status	☐ Published ☐ Accepted for Publication ☐ Submitted for Publication ☑ Unpublished and Unsubmitted work written in manuscript style
Publication Details	This draft manuscript reports on our investigation into the role of the Tum antirepressor and the significance of activation of the host SOS response during the process of 186 prophage induction.

Principal Author

Principal Author (1)	**Alejandra Isabel (Candidate)**		
Contribution to the Paper	Engineered and characterised the cumic acid-inducible 186$^{p.cym}$ phage, performed lacZ assays, phage production assays. Performed data analysis, prepared the results for publication, designed the explanatory figures and diagrams and contributed to writing the manuscript.		
Overall percentage (%)	40%		
Certification:	This paper reports on original research I conducted during the period of my Higher Degree by Research candidature and is not subject to any obligations or contractual agreements with a third party that would constrain its inclusion in this thesis. I am the primary author of this paper.		
Signature		Date	30 / 07 / 2020

Principal Author (2)	**Danna Lee**		
Contribution to the Paper	Engineered and characterised the chromosomally-integrated single-copy minimal reporter and *tum* expression modules, performed data analysis and contributed to writing the manuscript.		
Overall percentage (%)	40%		
Signature		Date	03/08/2020

Co-Author Contributions

By signing the Statement of Authorship, each author certifies that:

i. the candidate's stated contribution to the publication is accurate (as detailed above);
ii. permission is granted for the candidate in include the publication in the thesis; and
iii. the sum of all co-author contributions is equal to 100% less the candidate's stated contribution.

Name of Co-Author	Dr. Keith E. Shearwin		
Contribution to the Paper	Designed research, drafted the manuscript, contributed new reagents/analytic tools.		
Overall percentage (%)	10%		
Signature		Date	03/08/2020

Name of Co-Author	Dr. Ian B. Dodd		
Contribution to the Paper	Designed research, drafted the manuscript, contributed new reagents/analytic tools.		
Overall percentage (%)	10%		
Signature		Date	04/08/2020

Tum-dependent prophage induction of bacteriophage 186 is not enhanced by SOS activation

Danna Lee[1], Alejandra Isabel[1], Keith E. Shearwin[1,*], Ian B. Dodd[1]
1 Department of Molecular and Biomedical Science, University of Adelaide, Adelaide, South Australia 5005
* E-mail: keith.shearwin@adelaide.edu.au

Abstract

Prophage induction is the ability of temperate bacteriophage to switch from lysogenic to lytic development and for many phage occurs upon activation of the host SOS system. In phage 186 - which provided one of the first examples of induction by an SOS-controlled phage-encoded antirepressor - the *tum* gene is repressed by LexA and encodes a protein that reversibly inactivates the 186 CI immunity repressor. We showed previously that *tum* is necessary and sufficient to initiate 186 prophage induction. Induction by Tum in the absence of SOS activation however, has only been tested with high Tum expression levels. Hence, it is unclear whether SOS activation contributes to 186 prophage induction in ways other than by inducing *tum* expression. By engineering a minimal chromosomally-integrated, single-copy inducible system and by constructing a chemically inducible 186 phage, we further characterised the role of SOS activation and Tum in 186 prophage induction. We demonstrated that the fundamental role of SOS activation is to activate the expression of Tum.

Introduction

Many temperate phage have the ability to switch from lysogenic to lytic development in response to external stressors and internal cellular signals, a process termed prophage induction. In many phage, prophage induction is initiated when a stressor activates the host SOS system in response to DNA damage. Such stressors include changes in nutrients, pH or temperature, exposure to H_2O_2, foreign DNA, antibiotics or DNA damaging agents like UV and mitomycin C (Casjens and Hendrix, 2015; Howard-Varona et al., 2017). It is important to note, not all temperate phage are SOS-inducible. Well known examples in *E. coli* are Mu and P2, both of which exhibit spontaneous induction that is independent of SOS activation (Christie and Dokland, 2012; Liu et al., 1997; Ljungquist and Bukhari, 1977; Rozanov et al., 1998).

In the case of SOS-inducible phage, when the host's DNA is damaged this causes the RecA DNA repair protein to stimulate autoproteolysis of the LexA transcriptional repressor, derepressing the SOS regulon (Little et al., 1980; Little and Mount, 1982). Phage have developed three known strategies to respond to this system. In phage lambda (λ) and P22, their immunity repressor is like LexA and undergoes autoproteolysis in response to RecA (Galkin et al., 2009; Sauer, 1987). In phage CTXφ and GIL01, LexA acts as a co-repressor of the lytic operon and LexA cleavage by RecA derepresses lytic transcription (Fornelos et al., 2011; Quinones et al., 2005). Other phage (like 186) carry an antirepressor gene that is repressed by LexA, the product of which inactivates the immunity repressor (Lamont et al., 1989; Lemire et al., 2011; Mardanov and Ravin, 2007).

Coliphage 186 is a member of the P2 family (Nilsson and Haggård-Ljungquist, 2005) and forms an SOS-inducible, integrated prophage (Woods and Egan, 1974). The control of lytic and lysogenic development centres on two face-to-face promoters, *pR* and *pL* that direct transcription of the major early lytic and lysogenic operons respectively (Fig. 3.1A). The CI immunity repressor is required for maintenance of the stable lysogenic state through repression of *pR* as well as the late activator gene *B* (Shearwin et al., 1998). CI activates transcription of its own gene indirectly because repression of *pR* relieves transcriptional interference from *pR* on *pL* (Dodd and Egan, 2002). Apl is the 186 excisionase and also binds to the *pR.pL* region to reduce transcription from both promoters (Reed et al., 1997). CII is necessary for the establishment of lysogeny by activation of the alternative lysogenic operon promoter, *pE* (Murchland et al., 2014). The *tum* gene, along with another gene (*orf97*) is located on the 186 SOS operon. Both genes are under control of a LexA repressed promoter, *p95* that is overlapped by a LexA binding site (Fig. 3.1A) (Brumby et al., 1996; Lamont et al., 1989). The Orf97 protein has little effect on SOS-induction of 186; its expression rather, blocks 186 infection by an unknown mechanism (Brumby et al., 1996).

The *tum* gene is unusual as it has a number of internal translation initiation sites (Fig. 3.1B). Only the full-length product however, has antirepressor activity (Brumby et al., 1996), where Shearwin et al. (1998) showed purified full-length Tum reversibly inhibits CI binding to *pR* and *pB in vitro.* The high-expressed shorter Orf95.4 and Orf95.5 proteins are strongly similar to the *E. coli* DinI protein (Fig. 3.1B) and have been observed to have a mild inhibitory effect on SOS-induction of 186 (Brumby et al., 1996). Whilst the current evidence for DinI strongly suggests this protein is a physiological down-regulator of the SOS response (Voloshin et al., 2001), the function of DinI still remains unclear and the function of these short Tum proteins as well as the DinI-like C-terminal region of full-length Tum remains unknown.

The necessity of Tum for 186 prophage induction in response to SOS activation was shown by the inability of 186 prophage carrying point mutations or deletions in the *tum* gene to be induced by UV or mitomycin C, while retaining inducibility by temperature when the CI repressor carried the *cItsp* mutation (Brumby et al., 1996; Lamont et al., 1989; Woods and Egan, 1974). Furthermore, 186(*tum*$^{+}$) prophages were not SOS-inducible in the presence of a non-cleavable LexA mutant (Lamont et al., 1989). The sufficiency of Tum for SOS prophage induction of 186 was shown by the ability of plasmid-expressed Tum to induce the prophage and to cause derepression of the *pR* and *pB* promoters in the absence of SOS activation (Brumby et al., 1996; Lamont et al., 1989; Shearwin et al., 1998). These studies however, used high-copy plasmids and consequent high Tum levels, which left open the possibility that SOS activation may in some way aid in the action of Tum in its natural single-copy state in the prophage.

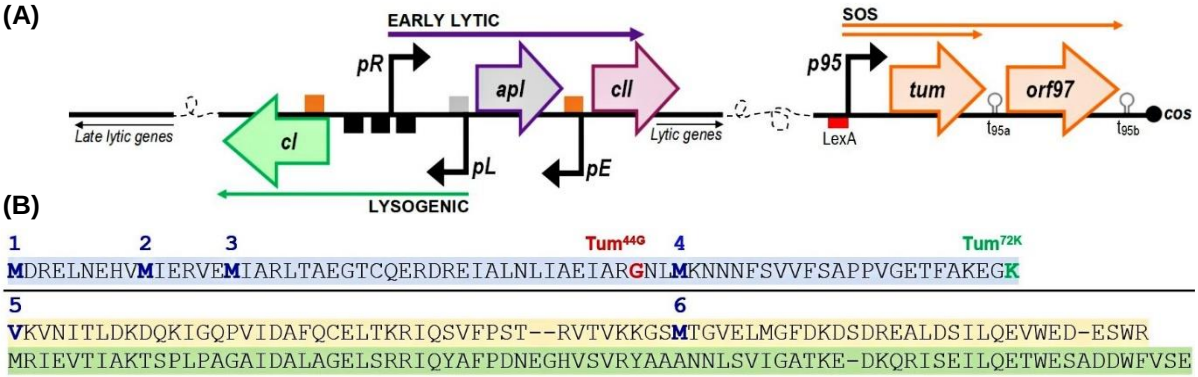

Figure 3.1: Details of the 186 switch, SOS operon and Tum. (A) A genetic map of the 186 switch (left) and SOS operon (right). During lytic development, *pR* is active and expresses the early lytic genes required to initiate lytic development. During lysogeny, CI (expressed from *pL*) inhibits lytic development by repressing *pR*. The SOS operon encodes *tum,* the product of which is the antirepressor protein, Tum produced upon activation of the host SOS response. During lysogeny, the host encoded LexA repressor represses *tum* expression from *p95*. Genes are shown as left-and-right facing arrows, promoters as right-angled arrows, their transcripts as arrows and terminators as stem loops. *pR* and *pB* operators are black boxes, the *pL* operator a grey box and CI *FL* and *FR* operator sites are orange boxes. The red rectangle positioned under *p95* is the LexA operator site. **(B)** Annotated amino acid sequence of the Tum (Orf95.1) protein. The N-terminus is highlighted blue and contains the nested translation start sites for Orf95.2, 3 and 4. The C-terminus is highlighted orange and contains the nested translation start sites for Orf95.5 and 6. The C-terminus displays homology to the *E. coli* DinI protein (highlighted green). Tum^{44*} and Tum^{72*} truncation sites are located in the N-terminus and are coloured red and green.

In this study we dissected the 186 prophage induction system by constructing and analysing the behaviours of chromosomally-integrated, single-copy minimal reporter and *tum* expression modules. We show UV induction of a single-copy *p95.tum*$^+$ construct is capable of efficiently switching a *cI*$^+$.***pR***$^+$.*pL*$^+$.*apl*$^+$ reporter from a lysogenic to a lytic transcription mode, and we used this system to examine the effects of different parts of the *tum* gene. We also confirmed *p95* is induced after SOS activation. Using chemical induction of *tum* expression, either from a minimal chromosomal *tum* gene expression module or by replacing *p95* with a controllable/inducible promoter on the prophage, we show 186 prophage induction is not enhanced by SOS activation.

Results

A minimal prophage induction reporter system

To assay prophage induction without the complication of prophage excision and full lytic development we constructed a minimal reporter of the lysogenic-lytic transcriptional transition. A DNA fragment encompassing the 186 *cIts.pR.pL.apl* region carried on a multi-copy plasmid was previously shown to exist in two transcriptional modes at the permissive temperature of CIts; a stable 'lysogenic' mode with *pR* repressed by CI expressed *pL;* and a semi-stable 'lytic' mode with *pR* active. A *galK* reporter placed downstream of *apl* and thus expressed from *pR* allowed these states to be observed by colony phenotype (Dodd et al., 1990). In this case, the lysogenic → lytic transition was achieved by transient temperature inactivation of CIts and the reverse transition occurred spontaneously at a slow rate. The semi-stable lytic state was not seen in the absence of *apl* and we believe Apl expressed from *pR* in the lytic state, combined with *pR* inhibition of *pL* by transcriptional interference dampens *pL* activity sufficiently to slow but not prevent CI accumulation (Callen et al., 2004).

To assay Tum's prophage induction activity, we used a similar *cI*$^{+}$*.pR.pL.apI* fragment with the *lacZ* reporter fused in-frame with *cII* downstream of *apI* (Fig. 3.2A) and inserted this fragment into the E4643 chromosome by CRIM-based plasmid integration at the λ attachment site (Haldimann and Wanner, 2001). This strain was isolated in the lysogenic transcriptional state (Fig. 3.2A1), giving stable white colonies on X-gal plates. A minimal Tum module containing a *p95.tum* fragment (or an empty control) was then inserted via plasmid integration at the primary 186 attachment site.

Treatment of cells with UV followed by plating on X-gal plates produced a mixture of white, blue and blue/white colonies after overnight incubation at 37°C (Fig. 3.2B). In the absence of UV or *tum,* only white colonies and occasional pale blue colonies were observed. We tested up to 60s of UV exposure (~7.8 J/m^{2}; at which cell death becomes substantial) and found maximal switching for *tum*$^{+}$ of ~50% at 40s (Fig. 3.2C; blue/white colonies were scored as switched). Restreaking of white colonies gave white colonies, while restreaking of blue colonies gave a majority of white colonies and variable proportions of blue colonies (data not shown). This and the sectoring of the blue/white colonies, indicates the lytic state of the reporter was semi-stable (Fig. 3.2A3), as seen previously (Dodd et al., 1990). We expect the lytic state of the reporter causes the colony assay to underestimate switching because lytic cells that revert to the lysogenic state soon after plating may not produce detectable blueness in the colony. As seen before, the semi-stable lytic state also required an active *apI* gene, as a reporter carrying the *apI*$^{-}$ HTH mutation gave only white colonies after UV. These experiments show UV-induced production of Tum from *p95.tum*$^{+}$ in single-copy is able to switch 186 from lysogenic to lytic transcription in the absence of other phage functions.

Inhibition of lysogenic → lytic switching by C-terminal portions of Tum

Brumby et al. (1996) constructed a mutant *tum* gene (*tum*$^{4\text{-}5\text{-}}$), which prevented the production of the C-terminal Orf95.4 and Orf95.5 proteins by ribosome binding site mutations. In the same study, a 186 phage carrying these mutations showed ~2-fold enhanced phage yield after prophage induction by UV. Introduction of these mutations into the *p95.tum* module gave increased lysogenic → lytic switching after UV in our minimal prophage induction system (Fig. 3.2C), showing production of the Orf95.4 and Orf95.5 proteins inhibit Tum's transcriptional effects after SOS activation.

Previous work in our laboratory (Julian Pietsch, unpublished) indicated the N-terminal region of Tum is sufficient for inactivation of CI. To test this in our system, we used a version of the *tum* gene truncated at codon 72, which removes the entire DinI homology region (Fig. 3.1B). This Tum^{72*} variant showed ~2-fold higher level of lysogenic → lytic switching after UV compared to full-length Tum, with a stronger enhancement at lower doses and even some switching (~8.0%) in the absence of UV (Fig. 3.2C). Switching was enhanced relative to the Tum$^{4\text{-}5\text{-}}$ variant, indicating the DinI-like portion has an inhibitory effect in the context of full-length Tum.

We have not tested the relative expression levels or stabilities of full-length versus truncated Tum. A version of *tum* truncated at 44 amino acids (Fig. 3.1B), showed no switching activity in our assay (Fig. 3.2C). We also tested the effect of *tum*$^{+}$ gene dosage by inserting a second copy of the *p95.tum*$^{+}$ fragment at the secondary 186 attachment site. This increased lysogenic → lytic switching after UV to a level similar to *tum*^{72*}, indicating the efficiency of SOS-induction is dependent upon Tum protein concentration, and that a single-copy of *tum*$^{+}$ is suboptimal for its transcriptional effects.

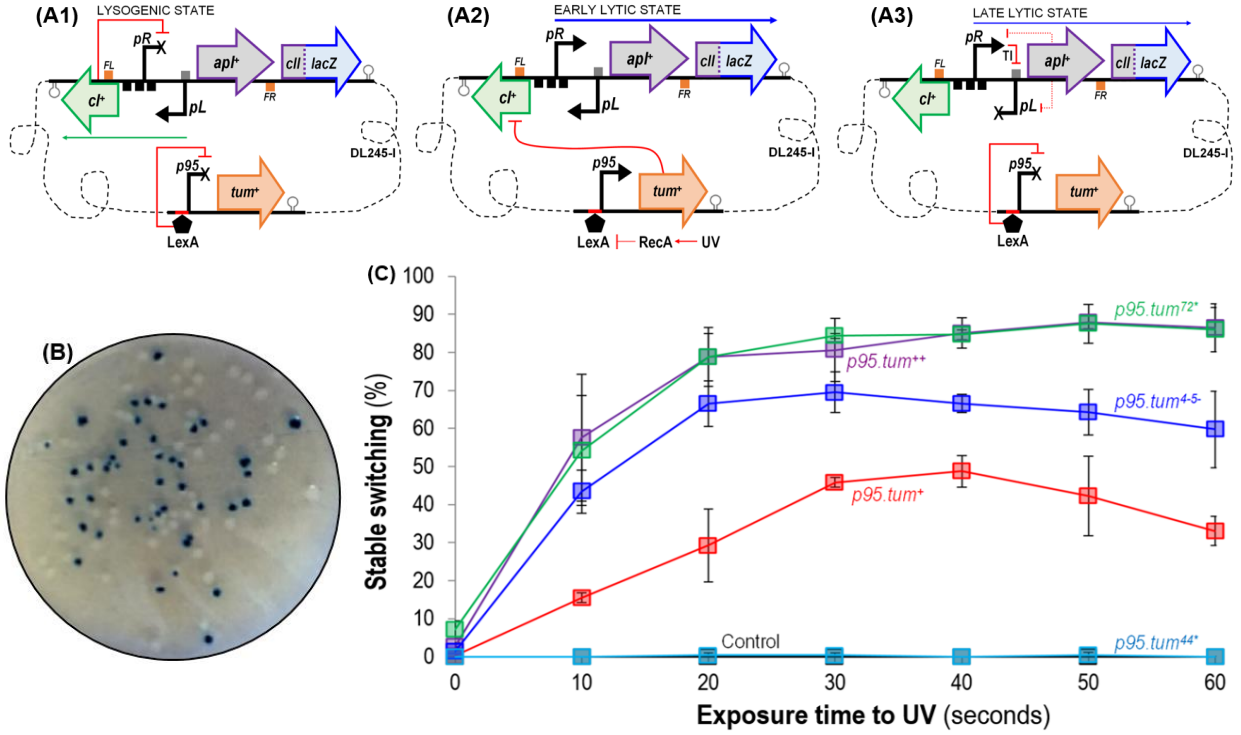

Figure 3.2: UV induced switching of the SOS switch reporter linked to a UV induction module encoding different *tum* copy numbers and variants. (A) The two-module chromosomally-integrated minimal reporter system consists of the λ integrated *cI*$^{+}$.***pR***$^{+}$.*pL*$^{+}$.*apl*$^{+}$.*cII::lacZ* reporter and a UV inducible *p95.tum* module integrated at the primary 186 attachment site. In the lysogenic state (1), LexA represses *p95.tum* expression. Active CI represses *pR*, inhibiting expression of *apl* and *cII::lacZ*. In the 'early' lytic state (2) LexA is degraded and *tum* is expressed from a derepressed *p95.* With CI inactivated by Tum, *pR* is derepressed and *apl* and *cII::lacZ* are expressed. In the 'late' semi-stable lytic state (3), LexA re-establishes repression of *p95,* shutting down *tum* expression. There is little/no expression of *cI* as Apl weakly represses *pR.pL* and any *pR* activity represses *pL* via transcriptional interference (TI). **(B)** X-gal plate with *p95.tum*$^{+}$ (DL245-I) post 40s UV (~5.2 J/m^2). **(C)** The percentage of UV-induced switching at different UV doses. The negative control (DL243; *n=2)* has no *p95.tum.* The *tum* variants are *tum*$^{+}$, *tum*$^{4-5-}$, *tum*^{72*} (DL245-I, DL245, DL255; *n=3*), *tum*^{44*} (DL244; *n=2*) and 2 x *p95.tum*$^{+}$ (DL245-II; *n=5*). The DL244 and negative control plots are superimposed. Error bars are 95% confidence intervals when *n>2*.

The timing of *p95* and *pR* activity after UV

A strong match to the consensus LexA binding site (Lewis et al., 1994) overlaps with the *p95* promoter (from -10 to +6), and *tum* expression has been shown genetically to be dependent on LexA inactivation (Lamont et al., 1989). The SOS-dependent derepression of *p95* however, and its timing and magnitude has not been measured directly. To characterise this, we constructed a single-copy *p95.tum*$^{+}$.*lacZ* reporter by plasmid integration into the primary 186 attachment site of E4643 (Fig. 3.3A). LacZ activity of this reporter strain (DL258) was followed over a 3hr timecourse after UV treatment (40s; ~5.2 J/m^2). LacZ activity rose steeply within 20min from a pre-UV level of ~75 units to a peak of ~750 units 60mins after UV and decreased thereafter (Fig. 3.3B).

Since LacZ is a highly stable protein, the activity of *p95* at any time point is best judged from the slope of the LacZ units versus time curve. On this basis, *p95* activity is high from some point before 20min up to 40min after UV and then decreases, with LexA repression likely fully repressed by 60min, causing the LacZ units to decrease by dilution due to culture growth. This profile is consistent with Western bot measurements of LexA repressor levels in cells treated with 5 J/m^2 UV, which show a rapid decrease to a minimum at 10min post-UV, and a slow restoration to normal LexA levels by 60min (Sassanfar and Roberts, 1990). The low level of LacZ activity in the absence of UV suggests incomplete repression of *p95* by LexA, though we cannot exclude the existence of other, weak promoters upstream of the *lacZ* reporter. The low level of lysogenic → lytic switching in the presence of two copies of *p95.tum*$^+$ in the absence of UV (Fig. 3.2C) supports the idea of incomplete LexA repression. It should be noted the ~10-fold increase in LacZ units from pre-UV to the 60min peak underestimates the strength of repression of *p95* by LexA, as the LacZ peak would likely be substantially higher with continued high *p95* activity.

We used the minimal prophage induction reporter system to compare the timing of *p95* expression after UV, with the kinetics of Tum derepression of *pR.* Instead of measuring colony switching we followed *pR* activity with a similar LacZ timecourse (Fig. 3.3B and C). As presented in Figure 3.3B, *pR* LacZ activity in the presence of the *p95.tum*$^+$ module steadily increased after 40s UV and peaked at ~45 LacZ units at 120min. Derepression of *pR* was delayed by 20min or more compared to *p95*, consistent with the time needed for Tum accumulation and CI inactivation. No derepression of *pR* LacZ activity was observed for the no-*tum* control, while full derepression by 39°C temperature induction of the *cIts* variant of the reporter gave ~100 LacZ units (Fig. 3.3C). Note the difference in LacZ units between the *p95.tum*$^+$*.lacZ* reporter and the *pR.cII::lacZ* translational fusion reporter is most likely due to low translation of the *cII::lacZ* fusion; we generally see ~1000 LacZ units in *pR* operon fusions, indicating *p95* and *pR* are similarly strong promoters. We interpret the gradual decrease in *pR* activity after 90min as due to re-establishment of the CI-dominated lysogenic transcriptional state of the reporter, which becomes possible once Tum levels fall after re-establishment of LexA repression of *p95*. Judging from the colony switching behaviour of the reporter (Fig. 3.2B), we imagine this lytic → lysogenic switch occurs stochastically in individual cells.

We also examined the kinetics of *pR* activity after UV in the presence of the *p95.tum* variants. Consistent with the colony switching assay, *tum*^{72*} gave the strongest *pR* derepression, followed by *tum*$^{4\text{-}5\text{-}}$, both elevated compared to *tum*$^+$*,* while *tum*^{44*} gave no *pR* derepression (Fig. 3.3C). Strikingly, the effect of *tum*^{72*} was as strong as temperature inactivation of CIts. For reasons we do not understand, the effect of two copies of the *p95.tum*$^+$ module on *pR* derepression was weaker compared to the other variants than in the colony-switching assay.

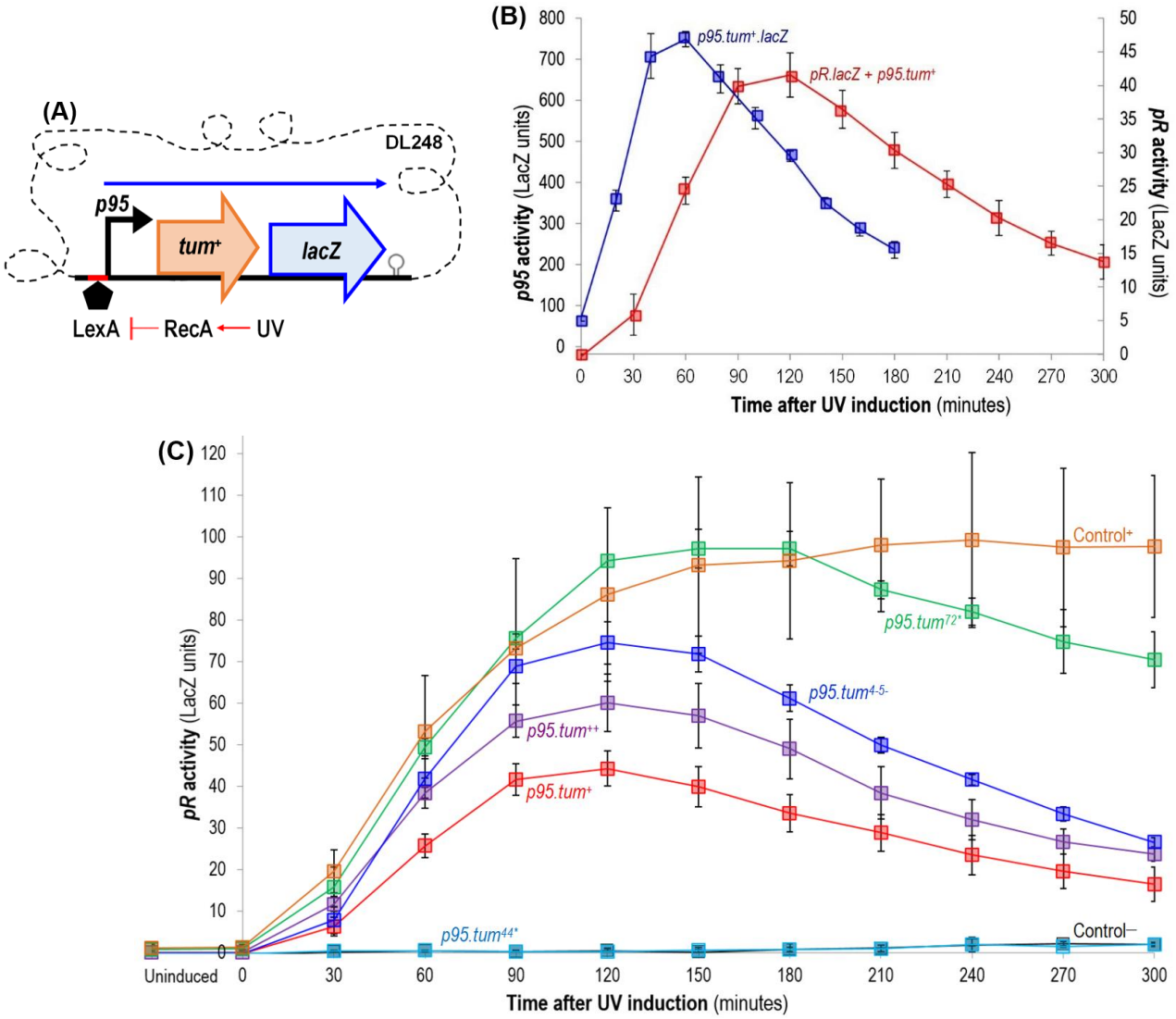

Figure 3.3: Kinetics of *p95* and *pR* following UV induction. (A) Schematic of the *p95.tum*$^{+}$*.lacZ* reporter integrated at the primary 186 attachment site used to characterise *p95* (DL258). The [*cI*$^{+}$.***pR***.*pL.apl.cII::lacZ*] + [*p95.tum*$^{+}$] system (DL245-I, Fig. 2A) was used to characterise *pR*. **(B)** *p95* and *pR* LacZ activity was followed for 3 or 5hrs after 40s UV (~5.2 J/m^{2}). After UV, cultures were grown at 37°C in M9MM-20, with regular dilution to maintain logarithmic growth and aliquots stored on ice for later LacZ assay. Error bars are 95% confidence intervals (DL258; *n=3,* DL245-I; *n=10*). **(C)** *pR* LacZ activity following 40s UV for *p95.tum* variants. Strains are as in Fig. 2C, except here the positive control strain (DL249) is a reporter with a temperature sensitive CI (*cIts*) [*cIts.***pR**.*pL.apl.cII::lacZ*] + [*p95.tum*$^{+}$], which was induced by growth at 39°C. Error bars are 95% confidence intervals when *n*>2: no-*tum, tum*^{44*} (DL244, DL243; *n=2*), *tum*$^{4-5-}$*, tum*^{72*} (DL254, DL255; *n=3*), *tum*$^{+}$ (DL245-I; *n=10*), 2 x *tum*$^{+}$ (DL245-II; *n=4*), and *cIts* (DL249; *n=5*).

Depression of *pR* by chemical induction of *tum* expression is not affected by SOS activation

To investigate whether SOS activation affects 186 prophage induction in ways other than through derepression of *p95,* we replaced *p95* with a LacI repressed promoter. We used the $P_{LlacO-1}$ promoter; a synthetic derivative of the λP_L promoter containing two copies of the *lacO-1* operator (Lutz and Bujard, 1997). The $P_{LlacO-1}$ promoter replaced the *p95* promoter of the *p95.tum*$^{+}$*.lacZ* reporter (Fig. 3.3A) in a strain with a plasmid module expressing LacI from the *PlacI*^{q} promoter (Priest et al., 2013) integrated into the HK022 attachment site. Induction of this promoter with 300μM IPTG gave ~800 LacZ units after 120mins (~600 units after 60mins), a level similar to that produced by *p95* after UV induction (Fig. 3.3B). We noted a substantial level of uninduced activity of ~50 units in this system.

We then removed the *lacZ* gene from the $P_{LlacO\text{-}1}$.*tum*$^{+}$.*lacZ* module and combined it with the *cI*$^{+}$.***pR***.*pL.apl.cII::lacZ* reporter and the *PlacI*^{q}.*lacI* module (Fig. 3.4A) to examine *pR* activity. The addition of 300μM IPTG produced a steady increase in LacZ activity to a plateau of ~75 units after 80min (Fig. 3.4B). The early stages of *pR* derepression by IPTG are similar to that seen by UV induction with *p95.tum*$^{+}$ (replotted from Fig. 3.3C); however, the constant presence of IPTG resulted in an eventual higher accumulation of LacZ. This result shows that a level of *tum*$^{+}$ expression similar to that produced by UV is able to derepress *pR* in the absence of SOS activation. Furthermore, combining IPTG induction with 40s UV treatment had no observable effect on *pR* derepression (Fig. 3.4B); showing Tum action is neither augmented nor inhibited by SOS activation.

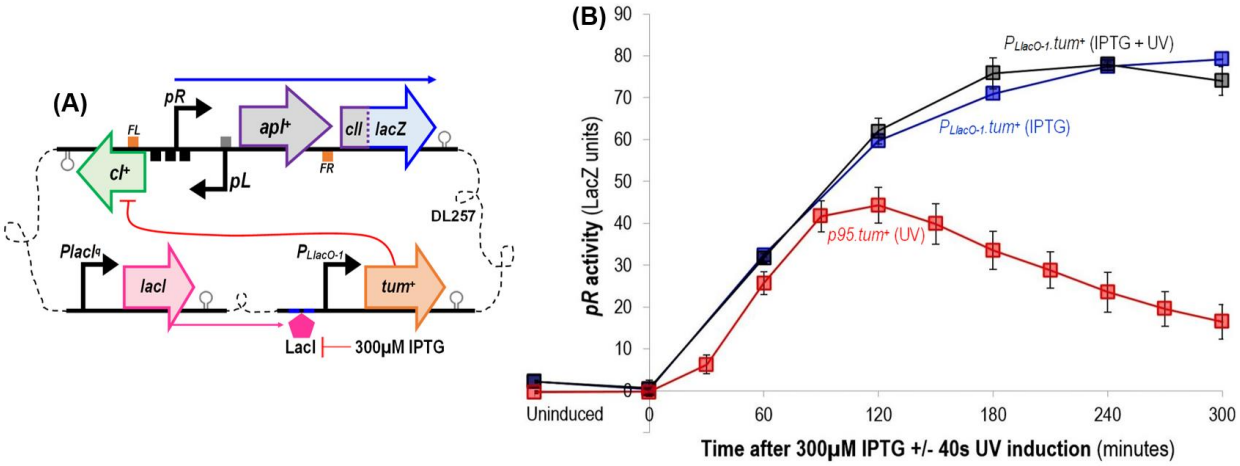

Figure 3.4: *pR* expression by LacI/IPTG induction of Tum expression is not affected by UV. (A) Schematic of the DL257 strain carrying the $P_{LlacO\text{-}1}$.*tum*$^{+}$ induction module, the *cI*$^{+}$.***pR***.*pL.apl.cII::lacZ* reporter and the *PlacI*^{q}.*lacI* module. **(B)** The timecourse of LacZ activity of DL257 induced with 300μM IPTG ±40s UV. Error bars are standard deviation (*n*=2). The *p95.tum*$^{+}$ curve from Fig. 3C was replotted for comparison. The uninduced timepoints represent samples taken immediately prior to induction.

Chemical induction of an engineered 186 prophage is not affected by SOS activation

While SOS activation does not affect *tum*-dependent induction of our minimal prophage induction system, it remained possible SOS activation might have effects in the presence of other phage functions. To examine this, our strategy was to replace the *p95* promoter on the 186 prophage with a promoter under control of a repressor expressed from the bacterial chromosome. This mimics the natural LexA-*p95.tum*$^{+}$ situation in which prophage induction results in expression of the *tum* gene but not of the host repressor gene. Our initial attempts to use the $P_{LlacO\text{-}1}$ promoter for this purpose resulted in lysogen instability, presumably due to 'leaky' *tum* expression in the absence of IPTG (see above). Thus, we turned to a CymR-cumic acid (CA) repressor-inducer system that we had modified from that of Choi et al. (2010).

We first tested the system's ability to control Tum induction of *pR* depression. The *cymR.tum*$^{+}$ expression module contains the *Pseudomonas putida cymR* gene expressed from a synthetic constitutive promoter (*proA*), in divergent orientation with *tum* expressed from a synthetic T5-based promoter (*T5-1*) with a CymR operator (*cymO*) conferring tight repression by CymR (Fig. 3.5A). This module was integrated at the φ21 attachment site and combined with the *cI*$^{+}$.***pR***.*pL.apl.cII::lacZ* reporter. Treatment with 150μM CA (which gives maximal induction) over a 3hr timecourse gave very similar *pR* derepression to that seen with the LacI system (Fig. 3.5B, compare with Fig. 3.4B). To better mimic the rise and fall of Tum expression after UV, we found treatment with 150μM CA for 20min, followed by centrifugation and resuspension in medium without CA, gave a very similar *pR* induction curve to that obtained by 40s UV (Fig. 3.5B). We believe the lower level of *pR* depression by UV induction compared with Fig. 3.3C is due to UV lamp variation.

To construct the CymR-controlled 186 prophage, an empty *cymR* construct was first integrated at the φ21 attachment site of a wildtype E4643(186^{+}) lysogen to supply CymR. The *p95* promoter on the prophage was next replaced with a *loxP.chlor*^{R}*.loxP.T5-1* cassette by recombineering. The *chlor*^{R} gene was removed by transient transformation with a Cre-expressing plasmid, leaving a 34bp *loxP* scar 6bp upstream of *T5-1* (Fig. 3.5C/D; Experimental procedures). We then compared phage production from this E4643::*cymR*(186$^{p.cym}$) lysogen and a wildtype E4643(186^{+}) lysogen after induction by CA or UV. As expected, spontaneous phage production was low in both lysogens (Fig. 3.5E). For the wildtype lysogen, the titre of plaque forming units (PFU) was ~1% of the number of viable cells, similar to previous results with 186 (Woods and Egan, 1974). Spontaneous phage production was some 20-fold lower in the E4643::*cymR*(186$^{p.cym}$) lysogen. We expect that uninduced expression of *tum* is less leaky with CymR repression of *T5-1* compared to LexA repression of *p95*. Occasional full or partial SOS activation in a small fraction of cells could potentially contribute to leaky repression of *p95*.

Treatment of the E4643::*cymR*(186$^{p.cym}$) lysogen with 150μM CA for 20min caused induction of ~100% of the cells, shown by the early time PFU titres being close to the CFU titres. Thus, the synthetic CymR-CA system provides for tightly controlled and efficient prophage induction. The phage burst occurs between 30 and 60mins, with a burst size of ~19 PFU/induced cell. When these lysogens were treated with UV as well as CA, the burst size was smaller, ~12 PFU/induced cell. Thus, SOS activation does not enhance 186 prophage induction when Tum expression is decoupled from LexA inactivation. For reasons not yet understood, 186 DNA replication is delayed in a UV-treated cell, even after infection by phage not exposed to UV (Hooper et al., 1981) and this effect may explain the reduced burst size observed after UV + CA induction.

UV induction of the wildtype prophage was fairly inefficient, with only ~30% of the cells induced (Fig. 3.5E), presumably because the UV dose was sub-optimal. Induction was not obviously affected by the presence of CA. Phage production occurred between 60 and 80mins, giving burst sizes of ~20 PFU/induced cell. The latent period was longer than seen for CA + UV induction of the E4643::*cymR*(186$^{p.cym}$) lysogen, supporting a more efficient induction of Tum expression by CA compared to UV in this experiment. We note the burst sizes for the E4643::*cymR*(186$^{p.cym}$) and wildtype lysogens were substantially lower than previous measurements of ~100 PFU/induced cell (Reed et al., 1997), most likely due to the use of minimal rather than rich medium in our experiments.

Phage production after treatment of the lysogens with the 'wrong' inducer remained at low levels (Fig. 3.5E). Treatment of the wildtype lysogen with CA alone gave no immediate increase in PFU titre. The ~2-fold increase in titre over the timecourse is probably due to culture growth. Treatment of the E4643::*cymR*(186$^{p.cym}$) lysogen with UV alone, produced a ~20-fold increase in PFU. Though this is a large fold change, the number of PFU per CFU remained low at ~0.4%, the same level as spontaneous production from the wildtype lysogen. We do not understand the reason for this increase in phage production but suspect UV may disrupt the maintenance of repression by CymR or CI in some cells.

Repression of *tum* is required for lysogenisation

Wildtype 186 forms turbid plaques on *lexA*$^{+}$ strains, but clear plaques on a strain with defective LexA repressor, with turbid plaques restored in 186*tum*$^{-}$ mutants (Lamont et al., 1989). While this result is consistent with Tum expression preventing establishment of 186 lysogenic transcription after infection, host SOS proteins produced in the absence of LexA may also be having an effect. We observed an equivalent effect however, with the 186$^{p.cym}$ phage: 186$^{p.cym}$ forms clear plaques on E4643, but turbid plaques on E4643::*cymR.* This confirms expression of the 186 SOS operon (*tum* and *orf97* genes) is sufficient to substantially reduce lysogenisation after infection. The virulence experiment however, was done differently to the normal approach, where normally, we would purify the 186$^{p.cym}$ phage and plate it on E4643 and E4643(186^{+}) to compare the efficiency of plaquing. In this instance, E4643::*cymR*(186$^{p.cym}$) was induced with CA and then plated on an E4643(186^{+}) lysogen lawn. The normal method gives an MOI=1 (at least initially), while inducing a 186$^{p.cym}$ lysogen produces many phage, so the first infection may have a MOI>1. What we did find from our virulence assays is that 186$^{p.cym}$ is virulent, meaning it is able to form plaques on an E4643(186^{+}) lysogen. This indicates that unrepressed expression of Tum (and Orf97) from an infecting 186$^{p.cym}$ phage is able to efficiently overcome CI expression from two copies of the *cI* gene (186^{+} prophage + 186$^{p.cym}$ infecting phage).

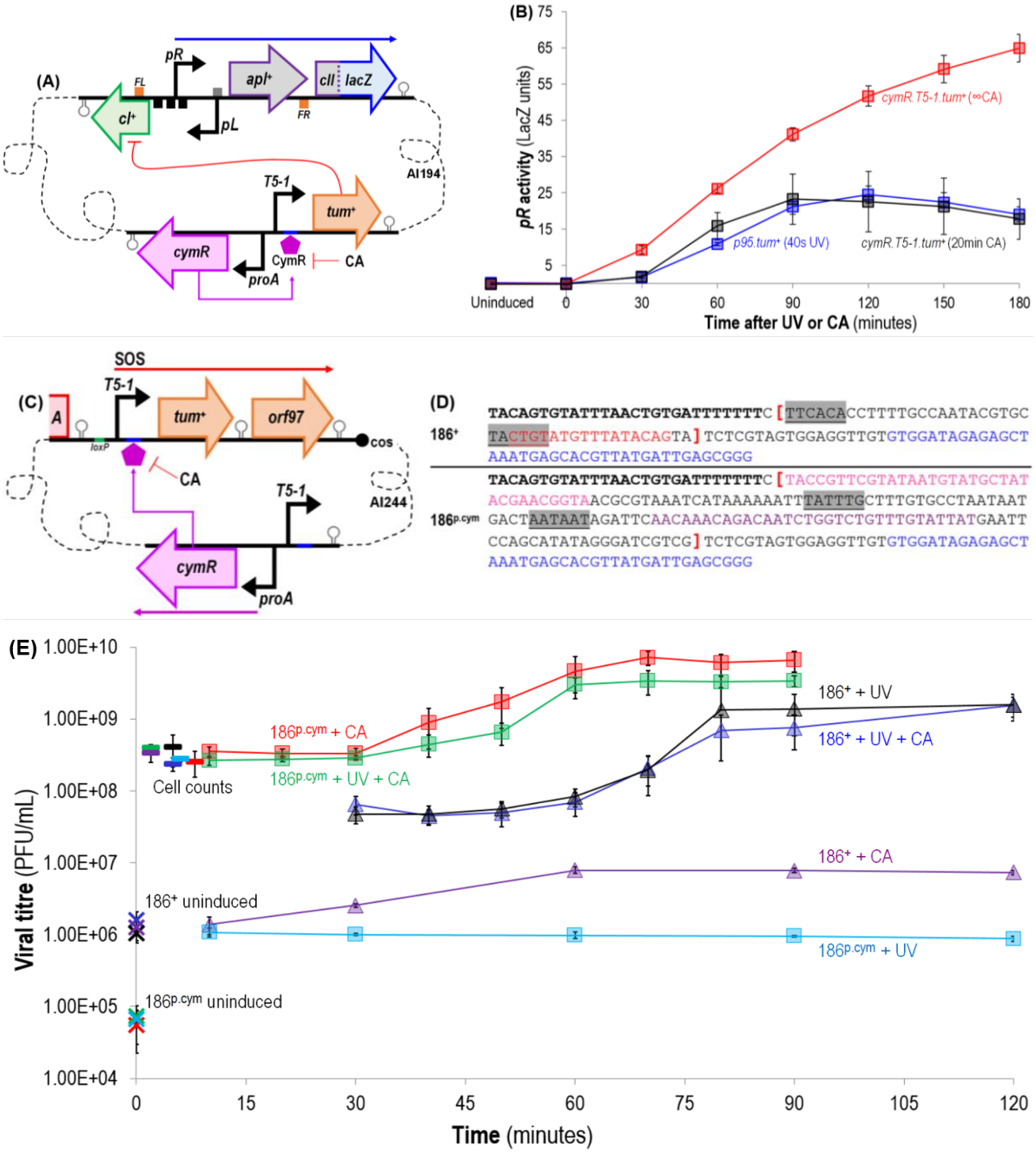

Figure 3.5: Cumic acid-induction of an engineered prophage is not affected by UV. Testing *pR* derepression by the CymR-cumic acid (CA) Tum expression system. **(A)** Schematic of strain AI194, which carries the φ21 integrated *cymR.T5-1.tum*$^{+}$ expression module and the λ integrated *cI*$^{+}$.***pR***.*pL.apl.cII::lacZ* reporter. **(B)** LacZ timecourses show AI194 induced with 150μM CA for 20mins or indefinitely, and DL245-I induced with 40s UV. CA removed 20min after induction by pelleting cells and resuspending in M9MM-20. Uninduced samples taken immediately prior to induction. Error bars are 95% confidence intervals (DL245-I; *n=8,* AI194; *n=6*). **(C)** Schematic of the 186$^{p.cym}$ prophage with *p95* replaced by the *T5-1* CymR-repressed promoter. The 34bp *loxP* scar lies at the -6 position of *T5-1,* immediately downstream of the terminator for the early lytic operon. **(D)** Sequence comparison of 186$^{p.cym}$ with 186^{+} genome at the SOS operon starting from the start of the gene *A* terminator and ending 40bp downstream of *tum* GTG start codon. Sequence in red squared brackets is the region of the 186$^{p.cym}$ genome that differs from 186^{+}. *tM* (bold), *loxP* sites (pink), *chlor*^{R} (green), *tum*$^{+}$ (blue), LexA site (red), CymR site (purple) and promoters *T5-1* and *p95* -10 and -35 (grey, underlined). See Fig. 3.6 for sequence of full-length *tM.loxP.chlor*^{R}*.loxP.T5-1.tum*$^{+}$ cassette used to generate the 186$^{p.cym}$ phage. **(E)** Single-step phage production curves after induction of E4643(186^{+}) and E4643(186$^{p.cym}$) lysogens (strains HB59 and AI244 respectively). UV and/or CA induction was obtained by treating cultures grown to OD_{600} in 0.30 in M9MM-20 with 40s UV and/or 150μM CA, with plaque forming units (PFU) or colony forming units (CFU) titred by standard plating assays with or without E4643 indicator. The T0 values show PFU/mL (X) and CFU/mL (—) of pre-treatment cultures. Cultures were diluted (10^{-4}) 10mins after treatment, effectively removing CA. PFU/mL for treated cultures over time: (Δ blue) 186^{+} treated with UV, (Δ black) 186^{+} treated with UV and CA, (Δ purple) 186^{+} treated with CA, (□ red) 186$^{p.cym}$ treated with CA, (□ green) 186$^{p.cym}$ treated with UV and CA, and (□ aqua) 186$^{p.cym}$ treated with UV. Error bars show 95% confidence limits (*n*=4-6).

Discussion

SOS control of *p95*

Our results confirm *p95* is under SOS control, with the kinetics of its activity consistent with previous measurements of intact LexA after a similar UV dose (Sassanfar and Roberts, 1990). The apparent leakiness of LexA repression (~10% of the maximal expression level, Fig. 3.3B) is surprising, given the strong match of the LexA site to consensus (Lewis et al., 1994) and the large overlap between the site and the promoter elements. It is possible there is a natural weak promoter, or a promoter introduced by construction, located downstream of *p95* in our reporter system. Some leak of Tum from *p95.tum* however, is supported by the lower level of spontaneous phage production observed when *tum* is repressed by CymR in the 186$^{p.cym}$ prophage (Fig. 3.5E). In theory, leaky *tum* expression could be due to tight control in most cells, and some level of SOS induction in a few cells. In a *lexA3* strain that is SOS non-inducible however, Lamont et al. (1989) observed ~10x higher free phage levels produced by a *tum*$^{+}$ prophage compared to a *tum*$^{-}$ prophage, indicating there is some Tum expressed even in the absence of SOS induction. This suggests 186 may have evolved some Tum expression in the prophage to set a particular level of spontaneous prophage induction.

Bistability in CI regulation of lytic and lysogenic transcription

Our results reproduce our previous observations of the bistability of the transcription state of the 186 *cI.pR.pL.apl* 'switch' region (Dodd et al., 1990). In the previous study, the switch fragment was carried on a multi-copy plasmid, contained the *cIts* allele and was flipped from lysogenic → lytic transcription using a transient temperature shift. Our present results show that bistability is also a feature of a more natural condition, with a single-copy wildtype *cI.pR.pL.apl* region showing a stable lysogenic transcription state can be flipped to a semi-stable lytic transcription state by SOS-induction of *tum*$^{+}$ expression. As in the previous study, *apl* is needed for the 'lytic' colony phenotype (blue), showing this phenotype is not simply due to a transient pulse of LacZ expressed from *pR,* but represents a stable state. The low fraction of blue colonies seen when a blue colony is restreaked and the CI-dependent decrease in *pR* activity after UV (Fig. 3.2B/C), show this state reverts slowly to the lysogenic state. The impact of this bistability on phage function is unclear, but the semi-stable lytic state is not necessary for lytic development of the phage after infection, as 186*apl*$^{-}$ phage are competent for lytic development (Dodd et al., 1993).

A single-copy of SOS induced *tum* is sufficient to initiate lytic development

Our minimal prophage induction assay system showed for the first time that a single-copy UV-induced *p95.tum* can efficiently flip transcription from the lysogenic to the lytic mode in the absence of other phage functions. Previously, the ability of Tum to derepress *pR* without other phage proteins was shown only using Tum expression from multi-copy plasmids (Shearwin et al., 1998), and high Tum expression may have made assistance by an accessory phage protein unnecessary.

Increasing the dose of *p95.tum*$^{+}$ to two copies increased lytic switching after UV in the colony assay (Fig. 3.2C) and also increased *pR* activity (Fig. 3.3C). For reasons we do not understand, the effect of two copies was stronger in the colony assay.

Tum activity resides in its N-terminal region

Our results show the N-terminal, non-DinI portion of Tum is sufficient for its anti-CI activity. This result is consistent with studies in our laboratory of a more extensive series of Tum truncations (Julian Pietsch, manuscript in preparation). Interestingly, while the truncated Tum^{44*} mutant was completely inactive in our assay, a His_6 Tum^{44*} was fully active when used in a different *pR* derepression assay (Julian Pietsch, personal communication). We suspect the higher expression level in the Pietsch study and possible effects of the amino acid differences (e.g. protein stabilisation by an N-terminal His_6 tag) are likely to explain these differences. These results however, do suggest the 45-72 amino acid region of Tum helps to stabilise the protein *in vivo.*

The function of Tum's DinI-like elements

Our results confirm the DinI-like proteins are inhibitory for *tum*-dependent derepression of *pR* after UV (Brumby et al., 1996). In addition, increased activity of the Tum^{72*} variant suggests the presence of the DinI-like domain on full-length Tum is also inhibitory. It is not clear from these or previous results as to whether the DinI-like elements act at the level of Tum or at the level of SOS induction. There are various ways in which the effects observed could reflect differences in the amount of active Tum produced per *tum* mRNA. The *tum*$^{4\text{-}5\text{-}}$ mutations and *tum*^{72*} truncation could affect stability or translation efficiency of *tum* mRNA. Tum^{72*} could be more stable or have higher specific activity than full-length Tum and Tum^{4} and Tum^{5} might interact with full-length Tum to destabilise or inhibit its activity. We favour the possibility however, that the 186 DinI-like elements act by being inhibitory to the SOS response, resulting in the production of fewer *tum* mRNAs. This more general effect is consistent with the presence of *dinI*-like genes in plasmid SOS-inducible operons, which do not encode Tum-like proteins (Runyen-Janecky et al., 1999), and also with observed inhibitory effects of overexpression of the *E. coli* DinI protein on SOS induction (Yasuda et al., 1998).

Chemical induction of prophage is not enhanced by SOS activation

In previous experiments, a single-copy of *tum* was shown to be capable of causing prophage induction, in the presence of all phage genes and when the SOS system was activated by UV, mitomycin C or a defective *lexA* mutant (Lamont et al., 1989). This leaves open the possibility that a host SOS function is required to assist the activity of the expressed Tum. While experiments with IPTG/LacI induction of Tum expression (Brumby et al., 1996; Shearwin et al., 1998) showed SOS activation is not necessary for *pR* depression or prophage induction, in these cases, Tum was expressed from multi-copy plasmids. High levels of Tum may reduce the need for assistance by an SOS function.

To eliminate this possibility, we used a single-copy LacI controlled *tum*$^{+}$ expression construct and showed induction by IPTG could mimic UV depression of *pR* in the absence of SOS activation. UV irradiation did not increase IPTG induction of *pR,* indicating the lack of an accessory role for SOS activation beyond its normal primary role of causing *tum* expression (Fig. 3.4B). It remained possible an accessory role for SOS activation may require the presence of other phage genes. Hence, we replaced the *p95.lexA* operator on the wildtype phage with a CymR-repressible CA-inducible promoter (*T5-1*). Stable lysogens of this 186$^{p.cym}$ phage were obtained in strains expressing CymR from the bacterial chromosome. Treatment of these lysogens with CA caused prophage induction in all cells, while the prophage was induced in <1% of cells treated with UV. Importantly, in cells induced with CA, additional treatment with UV did not improve the number of phage produced.

Overall, the outcomes of this study in conjunction with previous work provide strong evidence that transient expression of *tum*$^{+}$ in single-copy from a derepressed *p95* promoter is sufficient for 186 developmental switching. By achieving chemical induction of *tum* expression using a synthetic reporter system and the 186$^{p.cym}$ phage we demonstrated 186 prophage induction is not enhanced by SOS activation. Rather, the fundamental role of the host SOS response in wildtype 186 is to activate the expression of *tum.* This outcome suggests SOS activation is not necessarily a mandatory requirement for 186 prophage induction, instead it is an outcome of evolution simply making use of what is available to develop a system that optimises phage fitness and survival.

Experimental procedures

Bacterial strains

E4643 is MG1655 *rph+ ΔlacIZYA* (Priest et al., 2013). To test for integration of the 186 prophage in HB59 occurred at the primary 186 *attB* site (within the *IleY* gene) and not the secondary *attB* site (within the *IleX* gene) (St-Pierre et al., 2013), P2 and P3 primers specific for 186 phage #598 (P2) GCTCATCCATGGGCGATGGTTCTGAGTAACAGATAATAGAATGG and #597 (P3) GCTCAGCTAGC TATGCACTCCTCAGGAAAGTGG were used in combination with P1 and P4 primers for these sites (St-Pierre et al., 2013). E4644 is EC100D: *mcrAΔ(mrr-hsdRMS-mcrBC) ϕ80dlacZΔM15 ΔlacX74 recA1endA1 araD139Δ(ara,leu)7697 galU galK* λ^{-} *rpsL nupG pir+* (DHFR; Epicentre). Table 3.1 lists the bacterial strains constructed in this study.

Table 3.1: *E. coli* strains constructed in this study. Chromosomally integrated modules are encased with squared brackets, with the ending subscript indicating the site of integration. pIT3/4 plasmids harbouring gene reporters and induction modules were integrated into the genome of E4643 strain at the λ, φ21, HK022, 186.1 or 186.2 *attB* site.

Name	Genotype
DL243	E4643 + [pIT3-CL-186*cI*$^{+}$.***pR***$^{+}$.*pL*$^{+}$.*apl*$^{+}$.*cII::lacZ*]$_{\lambda}$ +[pIT3-TO]$_{186.1}$
DL244	E4643 + [pIT3-CL-186*cI*$^{+}$.***pR***$^{+}$.*pL*$^{+}$.*apl*$^{+}$.*cII::lacZ*]$_{\lambda}$ +[pIT3-TO-*p95.tum*^{44*}]$_{186.1}$
DL245-I	E4643 + [pIT3-CL-186*cI*$^{+}$.***pR***$^{+}$.*pL*$^{+}$.*apl*$^{+}$.*cII::lacZ*]$_{\lambda}$ +[pIT3-TO-*p95.tum*$^{+}$]$_{186.1}$
DL245-II	E4643 + [pIT3-CL-186*cI*$^{+}$.***pR***$^{+}$.*pL*$^{+}$.*apl*$^{+}$.*cII::lacZ*]$_{\lambda}$ +[pIT3-TO-*p95.tum*$^{+}$]$_{186.1}$ + [pIT3-TO-*p95.tum*$^{+}$]$_{186.2}$
DL249	E4643 + [pIT3-CL-186*clts.****pR***$^{+}$.*pL*$^{+}$.*apl*$^{+}$.*cII::lacZ*]$_{\lambda}$ +[pIT3-TO]$_{186.1}$

Name	Genotype
DL254	E4643 + [pIT3-CL-186*cI*$^+$.***pR***$^+$.*pL*$^+$.*apI*$^+$.*cII::lacZ*]$_\lambda$ +[pIT3-TO-*p95.tum*$^{4\text{-}5\text{-}}$]$_{186.1}$
DL255	E4643 + [pIT3-CL-186*cI*$^+$.***pR***$^+$.*pL*$^+$.*apI*$^+$.*cII::lacZ*]$_\lambda$ +[pIT3-TO-*p95.tum*$^{72^+}$]$_{186.1}$
DL257	E4643 + [pIT3-CL-186*cI*$^+$.***pR***$^+$.*pL*$^+$.*apI*$^+$.*cII::lacZ*]$_\lambda$ + [pIT3-TO-$P_{LlacO\text{-}1}$.*tum*$^+$]$_{186.1}$ + [pIT3-SH-*PlacI*^{q}.*lacI*]$_{HK022}$
DL258	E4643 + [pIT3-CL]$_\lambda$ + [pIT3-TO-*p95.tum*$^+$.*lacZ*]$_{186.1}$ +[pIT3-SH-*PlacI*^{q}.*lacI*]$_{HK022}$
AI194	E4643 + [pIT3-CL-186*cI*$^+$.***pR***$^+$.*pL*$^+$.*apI*$^+$.*cII::lacZ*]$_\lambda$ + [pIT4-KT-*cymR.T5-1.tum*$^+$]$_{\varphi21}$
HB59	E4643 + [186$^+$]$_{186.1}$
AI239	E4643 + [186$^+$]$_{186.1}$ +[pIT4-KT-*cymR.T5-1*] $_{\varphi21}$
AI243	E4643 + [186$^{loxP.chlorR.loxP.T5\text{-}1.tum+}$]$_{186.1}$ +[pIT4-KT-*cymR.T5-1*]$_{\varphi21}$
AI244	E4643 + [186$^{loxP.T5\text{-}1.tum+}$]$_{186.1}$ +[pIT4-KT-*cymR.T5-1*]$_{\varphi21}$
AI292	E4643 + [pIT4-KT-*cymR.T5-1*]$_{\varphi21}$

Growth media

M9MM-1, M9MM-2 and M9MM-20 are M9MM supplemented with 1mM, 2mM or 20mM glucose respectively. M9MM = 1 x M9 salts (10x M9 salts = 67.8g of NaH_2PO_4, 30.0g of KH_2PO_4, 10g NH4Cl and 5g NaCl/L H_2O), 2mM $MgSO_4$, 0.1mM $CaCl_2$, 0.01mM $(NH_4)_2Fe(SO_4)_2$•$6H_2O$. For general cloning procedures and plasmid propagation, bacteria were grown in LB broth (1% (w/v) Bactotryptone, 1% NaCl, 0.5% (w/v) yeast extract, pH 7.0) with the appropriate antibiotic(s) at 37°C or 30°C. The antibiotics used (in LB/M9MM) were ampicillin (100µg/mL), chloramphenicol (30/20/10µg/mL), kanamycin (50/20µg/mL) and tetracycline (4µg/mL).

Reporter and expression constructs

The reporters and expression constructs for Tum, LacI and CymR were made using a plasmid integration system (Priest et al., 2013; St-Pierre et al., 2013) developed from the CRIM system (Haldimann and Wanner, 2001) and components from the pZ plasmid series (Lutz and Bujard, 1997). Plasmid pIT3-TO (Cui et al., 2013) encodes tetracycline resistance and carries the 186 *attP* site for integration into the 186 *attB* sites. pIT3-TO-*lacZ* carries in addition an *O2*$^-$*lacZ* reporter gene (Müller et al., 1996) preceded by an RNaseIII cleavage site (Linn and St Pierre, 1990). pIT3-CL-*lacZ*trimfuse (Priest et al., 2013) carries an N-terminally truncated *O2*$^-$*lacZ* gene for translational fusions, encodes chloramphenicol resistance and carries the λ *attP* site. pIT3-SH-*PlacI*^{q} (Priest et al., 2013) carries the *lacI* gene expressed from the *PlacI*^{q} promoter, encodes spectinomycin resistance and carries the HK022 *attP* site. Plasmid pIT4-KT-*cymR.T5-1* (integrated in Fig. 3.5A) carries the *cymR* gene expressed from the constitutive *proA* promoter, arranged divergently with a CymR repressed promoter. It encodes kanamycin resistance and contains the φ21 *attP* site. These *pir*-dependent plasmids and their derivatives were propagated in a *pir*$^+$ strain E4644 and were integrated into the E4643 bacterial chromosome using original or modified CRIM integrase plasmids and PCR screening for correct single-copy integrants (Haldimann and Wanner, 2001; St-Pierre et al., 2013).

To make the *cI.**pR**.pL.apl.cII::lacZ* switch reporters (Fig. 3.2A), 186 DNA fragments (*cI*$^+$ or *cIts*) extending from the left end of the *cI* gene to the start of the *cII* gene were inserted into *Bam*HI digested pIT3-CL-*lacZ*trimfuse (Priest et al., 2013) such that the start codon of *cII* is fused to the ninth codon of *O2*$^-$*lacZ*. To make pIT3-TO-*p95.tum*$^+$, pIT3-TO-*p95.tum*$^{4\text{-}5\text{-}}$, pIT3-TO-*p95.tum*^{72*}, pIT3-TO-*p95.tum*^{44*}, and pIT3-TO-*p95.tum*$^+$*.lacZ*, PCR fragments with *Xba*I and *Pst*I tails, starting from the -72 position of *p95* and ending at the *tum* stop codon (or earlier for truncations) were amplified from lysogens of 186$^+$ or 186(*tum*$^{4\text{-}5\text{-}}$) (Brumby et al., 1996) and ligated into *Xba*I/*Pst*I digested pIT3-TO or pIT3-TO-*lacZ*. To make pIT3-TO-$P_{LlacO\text{-}1}$*.tum*$^+$ and pIT3-TO- $P_{LlacO\text{-}1}$*.tum*$^+$*.lacZ*, a PCR fragment with the $P_{LlacO\text{-}1}$ promoter, a variant of the λ*pL* promoter carrying two copies of the *lacO-1* operator was obtained from pZE12-*luc* (Lutz and Bujard, 1997) and assembled with a *tum*$^+$ gene PCR fragment into pIT3-TO or pIT3-TO-*lacZ*. The -72 to -1 sequence of $P_{LlacO\text{-}1}$ is fused to the +1 position of *tum*, maintaining the natural *tum* mRNA. All pIT3-TO constructs were integrated into the primary 186 *attB* site in the E4643 chromosome, except for DL245-II which harbours an additional pIT3-TO-*p95.tum*$^+$ at the secondary 186 *attB* site. To make pIT4-KT-*cymR.T5-1.tum*$^+$ a *tum*$^+$ gene PCR fragment obtained from pIT3-TO-*p95.tum*$^+$ was assembled with the *Spe*I digested pIT4-KT-*cymR.T5-1* module (gift from Dr. Ian Dodd, Shearwin laboratory). The plasmid was integrated into the φ21 *attB* site in the E4643 chromosome.

Inductions for gene expression assays

For the reporter induction assays, bacteria were grown overnight in M9MM-1 or M9MM-2 and subcultured in M9MM-20 to OD_{600} ~0.40 at 37°C (M9MM supplemented with 10μg/mL chloramphenicol). For UV-irradiation, 5mL neat or diluted cultures (in M9MM-20) were mixed with 1μL 10% TWEEN-20 in a 90mm Petri dish and exposed for 0 to 60s to a germicidal lamp (~7.5 J/m^2/min measured using the UVX-25 Digital Radiometer (UVP, Inc. serial# 031019). *Switching assay:* Diluted cultures were UV irradiated, stored on ice, and aliquots spread onto LB plates with 40μg/mL X-gal (5-bromo-4-chloro-3-indolyl-β-D-galactopyranoside). Plates were incubated overnight at 37°C and stored at 4°C for 1-2 days before being scored for blue/white colonies. *UV induction for LacZ assays:* After UV, cultures were diluted periodically with pre-warmed M9MM-20 to maintain log phase growth and ensure a sample OD_{600} ~0.40. Samples taken before and after UV were stored on ice until the LacZ assay. *Temperature induction for LacZ assays:* DL249 grown at 30°C was diluted into 39°C medium and incubation continued with periodical dilution with pre-warmed medium, as above. Samples were stored on ice until the LacZ assay. *IPTG/CA induction for LacZ assays:* IPTG (Sigma Aldrich) or CA (Sigma Aldrich) was added (after UV, if present) by dilution into M9MM-20 to give a final IPTG concentration of 300μM or CA concentration of 150μM. Periodical dilution was with pre-warmed M9MM-20 containing 300μM IPTG or 150μM CA, as above.

LacZ assays

Kinetic *LacZ* assays in 96-well microtitre plates were performed as previously described (Dodd et al., 2001), except cultures were grown in M9MM and stored on ice prior to the assay.

Construction of the 186$^{p.cym}$ bacteriophage

A *tM.loxP.chlor^R.loxP.T5-1.tum$^+$* DNA cassette (Fig. 3.6), prepared from two gBlocks (IDT) by high fidelity overlap extension PCR, was used to replace *p95* in the 186 prophage of AI239, using recombineering with the pSIM6 plasmid (Sharan et al., 2009) and selection for chloramphenicol resistance. The *loxP* cassette was excised by transient transformation with pKD46-*pE-Cre*, which expresses Cre recombinase constitutively from the phage P2 *pE* promoter and is removed by growth at 37°C. pKD46-*pE-Cre* was derived from pKD46-*pE-Flp* (St-Pierre et al., 2013) by Nan Hao (Shearwin laboratory). The location of the *cymR* operator in the *T5-1* promoter makes it impossible for this construct to produce mRNA with the same sequence as from *p95*. To make the translation rates similar we used the Salis Lab RBS Calculator v2.0 using the MG1655 ACCTCCTTA 16S RNA sequence setting (Borujeni et al., 2014) to design a leader for the *tum* coding sequence with a strength of 2392AUs, comparable to the wildtype strength of 2260AUs. The wildtype leader sequence from -18 to -1 was retained. The sequence of the *p95* replacement in the prophage was confirmed by Sanger sequencing.

Figure 3.6: The full-length *tM.loxP.chlor^R.loxP.T5-1.tum$^+$* cassette used to generate the 186$^{p.cym}$ phage. The cassette was prepared from two gBlocks (*tM.loxP.chlor^R* and *loxP.T5-1.tum*) by high fidelity overlap extension PCR. Sequence written 5' to 3', *tM* (bold), *loxP* sites (pink), *chlor^R* (green), *tum$^+$* (blue), CymR site (purple) and *T5-1* -10 and -35 sites (grey, underlined),

CCGCTAATATTCATCCATATCATGTACA**TACAGTGTATTTAACTGTGATTTTTTT**C**TACCGTTCGTAT**
AATGTATGCTATACGAAGTTATGATATCTGGCGAAAATGAGACGTTGATCGGCACGTAAGAGGTTCCA
ACTTTCACCATAATGAAATAAGATCACTACCGGGCGTATTTTTTGAGTTATCGAGATTTTCAGGAGCT
AAGGAAGCTAAAATGGAGAAAAAAATTACTGGGTATACAACCGTAGACATTTCGCAGTGGCACCGCAA
GGAACATTTTGAAGCGTTCCAGTCGGTGGCGCAATGCACATATAACCAAACTGTyCCAATTGGACATT
ACTGCGTTTTTGAAGACTGTCAAGAAAAATAAACACAAGTTCTACCCTGCGTTTATTCATATCCTGGC
TCGTCTGATGAATGCACACCCTGAGTTCCGCATGGCCATGAAGGACGGCGAATTGGTTATCTGGGACA
GCGTTCATCCCTGCTACACTGTGTTTCACGAGCAGACTGAAACATTCTCCTCACTTTGGTCAGAGTAC
CATGACGACTTTCGCCAATTCTTACATATTTATTCGCAGGACGTAGCCTGTTATGGAGAGAATCTTGC
GTATTTTCCGAAGGGGTTCATCGAGAACATGTTTTTTGTGAGTGCGAACCCTTGGGTGTCATTTACGT
CGTTTGATCTGAACGTGGCCAATATGGATAACTTCTTTGCCCCTGTGTTCACTATGGGCAAGTACTAC
ACTCAAGGAGACAAAGTTCTGATGCCTCTTGCTATCCAAGTACACCACGCAGTCTGTGATGGCTTCCA
CGTTGGGCGTATGTTGAATGAACTGCAACAGTACTGCGATGAATGGCAGGGCGGGGCTTAATAAGAAT
TAGGAAG**ATAACTTCGTATAATGTATGCTATACGAACGGTA**ACGCGTAAATCATAAAAAATTTATTTG
CTTTGTGCCTAATAATGACTAATAATAGATTC**AACAAACAGACAATCTGGTCTGTTTGTATTAT**GAAT
TCCAGCATATAGGGATCGTCGTCTCGTAGTGGAGGTTGT**GTGGATAGAGAGCTAAATGAGCACGTTAT**
GATTGAGCGGG

Prophage induction assays

HB59 and AI244 lysogens grown overnight in M9MM-2 were diluted to OD_{600} 0.15 in M9MM-20 and incubated with aeration at 37°C to OD_{600} ~0.30. Prior to UV or CA induction, cell counts were obtained by spreading dilutions in M9MM-20 onto LB and counting colonies after incubation overnight at 37°C. PFU titres were determined by mixing diluted samples with E4643 indicator in LB and 3mL molten soft agar (0.5% at 48°C), pouring onto LB plates and counting plaques after incubation at 37°C overnight. Uninduced PFU titres (free phage and spontaneously inducing lysogens) were obtained just prior to UV or CA treatment. Uninduced free phage levels were measured using supernatants after the addition of a few drops of chloroform and brief centrifugation. For UV induction, 5mL of each culture (+1µL 10% TWEEN-20) was irradiated for 40s in a Petri dish.

For CA induction, 150µM CA was added after UV (if present). After induction, cultures were incubated in tubes with rolling at 37ºC and 10mins after induction, culture were diluted (10^{-4}) in pre-warmed M9MM-20 and incubation continued. Samples were taken at various times for PFU titres.

The phage induction assay to determine virulence

HB59 and AI244 lysogens were plated on indicator lawns consisting of four different host strains (E4643, AI06, HB59 and AI244). To prepare the indicator strains, O/N cultures of E4643, AI06, HB59 and AI244 were diluted to OD_{600} 0.05 in LB and incubated with aeration at 37°C to OD_{600} ~0.60. To prepare the E4643 lysogens, O/N cultures of HB59 and AI244 were diluted to OD_{600} 0.15 in M9MM-20 and incubated with aeration at 37°C to OD_{600} ~0.30. Prior to induction, untreated HB59 and AI244 cultures (at OD_{600} 0.30) were diluted 10^{-2} and 10^{-1} respectively. For UV induction 5mL of the HB59 culture (+1µL 10% TWEEN-20) was irradiated for 40s in a Petri dish. For CA induction, 150µM CA was added to the AI244 culture. Induced cultures were incubated for 30mins at 37°C and then diluted 10^{-4}. Plating was performed by mixing the diluted samples with each indicator in LB and 3mL molten soft agar (0.5% at 48°C), pouring onto LB plates and counting plaques after incubation at 37°C overnight.

Acknowledgements

This work was supported by grants DP110100824 and DP160101450 from the Australian Research Council. The authors wish to thank Julian Pietsch for communicating unpublished results, Nan Hao for pKD46-*pE-Cre* and pIT4-*cymR,* Hannah Bonham for HB59 lysogen and Barry Wanner and Hermann Bujard for their gifts of plasmids.

References

Brumby, A.M., Lamont, I., Dodd, I.B., Egan, J.B., 1996. Defining the SOS Operon of Coliphage 186. *Virology* **219**, 105–114.

Callen, B.P., Shearwin, K.E., Egan, J.B., 2004. Transcriptional interference between convergent promoters caused by elongation over the promoter. *Molecular Cell* **14**, 647–656.

Casjens, S.R., Hendrix, R.W., 2015. Bacteriophage lambda: Early pioneer and still relevant. *Virology* **479–480**, 310–330.

Choi, Y.J., Morel, L., Le Francois, T., Bourque, D., Bourget, L., Groleau, D., Massie, B., Miguez, C.B., 2010. Novel, Versatile, and Tightly Regulated Expression System for *Escherichia coli* Strains. *Applied and Environmental Microbiology* **76**, 5058–5066.

Christie, G.E., Dokland, T., 2012. Pirates of the Caudovirales. *Virology* **434**, 210–221.

Cui, L., Murchland, I., Shearwin, K.E., Dodd, I.B., 2013. Enhancer-like long-range transcriptional activation by CI-mediated DNA looping. *PNAS* **110**, 2922–2927.

Dodd, I.B., Egan, J.B., 2002. Action at a distance in CI repressor regulation of the bacteriophage 186 genetic switch. *Molecular Microbiology* **45**, 697–710.

Dodd, I.B., Kalionis, B., Egan, J.B., 1990. Control of gene expression in the temperate coliphage 186: VIII. Control of lysis and lysogeny by a transcriptional switch involving face-to-face promoters. *Journal of Molecular Biology* **214**, 27–37.

Dodd, I.B., Perkins, A.J., Tsemitsidis, D., Egan, J.B., 2001. Octamerization of λ CI repressor is needed for effective repression of PRM and efficient switching from lysogeny. *Genes & Development* **15**, 3013–3022.

Dodd, I.B., Reed, M.R., Egan, J.B., 1993. The Cro-like Apl repressor of coliphage 186 is required for prophage excision and binds near the phage attachment site. *Molecular Microbiology* **10**, 1139–1150.

Espah Borujeni, A., Channarasappa, A.S., Salis, H.M., 2014. Translation rate is controlled by coupled trade-offs between site accessibility, selective RNA unfolding and sliding at upstream standby sites. *Nucleic Acids Research* **42**, 2646–2659.

Fornelos, N., Bamford, J.K.H., Mahillon, J., 2011. Phage-Borne Factors and Host LexA Regulate the Lytic Switch in Phage GIL01. *Journal of Bacteriology* **193**, 6008–6019.

Galkin, V.E., Yu, X., Bielnicki, J., Ndjonka, D., Bell, C.E., Egelman, E.H., 2009. Cleavage of Bacteriophage λ cI Repressor Involves the RecA C-terminal Domain. *Journal of Molecular Biology* **385**, 779–787.

Haldimann, A., Wanner, B.L., 2001. Conditional-Replication, Integration, Excision, and Retrieval Plasmid-Host Systems for Gene Structure-Function Studies of Bacteria. *Journal of Bacteriology* **183**, 6384–6393.

Hooper, I., Woods, W.H., Egan, B., 1981. Coliphage 186 Replication is delayed when the host cell is UV irradiated before infection. *Journal of Virology* **40**, 341–349.

Howard-Varona, C., Hargreaves, K.R., Abedon, S.T., Sullivan, M.B., 2017. Lysogeny in nature: mechanisms, impact and ecology of temperate phages. *The ISME Journal* **11**, 1511–1520.

Lamont, I., Brumby, A.M., Egan, J.B., 1989. UV induction of coliphage 186: prophage induction as an SOS function. *PNAS U.S.A.* **86**, 5492–5496.

Lemire, S., Figueroa-Bossi, N., Bossi, L., 2011. Bacteriophage Crosstalk: Coordination of Prophage Induction by Trans-Acting Antirepressors. PLoS Genetics **7**, e1002149.

Lewis, L.K., Harlow, G.R., Gregg-Jolly, L.A., Mount, D.W., 1994. Identification of high affinity binding sites for LexA which define new DNA damage-inducible genes in Escherichia coli. *Journal of Molecular Biology* **241**, 507–523.

Linn, T., St Pierre, R., 1990. Improved vector system for constructing transcriptional fusions that ensures independent translation of lacZ. *Journal of Bacteriology* **172**, 1077–1084.

Little, J.W., Edmiston, S.H., Pacelli, L.Z., Mount, D.W., 1980. Cleavage of the Escherichia coli lexA protein by the recA protease. *PNAS* **77**, 3225–3229.

Little, J.W., Mount, D.W., 1982. The SOS regulatory system of Escherichia coli. *Cell* **29**, 11–22.

Liu, C., Sun, D., Zhu, J., Liu, W., 2019. Two-Component Signal Transduction Systems: A Major Strategy for Connecting Input Stimuli to Biofilm Formation. *Frontiers in Microbiology* **9**, 3279.

Liu, T., Renberg, S.K., Haggård-Ljungquist, E., 1997. Derepression of prophage P2 by satellite phage P4: cloning of the P4 epsilon gene and identification of its product. *Journal of Virology* **71**, 4502–4508.

Ljungquist, E., Bukhari, A.I., 1977. State of prophage Mu DNA upon induction. *PNAS U.S.A.* **74**, 3143–3147.

Lutz, R., Bujard, H., 1997. Independent and tight regulation of transcriptional units in Escherichia coli via the LacR/O, the TetR/O and AraC/I1-I2 regulatory elements. *Nucleic Acids Research* **25**, 1203–1210.

Mardanov, A.V., Ravin, N.V., 2007. The Antirepressor Needed for Induction of Linear Plasmid-Prophage N15 Belongs to the SOS Regulon. *Journal of Bacteriology* **189**, 6333–6338.

Müller, J., Oehler, S., Müller-Hill, B., 1996. Repression of lac promoter as a function of distance, phase and quality of an auxiliary lac operator. *Journal of Molecular Biology* **257**, 21–29.

Murchland, I., Ahlgren-Berg, A., Priest, D.G., Dodd, I.B., Shearwin, K.E., 2014. Promoter Activation by CII, a Potent Transcriptional Activator from Bacteriophage 186. J*ournal of Biological Chemistry* **289**, 32094–32108.

Nilsson, A., Haggård-Ljungquist, E., 2005. The P2-like bacteriophages, In: Calendar, R.L., The Bacteriophages. Oxford University Press Incorporated, Oxford, United States.

Priest, D.G., Cui, L., Kumar, S., Dunlap, D.D., Dodd, I.B., Shearwin, K.E., 2014. Quantitation of the DNA tethering effect in long-range DNA looping in vivo and in vitro using the Lac and λ repressors. *PNAS U.S.A.* **111**, 349–54.

Quinones, M., Kimsey, H.H., Waldor, M.K., 2005. LexA cleavage is required for CTX prophage induction. *Molecular Cell* **17**, 291–300.

Reed, M.R., 1994. Apl: a multifunctional repressor and excisionase essential for prophage induction of temperate coliphage 186. The University of Adelaide.

Reed, M.R., Shearwin, K.E., Pell, L.M., Egan, J.B., 1997. The dual role of Apl in prophage induction of coliphage 186. *Molecular Microbiology* **23**, 669–81.

Rozanov, D.V., D'Ari, R., Sineoky, S.P., 1998. RecA-Independent Pathways of Lambdoid Prophage Induction in Escherichia coli. *Journal of Bacteriology* **180**, 6306–6315.

Runyen-Janecky, L.J., Hong, M., Payne, S.M., 1999. The Virulence Plasmid-Encoded impCAB Operon Enhances Survival and Induced Mutagenesis in Shigella flexneri after Exposure to UV Radiation. *Infection and Immunity* **67**, 1415–1423.

Sassanfar, M., Roberts, J.W., 1990. Nature of the SOS-inducing signal in Escherichia coli. The involvement of DNA replication. *Journal of Molecular Biology* **212**, 79–96.

Sauer, B., 1987. Functional expression of the cre-lox site-specific recombination system in the yeast Saccharomyces cerevisiae. *Molecular Cell Biology* **7**, 2087–2096.

Sharan, S.K., Thomason, L.C., Kuznetsov, S.G., Court, D.L., 2009. Recombineering: A Homologous Recombination-Based Method of Genetic Engineering. *Nature Protocols* **4**, 206–223.

Shearwin, K.E., Brumby, A.M., Egan, J.B., 1998. The Tum protein of coliphage 186 is an antirepressor. *Journal of Biological Chemistry* **273**, 5708–5715.

St-Pierre, F., Cui, L., Priest, D.G., Endy, D., Dodd, I.B., Shearwin, K.E., 2013. One-Step Cloning and Chromosomal Integration of DNA. *ACS Synthetic Biology* **2**, 537–541.

Voloshin, O.N., Ramirez, B.E., Bax, A., Camerini-Otero, R.D., 2001. A model for the abrogation of the SOS response by an SOS protein: a negatively charged helix in DinI mimics DNA in its interaction with RecA. *Genes & Development* **15**, 415–427.

Woods, W.H., Egan, J.B., 1974. Prophage Induction of Noninducible Coliphage 186. *Journal of Virology* **14**, 1349–1356.

Yasuda, T., Morimatsu, K., Horii, T., Nagata, T., Ohmori, H., 1998. Inhibition of Escherichia coli RecA coprotease activities by DinI. *The EMBO Journal* **17**, 3207–3216.

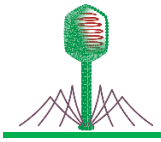

Chapter 4

Investigating the role of CII in the process of 186 prophage induction

The following chapter presents a draft manuscript of our investigation into the role of CII during the establishment of lysogeny and prophage induction. This draft has been written with the intent to submit to the Proceedings of the National Academy of Sciences of the United States of America. I had a minor contribution to this study by engineering and characterising the ***pL/pE***.*apl*$^{+/-}$.*cII*$^{+/-/145}$ LacZ reporter modules (Fig. 4.5D). The draft manuscript has not yet been submitted.

Statement of Authorship

Title of Paper	Instability of CII is needed for efficient switching between lytic and lysogenic development in bacteriophage 186.
Publication Status	☐ Published ☐ Accepted for Publication ☐ Submitted for Publication ☑ Unpublished and Unsubmitted work written in manuscript style
Publication Details	This draft manuscript reports on our investigation into the significance of the 186 bacteriophage having a short-lived/protease sensitive CII protein. In particular, we investigated how having a short half-life is important for 186 to make appropriate developmental decisions and to undergo prophage induction efficiently.

Principal Author

Principal Author	Iain M. Murchland		
Contribution to the Paper	Designed research, performed experiments (cloning, lacZ assays, Western blots, phage assays) developed modelling of phage infections. Prepared figures, drafted manuscript.		
Overall percentage (%)	35		
Signature		Date	03/08/2020

Co-Author Contributions

By signing the Statement of Authorship, each author certifies that:

i. the candidate's stated contribution to the publication is accurate (as detailed above);
ii. permission is granted for the candidate in include the publication in the thesis; and
iii. the sum of all co-author contributions is equal to 100% less the candidate's stated contribution.

Name of Co-Author	Alexander Ahlgren-Berg		
Contribution to the Paper	Designed research, identified proteases responsible for CII degradation, performed Western blots, yield of lysogen experiments, prepared figures.		
Overall percentage (%)	20		
Signature	No response received. Could not be contacted. Primary supervisor Shearwin signing on behalf of Dr. Alhgren-Berg.	Date	03/08/2020

Name of Co-Author	Julian M.J. Pietsch		
Contribution to the Paper	Developed mathematical model of phage infection, prepared figures.		
Overall percentage (%)	15		
Signature		Date	03/08/2020

Name of Co-Author	Alejandra Isabel (Candidate)		
Contribution to the Paper	Engineered and characterised the ***pL/pE***.*apl*$^{+/-}$.*cII*$^{+/-/145}$ LacZ reporter modules. Figure 4.5D. Assisted with manuscript drafting.		
Overall percentage (%)	10%		
Certification:	This paper reports on original research I conducted during the period of my Higher Degree by Research candidature and is not subject to any obligations or contractual agreements with a third party that would constrain its inclusion in this thesis.		
Signature		Date	30 / 07 / 2020

Name of Co-Author	Dr. Ian Dodd		
Contribution to the Paper	Designed research, drafted the manuscript, contributed new reagents/analytic tools.		
Overall percentage (%)	10		
Signature		Date	03/08/2020

Name of Co-Author	Dr. Keith E. Shearwin		
Contribution to the Paper	Designed research, drafted the manuscript, contributed new reagents/analytic tools.		
Overall percentage (%)	10		
Signature		Date	03/08/2020

Instability of CII is needed for efficient switching between lytic and lysogenic development in bacteriophage 186

Iain M. Murchland, Alexandra Ahlgren-Berg, Julian M. J. Pietsch[2], Alejandra Isabel, Ian B. Dodd, Keith E. Shearwin[1]
Department of Molecular and Biomedical Science, University of Adelaide, Adelaide, South Australia 5005
1 Corresponding author: keith.shearwin@adelaide.edu.au, +61 8 8313 5361
2 Current address: SynthSys-Synthetic and Systems Biology, University of Edinburgh, Edinburgh EH9 3BF, United Kingdom

Abstract

The CII protein of temperate coliphage 186, like the unrelated CII protein of phage λ, is a transcriptional activator that primes expression of the CI immunity repressor and is critical for efficient establishment of lysogeny. 186-CII is also highly unstable, and we show that *in vivo* degradation is mediated by FtsH and RseP. We investigated the role of CII instability by constructing a 186 phage encoding a protease resistant CII. The stabilised-CII phage was defective in the lysis-lysogeny decision: choosing lysogeny with close to 100% frequency after infection, and forming prophages that were defective in entering lytic development after UV treatment. While lysogenic CI concentration was unaffected by CII stabilisation, lysogenic transcription and CI expression was elevated after UV. A stochastic model of the 186 network after infection indicated that an unstable CII allowed a rapid increase in CI expression without a large overshoot of the lysogenic level, suggesting that instability enables a decisive commitment to lysogeny with a rapid attainment of sensitivity to prophage induction.

Introduction

The genetic and molecular machinery that governs the lytic/lysogenic life cycle decision of temperate phage has proven to be fertile ground for analysing the operation of genetic switches. The switch region of the λ phage in particular has yielded many insights into the principles and phenomena that underpin the effective function of a bistable switch (1-3) (4). The λCII protein is a critical component of the decision-making circuit, being a pro-lysogenic factor necessary for establishing lysogeny after infection. λCII primes production of the lysogenic repressor CI, inhibits expression of late lytic genes and activates expression of the integrase gene (1, 5) (Fig. 4.1A). λCII is encoded on the lytic transcript, thus creating a delayed negative feedback on lytic development. λCII is rapidly degraded *in vivo* by the protease FtsH, and is protected from FtsH by the λCIII protein (6-8).

The developmental switch of phage 186 has a very similar topology, encoding a proteolytically degraded, pro-lysogenic factor CII on the lytic transcript (9, 10) (Fig. 4.1B). Yet phage 186 belongs to the P2-related family of bacteriophage, and is evolutionarily distinct from λ, with analogous factors from the two phage typically possessing very little sequence homology (11). The developmental switch from 186-related temperate phage P2 lacks a CII-like factor and the associated delayed negative feedback (12) (Fig. 4.1C), demonstrating that a CII-like factor is not a necessary component of a genetic switch governing two alternative, stable states.

From an evolutionary perspective, we would therefore expect the presence of *cII* in the genetic switch to correlate with additional or improved functionality of the switch in some way. Additionally, the coincidence of proteolytic degradation of both λCII and 186-CII suggests a functional or evolutionary constraint on the half-life of CII. It is tempting to speculate that a rapidly degraded CII may be related to the SOS-inducible phenotype of 186 and λ, which P2 lacks (12-15). Yet the link between genotype and phenotype is not readily apparent, and the overall functionality imparted by CII on this class of genetic switch remains poorly described.

Studies of λ*cII* and λ*cIII* mutants have suggested that proteolysis of λCII affects the relative frequencies with which different developmental fates arise, resulting in changes to the phage frequency of lysogeny (6-8). However the complexity of the phage λ genetic network does not allow this effect to be directly linked to the behaviour of the core developmental switch (*cI-pRM-pR-cro-pRE-cII*), since λCII is also active at pro-lysogenic promoters *paQ* and *pI* (16), outside the switch region (Fig. 4.1A). It is therefore unclear whether the loss of λ plaque formation in response to λCII stabilisation (7) is a result of changes in the fate of the switch, or whether the activity of λCII at other promoters disrupts the lytic pathway in other ways. The 186 developmental switch, on the other hand, presents a substantially simpler system for the functional analysis of CII, possessing only a single CII-activated promoter (*pE*), and no CIII-like factor (17).

We have observed a renewed interest in phage biology as a rich source of components for use in synthetic biology, and an associated desire to understand how the properties of individual components affect the emergent properties of small reusable genetic networks. In this work, we seek to characterise the proteolysis of 186-CII and its functional consequences in an effort to further understand the role of CII and its degradation in the 186 switch, and switches with similar delayed negative feedback topologies.

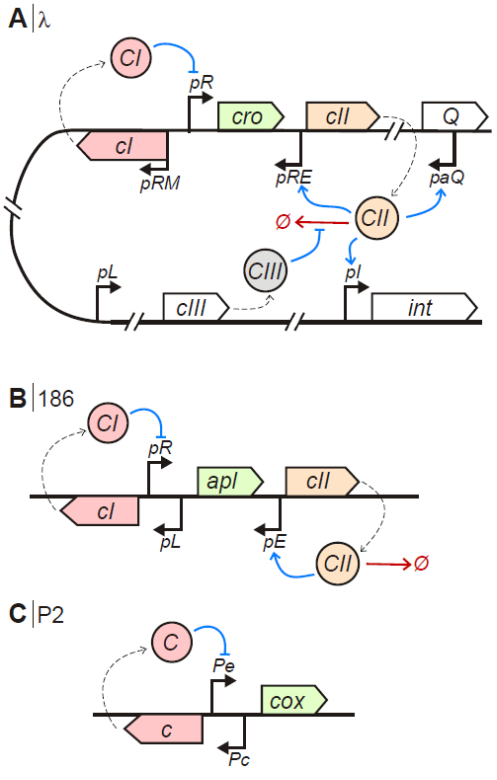

Figure 4.1: Schematic diagram of the switch regions of the temperate bacteriophage. (A) λ; **(B)** 186; **(C)** P2. In all cases, rightward transcription represents lytic transcripts, while leftward transcription represents lysogenic transcripts.

Results

186-CII is degraded by FtsH

We have previously shown that 186-CII is rapidly degraded *in vivo* by an unknown protease (9). λCII is known to be degraded by the *E. coli* protease FtsH/HflB (6), and strains with mutations in *ftsH* yield plaques with increased turbidity relative to parental strains when plated with λ phage (6, 7). We therefore hypothesised that FtsH may also be responsible for degradation of 186-CII. To test this hypothesis, we investigated the *in vivo* half-life of CII in the *ΔftsH* strain A8926, and the parental strain A8925 using Western blot analysis following addition of a translation inhibitor. CII degradation results in the formation of a specific, inactive product of proteolysis, corresponding to the first 135 amino acids of the protein (Fig. 4.2A) (9). In the *ΔftsH* strain, this degradation product was still evident, along with an additional degradation product migrating at an apparent molecular weight in between that of full-length CII and the previously characterised degradation product. Nonetheless, quantitative analysis of the full-length CII band shows that degradation is much slower in the *ΔftsH* strain than the control strain (Fig. 4.2A), leading us to conclude that CII is degraded by FtsH.

We further sought to evaluate the effect of stabilisation of CII on the behaviour of the 186 developmental switch. Given the pro-lysogenic function of CII, and the apparent high frequency of lysogeny phenotype of λ in mutants of *ftsH*, we expected that 186 would also exhibit a high yield of lysogens in a *ΔftsH* strain. However, our results show no statistically significant difference between the yield of 186 lysogens in strains A8926 and A8925 (n=4; p=0.93; t=0.075, df=6; unpaired, two-tailed t-test) (Fig. 4.2B). Consistent with this finding, there was also no observable difference in 186 plaque morphology on the two strains.

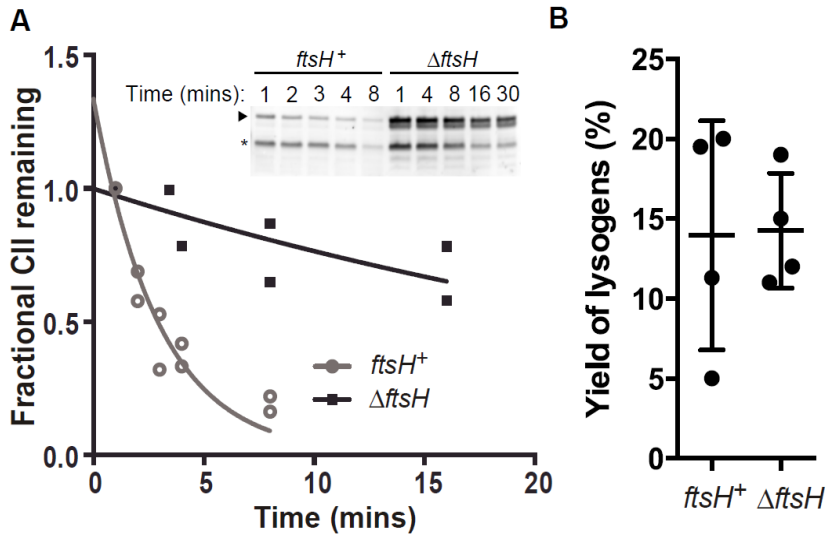

Figure 4.2: CII is degraded by FtsH. (A) *In vivo* degradation assays using A8925 (*ftsH*⁺) (lanes 1-5) or A8926 (*ΔftsH*) (lanes 6-10) expressing CII from pZS45-CII169 with translation inhibited by 100μg/mL chloramphenicol at time –1min. Full-length CII is indicated by the arrow; the major degradation product by an asterisk. Volumetric analysis of the full-length CII band shows that the host lacking *ftsH* degrades CII more slowly than the parental strain. Points represent individual measurements, lines show best fit of a one phase exponential decay to a plateau constrained to y=0. Best-fit (95% CI) values for half-lives were 2.1 (1.5-3.1) min for *ftsH*⁺ and 25.9 (14.0-180.0) min for *ΔftsH*. **(B)** 186+ was used to measure the yield of lysogens from *ftsH*⁺ and *ΔftsH*. Data points represent independent experiments, lines show mean and standard deviation of the ensemble.

186-CII is degraded by RseP

Since degradation products of CII are still evident despite deletion of *ftsH*, we reasoned that other proteases may also degrade CII. Search approaches exploiting random transposon-based knockouts (18) or using knockouts of non-essential proteases from the Keio collection (19), and screening for changes in CII transcriptional activity or 186 plaque morphology, did not successfully identify additional proteases that degrade CII. A limitation of both approaches is that the role of proteases essential for host function cannot be examined. This explains why FtsH was not identified as a CII-degrading enzyme by these experiments, since *ftsH* deletion alone is lethal to the host; the *ΔftsH* strain A8926 we used carries the additional mutation *sfhC21*, which suppresses lethality of *ΔftsH*.

We therefore sought to determine whether DegS or RseP (formerly YaeL) degrade CII, since single-gene deletions of these proteases are also lethal to the host (20). Again taking advantage of additional mutations that suppress lethality of protease deletions, we investigated the *in vivo* degradation of CII in the *ΔrsePΔrseA* strain KK211 and the parental *ΔrseA* strain AD1811. Using Western blot analysis after addition of a translation inhibitor, we found that deletion of *rseP* resulted in the loss of the CII degradation product (Fig. 4.3A). Thus we conclude that RseP degrades CII, in addition to FtsH. Quantitative analysis of the full-length CII band does not show evidence that degradation of CII is slowed by genetic deletion of *rseP* (Fig. 4.3A), presumably due to redundancy in degradation of CII via the FtsH pathway. Direct experimentation to confirm this hypothesis was not possible, due to the fact that a dual *ΔrseP/ΔftsH* knockout is not viable (21).

Yield of lysogen experiments suggest that deletion of *rseP* results in a slight (40%) increase in 186 lysogenisation (Fig. 4.3B). Such a result is unexpected, given that we see no detectable stabilisation of CII in the Δ*rseP* strain, yet stabilisation of CII in the *ΔftsH* strain is not associated with a change in the yield of lysogens. Translation-stop *in vivo* degradation experiments using strain CU141 and its *ΔdegS* derivative KK372 show no increase in CII half-life, nor loss of the CII degradation product (Fig. 4.3C). Thus, we conclude that CII is not degraded by DegS.

Our conclusion from this set of results is that the use of protease deletion strains is an unreliable method of probing the effects of stabilising CII on the behaviour of the 186 switch. Both FtsH and RseP are involved in regulating stress response pathways to which 186 may have evolved to respond. We and others (21, 22) have observed that the deletion strains of the essential proteases *ftsH* and *rseP* exhibit substantially different growth rates and temperature sensitivity to their parental strains. Furthermore, both FtsH and RseP are responsible for processing sigma factors (20, 23), making us sceptical that the intracellular environment – particularly the transcriptional machinery that is central to the switch's function – is comparable between the protease deletion strains and their respective parental controls.

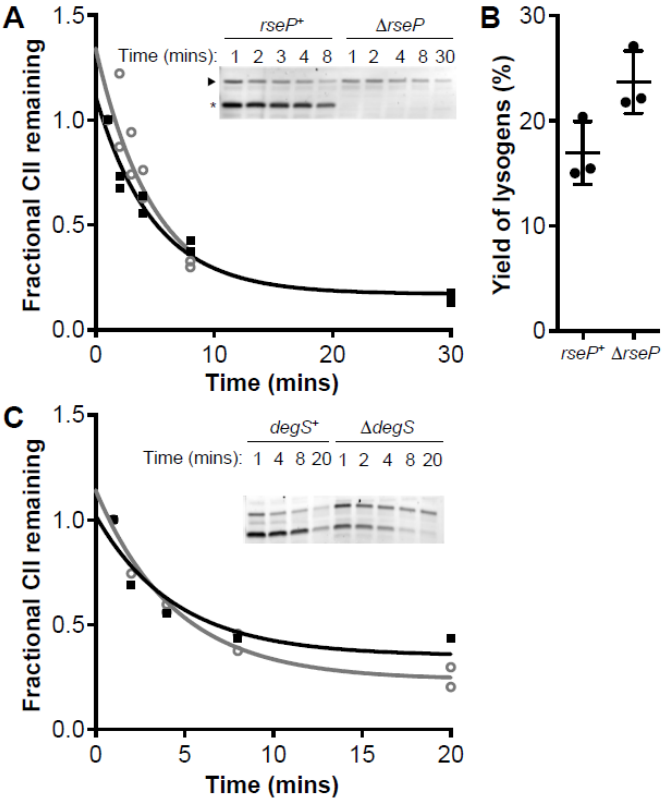

Figure 4.3: 186-CII is degraded by RseP. **(A)** *In vivo* degradation assays using AD1811 (lanes 1-5) or KK211 (lanes 6-10) expressing CII from pZS15-CII169 with translation inhibited by 200μg/mL spectinomycin at time –1 min. Volumetric analysis of the full-length CII band from *in vivo* degradation assays shows that degradation of full-length CII is not significantly slower in hosts lacking *rseP*. **(B)** 186+ was used to measure the yield of lysogens from AD1811 and K211. Data points represent independent experiments, lines show mean and standard deviation of the ensemble. Probability of no difference between means = 0.0505, unpaired *t*-test, *n*=3. (C) Translation stop *in vivo* degradation assays using CU141 (lanes 1-5) or KK372 (lanes 6-10) expressing CII from pZS15-CII169.

Poor prophage induction of a 186 with a stabilised CII

To better understand how reducing the rate of degradation of 186-CII changes the behaviour of the 186 developmental switch, we stabilised CII by alteration of the protein, rather than by alteration of the host. We have previously shown a C-terminal truncation of CII that retains the first 145 residues, termed CII145, to be stabilised yet retain the same specific activity as the full-length CII protein (9). Thus we created a mutant of the 186 phage, 186.*cII*^{145}, encoding the stabilised CII145 truncation of CII, using recombineering methods to alter a 186 prophage. Two independent 186.*cII*^{145} phage were created and characterised. We also created the chloramphenicol resistant phage variants 186.CmR, 186.*cII*$^{-}$.CmR and 186.*cII*^{145}.CmR, which carry a chloramphenicol acetyltransferase expression cassette in the untranscribed *cos* region of the 186 genome (position 126).

To characterise the phenotype of the 186.*cII*^{145} phage, we first compared induction of 186.*cII*^{145}.CmR, 186.CmR and 186.*cII*$^{-}$.CmR lysogens by UV irradiation. Assaying for induction by formation of plaques in a lawn of indicator after UV irradiation of lysogens, 186.*cII*^{145}.CmR did not show any sign of induction, while no consistent difference was observed between induction of 186.CmR and 186.*cII*$^{-}$.CmR (Fig. 4.4A). There are two possible explanations for this result. The first is that 186.*cII*^{145}.CmR simply cannot be induced to form viable daughter phage, while the second is that 186.*cII*^{145}.CmR induces, forms viable daughter phage, but cannot form plaques. Investigating the latter possibility, we again attempted to induce the phage (or a non-lysogen control) by UV irradiation, this time using a spectinomycin-resistant indicator strain, and selecting for lysogens that are the product of these infections by dual-resistance to chloramphenicol and spectinomycin.

Figure 4.4B shows that both spontaneous and UV-stimulated induction of 186.CmR is detectable by this method. The data also reveal that 186.*cII*^{145}.CmR induces spontaneously at a low level, and that this is not significantly increased by UV irradiation. However, the number of lysogen forming units (lfu) detected after irradiation of 186.*cII*^{145}.CmR is ~200-fold lower than that of 186.CmR, suggesting that induction is compromised in 186.*cII*^{145}.CmR. It is important to note that due to the design of this assay, we cannot be confident of the magnitude of this defect from this data alone, given that the number of lysogeny forming units is affected by other characteristics of the phage, such as its frequency of lysogeny.

Having established that 186.*cII*^{145}.CmR can be induced and produces infective virions, but with low efficiency, we used an artificial, more efficient method of induction which avoids the use of potentially mutagenic UV irradiation to create phage stocks of 186.*cII*^{145}.CmR for further experimentation. The method uses IPTG-induced over-expression of the dominant-negative C-terminal domain of the 186-CI lysogeny maintenance repressor (CI-CTD) to sequester wildtype CI in the lysogen, and de-repress the lytic promoters. Analysing the efficiency of this form of induction reveals no significant deficit in the number of lysogen forming units detected after induction of the 186.*cII*^{145}.CmR prophage compared to *cII*$^{+}$ (Fig. 4.4C). Again, care must be taken in the interpretation of these results due to the likelihood of differences in the frequencies of lysogeny of the two phages.

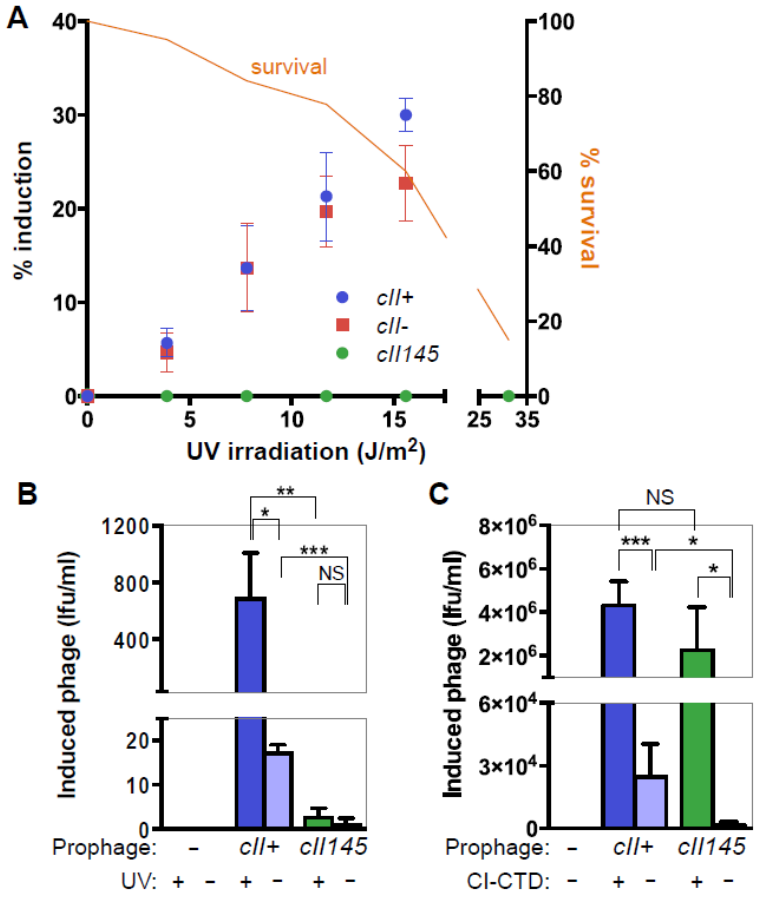

Figure 4.4: Induction of 186 prophage. Error bars are standard deviations. **(A)** Induction of 186.CmR, 186.*cII*$^{-}$.CmR and 186.*cII*^{145}.CmR prophages by UV irradiation and detection of plaque-forming units. % induction (left axis) is defined as number of plaques induced/number of input cells. Cell survival (right axis) is defined as number of colony-forming units following irradiation/number of input cells. **(B)** Induction of 186.CmR and 186.*cII*^{145}.CmR lysogens by UV irradiation (15.6 J/m^2) and detection of lysogen-forming units. * signifies $p < 0.05$; ** $p < 0.01$; *** $p < 0.001$ using an unpaired, two-tailed *t*-test (n=3 for *cII*$^{+}$ and 6 for *cII*^{145}). **(C)** Induction of 186.CmR and 186.*cII*^{145}.CmR lysogens by expression of CI-CTD (vs empty plasmid controls) and detection of lysogen-forming units. Note that a more dense culture was used for induction compared to (B). Statistics as in (B), except n=4.

186.*cII*^{145} frequency of lysogeny

Using the 186.*cII*^{145}.CmR and 186.CmR phage, we investigated how stabilisation of CII affects the frequency of lysogenisation after phage 186 infection. Frequencies of lysogeny were calculated by assaying an infection for the formation of lysogens by chloramphenicol resistance, for plaque formation, and for efficiency of infection. Consistent with the results of our induction experiments, we observed lysogens but no plaques due to infection with 186.*cII*^{145}.CmR, and thus derive a frequency of lysogeny of 100% for 186.*cII*^{145}.CmR, compared to ca. 10% for 186.CmR (Table 4.1).

Without proof that 186.*cII*^{145}.CmR is competent to produce a plaque, however, this result has multiple interpretations. It is possible that stabilisation of CII inhibits lytic development itself (for instance by transcriptional interference between *pR* and *pE*), rather than solely influencing the fate of the developmental switch. In this scenario, the true rate at which the switch resolves into the lysogenic state may be substantially lower than that revealed by experiment, but would be masked by 'abortive lytic' development, in which infections proceeding down a lytic path do not successfully produce a burst of daughter phage, thus yielding neither plaque nor lysogen.

Addressing this possibility, we repeated our frequency of lysogeny determination, but using a strain expressing CI-CTD as the indicator. Infections of this host should be directed more often to a lytic fate due to the dominant-negative action of CI-CTD (24) against the lysogeny maintenance repressor. Our results match this prediction exactly (Table 4.1). More importantly, using this strain we observed plaques of 186.*cII*^{145}.CmR, showing that the activity of CII145 itself does not prevent plaque formation, and suggesting that 186.*cII*^{145}.CmR does not undergo abortive lytic development (Table 4.1).

Table 4.1: Frequency of lysogeny of 186 variants.

Phage	**Host**	
	BW25113	BW25113 + pZE15-CI.CTD
186.CmR	9.64 ± 2.13%	0.03 ± 0.07%
186.*cII*^{145}.CmR	100 ± 0%	58.3 ± 3.13%

Understanding the prophage induction impairment of 186.*cII*^{145}

Having demonstrated that stabilisation of 186-CII results in an impairment of induction and an elevated frequency of lysogeny, we sought to explain the mechanism(s) by which these changes occur. In particular, impaired induction has multiple possible explanations. The simplest is that low, or 'leaky' levels of transcription from *pR* in the lysogenic state allows accumulation of CII145, in contrast to a wildtype prophage in which CII would be cleared by proteolysis. A prediction of this model is that on average, lysogens of 186.*cII*^{145}.CmR would have higher lysogenic concentrations of CI due to *pE* activity (Fig 4.1). Examining this using quantitative Western blot analysis, we find that there is no detectable change in relative lysogenic concentrations of CI in lysogens of 186.*cII*^{145}.CmR nor 186.*cII*-.CmR relative to 186.CmR (Fig. 4.5A).

Non-equilibrium effects of 186-CII stabilisation

Since the equilibrium lysogenic concentration of CI is unable to explain the impairment of 186.*cII*^{145}.CmR prophage induction we investigated the non-equilibrium effects of 186-CII stabilisation through the construction and characterisation of a minimal synthetic switch and *lacZ* reporter, integrated into the *E. coli* genome (Fig. 4.5B). Induction of 186 occurs via expression of the anti-CI factor Tum (14, 15), due to SOS mediated de-repression of the LexA-regulated *p95* promoter. Thus, integration of a *p95-tum* expression module alongside a switch construct allows investigation of the UV-induction process through reporter assays.

Following UV induction, expression of the switch reporter (Fig. 4.5B) was assayed over the ensuing 5 hours. For the wildtype construct, we expect that UV irradiation will induce expression of the antirepressor Tum, and a consequent de-repression of *pR* through Tum inhibition of CI. Our results show that de-repression of *pR* in response to UV irradiation is also detectable in the *cII*^{145} variant of the construct, but is of much lower magnitude than in the *cII*$^{+}$ or the *cII*$^{-}$ variants (Fig. 4.6B). Repression of *pR* is re-established once the SOS signal decays and *tum* becomes again repressed by LexA. This re-establishment of *pR* repression is faster in the *cII*^{145} variant.

We expected that the behaviour of the switch reporter in the *cII*^{145} variant is due to high expression of CI caused by high levels of CII-stimulated *pE* activity. Accordingly, observing the evolution of CI levels over time by Western blot, we found strongly elevated CI in the *cII*^{145} construct following induction (Fig. 4.5C). As a further test, we placed the *lac*Z gene at the left end of the switch construct to measure transcription of *cI* from *pL* and *pE* (Fig. 4.5D). This showed a large pulse of *cI* transcription in the *cII*^{145} variant, while the activity of the stable LacZ protein fell slowly in the *cII*$^{+}$ or and *cII*$^{-}$ variants. These results indicate that CII stabilisation reduces de-repression of *pR* after UV induction due to over-expression of CI to levels that exceed the sequestration capacity of Tum. Interestingly, no more than minor differences after induction are seen between the *cII*$^{+}$ and *cII*$^{-}$ variants (Fig. 4.5BCD), showing that in the presence of normal CII degradation the effects of a single copy of the wildtype *cII* gene are effectively nullified.

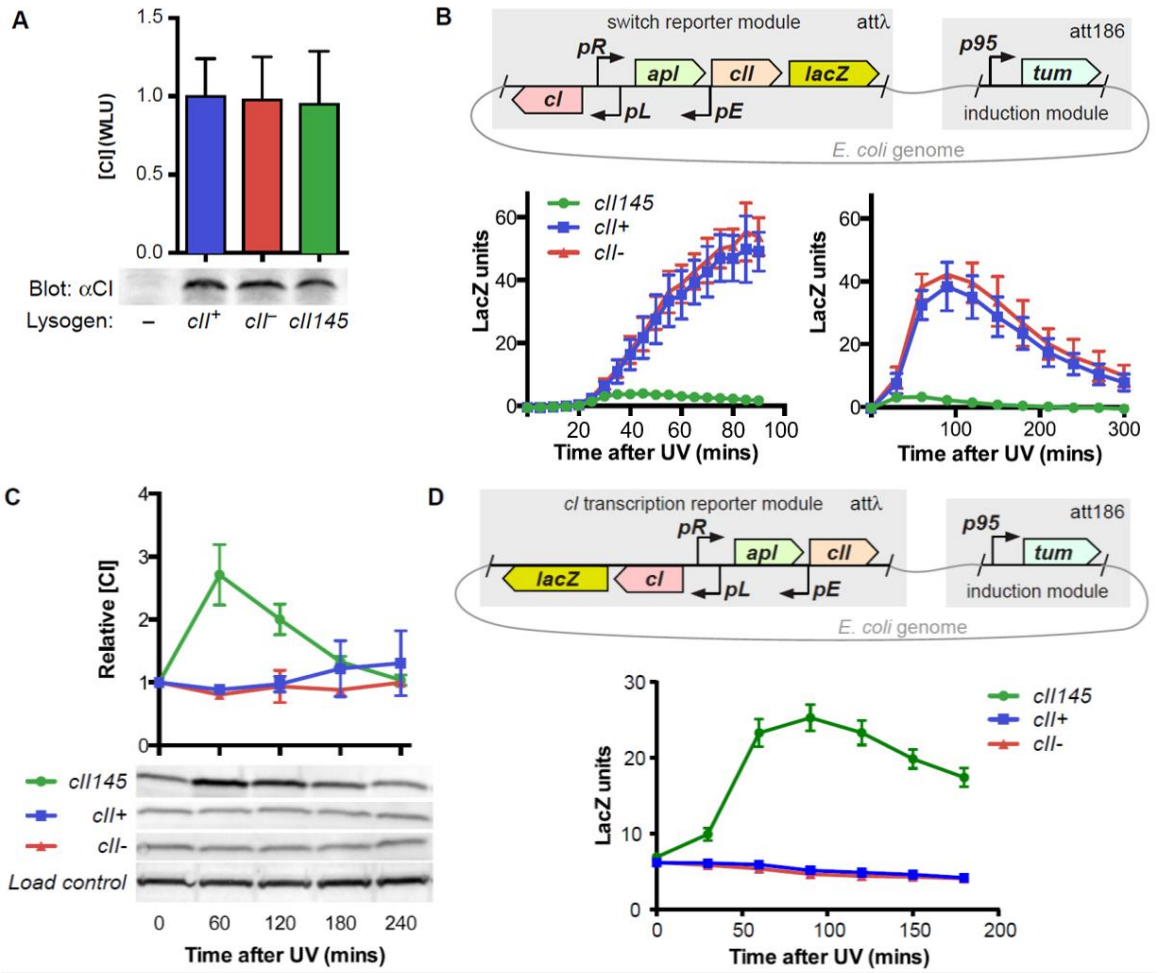

Figure 4.5: Regulatory effects of CII stabilisation. (A) Lysogenic CI concentrations of 186 variants. Relative levels of CI present in non-lysogens and lysogens of 186.CmR, 186.*cII*$^{-}$.CmR and 186.*cII*^{145}.CmR as detected by Western blot. Bars show mean and standard deviation (n=4) of quantitation of the CI band (expressed relative to 186.CmR) for experimental repeats. There was no statistically significant difference between CI levels in lysogens of 186.CmR and 186.*cII*$^{-}$.CmR (p=0.90; unpaired, two-tailed t-test), nor 186.CmR and 186.*cII*^{145}.CmR (p=0.82; unpaired, two-tailed t-test). **(B)** Timecourses of *pR* activity after UV induction. The schematic shows the switch reporter and the 186 *tum* induction module. The *lacZ* gene was translationally fused to the 186 *fil* gene. After UV irradiation (5.2 J/m^2) of strains, *pR* activity was measured by β-galactosidase assay every 5 or 30 minutes, for 90 or 300 minutes, respectively. **(C)** Expression of CI was measured by Western blot in the same irradiated cultures used for β-galactosidase assay in (B). Analysis of CI Western blots shows a significant elevation of CI in the *cII*^{145} variant following UV induction, but not in the *cII*$^{+}$ or *cII*$^{-}$ variants. Plots in (B) and (C) show mean and standard deviation (n=3). **(D)** As in (B), except the *lacZ* gene was a translational fusion to the 186 *int* gene in order to measure leftward transcription. Errors are 95% confidence limits (n=6-8).

An alternative, but not mutually exclusive mechanism for reduced de-repression of *pR* is transcriptional interference (25, 26). Because *pR* and *pE* are convergent promoters, it is possible that high levels of *pE* activity will reduce transcriptional activity from *pR*. Investigating this hypothesis, we used an integrated switch reporter construct lacking CI, and thus constitutively expressing CII, and reporting CII levels by way of a *pE-lacZ* reporter *in trans* (Fig. 4.6A). In this way, reduced *pR* activity can be detected by lower expression of the *lacZ* reporter, while the effect of *pE* activity on *pR* can be determined by mutation of the *pE* sequence in the switch construct. A confounding factor is the presence of the *apI* gene, encoding a weak repressor of *pR*, on the *pR* transcript. To address this, mutants of *apI* that abrogate DNA binding were also included in this experimental design.

For a construct encoding wildtype, unstable CII, abrogation of *pE* activity in the switch module has no detectable effect on reporter activity, while as expected, abrogation of Apl activity increases reporter activity (Fig. 4.6A). Using the *cII*^{145} variants, abrogation of neither *pE* nor Apl activity cause a statistically significant variation in reporter activity, demonstrating that even high levels of *pE* activity do not alter *pR* activity via transcriptional interference. We also compared the reporter activities from this experiment with standard curves derived by IPTG-inducible expression of 186-CII or CII145 from a plasmid (Fig. 4.6B) (9). This comparison allows us to calculate a level of IPTG induction (CII expression) that would give rise to the equivalent reporter activity as observed using the switch fragments. This analysis (Fig. 4.6) shows that the IPTG induction levels for CII and CII145 overlap, showing that the activity of *pR* is the same in the *cII*$^{+}$ and *cII*^{145} cases, adding further support to our conclusion that transcriptional interference of *pE* on *pR* is not significant.

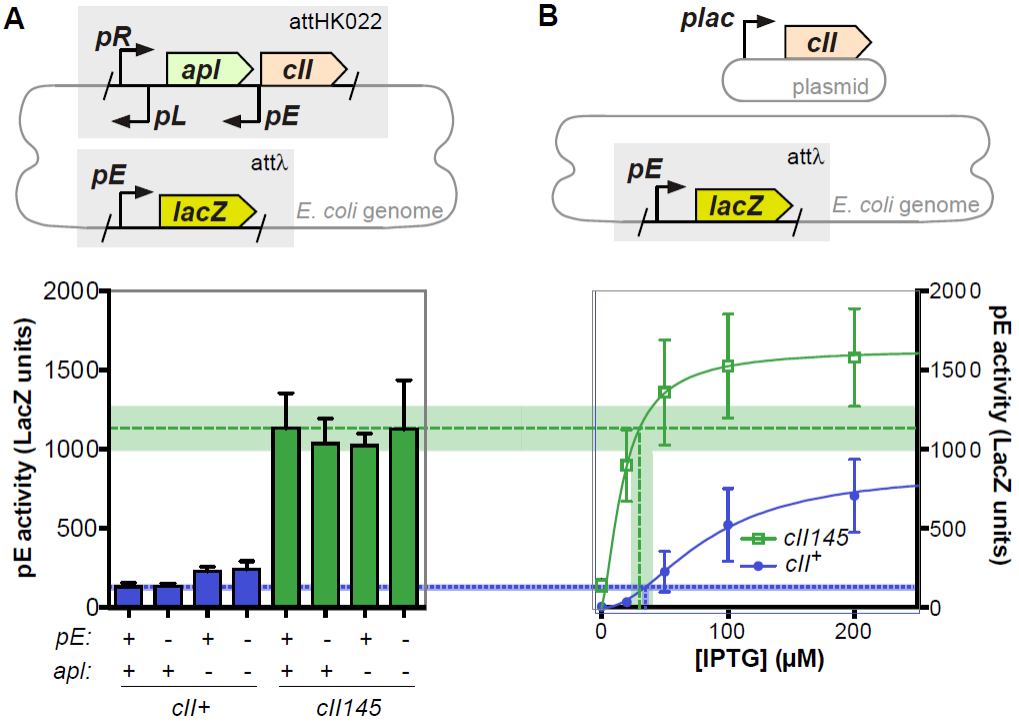

Figure 4.6: Steady-state CII activity. (A) The activity of CII expressed from the *pR* promoter in the absence of CI (upper module) was assayed by a *pE.lacZ* reporter *in trans* (lower module) by β-galactosidase assay at steady state. Bars show mean and standard deviation ($n \geq 11$). **(B)** The activity of CII expressed with IPTG induction from pZS45-CII169 or pZS45-CII145, assayed by the same reporter, as reported in (9). The plot shows the mean, standard deviation ($n \geq 6$) and Hill fits.

A mathematical model of the 186 switch

Our characterisation of 186.*cII*^{145} shows that stabilising CII both increases the frequency of lysogeny, and prevents induction of the prophage. A theoretical description of the decision-making gene network is a useful complement to these empirical observations to help better illuminate the functional consequences of CII stabilisation. In particular, it allows us to vary the parameters of any regulatory element precisely, without the constraint of what is biologically possible or evolutionarily accessible.

Such precision also allows us to incorporate pairs of changes that compensate for each other exactly, in order to preserve key characteristics of the network, while altering parameters of interest. In addition, it gives us ready, reliable and fine-scaled access to information about the dynamics of the network, especially over the short period after infection, which are technically difficult to access experimentally.

Most of the key, individual regulatory elements in the 186 switch region have previously been characterised quantitatively using empirical methods, or parameters describing their behaviour are available from previously published theoretical models. This motivated the construction of a hybrid stochastic-deterministic model of the gene regulatory network depicted in Figure 4.1B (equations are listed in Table 4.S1). The only known phenomena which were not captured in our model of the network were repression of *pE* by CI binding at its *FR* site (10), and transcriptional interference. In the case of CI binding at *FR*, a satisfactory quantitative description is not available for implementation. Transcriptional interference between *pR* and *pL* was not modelled explicitly, but a simplified treatment of its effects are inherent in the parameters used to describe CI regulation of *pL*. Short timescale events, and events driven by large numbers of molecules (protein-DNA binding equilibria, protein production and degradation) were modelled deterministically, while more sparse events (promoter firing, degradation of transcripts) were simulated stochastically as inhomogeneous Poisson processes according to a hybrid Gillespie algorithm (27).

Translation initiation rates have not previously been determined, so the measured lysogenic concentration of CI (28), the relative lysogenic concentrations of CI in variant lysogens (Fig. 4.5), and the *pE-lacZ* reporter construct data presented in Figure 4.6B were used as constraints to fit these parameters (Fig. 4.7A). Parameter optimisation was made tractable by exploiting the fact that the experimental measurements were all steady-state population averages. After verifying that over a wide parameter range the average behaviour of the stochastic model at steady state closely matched that of an equivalent deterministic model, we could fit the translation initiation rates using steady-state solutions of the deterministic model.

It should be noted that our theoretical model is not expected to exhibit clear bistability - that is, simulated infections based on the model do not yield observable, stable, distinct, 'lytic' and 'lysogenic' states. Rather, all simulations eventually produce long-run average CI concentrations corresponding to the lysogenic state, but the time taken to resolve into such a state varies between sister infection simulations. Recent experimental work (29, 30) suggests that the fate of the switch is not set in a single event, but is a consequence of a cascade of interrelated events. Under this paradigm, only lysogeny need be a genuinely stable state; the lytic cascade ends not in a stable state, but with the destruction of the host cell and release of daughter phage. Thus, the behaviour of our model can be seen as consistent with the absence of later lytic functions or any representation of phage replication in our model.

The mathematical model allowed us to explore the consequences of a wide range of alternative parameters relating to CII function. In addition to the *cII*^{145} (stabilised CII) and *cII*$^{-}$ variants examined in experiments, we are able to simulate networks in which CII is stabilised, but its activity is compromised in different ways, such as weaker binding to *pE* or lower maximal activity of *pE*. In this way, we can interrogate more directly the effects of CII half-life by constructing networks in which the equilibrium activity of *pE* is unaltered from that due to wildtype 186, but the half-life of CII is extended.

Modelling is consistent with the behaviour of CII145

We used the evolution of CI concentration over time, averaged across a population of simulated infections, as a proxy for the population's progress toward the lysogenic state to investigate the effects of CII stabilisation (Fig. 4.7B). Consistent with expectations and our experimental results, CII145 exhibited elevated CI concentrations following infection, before eventually equilibrating to a lysogenic CI concentration close to that of the wildtype network. A stabilised *cII* variant with a compensating reduction in production rate (to give steady-state CII levels equal to wildtype) did not give the overshoot in CI levels but gave a slower accumulation of CI than *cII*$^{+}$ (Fig. 4.7B), which we predict would correspond with a reduced frequency of lysogeny, as it does for the *cII*$^{-}$ variant.

Another way to view the function of CII in the network is as an additional layer of negative autoregulation of CI production (Fig. 4.1B). CI represses its own production via its action at the *pL* promoter. CI however, also represses CII production (via *pR*), which in turn causes CI production (via *pE*). Therefore, we used the model to simulate infections and examine the relationship between globally averaged CI concentrations and the net rate of CI production/loss for the network as a whole. Analysing the results this way (Fig. 4.7C) reiterates the findings described above that CII145 takes longer to equilibrate and overshoots the lysogenic concentration of CI. Additionally, however, this analysis highlights the maximal rate of net production of CI.

The significance of the maximal rate of net CI production is that in order to reduce CI concentrations to near-zero in the process of induction, the phage must produce the CI inhibitor Tum at or above this rate (or in the case of phage λ, induction must accelerate CI degradation by at least this amount). Failure to do so will result in a net accumulation of active CI and result in the phage being pushed back into the lysogenic state.

Figure 4.7C shows that the maximal CI production rate is greater than 2-fold higher for 186.*cII*^{145} relative to 186^{+}. This explains our experimental finding that UV induction is severely impaired, suggesting that only a small fraction of lysogens produce Tum at a sufficient rate to induce the phage after UV irradiation. In contrast, high rates of expression of CI-CTD from a high-copy number plasmid exceed even the 186.*cII*^{145} maximal CI production rate, yielding similar levels of induction to 186^{+}.

Modelling networks without 186-CII

Given our finding that a rapidly degraded CII helps the switch to rapidly reach yet not massively exceed the lysogenic concentration of CI, we sought to investigate whether these properties can be achieved without a CII-like factor, in a network resembling that of P2. That is, if we assume that faster equilibration to lysogenic CI concentrations is an evolutionary advantage for an inducible phage, can we expect to find inducible P2-like phages that lack a *cII* gene, but preserve the characteristics of *cII*-containing networks that we have identified here?

Without 186-CII present, the *pL* promoter would need to have a higher rate of maximal activity in order to produce CI at the requisite rate. However, simply increasing *pL* activity would also raises the equilibrium concentration of CI. Regulation of *pL* (like the analogous *pRM* promoter in phage λ) has a characteristic biphasic response to CI concentrations, with an activation phase at low [CI] and repression at higher [CI] (28, 31). Thus, increasing the strength of *pL* but increasing its repression by CI (through the EC_{50}) provides a mechanism for raising *pL* activity without a concomitant rise in equilibrium CI concentration. We adjusted these parameters to give the best fit to the 186^{+} CI concentration curve, finding that, for a *pL* strength of 1.5x, adjustments to the EC_{50} can indeed produce a close match with the average trajectory of the 186^{+} curve (Fig. 4.7D). Thus, we conclude that if faster equilibration of CI concentrations is the principal function of *cII*, then it is at least theoretically plausible for phage to evolve switch networks that lack a *cII*-like factor to achieve the same ends. However, we noticed that the rate of CI accumulation early in infection in the wildtype network was subject to less variation compared to the P2-like networks, shown by the time taken to reach 500nM CI in different simulation runs (Fig. 4.7D).

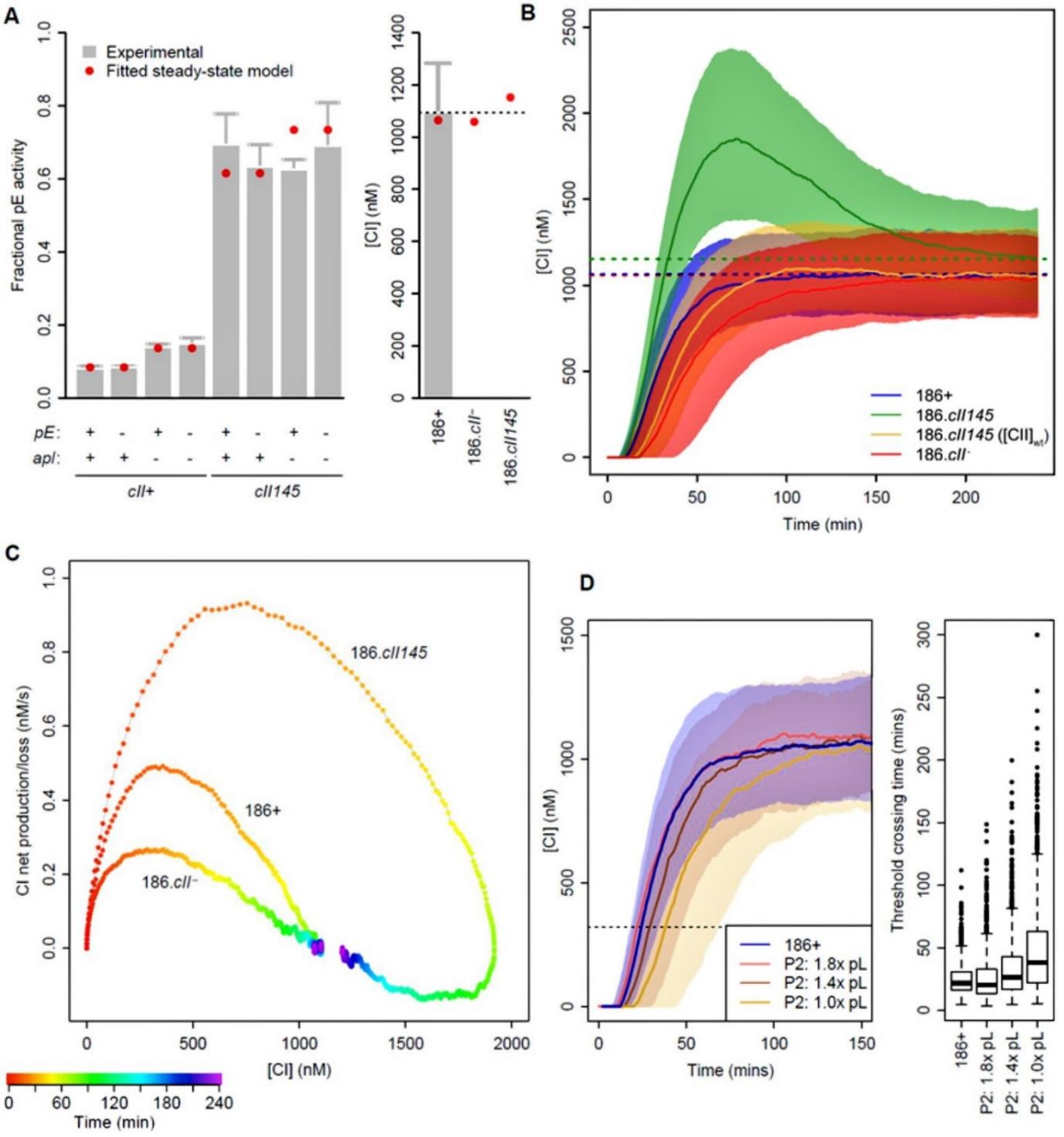

Figure 4.7: Mathematical modelling of the 186 genetic switch. (A) Translation initiation rate parameters of the model were optimised to fit (red circles) the measured *pE* activity of switch variants (left panel) and lysogenic CI concentrations (right panel). Experimental data is the same as that in Figures 4.6A and 4.5A; a fractional *pE* activity of 1 corresponds to 1635 LacZ units. **(B)** Plot of the evolution of median CI concentration over time in variants of the 186 genetic switch (*n*=3000 simulations per curve; shaded area is the interquartile range). Rapidly rising CI concentrations in the stable *cII*^{145} variant explain the high frequency of lysogeny phenotype. Slow increases in and equilibration of CI concentrations in other *cII*^{145} derivatives relative to *cII*$^{+}$ suggest a low frequency phenotype for these variants. Dotted lines indicate final lysogenic levels of CI. **(C)** Plot of CI concentration vs net CI production (*n*=3000 simulations per curve). High maximal CI production in *cII*^{145} provide an explanation for the impaired induction phenotype of this variant. **(D)** *cII*$^{-}$ gene network variants can achieve a similar evolution of CI concentrations to that of the 186+ network, in the case where *pL* activity is stronger and CI repression of *pL* is enhanced. Each curve shows median CI concentration from *n*=3000 simulations. The box plots on the right of panel D show the distribution of times at which [CI] = 320nM was reached in the simulations. This [CI] threshold represents 100x the EC_{50} for CI repression of *pR*.

Discussion

We have shown that CII is degraded by at least two essential proteases in *E. coli*, suggesting that maintenance of CII degradation is a strong evolutionary constraint on 186. Our data also show that the 186 yield of lysogens is remarkably resilient to deletions of either one of these proteases. As we have noted above, the nature of *ftsH* and *rseP* protease deletions and their phenotypes lead us to treat these data with some caution. Yet if any inference is to be drawn from these findings, it is that 186 does not use changes in protease abundance, localisation, or activity in the host to sense intracellular conditions and adjust the respective probabilities of the lytic or lysogenic fates, as is suggested to be the case for phage λ (1, 32-34).

Nonetheless, stabilisation of CII through deletion of the protease-recruiting C-terminal region yields a clearly demonstrable increase in frequency of lysogeny, and a resistance to induction through over-production of CI following the induction stimulus. Though we have reported a 100% frequency of lysogeny, the true frequency may be slightly lower than 100%. This is because visible plaques will cease to form at a true frequency of lysogeny below 100%, since at high frequencies of lysogeny, insufficient quantities of daughter phage will be produced through lytic development to continue the expansion of a plaque to a visible size.

A tightly specified mathematical model of the 186 switch genetic circuit matched experimental results from this and other studies closely. Our mathematical model can also explain both the increased frequency of lysogeny and impaired induction phenotypes of 186.*cII*^{145}. Simulations of 186 variants suggest that varying only the activity of CII results in a trade-off between quickly rising CI concentrations that enable an early decision upon infection, and fast establishment of a low but stable lysogenic CI concentration that facilitates induction. Fast degradation of a highly active CII reduces the severity of this trade-off, enabling fast-rising and fast-equilibrating CI concentration trajectories. Both of these properties are likely to be crucial in a competitive ecosystem with multiple phages. Fast lytic development is an obvious competitive advantage, but requires a commensurately rapid developmental decision.

Maximal CI production rates from 186+ and 186.*cII*^{145} trajectories satisfactorily explain the induction impairment of 186.*cII*^{145}, but falsely predict that 186.*cII*$^{-}$ will induce more readily than 186.*cII*+. This could be explained by suppression of CII activity by SOS-induced host factors during induction, in an analogous manner to that observed in phage λ (35), however such a phenomenon has not been tested in 186. One possibility is that inhibition of *pE* by CI binding at *FR* (10) reduces CI production during prophage induction due to CI activity that escapes inactivation by Tum. The λ phenomenon is saturable; over-expression of λCII restores its function during induction (35), which is directly analogous to our data showing CII145 activity following induction.

The results of infection simulations suggest that a key function of a highly active, rapidly degraded CII is to rapidly equilibrate CI concentrations in a lysogen. This has the advantage of ensuring that the lysogen is established and ready for induction as soon after infection as possible. One would expect this to be a more important property for SOS-inducible phages than non-inducible phages, which rely passively on spontaneous induction and so need not prefer an induction-ready state. An alternative mechanism to achieve rapid equilibration of CI concentrations is for CI itself to be rapidly degraded. Others however, have noted that a short CI half-life is likely to be detrimental to the lysogeny-maintenance function of CI, since a short-lived CI is more sensitive to stochastic noise in CI transcription (36).

Modelling of 186.*cII*$^{-}$ variants also suggests that rapid equilibration of CI concentrations could also be achieved by increasing *pL* activity, while increasing CI negative autoregulation through *pL* repression. While this is a simple adjustment to make in a theoretical model, the biological accessibility of this parameter space may well be more limited. CI repression of *pL* and *pR* is the product of a high-order multimer binding to five distinct operators (24, 37) and increased CI binding to *pL* is likely to also affect *pL* activation and *pR* repression. Thus, the addition of a delayed negative feedback such as the *cII-pE* system to the switch network may represent a more evolutionarily accessible solution. The use of an additional CII-like factor in the network has other advantages. The opportunity to respond differently during infection and induction is one such example, as described above in the case of SOS-induced inactivation of λCII at low concentrations. Our analysis suggests also that the CII-containing network showed reduced variability in the rate of CI accumulation, though whether this would be an advantage for the phage is not clear.

From a synthetic biology circuit design perspective, the use of a CII-like delayed negative feedback similarly presents a simple mechanism to create additional layers of pseudo-autoregulation, without needing to engineer complex promoters. Where the purpose of a CII-like delayed negative feedback is as a form of autoregulation, a short CII half-life is an essential element of this design. With rapid, continuous degradation of CII, the cellular concentration of CII most accurately encodes the immediate past activity of *pR*, and so is a reasonable approximation of current *pR* activity. In contrast, a stable CII results in cellular concentrations of CII that encode *pR* activity averaged over a long window of the past. If the aim is to regulate CI production with respect to its current concentration, then a stable CII builds into the genetic network an unwanted memory of past CI concentrations and *pR* activities.

Experimental procedures

Strains and constructs

A8295 = W3110 *sfhC zad-220::Tn10,* and A8296, its *ΔftsH3::kan* (38) derivative (= AR3291 and AR3289 of (22)), were obtained from Amos Oppenheim. KK211 is a *ΔrseP::kan* derivative of AD1811 *Δpro-lac thi ΔrseA::cat* /F'*lacI*^{q} ZM15 *Y*$^{+}$ *pro*$^{+}$ (20), obtained from Y. Akiyama (Kyoto University).

KK372 is a *ΔdegS::tet* derivative (20) of CU141 *araD139 Δ(argF-lac)$_{U169}$ rpsL150 relA1 flbB5301 deoC1 ptsF25 rbsR*/F'lacIq Z$^+$Y$^+$ pro$^+$ (39), obtained from Y. Akiyama (Kyoto University). Strains used for reporter assays were derivatives of *Escherichia coli* strain BW25113 *lacI^q rrnB$_{T14}$* Δ*lacZ$_{W316}$ hsdR514* Δ*araBAD$_{LD78}$* (40). The *cII$^-$* mutation was V36E/Q37S in the helix-turn-helix DNA-binding motif (9). The *apl$^-$* mutation was E28R/R29E/R33Q in the helix-turn-helix DNA-binding motif. The *pE$^-$* mutation was KS11 (41).

CII expression plasmids pZS45-CII169 (9) and pZS15-CII169 are pSC101 origin plasmids carrying spectinomycin or ampicillin resistance, respectively. Both express CII169 under the control of the wildtype *lac* promoter (with *O3* and *O1*) and the ribosome binding site from pET3a. pZE15-CI.CTD is pZE15-CI.CTDα, a colE1 origin plasmid carrying ampicillin resistance and expressing the 186 CI-CTD fused to the LacZα fragment (24), with promoter and RBS as for pZE15-CII169.

To make the switch reporter (Fig. 4.5B), 186 DNA fragments (*cII$^+$*, *cII$^-$* or *cII^{145}*) extending from the left end of the *cI* gene to the start of the *fil* gene (downstream of *cII*) were cloned into pIT3-CL*lac*Ztrimfuse (42) such that the first 3 codons of *fil* are fused to the 9th codon of *lacZ(O2$^-$)*. The plasmids were integrated into the λ*att* site. The leftward switch reporter (Fig. 4.5D) was made the same way except the 186 fragments are reversed, extending from the end of the *cII* gene, with codon 9 of *int* (downstream of *cI*) fused to codon 9 of *lacZ(O2$^-$)*. The *tum* induction module contains a wildtype 186 *p95.tum* fragment (Genbank: U32222.1 pos. 28984-29538) cloned into pIT3-TO (42) and inserted at the primary 186*att* site (43).

The *pE* reporter (Fig. 4.6) was pIT3-CL-*pE.lacZ* (9) integrated into the λ*att* site. The *pR.apl.cII* expression module (Fig. 4.6) contained 186 DNA (*apl$^+$/apl$^-$*, *pE$^+$/pE$^-$*) from codon 10 of *cI* to the end of *cII*, inserted into pIT3-TH (tetracycline resistant) and integrated into the HK022 *att* site.

Construction of phage mutants

186.*CmR* was constructed by insertion of a chloramphenicol resistance cassette into the sequence between *cos* and *tW* by recombineering with pKD46 (44). Construction of 186.*cII^{145}* and 186.*cII$^-$* mutants used a two-step recombineering protocol (45). In the first step, the *cII* gene of a wildtype 186 prophage was replaced with a *cII^{145}* or *cII$^-$* gene and a selection cassette containing both a chloramphenicol resistance gene and superfolder GFP. In the second step, the selection cassette was deleted from the prophage by recombineering with a single-stranded DNA oligonucleotide. Colonies were screened for a loss of GFP expression. Two independent 186.*cII^{145}* lysogens were obtained and the sequence of the entire switch region from *int* to *fil* confirmed. 186.*cII^{145}* and 186.*cII$^-$* phage were made CmR using pSIM6-based recombineering (46) using the same chloramphenicol resistance cassette described above.

In vivo degradation

In vivo CII degradation assays of Figure 4.2 were conducted as previously described (9), with pZS45-CII169-containing cells grown with 50µg/mL spectinomycin and 100µM IPTG to mid-log phase, and translation inhibited with chloramphenicol (100µg/mL). For Figure 4.3, pZS15-CII169-containing cells were grown with 100µg/mL ampicillin and 100µM IPTG, and translation was stopped using 200µg/mL spectinomycin.

Yield of lysogens

Yield of lysogens (the number of lysogens per added phage) was measured according to (47), where addition of 186*cI10* phage kills any non-lysogenic bacteria, but allows lysogens to grow.

Frequency of lysogeny

Frequency of lysogeny experiments were carried out using phage carrying chloramphenicol resistance as previously described (48), except that media were not supplemented with $MgSO_4$ or maltose, and indicator cultures were not concentrated prior to infection. Adsorption was 90-95% efficient. A strain harbouring the pZE15-CI.CTD plasmid was used as an indicator for infectious centre and free phage assays, with growth and plate media supplemented with ampicillin to 100µg/mL and IPTG to 200µM.

UV induction assays

Lysogens were cultured overnight at 37°C in M9 minimal media containing 0.5mM glucose, supplemented with 10µM $Fe(SO_4)_2$ and 10µg/mL chloramphenicol. Following overnight growth, cultures were supplemented with 20% glucose to a final glucose concentration of 20mM, and growth at 37°C was continued to log phase. Log phase cultures were diluted 1/1000 into fresh M9 minimal media (20mM glucose) + 0.1% TWEEN-20, and 5mL was UV irradiated (0.13 W/m^2) uncovered in a 90mm Petri dish for up to 4 minutes. Prior to and following UV treatment an aliquot was plated on LB agar to assay cell density and survival.

For plaque detection, irradiated cultures were added to BW25113 indicator and 0.7% top agar and immediately plated on TB agar. For lysogen detection, irradiated cultures were added to log phase cultures of the spectinomycin-resistant indicator BW25113 (pIT-SL), and infection was allowed to occur over 10 minutes. Lysogens were detected by plating on dual-selective LB agar media containing 10µg/mL chloramphenicol and 20µg/mL spectinomycin.

CI-CTD induction assays

Cultures of lysogens harbouring the pZE15-CI.CTD and pUHA-1 plasmids were grown overnight at 37°C in LB supplemented with 100µg/mL ampicillin and 50µg/mL kanamycin. Overnight cultures were collected by centrifugation and washed twice with an equal volume of fresh media to remove phage particles that may have accumulated due to spontaneous induction.

Cultures were diluted to OD_{600} 0.20 in LB + 100µg/mL ampicillin, 50µg/mL kanamycin and 200µM IPTG and cultured at 37°C for 2 hours. Phage stocks were prepared from these cultures by centrifugation and treatment with chloroform, and used to infect log-phase cultures of the indicator BW25113 (pIT-SL). Infection was allowed to occur over 10 minutes, before infection mixtures were plated on dual-selective LB agar media containing 10µg/mL chloramphenicol and 20µg/mL spectinomycin to select for new lysogens.

LacZ assays

Kinetic LacZ assays in 96-well microtitre plates were performed as previously described (26).

UV timecourse

Switch reporter strains were cultured overnight at 37°C in M9 minimal media containing 0.5mM glucose, supplemented with 10µM $Fe(SO_4)_2$, 10µg/mL chloramphenicol, and 4µg/mL tetracycline. (For the *cI* transcription reporter, overnight growth was in 1mM glucose and tetracycline was omitted). Following overnight growth, cultures were supplemented with 20% glucose to a final glucose concentration of 20mM, diluted to OD_{600} 0.15, and growth at 37°C was continued to early log phase (OD_{600} 0.30-0.40). 5mL culture + 0.1% TWEEN-20 as a wetting agent was transferred to a 90mm plastic Petri dish and an aliquot was taken and stored on ice. The culture was UV-irradiated (0.13 W/m^2) uncovered for 40 seconds, and returned to a flask for continued incubation with shaking at 37°C. The culture was occasionally diluted during longer incubations to maintain log phase growth. Aliquots were removed from culture at intervals, OD_{600} measured, and stored on ice for LacZ assay. For experiments conducted over 5 hours, the experimental culture was diluted to OD_{600} 0.30 and an aliquot was pelleted and stored at -20°C every hour. Cell pellets were subsequently analysed by Western blot.

Mathematical modelling

Simulations were conducted using a modified Gillespie algorithm that maintains well-synchronised discrete and continuous versions of each state variable to enable inter-related deterministic and stochastic calculations to take place. The hybrid algorithm numerically integrates deterministic equations between each stochastic event, and updates the cumulative hazard for stochastic events according to a time-dependent hazard function. The differential equations and hazard functions governing our model are described in Supplementary Table 4.S1. Variants of the wildtype 186 genetic circuit were modelled by altering model parameters, as described in Supplementary Table 4.S2.

Transcripts were modelled explicitly, and in the absence of data regarding degradation rates, were assumed to have mean lifetimes similar to the global average for *E. coli* (49). Further details of the mathematical modelling and fitting procedure are included in the Supplementary Information.

Acknowledgements

This work was funded by the Australian Research Council grants DP150103009 and DP160101450. We thank Prof. Yoshinori Akiyama (Kyoto University), Don Court (National Cancer Institute) and Amos Oppenheim (Hebrew University) for strains, Danna Lee for pIT3-TO-*p95.tum*, and Barry Egan, Nan Hao and Jia Truong for discussions.

Supplementary information

Mathematical model of the bacteriophage 186 switch region

Our model of the bacteriophage 186 switch region attempts to capture the most important known regulatory interactions that impact on the decision between lytic or lysogenic development upon infection of a bacterium. The decision made in a single cell is thought to be stochastic as a result of fluctuations at the molecular scale. Whilst much is understood about the average behaviour of the regulatory network, the primary sources of noise for bacteriophage 186 are unknown. Nonetheless, it is likely that stochastic production and degradation of the transcripts play a significant role, so for simplicity we limit the stochastic treatment to just those reactions, treating the remaining reactions deterministically. Custom software for simulation of hybrid stochastic-deterministic models using the 'next reaction' variant of Gillespie's algorithm was written in C++ with an API written for R to facilitate model specification. Software is available on request.

The reactions included in the model are listed in Table 4.S1 and describe regulation of the lytic (*pR*), lysogenic (*pL*) and establishment (*pE*) promoters by the products of the lytic transcript (Apl and CII) and by the product of the lysogenic transcript (CI). Variants from the wildtype phage were simulated by simple adjustments to the parameters as listed in Table 4.S2. The trans-*pE-lacZ* reporter strains were modelled as a CI^- network, taking the hazard for production of *pE* transcripts as proportional to LacZ activity, with equality when both are normalised by maximum promoter activity. In Figure 4.7C, the rate of production/loss of CI was calculated directly at each time point as the value of equation 8 in Table 4.S1. Regulation of *pR* and *pL* activity by the repressor CI is non-trivial, involving both multimerisation of the transcription factor at the DNA and transcriptional interference between the promoters. A detailed model of both processes has previously been described (51, 52) and was fit to population measurements of promoter activity for inducible concentrations of CI (28). For simplicity and clarity in this context, however, we chose instead to fit that data using Hill equations in the concentration of CI (equations 3 and 5 in Table 4.S1). The best least squares fit to the experimental data is shown in Figure 4.S1. Estimates for many of the other parameters have been determined previously. The degradation rate of CII was from (9), and the rates of loss of CI and Apl were assumed to be dilution limited. Promoter firing rates for *pR* and *pL* were from (51), with that for *pE* being estimated similarly by comparing promoter strengths. CII activation of the *pE* promoter was modelled as a Hill function with parameters fit to *in vitro* transcription data (9) repression was assumed to act equally on *pR* and *pL*, with parameters from a fit of 7-site gel shift data (53).

The protein translation rates and transcript degradation rates could not be determined from elsewhere. For the translation rates, we noted that over a broad range of parameters, simulations of the steady-state behaviour of lysogenic phage (corresponding to the variants in Fig. 4.5A) and of the *trans-pE* reporter strains (Fig. 4.6A) showed average behaviour that closely matched that of the equivalent deterministic model. As such, we were able to fit these parameters to reproduce the experimental data (Fig. 4.7A) by solving the equivalent deterministic model at steady state. A weighted least squares scheme was used in which residual errors were generally assumed to scale with the magnitude of the model output. Specifically, the following equation was minimised:

$$R^2 = \sum_{l \in L} \left(\frac{[CI]_t^{(l)}}{[CI]_t^{(expt)}} - 1 \right)^2 + \sum_{t \in T} \left(\frac{[Z]^{(t)}}{[Z]^{(expt,t)}} - 1 \right)^2, \qquad \textbf{(1)}$$

where $[CI]_t^{(l)}$ is the average total concentration of CI in each of the three lysogen variants, and $[Z]^{(t)}$ and $[Z]^{(expt,t)}$ are, respectively, the average values of *trans-pE* activity (normalised by maximum *pE* activity) for each of the eight *trans-pE* reporter variants. We had no data with which to fit the transcript degradation rates, so made them all equal, choosing a value typical of mRNA half-lives observed in *E. coli* (49). We note that within a biologically feasible range, the transcript degradation rates had little influence on the model outputs of interest.

Table 4.S1: Reactions included in the mathematical model of the bacteriophage 186 switch region.

Gene network component	Mathematical description	Parameter values
Stochastically modelled inhomogeneous Poisson processes with time-varying hazard $\lambda(t)$		
1. Production of *pE* transcripts. Each event yields one *pE* transcript (*pEt*).	$\lambda(t) = r_{pE} \times \frac{\left(\frac{[CII]_t}{EC50_{pE}}\right)^{h_{pE}}}{1 + \left(\frac{[CII]_t}{EC50_{pE}}\right)^{h_{pE}}}$	$r_{pE} = 0.030\text{s}^{-1}$ $EC50_{pE} = 12\text{nM}$ $h_{pE} = 1.17$
2. Degradation of *pE* transcripts. Each event destroys one *pEt*.	$\lambda(t) = \frac{\log 2}{\langle lifetime_{pEt} \rangle} [pEt]_t$	$\langle lifetime_{pEt} \rangle = 300\text{s}$
3. Production of *pL* transcripts. Each event yields one *pL* transcript (*pLt*).	$\lambda(t) = frac(Apl) \times r_{pL} \times \left(B_{pL(Act)} + \frac{\left(\frac{[CI]_t}{EC50_{pL(Act)}}\right)^{h_{pL(Act)}}}{1 + \left(\frac{[CI]_t}{EC50_{pL(Act)}}\right)^{h_{pL(Act)}}} \right) \times \frac{1}{1 + \left(\frac{[CI]_t}{EC50_{pL(Rep)}}\right)^{h_{pL(Rep)}}}$	$r_{pL} = 0.0056\ \text{s}^{-1}$ $B_{pL(Act)} = 0.12$ $EC50_{pL(Act)} = 144\text{nM}$ $h_{pL(Act)} = 1.00$ $EC50_{pL(Rep)} = 530\text{nM}$ $h_{pL(Rep)} = 1.23$
4. Degradation of *pL* transcripts. Each event destroys one *pLt*.	$\lambda(t) = \frac{\log 2}{\langle lifetime_{pLt} \rangle} [pLt]_t$	$\langle lifetime_{pLt} \rangle = 300\text{s}$
5. Production of *pR* transcripts. Each event yields one *pR* transcript (*pRt*).	$\lambda(t) = r_{pR} \times \frac{1}{1 + \left(\frac{[CI]_t}{EC50_{CI}}\right)^{h_{CI}}} \times frac(Apl)$	$r_{pR} = 0.056\ \text{s}^{-1}$ $EC50_{CI} = 3.2\text{nM}$ $h_{CI} = 0.73$

Gene network component	Mathematical description	Parameter values
6. Degradation of *pR* transcripts. Each event destroys one *pRt*.	$\lambda(t) = \frac{\log 2}{\langle lifetime_{pRt} \rangle}[pRt]_t$	$\langle lifetime_{pRt} \rangle = 300\text{s}$
Deterministically modelled processes		
7. Fractional inhibition of *pR*-*pL* by Apl.	$frac(Apl) = \frac{1}{1 + \left(\frac{[Apl]}{EC50_{Apl}}\right)^{h_{Apl}}}$	$EC50_{Apl} = 265\text{nM}$ $h_{Apl} = 2.8$
8. Production/degradation of CI from *pL* and *pE* transcripts.	$\frac{d[CI]}{dt} = \rho_{CI}([pLt]_t + [pEt]_t) - D_{CI}[CI]_t$	$\rho_{CI} = 0.56\ \text{nM.s}^{-1}$ $D_{CI} = 3.9 \times 10^{-4}\ \text{s}^{-1}$
9. Production of Apl from *pR* transcripts.	$\frac{d[Apl]}{dt} = \rho_{Apl}[pRt]_t - D_{Apl}[Apl]_t$	$\rho_{Apl} = 5.6 \times 10^{-3}\ \text{nM.s}^{-1}$ $D_{Apl} = 3.9 \times 10^{-4}\ \text{s}^{-1}$
10. Production of CII from *pR* transcripts.	$\frac{d[CII]}{dt} = \rho_{CII}[pRt]_t - D_{CII}[CII]_t$	$\rho_{CII} = 4.5 \times 10^{-4}\ \text{nM.s}^{-1}$ $D_{CII} = 4.4 \times 10^{-3}\ \text{s}^{-1}$

Table 4.S2: Parameter adjustments used to specify variants of the 186 switch genetic circuit.

Simulation variant	Parameter alteration(s) from wildtype
CI⁻	$\rho_{CI} = 0$
Apl⁻	$\rho_{Apl} = 0$
CII⁻	$\rho_{CII} = 0$
CII145	$D_{CII} = 3.9 \times 10^{-4}\ \text{s}^{-1}$
pE⁻	$\rho_{CII} = 0$
P2-like network (1.0x *pL*)	$\rho_{CII} = 0, EC50_{pL(Rep)} = 570\text{nM}$
P2-like network (1.4x *pL*)	$\rho_{CII} = 0, EC50_{pL(Rep)} = 390\text{nM}$
P2-like network (1.8x *pL*)	$\rho_{CII} = 0, EC50_{pL(Rep)} = 300\text{nM}$

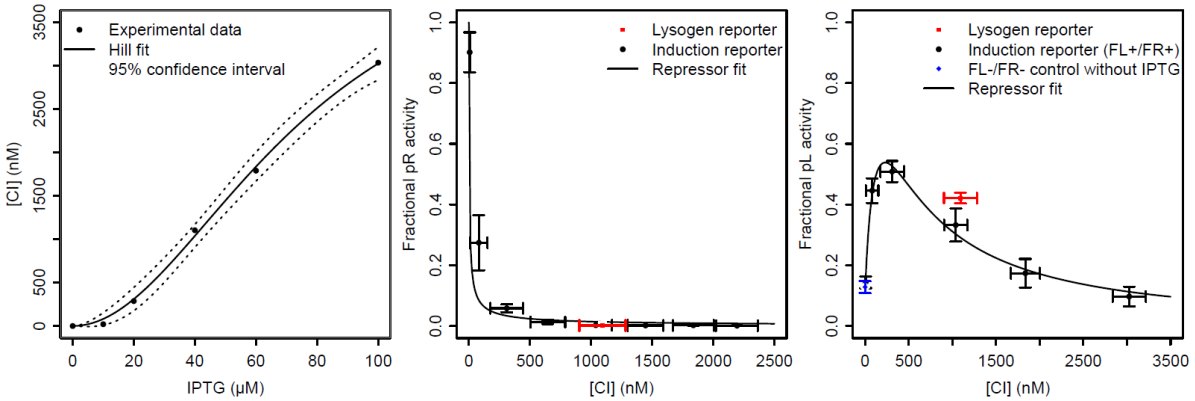

Figure 4.S1: Transcriptional interference and CI repression at *pL* and *pR* can be approximated using a combination of Hill functions. The left panel shows a Hill fit for protein induction ultra-sensitivity, relating inducer concentrations to concentrations of CI measured by Western blot (28) The middle and right panels show reporter data (28) for the switch region of bacteriophage 186 at the inducer concentrations shown in the left panel. Red squares indicate experimental measurements of promoter activity at lysogenic concentrations of CI. The black line shows the fit of the model.

References

1. Ptashne, M., 2004. A Genetic Switch Phage Lambda Revisited (Third Edition), In: Weisberg, R.A., The Quarterly Review of Biology **79**, 427-428. https://doi.org/10.1086/428187.

2. Bednarz, M., Halliday, J.A., Herman, C., Golding, I., 2014. Revisiting Bistability in the Lysis/Lysogeny Circuit of Bacteriophage Lambda. *PLoS ONE* **9**.

3. Balázsi, G., van Oudenaarden, A., Collins, J.J., 2011. Cellular Decision Making and Biological Noise: From Microbes to Mammals. *Cell* **144**, 910–925.

4. Golding, I., 2016. Single-Cell Studies of Phage λ: Hidden Treasures Under Occam's Rug. *Annual Review of Virology* **3**, 7.1-7.20.

5. Oppenheim, A.B., Kobiler, O., Stavans, J., Court, D.L., Adhya, S., 2005. Switches in Bacteriophage Lambda Development. *Annual Review of Genetics* **39**, 409–429.

6. Herman, C., Ogura, T., Tomoyasu, T., Hiraga, S., U.S.A., Y., Ito, K., Thomas, R., D'Ari, R., Bouloc, P., 1993. Cell growth and lambda phage development controlled by the same essential Escherichia coli gene, ftsH/hflB. *PNAS U.S.A.* **90**, 10861–10865.

7. Banuett, F., Hoyt, M.A, McFarlane, L., Echols, H., Herskowitz, I., 1986. hflB, a new *Escherichia coli* locus regulating lysogeny and the level of bacteriophage lambda cII protein. *Journal of Molecular Biology* **187**, 213–224.

8. Hoyt, M.A, Knight, D.M., Das, A., Miller, H.I., Echols, H., 1982. Control of phage lambda development by stability and synthesis of cII protein: role of the viral cIII and host hflA, himA and himD genes. *Cell* **31**, 565–573.

9. Murchland, I., Ahlgren-Berg, A., Priest, D.G., Dodd, I.B., Shearwin, K.E., 2014. Promoter Activation by CII, a Potent Transcriptional Activator from Bacteriophage 186. J*ournal of Biological Chemistry* **289**, 32094–32108.

10. Neufing, P.J., Shearwin, K.E., Camerotto, J., Egan, J.B., 1996. The CII protein of bacteriophage 186 establishes lysogeny by activating a promoter upstream of the lysogenic promoter. *Molecular Microbiology* **21**, 751–61.

11. Nilsson, H., Cardoso-Palacios, C., Haggård-Ljungquist, E., Nilsson, A.S., 2011. Phylogenetic structure and evolution of regulatory genes and integrases of P2-like phages. *Bacteriophage* **1**, 207–218.

12. Christie, G.E, Calendar, R., 2016. Bacteriophage P2. *Bacteriophage* **7081**, e1145782.

13. Roberts, J.W., Roberts, C.W., Craig, N.L., 1978. Escherichia coli recA gene product inactivates phage lambda repressor. *PNAS* **75**, 4717–4718.

14. Lamont, I., Brumby, A.M., Egan, J.B., 1989. UV induction of coliphage 186: prophage induction as an SOS function. *PNAS U.S.A.* **86**, 5492–5496.

15. Shearwin, K.E., Brumby, A.M., Egan, J.B., 1998. The Tum protein of coliphage 186 is an antirepressor. *Journal of Biological Chemistry* **273**, 5708–5715.

16. Kobiler, O., Rokney, A., Friedman, N., Court, D.L., Stavans, J., Oppenheim, A.B., 2005. Quantitative kinetic analysis of the bacteriophage λ genetic network. *PNAS* **102**, 4470–4475.

17. Lamont, I., Richardson, H., Carter, D.R., Egan, J.B., 1993. Genes for the establishment and maintenance of lysogeny by the temperate coliphage 186. *Journal of Bacteriology* **175**, 5286–5288.

18. Goryshin, I.Y., Jendrisak, J., Les, M., Meis, R., Reznikoff, W.S., 2000. Insertional transposon mutagenesis by electroporation of released Tn5 transposition complexes. *Nature Biotechnology* **18**, 97–100.

19. Baba, T., Ara, T., Hasegawa, M., Takai, Y., Okumura, Y., Baba, M., Datsenko, K.A., Tomita, M., Wanner, B.L., Mori, H., 2006. Construction of Escherichia coli K-12 in-frame, single-gene knockout mutants: The Keio collection. *Molecular Systems Biology* **2**.

20. Kanehara, K., Ito, K., Akiyama, Y., 2002. YaeL (EcfE) activates the sigma E pathway of stress response through a site-2 cleavage of anti-sigma E, RseA. *Genes & Development* **16**, 2147–2155.

21. Akiyama, Y., Kanehara, K., Ito, K., 2004. RseP (YaeL), an *Escherichia coli* RIP protease, cleaves transmembrane sequences. *The EMBO Journal* **23**, 4434–4442.

22. Ogura, T., Inoue, K., Tatsuta, T., Suzaki, T., Karata, K., Young, K., Su, L.-H., Fierke, C.A., Jackman, J.E., Raetz, C.R.H., Coleman, J., Tomoyasu, T., Matsuzawa, H., 1999. Balanced biosynthesis of major membrane components through regulated degradation of the committed enzyme of lipid A biosynthesis by the AAA protease FtsH (HflB) in Escherichia coli. *Molecular Microbiology* **31**, 833–844.

23. Herman, C., Thévenet, D., D'Ari, R., Bouloc, P., 1995. Degradation of sigma 32, the heat shock regulator in Escherichia coli, is governed by HflB. *PNAS U.S.A.* **92**, 3516–3520.

24. Pinkett, H.W., Shearwin, K.E., Stayrook, S., Dodd, I.B., Burr, T., Hochschild, A., Egan, J.B., Lewis, M., 2006. The structural basis of cooperative regulation at an alternate genetic switch. *Molecular Cell* **21**, 605–615.

25. Shearwin, K.E., Callen, B.P., Egan, J.B., 2005. Transcriptional interference - A crash course. *Trends in Genetics* **21**, 339–345.

26. Palmer, A.C., Ahlgren-Berg, A., Egan, J.B., Dodd, I.B., Shearwin, K.E., 2009. Potent Transcriptional Interference by Pausing of RNA Polymerases over a Downstream Promoter. *Molecular Cell* **34**, 545–555.

27. Kiehl, T.R., Mattheyses, R.M., Simmons, M.K., 2004. Hybrid simulation of cellular behavior. *Bioinformatics* **20**, 316–322.

28. Dodd, I.B., Egan, J.B., 2002. Action at a distance in CI repressor regulation of the bacteriophage 186 genetic switch. *Molecular Microbiology* **45**, 697–710.

29. Svenningsen, S.L., Semsey, S., 2014. Commitment to Lysogeny Is Preceded by a Prolonged Period of Sensitivity to the Late Lytic Regulator Q in Bacteriophage λ. *Journal of Bacteriology* **196**, 3582–3588.

30. Zeng, L., Skinner, S.O., Zong, C., Sippy, J., Feiss, M., Golding, I., 2010. Decision Making at a Subcellular Level Determines the Outcome of Bacteriophage Infection. Cell 141, 682–691.

31. Cui, L., Murchland, I., Shearwin, K.E., Dodd, I.B., 2013. Enhancer-like long-range transcriptional activation by CI-mediated DNA looping. *PNAS* **110**, 2922–2927.

32. St-Pierre, F., Endy, D., 2008. Determination of cell fate selection during phage lambda infection. *PNAS U.S.A.* **105**, 20705–20710.

33. Herskowitz, I., Hagen, D., 1980. The Lysis-Lysogeny Decision of Phage lambda: Explicit Programming and Responsiveness. An*nual Review of Genetics* **14**, 399–445.

34. Kobiler, O., Rokney, A., Oppenheim, A.B., 2007. Phage Lambda CIII: A Protease Inhibitor Regulating the Lysis-Lysogeny Decision. *PLoS ONE* **2**, e363.

35. Rokney, A., Kobiler, O., Amir, A., Court, D.L., Stavans, J., Adhya, S., Oppenheim, A.B., 2008. Host responses influence on the induction of lambda prophage. *Molecular Microbiology* **68**, 29–36.

36. Avlund, M., Krishna, S., Semsey, S., Dodd, I.B., Sneppen, K., 2010. Minimal Gene Regulatory Circuits for a Lysis-Lysogeny Choice in the Presence of Noise. *PLoS ONE* **5**, 1–7.

37. Wang, H., Dodd, I.B., Dunlap, D.D., Shearwin, K.E., Finzi, L., 2013. Single molecule analysis of DNA wrapping and looping by a circular 14mer wheel of the bacteriophage 186 CI repressor. *Nucleic Acids Research* **41**, 5746–5756.

38. Akiyama, Y., Ogura, T., Ito, K., 1994. Involvement of FtsH in protein assembly into and through the membrane. I. Mutations that reduce retention efficiency of a cytoplasmic reporter. *The Journal of Biological Chemistry* **269**, 5218–5224.

39. Akiyama, Y., Ito, K., 2003. Reconstitution of Membrane Proteolysis by FtsH. *Journal of Biological Chemistry* **278**, 18146–18153.

40. Datsenko, K.A., Wanner, B.L., 2000. One-step inactivation of chromosomal genes in Escherichia coli K-12 using PCR products. *PNAS* **97**, 6640–6645.

41. Shearwin, K.E., Egan, J.B., 2000. Establishment of lysogeny in bacteriophage 186 DNA binding and transcriptional activation by the CII protein. *Journal of Biological Chemistry* **275**, 29113–29122.

42. Priest, D.G., Cui, L., Kumar, S., Dunlap, D.D., Dodd, I.B., Shearwin, K.E., 2014. Quantitation of the DNA tethering effect in long-range DNA looping in vivo and in vitro using the Lac and λ repressors. *PNAS U.S.A.* **111**, 349–54.

43. St-Pierre, F., Cui, L., Priest, D.G., Endy, D., Dodd, I.B., Shearwin, K.E., 2013. One-Step Cloning and Chromosomal Integration of DNA. *ACS Synthetic Biology* **2**, 537–541.

44. Datsenko, K.A., Wanner, B.L., 2002. One-step inactivation of chromosomal genes in Escherichia coli K-12 using PCR products. *PNAS* **97**, 6640–6645.

45. Sharan, S.K., Thomason, L.C., Kuznetsov, S.G., Court, D.L., 2009. Recombineering: A Homologous Recombination-Based Method of Genetic Engineering. *Nature Protocols* **4**, 206–223.

46. Datta, S., Costantino, N., Court, D.L., 2006. A set of recombineering plasmids for gram-negative bacteria. *Gene* **379**, 109–115.

47. Dodd, I.B., Reed, M.R., Egan, J.B., 1993. The Cro-like Apl repressor of coliphage 186 is required for prophage excision and binds near the phage attachment site. *Molecular Microbiology* **10**, 1139–1150.

48. Schubert, R.A., Dodd, I.B., Egan, J.B., Shearwin, K.E., 2007. Cro's role in the CI–Cro bistable switch is critical for λ's transition from lysogeny to lytic development. *Genes & Development* **21**, 2461–2472.

49. Bernstein, J.A., Khodursky, A.B., Lin, P., Lin-chao, S., Cohen, S.N., 2002. Global analysis of mRNA decay and abundance in *Escherichia coli* at single-gene resolution using two-color fluorescent DNA microarrays. *PNAS U.S.A.* **99**, 9697–9702.

50. Dodd, I.B., Shearwin, K.E., Perkins, A.J., Burr, T., Hochschild, A. and Egan, J.B., 2004. Cooperativity in long-range gene regulation by the lambda CI repressor. *Genes & Development* **18**, 344–354.

51. Sneppen, K., Dodd, I.B., Shearwin, K.E., Palmer, A.C., Schubert, R.A., Callen, B.P., Egan, J.B., 2005. A mathematical model for transcriptional interference by RNA polymerase traffic in Escherichia coli. *Journal of Molecular Biology* **346**, 399–409.

52. Dodd, I.B., Shearwin, K.E., Sneppen, K., 2007. Modelling transcriptional Interference and DNA Looping in gene regulation. *Journal of Molecular Biology* **369**, 1200–1213.

53. Cutts, E.E., Barry Egan, J., Dodd, I.B., Shearwin, K.E., 2020. A quantitative binding model for the Apl protein, the dual purpose recombination-directionality factor and lysis-lysogeny regulator of bacteriophage 186. *Nucleic Acids Research* **48**, 8914–8926.

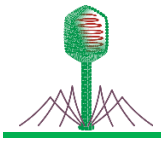

Chapter 5

Building synthetic memory - the design and construction of a 186 bacteriophage-based bistable mixed feedback switch

5.0 Introduction

Recent advances in SynBio are now enabling scientists to unleash their imagination, such that gene regulatory circuits with essentially any desired property can be constructed (potentially) from a registry of standardised biological devices and parts (IOM, 2011; iGEM, 2019). These components have been largely sourced from single-celled prokaryotic (e.g. bacteria) and eukaryotic organisms (e.g. yeast), but phage have also proven to be a rich reservoir, with many unique biological parts and devices discovered in networks evolved for precise control of gene expression and developmental fates (Citorik et al., 2014a). Since the birth of SynBio, scientists have worked to identify and characterise a great number of regulatory regions within bacterial and phage genomes. This has led to significant growth of the SynBio toolbox and increased the number of available biological 'building blocks', thereby facilitating the efforts of synthetic biologists in engineering novel synthetic circuitry.

Extensive studies of coliphage λ has made this phage a popular choice in engineering novel synthetic circuitry as we have a relatively comprehensive understanding of how this phage regulates its developmental decisions (Anderson and Yang, 2008; Dodd et al., 2001; Meyer et al., 2012; Oppenheim et al., 2005; Ptashne, 2006; Schubert et al., 2007; Svenningsen et al., 2005). The two key studies renowned for establishing the age of SynBio are that of Gardner et al. (2000) and Elowitz and Leibler (2000), both of which used promoter and protein components from the λ switch to construct their transcriptional toggle switch and oscillator, respectively. In later studies, Kotula et al. (2014) used λ to engineer a mammalian memory device and Noman et al. (2016) combined a pulse counter with a λ memory element to construct a one-counter circuit. Many other synthetic circuits have been engineered using DNA, RNA and protein components from the genomes of other phage. For example, Siuti et al. (2013) used the Bxb1 and φC31 phage recombinases to engineer an integrated AND logic gate and Bonnet et al. (2013) used unidirectional serine integrases from phage TP901-1 and Bxb1 to build a sophisticated genetic device, termed the Transcriptor. When used to control the transcriptional output of six types of logic gates they achieved digital genetic memory. Additionally, this system was later used to develop a series of bacterial biosensors (i.e. bactosensors) that could detect clinically relevant biomarkers in human urine and serum of diabetic patients (Courbet et al., 2015).

The virulent T7 phage has also been widely used in SynBio, where Ike et al. (2015) engineered a choline-inducible and repressible-T7-based induction system and Han et al. (2017) used T7 phage to generate a series of T7 RNA polymerase-based photoactivatable genetic switches. Schaerli et al. (2014) made a transcriptional AND gate using a split intein T7 RNA polymerase and Ortiz and Endy (2012) used T7 and the filamentous M13 phage to engineer an *E. coli* cell-cell communication platform.

As discussed in Section 1.2.3 of Chapter 1, there is a clear need for new technologies that serve as accurate preclinical disease detection and diagnostic tools. Since whole-cell biosensors (WCB) are ideal candidates for such technology, we endeavoured to develop an *E. coli* WCB using discrete components from the genome of coliphage 186. In this chapter, we describe the process that led to the successful engineering of *E. coli* with a bistable mixed feedback loop (MFL) linked to two induction modules. This system enables *E. coli* to detect and respond (with high sensitivity and specificity) to the presence of cumic acid (CA) and vanillic acid (VA) such that the bacterium can exist in one of two distinct alternate states and in the absence of the inducer stably maintain each state, thereby establishing a form of cellular memory.

As defined by François and Hakim (2005), in its simplest form, a MFL is a small two-protein feedback loop consisting of a protein-DNA interaction and a protein-protein interaction. Depending on the design of the system and kinetic parameters, MFLs can serve as bistable switches and molecular clocks (i.e. oscillators). They are a natural phenomenon employed by a wide range of simple to complex life forms to achieve precise regulatory control of gene expression. Presented in Figure 5.1 is a schematic of a simple bistable MFL that expresses two proteins, A and B. A bistable MFL is one that can establish memory of two mutually exclusive alternate states (ON or OFF) by stably expressing specific positive and negative control factors. To set the MFL in the OFF state (Fig. 5.1A) protein A is expressed from the constitutive *pA* promoter. To establish memory of the OFF state, A binds to DNA at the *pB* promoter to repress transcription of gene *B* (the protein-DNA interaction). To set the MFL in the ON state (Fig. 5.1B/C) gene *B* is expressed from *pB* and protein B forms a heterodimer with A (the protein-protein interaction) to prevent A from repressing the expression of *B* from *pB*. To switch the MFL between OFF and ON states, an additional component is required; termed the induction module (IM). An IM is typically designed to transiently express a protein factor (when exposed to a specific inducer) that influences the state of the MFL; usually by inhibiting the protein factor that regulates the alternate state. For example, to switch the MFL presented in Figure 5.1 from the A (OFF) state to the B (ON) state, the IM supplies protein C, a factor that could inhibit A either via an A-C protein-protein interaction (illustrated here), or by directly repressing production of A to induce expression of *B* from *pB* (Fig. 5.1B). Memory of the ON state would be established by the increased expression of *B* from *pB*, so that the A-B interaction keeps A inactivated when the IM is no longer expressing protein C (due to absence of the inducer, X) (Fig. 5.1C). To develop a more dynamic bistable MFL, one that can be toggled between two alternate states, a second IM (one that inhibits protein B) would be required for ON → OFF state switching.

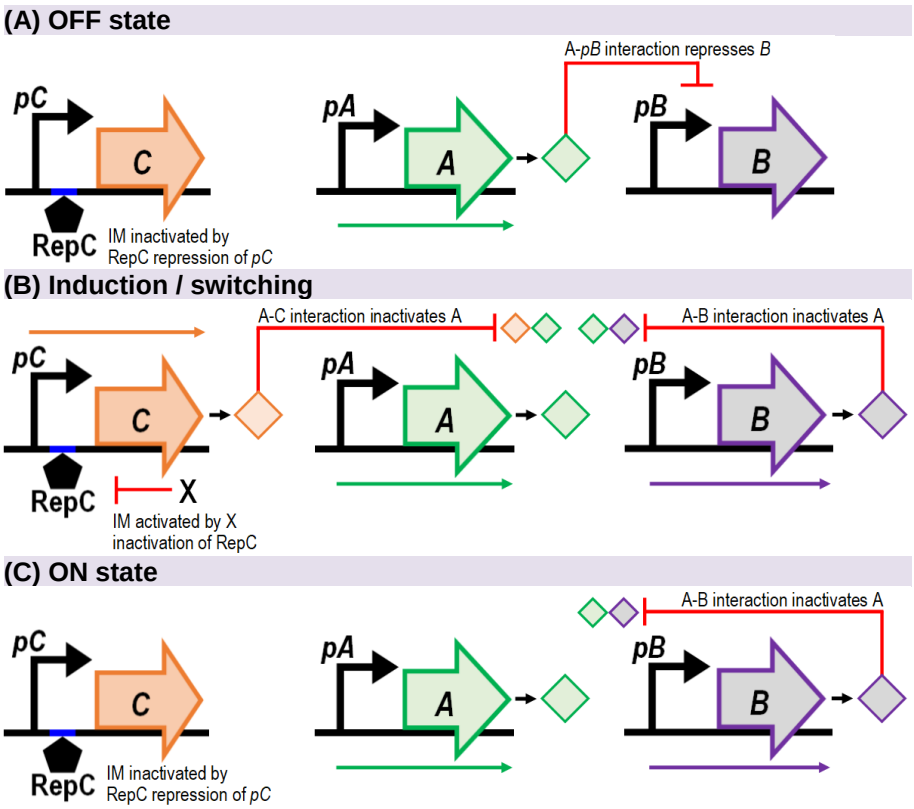

Figure 5.1: A schematic of an inducible bistable MFL. At minimum, a bistable MFL is a two-protein feedback system that entails a DNA-protein interaction and a protein-protein interaction and can exist in two mutually exclusive alternate states (ON OR OFF). **(A)** In the absence of inducer X, the IM is repressed by RepC and protein A dominates the system. To maintain the OFF state, A inhibits *B* expression by repressing *pB*. **(B)** In the presence of X, RepC is inactivated and *C* is expressed from *pC*. Protein C binds and inactivates A. With A inactivated, *B* is expressed from a derepressed *pB*. **(C)** Protein B binds A to form the inactive A-B complex. Protein B will maintain the ON state when inducer X is removed from the system and the IM is re-repressed by RepC. Genes are coloured left-and-right facing arrows respectively. Promoters are solid black right-angled arrows, with transcriptional output from each active promoter denoted with coloured arrows. Proteins are shown as coloured triangles, with heterodimers as paired triangles.

Like λ, extensive studies of 186 have revealed certain areas of its genome to be promising sources of biological components for the development of novel synthetic circuitry; in particular MFLs. Two regions of interest are the *cI.pR.pL.apl* region of the 186 switch and *p95.tum* of the SOS operon. Studies have revealed the 186 switch regulates the decision to undergo lytic or lysogenic development, where an active *pR* promoter is important for lytic development and CI is required for lysogeny (Dodd et al., 2007, 1993, 1990; Dodd and Egan, 2002, 1996; Neufing et al., 2001; Reed et al., 1997; Shearwin et al., 2005; Shearwin and Egan, 2000). Other studies have identified the SOS operon to be essential for prophage induction; where expression of *tum* from a derepressed *p95* promoter initiates the switch from lysogenic to lytic development (Brumby et al., 1996; Lamont et al., 1989; Shearwin et al., 1998; Voloshin et al., 2001). Using the information published in previous studies and from the research conducted in this thesis we inferred the *cI.pR.pL.apl* region of the 186 switch could serve as a potential MFL and *p95.tum* of the SOS operon could act as a potential IM.

This chapter details the progressive development of the 186-WCB. Section 5.1 introduces the initial working design, a chromosomally-integrated, two-module system consisting of a MFL LacZ reporter switch (derived from the 186 switch) coupled *in trans* to a UV-inducible IM (modelled from the SOS operon). When designing and engineering novel synthetic circuitry, optimisation is inevitable. A synthetic biologist must accept that the initial design is never the final version. This study was no exception, with the initial working design requiring extensive optimisation and characterisation to improve induction efficiency and bistability and reduce stochastic switching and system variability. After multiple rounds of optimisation and the shuffling, replacing and fine-tuning of component parts, we succeeded in developing a chromosomally-integrated, dynamic three-module system that exhibits impressive cellular memory. Given the ease with which this system can be adapted, we are optimistic our 186-WCB could serve as a 'memory diagnostic' in a real-life clinical setting by modification of one or both of the IMs, such that cells can selectively and sensitively detect a molecular analyte or condition unique to a disease of interest. Furthermore, this WCB could potentially serve as a monitoring device due to the ability of the system to establish a heritable form of cellular memory, such that in the absence of the inducer, cells (as they replicate and divide) can continue to maintain and report on the history of the system.

5.1 186-WCB engineering stage 1

5.1.1 Establishing an initial working module of the 186-WCB

5.1.1.1 To achieve ON state switching the *tum^{72K}* gene is an essential component part of WCB design

Based on our understanding of the 186 switch and the SOS operon, the initial design of the 186-WCB was a two-module system consisting of a MFL in the form of a ***pR***.*apl*$^{+/-}$.*tum*$^{72K/-}$-LacZ reporter linked to a *p95.tum*$^{+/72K}$ UV-IM integrated (at independent sites) into the chromosome of the *E. coli* 4643 (E4643) strain (Fig. 5.2). The MFL reporter mimics the 186 switch as it features the face-to-face *pR* and *pL* promoters, flanked by intact *FL* and *FR* sites. The *cI*$^{+}$ and *apl*$^{+}$ genes express wildtype CI and Apl respectively and to reduce reporter background expression a translational fusion of *lacZ* with *fil* (the third 186 lytic gene expressed from *pR*) was used to assay *pR* activity. To prevent activation of the *pE.cI* transcript, the native *cII* gene was replaced with *tum*^{72K}, which encodes a mutant Tum^{72K} variant that exhibits enhanced activity against CI (see Chapter 3). To determine whether *apl* and/or *tum*^{72K} are essential design components of the reporter switch, *apl*$^{-}$ and *tum*$^{-}$ reporters were also made, with the *apl*$^{-}$ gene encoding the Apl HTH mutant deficient in DNA binding and excision and the *tum*$^{-}$ gene encoding a truncated Tum^{72K} mutant made inactive by the D30G mutation. We hypothesised that to get the cells to establish long-term cellular memory of the lytic (i.e. ON) state, expression of Apl and Tum^{72K} from *pR* would be sufficient in keeping *pL* repressed and CI inactivated, respectively.

Since the 186 *cI.pR.pL.apl.cII* region does not itself constitute a MFL, we anticipated replacing *cII* with *tum*^{72K} would generate the *cI.pR.pL.apl.tum*^{72K} switch, which would act as a MFL. This is because, under non-induced conditions, CI would interact with its cognate DNA operator sites at *pR* to repress transcription of *apl* and *tum*^{72K} (the DNA-protein interaction). During and after UV induction, when *tum*^{72K} is expressed from a derepressed *pR,* Tum^{72K} would bind CI (the protein-protein interaction) to prevent CI from repressing the expression of *tum*^{72K} from *pR.* Hence, in this system, CI is analogous to protein A and Tum^{72K} is analogous to protein B (refer back to Fig. 5.1).

To develop an inducible bistable MFL, such that it has the ability to switch between and establish memory of OFF and ON states, an independent IM was required. For our system, the IM was remodelled from the SOS operon and features the LexA repressed *p95* promoter that drives *tum*$^{+/72K}$ expression following UV induction. A *tum*^{72K} version of the IM was made as we inferred the Tum^{72K} mutant would improve the switching efficiency of the WCB. The IM is analogous to a light switch, where when exposed to UV, it switches ON (equivalent to flicking the light switch with your finger). In the ON state, the IM expresses Tum, which transduces the 'switch ON' signal by acting *in trans* on the MFL reporter, by inactivating CI. With CI inactivated, *pR* is derepressed and *lacZ* expressed. Cells making LacZ are detected by growing as blue colonies on L-plates supplemented with X-gal, where the growth of blue colonies is analogous to a light globe emitting light. Referring back to Figure 5.1, the Tum expressed from the IM is analogous to protein C and is required for OFF → ON state switching, whilst the Tum^{72K} expressed from the MFL reporter is analogous to protein B and is required for maintaining (i.e. establishing memory) the ON state.

Genetic maps of the initial working modules of the 186-WCB are presented in Figure 5.2 and show the system in the lysogenic (i.e. OFF) state and lytic (i.e. ON) state. In the absence of UV, the MFL reporter exists/rests in the OFF state, where CI expressed from *pL* represses *pR* (inhibiting *apl, tum* and *lacZ* expression) and the host encoded LexA repressor inhibits expression of *tum* from *p95* (Fig. 5.2A). UV irradiation of the WCB strain inactivates LexA, which derepresses *p95* and allows for the expression of *tum* from the IM. In the presence of Tum, CI is inactivated, resulting in *pR* derepression and the expression of *apl, tum* and *lacZ,* thereby switching the reporter to the ON state (Fig. 5.2B). As the host SOS system repairs the DNA damage ensuing from UV irradiation, LexA repression of *p95* is gradually reinstated thereby progressively shutting down *tum* expression. Once the IM returns to its repressed state, the Apl and Tum^{72K} expressed from the MFL reporter are expected to maintain/establish memory of the ON state, where Tum^{72K} will continue to sequester CI into an inactive state and *cI* expression from *pL* is repressed by Apl and by *pR* transcriptional interference (TI) (Shearwin et al., 2005).

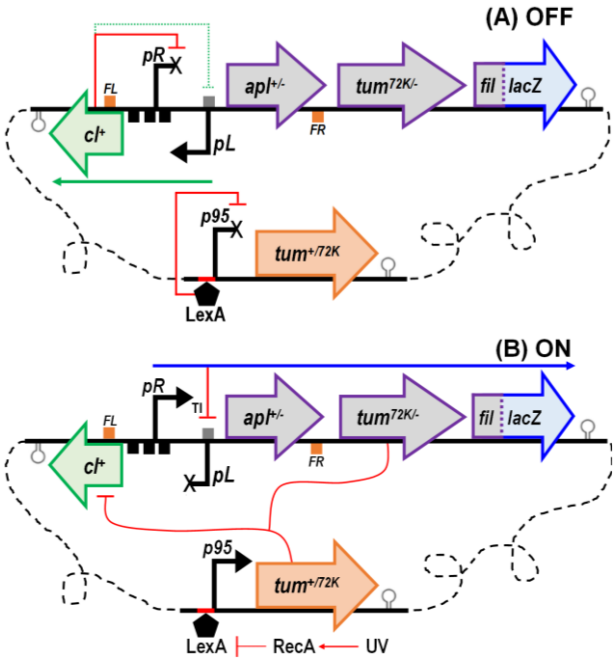

Figure 5.2: Schematics of the initial working modules of the 186-WCB. Each working module consists of a single-copy λ integrated ***pR***.*apl*$^{+/-}$.*tum*$^{72K/-}$ LacZ reporter and a 186 *attB1* integrated *p95.tum*$^{+/72K}$ UV-IM. **(A)** In the OFF state, LexA represses *p95.tum* and CI (expressed from *pL),* represses *pR* preventing the expression of *apl, tum* and *lacZ*. CI also weakly represses *pL* to negatively regulate its own expression; establishing an OFF-CI steady state. **(B)** Following UV, LexA is degraded, *p95* is derepressed and *tum* is expressed. Tum inactivates CI, which results in *pR* derepression and expression of *apl, tum* and *lacZ*. To maintain the ON state, *cI* expression from *pL* is repressed by Apl and *pR* transcriptional interference (TI), whilst Tum (expressed from *pR*) keeps CI inactivated. Symbolism defined in Table 5.12.

5.1.1.1.1 Determining OFF to ON state switching for the initial working modules of the 186-WCB

To detect which of the initial working modules of the 186-WCB (Table 5.1) could undergo OFF ⟶ ON state switching, blue/white switch plate assays and UV induction timecourse LacZ assays were performed. The blue/white switch plate assays provided a phenotypic picture of what proportion of cells switch to the ON state following UV irradiation. In these assays, the initial eight WCB strains were treated with 40s UV and plated on X-gal L-plates. The assay works on the principle that ON state cells will grow as blue colonies because the MFL reporter is expressing *lacZ* - the product of which will cleave the X-gal substrate to give a blue coloured precipitate. OFF state cells grow as white colonies because CI is repressing *pR.lacZ* expression. The optimal UV dose was determined by conducting a series of UV dose-response assays, where each WCB strain (Table 5.1) was exposed to 0 to 60s of UV, plated on X-gal L-plates and the proportion of blue to white colonies scored the next day. The outcome of these assays indicated exposure to 40s UV was sufficient for switching without causing excess cell death (data not shown). Unless otherwise specified, a 40s dosage (equivalent to ~7.5 J/m^2/min) was chosen as the standard UV dose for all UV induction experiments carried out in this study. LacZ assays were also performed to quantify *pR* activity over a defined timecourse following exposure to 40s UV. These assays allowed us to compare induction efficiencies between the initial eight WCB strains and ultimately determine what component parts are crucial to WCB performance.

Table 5.1: The initial 186-WCB strains. Strains that undergo stable OFF → ON state switching are shaded blue. Each module exists at single-copy in the E4643 chromosome; ending subscript indicates site of integration.

Name	Description
AI168	E4643 + [pIT3-TO-*p95.tum*$^{+}$]$_{186.1}$ + [pIT3-CL-*cI*$^{+}$.***pR***$^{+}$.*pL*$^{+}$.*apl*$^{+}$.*tum*^{72K}.*fil::lacZ*]$_{\lambda}$
AI169	E4643 + [pIT3-TO-*p95.tum*$^{+}$]$_{186.1}$ + [pIT3-CL-*cI*$^{+}$.***pR***$^{+}$.*pL*$^{+}$.*apl*$^{+}$.*tum*$^{-}$.*fil::lacZ*]$_{\lambda}$
AI170	E4643 + [pIT3-TO-*p95.tum*$^{+}$]$_{186.1}$ + [pIT3-CL-*cI*$^{+}$.***pR***$^{+}$.*pL*$^{+}$.*apl*$^{-}$.*tum*^{72K}.*fil::lacZ*]$_{\lambda}$
AI171	E4643 + [pIT3-TO-*p95.tum*$^{+}$]$_{186.1}$ + [pIT3-CL-*cI*$^{+}$.***pR***$^{+}$.*pL*$^{+}$.*apl*$^{-}$.*tum*$^{-}$.*fil::lacZ*]$_{\lambda}$
AI172	E4643 + [pIT3-TO-*p95.tum*^{72K}]$_{186.1}$ + [pIT3-CL-*cI*$^{+}$.***pR***$^{+}$.*pL*$^{+}$.*apl*$^{+}$.*tum*^{72K}.*fil::lacZ*]$_{\lambda}$
AI173	E4643 + [pIT3-TO-*p95.tum*^{72K}]$_{186.1}$ + [pIT3-CL-*cI*$^{+}$.***pR***$^{+}$.*pL*$^{+}$.*apl*$^{+}$.*tum*$^{-}$.*fil::lacZ*]$_{\lambda}$
AI174	E4643 + [pIT3-TO-*p95.tum*^{72K}]$_{186.1}$ + [pIT3-CL-*cI*$^{+}$.***pR***$^{+}$.*pL*$^{+}$.*apl*$^{-}$.*tum*^{72K}.*fil::lacZ*]$_{\lambda}$
AI175	E4643 + [pIT3-TO-*p95.tum*^{72K}]$_{186.1}$ + [pIT3-CL-*cI*$^{+}$.***pR***$^{+}$.*pL*$^{+}$.*apl*$^{-}$.*tum*$^{-}$.*fil::lacZ*]$_{\lambda}$

The results of the blue/white switch plate assays (Fig. 5.3) show successful OFF → ON state switching is only observed for WCB strains harbouring a ***pR***.*apl*$^{+/-}$.*tum*^{72K} reporter (AI168, AI170, AI172 and AI174). The switch plate data for strains harbouring a ***pR***.*apl*$^{+/-}$.*tum*$^{-}$ reporter (AI169, AI171, AI173 and AI175) has not been presented as these cells failed to stably switch to the ON state (UV-induced cultures grow as white colonies). This outcome indicates that to achieve stable OFF → ON state switching; only *tum*^{72K} (and not *apl*) is an essential design component of the MFL reporter.

The blue/white switch plate data also suggests the *p95.tum*^{72K} IM is superior to the *p95.tum*$^{+}$ IM because the two WCB strains featuring *p95.tum*^{72K} (AI172 and AI174) show improved switching (>90% of colonies coloured blue), whilst strains featuring *p95.tum*$^{+}$ only exhibit an ~32% switch rate (AI168 and AI170). Unfortunately, AI172 and AI174 exhibit a high rate of spontaneous switching with a significant proportion of uninduced colonies having a dark blue (induced) phenotype (>10%) or a light blue (partially induced) phenotype. This suggests the LexA-based UV-IM generates a high level of basal (i.e. leaky) *tum* expression, such that for AI172 and AI174 cells the degree of Tum^{72K} leak is sufficient to induce OFF → ON state switching. Whilst it appears expressing *tum*^{72K} from *pR* and *p95* is required for efficient switching, we also wanted to assess whether *tum*^{72K} expression from *pR* was sufficient for maintaining the ON state following re-repression of the UV-IM by LexA. To quickly assess ON state stability, blue colonies from each switch plate were resuspended in LB and re-plated on X-gal L-plates. For all WCBs (regardless of their IM), ~50% of colonies produced a blue phenotype (data not shown), suggesting the ON state is unstable – it cannot be maintained indefinitely in absence of the inducer - and optimisation of 186-WCB design was required.

Figure 5.4 presents the LacZ data for the initial eight 186-WCB strains, the results of which are comparable to the blue/white switch plate data (Fig. 5.3). As expected, each strain produces a rise in *pR* activity following UV induction, with the ***pR***.*apl*$^{+/-}$.*tum*^{72K} strains (AI168, AI170, AI172 and AI174) having enhanced *pR* induction profiles. Improved induction was also observed for WCB strains with the *p95.tum*^{72K} IM (Fig. 5.4B), where *pR* activity reaches ~90 LacZ units and starts to taper 210mins after induction compared to strains with the *p95.tum*$^{+}$ IM (Fig. 5.4A), where *pR* activity peaks at ~80 LacZ units and begins to taper 150mins after UV induction. The decline in *pR* activity observed for each WCB strain towards the end of the timecourse corresponds to the observation of re-plated induced (blue) cells growing back as a mix of blue and white colonies. This outcome indicates that for these initial WCB strains the ON state cannot be stably maintained by expressing *tum*^{72K} from *pR.*

Overall, WCB strains harbouring a ***pR***.*apl*$^{+/-}$.*tum*^{72K} reporter linked to the *p95.tum*$^{+}$ IM (AI168 and AI170) have an ~32% switch rate, ~1% spontaneous switch rate and exhibit maximal *pR* activity of ~80 LacZ units 150mins after UV induction (Fig. 5.3A/B, Fig. 5.4A). WCB strains harbouring a ***pR***.*apl*$^{+/-}$.*tum*^{72K} reporter linked to the *p95.tum*^{72K} IM (AI172 and AI174) have an ~95% switch rate, ~15% spontaneous switch rate and exhibit maximal *pR* activity of ~90 LacZ units 210mins after UV induction (Fig. 5.3C/D, Fig. 5.4B). WCB strains harbouring a ***pR***.*apl*$^{+/-}$.*tum*$^{-}$ reporter linked to a *p95.tum*$^{+}$ IM (AI169 and AI171) have reduced *pR* induction profiles, with maximal *pR* activity reaching ~52 LacZ units 120mins after induction (Fig. 5.4A). Strains harbouring a ***pR***.*apl*$^{+/-}$.*tum*$^{-}$ reporter linked to a *p95.tum*^{72K} IM (AI173 and AI175) display improved *pR* induction profiles, comparable to AI172 and AI174 but these cells cannot maintain this high level of *pR* activity for the entire timecourse, with *pR* activity starting to taper at the 180min mark (Fig. 5.4B). Furthermore, regardless of what UV-IM the ***pR***.*apl*$^{+/-}$.*tum*$^{-}$ reporter is linked to, all cells fail to grow as blue colonies following UV induction (data not shown).

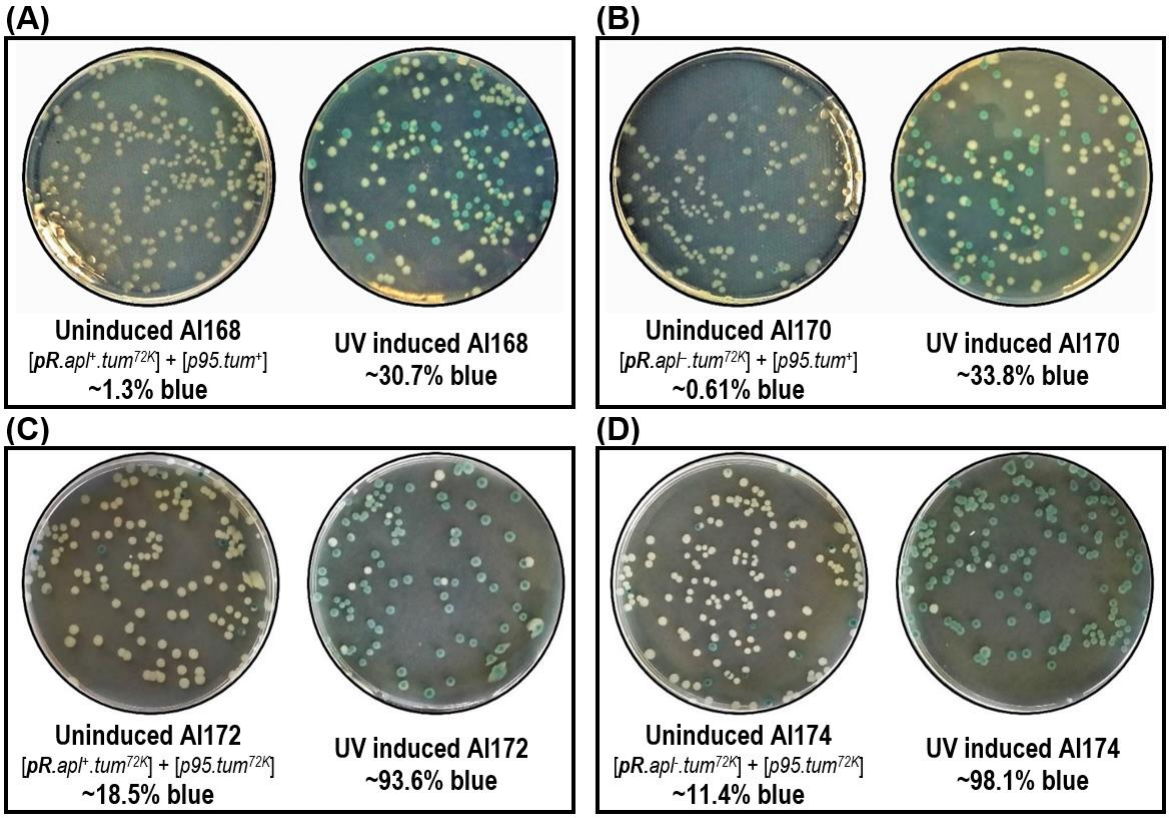

Figure 5.3: Blue/white switch plate data for the initial 186-WCB strains. OFF → ON state switching was observed only for strains harbouring a ***pR***.*apl*$^{+/-}$.*tum*^{72K} reporter. The elevated switch rate observed for AI172 and AI174 (>90%) suggests the *p95.tum*^{72K} IM improves switching efficiency, but the UV-IM appears to be somewhat 'leaky' as these strains have a high rate of spontaneous induction (>11%). To assess ON state stability a single blue colony from each plate was resuspended in LB and re-plated on X-gal L-plates. Regardless of the IM present, cells are sub-optimal in maintaining the ON state as only ~50% of cells grow as blue colonies (data not shown). Switching was assayed by growing cultures to OD_{600} 0.30 in M9MM-20, treated with 40s UV, diluted 10^{-4} and 10µL plated on L-plates with 40µg/mL X-gal and the growth of blue to white colonies scored the next day. Percentage values represent the approximate proportion of blue colonies observed on each switch plate presented.

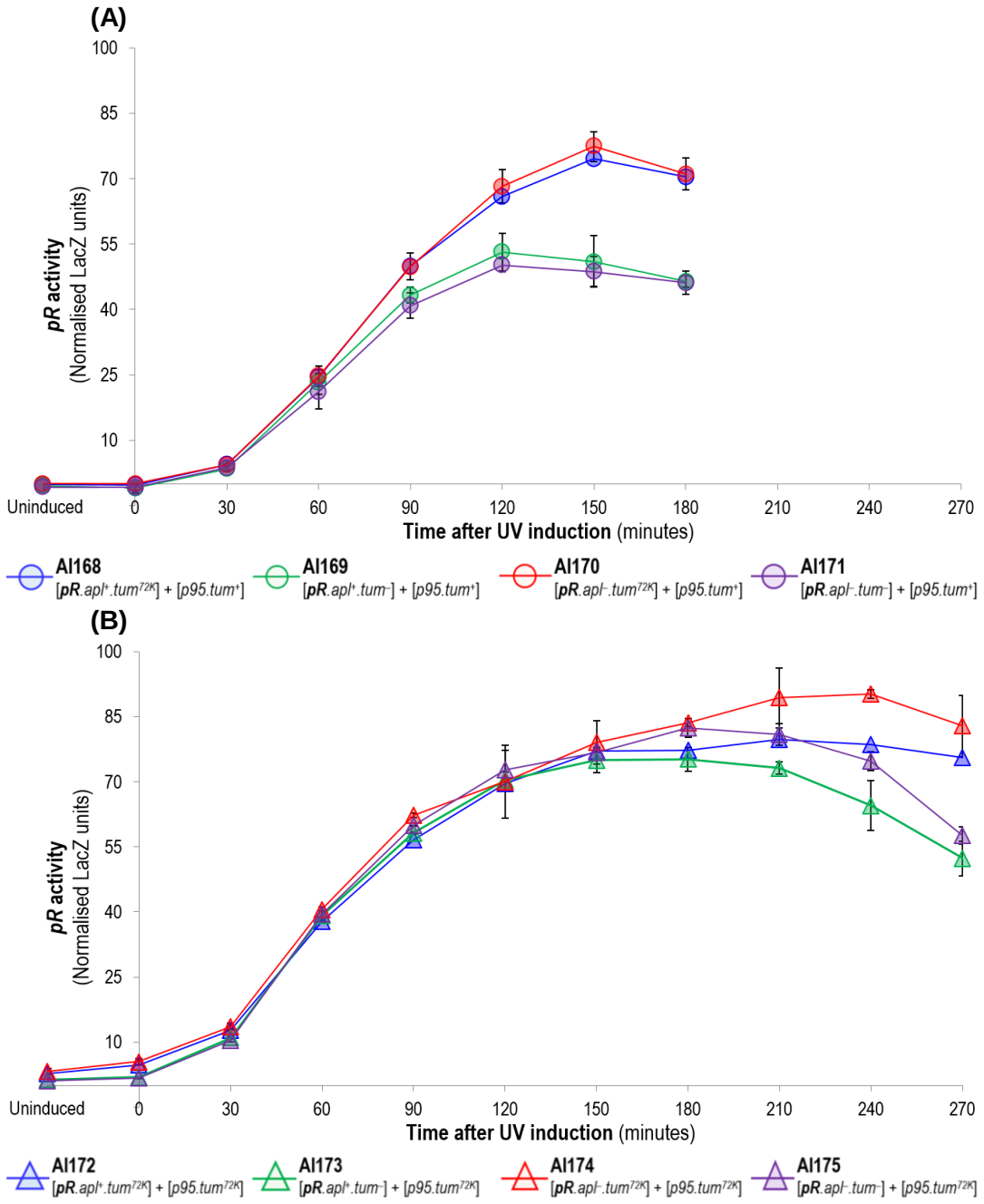

Figure 5.4: Observed *pR* LacZ activity for the initial 186-WCB strains. **(A)** *pR* induction profiles for WCB strains harbouring a *p95.tum*$^{+}$ UV-IM. **(B)** *pR* induction profiles for WCB strains harbouring a *p95.tum*^{72K} UV-IM. *pR* induction profiles were obtained by inducing cultures with 40s UV and tracking *pR* LacZ production over a 3hr or 4.5hr timecourse. The *pR* LacZ data complements the blue/white switch plate data, where comparison of strains harbouring *p95.tum*$^{+}$ (A) shows strains with a ***pR***.*apl*$^{+/-}$.*tum*^{72K} reporter have an enhanced *pR* induction profile, confirming *tum*^{72K} is a required component part of the reporter switch. AI168 and AI170 have identical *pR* induction profiles, which suggests *apl* is not required for switching. Comparison of the (A) *pR* LacZ data with the (B) *pR* LacZ data verifies *tum*^{72K} is the optimal *tum* variant for the UV-IM. Strains harbouring *p95.tum*^{72K} (AI172-AI175) (B) have elevated *pR* induction profiles and maintain high *pR* activity up to 210mins after UV induction, whilst *pR* activity starts to taper ~150mins after induction for AI168-AI171 strains (A). To reduce the day-to-day variation observed with these assays, the LacZ data for AI169, AI170, AI171 was normalised to the AI168 data (A) and the LacZ data for AI173, AI174 and AI175 was normalised to the AI172 data (B). Each data point represents an average of three independent assays, 95% confidence interval error bars are shown.

The blue/white switch plate data and *pR* LacZ data confirms that to achieve OFF → ON state switching, tum^{72K} must be included in the design of the MFL reporter as only WCB strains that express tum^{72K} from the reporter can successfully switch ON (AI168, AI170, AI172 and AI174). This suggests that following UV irradiation, Tum^{72K} helps stabilise the ON state even after LexA has re-established repression of *p95*. The LacZ data also shows Tum^{72K} does not provide long-term maintenance of the ON state as each WCB strain eventually starts to show a decline in *pR* activity. This outcome is reinforced by the fact that re-plated induced (blue) colonies are unable to grow back as homogenous populations of blue colonies, with ~50% of cells relapsing to the OFF state and growing as white colonies (data not shown).

From an Apl perspective, it appears the *apl* gene is not an essential component part of MFL design as ***pR***.apl^{-}.tum^{72K} WCB strains can successfully switch to the ON state (AI170 and AI174). Apl also does not appear to assist in stabilising the ON state because re-plated AI168, AI170, AI172 and AI174 blue cells all grow back as heterogeneous populations of blue and white colonies with similar proportions of each phenotype (data not shown). If Apl were assisting Tum^{72K} in stabilising the ON state then re-plated AI168 and AI172 induced cells (apl^{+}) should have returned a greater proportion (>50%) of blue to white colonies than that observed for AI170 and AI174 (apl^{-}). Overall, our analysis of the initial working 186-WCB modules strongly indicates that to achieve ON state switching the MFL reporter only needs to encode tum^{72K} (not *apl*). Since a Tum^{72K} reporter is only able to achieve short-term stability of the ON state, to improve this parameter we decided to increase tum^{72K} mRNA translation by optimising the strength of the Ribosomal Binding Site (RBS) (see Section 5.1.1.2).

In terms of the UV-IM, we created $p95.tum^{+}$ and $p95.tum^{72K}$ versions and inferred the latter would be the superior IM. Analysis of the switch plate and LacZ data supports our inference, as AI172 and AI174 exhibit improved switching efficiency (Fig. 5.3B/C) and all WCB strains harbouring $p95.tum^{72K}$ (AI172, AI173, AI174 and AI175) have elevated *pR* LacZ induction profiles (Fig. 5.4B). Unfortunately, despite the ability of Tum^{72K} to improve the WCB switch rate and induction efficiency, the high level of spontaneous (ON state) switching suggests the enhanced stability/half-life of Tum^{72K} is making the OFF state unstable. The elevated spontaneous switching observed for AI172 and AI174 is likely due to the system being hypersensitive to RecA, such that even the slightest derepression of *p95* via the RecA-LexA interaction could induce cells to switch ON. Spontaneous switching is possible because RecA expression is induced when the host SOS response is activated by any DNA damaging event caused by any mutagen that happens to inflict single-stranded breaks in the host DNA.

Another factor likely contributing to the system's stochastic switching is that repression of *p95* via LexA may be a relatively weak interaction. Evidence of this was provided by Danna Lee (see Chapter 3), where non-zero basal LacZ promoter activity was observed when characterising *p95* in the presence and absence of UV. To overcome this issue, the UV-IM (*p95.tum^{72K}*) was replaced with a cumic acid (CA) inducible-IM (*cymR.T5-1.tum^{72K}*). We predicted this CA-IM would retain the switching efficiency as seen for the UV-IM but restore stability of the OFF state by offering improved repression of *tum^{72K}* by removing any dependence the system has on the presence of RecA (see Section 5.2).

5.1.1.2 Enhancement of the *tum^{72K}* RBS improves ON state stability

The initial working modules of the 186-WCB confirmed *tum^{72K}* is an essential design component of the reporter switch because all ***pR***.*apl$^{+/-}$.tum^{-}* WCB strains failed to exhibit blue/white switching and have suboptimal *pR* induction profiles. Whilst expressing *tum^{72K}* from *pR* achieves ON state switching, it does not establish long-term ON state stability (i.e. cellular memory) with the LacZ data showing *pR* levels start to taper ~180mins after UV induction and re-plated induced (blue) colonies grow back as a mix of blue and white colonies. This suggests the level of *tum^{72K}* expressed from the MFL reporter is not sufficient to control CI and maintain the ON state. To improve ON state stability, a new set of 186-WCB strains were made (Table 5.2) by integrating E4643 with a ***pR***.*apl$^{+/-}$.tum*^{72K}* LacZ reporter featuring an enhanced *tum^{72K}* RBS (denoted as *tum*^{72K}*) coupled to a *p95.tum$^{+/72K}$* UV-IM. The *tum^{72K}* RBS was originally driven by the native weak *cII* RBS and was optimised from a strength of ~3,200 to ~55,600 (in arbitrary units; AUs) using the RBS Calculator v2.0 (Espah Borujeni et al., 2014) and the *E. coli* str. K-12 substr. MG1655 (ACCTCCTTA 16S RNA sequence) setting (Table 5.3).

Table 5.2: The *tum*^{72K}* RBS optimised 186-WCB strains. Each module exists at single-copy in the E4643 chromosome; ending subscript indicates site of integration.

Name	Description
AI208	E4643 + [pIT3-TO-*p95.tum^{+}*]$_{186.1}$ + [pIT3-CL-*cI^{+}*.***pR***$^{+}$.*pL^{+}.apl^{+}.tum*^{72K}.fil::lacZ*]$_{\lambda}$
AI209	E4643 + [pIT3-TO-*p95.tum^{+}*]$_{186.1}$ + [pIT3-CL-*cI^{+}*.***pR***$^{+}$.*pL^{+}.apl^{-}.tum*^{72K}.fil::lacZ*]$_{\lambda}$
AI210	E4643 + [pIT3-TO-*p95.tum^{72K}*]$_{186.1}$ + [pIT3-CL-*cI^{+}*.***pR***$^{+}$.*pL^{+}.apl^{+}.tum*^{72K}.fil::lacZ*]$_{\lambda}$
AI211	E4643 + [pIT3-TO-*p95.tum^{72K}*]$_{186.1}$ + [pIT3-CL-*cI^{+}*.***pR***$^{+}$.*pL^{+}.apl^{-}.tum*^{72K}.fil::lacZ*]$_{\lambda}$

Table 5.3: *tum*^{72K}* RBS optimisation. RBS strength was increased ~17-fold by optimising the *cII* RBS sequence using the Salis Lab RBS Calculator v2.0 (Espah Borujeni et al., 2014) and the *E. coli* str. K-12 substr. MG1655 (ACCTCCTTA 16S RNA sequence). DNA sequence written 5' to 3'. End of *apl* gene (TAA) (green), *FR* operator (grey), pre-sequence (red), RBS (bold), Shine-Delgarno sequence (bold, underlined), start of *tum* gene (ATG) (blue). *Strength refers to the RBS translation initiation rate listed in arbitrary units (AUs).

RBS	DNA sequence	*Strength
Native *cII*	TAATTCACTTTATGTGAATTGTAAGGATGCAAC**ATGGATAGAGAGCTAA**ATG	3,191
Optimised	TAATTCACTTTATGTGAATTGTAAGGATGCAAC**GATAAGCAACAGAAATAAG GACTATAGTA**ATG	55,569

To characterise the performance of the new ***pR***.*apl*$^{+/-}$.*tum*^{*72K} 186-WCB strains, blue/white switch plate assays and UV induction timecourse LacZ assays were performed. The blue/white switch plate data (Fig. 5.5) shows each of these new strains can successfully undergo OFF → ON state switching with *apl* offering no significant improvement to switching. As done previously, long-term ON state stability was assessed by re-plating a single induced (blue) colony (from each plate) on an X-gal L-plate and the growth of blue and white colonies scored the next day. The data shows that regardless of the UV-IM used, each strain showed an improvement in maintaining the ON state as a greater proportion of cells (~80%) retained the induced (blue) phenotype, in comparison to the initial working modules (Table 5.1), where only ~50% of colonies retained their blue colouration (data not shown). This suggests that increasing the level of *tum*^{72K} expressed from *pR* has improved ON state stability.

The blue/white switch plate data (Fig. 5.5A-D) also shows strains harbouring the *p95.tum*^{72K} UV-IM (AI210 and AI211) have an elevated switch rate of >90%, compared to the ~18% switch rate observed for AI208 and AI209 strains harbouring the *p95.tum*$^{+}$ UV-IM. This supports the previous finding (Fig. 5.3) that *p95.tum*^{72K} prevails over *p95.tum*$^{+}$ when it comes to achieving efficient OFF → ON state switching. As expected, AI210 and AI211 retain a high spontaneous induction rate (~4.8%), which we infer is due to a weak LexA-*p95* interaction and that these systems have RecA hypersensitivity due to their use of a UV-IM that encodes the *tum*^{72K}. Section 5.2 describes our efforts to optimise our IM system so to reduce the degree of spontaneous switching observed for WCB strains harbouring a *p95.tum*^{72K} UV-IM.

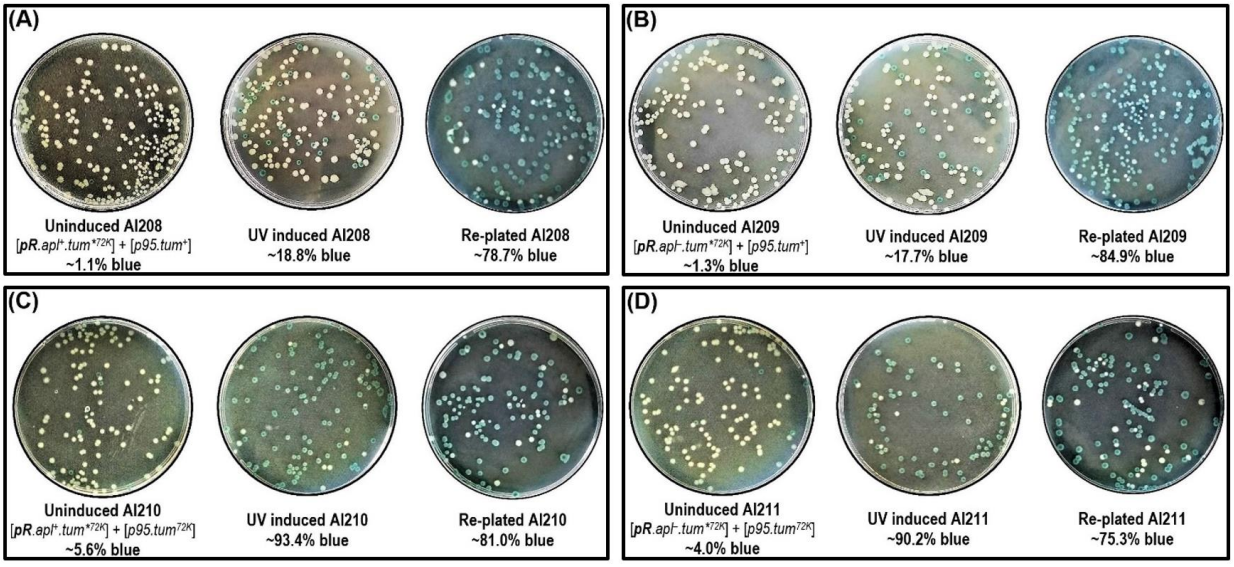

Figure 5.5: Blue/white switch plate data for the *tum*^{*72K} RBS optimised 186-WCB strains. Improved OFF → ON state switching (>90%) was observed for strains harbouring a *p95.tum*^{72K} UV-IM (C and D), but a high rate (>4.0%) of spontaneous switching was also observed. Regardless of the UV-IM present each strain shows an improvement in maintaining the ON state as a greater proportion (>75%) of re-plated colonies exhibit a blue phenotype, in comparison to the initial working modules (~50%). Switching was assayed as per the protocol described in Fig. 5.3. Percentage values represent the approximate proportion of blue colonies observed on each switch plate presented.

The *pR* LacZ data (Fig. 5.6B) shows WCB strains harbouring a ***pR***.*apl*$^{+/-}$.*tum*^{*72K} LacZ reporter linked to the *p95.tum*^{72K} UV-IM (AI210 and AI211) have similar enhanced *pR* profiles, with maximal LacZ activity ~1.3-fold greater than their *p95.tum*$^{+}$ UV-IM counterparts (AI208 and AI209 respectively). AI208 and AI209 have enhanced *pR* profiles in respect to *pR* stability but not activity when compared to the *pR* profiles of AI168 and AI170 (Fig. 5.4A). Whilst *pR* levels start to taper 150mins after UV induction for AI168 and AI170, the AI210 and AI211 strains are able to maintain a high level of *pR* activity for the entire 4.5hr timecourse. This extended period of *pR* activity complements the switch plate data and confirms optimisation of the *tum*^{72K} RBS is contributing to the stabilisation of the ON state, such that these WCB strains can remain ON, not indefinitely, but for a longer period-of-time.

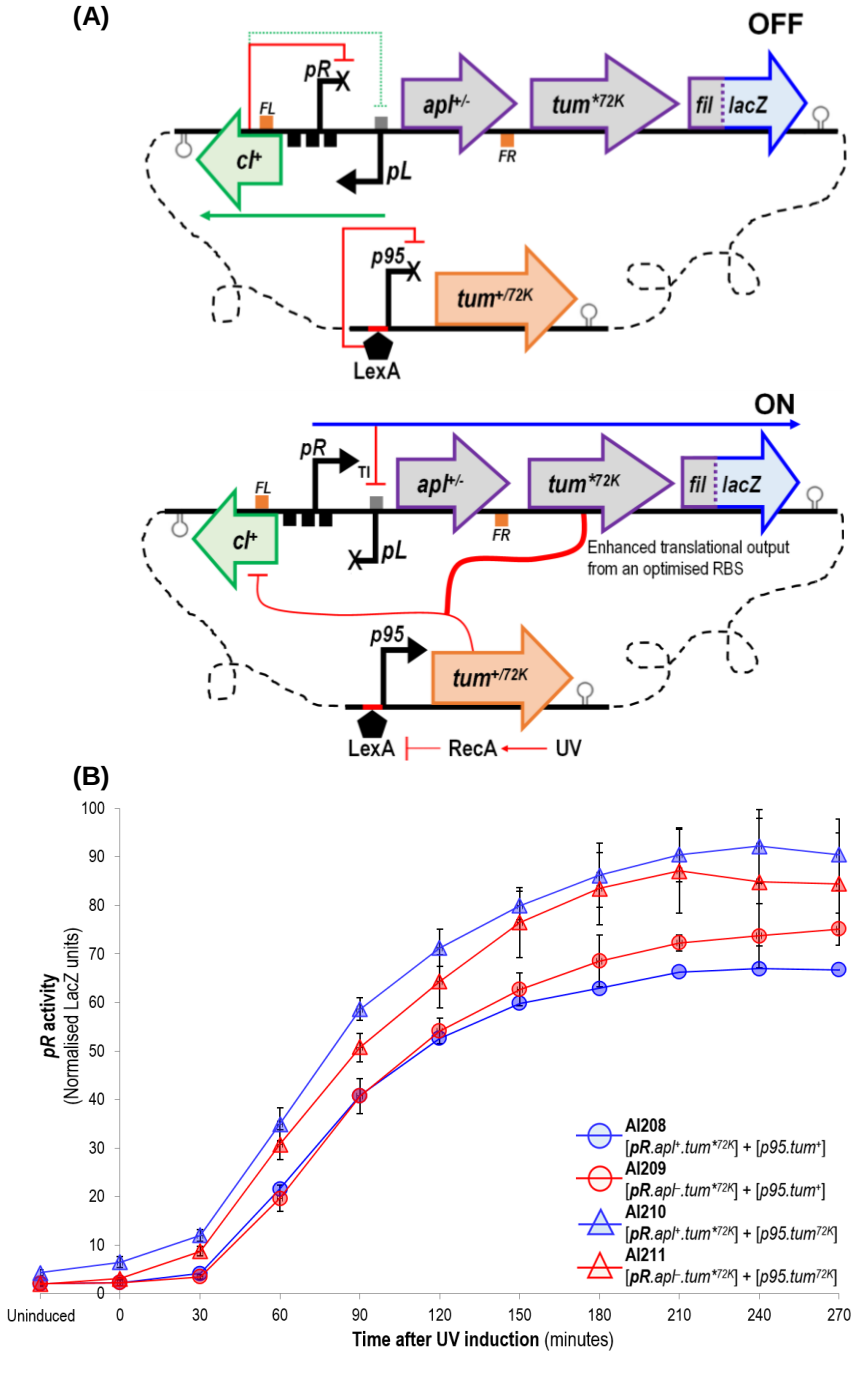

Figure 5.6: Observed *pR* LacZ activity for the *tum*^{*72K} RBS optimised 186-WCB strains. (A) OFF and ON state schematics of the optimised WCB. ON and OFF state cycling occurs exactly as described in Fig. 5.2, with elevated translational expression of *tum*^{*72K} mRNA expected to improve ON state stability. Symbolism defined in Table 5.12. **(B)** Observed *pR* LacZ activity of each *tum*^{*72K} RBS optimised WCB strain. *pR* induction profiles were obtained by inducing cultures with 40s UV and tracking *pR* LacZ production over a 4.5hr timecourse. Strains harbouring the *p95.tum*^{72K} UV-IM (AI210 and AI211) have similar enhanced *pR* profiles in comparison to AI208 and AI209 respectively. AI208 and AI209 have enhanced *pR* profiles in respect to *pR* stability but not activity when compared to the induction profiles of AI168 and AI170 (Fig. 5.4A). To reduce the day-to-day variation observed with these assays, the LacZ data for AI209, AI210 and AI211 was normalised to the AI208 data. Each data point represents an average of six independent assays, 95% confidence interval error bars are shown.

5.2 186-WCB engineering stage 2

5.2.1 Optimising the IM system of the 186-WCB

5.2.1.1 The use of a cumic acid IM system reduces spontaneous switching

LacZ analysis of the 186-WCB strains listed in Tables 5.1 and 5.3 revealed strains harbouring the *p95.tum*^{72K} UV-IM have enhanced *pR* induction profiles, which indicates *tum*^{72K} (rather than *tum*$^{+}$) is the preferred *tum* variant for the IM. The blue/white switch plate data also revealed these strains have a high rate of spontaneous OFF → ON state switching, which suggests the UV-IM system is somewhat leaky - likely due to a weak LexA-*p95* interaction - and tighter control of *tum*^{72K} expression is required. In an effort to reduce this spontaneous switching, the *tum*^{72K} UV-IM was replaced with the cumic acid (CA)-inducible IM encoding *tum*$^{+}$ or *tum*^{72K}.

The CA system was initially developed by Choi et al. (2010), where they developed a tightly regulated novel gene expression system compatible for a wide range of *E. coli* strains. In this study, regulatory elements derived from the *Pseudomonas putida* F1 *cym* and *cmt* operons were used to engineer a switch module (pNEW) that provides tight control of target gene expression (at the transcriptional level) and responds with high sensitivity and specificity to the non-toxic exogenous inducer, p-isopropylbenzoate (cumic acid; CA). In the pNEW system, a partial (strong) T5 phage promoter, linked (downstream) to a truncated operator fragment of the *cmt* operon, drives target gene expression. The CA repressor (CymR), a regulatory protein of the *Pseudomonas putida* F1 *cmt* operon, recognises the operator. Since CymR is not native to *E. coli,* the pNEW system was designed to express *cymR* from the weak constitutive promoter, P_{km}. In the absence of CA, target gene expression is inhibited because CymR is bound to its operator, thereby blocking RNAPs. Upon exposure to CA, the inducer rapidly alters the CymR-operator interaction, thereby dislodging the repressor from the DNA and allowing for target gene expression.

In later studies, independently undertaken by Ian Dodd (Shearwin laboratory), the pNEW system was modified to generate a series of three modules (1, 4 and 6) that featured a T5 phage promoter mutated to give different transcriptional outputs. The weak P_{km} promoter used to drive *cymR* expression was replaced with the stronger constitutive promoter, *proA*. To characterise each module, Dodd conducted preliminary LacZ assays by cloning *lacZ* immediately downstream of the *T5-1, 4* and *6* promoters. Testing a 0-250µM [CA] range, Dodd confirmed 150µM CA is sufficient to achieve maximal induction (data not shown). Comparison of the LacZ induction profiles for each T5 promoter variant revealed the *T5-1* system to have an enhanced induction profile and very low (almost zero) basal promoter activity. Using this data, we hypothesised that use of this tightly regulated system would help reduce spontaneous OFF → ON switching and achieve comparable (or perhaps improve) WCB switching efficiency.

Our new *cymR.T5-1.tum*$^{+/72K}$ CA-IMs were assembled with the *Spe*I digested pIT4-KT-*cymR.T5-1* module (made by Ian Dodd, Shearwin laboratory) and the *tum*$^{+/72K}$ gene PCR fragment sourced from pIT3-TO-*p95.tum*$^{+/72K}$ (made by Danna Lee, Shearwin laboratory). A *tum*$^{+}$ version was made to (again) compare induction efficiency between these two *tum* variants, the results of which are discussed in Section 5.2.1.1.3. Once assembled, each CA-IM was integrated into E4643 harbouring the RBS optimised ***pR***.*apl*$^{-}$.*tum*^{*72K} LacZ reporter to generate two new WCB strains (Table 5.4). Our decision to use the *apl*$^{-}$ version of the reporter was based on our earlier LacZ and switch plate assays (Section 5.1), which indicated *apl* plays no role in switching and ON state stability, whilst *tum*^{72K} is required for switching and when linked to an optimised RBS allows for improved ON state stability.

Table 5.4: The CA-inducible 186-WCB strains. Each module exists at single-copy in the E4643 chromosome; ending subscript indicates site of integration.

Name	Description
AI215	E4643 + [pIT4-KT-*cymR.T5-1.tum*$^{+}$]$_{\varphi 21}$ + [pIT3-CL-*cI*$^{+}$.***pR***$^{+}$.*pL*$^{+}$.*apl*$^{-}$.*tum*^{*72K}.*fil::lacZ*]$_{\lambda}$
AI219	E4643 + [pIT4-KT-*cymR.T5-1.tum*^{72K}]$_{\varphi 21}$ + [pIT3-CL-*cI*$^{+}$.***pR***$^{+}$.*pL*$^{+}$.*apl*$^{-}$.*tum*^{*72K}.*fil::lacZ*]$_{\lambda}$

As illustrated in Figure 5.7, these CA-inducible 186-WCB strains maintain the OFF state by expressing CymR from the constitutive *proA* promoter. CymR represses the *T5-1* promoter and inhibits *tum* expression by binding to its cognate operator site located immediately downstream of *T5-1*. In the presence of CA, CymR is inactivated resulting in the expression of *tum* from a derepressed *T5-1*. Tum inactivates CI, which results in *pR* derepression and the expression of *apl*$^{-}$, *tum*^{*72K} and *lacZ,* thereby switching the reporter to the ON state. Upon removal of CA, CymR repression of the CA-IM is reinstated. Rather than observe a decline in *pR* activity and reversion back to the OFF state, we anticipate the enhanced level of Tum^{*72K} expressed from the RBS optimised reporter will keep CI inactivated and the ON state stably maintained, thereby establishing cellular memory of the ON state.

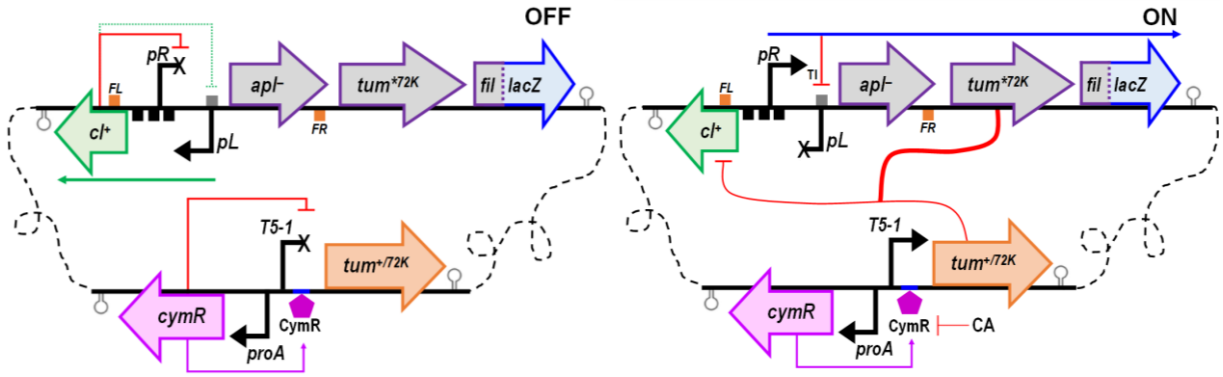

Figure 5.7: ON and OFF state schematics of the CA-inducible AI215 and AI219 186-WCB strains. In the OFF state, CymR inhibits *tum* expression from *T5-1* whilst an active CI (expressed from *pL*) inhibits expression of the *pR.apl*$^{-}$*.tum*^{*72K}*.fil::lacZ* transcript. Following CA induction, CymR is inactivated resulting in derepression of *T5-1* and expression of *tum*. Tum inactivates CI, resulting expression of the *pR.apl*$^{-}$*.tum*^{*72K}*.fil::lacZ* transcript. In the absence of CA, enhanced translation of *tum*^{72K} mRNA is expected to establish ON state cellular memory. Symbolism defined in Table 5.12.

5.2.1.1.1 Determining the CA dosage required for optimal OFF → ON state switching

Preliminary LacZ assays conducted by Ian Dodd for his CA systems confirmed 150µM CA is sufficient to achieve maximal induction. To determine how long our CA-IMs needed to be exposed to 150µM CA to achieve maximal switching, an 80min timecourse blue/white switch plate assay was performed for the AI219 WCB strain. As presented in Figure 5.8, maximal switching was observed 10-20mins after exposure to CA, leading us to conclude an exposure time of 20mins (to 150µM CA) is the optimal dosage for maximal induction. Furthermore, no blue colonies were observed on the uninduced plate, suggesting our CA-IM system significantly reduces/eliminates spontaneous OFF → ON state switching. Re-plated blue colonies (taken from the 10min or 20min switch plate) also returned a greater mix of blue (~91%) to white colonies indicating there is some improvement to ON state stability.

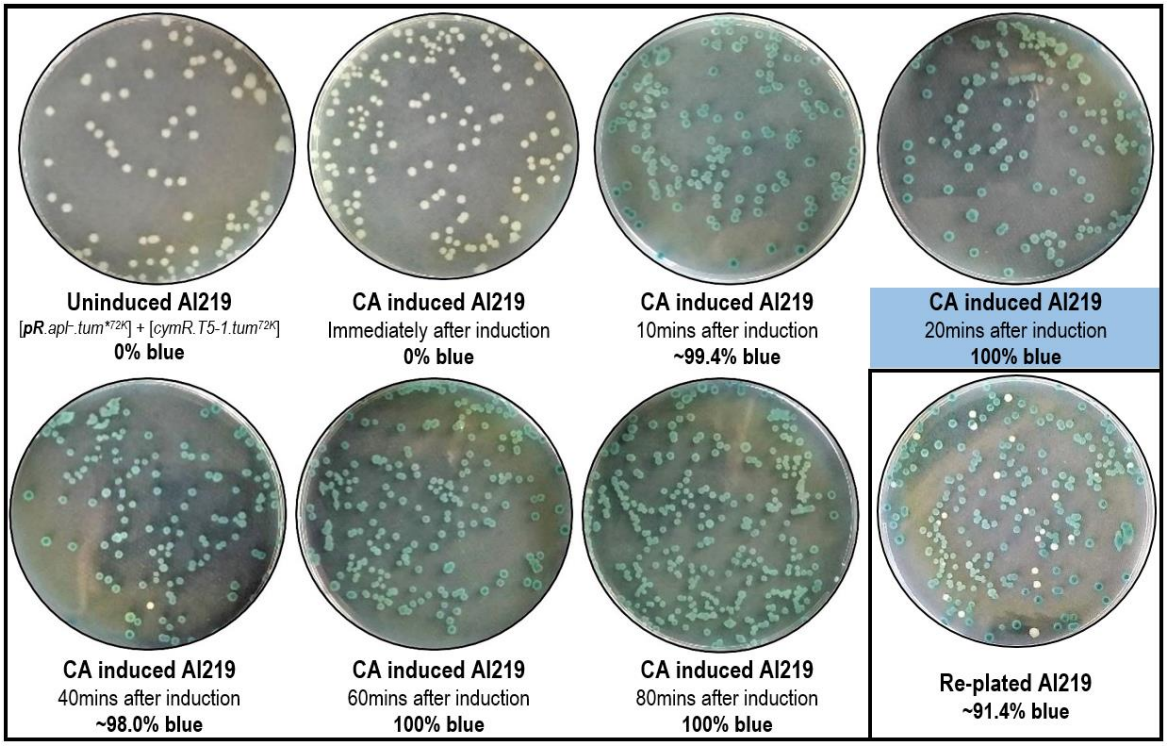

Figure 5.8: Blue/white switch plate timecourse data for the CA-inducible AI219 186-WCB strain. The data shows 20min exposure to 150µM CA is sufficient to achieve maximal (100%) OFF → ON state switching. The issue of spontaneous switching seems to have been eliminated as no blue colonies grew on the uninduced plate. There appears to be an improvement in ON state stability as the majority of colonies (~91%) produced from re-streaking a single blue colony retained the blue/induced phenotype, however, growth of a few white colonies is indicative of ON state instability. Switching was assayed by growing cultures to OD_{600} 0.30 in M9MM-20, treated (in culture) with 150µM CA and switching tracked for 80mins at 37°C. Uninduced and induced switch plates were prepared by diluting cultures 10^{-4}, plating 10µL on L-plates containing 40µg/mL X-gal, incubating O/N at 37°C and the growth of blue and white colonies scored the next day. Percentage values represent the approximate proportion of blue colonies observed on each switch plate presented.

5.2.1.1.2 Comparing ON state switching efficiency between the *tum*^{72K} UV and CA-IMs

To further our characterisation of the CA-IM system we compared the performance of the *tum*^{72K} CA-IM against the *tum*^{72K} UV-IM and confirmed 20mins exposure to 150µM CA achieves a comparable induction profile as observed with the UV system. This was carried out by linking each IM to a λ integrated minimal ***pR***.*apl*$^{+}$.*cII::lacZ* reporter to generate AI199 and AI195 strains (Table 5.5, Fig. 5.9) and to the WCB ***pR***.*apl*$^{-}$.*tum**^{72K} reporter to generate WCB strains AI211 and AI219 (Table 5.5, Fig. 5.10). To assay for induction, *pR* LacZ induction profiles were obtained for AI199 and AI195 (Fig. 5.9C) and AI211 and AI219 (Fig. 5.10C) by conducting concurrent 3hr and 5hr UV and CA-induction timecourse LacZ assays respectively. AI199 and AI211 cultures were induced with 40s UV and AI195 and AI219 cultures were induced with 150µM CA either indefinitely (CA not removed) or for 20mins.

Table 5.5: *E. coli* strains assayed to compare ON state switching efficiency between the *tum*^{72K} UV and CA-IMs. Each module exists at single-copy in the E4643 chromosome; ending subscript indicates site of integration.

Name	Description
AI199	E4643 + [pIT3-CL-*cI*$^{+}$.***pR***$^{+}$.*pL*$^{+}$.*apl*$^{+}$.*cII::lacZ*]$_{\lambda}$ + [pIT3-TO-*p95.tum*^{72K}]$_{186.1}$
AI195	E4643 + [pIT3-CL-*cI*$^{+}$.***pR***$^{+}$.*pL*$^{+}$.*apl*$^{+}$.*cII::lacZ*]$_{\lambda}$ + [pIT4-KT-*cymR.T5-1.tum*^{72K}]$_{\varphi 21}$
AI211	E4643 + [pIT3-CL-*cI*$^{+}$.***pR***$^{+}$.*pL*$^{+}$.*apl*$^{-}$.*tum*^{*72K}.*fil::lacZ*]$_{\lambda}$ + [pIT3-TO-*p95.tum*^{72K}]$_{186.1}$
AI219	E4643 + [pIT3-CL-*cI*$^{+}$.***pR***$^{+}$.*pL*$^{+}$.*apl*$^{-}$.*tum*^{*72K}.*fil::lacZ*]$_{\lambda}$ + [pIT4-KT-*cymR.T5-1.tum*^{72K}]$_{\varphi 21}$

The minimal *pR* LacZ reporter data presented in Figure 5.9C shows AI199 has a slightly elevated *pR* induction profile compared to AI195 treated with CA for 20mins. Continuous exposure to CA generates an enhanced induction profile for AI195, with *pR* activity reaching ~63 LacZ units, 1.2-fold greater than the highest *pR* activity observed for AI195 under transient CA exposure. This makes sense, because when CA is present indefinitely, the system is under constant induction and the reporter fed a continuous supply of Tum^{72K}. Under transient exposure, only a limited amount of Tum^{72K} is expressed (from *T5-1*) during the 20mins in which CA is present. Removing CA allows CymR to re-repress the CA-IM, leaving the system to rely on the limited pool of Tum^{72K} to keep CI inactivated and maintain *pR* activity. Most importantly, an undetectable level of *pR* activity was observed for uninduced AI195, demonstrating Dodd's system offers tight repression of *tum*^{72K} in the absence of CA. The WCB *pR* LacZ reporter data presented in Figure 5.10C shows AI211 and AI219 have identical induction profiles, with *pR* increasing steadily after induction, with levels peaking at ~87 LacZ units 210mins after induction and then stabilising for the remainder of the 5hr timecourse. The results confirm 20mins exposure to 150µM CA achieves a comparable level of induction as seen when the WCB ***pR***.*apl*$^{-}$.*tum**^{72K} reporter is linked to the *tum*^{72K} UV-IM and induced with 40s UV.

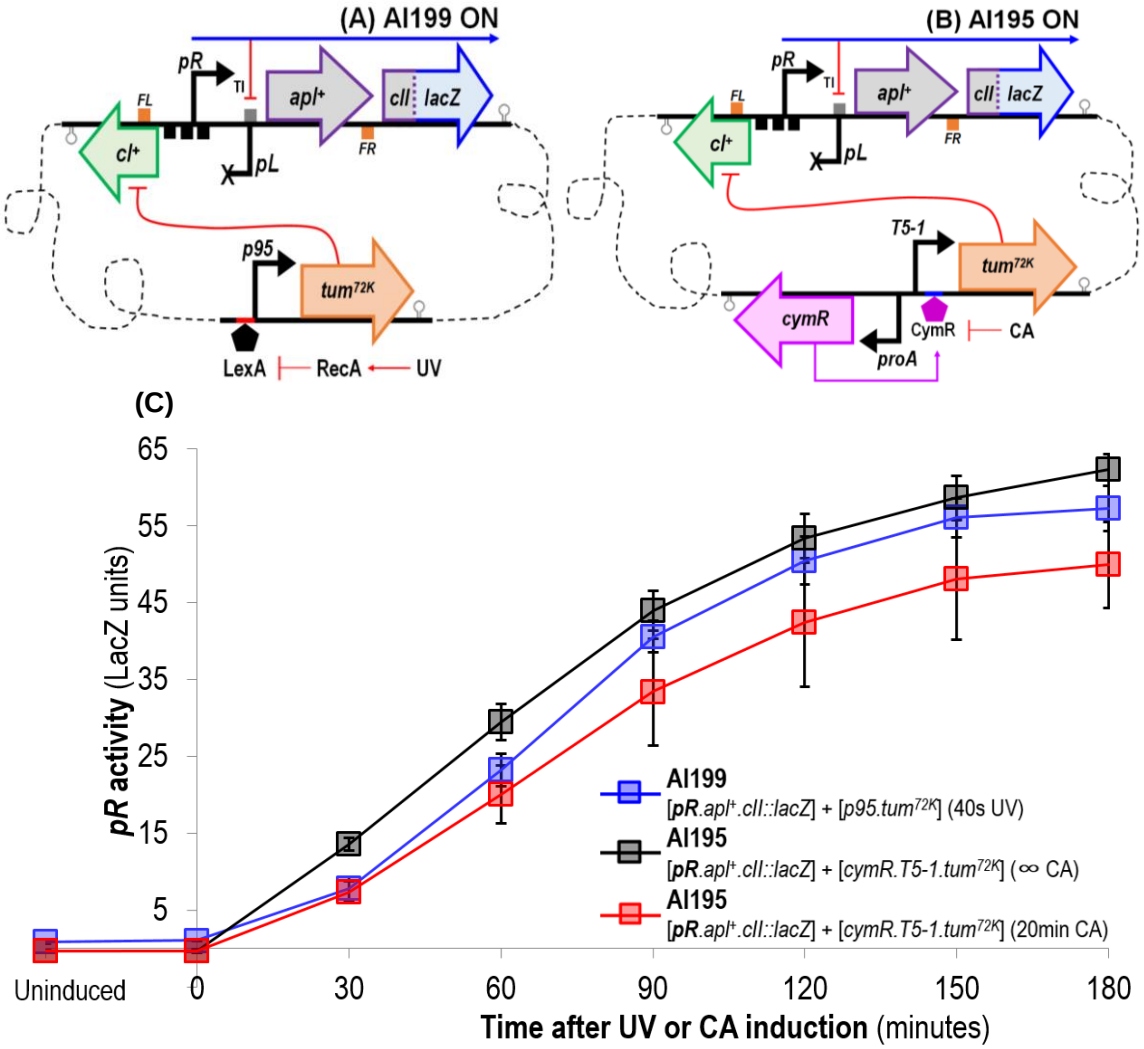

Figure 5.9: The minimal *pR* LacZ reporter strains used to characterise the *cymR.T5-1.tum^{72K}* CA-IM. (A/B) ON state schematics of strains harbouring a λ integrated minimal ***pR**.apl^{+}.cII::lacZ* reporter and a 186 *attB1* integrated *p95.tum^{72K}* UV-IM (AI199) or a φ21 integrated *cymR.T5-1.tum^{72K}* CA-IM (AI195). Symbolism defined in Table 5.12. **(C)** Observed *pR* LacZ activity for AI199 induced with 40s UV and AI195 induced with 150μM CA for 20mins or indefinitely. CA induction was done by adding 7.5μL of 100mM CA stock to 5mL of liquid culture and incubated at 37°C with aeration. The CA was removed by centrifuging cells to a pellet (3095rcf for 5min) at the 20min mark, removing all the S/N and resuspending cells in M9MM-20. Cultures were incubated at 37°C with agitation for the remainder of the timecourse, with samples taken every 30mins. The uninduced time point represents samples taken immediately prior to induction. Each data point represents six independent assays, 95% confidence interval error bars are shown.

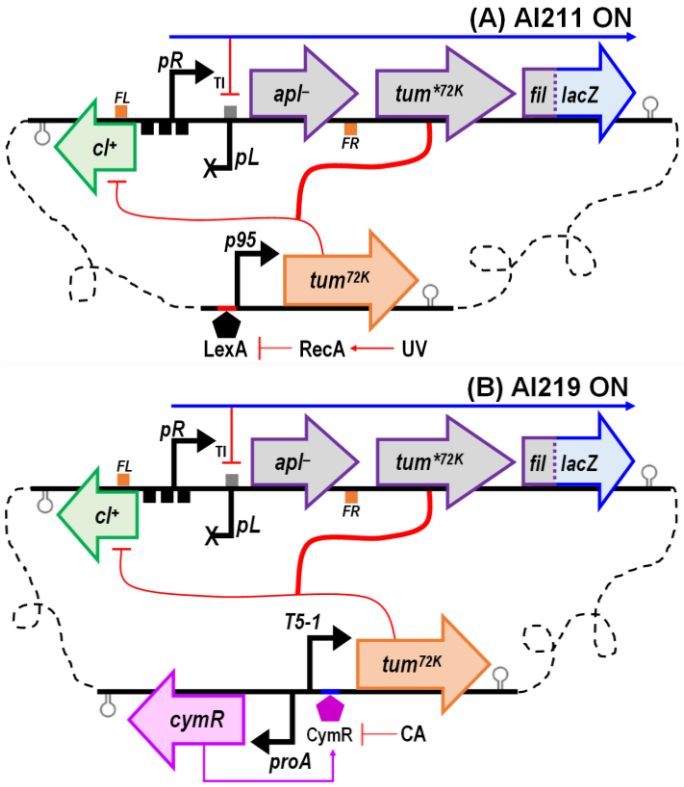

Figure 5.10: The AI211 and AI219 186-WCB strains used to characterise the *cymR.T5-1.tum^{72K}* CA-IM. (A/B) ON state schematics of strains harbouring a λ integrated ***pR***.*apl⁻.tum*^{72K}* reporter and a 186 *attB1* integrated *p95.tum^{72K}* UV-IM (AI211) or a φ21 integrated *cymR.T5-1.tum^{72K}* CA-IM (AI219). Symbolism defined in Table 5.12. **(C)** Observed *pR* LacZ activity for AI211 induced with 40s UV and AI219 induced with 150μM CA for 20mins. CA induction and removal performed exactly as described in Fig. 5.9. The uninduced time point represents samples taken immediately prior to induction. Each data point represents three (AI211) and twelve (AI219) independent assays, 95% confidence interval error bars are shown.

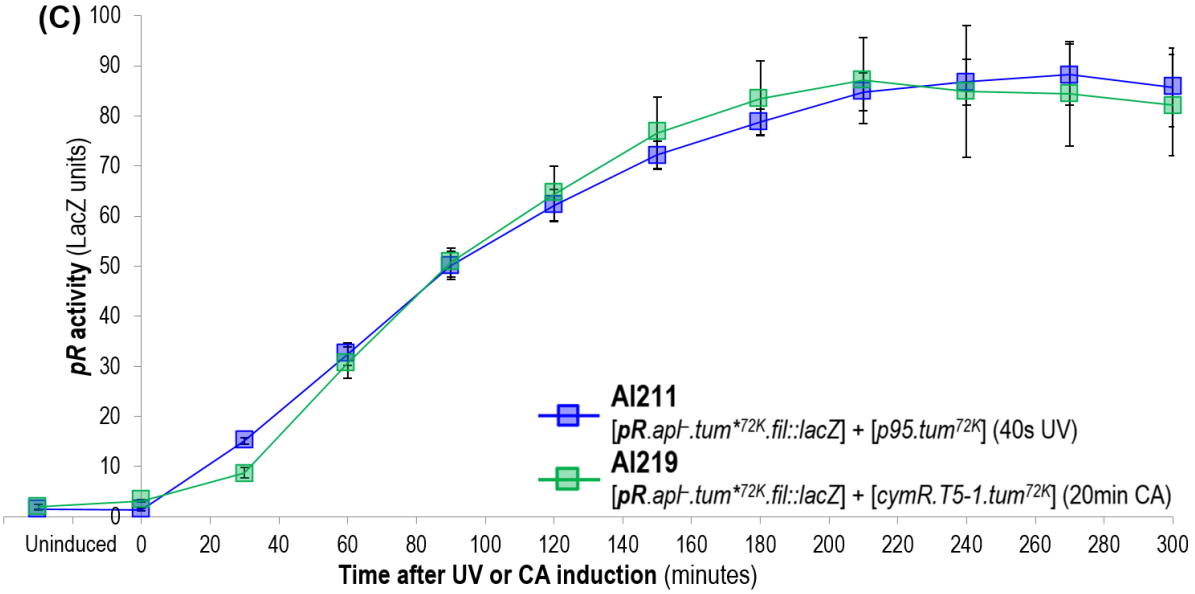

5.2.1.1.3 Comparing ON state switching efficiency between CA-IMs encoding *tum⁺* and *tum^{72K}*

Lastly, we wished to compare the performance of the *tum^{72K}* CA-IM against a *tum⁺* version to ultimately confirm *tum^{72K}* is the optimal *tum* variant for achieving maximal induction efficiency. To conduct this comparison, the *tum⁺* CA-IM was integrated into E4643 harbouring a λ integrated minimal ***pR***.*apl⁺.cII::lacZ* reporter or a WCB ***pR***.*apl⁻.tum*^{72K}* reporter (Table 5.6).

Table 5.6: *E. coli* strains assayed to compare ON state switching efficiency between *tum*⁺ and *tum*^{72K} CA-IMs. Each module exists at single-copy in the E4643 chromosome; ending subscript indicates site of integration.

Name	Description
AI194	E4643 + [pIT4-KT-*cymR.T5-1.tum*⁺]$_{\varphi 21}$ + [pIT3-CL-*cI*⁺.***pR***⁺.*pL*⁺.*apl*⁺.*cII::lacZ*]$_{\lambda}$
AI195	E4643 + [pIT4-KT-*cymR.T5-1.tum*^{72K}]$_{\varphi 21}$ + [pIT3-CL-*cI*⁺.***pR***⁺.*pL*⁺.*apl*⁺.*cII::lacZ*]$_{\lambda}$
AI215	E4643 + [pIT4-KT-*cymR.T5-1.tum*⁺]$_{\varphi 21}$+ [pIT3-CL-*cI*⁺.*apl*⁻.*tum*^{72K}.fil::lacZ*]$_{\lambda}$
AI219	E4643 + [pIT4-KT-*cymR.T5-1.tum*^{72K}]$_{\varphi 21}$ + [pIT3-CL-*cI*⁺.*apl*⁻.*tum*^{72K}.fil::lacZ*]$_{\lambda}$

To assay for induction, *pR* LacZ induction profiles were obtained for AI194 and AI195 (Fig. 5.11B) and AI215 and AI219 (Fig. 5.11D) by conducting 3hr CA-induction LacZ assays. AI194 and AI195 cultures were induced with 150µM CA either indefinitely or transiently (20mins), whilst AI215 and AI219 cultures were only induced transiently. The minimal *pR* LacZ reporter data (Fig. 5.11B) revealed that under continuous exposure to CA, AI194 (*tum*⁺) and AI195 (*tum*^{72K}) have identical induction profiles, with *pR* LacZ activity reaching ~65 LacZ units and exhibiting close-to-zero basal *pR* activity. When exposed to CA transiently however, both modules show reduced *pR* activity, with AI194 (*tum*⁺) exhibiting significant impaired induction efficiency, with *pR* activity peaking at ~23 LacZ units 90mins after induction. For AI195 (*tum*^{72K}), *pR* activity is less than that observed when continuously exposed to CA, but higher levels of *pR* activity are observed (~50 LacZ units) and maintained for the entire 3hr timecourse. Furthermore, the WCB *pR* LacZ reporter data (Fig. 5.11D) clearly shows that following transient exposure to CA, AI215 (*tum*⁺) has a suboptimal *pR* induction profile in comparison AI219 (*tum*^{72K}), with *pR* activity peaking at ~46 LacZ units, 1.9-fold less than that observed for AI219.

Our examination of the WCB strains made thus far confirms that expressing *tum*^{72K} from an RBS optimised WCB reporter offers improved stability of the ON state, whilst expressing *apl* does not offer any improvement to WCB performance. Switching to a CA-IM system significantly reduces/eliminates spontaneous induction and achieves comparable levels of *pR* activity as observed with the LexA-based UV-IM system. Lastly, engineering the CA-IM to express *tum*^{72K} (instead of *tum*⁺) significantly improves WCB OFF → ON state switching. Subsequently, for the continuation of this study, the WCB reporter will be the ***pR***.*apl*⁻.*tum**^{72K} version and the IM will exist as the CA-inducible *T5-1* system that encodes *tum*^{72K}

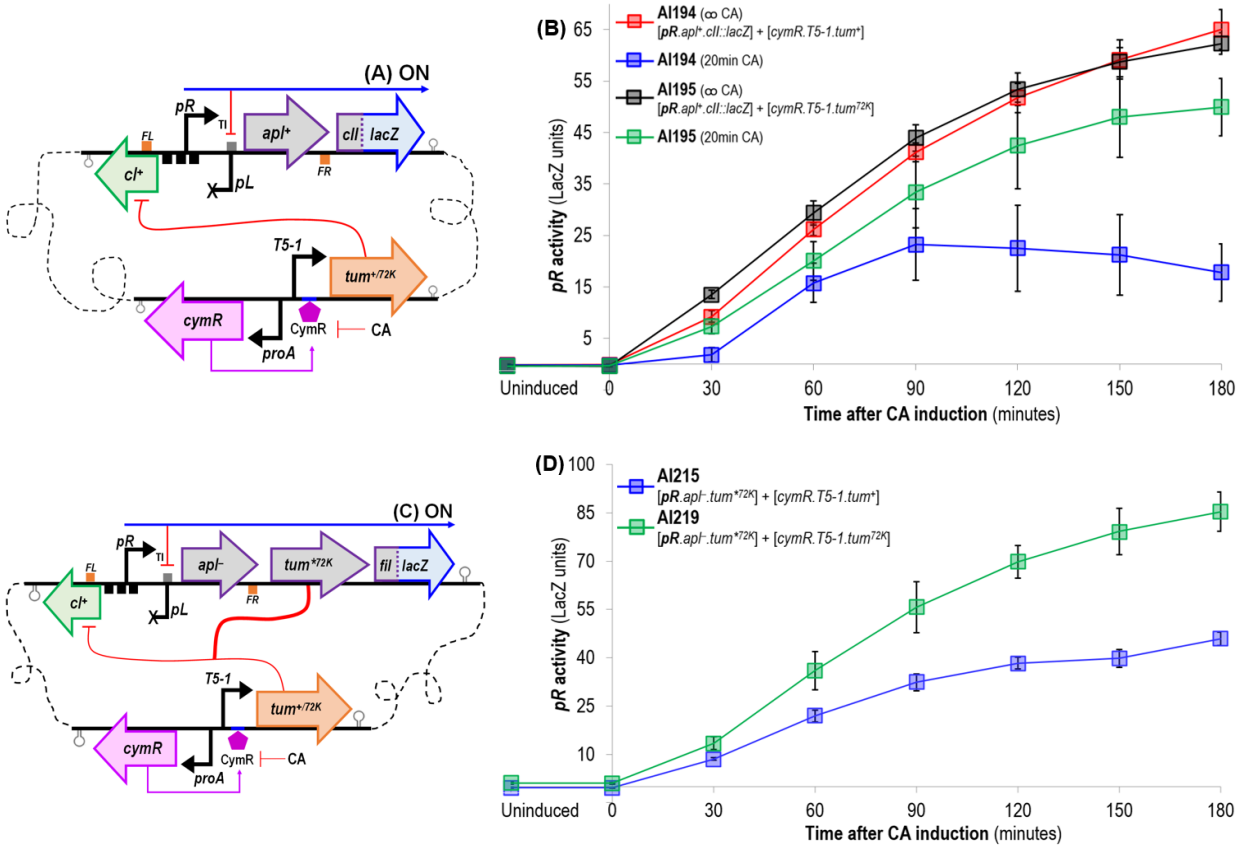

Figure 5.11: The minimal *pR* LacZ reporter strains and the 186-WCB strains used to characterise the *tum*⁺ and *tum*^{72K} CA-IMs. **(A)** ON state schematic of AI194 and AI195 strains harbouring a λ integrated minimal ***pR***.*apl*⁺.*cII::lacZ* reporter and a φ21 integrated *cymR.T5-1.tum*$^{+/72K}$ CA-IM. Symbolism defined in Table 5.12. **(B)** Observed *pR* LacZ activity for AI194 and AI195 following CA-induction. Liquid cultures were induced with 150μM CA transiently (20mins) or indefinitely and *pR* LacZ activity tracked over a 3hr timecourse. The data shows both strains have similar *pR* induction profiles when under continuous exposure to CA, but transient CA exposure results in reduced induction efficiency, especially for AI194 (*tum*⁺). Each data point represents six to eight independent assays, 95% confidence interval error bars are shown. **(C)** ON state schematic of AI215 and AI1219 strains harbouring a λ integrated WCB ***pR***.*apl*⁻.*tum**^{72K}.*fil::lacZ* reporter and a φ21 integrated *cymR.T5-1.tum*$^{+/72K}$ CA-IM. Symbolism defined in Table 5.12. **(D)** Observed *pR* LacZ activity for AI215 and AI219 following CA induction. Liquid cultures were induced with 150μM CA for 20mins and *pR* LacZ activity tracked over a 3hr timecourse. The data complements the (B) data, as the ***pR***.*apl*⁻.*tum**^{72K}.*fil::lacZ* reporter exhibits poor induction efficiency when linked to *cymR.T5-1.tum*⁺ (AI215). Improved induction efficiency is observed when the reporter is linked to *cymR.T5-1.tum*^{72K} (AI219). Each data point represents four independent assays, 95% confidence interval error bars are shown. For all strains, CA induction and removal was performed exactly as described in Fig. 5.9. The uninduced time point represents samples taken immediately prior to induction.

5.3 186-WCB engineering stage 3

5.3.1 Quantifying long-term ON state stability of the 186-WCB

5.3.1.1 The design of a stability assay to measure WCB long-term ON state stability following CA induction

So far, our assessment of WCB ON state stability remains confined to a 24hr period. To further our characterisation we wanted to determine whether cells could remain ON for days rather than hours. The third stage of this study focused on developing an assay that could accurately measure the long-term stability of the ON (or OFF) state of the WCB. In particular, we wanted to determine, for the most optimal WCB created thus far (AI219) (including its *tum*⁻ control, AI266) (Fig. 5.12), the ability this system has in establishing long-term memory of the ON state following transient exposure to CA.

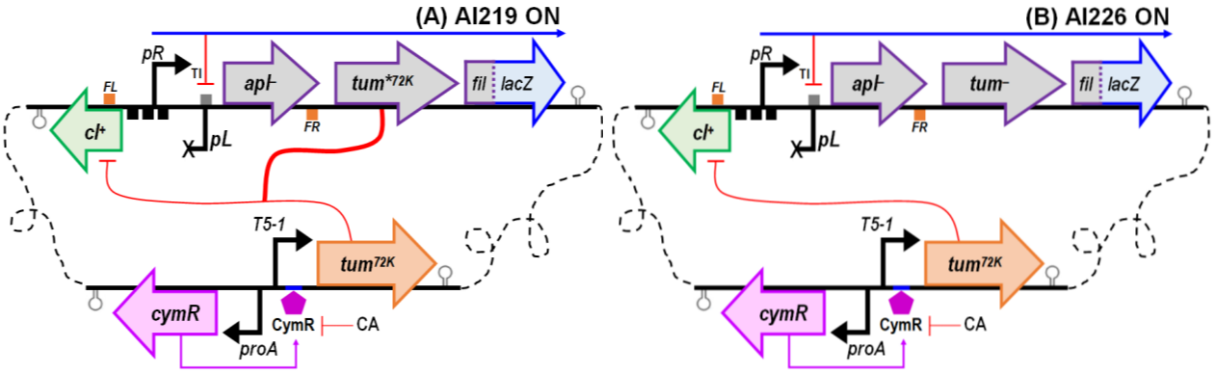

Figure 5.12: The AI219 and AI226 186-WCB strains used to test the stability assay. **(A)** ON state schematic of the AI219 strain, E4643 + [pIT4-KT-*cymR.T5-1.tum*^{72K}]$_{\varphi 21}$ + [pIT3-CL-*cI*$^{+}$.***pR***$^{+}$.*pL*$^{+}$.*apl*$^{-}$.*tum**^{72K}]$_{\lambda}$. **(B)** ON state schematic of the AI226 control strain, E4643 + [pIT4-KT-*cymR.T5-1.tum*^{72K}]$_{\varphi 21}$ + [pIT3-CL-*cI*$^{+}$.***pR***$^{+}$.*pL*$^{+}$.*apl*$^{-}$.*tum*$^{-}$]$_{\lambda}$. Symbolism defined in Table 5.12.

To assay long-term stability, we developed the stability assay (Fig. 5.13), a continuous experiment that can simultaneously measure and visualise ON or OFF state stability of WCB cells by conducting daily LacZ assays and preparing blue/white switch plates, respectively. In practical terms, the assay is relatively simple and works as follows:

1. An O/N culture is prepared by inoculating a single colony in M9MM-1.
   - Single colonies are sourced from a glycerol stock re-streaked on a L-plate with the appropriate antibiotic(s) and grown O/N at 37°C.
2. The O/N culture is prepared for induction by diluting cells to OD_{600} 0.15 in M9MM-20 and permitting growth to early-log phase (OD_{600} ~0.30).
3. Cells are induced with 150µM CA for 20mins to set the system in the ON state.
   - Induction parameters can be changed to switch cells that respond to different inducers.
4. To remove the CA, cells are centrifuged to a pellet and the S/N removed.
5. To assay system stability, cells are resuspended in M9MM-20 and LacZ production tracked for 5hrs each day.

- To quantify LacZ, samples are taken every 30mins, stored on ice and at the end of the timecourse a LacZ assay is performed (see Chapter 7, Section 7.0.6.2).
- To visualise the production of LacZ, a set of blue/white switch plates are prepared at various chosen timepoints (we recommend one plate/hr).

6. To continuously passage cells over multiple days, at the end of each 5hr timecourse, induced cells are subcultured in M9MM-1and grown O/N at 37°C.
7. To prepare for a second round of LacZ analysis the M9MM-1 O/N induced culture is diluted to OD_{600} 0.15 in M9MM-20 and grown to early-log phase (OD_{600} ~0.30).
8. At the correct cell density, another 5hr LacZ timecourse is started during which a set of blue/white switch plates are prepared and samples stored on ice for the LacZ assay.
9. At the end of the 5hr timecourse, cells are switched back to M9MM-1 for O/N growth and passaging to the third day.

System stability can be continuously tracked by repeating steps (7) to (9) for as many days as deemed appropriate. The decision to continuously switch the cells between M9MM-1 and M9MM-20 was a design feature intended for the control of cell growth. To accurately quantify LacZ production, it is a requirement that cells are assayed in log phase. Since it was unfeasible to manually control cell growth continuously we designed the assay such that cultures never exceeded OD_{600} 0.50. To prevent cells from entering stationary growth, O/N cells were cultured in M9MM-1, as the low level of glucose (1mM) would quickly become the limiting factor and halt cell growth - when cell density was measured the next day, values never exceeded OD_{600} 0.25. To prepare cells for LacZ analysis, each culture was diluted to OD_{600} 0.15 in M9MM-20, where the addition of more glucose (20mM) would encourage growth and allow cells to each a density of OD_{600} 0.40. To ensure cells did not exceed the absolute upper limit (OD_{600} 0.50) during the 5hr timecourse, cultures were periodically diluted (every 30mins) with pre-warmed M9MM-20 to OD_{600} 0.30. This not only ensured cells never entered the stationary phase but each sample for LacZ analysis fell within the required OD_{600} 0.30-0.40 range.

A key question that did arise was whether switching between M9MM-1 and M9MM-20 media would have an effect on WCB stability, such that, could it cause cells (especially when cultured in M9MM-1) to relapse to the OFF state? To assess the robustness of the AI219 WCB strain, a series of blue/white switch plates were prepared following growth in different media and at different growth phases (Fig. 5.14). The plates clearly show that (1) switching induced cells between M9MM-1 and M9MM-20 does not disrupt ON state stability (Fig. 5.14, steps 5A and 5B) and (2) log and stationary growth in M9MM-1, M9MM-20 and LB +20µg/mL chloramphenicol and kanamycin also does not affect ON state stability (Fig. 5.14, steps 6A to 6C).

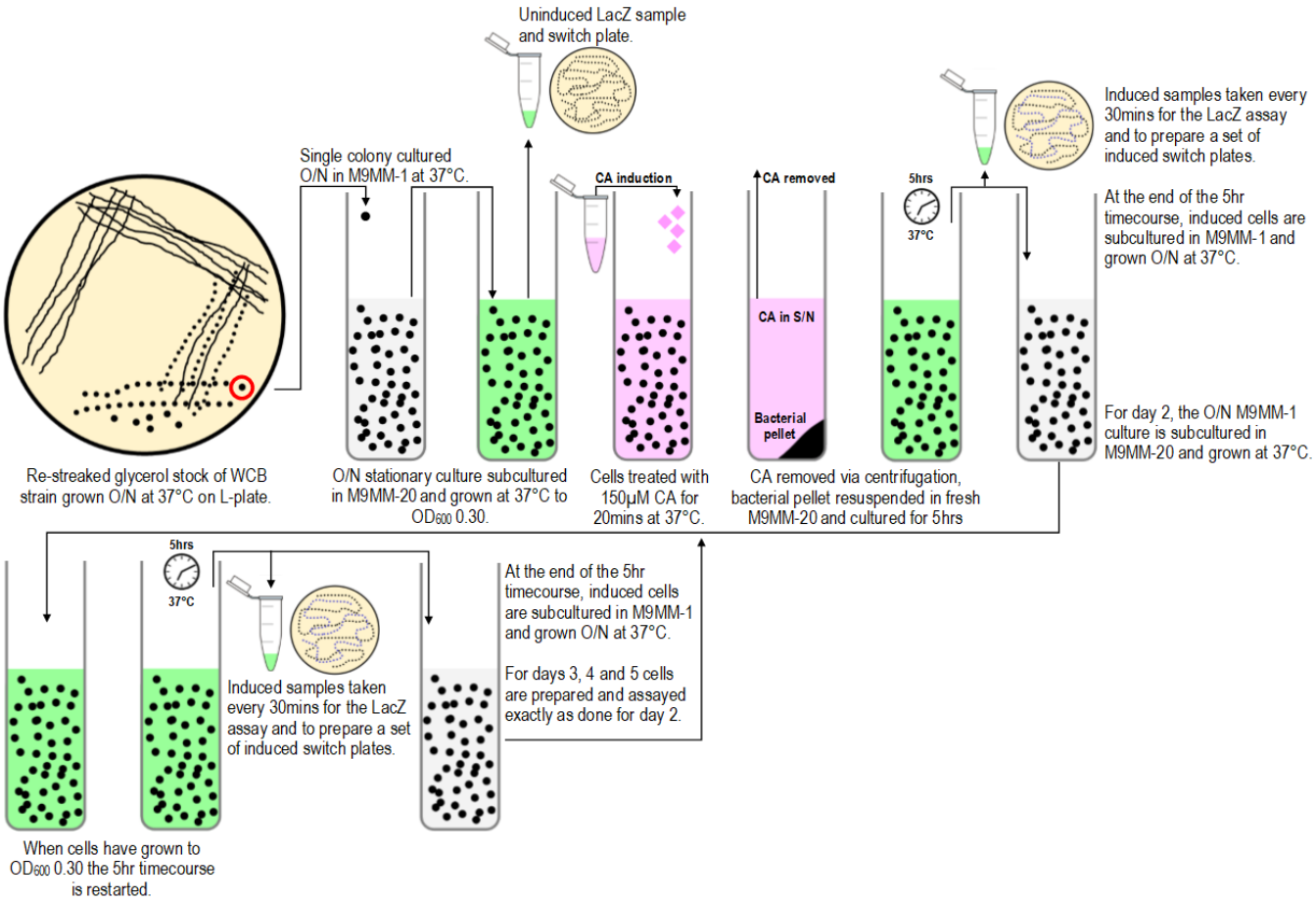

Figure 5.13: A flow diagram of the stability assay tested on the AI219 and AI226 186-WCB strains. To prepare for the assay, O/N stationary cultures are setup by growing cells in M9MM-1 at 37°C under agitation. To prepare for induction, each O/N culture is diluted to OD_{600} 0.15 in M9MM-20 and grown at 37°C under agitation until cells reach OD_{600} 0.30. To begin the assay, each culture is induced with 150µM CA for 20mins and to remove the CA, cells are centrifuged to a pellet (at 3095rpm for 5mins), all the S/N removed and the pellet resuspended in M9MM-20. Each culture is incubated at 37°C with agitation for 5hrs, with samples taken every 30mins. For LacZ analysis, samples are stored on ice and assayed as per the protocol described in Chapter 7, Section 7.0.6.2. To assay for blue/white switching, samples are diluted (10^{-4}) and 10µL plated on X-gal (40µg/mL) L-plates, incubated O/N at 37°C and the growth of blue and white colonies scored the next day. At the end of the 5hr timecourse, ~7mL M9MM-1 is inoculated with ~5µL of each induced culture and incubated O/N at 37°C with aeration. The next day, the O/N induced cultures are diluted to OD_{600} 0.15 in 7mL M9MM-20 and incubated at 37°C with aeration until cells reach OD_{600} 0.30. The second 5hr timecourse is started (without induction) by taking ~500µL samples every 30mins and storing them on ice for LacZ analysis and diluted (10^{-4}) to make a set of blue/white switch plates. To maintain log phase growth (OD_{600} ~0.40) throughout each timecourse, cultures are periodically diluted with pre-warmed M9MM-20 to OD_{600} 0.30.

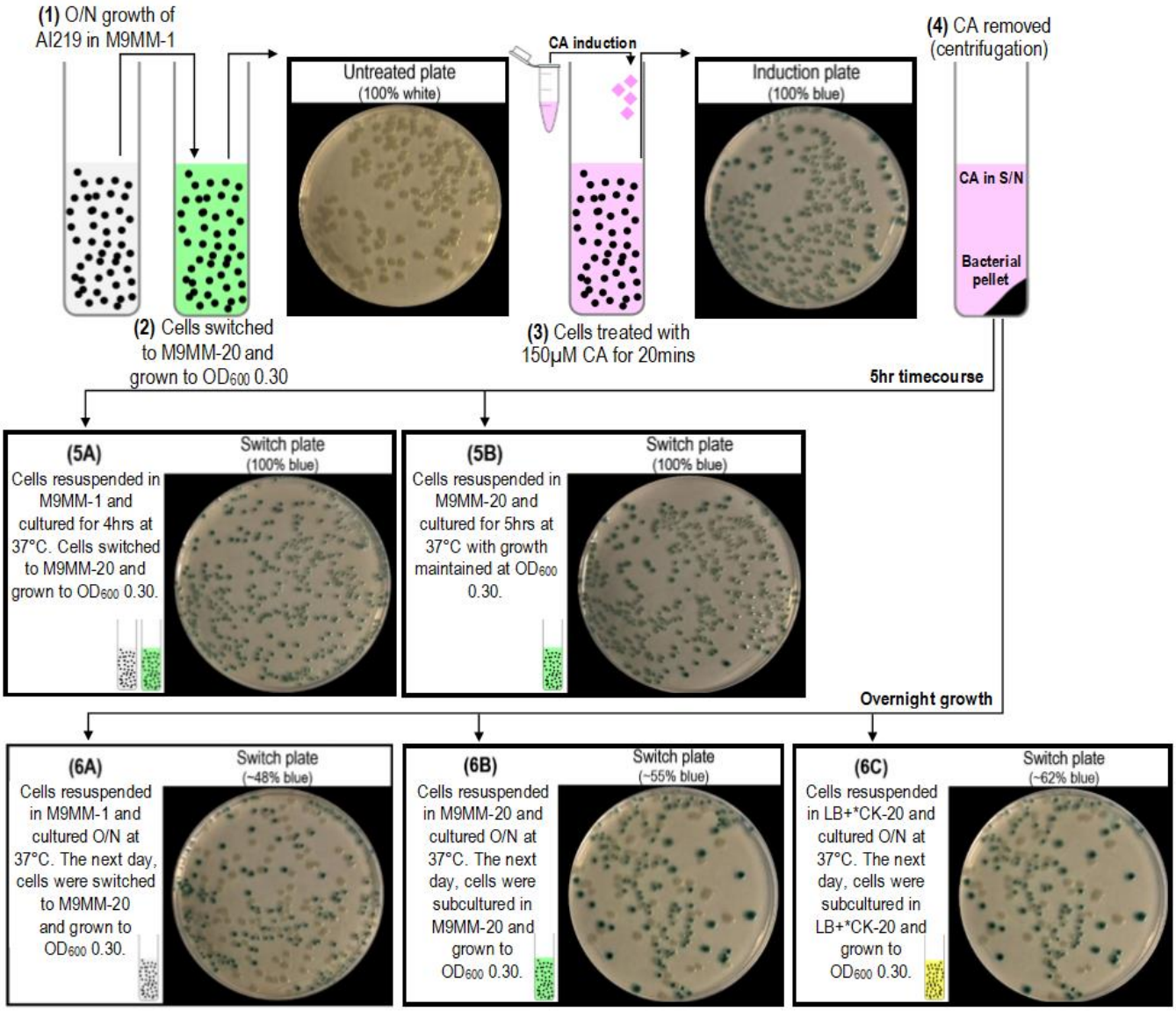

Figure 5.14: Assaying the robustness of the AI219 186-WCB strain. To confirm ON state stability is not compromised when cells are exposed to different media and/or cultured beyond log phase growth, CA-induced AI219 cells were cultured O/N in M9MM-1, M9MM-20 and LB+CK-20 and allowed to grow to OD_{600} >0.40. The results show that (1) switching cultures between M9MM-1 and M9MM-20 does not disrupt ON state stability and (2) log and stationary phase growth in M9MM-1, M9MM-20 and LB+CK-20 does not affect ON state stability. *CK-20 represents LB media supplemented with 20µg/mL of chloramphenicol and kanamycin.

5.3.1.1.1 The results of the AI219 WCB long-term ON state stability assay

As mentioned previously, the most optimal 186-WCB created thus far is AI219 (Fig. 5.12A), with previous experiments, showing this system has an impressive rate of OFF → ON state switching and a very low rate of spontaneous induction. Using this strain and its *tum*⁻ control (AI226) we tested our stability assay protocol, by inducing cells to the ON state with 150µM CA for 20mins (Fig. 5.15 and 5.16). Since AI226 does not encode tum^{72K} from the MFL reporter, we expected these cells to undergo OFF → ON state switching but be incapable of establishing long-term memory of the ON state.

As expected AI219 (tum^{72K}) exhibits maximal (100%) OFF → ON state switching after CA-induction. The progressive emergence of white colonies on the 24, 48, 72 and 96hr plates suggests the ON state is somewhat unstable (Fig. 5.15). The same data is presented graphically in Figure 5.16A, where AI219 has a near 100% induction rate, with the proportion of blue colonies reducing to ~60%, ~27%, ~10% and ~4% on days 2, 3, 4 and 5 respectively. AI219 also exhibited a significantly improved *pR* LacZ induction profile in comparison to AI229 (*tum*⁻), with *pR* activity peaking at ~111 LacZ units 300mins after CA-induction, which then declines to ~57, ~25, ~11 and ~7 LacZ units over days 2, 3, 4 and 5 respectively (Fig. 5.16B, ▲ data). We calculated ON state stability for AI219 to have an ~half-life of 26hrs.

The *pR* LacZ induction profile observed for AI226 (Fig. 5.16B, ▲ data), complements the switch plate data (Fig. 5.15), where an initial increase in *pR* activity (~80 LacZ units) is observed after CA-induction (indicative of OFF → ON state switching), which then declines to ~42 LacZ units at the end of day 1. During the day 2 timecourse, no *pR* LacZ activity was detected; indicating all cells were growing in the OFF state and had failed to establish long-term memory of the ON state. We calculated ON state stability for AI226 to have a very short half-life of ~2.5hrs.

Figure 5.16C presents a combined plot of the switch plate data and the LacZ data to illustrate that a strong agreement exists between the two data types. We were impressed to discover how well our protocol can reproducibly quantify and visualise (simultaneously) long-term WCB stability. Overall, during this stage of the project we successfully developed a stability assay that can accurately measure long-term WCB stability, such that when tested on the AI219 186-WCB strain we discovered these cells can sustain the ON state for tens of hours. The fact that the ON state is not maintained indefinitely however, is again indicative that more optimisation is required.

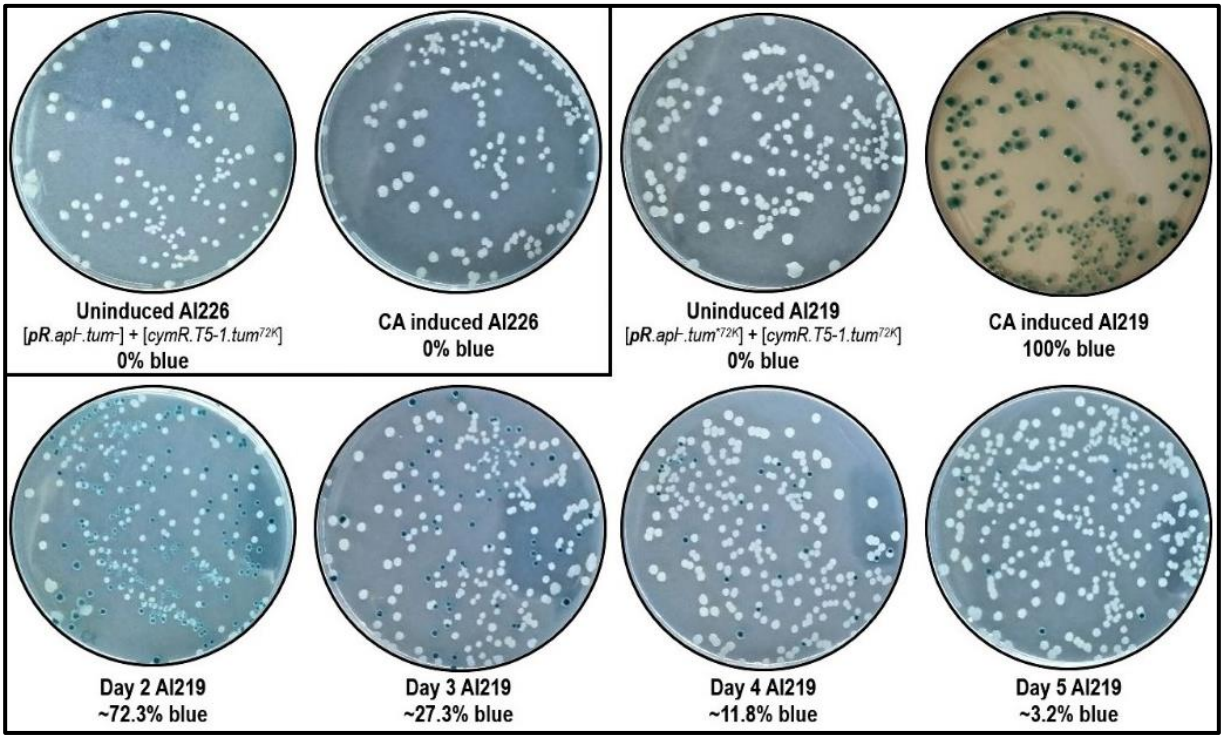

Figure 5.15: A set of long-term blue/white switch plates prepared for the AI219 and AI226 186-WCB strains. As expected, AI229 (*tum*$^{-}$) exhibited no stable OFF → ON state switching, with all cells growing as white colonies. All colonies appear white on the uninduced AI219 (*tum*^{*72K}) plate confirming the system has a very low level of spontaneous switching. The first AI219 induced switch plate (made immediately after 20mins exposure to 150uM CA) displays maximal (100%) OFF → ON state switching. Plates prepared 24, 48, 72 and 90hrs after CA-induction show a gradual decline in blue colonies, with almost all cells relapsing to the OFF state at the end of the passaging period. The gradual emergence of white colonies demonstrates AI219 cells are unable to maintain the ON state indefinitely. The assay was performed exactly as described in Fig. 5.13. Percentage values represent the approximate proportion of blue colonies observed on each switch plate presented.

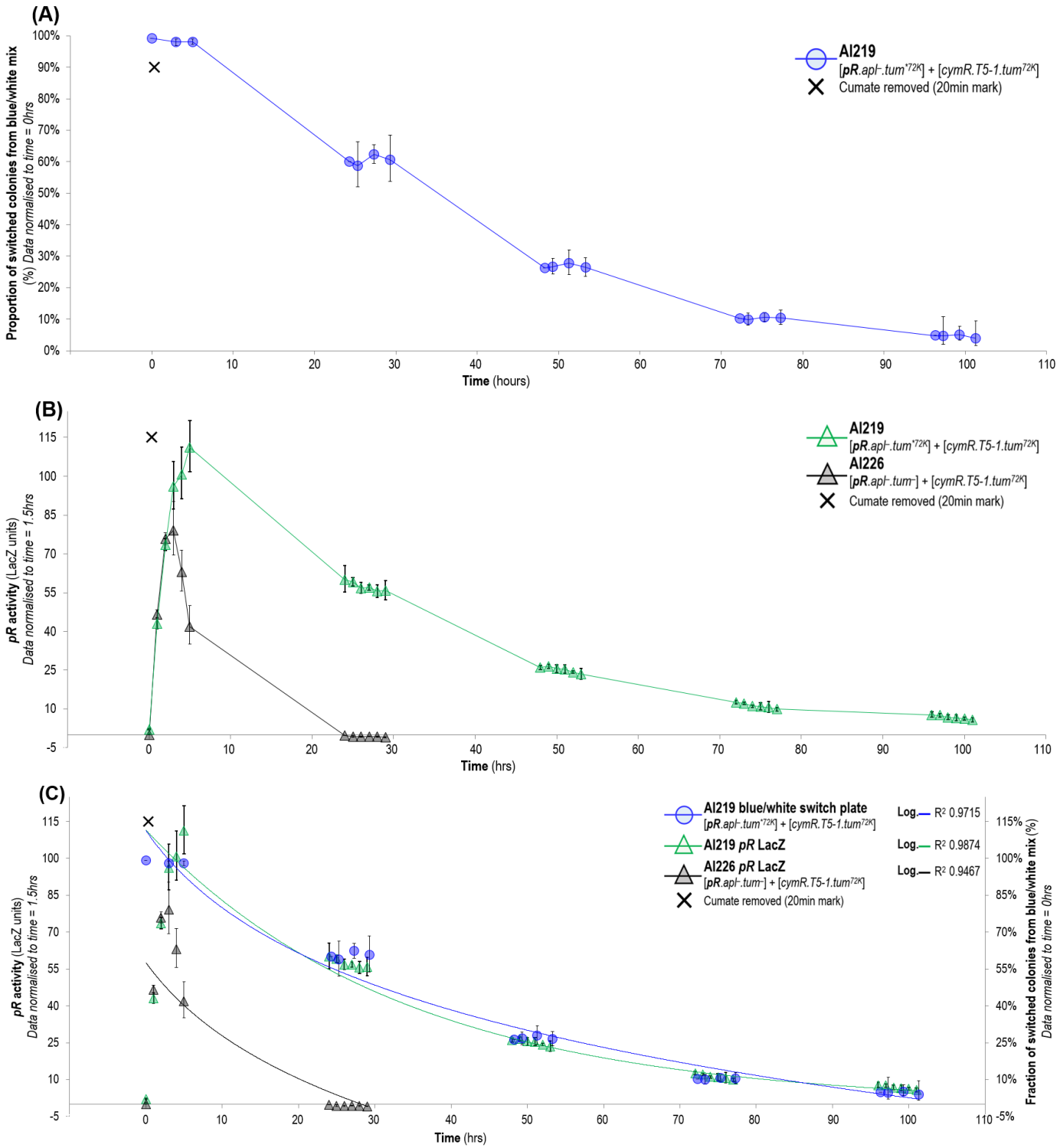

Figure 5.16: Observed blue/white switching and *pR* LacZ activity for the AI219 and AI226 186-WCB strains. **(A)** The proportion of AI219 (*tum*^{72K}) colonies observed on blue/white switch plates prepared before and after CA-induction. The AI226 (*tum*$^{-}$) switch plate data has not been plotted as growth of blue colonies was not observed. CA-induction of AI219 cells results in maximal (100%) OFF → ON state switching, but the proportion of ON state cells gradually declines each day, with ~97% of cells having switched OFF at the end of day 5. The data has been plotted as the average proportion (%) of blue colonies observed on each switch plate. To reduce the day-to-day variation observed, the data for each independent assay was normalised to the time = 0hr mark. Each data point represents an average of four independent assays, 95% confidence interval error bars are shown. **(B)** Observed *pR* LacZ activity for AI219 and AI226 following CA-induction. Liquid cultures were induced with 150µM CA for 20mins and *pR* LacZ activity monitored for 5 days by conducting 5hr timecourse LacZ assays each day. AI226 exhibits poor ON state stability, whilst AI219 has an enhanced *pR* induction profile and can maintain the ON state for tens of hours. ON state stability for AI226 and AI219 were calculated to have a half-life of ~2.5hrs and ~26hrs respectively. To reduce the day-to-day variation observed, the data for each independent assay was normalised to the time = 1.5hr (90mins) mark. Each data point represents an average of three independent assays, 95% confidence interval error bars are shown. **(C)** A combined scatter plot of the blue/white switch plate data (from A) and the *pR* LacZ data (from B) plotted on the same time scale. R^2 values are shown for each data set, all of which are >0.90.

5.4 186-WCB engineering stage 4

5.4.1 Exploring WCB adaptability to assess the potential for real-life applications

5.4.1.1 The use of vanillic acid and salicylic acid IMs demonstrates the WCB can be adapted to respond to other signals

In our efforts to engineer a WCB that can establish long-term cellular memory of two mutually exclusive ON and OFF states, we have (so far) successfully built a MFL reporter switch with several desirable properties. First, the AI211 and AI219 WCB strains demonstrate efficient OFF → ON state switching when induced with UV or CA respectively. AI219 is the preferred WCB as it exhibits a very low rate of spontaneous switching, which suggests the CA-IM offers tight control of *tum*^{72K} expression in the absence of CA. The AI219 stability assays also revealed this WCB strain is capable of establishing memory of the ON state that lasts for tens of hours. Having created a MFL reporter switch that can respond with high efficiency to UV or CA, we wanted to determine if the system could be adapted to respond to other small molecules. Using the Meyer et al. (2019) paper as inspiration we engineered two new IMs that could be induced with vanillic acid (VA) or salicylic acid (SA). Of the twelve different IMs developed by Meyer et al. (2019) (each induced by a different compound) the VA- and SA-IMs were chosen because their induction profiles exhibited very low levels of basal activity and achieved high activation of promoter activity following induction. Furthermore, VA and SA are compounds that are readily available and inexpensive.

The design of our VA-IM (pIT4-KT-*vanR.pVan*^{CC}*.tum*^{72K}) and SA-IM [pIT4-KT-*nahR.pSal*^{TTC}*.tum*^{72K}] was very similar to the CA-IM *(*pIT4-KT-*cymR.T5-1.tum*^{72K}) (Fig. 5.17). In these systems, the constitutive *proA* promoter expresses the VA repressor (VanR) or the SA repressor (NahR), with *tum*^{72K} expression under the control of the VanR regulated *pVan*^{CC} promoter or the NahR regulated *pSal*^{TTC} promoter. The VA- and SA-IMs were assembled with the *Kpn*I and *Xma*I digested pIT4-KT-*cymR.T5-1.tum*^{72K} module and gBlock 15 or gBlock 16 respectively (see Chapter 7, Table 7.12). These gBlocks contained the DNA sequences encoding VanR and *pVan*^{CC} (15) and NahR and *pSal*^{TTC} (16), which we derived from Meyer et al. (2019). The new IMs were integrated into the φ21 *attB* site of E4643 already harbouring the WCB ***pR***.*apl*$^{-}$*.tum*^{*72K} LacZ reporter to develop two new WCB strains, AI256 and AI260 (Fig. 5.17).

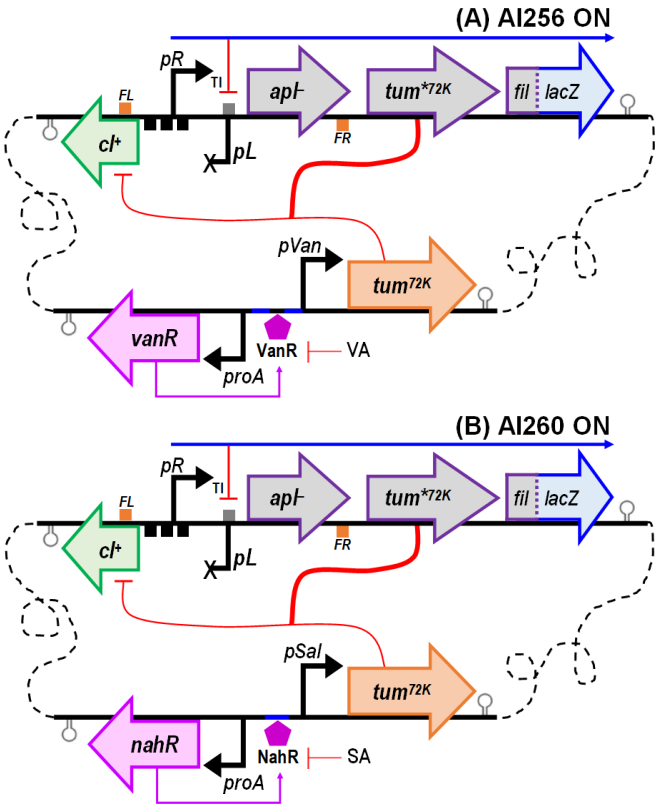

Figure 5.17: The VA- and SA-inducible 186-WCB strains. **(A)** ON state schematic of the AI256 strain, E4643 + [pIT4-KT-*vanR.pVan*^{CC}*. tum*^{72K}]$_{\varphi 21}$ + [pIT3-CL-*cI*$^{+}$.***pR***$^{+}$*.pL*$^{+}$*.apl*$^{-}$*. tum*^{*72K}*. fil::lacZ*]$_{\lambda}$. **(B)** ON state schematic of the AI260 strain, E4643 + [pIT4-KT-*nahR. pSal*^{TTC}*.tum*^{72K}] $_{\varphi 21}$ + [pIT3-CL-*cI*$^{+}$.***pR***$^{+}$*.pL*$^{+}$*.apl*$^{-}$*.tum*^{*72K}*.fil::lacZ*]$_{\lambda}$. In the presence of VA or SA, AI256 and AI260 are induced to undergo OFF → ON state switching respectively. Following induction, the repressor is inactivated and *tum*^{72K} expressed from a depressed *pVan* or *pSal* promoter. Tum^{72K} inactivates CI, which results in expression of more *tum*^{72K} and *lacZ* from a derepressed *pR*. Symbolism defined in Table 5.12.

5.4.1.1.1 Determining the VA and SA dosage required for optimal 186-WCB ON state switching

Since Meyer et al. (2019) used 100µM VA or SA to achieve maximal induction of their VA and SA systems, we assumed an inducer concentration ≥100µM would also achieve maximal induction of our new (yet similar) IMs. As determined previously, the optimal dosage for our CA-IM was set at 20mins 150µM CA (see Section 5.2.1.1.1, Fig. 5.8). For consistency purposes, we decided to treat each new IM with 150µM of their respective inducer and determine the optimal exposure time each IM required to achieve maximal switching. To determine dosage time, a 60min timecourse blue/white switch plate assay was performed for the VA-inducible AI256 and the SA-inducible AI260 WCB strains (see Fig. 517). As presented in Figure 5.18, maximal switching (100%) was observed for AI256 40mins after exposure to VA and for AI260 60mins after exposure to SA, with spontaneous switching being non-existent for both systems. From these assays, we concluded an exposure time of 40mins to 150µM VA and 60mins to 150µM SA is the optimal dosage to achieve maximal induction of AI256 and AI260 respectively.

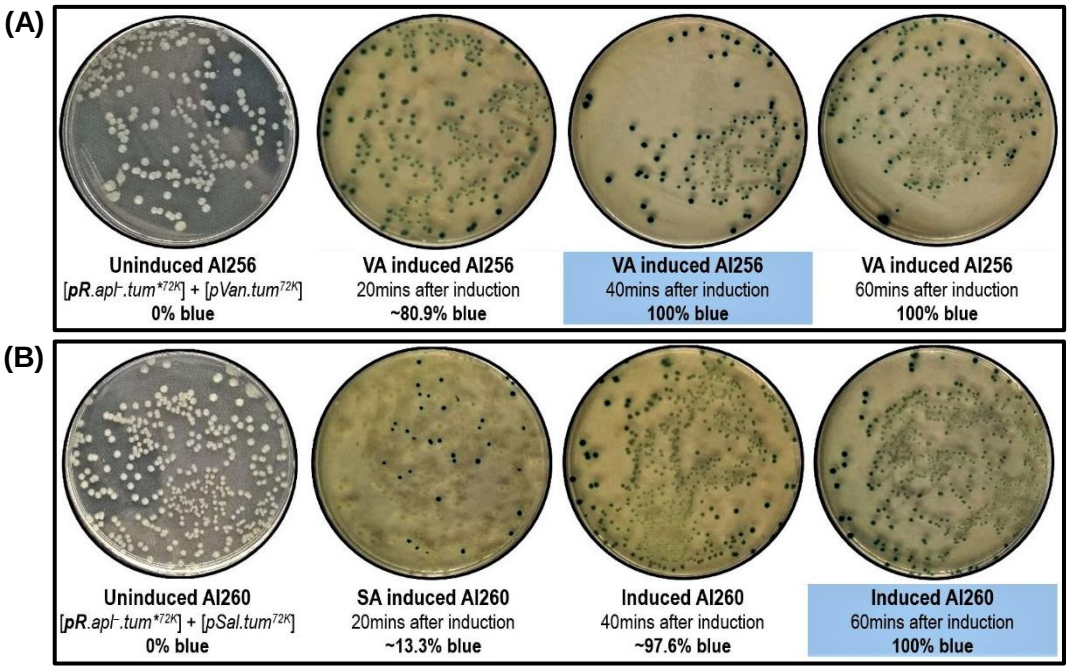

Figure 5.18: Blue/white switch plate timecourse data for the VA-inducible AI256 and SA-inducible AI260 186-WCB strains. The data shows 40mins exposure to 150µM VA **(A)** and 60mins exposure to 150µM SA **(B)** is required to achieve maximal (100%) OFF → ON state switching. Both IMs appear to offer tight control of *tum*^{72K} expression as no blue colonies grew on the uninduced plates. Switching was assayed by growing cells to OD_{600} 0.30 in M9MM-20, treated with 150µM VA or SA (in culture) and switching tracked for 60mins. To evaluate spontaneous induction, a switch plate of the uninduced culture was prepared. Switch plates were prepared by diluting the culture (10^{-4}), plating 10µL on X-gal L-plates, incubating O/N at 37°C and the growth of blue and white colonies scored the next day. Percentage values represent the approximate proportion of blue colonies observed on each switch plate.

5.4.1.1.2 Comparing ON state switching efficiency between UV, CA, VA and SA-IMs encoding *tum*^{72K}

To compare the performance of the new IMs with the previously used UV- and CA-IMs, a series of 4.5hr timecourse LacZ assays were performed for the AI211, AI219, AI256 and AI260 WCB strains (Table 5.7). The observed *pR* induction profiles for the new IMs (Fig. 5.19) are rather languid in comparison to the AI211 (UV) and the AI219 (CA) strains, where *pR* activity peaks at ~87 LacZ units 210mins after induction. For AI256 (VA), *pR* LacZ activity reaches ~76 LacZ units 240mins after induction and for AI260 (SA), *pR* activity reaches ~66 LacZ units 260mins after induction. The lower *pR* activity observed for these new IMs is likely due to a number of factors. First, the system's kinetics may explain why each IM requires a longer exposure time than the CA-IM system, where more time is required for the VA or SA to enter *E. coli,* locate, bind and disengage their respective repressor from the DNA. Secondly, in the CA-IM system *tum*^{72K} expression is driven by the *T5-1* promoter, which may offer a stronger rate of transcription than the *pVan* and *pSal* promoters designed by Meyer et al. (2019). Overall, introducing these new IMs clearly demonstrates that our 186-WCB can be easily adapted to respond to different sensor molecules.

Table 5.7: The 186-WCB strains assayed to compare OFF → ON state switching efficiency between the *tum^{72K}* UV, CA, VA and SA-IMs. Each module exists at single-copy in the E4643 chromosome; ending subscript indicates site of integration.

Name	Description
AI211	E4643 + [pIT3-TO-*p95.tum^{72K}*]$_{186.1}$ + [pIT3-CL-*cI^{+}.**pR**$^{+}$.pL^{+}.apI^{-}.tum^{*72K}.fil::lacZ*]$_{\lambda}$
AI219	E4643 + [pIT4-KT-*cymR.T5-1.tum^{72K}*]$_{\varphi 21}$ + [pIT3-CL-*cI^{+}.**pR**$^{+}$.pL^{+}.apI^{-}.tum^{*72K}.fil::lacZ*]$_{\lambda}$
AI256	E4643 + [pIT4-KT-*vanR.pVan^{CC}.tum^{72K}*]$_{\varphi 21}$ + [pIT3-CL-*cI^{+}.**pR**$^{+}$.pL^{+}.apI^{-}.tum^{*72K}.fil::lacZ*]$_{\lambda}$
AI260	E4643 + [pIT4-KT-*nahR.pSal^{TTC}.tum^{72K}*]$_{\varphi 21}$ + [pIT3-CL-*cI^{+}.**pR**$^{+}$.pL^{+}.apI^{-}.tum^{*72K}.fil::lacZ*]$_{\lambda}$

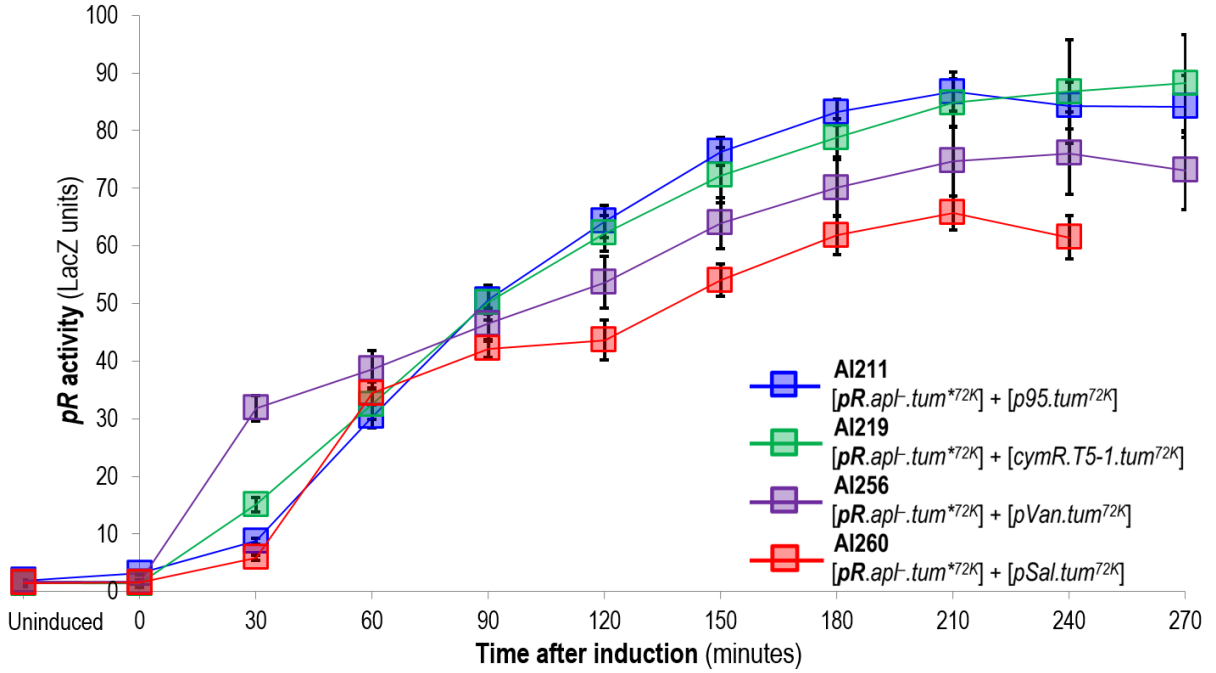

Figure 5.19: Observed *pR* LacZ activity for the 186-WCB strains harbouring a *tum^{72K}* UV, CA, VA and SA-IM. *pR* LacZ activity was assayed for 4.5hrs following induction with 40s UV (AI211), 20mins 150µM CA (AI219), 40mins 150µM VA (AI256) and 60mins 150µM SA (AI260). As observed previously, AI211 (UV) and AI219 (CA) have similar induction profiles (Fig. 5.10C), with AI211 (UV) having a slightly higher level of basal *pR* LacZ activity. Whilst AI256 (VA) and AI260 (SA) have lower *pR* induction profiles, both have low basal *pR* LacZ activity suggesting they also offer tight control of *tum^{72K}* expression. The CA, VA and SA was removed by centrifuging cells to a pellet (at 3095rcf for 5min), removing all the S/N and resuspending cells in M9MM-20. Cultures were incubated at 37°C with agitation for the remainder of the timecourse, with samples taken every 30mins. The uninduced time point represents samples taken immediately prior to induction. Each data point represents three (AI211), twelve (AI219) and nine (AI256 and AI260) independent assays, 95% confidence interval error bars are shown.

5.5 186-WCB engineering stage 5

5.5.1 Engineering the fluorescent 186-WCB reporter

5.5.1.1 The ability of the WCB to report fluorescently was achieved by replacing *lacZ* with *mCherry*

The third stage of this project revealed the 186-WCB system can be easily adapted to respond to different small sensory molecules, where we demonstrated the ***pR***.*apI^{-}.tum^{*72K}* LacZ reporter can undergo OFF → ON state switching when linked to different IMs (Fig. 5.19). This outcome was encouraging, as system adaptability is an important attribute of biosensor design, especially when applying the technology to a real-life setting. To optimise our WCB for a real-life application, we decided the reporter module should report on the current state of the system by emitting a fluorescent (rather than a colourimetric) readout.

To make this modification the ***pR***.*apl⁻*.*tum*72K* LacZ reporter module (and the *tum⁻* control) was modified by replacing *lacZ* with *mCherry* (Fig. 5.20), the product of which is MCherry, a 26.7kDa red-fluorescent protein originally derived from DsRed of *Discosoma* sea anemones (Shaner et al., 2004). This would adapt the *E. coli* to emit a red-fluorescent signal when switched to the ON state, rather than grow as blue colonies when plated on X-gal L-plates. To maximise the red-fluorescent signal, transcriptional expression of *mCherry* was driven from the strong *pR* promoter and mRNA translation was enhanced by using the strong pET RBS. Using the Salis Lab RBS Calculator v2.0 (Espah Borujeni et al., 2014) and the *E. coli* str. K-12 substr. MG1655 (ACCTCCTTA 16S RNA sequence) we determined this RBS to have a strength of ~46,000AUs. To have the cells fluorescently report on the OFF state of the system, we also cloned the *superfolder-gfp* downstream of *cI*, such that OFF state cells would emit a green-fluorescent signal. To test our fluorescent system, the new ***pR***.*apl⁻*.*tum*72K* MCherry reporter (and the *tum⁻* control) was integrated at the λ *attB* site of E4643 already integrated with a *tum*72K* UV, CA, VA and SA-IM to generate a new series of fluorescent 186-WCB strains (Table 5.8).

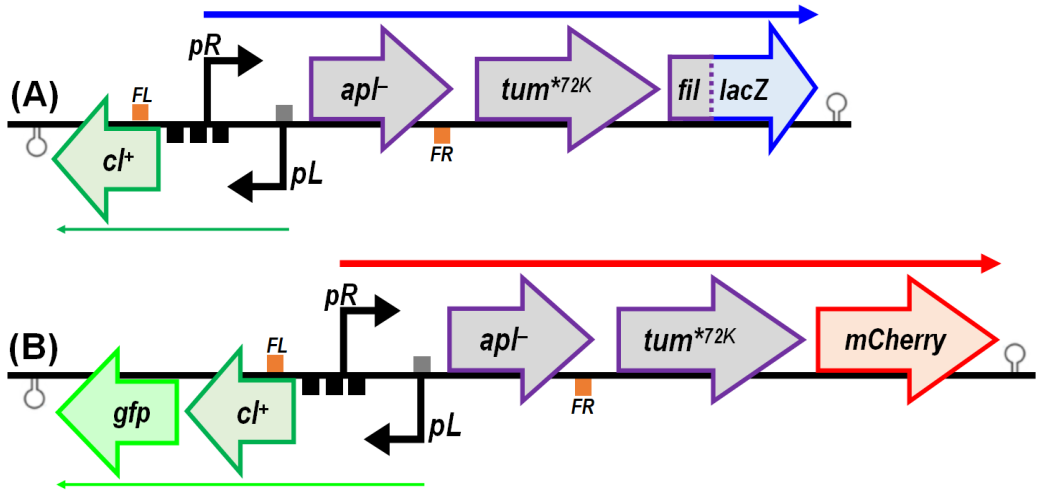

Figure 5.20: Optimising the 186-WCB MFL reporter module. **(A)** Schematic of the original colourimetric ***pR***.*apl⁻*.*tum*72K* LacZ reporter. **(B)** Schematic of the new fluorescent ***pR***.*apl⁻*.*tum*72K* MCherry reporter. The reporter module was modified by replacing *lacZ* with *mCherry* and cloning the *superfolder-gfp* gene immediately downstream of *cI*. *E. coli* integrated with this fluorescent reporter are expected to emit a stable green-fluorescent or a red-fluorescent signal when growing in the OFF or ON state respectively. To characterise the performance of the new fluorescent reporter, a *tum⁻* version was made. Symbolism defined in Table 5.12.

Table 5.8: The fluorescent 186-WCB strains. Each module exists at single-copy in the E4643 chromosome; ending subscript indicates site of integration.

Name	Description
AI233	E4643 + [pIT3-TO-*p95.tum*72K*]$_{186.1}$+ [pIT3-CL-*SF(gfp).cI⁺.**pR**⁺.pL⁺.apl⁻.tum*72K.mCherry*]$_{λ}$
AI234	E4643 + [pIT3-TO-*p95.tum*72K*]$_{186.1}$ + [pIT3-CL-*SF(gfp).cI⁺.**pR**⁺.pL⁺.apl⁻.tum⁻.mCherry*]$_{λ}$
AI235	E4643 + [pIT4-KT-*cymR.T5-1.tum*72K*]$_{φ21}$+ [pIT3-CL-*SF(gfp).cI⁺.**pR**⁺.pL⁺.apl⁻.tum*72K.mCherry*]$_{λ}$
AI236	E4643 + [pIT4-KT-*cymR.T5-1.tum*72K*]$_{φ21}$+ [pIT3-CL-*SF(gfp).cI⁺.**pR**⁺.pL⁺.apl⁻.tum⁻.mCherry*]$_{λ}$
AI258	E4643 + [pIT4-KT-*vanR.pVan^{CC}.tum*72K*]$_{φ21}$ + [pIT3-CL-*SF(gfp).cI⁺.**pR**⁺.pL⁺.apl⁻.tum*72K.mCherry*]$_{λ}$
AI259	E4643 + [pIT4-KT-*vanR.pVan^{CC}.tum*72K*]$_{φ21}$+ [pIT3-CL-*SF(gfp).cI⁺.**pR**⁺.pL⁺.apl⁻.tum⁻.mCherry*]
AI262	E4643 + [pIT4-KT-*nahR.pSal^{TTC}.tum*72K*]$_{φ21}$ + [pIT3-CL-*SF(gfp).cI⁺.**pR**⁺.pL⁺.apl⁻.tum*72K.mCherry*]$_{λ}$
AI263	E4643 + [pIT4-KT-*nahR.pSal^{TTC}.tum*72K*]$_{φ21}$+ [pIT3-CL-*SF(gfp).cI⁺.**pR**⁺.pL⁺.apl⁻.tum⁻.mCherry*]$_{λ}$

To assay the performance of the new fluorescent WCB strains a series of fluorescent switch plate assays were performed. These switch plate assays were performed exactly as per the blue/white switch plate assays, with the exception that cells were plated on L-plates without X-gal. Rather than looking for the growth of blue colonies, red-fluorescence (via expression of *mCherry*) was visualised on the SYPRO Ruby (Green Epi illumination with 605/50 filter at 1sec exposure) channel linked to the ChemiDoc™ MP Imaging System (BioRad). It is important to note, the SF-GFP switch plate data has not been presented because expression of *superfolder-gfp* from the weak *pL* promoter and a weak RBS (strength ~3100AUs, Espah Borujeni et al., 2014) failed to generate a green-fluorescent signal that could be easily distinguished from the relatively high intrinsic background fluorescence of *E. coli.* As a result, we decided to use *mCherry* as the primary reporter gene, with cells identified as OFF or ON by growing on L-plates as non-fluorescent or red-fluorescent colonies respectively.

The results of the fluorescent switch plate assays (Fig. 5.21, 5.22, 5.23 and 5.24) clearly demonstrate the new fluorescent MFL reporter is functional, meaning it can successfully express active MCherry when induced with UV, CA, VA or SA. As expected, all WCB strains containing the ***pR***.*apl*$^{-}$.*tum*$^{-}$ MCherry reporter fail to exhibit stable OFF → ON state switching, whilst strains harbouring the ***pR***.*apl*$^{-}$.*tum*^{*72K} MCherry reporter exhibit an impressive rate of switching with >95% of cells emitting a red-fluorescent signal following induction. The least optimal system appears to be AI233 (UV) (Fig. 5.21), as we observed a high rate of spontaneous induction, with ~20% of colonies on the uninduced plate emitting a red-fluorescent signal. This outcome is consistent with the high rate of spontaneous OFF → ON state switching observed for the *lacZ* version (AI211) (Fig. 5.5D). The very low rate of spontaneous induction observed for AI235 (CA), AI258 (VA) and AI262 (SA) is consistent with the previous switch plate assays performed for their respective *lacZ* versions AI219 (CA), AI256 (VA) and AI260 (SA). For all 'switchable' WCB strains, re-streaked red-fluorescent colonies (taken from the induced switch plate) returned a mix of red- and non-fluorescent colonies. Whilst the majority of cells (>84%) continued to emit a red-fluorescent signal the loss of fluorescence in some cells is again indicative of ON state instability, prompting further optimisation of biosensor design.

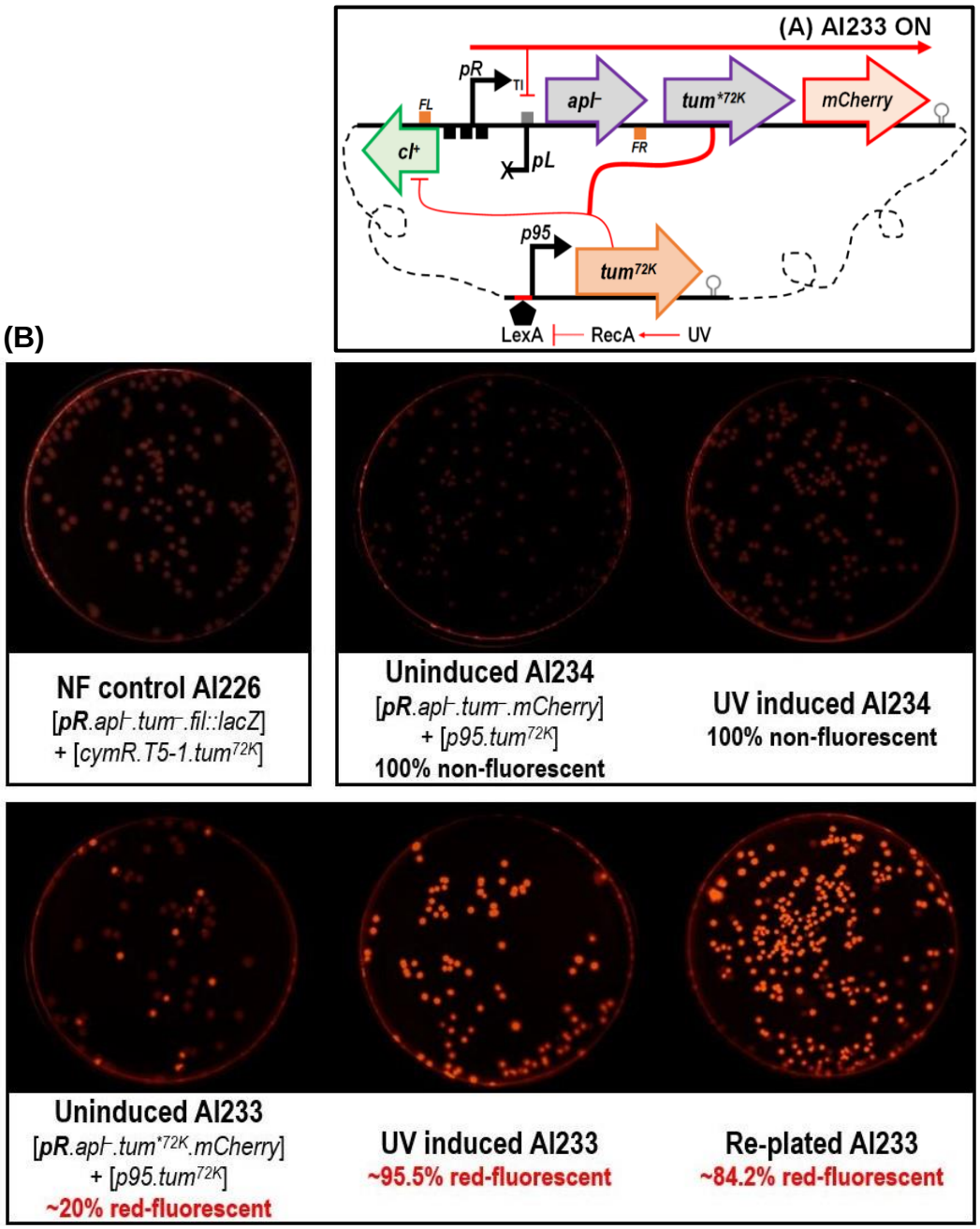

Figure 5.21: Testing for fluorescent switching of the UV-inducible AI233 and AI234 186-WCB strains. **(A)** ON state schematic of AI233 harbouring the λ integrated ***pR***.*apl⁻.tum*72K* MCherry reporter and a 186 *attB1* integrated *p95.tum72K* UV-IM. Symbolism defined in Table 5.12. **(B)** A set of switch plates for AI233 and AI234. Only AI233 (*tum72K*) exhibited stable OFF → ON state switching, but this strain has an unwarranted degree of spontaneous switching with ~20% of uninduced colonies being red-fluorescent. The ON state appears to be somewhat unstable as only ~84% of re-plated cells continue to emit a red-fluorescent signal. Switching was assayed by growing cultures to OD_{600} 0.30 in M9MM-20, treated with 40s UV, diluted 10^{-4}, 10µL plated on L-plates and the growth of red-fluorescent colonies counted the next day. Percentage values represent the proportion of red-fluorescent colonies observed on each switch plate presented. To differentiate background from 'true' fluorescence a switch plate of the non-fluorescent (NF) AI226 WCB strain was prepared.

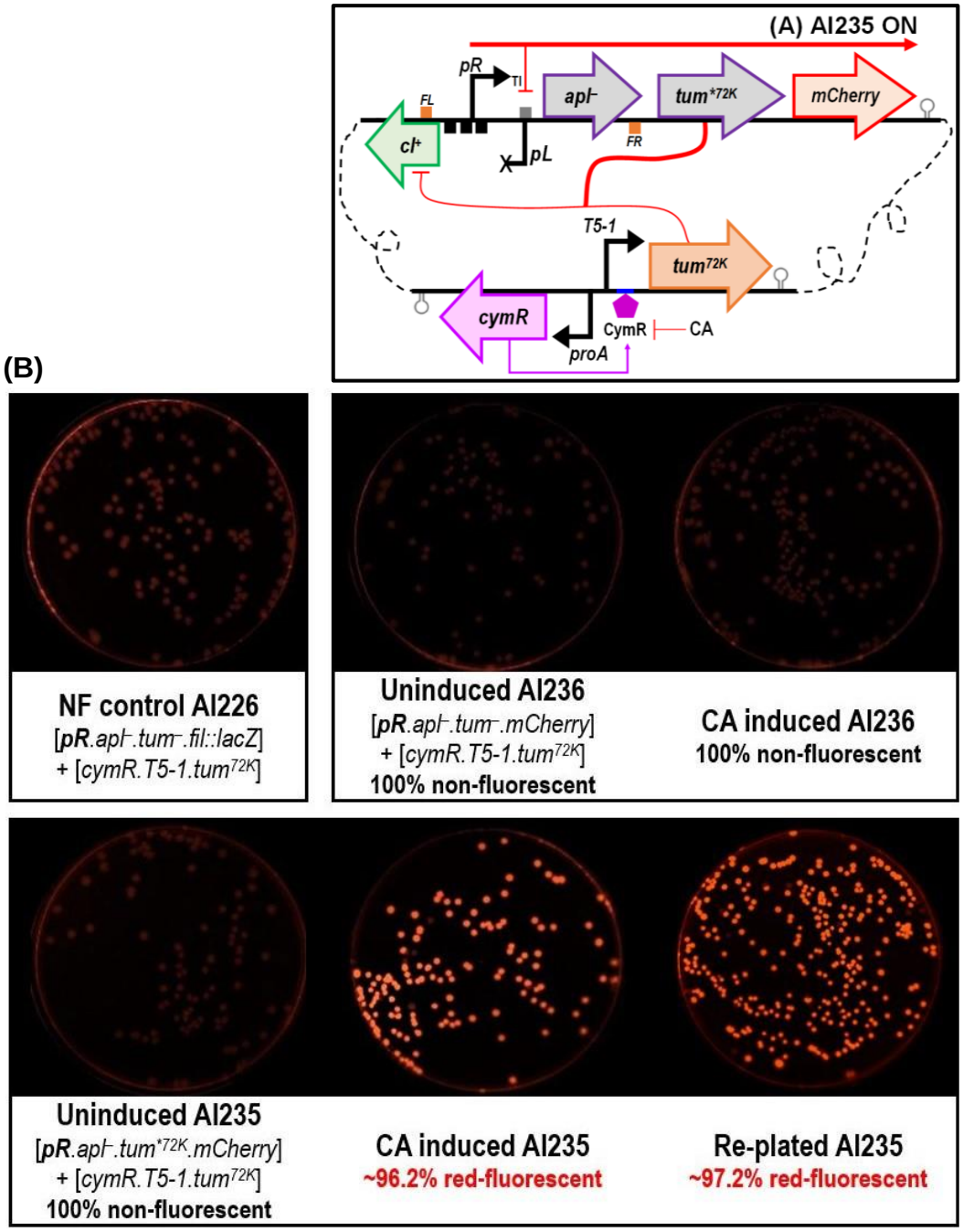

Figure 5.22: Testing for fluorescent switching of the CA-inducible AI235 and AI236 186-WCB strains. **(A)** ON state schematic of AI235 harbouring the λ integrated ***pR***.*apl⁻.tum*72K* MCherry reporter and a φ21 integrated *cymR.T5-1.tum72K* CA-IM. Symbolism defined in Table 5.12. **(B)** A set of switch plates for AI235 and AI236. Only AI235 (*tum72K*) exhibited stable OFF → ON state switching and no spontaneous switching. The ON state appears to be relatively stable as ~97% of re-plated cells continue to emit a red-fluorescent signal. Switching was assayed exactly as described in Fig. 5.21, with the exception that cultures were induced with 150μM CA for 20min. Percentage values represent the proportion of red-fluorescent colonies observed on each switch plate presented. To differentiate background from 'true' fluorescence a switch plate of the non-fluorescent (NF) AI226 WCB strain was prepared.

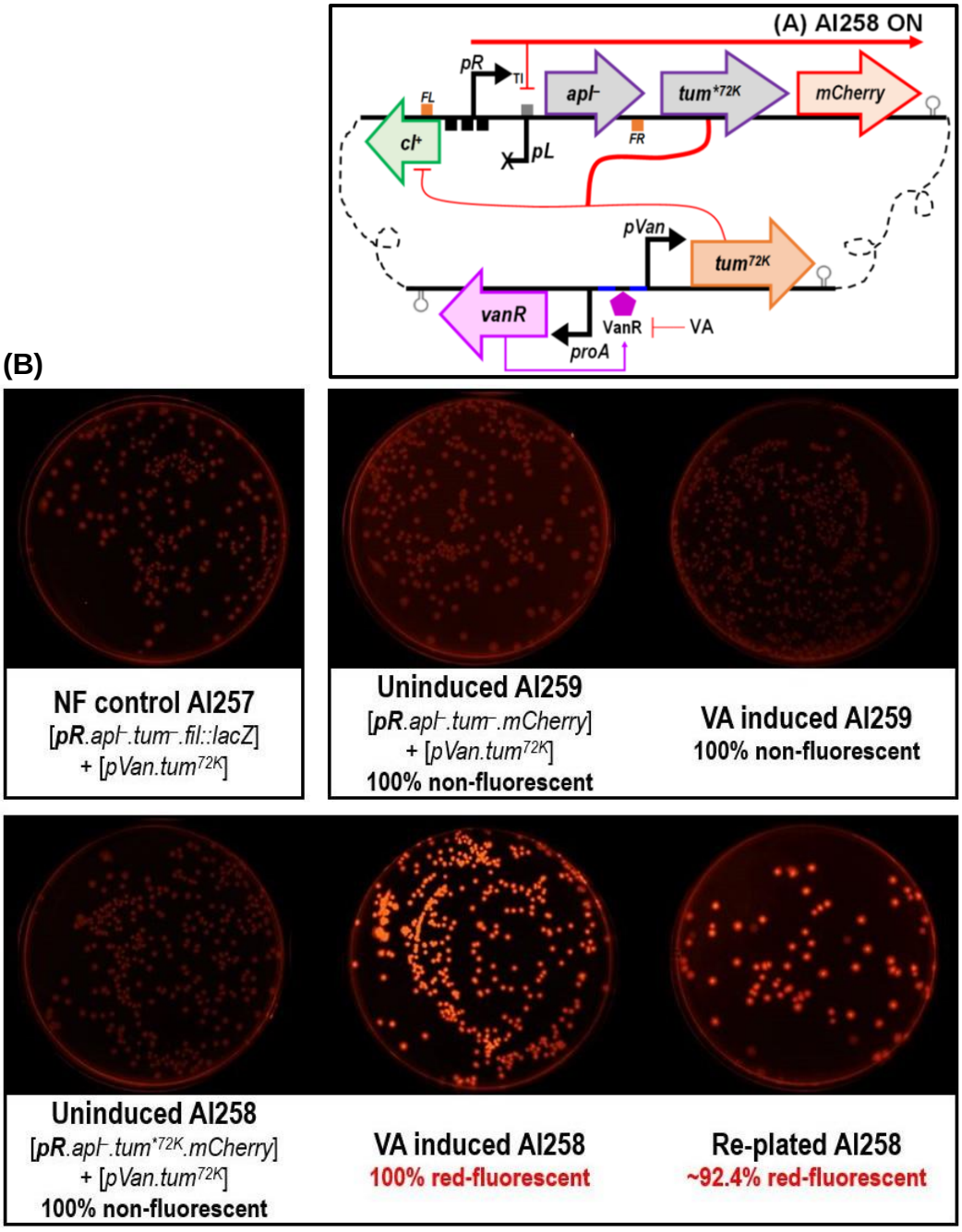

Figure 5.23: Testing for fluorescent switching of the VA-inducible AI258 and AI259 186-WCB strains. **(A)** ON state schematic of AI258 harbouring the λ integrated ***pR***.*apl⁻.tum*72K* MCherry reporter and a φ21 integrated *pVan.tum72K* VA-IM. Symbolism defined in Table 5.12. **(B)** A set of switch plates for AI258 and AI259. Only AI258 (*tum72K*) exhibited stable OFF → ON state switching and no spontaneous switching. The ON state appears to be relatively stable as ~92% of re-plated cells continue to emit a red-fluorescent signal. Switching was assayed exactly as described in Fig. 5.21, with the exception that cultures were induced with 150µM VA for 40min. Percentage values represent the proportion of red-fluorescent colonies observed on each switch plate presented. To differentiate background from 'true' fluorescence a switch plate of the non-fluorescent (NF) AI257 WCB strain was prepared.

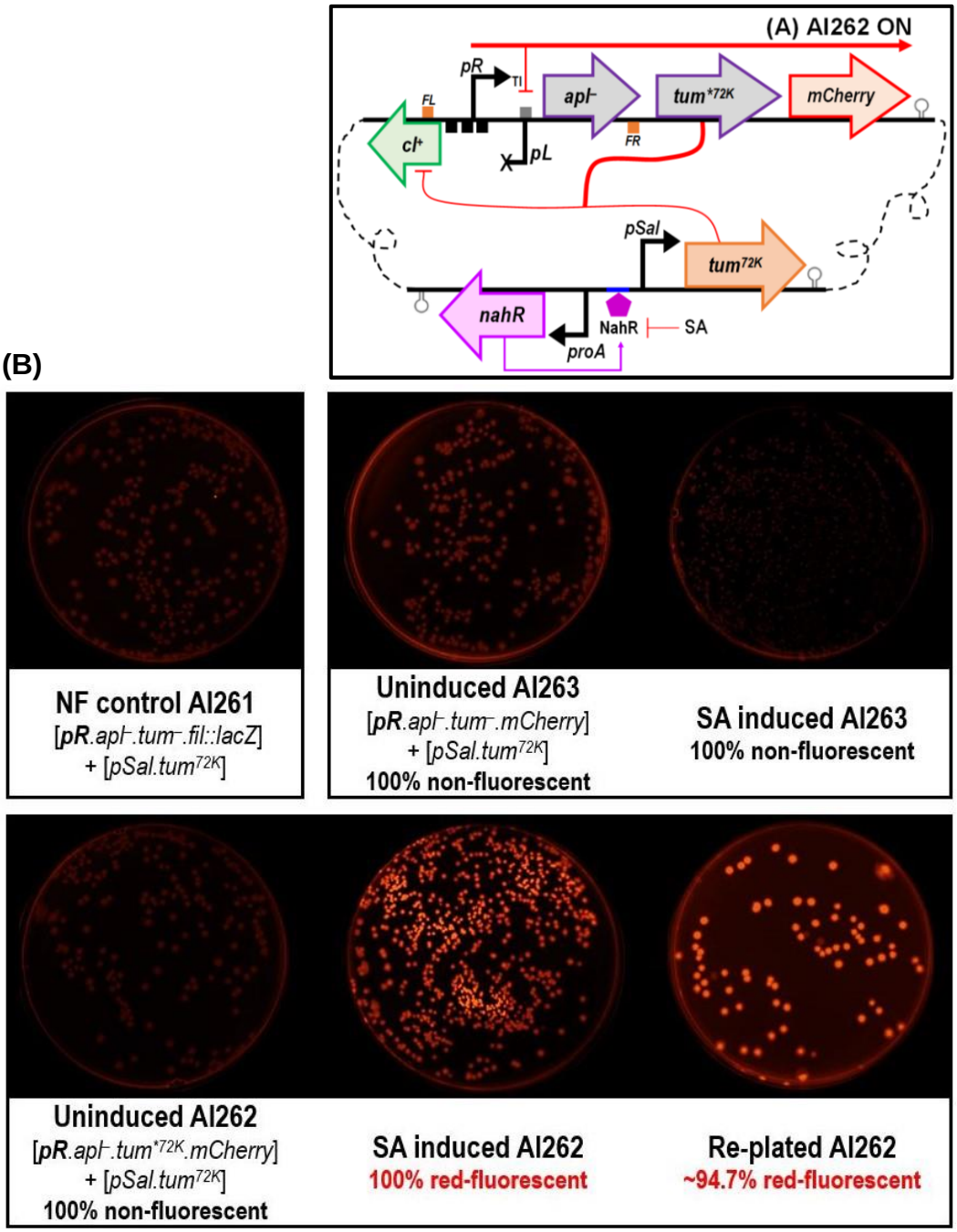

Figure 5.24: Testing for fluorescent switching of the SA-inducible AI262 and AI263 186-WCB strains. **(A)** ON state schematic of AI262 harbouring the λ integrated ***pR***.*apl*$^{-}$.*tum*^{*72K} MCherry reporter and a φ21 integrated *pSal.tum*^{72K} SA-IM. Symbolism defined in Table 5.12. **(B)** A set of switch plates for AI262 and AI263. Only AI262 (*tum*^{72K}) exhibited stable OFF → ON state switching and no spontaneous switching. The ON state appears to be relatively stable as ~95% of re-plated cells continue to emit a red-fluorescent signal. Switching was assayed exactly as described in Fig. 5.21, with the exception that cultures were induced with 150μM SA for 60min. Percentage values represent the proportion of red-fluorescent colonies observed on each switch plate presented. To differentiate background from 'true' fluorescence a switch plate of the non-fluorescent (NF) AI261 WCB strain was prepared.

5.6 186-WCB engineering stage 6

5.6.1 Establishing an ON resting state for the 186-WCB

To summarise the project so far, our 186-WCB started out as a simple UV-inducible MFL switch modelled from coliphage 186. To optimise a number of performance parameters, we have progressively modified our initial working module (Fig. 5.2) into a system that can be induced to undergo efficient OFF → ON state switching and establish a cellular form of ON state memory that lasts for tens of hours. The system is robust, as induced cells can remain switched ON when grown to different growth phases and in different growth media (Fig. 5.14). The system exhibits impressive adaptability as we demonstrated the MFL reporter could respond to a number of different inducers when linked to a UV, CA, VA or SA-IM. All (except the UV-IM) appear to offer tight control of *tum*^{72K} as they exhibit very low rates of spontaneous induction and record near-zero basal LacZ promoter activity under non-induced conditions (Fig. 5.19). To optimise the system further, we also successfully converted the MFL LacZ reporter into the MCherry reporter; switching the system's mode of reporting from a colourimetric to a fluorescent means.

The primary issued faced (thus far) in engineering our WCB is achieving bistability, such that each mutually exclusive state (ON and OFF) can be maintained indefinitely in the absence of the inducer. Previous studies by the Egan/Dodd/Shearwin laboratory have also attempted to reconfigure the 186 switch to create bistable switches, but unfortunately, achieving bistability has remained a challenge largely because 186 naturally maintains lysogeny by establishing a negative feedback regulatory loop using the highly stable CI immunity repressor. Modifying the 186 switch such that the lytic/ON state can dominate the lysogenic/OFF state is a significant challenge and one that has definitely afflicted this study. So far, most of our optimisation has focused on improving ON state stability, so the MFL reporter can overcome the stability of CI. Currently, all versions of the WCB naturally rest in the OFF state - defined as the state in which the system cycles naturally in the absence of the inducer - and is switched to the ON state when treated with UV, CA, VA or SA. Our assays of WCB performance continue to indicate there is ON state instability, with the latest switch plate data (Fig. 5.21, 5.22, 5.23 and 5.24) confirming the issue persists, as all re-plated L-plates grow a mix of red- and non-fluorescent colonies. Furthermore, the long-term ON state stability profile for the AI219 WCB strain (Fig. 5.16) showed that overtime there is a gradual decline in ON state cells, which is due to CI gradually regaining repression of *pR* and thus inhibiting the expression of *tum*^{72K}, which is required to keep CI inactivated. Whilst our attempts to optimise the system have improved ON state stability, we are yet to reach a design where the ON state is 'digital', meaning cells can continue to red-fluoresce indefinitely in the absence of the inducer.

To tackle the issue of CI stability and consequential ON state instability, we decided to take a different approach in our optimisation of the 186-WCB by working to design a dynamic bistable system that has a resting ON state, and can (ideally) establish ON/OFF bistability. To achieve this, the design of the WCB was adapted by (1) modifying the MFL reporter to reduce active CI levels further by replacing *apl* with the gene encoding the 186CI C-terminal domain (*cI-CTD*) and (2) introducing a second IM to develop a system that can be chemically switched in both directions (ON → OFF and OFF → ON).

5.6.1.1 Replacing *apl* with *cI-CTD* establishes an ON resting state and improves ON state stability

In the effort to improve ON state stability, the MFL reporter was modified by replacing *apl* with the *cI-CTD* gene (Fig. 5.25A) as we determined early on in this study that *apl* offered no improvement to ON state switching and stability. The *cI-CTD* gene encodes the last 111 amino acids of the CI protein and acts as a dominant-negative to the full-length repressor (Pinkett et al., 2006). We expected its co-expression with tum^{72K} (from *pR*) would provide a second means of keeping CI inactivated and thus stabilise the ON state. To preserve *pL* functionality, the first 27bp of *apl* was retained as it contains the *pL* -35 site. The *apl* start codon was changed to TGT to prevent this pre-sequence from interfering with *cI-CTD* expression. To conserve proper CI regulation, the *FR* site was repositioned immediately after the *cI-CTD* stop codon, which increased the spacing between the CI-*pL* operator and *FR* site by 116bp. We reasoned this minor extension would not affect CI regulation, as Dodd and Egan (2002) showed loss of the *FR* site only has a minor effect on the ability of CI to control *pR* and *pL.* The pET RBS was chosen to drive *cI-CTD* mRNA translation as it is stronger (~12,500AUs) than the weak *apl* RBS (~900AUs) (Espah Borujeni et al., 2014). To mitigate DNA synthesis and assembly issues, the *cI-CTD* gene sequence was codon optimised using the IDT codon optimisation tool (IDT, 2019), which reduced the degree of DNA sequence homology that exists between full-length *cI* and *cI-CTD* (see Chapter 7, Table 7.12 for sequence). For control purposes, a fluorescent version with a ***pR***.*cI-CTD.tum*$^{-}$ reporter was also assembled.

Before linking the new ***pR***.*cI-CTD.tum*^{*72K} MCherry reporter with any one of the four tum^{72K} IMs, we needed to verify the resting state of the new reporter as it is possible that substituting *apl* for *cI-CTD* could have switched the original OFF resting state to the ON state. If the reporter retained an OFF resting state then any of the tum^{72K} IMs would be compatible for OFF → ON state switching. If the reporter were to rest in the ON state, a different IM would need to be made to allow for ON → OFF state switching. To verify the resting state of the new reporter (including the *tum*$^{-}$ control), each reporter was λ integrated into E4643 to generate the AI278 (***pR***.*cI-CTD.tum*^{*72K}) and AI279 reporter strains (***pR***.*cI-CTD.tum*$^{-}$). The resting state was determined by re-streaking the glycerol stocks of AI278 and AI279 on L-plates and scanning the plates for red-fluorescent colonies the next day.

The images of the AI278 and AI279 resting state L-plates clearly show both versions of the new reporter have an ON resting state (Fig. 5.25B). To assess the stability of the resting ON state, a single colony from the re-streaked glycerol stock L-plate was re-plated and the growth of red-fluorescent colonies observed the next day. For both strains, all colonies continue to emit a red-fluorescent signal, which suggests the CI-CTD is acting as a potent inactivator of CI and is having a significant effect on improving ON state stability. With the new reporters having an ON resting state, this indicated the *tum*^{72K} IMs were no longer compatible and a new IM was required to develop a new series of WCB strains than can undergo ON → OFF state switching.

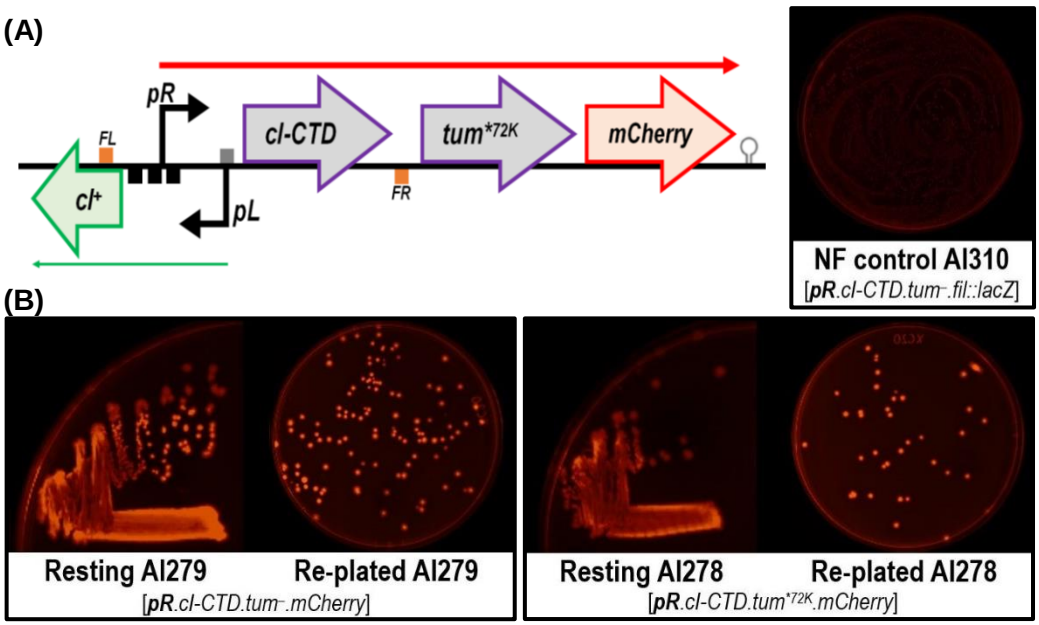

Figure 5.25: Determining the resting state of *E. coli* harbouring a new fluorescent 186-WCB reporter encoding the *cI-CTD* gene. **(A)** Schematic of the new fluorescent ***pR***.*cI-CTD.tum*^{*72K} MCherry reporter. In the effort to achieve tight control of CI, *apl* was replaced with *cI-CTD,* which is expected to assist Tum^{72K} in keeping CI inactive and thus improve ON state stability. To characterise the performance of the new reporter, a *tum*$^{-}$ version was made. Symbolism defined in Table 5.12. **(B)** Resting L-plates of re-streaked glycerol stocks of AI278 and AI279 and L-plates of a single red-fluorescent colony re-plated from each resting L-plate. The results show both reporter modules have a stable ON resting state. To differentiate background from 'true' fluorescence a L-plate of the non-fluorescent (NF) AI310 WCB strain was prepared.

5.6.1.2 Engineering an IM that encodes *cI* to achieve ON → OFF state switching

Having created a fluorescent MFL reporter that naturally cycles/rests in the ON state, a new IM system was required for OFF → ON state switching. To engineer this IM we decided to use a modified CA-IM system (hereon denoted as ^{1}CA^{OFF}-IM). This system was adapted and assembled for other purposes by Andrew Hao (Shearwin laboratory) and has an architecture inspired by the Meyer et al. (2019) study. In this system, *cI* is expressed from the *pcymR*^{C} promoter, which features two CymR operator sites. We anticipated the use of two operator sites would allow for tighter control of *cI*, thereby reducing the degree of *cI* expressed in the absence of CA. CymR is supplied from the same module where expression is driven from the *PlacI*^{q} promoter. To assemble the ^{1}CA^{OFF}-IM (pIT4-*loxP*-KH-*pcymR*^{C}.*cI*$^{+}$.*PlacI*^{q}.*cymR*^{AM}) a PCR fragment containing the *cI* gene was cloned downstream of *pcymR*^{C} at the *Xba*I restriction site (Fig. 5.26A).

A new pair of WCB strains (AI316 and AI317) were made by integrating the $^{1}CA^{OFF}$-IM into E4643 already integrated with a ***pR***.*cI-CTD.tum*^{72K}* MCherry reporter (including the *tum*$^{-}$ control). To characterise these new strains, we needed to first verify their resting state, to ensure any basal *cI* expression generated from the $^{1}CA^{OFF}$-IM did not alter the reporter's resting ON state. Unfortunately, both strains were found to have an OFF resting state, determined exactly as done for AI278 and AI279 (Fig. 5.26B). Whilst this indicated the $^{1}CA^{OFF}$-IM is functional (it can successfully express the full-length CI repressor), cells having an OFF resting state suggests the IM generates a significant degree of basal *cI* expression that compromises ON state stability. This means, the CI 'leak' from the $^{1}CA^{OFF}$-IM (in the absence of CA) is sufficient to establish a level of CI that can repress *pR* by outcompeting CI-CTD and Tum^{72K}. This outcome indicated that to engineer an IM that features an inducible promoter that offers tighter control of *cI* the design of the $^{1}CA^{OFF}$-IM would need to be modified.

Table 5.9: The fluorescent 186-WCB strains harbouring the $^{1}CA^{OFF}$-IM. Each module exists at single-copy in the E4643 chromosome; ending subscript indicates site of integration.

Name	Description
AI316	E4643 + [pIT4-KH-*pcymR^{C}.cI^{+}.PlacI^{q}.cymR^{AM}*]$_{\varphi 21}$ + [pIT3-CL-*cI^{+}.**pR**$^{+}$.pL^{+}.cI-CTD.tum*^{72K}.mCherry*]$_{\lambda}$
AI317	E4643 + [pIT4-KH-*pcymR^{C}.cI^{+}.PlacI^{q}.cymR^{AM}*]$_{\varphi 21}$ + [pIT3-CL-*cI^{+}.**pR**$^{+}$.pL^{+}.cI-CTD.tum^{-}.mCherry*]$_{\lambda}$

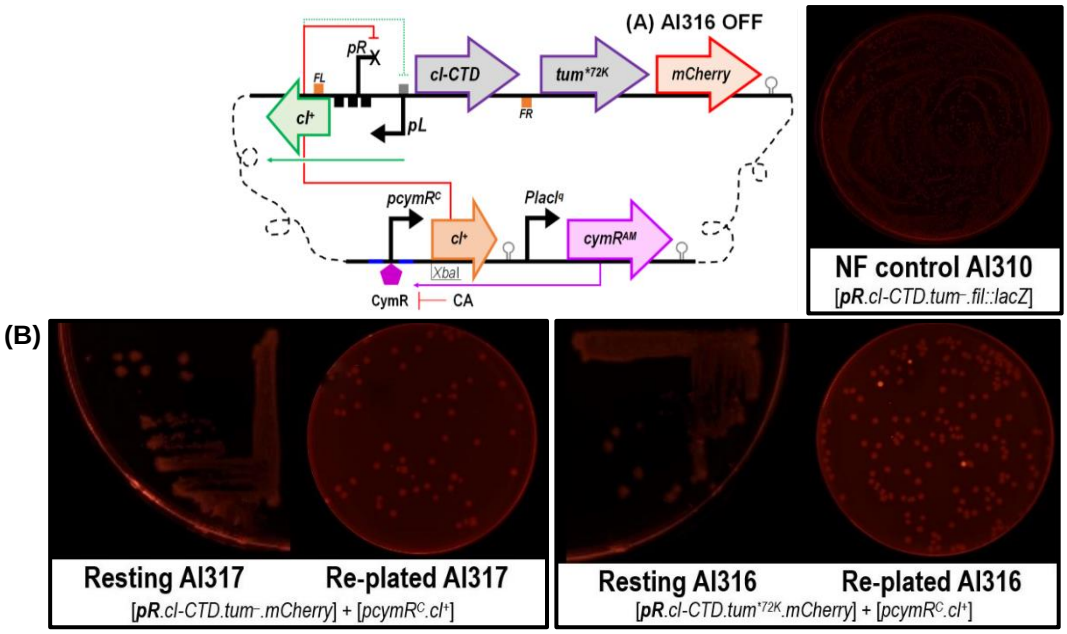

Figure 5.26: The fluorescent AI316 and AI317 186-WCB strains harbouring the $^{1}CA^{OFF}$-IM. (A) OFF state schematic of AI316 harbouring the λ integrated ***pR***.*cI-CTD.tum*^{72K}* MCherry reporter and a HK022 integrated $^{1}CA^{OFF}$ -IM. AI317 is the *tum*$^{-}$ control strain. Symbolism defined in Table 5.12. **(B)** Resting L-plates of re-streaked glycerol stocks of AI316 and AI317 and L-plates of a single non-fluorescent colony re-plated from each resting L-plate. The results show both strains have an OFF resting state (CI dominates the system). To differentiate background from 'true' fluorescence a L-plate of the non-fluorescent (NF) AI310 WCB strain was prepared.

5.6.1.3 A 186-WCB integrated with two independent IMs exhibits hysteretic behaviour and allows for ON → OFF state switching

Before approaching the issue of leaky *cI* expression from the $^{1}CA^{OFF}$-IM, we decided that since we already had an established collection of tum^{72K} IMs for ON → OFF state switching, we would construct a WCB that could be switched ON OR OFF using different inducers. This would develop a much more dynamic system as we would now have the ability to switch cells between two alternate states rather than only switch cells in one direction. To do this, the ***pR***.*cI-CTD.tum**^{72K} MCherry reporter (including the tum^{-} control) was linked to the $^{1}CA^{OFF}$-IM (encodes *cI*) and the *pVan.tum*^{72K} VA-IM (hereon denoted as VA^{ON}-IM). This led to the development of a three-module WCB (strain AI311; Fig. 5.27), which (in theory) could be induced to undergo OFF → ON state switching with VA and ON → OFF state switching with CA. To characterise AI311, the first step was to verify the resting state as any basal/leaky expression of tum^{72K} from the VA^{ON}-IM could possibly influence the resting state of the fluorescent MFL reporter. Interestingly, the resting L-plates revealed AI312 (tum^{-}) has an OFF resting state, whilst AI311 (tum^{72K}) has a heterogeneous resting state (some cells are ON whilst others are OFF) (Fig. 5.28). Furthermore, when a single AI311-OFF colony was re-plated, these cells were able to retain their resting OFF state by growing back as non-fluorescent colonies, whilst a re-plated AI311-ON colony grew back as a mix of red- and non-fluorescent colonies.

This outcome is indicative of hysteresis, a feature diagnostic for a bistable circuit. This phenomenon is found in a wide variety of natural and constructed systems and is defined as the ability of a system to establish memory of its past state when positive and negative control parameters are varied (Ferrell, 2002; Morris, 2011). A system exhibits hysteretic behaviour when the characteristic looping behaviour of an input-output graph is observed (Fig. 5.29) and (depending on the system) can be due to a variety of unique causes (Morris, 2011). For AI311, the intricate interaction between the positive/ON control elements (Tum^{72K} and CI-CTD) with the negative/OFF control element (CI) underlies the system's hysteretic resting behaviour. To illustrate this phenomenon, Figure 5.29 presents a simple relay of AI311 exhibiting hysteretic behaviour in the context of varying CI production. The relay consists of a bistable region flanked by two monostable ON and OFF states, where cells follow independent (non-overlapping) ON → OFF (red) or OFF → ON (grey) paths depending on the level of CI.

In the AI311 system, what ultimately determines the resting state of a single cell is whether the system is dominated by CI (the OFF regulator) or by CI-CTD and Tum^{72K} (the ON regulators). When CI production is low, cells will rest in the ON state because the ON regulators will dominate and keep CI inactivated, whilst transcriptional interference from an active *pR* will inhibit further expression of *cI* from the weak *pL* promoter (Fig. 5.27A).

When CI production is high, cells will rest in the OFF state because CI will dominate and inhibit expression of the ON regulators by strongly repressing *pR* (Fig. 5.27B). Referring to Figure 5.29, as CI production increases, cells will follow the ON → OFF (red) path and eventually grow as non-fluorescent colonies. As CI production decreases, cells will follow the OFF → ON (grey) path and eventually grow as red-fluorescent colonies. If all cells grow as OFF (non-fluorescent) or ON (red-fluorescent) colonies then the system exists in one of two mutually exclusive monostable states. If cells grow as a mix of OFF and ON colonies this indicates the system has established an equilibrium within the bistable region, where because of stochastic variation in intracellular concentrations, in some cells CI dominates and in other cells CI-CTD and Tum^{72K} dominate. Whilst it is difficult to determine precisely where within the bistable region the AI311 system rests, we reason it may sit within the second or third quadrant of the bistable region simply because the AI311-OFF re-plate generated homogenous growth of non-fluorescent colonies, whilst the AI311-ON re-plate generated a heterogeneous population of colonies. This suggests that for the AI311 system the OFF state is perhaps the preferred/more stable state.

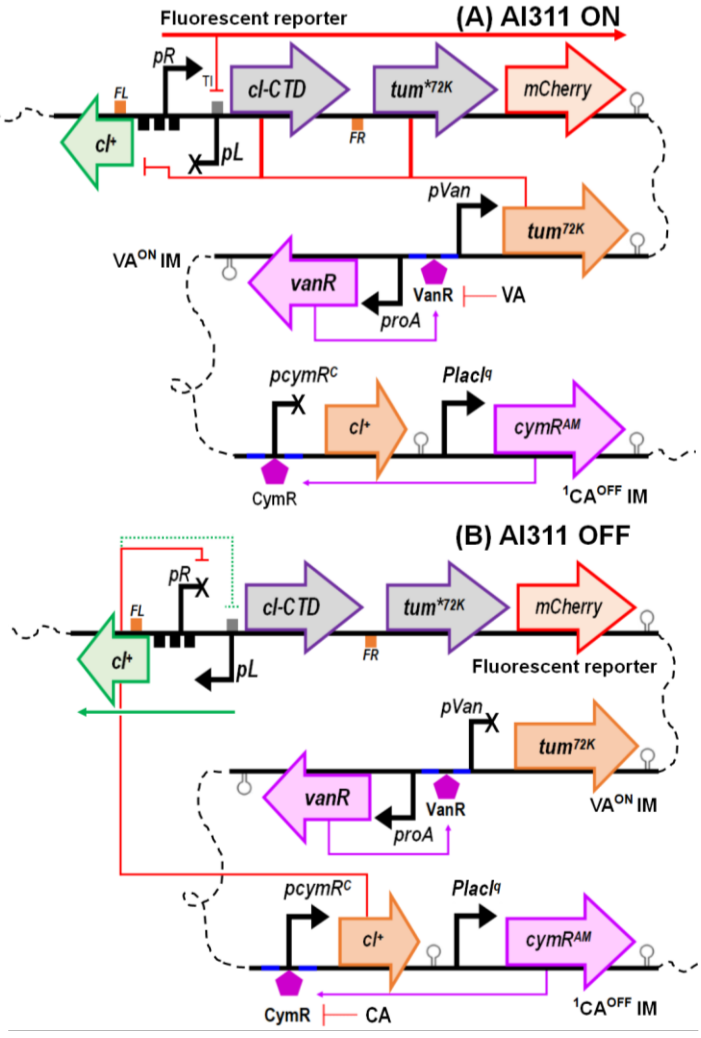

Figure 5.27: The three-module fluorescent AI311 186-WCB strain. This strain harbours a λ integrated ***pR***.*cI-CTD.tum*72K* MCherry reporter, a φ21 integrated VA^{ON}-IM and a HK022 integrated ^{1}CA^{OFF}-IM. AI312 is the *tum*$^{-}$ control strain. **(A)** ON state schematic of AI311, where following VA induction, VanR is inactivated and the *pVan.tum*^{72K} transcript expressed. Tum^{72K} inactivates CI, *pR* is derepressed and *cI-CTD*, *tum*^{72K} and *mCherry* genes are expressed. To control CI and establish memory of the ON state, *cI-CTD* and *tum*^{72K} expression continues from *pR*, whilst transcriptional interference (TI) from an active *pR* inhibits expression of *cI* from *pL*. **(B)** OFF state schematic of AI311, where following CA induction, CymR^{AM} is inactivated and the *pcymR*^{C}*.cI*$^{+}$ transcript expressed. CI represses *pR* to inhibit expression of *cI-CTD*, *tum*^{72K} and *mCherry*. To establish memory of the OFF state, *cI* expression continues from *pL*, which is under CI positive and negative feedback autoregulation. Symbolism defined in Table 5.12.

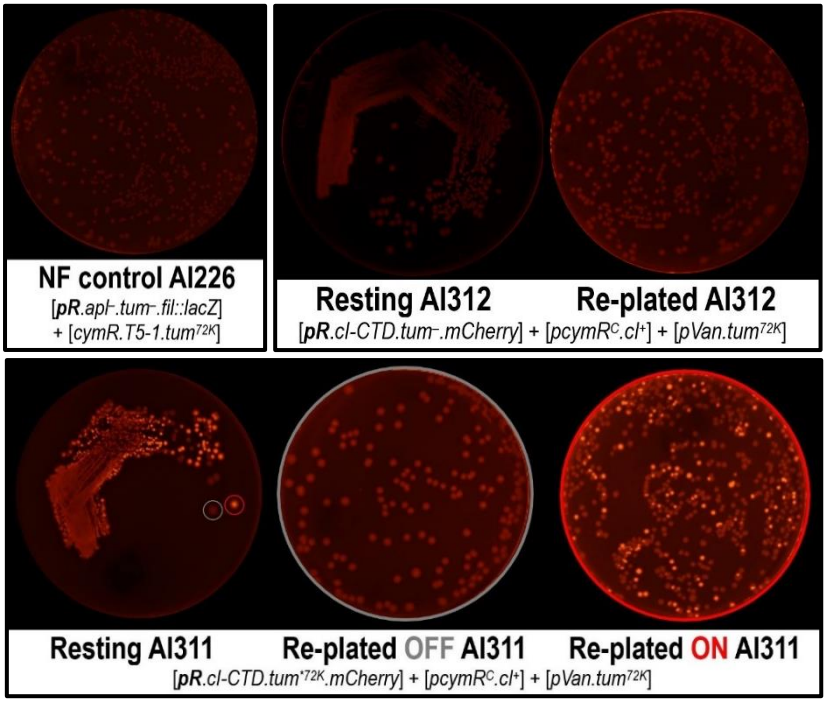

Figure 5.28: Determining the resting state of the three-module fluorescent 186-WCB strains. **(A)** Resting L-plates of re-streaked glycerol stocks of AI311 and AI312 and L-plates of single non- and red-fluorescent colonies re-plated from each resting L-plate. The results show AI312 (*tum*⁻) has an OFF resting state and AI311 (*tum*^{72K}) has a bistable resting state. For both strains, the OFF state appears stable as re-plated OFF colonies all grow back non-fluorescent. For AI311, a mix of red- and non-fluorescence colonies grow when a single red-fluorescent colony is re-plated. To differentiate background from 'true' fluorescence a L-plate of the non-fluorescent (NF) AI226 WCB strain was prepared.

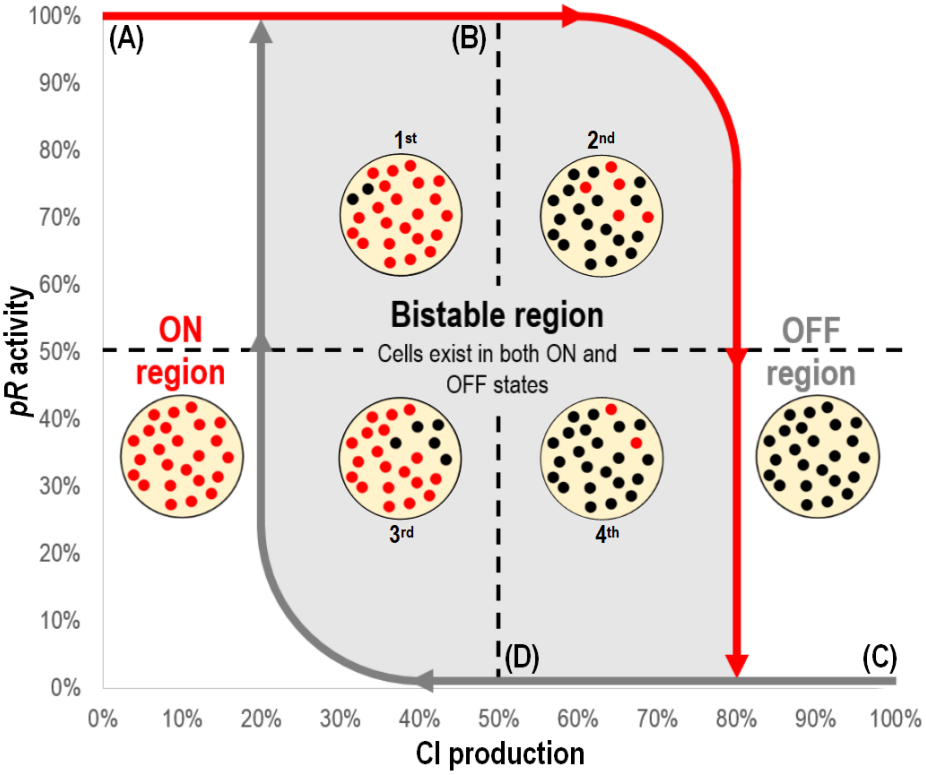

Figure 5.29: A simple relay explaining the AI311 resting hysteretic behaviour in the context of varying CI production rate. The system consists of a bistable region flanked by monostable ON and OFF states, where cells follow independent (non-overlapping) ON → OFF (red) or OFF → ON (grey) paths depending on the initial CI production level. At low CI production **(A)**, CI-CTD and Tum^{72K} dominate the system. *pR* is active, *mCherry* is expressed and cells grow as red-fluorescent colonies. As CI production increases **(B)**, cells enter the bistable region, where (in some cells) CI starts to dominate the system causing cells to switch OFF. At higher CI production, a greater proportion of cells will grow as non-fluorescent colonies as the population moves towards the OFF region. At high CI production **(C)**, CI dominates the system. *pR* is repressed, *mCherry* expression is inhibited and cells grow as non-fluorescent colonies. As CI production decreases **(D)**, cells enter the bistable region, where (in some cells) CI-CTD and Tum^{72K} start to dominate the system causing cells to switch ON. At lower CI production, a greater proportion of cells will grow as red-fluorescent colonies as the population moves towards the ON region. Given the growth outcomes observed on the re-plated ON and OFF plates we reason the AI311 system may have established a resting equilibrium within the second or third quadrant of the bistable region, with the system still presenting a bias towards the OFF state. Image adapted from Morris (2011) and Pietsch (2015).

With the ultimate goal being to develop a system that rests in the ON state and be can induced OFF and ON using CA and VA respectively, the AI311 bistable resting state was not ideal. It does however; indicate that we are heading in the right direction, where we anticipate cells are moving along the OFF → ON (red) path towards the monostable ON region. Evidently, a resting L-plate is by no means sufficient to characterise the hysteretic behaviour of AI311. To do this, a series of stability assays were performed, using the protocol as described in Section 5.3.1.1. Since AI311 harbours a fluorescent reporter, LacZ analysis was not applicable. Since we observed a high agreement between the switch plate data and the LacZ data, we reasoned that preparing a set of fluorescent switch plates each day for five days and counting the growth of non- and red-fluorescence colonies would be sufficient to quantify OFF and ON state long-term stability respectively.

Table 5.10 lists the control strains used to characterise AI311 bistability. AI312 was used as a negative control because we expected this WCB strain would exhibit no stable OFF → ON state switching has it harbours a ***pR***.*cI-CTD.tum*$^{-}$ MCherry reporter. AI235 was used as a positive control for OFF → ON state switching as it is the fluorescent equivalent of AI219 (*lacZ* version). In Section 5.3.1.1.1, we characterised the long-term ON state stability of AI219 and calculated ON state stability to have a half-life of ~26hrs. If the tight agreement between the LacZ data and switch plate data holds true we then expected AI235 to exhibit the same degree of ON state stability when induced with CA.

Table 5.10: The 186-WCB strains used to characterise long-term bistability of the AI311 186-WCB strain. AI312 is the negative control strain, AI253 is the positive control strain and AI226 is the non-fluorescent control strain used to differentiate background fluorescence from 'true' red-fluorescence. Each module exists at single-copy in the E4643 chromosome; ending subscript indicates site of integration.

Name	Description
AI311	E4643 + [pIT4-T-*vanR.pVan*^{CC}*.tum*^{72K}]$_{\varphi 21}$ + [pIT4-KH-*pcymR*^{C}*.cI*$^{+}$*.PlacI*^{q}*-cymR*^{AM}]$_{HK022}$ + [pIT3-CL-*cI*$^{+}$*.**pR***$^{+}$*.pL*$^{+}$*.cI-CTD.tum*^{*72K}*.mCherry*]$_{\lambda}$
AI312	E4643 + [pIT4-T-*vanR.pVan*^{CC}*.tum*^{72K}] $_{\varphi 21}$ + [pIT4-KH-*pcymR*^{C}*.cI*$^{+}$*.PlacI*^{q}*-cymR*^{AM}]$_{HK022}$ + [pIT3-CL-*cI*$^{+}$*.**pR***$^{+}$*.pL*$^{+}$*.cI-CTD.tum–.mCherry*]$_{\lambda}$
AI235	E4643 + [pIT4-KT-*cymR.T5-1.tum*^{72K}]$_{\varphi 21}$ + [pIT3-CL-*cI*$^{+}$*.**pR***$^{+}$*.pL*$^{+}$*.apI*$^{-}$*.tum*^{*72K}*.mCherry*]$_{\lambda}$
AI226	E4643 + [pIT4-KT-*cymR.T5-1.tum*^{72K}]$_{\varphi 21}$ + [pIT3-CL-*cI*$^{+}$*.**pR***$^{+}$*.pL*$^{+}$*.apI*$^{-}$*.tum*$^{-}$*.fil::lacZ*]$_{\lambda}$

To assay AI311 long-term OFF state stability, liquid cultures of resting ON state colonies were grown O/N in M9MM-1, switched to M9MM-20, induced with 150μM CA for 20mins and passaged continuously for five days with a set of fluorescent switch plates prepared over a 4hr timecourse each day. To assay AI311 long-term ON state stability, liquid cultures of resting OFF state colonies were grown O/N in M9MM-1, switched to M9MM-20, induced with 150μM VA for 40mins and passaged continuously for five days with a set of fluorescent switch plates prepared over a 4hr timecourse each day.

To assay AI235 long-term ON state stability, liquid cultures of resting OFF state colonies were grown O/N in M9MM-1, switched to M9MM-20, induced with 150µM CA for 20mins and passaged continuously for five days with a set of fluorescent switch plates prepared over a 4hr timecourse each day. For all cultures, cell growth was controlled by switching between M9MM-1 (for O/N growth) and M9MM-20 (for daily growth) and periodically diluting each culture in M9MM-20 during the 4hr timecourse to ensure cells did not exceed OD_{600} 0.50.

The results of the long-term ON and OFF AI311 stability assays are presented in Figures 5.30 to 5.34. Starting with the AI235 positive control, in this system, all cells have a resting OFF state and all (100%) successfully undergo OFF → ON state switching following CA induction of Tum^{72K} (Fig. 5.30). The ON state however, is unstable as the proportion of red-fluorescent cells drops to ~75%, ~51%, ~34% and ~25% on days 2, 3, 4 and 5 respectively (Fig. 5.34, ● data). Interestingly, the ON state half-life averaged at ~52hrs, which is ~26hrs longer than AI219 (*lacZ* version). We account this variation to be due to differences in the *pR.fil::lacZ* reporter mRNA transcript and/or differences in reporter protein stability. Hence, if the *pR.mCherry* mRNA transcript is more readily translated than the *pR.fil::lacZ* mRNA transcript and/or if MCherry is more stable than Fil::LacZ, then cells will continue to emit a red-fluorescent signal (for some time) even after the reporter has switched back to the OFF state, thus extending the apparent half-life of the ON state. Regardless of this difference in half-life, the AI235 control did behave as expected, confirming that preparing switch plate data sets for each WCB strain is a sufficient means to assay ON and OFF state long-term stability.

Our characterisation of AI311 revealed this WCB has an impressive OFF state stability profile. Starting with ~25% of cells resting in the ON state, maximal (100%) ON → OFF state switching was observed when CI was induced with CA. The OFF state exhibits almost complete stability as ~99% of cells continued to grow as non-fluorescent colonies at the end of day 5 (Fig. 5.31 and Fig. 5.34, ● data). To assess whether AI311-OFF cells could be switched back ON, each culture was induced with VA (at the end of day 5) to induce Tum^{72K} expression. Whilst maximal switching was not observed, ~87% of cells did successfully switch back ON, growing as red-fluorescent colonies. Assaying the ON state of AI311 revealed a less impressive stability profile (Fig. 5.32 and Fig. 5.34, ● data). Starting with ~92% of cells resting in the OFF state; suboptimal OFF → ON state switching (~80%) was observed when Tum^{72K} was induced with VA. The ON state exhibits high instability as only ~2% of cells remain ON at the end of day 4. To assess whether these AI311-OFF cells could be switched back ON, each culture was re-induced with VA (at the end of day 4). Suboptimal OFF → ON state switching was observed, with only ~59% of cells growing as red-fluorescent. For AI311, we calculated the ON state to have a half-life of ~12hrs. Poor ON state stability suggests there must still be a significant degree of basal/leaky *cI* expression from the $^{1}CA^{OFF}$-IM, such that this pool of CI, in combination with some *cI*

expressed from a weakly repressed *pL,* gradually outcompetes the CI-CTD and Tum^{72K}, resulting in cells relapsing OFF shortly after VA induction. As expected, the AI312 (*tum*$^{-}$) negative control, failed to exhibit stable OFF → ON state switching when Tum^{72K} was induced with VA (Fig. 5.33 and Fig. 5.34, ● data). This outcome does not mean these cells are uninducible, but rather indicates the ON state is so unstable that cells cannot grow as red-fluorescent colonies after an O/N incubation of ~12hrs. This outcome suggests that for this particular three-module system, without expression of *cI-CTD* AND *tum*^{72K} from the MFL reporter, cells cannot establish long-term memory of the ON state. Whilst AI311 has a near digital OFF state, an unstable ON state confirms our optimisation efforts are yet to produce a truly dynamic bistable system, with the issue of CI stability proving difficult to fine-tune and counteract. To continue with our optimisation we considered two key approaches. First, we wanted to determine whether the system could be fine-tuned with VA. If unsuccessful, the second approach would be to revise the design of the ^{1}CA^{OFF}-IM, so to develop a system that offers tighter control of *cI.*

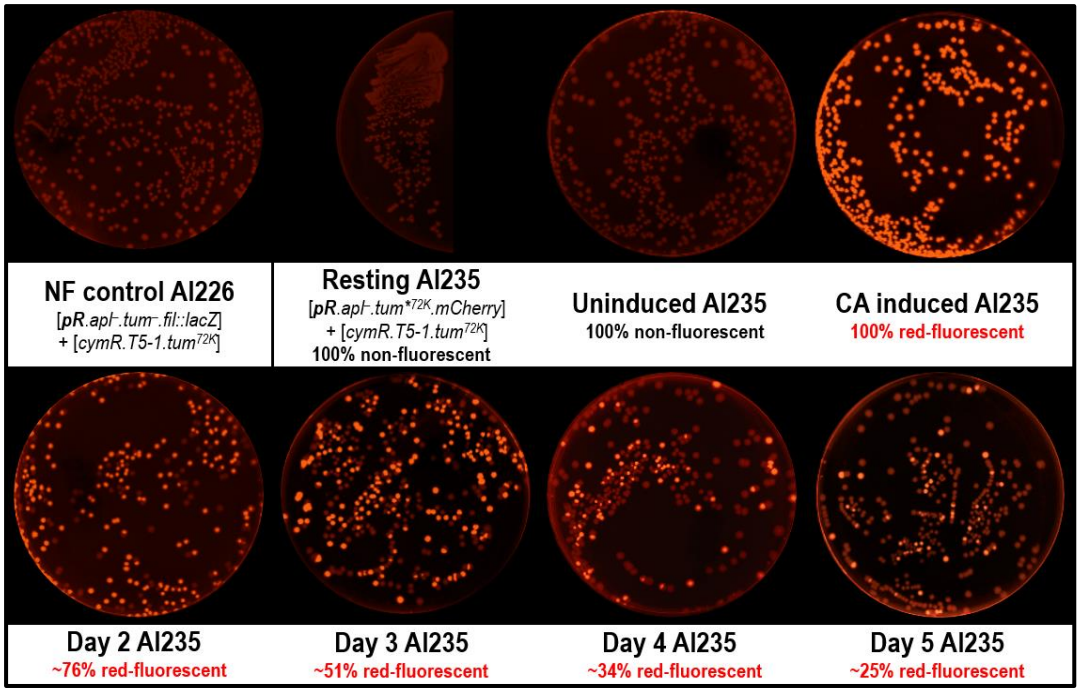

Figure 5.30: OFF → ON state switching and ON state stability plates for the positive control AI235 186-WCB strain. The plates confirm AI235 has an OFF resting state and achieves maximal (100%) OFF → ON state switching when induced with 150µM CA for 20mins. The ON state is unstable as a mix of non- and red-fluorescent colonies appear on the day 2, 3, 4 and 5 plates, with the proportion of non-fluorescent cells increasing over time. The resting plate was prepared by restreaking the AI235 glycerol stock on a L-plate and grown O/N at 37°C. Liquid cultures were prepared by taking a single OFF colony from the resting L-plate and culturing O/N in M9MM-1 at 37°C with aeration. To prepare for induction, each culture was diluted to OD_{600} 0.15 in M9MM-20 and grown to OD_{600} 0.30. The uninduced plate represents a sample of the culture taken immediately prior to induction. Day 2, 3, 4 and 5 plates represent induced cells cultured in M9MM-1/20 in the absence of the inducer. To remove the inducer, cells were centrifuged to a pellet (3095rpm for 5mins), the S/N removed and cells resuspended in M9MM-20. Switch plates were prepared by diluting a sample of the culture 10^{-4}, plating 10µL on a L-plate and incubating O/N at 37°C. Fluorescence was visualised on the SYPRO Ruby (Green Epi illumination with 605/50 filter at 1sec exposure) channel linked to the ChemiDoc™ MP Imaging System (BioRad). Percentage values represent the approximate proportion of non- or red-fluorescent colonies observed on each switch plate presented. To differentiate background from 'true' fluorescence a L-plate of the non-fluorescent (NF) AI226 WCB strain was prepared.

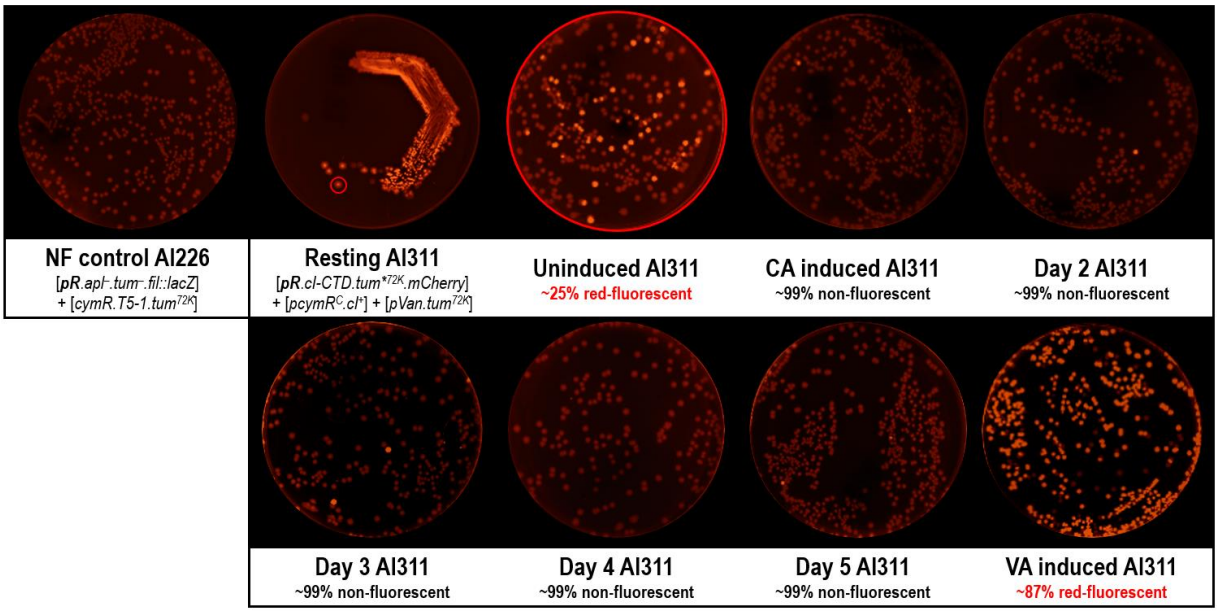

Figure 5.31: ON → OFF state switching and OFF state stability plates for the AI311 186-WCB strain. The plates confirm AI311 has a bistable resting state and the uninduced plate confirms starting cultures prepared from a single ON colony grow as a mixed population of OFF/ON state cells, which suggests the ON state is unstable in this system. From the ON cells available, induction with CA achieves maximal (~99%) ON → OFF state switching. The OFF state appears to be very stable, with ~99% of cells continuing to grow as non-fluorescent colonies over days 2, 3, 4 and 5. The VA-induced plate confirms CA-induced OFF state cells can successfully undergo OFF → ON state switching when induced with 150µM VA for 40mins. The resting, uninduced and induced L-plates were prepared and fluorescence visualised as described in Fig. 5.30, with the exception that O/N cultures were prepared by taking a single ON colony from the resting L-plate and culturing O/N in M9MM-1 at 37°C with aeration. Percentage values represent the approximate proportion of non- or red-fluorescent colonies observed on each switch plate presented. To differentiate background from 'true' fluorescence a L-plate of the non-fluorescent (NF) AI226 WCB strain was prepared.

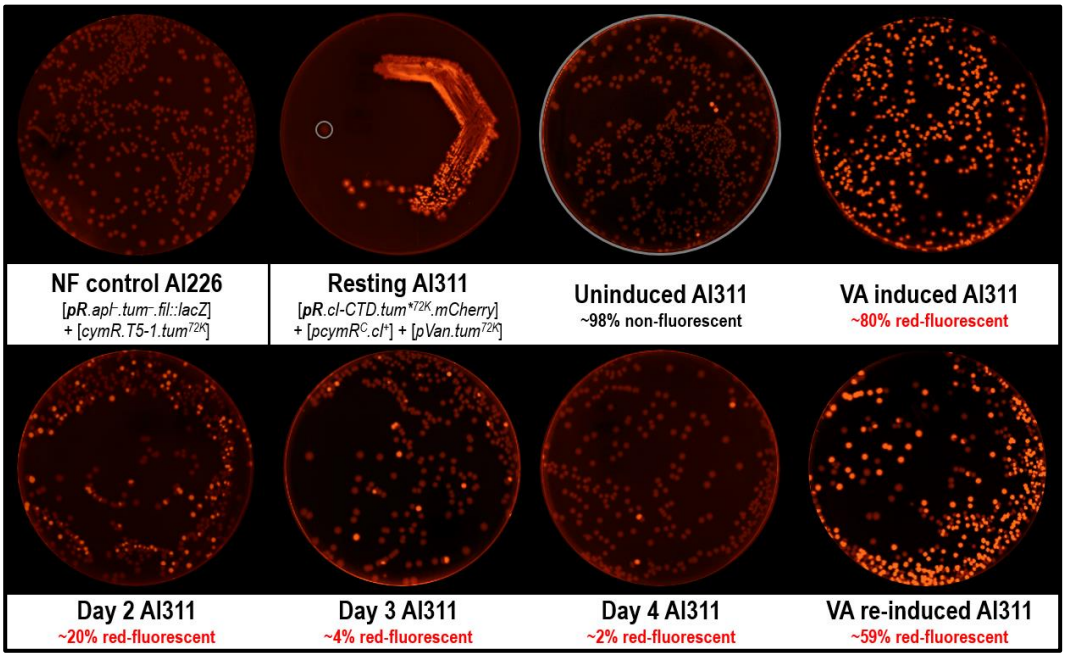

Figure 5.32: OFF → ON state switching and ON state stability plates for the AI311 186-WCB strain. The resting plate reconfirms AI311 has an bistable resting state and the uninduced plate confirms starting cultures prepared from a single OFF colony grow as a homogeneous population of non-fluorescent cells, suggesting the OFF state is the more stable state in this system. When induced with 150µM VA for 40mins, suboptimal OFF → ON state switching (~80%) is observed. The ON state is unstable as cells quickly relapse to the OFF state, with only ~2% of cells retaining their red-fluorescence at the end of day 4. The VA re-induced plate confirms relapsed-OFF state cells can be switched back ON, but switching is suboptimal. The resting, uninduced and induced L-plates were prepared and fluorescence visualised as described in Fig. 5.30. Percentage values represent the approximate proportion of non- or red-fluorescent colonies observed on each switch plate presented. To differentiate background from 'true' fluorescence a L-plate of the non-fluorescent (NF) AI226 WCB strain was prepared.

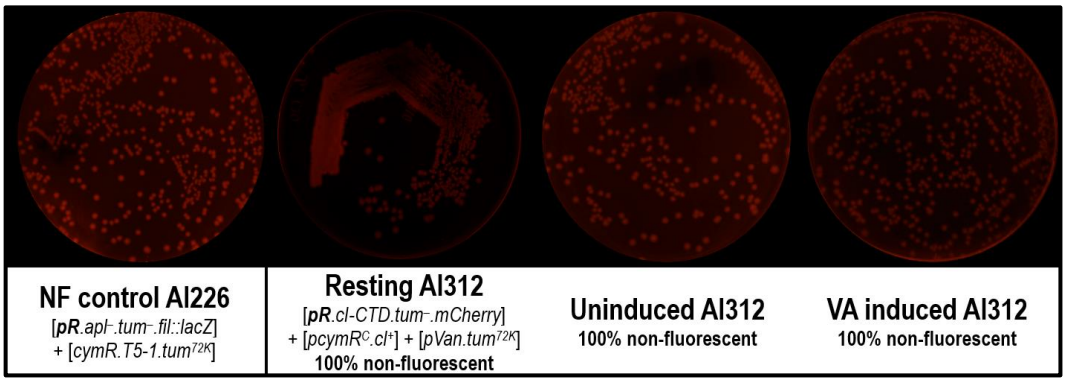

Figure 5.33: OFF → ON state switching and ON state stability plates for the AI312 186-WCB strain. The plates confirm AI312 has an OFF resting state and as expected does not exhibit stable OFF → ON state switching when induced with 150µM VA for 40mins due the presence of the *tum⁻* reporter. The resting, uninduced and induced L-plates were prepared and fluorescence visualised as described in Fig. 5.30. Percentage values represent the approximate proportion of non-fluorescent colonies observed on each switch plate presented. To differentiate background from 'true' fluorescence a L-plate of the non-fluorescent (NF) AI226 WCB strain was prepared.

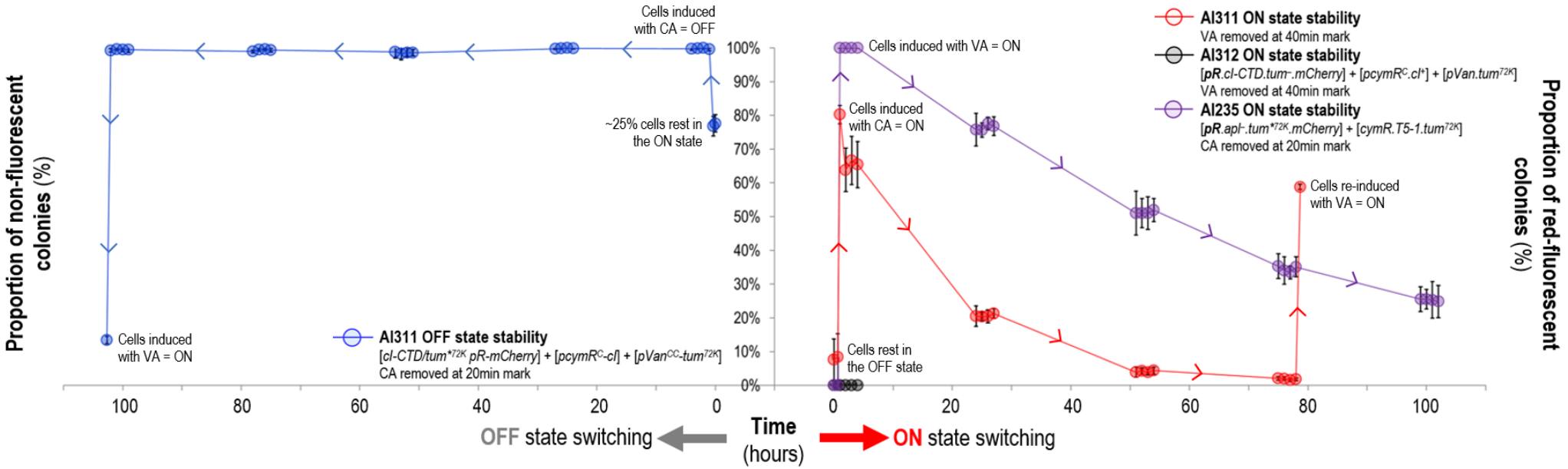

Figure 5.34: ON and OFF state long-term stability profiles for the AI311 186-WCB strain. A graphical representation of the ON and OFF state fluorescent stability plates prepared for AI235, AI311 and AI312. AI235 (positive control, ● profile) displayed maximal OFF → ON state switching when induced with CA. ON state instability exists as cells gradually switch OFF over the 5-day passaging period. ON state half-life was calculated to be ~52hrs (R^2 .0.9957). As expected, AI312 (negative control, ● profile) failed to exhibit stable OFF → ON state switching when induced with VA. AI311 (● profile) has a stable OFF state, with maximal ON → OFF state switching observed when CI is induced with CA, with almost all cells maintaining this state over the 5-day passaging period. Induction of Tum^{72K} with VA at the end of day 5 confirmed CA-induced OFF state cells can be switched back ON. In contrast, AI311 OFF → ON state switching (● profile) is suboptimal, with ~80% of cells switching ON when Tum^{72K} is induced with VA. ON state instability is evident as cells rapidly switch OFF over the 5-day passaging period, with only ~2% of cells growing red-fluorescent at the end of day 4. A second round Tum^{72K} induction (with VA) at the end of day 4 demonstrated cells can be switched back ON after relapsing OFF. ON state half-life averaged at ~12hrs (R^2 .0.9861). Liquid cultures were prepared by taking a single OFF or ON colony from a re-streaked glycerol stock L-plate and culturing O/N in M9MM-1 at 37°C with aeration. To prepare for induction, O/N cultures were subcultured to OD_{600} 0.15 in M9MM-20 and grown to OD_{600} 0.30 at 37°C with aeration. Immediately prior to induction, an untreated switch plate was prepared to confirm each WCB strain was in the correct resting state. For induction, cultures were treated with 150µM CA or 150µM VA for 20mins and 40mins respectively at 37°C with aeration and induction plates prepared immediately after. To remove the inducer, cells were centrifuged to a pellet (3095rpm for 5mins), the S/N removed and cells resuspended in M9MM-20. Each culture was incubated at 37°C with aeration for 4hrs, with stability plates prepared every hour. To track the fluorescent status of cells over multiple days, at the end of each timecourse, 7mL M9MM-1 was inoculated with ~5µL of each induced culture and incubated O/N at 37°C with aeration. The next day, each O/N induced culture was diluted to OD_{600} 0.15 in M9MM-20 and incubated at 37°C with aeration until cells reached OD_{600} 0.30. Fluorescence was monitored for 4hrs by preparing stability plates every hour (x4 plates/day). Untreated, induction and stability plates were made by taking ~100µL samples of each culture, preparing a 10^{-4} dilution in M9MM-20, plating 10µL on a L-plate and incubated O/N at 37°C. To maintain log phase growth throughout each timecourse cultures were diluted every 30mins with pre-warmed M9MM-20 to OD_{600} 0.30. Fluorescence was determined by visualising MCherry expression on the SYPRO Ruby (Green Epi illumination with 605/50 filter at 1sec exposure) channel linked to the ChemiDoc™ MP Imaging System (BioRad). To quantify OFF or ON state stability, the growth of non-fluorescent or red-fluorescent cells were counted and plotted against a 110hr time scale. Each data point represents four (AI234, AI312), six (A311 OFF) and eight (AI311 ON) independent assays with 95% confidence interval error bars shown.

5.7 186-WCB engineering stage 7

5.7.1 Optimisation of the AI311 186-WCB strain

5.7.1.1 Fine-tuning the AI311 WCB strain with VA to improve ON state stability

In the effort to improve ON state stability of the AI311 system, we considered culturing AI311 with a low level of Tum^{72K}, by continuously expressing *tum*^{72K} at a low level from the VA^{ON}-IM by supplementing M9MM with a defined concentration of VA ([VA]). We reasoned that supplying cells with a constant low supply of Tum^{72K} would counteract the CI leaked from the $^{1}CA^{OFF}$-IM and allow these cells to establish indefinite memory of the ON state.

A [VA] of 10µM was initially determined by conducting a VA dose-response stability assay. In this assay, AI311 cultures were induced with 150µM VA for 40mins, the VA removed by centrifugation, the cells resuspended in M9MM-20 supplemented with various [VA] (0, 2, 10, 25, 50, 80, 120 and 150µM) and the growth of red-fluorescent colonies tracked for three days. The results indicated that following Tum^{72K} induction (with 150µM VA), growth in M9MM-1/20 +10µM VA was sufficient to maintain the ON state without causing any cells that failed to switch initially, to undergo OFF → ON state switching at 10µM VA (data not shown).

A fluorescent ON state stability profile for AI311 continuously cultured in M9MM-1/20 +10µM VA was then obtained (Fig. 5.35A/B, ● data). An improved ON state half-life of ~64hrs was observed, but only ~31% of cells remained red-fluorescent at the end of day 5. This outcome implied that the degree of Tum^{72K} induction provided by 10µM VA was not sufficient to control the CI leaked from the $^{1}CA^{OFF}$-IM; hence, we inferred a higher [VA] was required to counteract this leak. It is important to note, with a higher [VA] required, we needed to ensure this level did not have an 'inductive' effect on cells. In other words, the optimal [VA] should only facilitate ON state stability (keep cells switched ON) and not be too high to induce OFF → ON state switching. To determine the optimal [VA], a VA dose-response induction assay was performed on AI311, where we assayed for <u>no</u> OFF → ON state switching when cells were exposed to [VA] of 10, 15, 20, 25, 30, 35, 40, 50, 60, 70, 80, 100µM for 60mins (exposure time increased to maximise induction). Fluorescent switch plates were prepared and the growth of non- and red-fluorescent colonies visualised the following day. Unfortunately, red-fluorescent colonies (~50%) were observed when AI311 was treated with the lowest [VA] tested (10µM) (data not shown). This outcome verified the AI311 system could not be fine-tuned with VA because the [VA] required to overcome the CI leaked from the $^{1}CA^{OFF}$-IM is too high, such that Tum^{72K} induction with 10µM VA is in fact sufficient for stable OFF → ON state switching. The next option was to reconfigure the $^{1}CA^{OFF}$-IM to create a system that offered tighter control of *cI*.

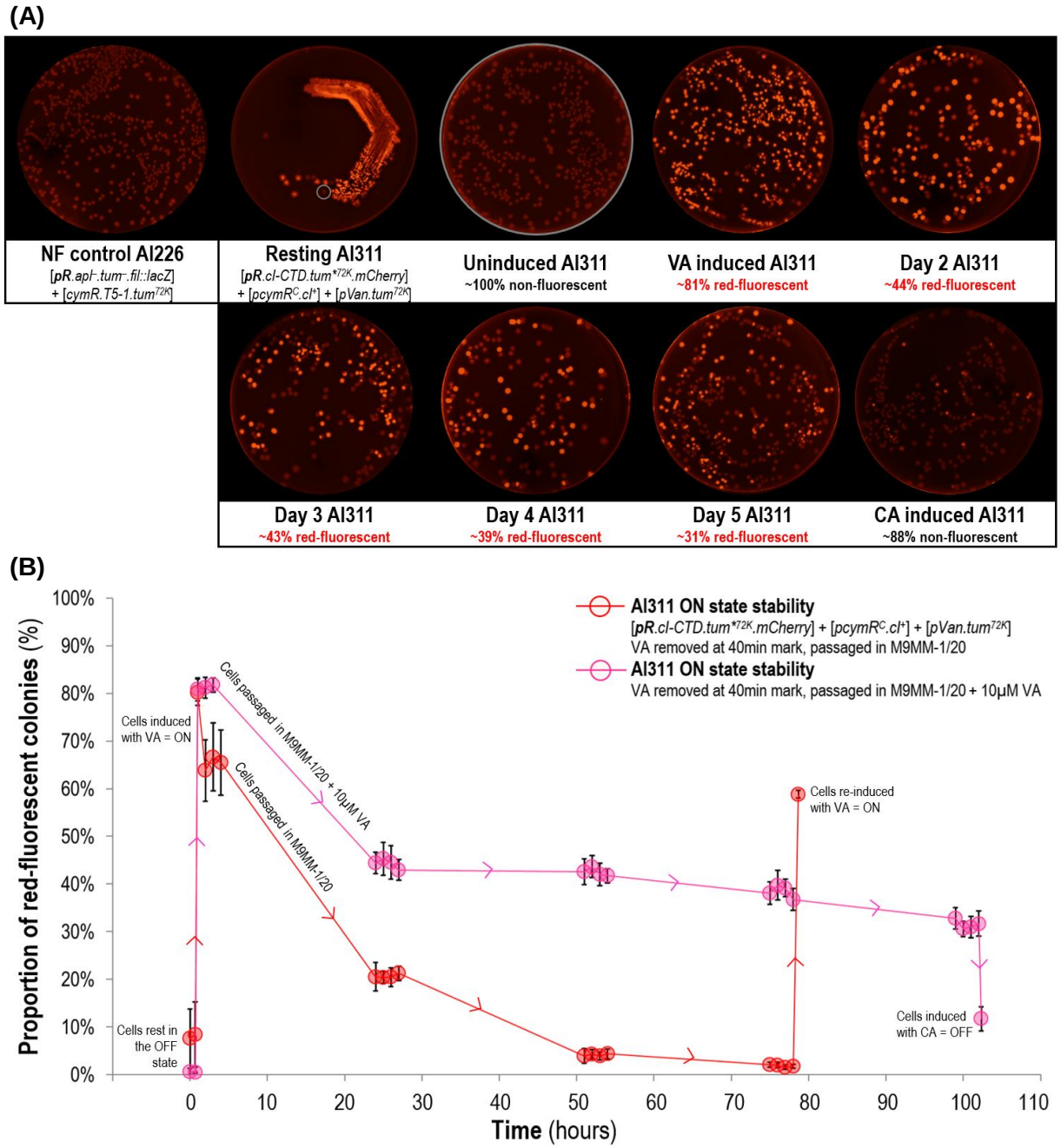

Figure 5.35: Long-term ON state stability profile for the AI311 186-WCB strain cultured in M9MM supplemented with 10µM VA. **(A)** ON state fluorescent switching and stability plates for AI311 following Tum^{72K} induction with 150µM VA for 40mins and continuous passaging in M9MM-1/20 +10µM VA. As observed previously, OFF → ON state switching is suboptimal with ~81% of cells emitting red-fluorescence after Tum^{72K} induction with VA, with ~31% of cells continuing to emit a red-fluorescent signal at the end of day 5. CI induction with 150µM CA for 20mins results in ~88% of cells undergoing ON → OFF state switching. The resting, uninduced and induced L-plates were prepared and fluorescence visualised as described in Fig. 5.30. Percentage values represent the approximate proportion of non- or red-fluorescent colonies observed on each switch plate presented. To differentiate background from 'true' fluorescence a L-plate of the non-fluorescent (NF) AI226 WCB strain was prepared. **(B)** A graphical representation of the proportion of red-fluorescent colonies observed on each switch plate. For comparison, the AI235 data (● profile) from Fig. 5.34 has been reproduced to show passaging VA-induced AI311 cells in M9MM +10µM VA (● profile) improves ON state stability; extending the half-life from ~12hrs to ~64hrs (R^2 0.7959). Since a proportion of cells switch OFF each day, it appears cells need to be cultured in M9MM supplemented with a higher [VA]. These assays were performed exactly as described in Fig. 5.34, with the exception that following VA induction and removal, cells were resuspended and continuously passaged in M9MM-1/20 +10µM VA for 5 days. To quantify ON state stability, the growth of red-fluorescent cells on each plate was counted and plotted against a 120hr time scale. Each ● data point represents six independent assays with 95% confidence interval error bars shown.

5.7.1.2 Better control of the CA^{OFF}-IM achieves an ON resting state and optimises system stability

The AI311 ON and OFF long-term stability assays (Fig. 5.34) revealed this WCB has a digital OFF state but an unstable ON state. Whilst supplementation of Tum^{72K} with 10µM VA does improve ON state stability (Fig. 5.35), this approach is not practical for optimising WCB performance as the VA dose-response induction assay (data not shown) revealed 10µM VA is sufficient to induce *tum^{72K}* expression to a level that allows for stable OFF → ON state switching. This outcome confirmed AI311 ON state stability is difficult to improve with VA. We suspect AI311 ON state instability is due to the architecture of the ^{1}CA^{OFF}-IM, where use of the *pcymR^{C}* promoter, which harbours two CymR operator sites, is unable to provide tight enough control of *cI*.

To improve ON state stability another round of optimisation was required, such that the design of the ^{1}CA^{OFF}-IM needed reconfiguring. Ultimately, we wanted to engineer a new CA-IM that featured an inducible promoter that could achieve two things. First, offer tighter control of *cI* in the absence of CA, to reduce the degree of basal/leaky *cI* expression. Second, exhibit a weak expression profile, where in the presence of CA, a lower level of *cI* is expressed that is sufficient for stable ON → OFF state switching but does not compromise OFF → ON state switching and stability. To source this 'weak' ^{2}CA^{OFF}-IM, we returned to Ian Dodd's series of CA systems (pIT4-KT-*cymR.T5-1, 4* and *6*). As discussed in Section 5.2.1.1, CA-induction profiles for each system were obtained by cloning *lac*Z immediately downstream of each T5 promoter (Ian Dodd, unpublished data). The outcome of these tests led to the rejection of the *T5-1* and *T5-4* promoter variants as they both exhibited strong expression profiles and the latter also exhibited a high level of basal activity.

The *T5-6* promoter variant looked promising, as it exhibited a weak expression profile and had a very low level of basal promoter activity, similar to the *T5-1* promoter variant used to generate the *cymR.T5-1.tum^{72K}* CA-IM (Fig. 5.7). Dodd's *T5-6* system was converted to the ^{2}CA^{OFF}-IM (pIT4-KH-*cymR.T5-6.cI^{+}*) by assembling the *Spe*I-HF and *Nar*I digested pIT4-KT-*cymR.T5-6.φK02CB* backbone (made by Ian Dodd) with a *cI^{+}* gene PCR fragment. A new set of WCB strains were made by integrating the ^{2}CA^{OFF}-IM into E4643 already harbouring the VA^{ON}-IM (encodes *tum^{72K}*) and the ***pR**.cI-CTD.tum*^{72K}* MCherry reporter (or the *tum^{-}* control) (see Table 5.10 and Fig. 5.36).

Table 5.10: The 186-WCB strains harbouring the ^{2}CA^{OFF}-IM. Each module exists at single-copy in the E4643 chromosome; ending subscript indicates site of integration.

Name	Description
AI322	E4643 + [pIT4-T-*vanR.pVan^{CC}.tum^{72K}*]$_{φ21}$ + [pIT4-KH-*cymR.T5-6.cI^{+}*]$_{HK022}$ + [pIT3-CL-*cI^{+}.**pR**$^{+}$.pL^{+}.cI-CTD.tum*^{72K}.mCherry*]$_{λ}$
AI323	E4643 + [pIT4-T-*vanR.pVan^{CC}.tum^{72K}*]$_{φ21}$ + [pIT4-KH-*cymR.T5-6.cI^{+}*]$_{HK022}$ + [pIT3-CL-*cI^{+}.**pR**$^{+}$.pL^{+}.cI-CTD.tum–.mCherry*]$_{λ}$

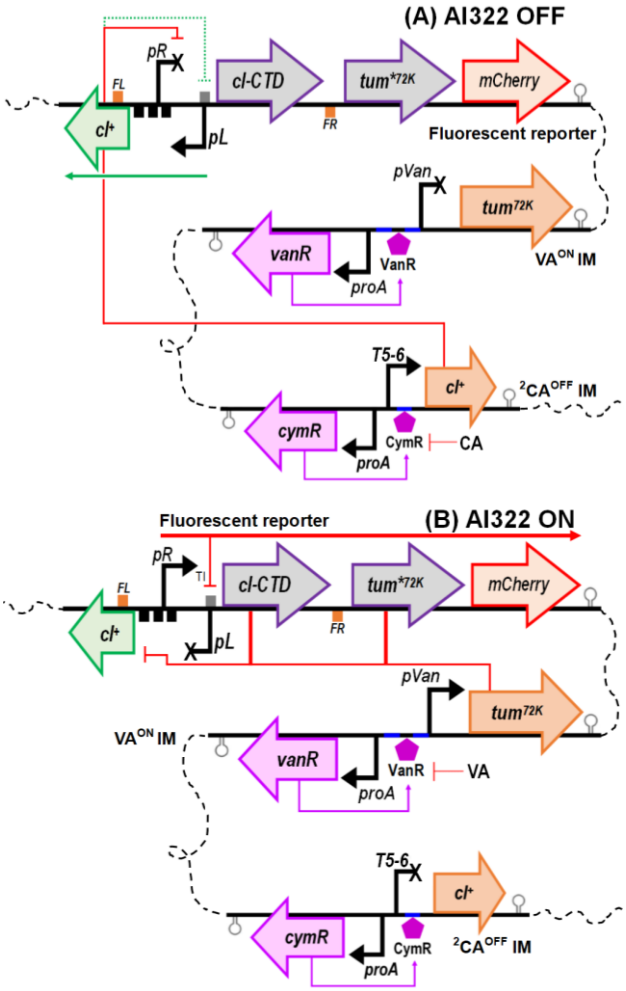

Figure 5.36: The three-module fluorescent AI322 186-WCB strain. AI322 harbours λ integrated ***pR***.*cI-CTD.tum*72K* MCherry reporter, the φ21 integrated VA^{ON}-IM and the HK022 integrated weak ^{2}CA^{OFF}-IM. AI323 is the *tum*$^{-}$ control strain. **(A)** OFF state schematic of AI322, where in the presence of CA, cells undergo ON → OFF state switching. An inactivated CymR (by CA) results in expression of the *T5-6.cI*$^{+}$ transcript. Active CI represses *pR*, inhibiting the expression of *cI-CTD, tum*^{72K} and *mCherry*. OFF state memory is established by expressing more *cI* from *pL*, which is under CI positive and negative feedback autoregulation. **(B)** ON state schematic of AI322, where in the presence of VA, cells undergo OFF → ON state switching. An inactivated VanR (by VA) results in expression of the *pVan.tum*^{72K} transcript. Active Tum^{72K} inactivates CI, resulting in *pR* depression and the expression of *cI-CTD, tum*^{72K} and *mCherry*. ON state memory is established by expressing *cI-CTD* and *tum*^{72K} from *pR*, which will keep CI inactivated, whilst transcriptional interference (TI) from an active *pR* will inhibit the expression of *cI* from *pL*. Symbolism defined in Table 5.12.

Upon restreaking AI322 and AI323 glycerol stocks on L-plates, we discovered these WCB strains have a resting ON state (Fig. 5.37A/B), which indicates the ^{2}CA^{OFF}-IM is generating less *cI* in the absence of CA, such that the reporter can return to its natural ON resting state as observed previously (Fig. 5.28). To characterise the performance of AI322 and AI323, ON and OFF state long-term stability profiles were obtained by performing a series of fluorescent stability assays as done for the AI311 WCB strain (Fig. 5.34). Preliminary switch tests however, revealed a longer exposure time of 30mins to CA was required to achieve maximal switching (data not shown). To assay the OFF state, O/N cultures of resting ON state colonies were grown in M9MM-1, switched to M9MM-20, induced with 150µM CA for 30mins and passaged continuously for five days with a set of fluorescent switch plates prepared over a 4hr timecourse each day. To assay ON state stability, on day five, each culture was induced with 150µM VA for 40mins and cultures passaged continuously for another five days with a set of fluorescent switch plates prepared over a 4hr timecourse each day (plate set reduced to x2 plates/day).

The protocol differed slightly, because AI322 and AI323 have an ON resting state, so ON and OFF state stability was assayed by passaging cultures for nine days, with days one to five assaying OFF state stability and days five to nine assaying ON state stability. For AI311, since this strain has a bistable resting state, independent cultures were setup to assay the ON or OFF state, meaning cells were not passaged beyond five days.

The results of the AI322 and AI323 ON and OFF state long-term stability assays are presented in Figure 5.37A to C. The results clearly show both strains have very similar ON and OFF state stability profiles. The OFF state stability profiles show that in the absence of CA, all cells emit a red-fluorescent signal and following exposure to CA, maximal (100%) ON → OFF state switching is observed with all cells growing non-fluorescent. The ability of each WCB strain to maintain the OFF state is somewhat unstable, with ~43% of cells continuing to grow as non-fluorescent colonies at the end of the passaging period (day 5). For AI322, the OFF state half-life averaged at ~92hrs, which was slightly longer than AI323, which averaged an OFF state half-life of ~90hrs. Improved OFF state stability for AI322 was expected because it has the ***pR***.*cI-CTD.tum*^{72K}* MCherry reporter whilst AI323 has the *tum*$^{-}$ version, hence AI322 has the added assistance of Tum^{72K} to dampen the effects of CI.

The ON state stability profiles for AI322 and AI323 show that when the remaining OFF state cells (~43% present in the day 5 OFF induced cultures) were treated with VA, maximal (100%) OFF → ON state switching was observed. The ON state is clearly digital, as ~99% of cells continue to emit a red-fluorescent signal at the end of the passaging period (day 9). The dynamic nature of these WCB strains is clear as almost all cells (~97%) can be switched OFF when re-induced with CA. The performance of the AI322 and AI323 WCB strains is an impressive improvement from that of the AI311 WCB, as these optimised strains have the desired ON resting state, can establish infinite long-term memory of the ON state and establish memory of the OFF state that although not digital, has an impressive half-life of >90hrs.

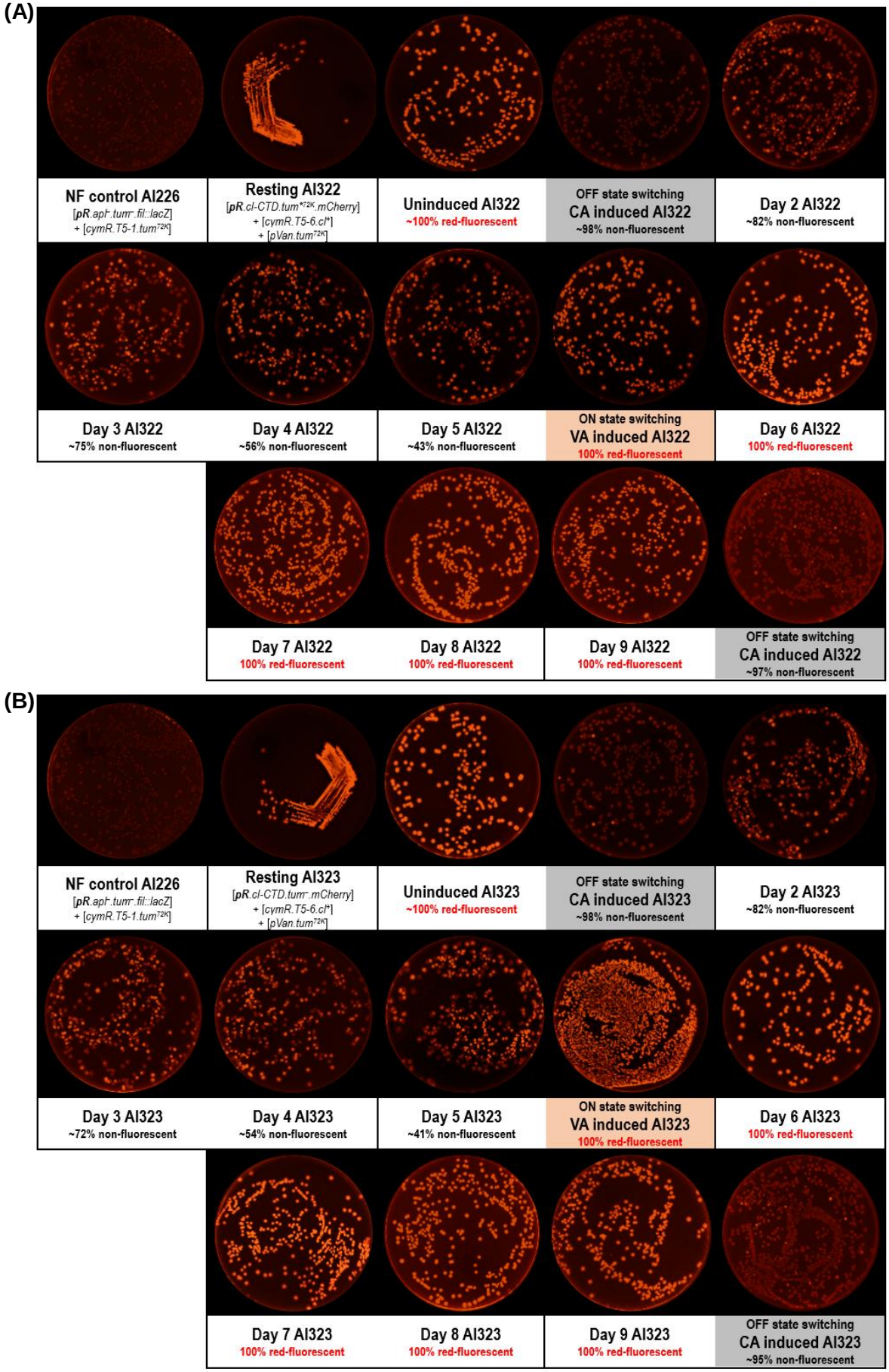

Continued to next page.

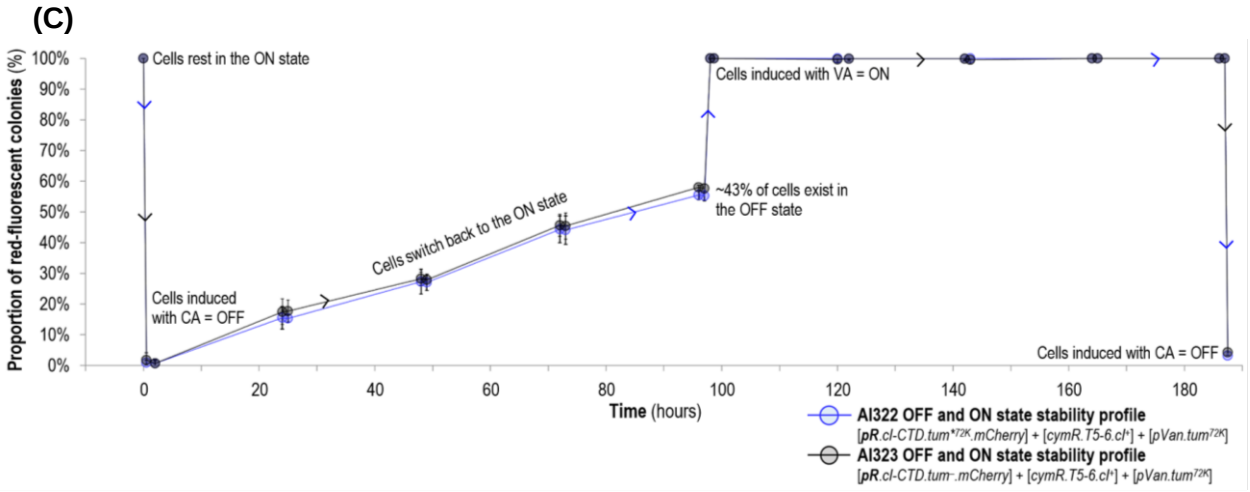

Figure 5.37: Long-term OFF and ON state stability profiles for the AI322 and AI323 186-WCB strains. **(A)** and **(B)** present images of the OFF and ON state fluorescent switching and stability plates prepared for AI322 and AI323 respectively. The resting plates confirm these strains have an ON resting state. Each culture was initially switched OFF with CA and continuously passaged for 5 days and then switched back ON with VA and continuously passaged for another 5 days. The resting, uninduced and induced L-plates were prepared and fluorescence visualised as described in Fig. 5.30. Percentage values represent the approximate proportion of non- or red-fluorescent colonies observed on each switch plate presented. To differentiate background from 'true' fluorescence a L-plate of the non-fluorescent (NF) AI226 WCB strain was prepared. **(C)** A graphical representation of the proportion of red-fluorescent colonies observed on each plate during the OFF and ON state passaging periods. The data shows, CA induction achieves maximal ON → OFF state switching, with ~99% of cells growing as non-fluorescent colonies. Cells gradually switch back ON, with ~43% of cells remaining non-fluorescent at the end of day 5. OFF state stability for AI322 and AI323 was calculated to have a half-life of ~92hrs and ~90hrs respectively. ON state stability was assayed by inducing day 5 cultures (a mix of ~43% OFF and ~57% ON cells) with VA. Following VA induction, maximal OFF → ON state switching was observed, with all cells emitting a red-fluorescent signal, which is stably maintained over days 6 to 9. At the end of day 9, cells were successfully switched OFF with CA. These assays were performed exactly as described in Fig. 5.34; with the exception that cells were induced OFF with 30min exposure to 150µM CA. ON and OFF state stability was assayed using the same cultures passaged continuously for 9 days, with days 1 to 5 assaying OFF state switching and stability and days 5 to 9 assaying ON state switching and stability. To quantify ON and OFF state stability, the growth of red-fluorescent cells on each plate was counted and plotted against a 190hr time scale. Each data point represents four independent assays with 95% confidence interval error bars shown.

To observe AI322 and AI323 to have near identical ON and OFF state stability profiles was an unexpected outcome (Fig. 5.37C). This indicates that for this particular configuration of synthetic circuitry, *cI-CTD* expressed alone from the MFL reporter is sufficient to control CI, meaning *tum*^{72K} is no longer required for ON state stability. These WCB strains however, are yet to achieve digital ON and OFF state stability as cells slowly relapse to the ON state after being switched OFF with CA. This led us to question, have we over stabilised the system such that these cells are now too good at maintaining the ON state? Would expression of *tum*^{72K} (rather than *cI-CTD*) from the MFL reporter be sufficient to achieve digital ON state stability, but with its 'weaker' control of CI allow for a more stable OFF state? To test this, we engineered the AI326 WCB, which features the ***pR***.*apl*$^{-}$.*tum*^{*72K} MCherry reporter linked to the VA^{ON}-IM and the ^{2}CA^{OFF}-IM (Fig. 5.38A). Surprisingly, upon restreaking the AI326 glycerol stock we found cells rest in the OFF state (Fig. 5.38B). To characterise the performance of the AI326 ON state, a set of fluorescent stability assays was performed exactly as described in Figure 5.34, with cells induced with 150µM VA for 40mins and the growth of red-fluorescent colonies tracked for 4hrs each day (plate set reduced to x2 plates/day) over four days.

The outcome of these assays clearly shows AI326 does not outperform AI322 and AI323 with the ON state averaging a short half-life of ~31hrs (Fig. 5.38B/C, ● profile), which confirms the CI-CTD is a more potent control factor for CI than Tum^{72K}. Furthermore, with the expression of Tum^{72K} alone from the MFL reporter introducing ON state instability, this demonstrates Dodd's *T5-6* IM system is also somewhat 'leaky', such that it spontaneously expresses *cI* at a 'lower' level that is tolerated by the CI-CTD but not by Tum^{72K}. Following this final test, we can confidently confirm the AI322 system remains the most optimal 186-WCB.

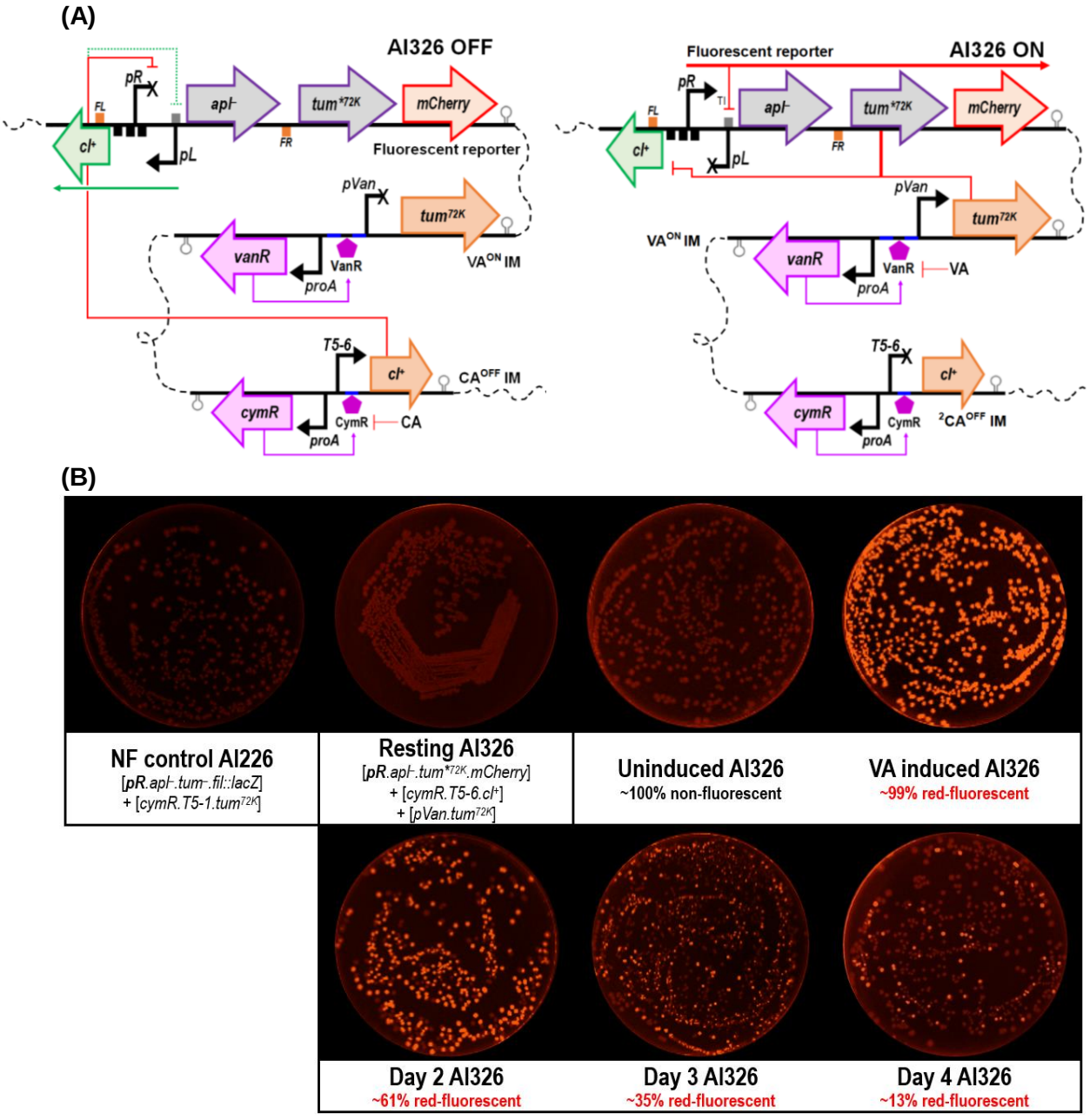

Continued to next page.

(C)

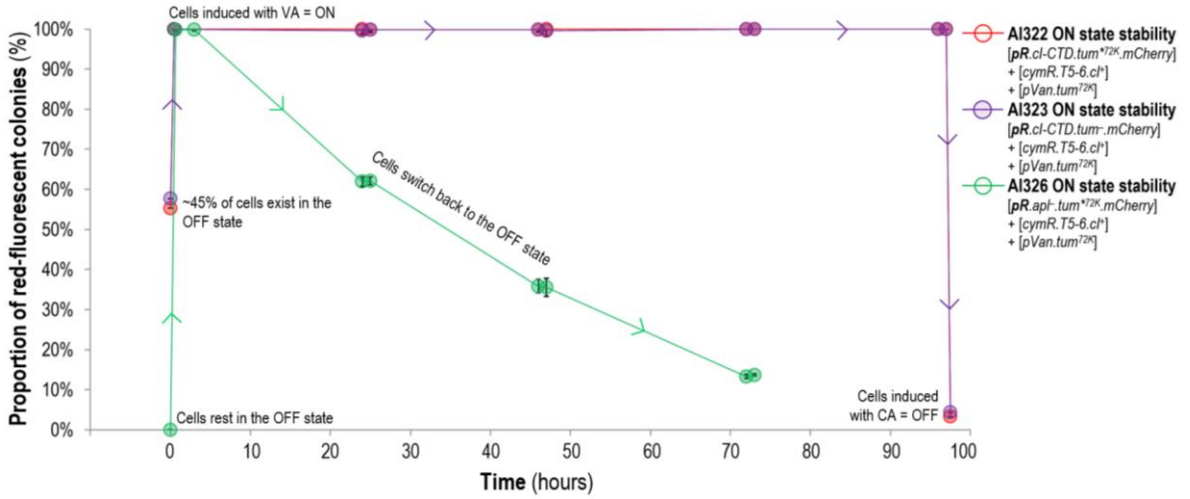

Figure 5.38: Long-term ON state stability profile for the AI326 186-WCB strain. This strain harbours the ***pR***.*apl⁻.tum*72K* MCherry reporter, a VA^{ON}-IM and a ^{2}CA^{OFF}-IM integrated at the λ, φ21 and HK022 *attB* sites respectively. **(A)** OFF and ON state schematics of AI326. In the presence of CA, cells undergo ON → OFF state switching and in the presence of VA, cells undergo OFF → ON state switching. In this system, it expected ON state memory will be established when more *tum^{72K}* is expressed from *pR,* to keep CI inactivated and transcriptional interference (TI) from an active *pR* inhibits further expression of *cI* from *pL*. Symbolism defined in Table 5.12. **(B)** Images of the ON state fluorescent switch and stability plates prepared for AI326. The resting plate confirms this WCB has an OFF resting state. To assay ON state stability, OFF state cultures were switched ON with VA and continuously passaged for 4 days The resting, uninduced and induced L-plates were prepared and fluorescence visualised as described in Fig. 5.30. Percentage values represent the approximate proportion of non- or red-fluorescent colonies observed on each switch plate presented. To differentiate background from 'true' fluorescence a L-plate of the non-fluorescent (NF) AI226 WCB strain was prepared. **(C)** A graphical representation of the proportion of red-fluorescent colonies observed on each switch plate. For comparison, the AI322 and AI323 ON state data from Fig. 5.37C was reproduced to show the ***pR***.*apl⁻.tum*72K* MCherry reporter does not result in a better (more stable) system. The data shows induction with VA achieves maximal OFF → ON state switching, but the ON state in unstable, averaging a half-life of ~31hrs (R^2 0.9814). These assays were performed exactly as described in Fig. 5.34, with OFF state cells induced ON with 150μM VA for 40mins. To quantify ON state stability, the growth of red-fluorescent cells on each plate was counted and plotted against a 100hr time scale. Each ● data point represents six independent assays with 95% confidence interval error bars shown.

5.8 Conclusion

In our efforts to harness the biology of the 186 coliphage, over seven stages of optimisation and characterisation we successfully developed a synthetic MFL transcriptional switch that responds to CA and VA with high sensitively and specificity. When integrated into *E. coli* (strain AI322) this system achieves the desired ON resting state and enables cells to undergo efficient switching between alternate OFF and ON states. The system exhibits impressive cellular memory, where the ON state is 'digital' and the OFF state averages a half-life of >90hrs. Whilst the performance of our 186-WCB is impressive, further optimisation is required to develop a system that can establish indefinite memory of the OFF state. To achieve permanent cellular memory of two alternate states a number of approaches (as listed below) could be undertaken. We anticipate these approaches could increase the bistable region of the system (see Fig. 5.29), which would ensure cells only undergo stable switching when exposed to the appropriate signal threshold and thus minimise cells from stochastically switching between alternate states when within the bistable region.

1. Reconfigure the $^{2}CA^{OFF}$-IM with an inducible promoter that gives even tighter control of *cI*.
2. Integrate a second copy of the VA^{ON}-IM to more closely match the 'leak' of CI with Tum^{72K}.
3. Mutate *pL* at the -10 or -35 sites to reduce *cI* expression.
4. Reduce translational output of *cI-CTD* mRNA by using a weaker RBS.

Whilst these approaches may result in a new system that outperforms AI322, we believe the current system claims an impressive performance profile and has the potential to be applied to a real-life setting. Given the ease at which the system can be adapted, AI322 could serve as a diagnostic tool by modifying one or both of the IMs, such that cells are adapted to detect a molecular analyte or condition unique to a disease of interest. Furthermore, AI322 could potentially act as a monitoring device due to the ability of the system to establish a heritable form of cellular memory. The system could be used to report on whether a specific 'event' occurred by emitting a non- or red-fluorescent signal. This 'event' could be in the form of detecting a disease specific analyte or detecting the presence of an environmental contaminant in water, food or soil for example. The key challenge in applying this technology to a real-life setting however, is engineering a compatible IM. If this is possible, we are confident our system could serve as a biosensor applicable to the industries of medicine, agriculture, food quality and control, water sanitation, environmental sustainability and industrial processing and monitoring.

Table 5.12: Glossary of definitions and symbols. A list of the characters, codes and symbols used to illustrate the various synthetic gene modules presented in this chapter and the definitions of each gene and genetic component.

Symbolism				
Lytic gene 	Lysogenic gene 	Induction gene 	Repressor gene 	Reporter gene 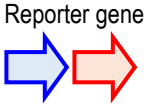
Active promoter 	Inactive promoter 	*E. coli* chromosome 	Repressor protein 	*FL* or *FR* operator 
Repressor operator 	*pR* operators 	*pL* operator 	Terminator 	Inhibitory sign 

Definitions	
apl^{+}	Encodes 186 wildtype excisionase, Apl
apl^{-}	Encodes 186 inactive excisionase, Apl HTH mutant
cI^{+}	Encodes 186 wildtype immunity repressor, CI
cI-CTD	Encodes CTD of 186 CI immunity repressor, a dominant negative to wildtype CI
cII::lacZ	Encodes CII::LacZ fusion reporter protein; the CII RBS and first codon of CII linked to the ninth codon of LacZ.
cymR	Encodes the cumic acid repressor, CymR
cymR^{AM}	Encodes the optimised cumic acid repressor, $CymR^{AM}$
fil::lacZ	Encodes Fil::LacZ fusion reporter protein; the Fil RBS and first three amino acids of Fil linked to the ninth codon of LacZ.
FR and *FL*	Right and left intact 186 CI operator sites
gfp	Encodes the green-fluorescent reporter protein, SF-GFP
mCherry	Encodes the red-fluorescent reporter protein, MCherry
nahR	Encodes the salicylic acid repressor, NahR
p95	LexA repressed 186 SOS promoter
pcymR^{C}	Strong cumic acid inducible promoter, repressed by $CymR^{AM}$

Definitions	
pL	Weak leftward 186 lysogenic promoter
placIq	IPTG inducible promoter, repressed by LacI
pR	Strong rightward 186 lytic promoter
proA	Constitutive promoter
pSal	Salicylic acid inducible promoter, repressed by NahR
pVan	Vanillic acid inducible promoter, repressed by VanR
T5-1	Strong cumic acid inducible promoter, repressed by CymR
T5-6	Weak cumic acid inducible promoter, repressed by CymR
tum^{+}	Encodes the 186 anti-CI protein
tum^{72K}	Encodes hyperactive Tum^{72K} mutant, truncated to its first 72 residues, removing most of its DinI-like CTD
tum^{-}	Encodes inactive Tum^{72K} mutant, due to the presence of the inactivating ΔD30G mutation
tum^{72K}*	Encodes Tum^{72K} linked to an optimised RBS
vanR	Encodes the vanillic acid repressor, VanR

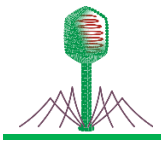

Chapter 6

Conclusions and future directions

6.0 Understanding bacteriophage 186

Temperate phage, like coliphage λ and 186 serve as model organisms for the study of prokaryotic gene regulatory control; largely because of their ability to 'decide' on two alternative modes of development, lytic or lysogenic. The ability of 186 to make appropriate developmental decisions has come about through the evolution of a transcriptional lytic/lysogenic switch and an inducible SOS operon. Each exist as independent modules in the 186 genome, where the switch entails a complex interplay of regulatory proteins to enforce lytic or lysogenic development and the SOS operon encodes Tum, the CI antirepressor essential for prophage induction.

Like most temperate phage, 186 makes its developmental decisions early after infection. Lytic development is the developmental default state and follows the typical cycle of rapid DNA replication, mass assembly of new phage progeny and their release into the extracellular environment via host cell lysis. Lysogeny is the alternate developmental state that occurs in ~10% of infections (Reed, 1994). In this cycle, the phage genome integrates into the host chromosome and exists in a state of dormancy, establishing a lysogen-prophage symbiosis. Despite lysogeny being an extremely stable mode of development that can persist for thousands of generations, it remains reversible, meaning the phage can rapidly switch to the lytic development mode; a process termed prophage induction. In 186, this process occurs when the host SOS system is activated, usually by a DNA damaging event (e.g. UV irradiation). Activation of the SOS response results in activation of the 186 SOS operon, where expression of the *tum* gene, resets the 186 switch (from the lysogenic) to the lytic state.

6.0.1 Investigating the role of key regulatory factors in 186 bacteriophage development

Phage 186 is used as a model organism to investigate the properties of natural regulatory circuits and to design and engineer novel biological circuits, systems and switches. Over the last four decades, studies of 186 by the Egan/Dodd/Shearwin laboratory have provided a detailed picture of how the lytic and lysogenic cycles are regulated in this phage. Whilst these studies have revealed the switch to exhibit many characteristics comparable with those of P2 and λ, it also has a number of unique aspects for which our understanding remained incomplete.

In this thesis, four studies were undertaken to answer key questions concerning the action of four key regulatory proteins (CI, Apl, Tum and CII) at the 186 switch and in particular, during prophage induction. We anticipated these studies would provide us with new information that would contribute to our understanding of specific areas of 186 development. Furthermore, using this information (in combination with data obtained from previous studies) a fifth study was undertaken, where we applied the principles of synthetic biology (SynBio) to develop a whole-cell biosensor (WCB) using discrete components of the 186 genome. The efforts to build such a system proved successful, with the final (most optimal) system having the capacity to program *E. coli* to exhibit high specificity and sensitivity to specific chemical inducers, such that when induced, cells are able to switch between and establish long-term cellular memory of two alternate states.

The key outcome obtained from these studies of 186 is how modest changes in the levels of key regulatory factors (or alteration of their biological properties) can introduce bias towards lytic or lysogenic development and/or compromise phage survival (by antagonising prophage induction efficiency). Over evolutionary time, 186 has been precisely fine-tuning its decision-making parameters, where critical regulatory proteins are expressed at optimum levels to allow for maximal switching efficiency and to establish the right balance of lytic versus lysogenic development. The ability of 186 to go lytic or lysogenic is a highly coordinated decision negatively impacted when key regulatory factors are expressed at inappropriate times and/or at suboptimal or elevated quantities. The research described in Chapters 2, 3 and 4 of this thesis not only contributed to our understanding of the extreme precision associated with prokaryotic gene regulatory control systems, but also served as the basis for the design and optimisation our 186-inspired WCB.

6.0.1.1 Concluding remarks on the role of CI and Apl at the 186 switch during prophage induction

Chapter 2 presented the results of our investigation into CI, Apl and the *goa8* mutation. In the CI study, we re-examined the mechanics of CI regulation at *pR* and *pL* using a chromosomally-integrated CI expression-wildtype *pR.pL* LacZ reporter system. We anticipated this system would give an improved insight into CI's action at the 186 switch as chromosomal integration of the synthetic componentry would circumvent the biological noise associated with plasmid-based systems. The concluding outcomes of this investigation were comparable with the Dodd and Egan (2002) study and are as follows:

- In the absence of CI, *pR* activity is high.
- In the presence of CI, *pR* activity decreases as CI levels increase.
- In the absence of *pR* transcriptional interference and CI, *pL* activity is high.
- In the presence of *pR* transcriptional interference and absence of CI, *pL* activity is low.

- At intermediate/lysogenic CI levels, *pL* activity increases.
- At high CI levels, *pL* activity decreases.

The second (concurrent) investigation confirmed that the poor prophage induction efficiency observed by Reed et al. (1997) for their C600(186^{goa8}) lysogen was due to the *goa8* mutation disrupting CI negative autoregulation, rather than disrupting Apl *pR.pL* repression. Using a chromosomally-integrated CI expression-*goa8 pR.pL* LacZ reporter system we provided clear evidence the *goa8* mutation significantly disrupts CI's repression of *pL*, but does not affect CI's ability to repress *pR* (Fig. 2.6). We reasoned the impaired repression of *pL* by CI in the presence of *goa8* was due to the loss of the CI-*pR.pL* repressive complex, where *goa8* disrupts the precise spacing required for the *pL* operator to correctly wrap onto the CI-*pR* wheel. We inferred *goa8* does not disrupt CI *pR* repression because the CI-*pR.FL* and CI-*pR.FR* wheels can still sufficiently shut down *pR* activity and so rescue the loss of the CI-*pR.pL* wheel.

A quantitative Western blot analysis of C600(186^{+}) and C600(186^{goa8}) lysogens supported the idea that disrupting CI negative autoregulation would establish a higher lysogenic [CI]. In this instance, the C600(186^{goa8}) lysogen was found to express CI at a level 1.65-fold higher than that of wildtype (Fig. 2.8). To assess the extent to which this increase in [CI] affected prophage induction efficiency, we assayed our *goa8*$^{+/-}$ ***pR***.*apl*$^{+}$.*cII*$^{+}$ minimal prophage induction reporter modules and observed *pR* derepression to be reduced by ~51% in the presence of *goa8* (Fig. 2.9). We interpreted this outcome to be a consequence of cells having an elevated steady state level of CI, such that the sequestering capacity of Tum is exceeded. With Tum unable to inactivate a sufficient fraction of the CI in the cell, *pR* is only partially derepressed, resulting in reduced expression of the lytic genes, including *apl.* With insufficient Apl available to bind Int and form the excisionase complex, and likely insufficient *A* gene (DNA replication initiator) product, the prophage is more likely to remain integrated within the host chromosome and be unable to proceed with lytic development.

Having determined that the *goa8* mutation likely affects 186 prophage induction efficiency more by disrupting CI negative autoregulation than by disrupting Apl binding at *pR.pL,* it was clear a renewed investigation of Apl's second role as a transcriptional repressor at *pR* and *pL* during prophage induction was required. Three key hypothesises were formulated and focused on the idea that Apl binding at *pR.pL* is required to control *cII, cI* and/or *int* gene expression during prophage induction (Table 2.3). To test these theories we expanded our minimal prophage induction module to study *pR* and *pL/pE* activity during induction in the presence and absence of Apl and/or CII. Analysis of the results however, led to the rejection of all three hypotheses (Fig. 2.10 and Fig. 2.11).

Combining the outcomes observed in this study and from previous studies of Apl, the following conclusions can be drawn.

- Apl represses transcription from *pR* and *pL*, a function analogous to λCro (Dodd et al., 1990).
- Apl is not essential for lytic development, but is required (as the RDF) during prophage induction to excise the prophage from the host chromosome (Dodd et al., 1993; Reed et al., 1997).
- During 186 prophage induction, Apl's role *is not* to aid Tum-mediated *pR* depression by repressing *cI* gene expression from *pL.*
- During 186 prophage induction, Apl's role *is not* to prevent over activation of *cI* and/or *int* gene expression from a CII-activated *pE.*
- During 186 prophage induction, Apl's role *is not* to control *int* gene expression from *pL* to facilitate efficient excision of the prophage from the host chromosome.

Whilst these conclusions *do not* define the role of Apl as a transcriptional repressor at *pR.pL* during prophage induction, we remain hopeful that as we formulate and test new hypotheses we will eventually uncover this mystery. As discussed in the *Conclusion* of Chapter 2, since the *goa8* mutation disrupts both Apl regulation and CI regulation at the 186 switch, it is not the ideal mutation to use to study Apl and CI in isolation. To investigate CI further, the next logical step would be to create a CI *pL* operator mutant to study what happens to prophage induction efficiency when CI negative autoregulation is disrupted. Creating this mutant would allow us to confirm 186 expresses CI at a tightly-controlled steady state to maintain lysogeny and keep the prophage primed for prophage induction. To determine why Apl acts as a transcriptional repressor at *pR.pL,* it would also be ideal to create Apl operator mutants, where Apl repression of *pR* and *pL* is lost/disrupted, but CI regulation remains unaffected. This region of DNA however, is genetically dense, and the best approach to disrupting Apl binding while minimising any effects on promoter activity would be to mutate the central three Apl operator sites (Fig. 2.12).

6.0.1.2 Concluding remarks on the role of Tum at the 186 switch during prophage induction

Chapter 3 presented a draft manuscript of the Tum study, where in the context of 186 prophage induction, the role of Tum and the host SOS response were investigated. To conduct this study, we engineered a series of 186-like UV- and chemically-inducible, chromosomally-integrated minimal reporter systems and a cumic acid (CA)-inducible $186^{p.cym}$ phage. Using these molecular tools, we analysed different parts of the *tum* gene and investigated whether activation of the host SOS response only serves to induce *tum* expression or whether other accessory role(s) exist.

These experiments, in both a minimal reporter and whole phage setting, have revealed more detail on the mechanism of 186 prophage induction. While 186 utilises the host SOS system, the process differed from that of phage λ, as RecA does not catalyse the autoproteolysis of 186CI, instead the 186 repressor is reversibly inactivated by Tum (Lamont et al., 1989; Shearwin et al., 1998). Tum is a *trans*-acting antirepressor whose gene is controlled by the LexA repressed *p95* promoter. Transient expression of full-length *tum* in single-copy from a derepressed *p95* is sufficient for 186 lysogenic → lytic switching. The structure of the *tum* gene is unusual as it displays five additional potential start sites with *orf95.2, orf95.4* and *orf95.5* actively expressed. Whilst Orf95.2 has a stimulatory effect on Tum activity, Orf95.4 and Orf95.5 have an inhibitory effect as observed in our study and that of Brumby et al. (1996). Tum's antirepressor activity is thought to reside within the N-terminus, as our experiments suggest the DinI-like C-terminus on full-length Tum is inhibitory.

Naturally, 186 prophage induction is linked to the host SOS response. However, when this connection was broken and replaced by chemical induction (IPTG and CA), a single-copy full-length *tum* expression module was successful in (1) activating the *p95.tum*$^{+}$ minimal reporter system (DL245-I) to undergo stable lysogenic → lytic switching and (2) triggering induction of a 186$^{p.cym}$ prophage, with similar phage production profiles observed for 186$^{p.cym}$ under CA ±UV conditions. These outcomes confirmed that no accessory role(s) exists for SOS activation, the fundamental role of this response is to induce *tum* gene expression.

Whilst this study did answer a number of unknowns about the process of 186 prophage induction, our knowledge of Tum functionality still remains incomplete. In particular, we are yet to determine the exact role of the Tum^{4} (Orf95.4) and Tum^{5} (Orf95.5) proteins and what consequence their inhibitory effect on full-length Tum activity has on the process of 186 prophage induction. At present, it is unclear if these DinI-like elements act at the level of Tum or at the level of SOS induction. In the Brumby et al. (1996) study, an inhibitory effect for Tum^{4} and Tum^{5} was observed, which led to the prediction that active Tum^{1} (Orf95.1) exists as a homodimer, where heterodimers of full-length Tum^{1} with Tum^{4} or Tum^{5} are inactive and Tum^{2} (Orf95.2) stimulates Tum^{1} activity by titrating Tum^{4} and Tum^{5} into Tum^{2} heterodimers; reducing their inhibition of full-length Tum^{1}.

An alternate idea is that the DinI-like proteins are inhibitory to the SOS response, thereby resulting in the production of fewer *tum* mRNAs. Since Brumby et al. (1996) also observed Tum^{4-} and Tum^{5-} mutants to exhibit a 2-fold increase in phage production after UV exposure it was suggested the dampening of *tum* expression during 186 prophage induction may be related to dampening the SOS response to perhaps reduce unnecessary prophage induction.

To investigate the inhibitory role of the Tum^4 and Tum^5 proteins, the logical approach would be to induce expression of *tum^4* and *tum^5* via use of a chromosomally-integrated CA-inducible gene expression module (like the *cymR.T5-1* system) and linking these modules (*cymR.T5-1.tum^4* and *cymR.T5-1.tum^5*) to a *p95.lacZ* reporter integrated at another site in the *E. coli* chromosome. To assay the effect Tum^4 and Tum^5 have on the SOS response, LacZ timecourse assays under UV ±CA induction conditions would be performed, where we predict these short Tum proteins would decrease the UV response and thus reduce expression of *lacZ* from *p95.* Overall, from this current study, we can confidently conclude that (1) Tum is essential and sufficient in single-copy for stable 186 lysogenic → lytic switching and (2) the fundamental role of host SOS activation is to induce expression of the *tum* gene.

6.0.1.3 Concluding remarks on the role of CII at the 186 switch during the establishment of lysogeny and prophage induction

Chapter 4 presented a draft manuscript of a study focused on CII, which investigated the role of CII at the 186 switch during the establishment of lysogeny and prophage induction. This study addressed the apparent paradox of how 186 can encode the pro-lysogenic CII protein from *pR* and yet avoid introducing bias towards lysogeny. The study began by identifying FtsH and RseP as the two key *E. coli* proteases that degrade 186CII and confer on it a very short (~2min) *in vivo* half-life. The significance of 186 (and λ) having a protease-sensitive CII was modelled, asking, does a short-lived CII factor prevent over-activation of *pE* early after infection to prevent 186 from establishing lysogeny inappropriately? I was not involved in this part of the study.

Using a series of ***pR***.*apl$^+$.cII$^{+/-/145}$* LacZ reporter switches, *E. coli* harbouring a long-lived CII145 variant were found to exhibit very poor *pR* derepression following UV induction. To determine what effect CII145 has on CI levels following induction of a 186 variant carrying CII145, the change in [CI] over time was quantified by Western blot; with the results revealing significantly higher levels of CI following UV induction. We reasoned that in the presence of CII145 there is enhanced expression of *cI* from an over-activated *pE.* We tested this by conducting LacZ assays of a series of ***pL/pE***.*apl$^+$.cII$^{+/-/145}$* LacZ reporter switches, where *E. coli* expressing *cII^{145}* had a significantly enhanced *pL/pE* LacZ UV induction response in comparison to cells expressing wildtype *cII*. It appears the consequence of over-activation of *pE,* is an elevated level of CI that exceeds the sequestration capacity of Tum. The extra CI (not inactivated by Tum) then impedes derepression of *pR* following UV induction. Using the experimental data generated in this study, simulations suggest a key function of having a highly active, rapidly degraded CII factor is to quickly equilibrate [CI] in a lysogen. This has the advantage of ensuring the lysogen is established and ready for induction as soon after infection as possible.

Overall, this study demonstrated CII protease sensitivity is an important control strategy, as early after infection, inappropriate activation of *cI* expression from *pE* could bias the phage too heavily towards lysogeny. Whilst lysogeny offers a number of advantages, from an evolutionary perspective there is likely to be an optimal frequency of lysogeny. During prophage induction, inappropriate activation of *pE* could pose a significant threat to phage survival, if expression of *cI* (from *pE*) exceeds the sequestering capacity of Tum. If this were to happen (as observed in our CII145 systems), inefficient prophage induction would follow.

A key unknown of 186 developmental decision-making, is the exact 'signal/condition' that prompts 186 to establish lysogeny. Whilst relying on host factors to adjust the frequency of lysogeny makes sense, making developmental decisions based on the levels of host proteases does appear to be a somewhat disconnected and indirect measure. An alternate theory to explain how 186 opts for the lytic or lysogenic pathway relates to whether *tum* is expressed or repressed early after infection, with CII playing an important role as a 'calibrator' of the SOS operon to ensure [Tum] is an accurate and appropriate indicator of host stability. For instance, upon infection, a short-lived CII protein may encourage some expression of *cI* from *pE*, which could result in two mutually exclusive outcomes. If Tum levels were high enough to inactivate the CI expressed from *pE,* this would prevent CI from repressing the early lytic promoters, *pR* and *pB* and thus drive the lytic decision. We would expect high Tum levels to facilitate lytic development, because if LexA were being inactivated by RecA (for example), this would indicate the host has sustained DNA damage and is in a vulnerable state (and not suitable for lysogeny). If Tum levels were low however, such that some of the CI expressed from *pE* remained active, this would result in the repression of *pR* and *pB* and thus drive the lysogenic decision. Hence, having CII transiently activate *pE* to establish a small pool of CI in the cell early after infection is perhaps a means to calibrate the system to ensure whatever Tum is present is at the appropriate threshold for directing 186 to make the correct developmental decision. Whilst this theory makes sense, it is just a theory and requires investigation. Engineering a set of 186 phage mutants encoding various combinations of cII^{+}, cII^{-}, cII^{145} and/or tum^{+} or tum^{-} would allow us to assay the frequency in which these phage establish lytic or lysogenic development and investigate whether Tum is 'the' or 'a' condition used by 186 to measure host stability and suitability for lysogeny.

6.1 The design and engineering of the 186-WCB

Phage are the planet's most abundant organisms. The relative simplicity of phage however, is what makes them model organisms for the study of prokaryotic gene regulatory control, whilst the mosaic nature of their genomes makes them fruitful sources of genetic componentry.

Applying the principles of engineering, mathematics and biology, synthetic biologists have already utilised countless 'parts' and 'modules' from well-charactered phage (e.g. λ and T7) to design and construct novel synthetic biological switches and systems (Elowitz and Leibler, 2000; Gardner et al., 2000; Han et al., 2017; Ike et al., 2015; Kotula et al., 2014; Ortiz and Endy, 2012). With so many phage yet to be discovered, phage clearly have the potential to power the future advancement of SynBio. By making new phage discoveries, we will be able to grow our toolbox of biological building blocks and components, thereby facilitating the development of more sophisticated and complex synthetic networks that predictably perform to fulfil predefined outcomes.

Temperate phage are of particular interest when sourcing novel genetic componentry as these phage require a switchable memory circuit to maintain the lysogenic state. Coliphage 186 and λ have evolved sophisticated genetic switches to control their ability to make developmental decisions and both are model examples of how similar outcomes can be achieved by different means. Extensive studies of 186 have provided the scientific community with detailed information on how this phage develops in a lytic and lysogenic manner. Using the information published in previous studies and from the research conducted in this thesis two specific regions of the 186 genome were identified to be promising sources of biological componentry for the development of a WCB. Such a biosensor could potentially be based on a mixed feedback loop (MFL) design and be programmed to report on the presence of a specific ligand by switching between two alternate states of gene expression.

As discussed in the *Introduction* of Chapter 5, the MFL is a common composite motif utilised by prokaryotic and eukaryotic organisms to achieve two alternative states of gene expression. In its simplest form, it is a positive feedback loop consisting of a protein-protein interaction and a protein-DNA interaction (François and Hakim, 2005). To engineer an inducible MFL, an induction module (IM) is required, such that it expresses a control factor that enables the MFL to switch from its current state to the alternate state. In fulfilling these requirements, we developed our initial working WCB modules as two-module systems consisting of a chromosomally-integrated MFL in the form of a cI^{+}.***pR***$^{+}$.pL^{+}.$apl^{+/-}$.$tum^{72K/-}$ LacZ reporter linked to an integrated $p95.tum^{+/-72K}$ UV-IM (Fig. 5.39A). Working from this initial design, the system was progressively optimised over seven stages of engineering to reach the final (most optimal) system (Fig. 5.39B). The final three-module system consists of an integrated fluorescent MFL in the form of a cI^{+}.***pR***$^{+}$.pL^{+}.*cI-CTD*.tum^{72K} MCherry reporter linked to two integrated IMs, one that encodes cI^{+} for ON → OFF state switching and another that encodes tum^{72K} for OFF → ON state switching. During each optimisation stage, the system's design was modified to improve induction efficiency, bidirectional switching and bistability and reduce stochastic switching and system variability. These performance parameters were improved by determining which design components were essential for MFL and IM design, what elements could be replaced with components that could offer improved performance and what configuration of the MFL and IMs could achieve superior system performance.

Adopting a progressive approach for system optimisation and continuously using WCB strains encoding the *tum*⁻ gene allowed us to characterise the performance of the system and determine whether our design modifications resulted in an improved system. It also assisted in identifying design flaws and how best to adapt these areas to develop a more stable and predictable system. The development of the stability assay proved to be an important protocol for characterising system bistability. The agreement observed between the LacZ data and the switch plate data (Fig. 5.16C) was impressive, and the ease at which the assay could be performed and its accurate quantification of system stability. The assay not only allowed us to develop ON and OFF state long-term stability profiles, but it also proved appropriate to a wide range of systems and was useful in determining system dynamics, variability and tolerance (i.e. robustness).

6.1.1 The influence of past and present studies of 186 on the design and optimisation of the 186-WCB

The design of the 186-WCB was largely influenced by the research conducted on 186, both previously and in this thesis. To develop the initial working modules, the available evidence indicated the use of CI, Tum and the *cI.pR.pL* feedback motif of the 186 switch could theoretically produce a bistable network. Furthermore, since CI and Tum show few interactions with the host *E. coli* network they presented as ideal choices for the development of a synthetic switch that works in isolation.

Previous studies of CI from a functional and structural perspective have shown CI cooperatively interacts with three high affinity operator sites at *pR* to inhibit lytic development and interacts with a weak putative operator at *pL* to positively and negatively regulate the expression of its own gene. Our study of CI *pR* and *pL* regulation and our investigation into the molecular consequences of the *goa8* mutation on prophage induction efficiency, revealed outcomes that suggested CI negative autoregulation is not only important for maintaining lysogeny, but is also important for keeping the prophage optimally primed for prophage induction. The CI autoregulatory loop, in conjunction with the precise face-to-face arrangement of the *pR* and *pL* promoters were deemed to be central design components to constitute a functional MFL, as establishing the correct lysogenic [CI] would allow for maintenance of the lysogenic/OFF state whilst keeping cells primed for lysogenic/OFF → lytic/ON switching. With the marginal increase in the lysogenic [CI] observed in the presence of the *goa8* mutation having a negative impact on prophage induction efficiency, this further demonstrated that to engineer a bistable MFL, ON state stability would need to be achieved by employing ON state control elements capable of keeping CI activity and *cI* expression under tight control. Without tight control of CI, the system would exhibit bias towards lysogeny (i.e. the OFF state). Reducing ON state instability was undoubtedly a persistent challenge encountered throughout each stage of optimisation.

The Tum and Apl factors of 186 were initially considered to be the appropriate ON state control elements, as we believed they would allow for tight control of CI and *cI* expression respectively and thus achieve long-term ON state stability. In the Tum study (Chapter 3), we demonstrated Tum is necessary and sufficient for 186 prophage induction. Our analysis of Tum's action at the 186 switch during this process lead to the following considerations for 186-WCB design:

1. To establish an inducible MFL, Tum would need to be expressed from the IM to induce OFF → ON switching by transient inactivation of CI.
2. To establish a bistable MFL, Tum would need to be expressed from the MFL reporter to keep CI inactivated and allow cells to establish long-term memory of the ON state.

The decision to replace the *cII* gene with the *tum* gene was based on the CII study (Chapter 4), where we demonstrated CII is not a constituent part for the MFL, as CII's role is to establish lysogeny by facilitating *cI* expression from an activated *pE* promoter. Replacing *cII* with tum^{72K} would not only eliminate any *pE.cI* expression following induction (which would compromise ON state switching and stability), but rather, Tum would establish the inhibitory CI-Tum interaction; fulfilling the protein-protein interaction required to constitute a functional MFL. The decision to use Tum^{72K} was influenced by the Tum study (Chapter 3), as this mutant consistently exhibited enhanced activity against CI. We inferred Tum^{72K} would allow us to develop a WCB that exhibited more efficient OFF → ON state switching and achieve a more stable ON state by providing better control of CI in the absence of the inducer.

From an Apl perspective, despite the outcomes of our Apl experiments resulting in the rejection of all three hypotheses, the information gained from this study did assist with the initial design and subsequent optimisation of the WCB. Initially, we inferred Apl repression of *pL* would facilitate OFF → ON state switching and enhance ON state stability by assisting Tum in keeping CI inactivated by inhibiting further expression of *cI* from *pL.* When testing for the importance of Apl and Tum in WCB design, we found Apl offered no assistance to OFF → ON state switching and ON state stability, ruling Tum as the sole factor important for the design of a working MFL (Fig. 5.3 and Fig 5.4). This outcome was consistent with the results obtained from our LacZ analysis of our minimal prophage induction *pR* and *pL/pE* modules (Fig. 2.10 and Fig. 2.11). With *apl* not a required component for the MFL, this provided an avenue for WCB optimisation as it was easily replaced with the *cI-CTD* gene, which significantly improved ON state stability and overall system performance.

6.1.2 The 186-WCB now and into the future

E. coli harbouring the final (most optimal) working module of the 186-WCB (Fig. 5.39B) exhibit remarkable cellular performance, as they can readily switch between ON and OFF states and establish long-term cellular memory of each alternate state. Specifically, the system exhibits impressive cellular memory, where the ON state can be maintained indefinitely and the OFF state exhibits an average half-life of >90hrs. Whilst the performance of our WCB is impressive, further optimisation is likely to be required for cells to establish indefinite memory of the OFF state; suggestions for future optimisation are listed in Chapter 5, Section 5.7.

With the task of balancing the requirements for CI, Tum^{72K} and CI-CTD production rates to achieve bistability being a prominent challenge, developing a mathematical model of the system could prove useful in determining how best to optimise the system to achieve indefinite/digital ON and OFF state stability. Rather than adopting a 'build and test' approach, we could run specific simulations by varying the parameters of CI, Tum^{72K} and CI-CTD to reach a more bistable system and then work experimentally to apply these parameters to the system. Developing a full mathematical model would be a complex task as there are a number parameters to consider, some of which have unknown values. However, even a simplified model, such as that developed in Chapter 4, would allow us to scan a range of parameter values and test the underlying assumptions.

Whilst there is room for improvement, we believe the current system exhibits an impressive performance profile and has the potential to be applied to a real-life setting. A desirable property of our WCB is that it can be efficiently switched OFF → ON and ON → OFF when exposed to VA and CA respectively. In contrast, synthetic systems that use phage integrases induce a permanent change (by causing DNA inversions, insertions and deletions) (Merrick et al., 2018; Yang et al., 2014), thereby rendering them as 'single-use' systems in the absence of the corresponding RDF. Our WCB is in a sense 'recyclable' as neither ON or OFF states are permanent; rather cells can be 'toggled' between each alternate state depending on which inducer they are exposed to. Given the ease at which this system can be adapted, our WCB could serve as a diagnostic tool by modifying one or both of the IMs, thereby adapting cells to detect a molecular analyte or condition unique to a disease of interest. Our WCB could also act as a monitoring device due to the system being able to establish a heritable (yet reversible) form of cellular memory. To demonstrate the potential application of the WCB to a real-life setting, the final section of this chapter presents two hypothetical systems, where I propose that the MFL reporter could be integrated into (1) a two-component signal-transduction system designed to detect microplastic compounds and (2) a dual-sensory system designed to detect cancer.

6.1.2.1 The 186-WCB as an environmental biosensor

In today's society, with our excessive use and careless disposal of plastic products, a major concern is that the microplastics produced from these waste products (as they slowly degrade) are leaching into our waterways and making their way into our food and beverage sources. Studies are being conducted to investigate whether consuming these plastic particles are harmful to human health (Campanale et al., 2020; Hwang et al., 2020; Shams et al., 2020; Smith et al., 2018), but without any clear and complete studies available to support this claim more evidence is required. I do believe that for a better future - one that promotes healthy living and sustainable environmental practises - the development of biosensors that can detect and report on the presence of plastics and other harmful compounds is a relevant and important area of study.

I believe our 186-WCB could be adapted to act as an environmental biosensor that is sensitive enough to detect plastic derived compounds at low concentrations. As presented in Figure 6.1, the hypothetical system features the MFL reporter linked to a typical bacterial two-component signal-transduction system (Liu et al., 2019; Mitrophanov and Groisman, 2008; Zschiedrich et al., 2016). The first component consists of a novel membrane-bound sensor histidine kinase, where exposed on the cell surface is the sensory domain and suspended in the cytoplasm is the signal-transduction kinase domain. The second component is the novel response regulator (RR), which (when activated) acts as a potent transcriptional activator of an inducible promoter, where its gene output will influence the state of the MFL reporter.

Bacteria (e.g. *E. coli*) engineered with this system would emit a red-fluorescent signal when the receptor's sensor domain detects the presence of a plastic compound. This interaction will induce a conformational change that activates the kinase domain, causing it autophosphorylate at a conserved histidine residue. The phosphate is then transferred to a conserved aspartate residue within the receiving domain of the RR, which when phosphorylated becomes an active transcription factor of the *pON* promoter. When *pON* is active, the tum^{72K} gene is expressed and Tum^{72K} acts on the MFL reporter by inactivating CI. With CI inactive, *pR* is derepressed and the *cI-CTD,* tum^{72K} and *mCherry* genes are expressed (including perhaps expression of enzymes for bioremediation). Cells expressing *mCherry* will emit a red-fluorescent signal, indicating the sample being tested contains plastic compounds. It is important to note, this system is purely hypothetical with a key assumption being that the right sensor/receptor can be developed and actively expressed in *E. coli* or another (more suitable) bacterial chassis.

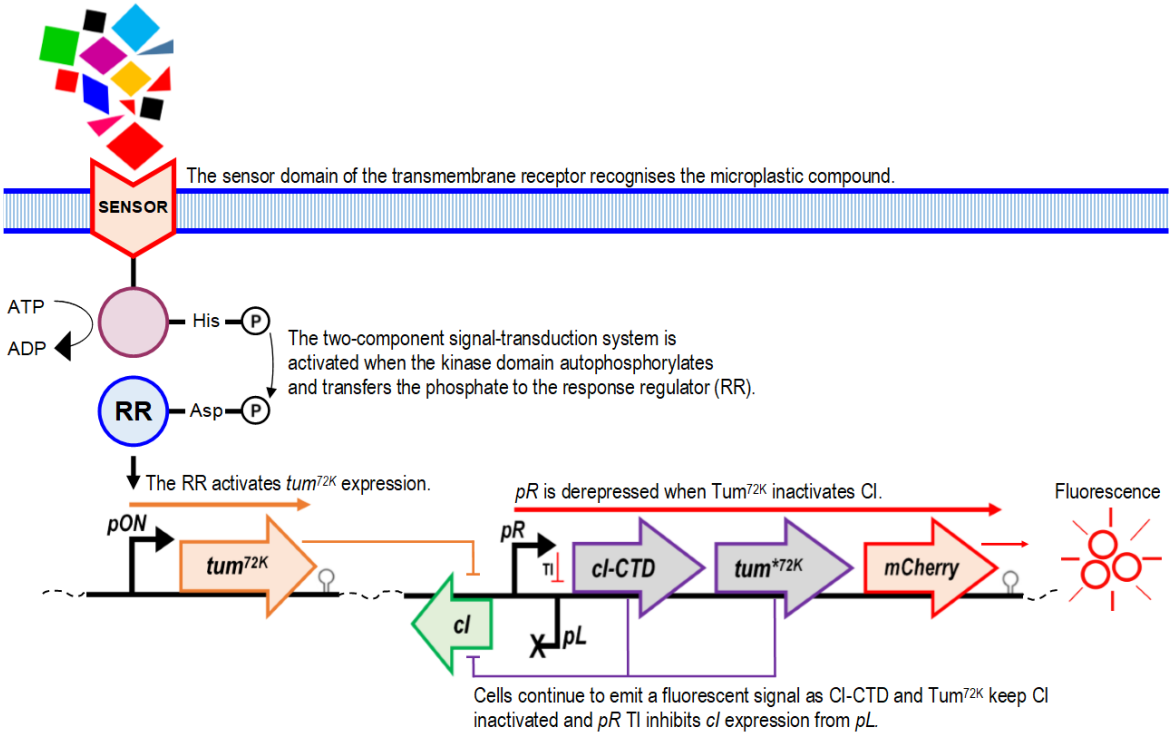

Figure 6.1: The hypothetical environmental 186-WCB as a detector of microplastic compounds. A schematic of the 186-WCB as a two-component signal-transduction system, where cells are expected to emit a red-fluorescent signal in the presence of a microplastic compound. In theory, cells are expected to exhibit OFF → ON state switching when the microplastic interacts with the receptor's sensor domain. This interaction induces a conformation change that causes the kinase domain to autophosphorylate. When the phosphate is transferred to the response regulator (RR) it becomes an active transcription factor and activates expression of *tum*^{72K} from the *pON* promoter. When Tum^{72K} inactivates CI (expressed from *pL*), *pR* is derepressed and the *cI-CTD.tum*^{72K}*.mCherry* transcript expressed. Cells expressing *mCherry* will emit a red-fluorescent signal, indicating the sample tested contains plastic compounds. Cells will remain fluorescent as the CI-CTD and Tum^{72K} keep CI inactivated and transcriptional inference (TI) from *pR* inhibits *cI* expression from *pL*.

6.1.2.2 The 186-WCB as a cancer biosensor

The use of biosensors in cancer detection and diagnosis is a very real possibility and an attractive avenue of SynBio. Whilst significant advances in cancer therapy have been made over recent decades (Burney and Al-Moundhri, 2008; Kruger et al., 2019; Markham et al., 2020), many cancers are still diagnosed only after they appear as a visible mass and/or have metastasised throughout the body. As discussed in Chapter 1, Section 1.2.3, the key to curing cancer is detecting the disease during the preclinical stage - the interval when the disease is detectable by screening but the patient remains asymptomatic (Herman, 2006). To detect cancer at this early stage, the analyte to be detected (by the biosensor) is called a tumour biomarker (TB), defined by the National Cancer Institute, as *'a substance found in tissue, blood, bone marrow, or other body fluids that may be a sign of cancer'* (NCI, 2019). TBs can come in many forms (e.g. DNA, RNA, protein or biochemical) and are used to not only diagnose cancer, but also help develop treatment plans, forecast prognosis and assess treatment effectiveness. Examples of some common TBs include BRCA1/2 and CA 15-3 (for breast cancer), CEA and CA 19-9 (for colon cancer), CEA and SCC (for lung cancer), CA 125 and HCG (for ovarian cancer) and PSA (for prostate cancer) (Bohunicky and Mousa, 2010).

Due to the complex nature of cancer, each cancer type *is not* simply defined by a single TB, but rather by a unique set of TBs, commonly referred to as a 'molecular signature'. Unfortunately, due to the intertumour and intratumour heterogenic nature of cancer, tumours (of the same type) often exhibit different 'molecular signatures'. It makes sense that engineering biosensors that can detect multiple TBs would prove useful in cancer diagnosis. With advances in SynBio, there is the potential to engineer multi-sensory biosensors that can serve as more accurate/reliable (early) detectors of cancer by sensing and reporting on the presence of a 'TB signature', rather than relying on the presence of a single TB. Given the ease with which our WCB could be adapted to sense different small molecules (see Chapter 5, Section 5.4) I believe our system has the potential to work as a cancer biosensor by modifying the IMs to respond to specific TBs.

Taking inspiration from the synthetic transcriptional AND system designed by Anderson et al. (2007), I propose the MFL reporter of the 186-WCB could work as a dual-sensory cancer biosensor that only responds to the presence of two TBs that are characteristic for a specific type of cancer. Presented in Figure 6.2 is a schematic of this hypothetical system, where cells are only expected to emit a red-fluorescent signal when TBs X AND Y are present. The first promoter (*pX*) is activated by X and drives transcription of a T7 RNA polymerase (*T7pol*) gene, but transcription is blocked due to the presence of two internal amber stop codons. The second promoter (*pY*) is activated by Y and drives expression of the *supD* gene, which encodes the SupD amber suppressor tRNA.

SupD can essentially 'override' the amber stop codons and thus allow for complete translation of the *T7pol* mRNA. Hence, only when X AND Y are present is the full-length T7 RNA polymerase synthesised and able to activate tum^{72K} gene expression from the T7 promoter. Tum^{72K} will act on the MFL reporter by inactivating CI. With CI inactivated, *pR* is depressed and the *cI-CTD,* tum^{72K} and *mCherry* genes expressed. Cells expressing *mCherry* will emit a red-fluorescent signal, thereby indicating that the patient is positive for a particular type of cancer. Again, it is important to note that this system is purely hypothetical and entails a number of assumptions. A key assumption is that a suitable set of TBs with the ability to influence gene transcription can be identified for the cancer of interest and that these TBs can be sourced from a bodily fluid that is easy to sample from an individual (e.g. blood, urine, saliva or faeces).

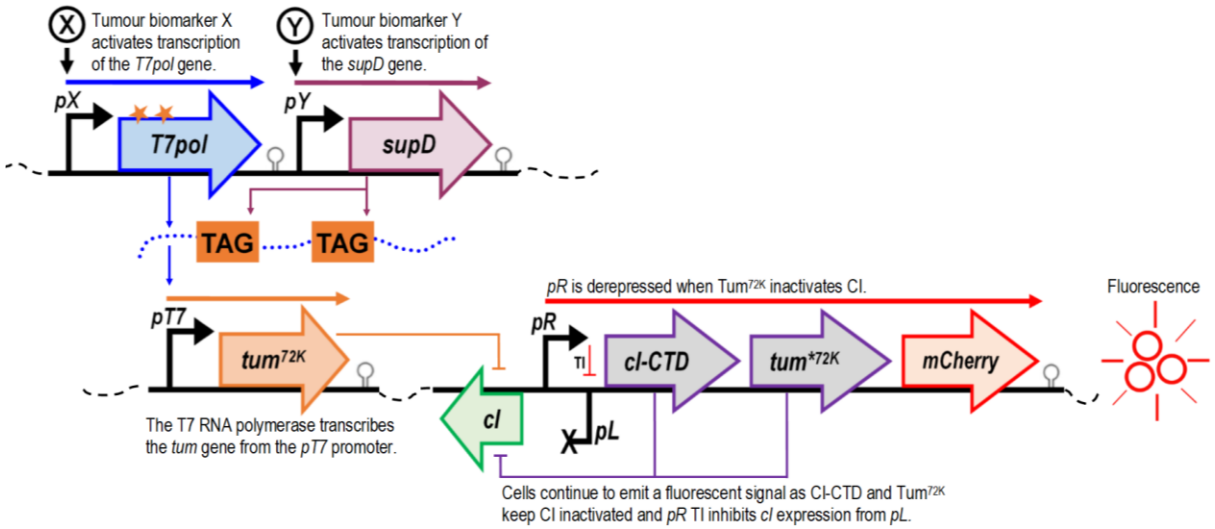

Figure 6.2: The hypothetical cancer 186-WCB. A schematic of the 186-WCB as a dual-sensor, transcriptional AND switch system, where cells are only expected to emit a red-fluorescent signal in the presence of two tumour biomarkers (X and Y) that are characteristic for a specific type of cancer. In theory, cells are expected to exhibit OFF → ON state switching when X activates *pX* AND Y activates *pY*. The *supD* gene encodes the SupD amber suppressor tRNA, which overrides the amber stop codons present in the *T7pol* gene sequence that encodes the T7 RNA polymerase. Only in the presence of SupD can the *T7pol* mRNA be faithfully translated. The full-length T7 RNA polymerase activates transcription of tum^{72K} from *pT7*. When Tum^{72K} inactivates CI (expressed from *pL*), *pR* is derepressed and the *cI-CTD.*tum^{72K}*.mCherry* transcript expressed. Cells expressing *mCherry* will emit a red-fluorescent signal, indicating the patient is positive for the cancer type under investigation. Cells will remain fluorescent as CI-CTD and Tum^{72K} keep CI inactivated and transcriptional inference (TI) from *pR* inhibits *cI* expression from *pL*. The design of the hypothetical cancer 186-WCB was adapted from Anderson et al. (2007).

Overall, the work undertaken in this thesis on 186 and the use of this phage for the development of a novel WCB, demonstrates the potential nature can offer humanity for the discovery of new genes and gene control pathways. With the rate at which SynBio is advancing, it is possible to assemble genetic components (from any foreign organism) into systems that perform given tasks and generate specific outputs based on the detection of defined signals, with superior sensitivity and specificity. With phage being so small and seemingly insignificant, clearly we have demonstrated that size means nothing when it comes to exploiting the potential benefits phage have to offer. Their genomes are mosaic treasures of biological componentry and with many more yet to be discovered, phage are not only fascinating creatures but are of incredible importance to humanity, now and into the future.

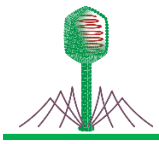

Chapter 7

Materials and methods

7.0 Methods

7.0.1 Bacterial procedures

7.0.1.1 Storage of bacterial stocks

Bacterial colonies were maintained short-term on Luria-Bertani (LB) plates (L-plates) with the appropriate antibiotics at 4°C. For long-term storage, single colonies were grown in LB broth with the appropriate antibiotic(s) and incubated O/N to stationary phase. A glycerol stock was prepared by adding 500µL O/N culture to 500µL 80% glycerol in a sterile, screw cap 1.5mL microcentrifuge tube and stored at -80°C.

7.0.1.2 Growth of bacterial strains

Frozen bacterial glycerol stocks were restreaked on fresh L-plates with the appropriate antibiotic(s) and grown O/N at 37°C or 30°C for strains carrying constructs with a temperature sensitive origin of replication (*orits*). L-plates were prepared by adding the required antibiotic(s) to molten 1.5% LB agar (48°C), pouring into petri dishes, allowing 30mins to set at RT and then drying for 15-30mins at 37°C. Table 7.1 lists the concentrations of antibiotics used for plasmid maintenance and chromosomal integration in this thesis.

Table 7.1: Antibiotic concentrations (µg/mL) used in this thesis for plasmid maintenance and chromosomal integration.

Antibiotic	Plasmid	Integration
Ampicillin	100	-
Chloramphenicol	30	20
Kanamycin	50	20
Spectinomycin	50	10
Tetracyclin	20	4

Unless specified otherwise, stationary-phase cultures were prepared by inoculating a single colony in LB with the appropriate antibiotic(s) and grown O/N with aeration at 37°C or 30°C. Log-phase cultures were prepared by diluting a fresh O/N stationary phase culture in LB with the appropriate antibiotic(s) and grown to the desired cell density (OD_{600} 0.40-0.60) at 37°C with aeration. OD_{600} was determined by pipetting 100µL of culture into the wells of a flat-bottomed 96-well microtitre plate and measuring the absorbance at 620nm (A_{620}) using a Multiskan Ascent V1.22 plate reader (Labsystems). The A_{620s} were converted back to OD_{600s} using an empirically determined relationship (Dodd et al., 2001).

7.0.1.3 Preparation and transformation of TSS competent cells

For transformation and/or integration of assembled pIT3/4 CRIM plasmids, chemically competent *E. coli* were prepared using the Transformation and Storage Solution (TSS) method (Chung et al., 1989). Chemically competent cells were prepared by diluting (10^{-2}) a fresh O/N stationary culture in LB with the appropriate antibiotic(s) and grown to early log phase (OD_{600} ~0.40). For bacteria containing a CRIM helper plasmid, an additional heat induction step was performed (15min incubation at 45ºC) to activate *int* expression. Cells were chilled on ice for 15mins and then pelleted at 3095rcf using an Eppendorf 5810R centrifuge at 4°C for 10mins. Cells were kept on ice and resuspended in 1/10th of the original culture volume of chilled TSS buffer. 500µL aliquots of cells were stored in 1.5mL Eppendorf tubes and frozen at -80°C. For bacterial transformation, cells were thawed on ice and 100µL mixed with 1 to 10µL of DNA solution. The cell/DNA mix was incubated on ice for 15mins and heat shocked at 42°C for 45s. Cells were recovered in 1mL SOC media followed by incubation at 37°C or 30°C for 1hr. Cells were pelleted at 1306rcf in an Eppendorf 5424R centrifuge for 5mins, resuspended in ~100µL of S/N and plated on L-plates with the appropriate antibiotic(s).

7.0.1.4 Preparation and transformation of electrocompetent cells

Electrocompetent *E. coli* cells were prepared for applications that required a higher degree of competency, such as the transformation of ssDNA or dsDNA for recombineering purposes or large multi-fragment assembled pIT3/4 plasmids. Electrocompetent *E. coli* were prepared by diluting (1/250) a fresh O/N stationary culture in LB with the appropriate antibiotic(s), grown to early/mid-log phase (OD_{600} ~0.40-0.60), chilled on ice for 15-30mins and then pelleted at 3095rcf using an Eppendorf 5810R centrifuge at 4°C for 10mins. For bacteria containing a CRIM helper plasmid, prior to centrifugation, an additional heat induction step was performed (15min incubation at 45ºC) to activate *int* expression. To remove the salt from the growth media (which would otherwise cause arcing in the electroporation apparatus) multiple washes were required. Cells were first washed twice in ice cold MQ H_2O, using the same volume as the original culture and pelleted at 3095rcf (Eppendorf 5810R centrifuge) at 4°C for 10mins. After the second wash, cells were resuspended in 10mL 10% glycerol solution and centrifuged at 3095rcf (Eppendorf 5810R centrifuge) at 4°C for 10mins. The final pellet was resuspended in 1/200th of the starting culture volume of ice-cold 10% glycerol solution and ~40µL aliquots of cells stored in 1.5mL Eppendorf tubes and frozen at -80°C. For electroporation, 40µL of electrocompetent cells were thawed on ice and mixed with 1 to 3µL of DNA solubilised in a low ionic strength medium (e.g. TE or MQ H_2O) and mixed briefly by flicking the Eppendorf tube. The cell/DNA mix was transferred to an ice-cold sterile 1mm electroporation cuvette and electrotransformed using the BioRad Micropulser set to the recommended bacterial setting (1.8kv, 200Ω, 25µF) and the time constant of the shock recorded (should range from 5 to 7ms, otherwise an electric arc has probably occurred).

Immediately after electroporation, cells were flushed from the cuvette using 1mL SOC media, transferred to an Eppendorf tube and recovered at 37°C or 30°C for 1hr. Cells were pelleted at 1306rcf in an Eppendorf 5424R centrifuge for 5mins, resuspended in ~100µL of S/N and plated on L-plates with the appropriate antibiotic(s).

7.0.1.5 Chromosomal integration

Integration of recombinant gene constructs and circuits into the *E. coli* chromosome offers stable, single-copy expression of target genes, thereby making it a preferable strategy to overcome the drawbacks of plasmid-based expression systems. In this thesis, integration of pIT3/4 plasmids was achieved through integrase-mediated site-specific recombination using one of four potential bacteriophage Integrase (Int) proteins, which were supplied from a series of CRIM (conditional-replication, integration and modular) plasmids propagated and extracted from the *E. coli* host strain BW23473 (Haldimann and Wanner, 2001) (Table 7.2). Strains harbouring a CRIM helper plasmid were always cultured in LB supplemented with 100µg/mL ampicillin and incubated at 30°C due to the presence of the R101 *orits*

Table 7.2: Bacteriophage chromosomal integration (*attB*) sites used in this thesis for the integration of pIT3/4 CRIM plasmids. Integration can be achieved at four possible *attB* sites within the *E. coli* chromosome. Each site is specific to a particular phage, as each phage Int has a site-specific DNA recognition site. Unless specified otherwise, each CRIM helper plasmid encodes an *int* gene driven by λ*pR* promoter, which at 30°C is repressed by the temperature sensitive λ*cI857* repressor (also borne by these plasmids). Int synthesis is induced at elevated temperatures (37°C) allowing for recombination of the transformed DNA to take place (Haldimann and Wanner, 2001). *The *E. coli* genome harbours two 186 *attB* sites.

Integration site	Abbrev.	Plasmid	Description
186*	O	p186*int*-λ*clts*	186*int* expressed from λ*cI857* repressed λ*pR* promoter
Lambda (λ)	L	pINT-ts	λ*int* expressed from λ*cI857* repressed λ*pR* promoter
		pλ*int*-186*clts*	λ*int* expressed from 186*clts* repressed 186*pR* promoter
φ21	T	pAH121	φ21*int* expressed from λ*cI857* repressed λ*pR* promoter
HK022	H	pAH69	HK022*int* expressed from λ*cI857* repressed λ*pR* promoter

To prepare cells for chromosomal integration, chemically competent *E. coli* 4643 (E4643) were transformed with the appropriate CRIM helper plasmid, which is dependent on the site chosen for integration (e.g. integration of pIT3-CL CRIM plasmid into λ *attB* site would require transformation with pINT-ts). Helper plasmid transformation was performed according to the standard TSS transformation protocol, with cells recovered at 30°C and plated on L-plates with 100µg/mL ampicillin. O/N colonies were re-streaked on L-plates with 100µg/mL ampicillin and incubated O/N at 30°C. Chemically competent E4643 helper cells were made according to the TSS competent protocol, including the heat induction step (15min incubation at 45°C) and maintaining growth at 30°C in LB with 100µg/mL ampicillin. Chromosomal integration was performed according to the standard TSS transformation protocol with cells recovered at 37°C to induce Int synthesis. Since CRIM helper plasmids are temperature sensitive for replication an O/N incubation at 37°C simultaneously cures the resulting transformants of the helper plasmid. Integrants were validated by PCR screening as described in Section 7.0.2.7.

7.0.2 DNA manipulation

7.0.2.1 Preparation and purification of plasmid DNA

Small-scale preparations of plasmid DNA were performed by pelleting a 5mL O/N stationary LB culture (at 3095rcf for 10mins) and using the QIAprep® Spin Miniprep Kit (Qiagen) or GenElute™ HP Plasmid Miniprep Kit (Sigma Aldrich-Aldrich) for DNA extraction. Larger-scale preparations of plasmid DNA were made by pelleting a 100mL O/N stationary LB culture (at 3095rcf for 10mins) and using the ZymoPURE™ Plasmid Midiprep Kit (ZYMO research) for DNA extraction. All kits were used in accordance with the manufacturer's instructions. Small and large-scale preparations were eluted in 50 to 100µL MQ H_2O and 200µL H_2O or the supplied elution buffer respectively. All DNA plasmid preparations were stored at -20°C.

7.0.2.2 Electrophoresis of DNA

DNA samples, generally in the form of a PCR amplicon or linear restriction digest product were assessed for size and purity using agarose gel electrophoresis. 1 to 2.5% agarose gels were prepared by mixing agarose power with 1X TAE (Table 7.16), heating in a microwave oven and then casting the mix into 15-welled mini-gels. DNA samples were prepared for electrophoresis by adding EZ-Vision 6X DNA Dye as Loading Buffer (Amresco). Either 2-Log DNA molecular makers (NEB) or the Gold Standard DNA ladder (Alchemy Biosciences) were used for size comparison and approximation of concentration. Electrophoresis was performed with a Mini-Sub Gel GT (BioRad) electrophoresis device in 1X TAE running buffer at 90 to 120V. DNA fragments were visualised using the ChemiDoc™ MP Imaging System (BioRad).

7.0.2.3 Purification of DNA

DNA was routinely spin column purified using the DNA Clean and Concentrator™-5 kit (ZYMO research) or the Monarch® PCR and DNA Cleanup Kit (BioLabs) in accordance with the manufacturer's instructions.

For DNA manipulation reactions that generated multiple bands, gel extraction was used to isolate and purify the DNA fragment of interest. Gel extraction was performed by casting mini-gels (1 to 2.5% agarose) with larger wells and loading each well with 20µL DNA sample with 6X Blue Vision dye and running at 90 to 120V for 30 to 45mins. For staining of DNA bands, the gel was submerged in 1X SYBR Safe DNA gel stain (Invitrogen) made up in 1X TAE for ~20mins and visualised using the Safe Imager Bright Light Transilluminator (Invitrogen). The bands were excised from the gel using a sterile scalpel blade and the DNA purified using the Zymoclean™ Gel DNA Recovery Kit (ZYMO research) or the NucleoSpin® Gel and PCR clean up kit (Macherey-Nagel). All purified DNA samples were eluted in 10 to 20µL of MQ H_2O and stored at -20°C. Accurate measurement of DNA concentration and purity was performed using the NanoDrop 2000 spectrophotometer (Thermo Scientific).

7.0.2.4 Restriction enzyme digestion

New England Biolabs (NEB) restriction endonucleases were used to digest DNA using 2 to 5U of enzyme with incubation times ranging from 1hr to O/N. Reaction conditions and incubation temperatures were as specified by the manufacturer. Digested DNA was examined by gel electrophoresis, spin column purified or gel extracted and the DNA quality and quantity determined using the NanoDrop 2000 spectrophotometer (Thermo Scientific).

7.0.2.5 DNA ligation

For ligation of DNA, 20µL reactions were prepared using a 3:1 molar ratio of insert to vector DNA (with the concentration of vector DNA within a 10-50ng range) combined with 0.2µL T4 DNA ligase (NEB) and 2µL ligase buffer (10X stock). For sticky-end ligation, reactions were incubated at 16°C for 1hr and for blunt-end ligation, reactions were incubated O/N at 16°C. To achieve 'self' ligation of a single DNA fragment, the DNA template was diluted (10^{-1}), left at RT for 15mins and then incubated O/N at 16°C. 10µL of the crude ligation reaction or 5µL of the spin column purified ligation reaction was transformed into TSS treated E4644.

7.0.2.6 Gibson isothermal assembly of DNA fragments

Gibson isothermal assembly is an extremely useful and highly efficient molecular cloning method developed by Dr. Daniel G. Gibson at the J. Craig Venter Institute (Gibson et al., 2009), and was used to assemble the majority of the plasmid protein expression constructs, LacZ reporters and biosensor modules used in this thesis. The technique can be used to generate linear or closed circular molecules by allowing the joining of multiple DNA fragments in a single, isothermal reaction under the condition that each DNA fragment contains 20 to 40bp overlap with its adjacent DNA fragment(s). These homologous ends are easily generated by incorporating them into the 'tails' of PCR primers. For assembly to occur, the linear homologous DNA fragments are mixed with an 'assembly mix' that contains the T5 exonuclease (Epicentre), Phusion DNA polymerase (NEB) and Taq DNA ligase (NEB). First, the T5 exonuclease chews back DNA from the 5' end to generate single-stranded complementary overhangs between the assembly fragments. The Phusion DNA polymerase then incorporates nucleotides to fill in any gaps, which are generated when the T5 exonuclease chews back further than the 20 to 40bp homology between the assembly fragments. The Taq DNA ligase covalently joins the DNA fragments, removing any single-stranded nicks in the assembled DNA.

20µL Gibson isothermal assembly reactions were performed in 0.2mL PCR tubes by combining vector and insert DNA in a 1:1 molar ratio (aiming for a total of 130ng DNA) with 15µL of Gibson Assembly Super Mix. Isothermal assembly was performed at 50°C for 1hr. 10µL of the crude assembly reaction or 5µL of the spin column purified assembly reaction was then transformed into TSS E4644.

7.0.2.7 Polymerase Chain Reactions

Polymerase chain reactions (PCR) were used to screen and verify bacterial clones (from colonies), to prepare DNA templates for Sanger sequencing and to amplify DNA fragments (mutagenic or non-mutagenic) using specially designed primers for cloning and Gibson isothermal assembly. For routine screening of bacterial clones transformed with a plasmid construct and for the preparation of DNA templates for Sanger sequencing, colony PCR was performed using the KAPA2G Robust PCR Kit (KAPA Biosystems). To generate DNA fragments for cloning and Gibson isothermal assembly high-fidelity PCR was performed using the KAPA HiFi™ PCR Kit (KAPA Biosystems) or the Phusion® High-Fidelity PCR Kit (NEB). In accordance with the manufacturer's recommendations, Table 7.3 lists the standard reaction set-up and cycling conditions used for each PCR kit. 10 to 20µL PCR reactions were set up in 0.2mL PCR tubes and cycled using a Bio-Rad DNA Engine thermal cycler (BioRad).

Table 7.3: Standard reaction setup and cycling conditions for each PCR kit used in this thesis. *The additional of DMSO is recommended for PCR of GC rich amplicons or when using GC-rich primers.

KAPA2G Robust PCR Kit (KAPA Biosystems) for screening bacterial clones and preparation of DNA templates for Sanger sequencing.			
Reaction component	**10µL reaction**		**Final conc.**
MQ H_2O	Up to 10µL		
5X KAPA2G (GC) buffer	2.0µL		1X
10mM KAPA dNTP mix	0.2µL		0.2mM each
10µM forward primer	1.0µL		1µM
10µM reverse primer	1.0µL		1µM
1U/µL KAPA Robust DNA polymerase	0.04µL		0.05U
DMSO* *(optional)*	0.5µL		5%
Single bacterial colony	As required		
Cycling protocol	**Temp.**	**Time**	**Cycles**
Initial denaturation	95°C	3min	1
Denaturation	95°C	20s	
Annealing	58°C	15s	30
Extension	72°C	1min/kb	
Final extension	72°C	1min/kb	1

KAPA HiFi™ PCR Kit (KAPA Biosystems) for high-fidelity amplification of DNA for cloning and Gibson isothermal assembly.			
Reaction component	**20µL reaction**		**Final conc.**
MQ H_2O	Up to 20µL		
5X KAPA HiFi buffer *(fidelity or GC)*	4.0µL		1X
10mM KAPA dNTP mix	0.6µL		0.3mM each
10µM forward primer	1.0µL		0.5µM
10µM reverse primer	1.0µL		0.5µM
1U/µL KAPA HiFi DNA polymerase	0.4 µL		0.4U
1-2ng DNA or bacterial colony	As required		
Cycling protocol	**Temp.**	**Time**	**Cycles**
Initial denaturation	95°C	3min	1
Denaturation	95°C	20s	
Annealing	58°C	15s	30
Extension	72°C	1min/kb	
Final extension	72°C	1min/kb	1

Phusion® High-Fidelity PCR Kit (NEB) for high-fidelity amplification of DNA for cloning and Gibson isothermal assembly.			
Reaction component	**20µL reaction**		**Final conc**.
MQ H_2O	Up to 20µL		
5X Phusion HF buffer	4 µL		1X
10mM KAPA dNTP mix	0.4µL		0.2mM each
10µM forward primer	1.0µL		0.5µM
10µM reverse primer	1.0µL		0.5µM
1U/µL Phusion DNA polymerase	0.2 µL		0.4U
DMSO* *(optional)*	0.5µL		5%
1/100 dilution of template DNA	1.0µL		
Cycling protocol	**Temp**.	**Time**	**Cycles**
Initial denaturation	95°C	3min	1
Denaturation	95°C	20s	
Annealing	58°C	15s	30
Extension	72°C	1min/kb	
Final extension	72°C	1min/kb	1

To screen for recombinant bacterial clones transformed with a plasmid construct, 10µL KAPA2G Robust colony PCR reactions were prepared using PCR primers designed to amplify the DNA region of interest. Positive clones were identified by generating a PCR product of the correct size or by diagnostic restriction enzyme digest of the PCR product. For the latter, 1µL of the chosen restriction enzyme was added directly to the PCR reaction, incubated at the required temperature for at least 4hrs and analysed by gel electrophoresis.

To test for single-copy chromosomal integration of 186 phage or protein expression constructs and LacZ reporters retained on pIT3/4 CRIM integration plasmids, 10µL KAPA2G Robust colony PCR reactions with a slightly amended protocol (Table 7.4) were performed with specific sets of integration primers. As presented in Figure 7.1, each primer set contained four oligonucleotides (P1, P2, P3 and P4) designed to amplify the *attP*, *attB* or *attR* and *attL* sites for each region of integration. Single-copy integrants were identified as integrants that generate the P1-P2 and P3-P4 PCR products, which correspond to the *attL* and *attR* junctions respectively. Non-integrants were revealed by generating the P1-P4 fragment, which corresponds to the intact *attB* site and multiple integrants were revealed by producing a third P2-P3 fragment, characteristic of the *attP* site (Haldimann and Wanner, 2001; St-Pierre et al., 2013). Table 7.5 lists the integration primer sets used for each integration site and the expected size for each *attP*, *attB*, *attR* and *attL* PCR product.

Table 7.4: Standard reaction setup and cycling conditions used to screen for single-copy chromosomal integration of 186 phage or foreign constructs residing on pIT3/4 CRIM integration plasmids. PCR performed using the KAPA2G Robust PCR Kit (KAPA Biosystems).

Reaction component	10µL reaction		Final conc.
MQ H_2O	Up to 10µL		
5X KAPA2G (GC) buffer	2µL		1X
10mM KAPA dNTP mix	0.2µL		0.2mM each
10µM P1-P4 λ, φ21, HK022, 186 primer mix	1µL		1µM
1U/µL KAPA Robust DNA polymerase	0.04µL		0.05U
Single bacterial colony	As required		
Cycling protocol	**Temp.**	**Time**	**Cycles**
Initial denaturation	95°C	3min	1
Denaturation	95°C	20s	
Annealing	58°C	15s	30
Extension	72°C	1min/kb	
Final extension	72°C	1min/kb	1

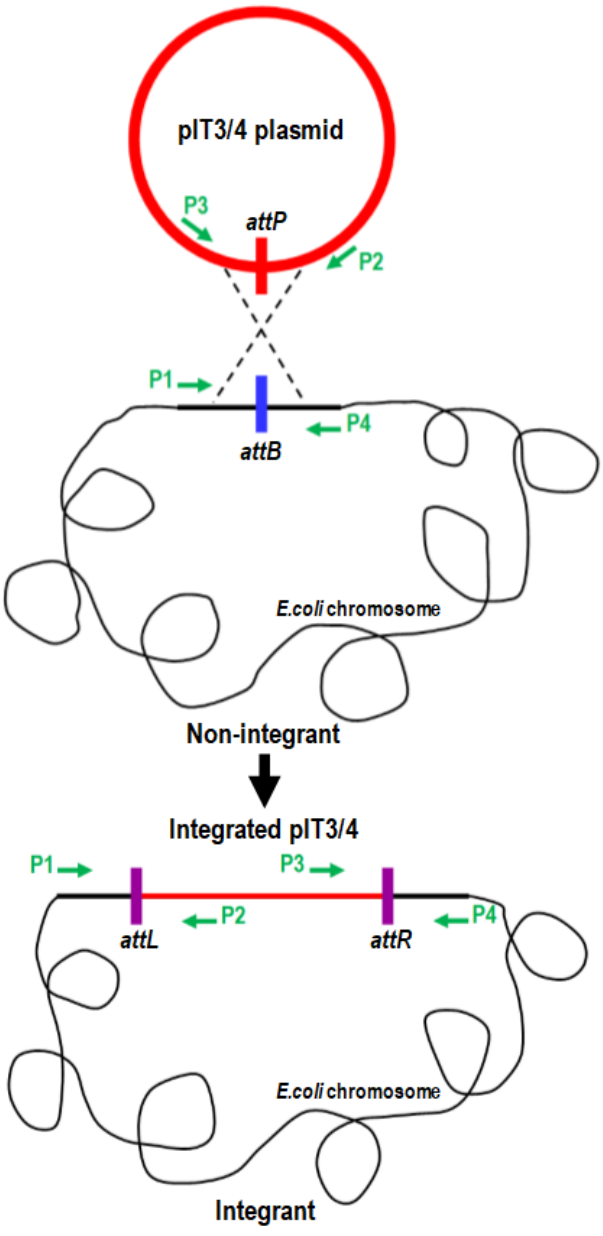

Figure 7.1: Screening for chromosomal integration events by PCR. To verify chromosomal integration of 186 prophage or pIT3/4 constructs, colony PCR using a set of four integration primers (P1, P2, P3 and P4) was performed. A non-integrant will generate *attP* and *attB* PCR products from primer pairs P2 + P3 and P1 + P4 respectively. A single integrant will generate *attL* and *attR* PCR products from primer pairs P1 + P2 and P3 + P4 respectively. The presence of a third *attP* PCR product is indicative of multiple integration. Adapted from St-Pierre et al. (2013).

Table 7.5: The integration primer sets and expected product sizes used to screen for chromosomal integration by PCR. To test for single-copy chromosomal integration events at phage 186, λ, φ21 and HK022 integration sites a single PCR with a set of four primers was performed to generate *attB, attP, attL* and *attR* PCR products. Each PCR product is generated by a specific primer pair, where P2 + P3 = *attP,* P1 + P4 = *attB,* P1 + P2 = *attL* and P3 + P4 = *attR*. Listed are the primer sets for each integration site and the expected size (in base pairs) of each PCR product (for primer sequences see Table 7.11). Unless specified otherwise, all primer sets are for integration into *E. coli* MG1655, with the majority of primers obtained from Haldimann and Wanner (2001). Underlined primers were designed to create an optimised primer set that clearly differentiates between single, multiple and no integration events. *186 has two integration primer sets to test for integration at the primary and secondary sites. Primer 2404 is an alternate φ21 P4 primer that gives alternate *attB* (402) and *attR* (1025) PCR products.

Integration site	PCR product	Primer set	Expected size
Primary 186.1	*attP*	598 + 597	335
	attB	610 + 611	242
	attL	610 + 598	317
	attR	597 + 611	260
Secondary 186.2	*attP*	598 + 597	335
	attB	1104 + 1103	602
	attL	1104 + 598	576
	attR	597 + 1103	361
λ	*attP*	467 + 468	502
	attB	466 + 469	741
	attL	466 + 467	577
	attR	468 + 469	666
φ21	*attP*	467 + 465	1226
	attB	871 + 872 (2404)	506bp (402)
	attL	871 + 467	622bp
	attR	465 + 872 (2404)	1110 (1025)
HK022	*attP*	467 + 468	427bp
	attB	585 + 586	740bp
	attL	585 + 467	824bp
	attR	468 + 586	343bp

Sanger sequencing of DNA was outsourced to the Australian Genome Research Facility (AGRF) using their PD sequencing service (AGRF, 2014). To prepare DNA templates for PD sequencing, 10µL KAPA2G Robust PCR reactions were prepared from bacterial colonies or from plasmid DNA. Each PCR was verified for the presence of a DNA template of the expected size via gel electrophoresis; spin column purified using the DNA Clean and Concentrator™-5 kit (ZYMO research) and quantified using the NanoDrop2000 spectrophotometer (Thermo Scientific). For PCR products >800bp, 30 to 75ng of the purified template was mixed with 1µL 10µM sequencing primer and with MQ H_2O to a final volume of 12uL in a 1.5mL Eppendorf tube and stored at 4°C (ready for delivery). Sequencing results were retrieved electronically and the data analysed using the Ape-A plasmid editor program (v2.0.55) (Davis, 2018).

7.0.3 Bacteriophage procedures

7.0.3.1 Preparation and storage of 186 phage stocks

To prepare a high titre wildtype 186 phage stock, two rounds of infection are performed. To begin, an *E. coli* 186^{+} lysogen (e.g. E0573 or HB59) and an *E. coli* indicator strain (e.g. C600 or E4643) were restreaked on L-plates and grown O/N at 37°C. O/N cultures of the lysogen and indicator were setup by inoculating 5mL LB with a single colony and grown O/N at 37ºC. The indicator strain was prepared for infection by diluting (10^{-2}) the O/N stationary culture in LB and incubated with aeration at 37°C until log phase growth (OD_{600} ~0.60). 186 phage were prepared by pelleting the O/N stationary lysogen culture at 3095rcf using an Eppendorf 5810R centrifuge for 10mins and the S/N carefully transferred to a 1.5mL Eppendorf tube. Using a glass test tube, 100µL of the S/N was mixed with 200µL of the indicator strain and 3mL molten 0.7% top agar (48°C) supplemented with 10mM $MgSO_4$. The cells/agar mix was poured over a fresh L-plate, left to set at RT for ~30mins and incubated O/N at 37°C. The following day, a single plaque was picked using the tip of a sterile glass pipette and resuspended in 100µL 1X TM buffer (50mM TRIS pH 7.5 +10mM $MgSO_4$). The resuspended phage were centrifuged briefly and all the S/N collected and combined (in a glass test tube) with 200µL of the indicator strain (prepared from a fresh O/N culture, diluted 10^{-2} in LB and grown to OD_{600} ~0.60) and 3mL molten 0.7% top agar (48°C) supplemented with 10mM $MgSO_4$. The cells/agar mix was poured over a fresh L-plate, left to set at RT for ~30mins and incubated O/N at 37°C. The next day, to collect and isolate the phage, 5mL 1X TM buffer was added directly to the phage plate and left at RT for 15mins. All the liquid and top agar was scraped off and dispensed into a sterile 10mL screw cap centrifuge tube, treated with ~5µL chloroform and vortexed thoroughly to ensure any potentially remaining live cells were killed. The entire mixture was centrifuged at 3095rcf for 10mins and the S/N carefully transferred to a sterile 10mL screw cap centrifuge tube and stored at 4ºC.

7.0.3.2 Making *E. coli* 4643 186^{+} lysogens

E4643(186^{+}) lysogens were prepared by diluting (10^{-2}) a fresh O/N stationary culture of the indicator strain in fresh LB and incubated with aeration at 37°C until log phase growth (OD_{600} ~0.60). 200µL of the indicator strain was combined with 3mL molten 0.7% top agar (48°C) supplemented with 10mM $MgSO_4$ and poured over a fresh L-plate and left to set at RT for ~30mins. Undiluted, 10^{-1} and 10^{-2} 186^{+} phage stock dilution samples were prepared in 1X TM buffer and 10µL spotted onto the lawn of indicator. Plates were left to dry at RT for ~30mins and then incubated O/N at 37°C. Single colonies of potential lysogens were restreaked from the centre of a turbid plaque and the lysogens validated by PCR. Given that *E. coli* harbours two 186 *attB1/2* sites, KAPA2G Robust colony PCR (KAPA Biosystems) using two specific sets of integration primers was performed to select for single-copy integration of 186^{+} prophage at the 186 *attB1* integration site (see Figure 7.1 and Table 7.5 for details).

Lysogens harbouring a prophage were identified by generating the P1-P2 and P3-P4 PCR products, which correspond to the *attL* and *attR* junctions respectively. Non-integrants were revealed by generating the P1-P4 fragment, which corresponds to the intact *attB* site (St-Pierre et al., 2013). For example, an E4643 lysogen harbouring 186^{+} prophage at the 186 *attB1* site generated the 186.1 P1-P2 and P3-P4 PCR products and the 186.2 P1-P4 PCR product.

7.0.3.3 Recombineering the cumic acid-inducible 186$^{p.cym}$ prophage

A single-step recombineering method (Sharan et al., 2009) was used to engineer the cumic acid (CA)-inducible 186 phage (186$^{p.cym}$). Cassette 17 - *loxP.chlor^{R}.loxP.T5-1* (Table 7.12) was used to replace the natural UV-inducible *p95.tum* locus with the CA-inducible *T5-1.tum* cassette. To maintain lysogeny, the E4643 host strain was φ21 integrated with the pIT4-KT-*cymR.T5-1* plasmid to supply the 186$^{p.cym}$ prophage with CymR to repress *tum* expression until induced with CA.

7.0.3.3.1 The design and generation of the linear dsDNA substrate for recombineering

The *loxP.chlor^{R}.loxP.T5-1.tum* cassette (Table 7.12) features the chloramphenicol resistance marker (*chlor^{R}*) flanked by a direct repeat of *loxP* sites, allowing for its deletion when treated with the P1 phage cyclization recombination (Cre) recombinase. Downstream is the *T5-1* promoter, which features a single *cymR* operator site and a short 40bp segment of the wildtype *tum* N-terminus. For recombineering, each end of the cassette shares 60bp homology to the desired recombineering site on the 186 genome. The *tum* ribosomal binding site (RBS) was optimised to a strength of ~2,330AUs using the Salis Lab RBS Calculator v2.0 (Espah Borujeni et al., 2014) and the *E. coli* str. K-12 substr. MG1655 (ACCTCCTTA 16S RNA sequence) setting (Table 7.6). The 'pre-sequence' included the first 40bp upstream of the *tum* GTG. The 'desired strength' was set to 2,200AUs, which is the approximate RBS strength calculated for the native *tum* gene in wildtype 186. The strength of the native *tum* RBS was also calculated using the RBS Calculator v2.0 (Espah Borujeni et al., 2014) and the *E. coli* str. K-12 substr. MG1655 (ACCTCCTTA 16S RNA sequence) setting. The 'pre-sequence' included the first 40bp upstream of the *tum* GTG and returned a strength of ~2260AUs.

Table 7.6: Optimising the *tum*$^{+}$ RBS. Optimisation performed using the Salis Lab RBS Calculator v2.0 (Espah Borujeni et al., 2014) and the *E. coli* str. K-12 substr. MG1655 (ACCTCCTTA 16S RNA sequence). Pre-sequence (red), RBS (underlined), start of *tum* gene (GTG) (blue). *Strength refers to the RBS translation initiation rate listed in arbitrary units (AUs).

tum RBS	DNA sequence	Strength
Wildtype	CGTGCTACTGTATGTTTATACAGTATCTCGTAGTGGAGGTTGTGTG	2260.13
Optimised	GAATTCCAGCATATAGGGATCGTCGTCTCGTAGTGGAGGTTGTGTG	2329.32

To generate the *loxP.chlor*^{R}*.loxP.T5-1.tum* cassette high-fidelity overlap PCR was performed with gBlocks 17B - *loxP.chlor*^{R} and 17C - *loxP.T5-1.tum* (synthesised by IDT, see Table 7.12 for sequence details). Each gBlock harbours 23bp homology at the 3' or 5' end and were combined with primers #2797 and #2798 (see Table 7.11 for sequences). 20µL overlap PCR reactions were performed according to the Phusion® High-Fidelity PCR Kit (NEB) protocol. The *loxP.chlor*^{R}*.loxP.T5-1.tum* PCR product was purified in 15µL MQ H_2O using the DNA Clean and Concentrator™-5 kit (ZYMO Research), quantified using the NanoDrop2000 spectrophotometer (Thermo Scientific) and stored at -20ºC.

7.0.3.3.2 Chromosomal integration of AI238 with the pIT4-KT-*cymR.T5-1* plasmid expressing the CymR repressor

CymR was supplied *in trans* to the prophage via the φ21 integrated pIT4-KT-*cymR.T5-1* plasmid using the CRIM system (Haldimann and Wanner, 2001). To prepare for integration, the AI238 strain (see Table 7.9 for genotype) was made chemically competent using the Transformation and Storage Solution (TSS) method (Chung et al., 1989) as described in Section 7.0.1.3. Integration was performed as described in Section 7.0.1.5, with cells plated on a L-plate with kanamycin (20ug/mL) and incubated O/N at 37°C. Selected colonies were restreaked on L-plates with kanamycin (20ug/mL) and incubated O/N at 37°C. To screen for single-copy chromosomal integration, 10µL colony PCR was performed according to the KAPA2G Robust PCR Kit (KAPABiosystems) using four integration primers; #871 (P1), #467 (P2), #465 (P3) and #872 (P4) (Haldimann and Wanner, 2001) (see Table 7.11 for sequences). Single integrant AI239 clones generated the P1-P2 (*attL*) and P3-P4 (*attR*) PCR products (refer to Figure 7.1).

7.0.3.3.3 Transformation of AI239 with pSIM6 plasmid expressing the λRed enzymes

The λRed recombineering system was supplied to the prophage via the pSIM6 plasmid (Sharan et al., 2009). The AI239 strain (see Table 7.9 for genotype) was made chemically competent using the Transformation and Storage Solution (TSS) method (Chung et al., 1989) and transformed with purified pSIM6 as described in Section 7.0.1.3. Transformed cells were plated on a L-plate with ampicillin (100ug/mL) and incubated O/N at 30°C. Selected colonies were restreaked on L-plates with ampicillin (100ug/mL) and incubated O/N at 30°C. For long-term storage, O/N cultures of the AI241 strain were transferred to 1:1 glycerol stocks and frozen at -80°C.

7.0.3.3.4 Preparation of electrocompetent AI241 for recombineering

For induction of λRed *exo*, *bet*, and *gam* genes from pSIM6, the AI241 strain (see Table 7.9 for genotype) was prepared by diluting an O/N stationary culture (10^{-2}) in fresh LB with ampicillin (100ug/mL), grown at 30°C with aeration to OD_{600} ~0.50 and then incubated in a 45°C water bath for 15mins.

To make electrocompetent, the cells were centrifuged to a pellet (at 3095rcf, 4°C for 10mins), the S/N removed and the pellet resuspended in the original culture volume of ice-cold MQ H_2O (repeated twice). After the second wash, the pellet was resuspended in ice-cold 10mL 10% glycerol solution and centrifuged to a pellet (at 3095rcf, 4°C for 10mins). The S/N was carefully discarded and the bacterial pellet resuspended in 1/200th of the starting culture volume of ice-cold 10% glycerol solution. 40µL aliquots of cells were stored in 1.5mL Eppendorf tubes and frozen at -80°C.

7.0.3.3.5 Electroporation of AI241 with linear dsDNA substrate

For electroporation with the *loxP.chlor^R.loxP.T5-1.tum* cassette, electrocompetent AI241 cells were thawed on ice and electroporated with purified cassette 17 DNA as described in Section 7.0.1.4. Cells were plated on a L-plate with chloramphenicol (20ug/mL) and incubated O/N at 37°C. To ensure cells were cured of the pSIM6 plasmid (carries an *orits*) selected colonies were restreaked on L-plates with chloramphenicol (20ug/mL) and incubated O/N at 37°C. To screen for successful recombineering, 10µL colony PCR was performed according to the KAPA2G Robust PCR Kit (KAPABiosystems) using primers #148 and #1963 (see Table 7.11 for sequences). Selected clones were also Sanger sequenced in accordance with the PD sequencing service provided by AGRF (AGRF, 2014).

7.0.3.3.6 Removal of the drug resistance cassette from AI243

The *loxP*-flanked *chlor^R* marker was removed using Cre supplied from the *pE-Cre* plasmid (Shearwin laboratory, unpublished) (Table 7.10). The AI243 strain (see Table 7.9 for genotype) was made chemically competent using the Transformation and Storage Solution (TSS) method (Chung et al., 1989). For transformation, 100µL AI243 cells were mixed with 1µL (~20ng) purified *pE-Cre*, incubated for 15mins on ice and heat shocked at 42°C for 45s followed by 1hr recovery at 30°C in 1mL SOC media. Cells were centrifuged to a pellet (at 1306rcf, 4°C for 10mins), the S/N discarded and the pellet resuspended in residual S/N, plated on L-plate with ampicillin (100ug/mL) and incubated O/N at 30°C. To cure cells of the *pE-Cre* plasmid, selected colonies were restreaked on L-plates with kanamycin (20ug/mL) and incubated O/N at 37°C.To screen for successful removal of the *chlor^R* marker, 10µL colony PCR was performed according to the KAPA2G Robust PCR Kit (KAPABiosystems) using primers #148 and #1963 (see Table 7.11 for sequences). O/N cultures of verified AI244 clones were transferred to 1:1 glycerol stocks and frozen at -80°C.

7.0.3.4 Characterising the cumic acid-inducible $186^{p.cym}$ prophage

7.0.3.4.1 Phage induction timecourse assay to characterise lytic development and define burst size

To characterise lytic development and quantify the burst size for 186^{+} and $186^{p.cym}$ phage, single-step phage production curves were generated by tracking phage titre following induction with UV and/or CA. For this assay, E4643 was the standard indicator strain; however, to demonstrate $186^{p.cym}$ is a temperate phage, induction was also assayed on a lawn of AI292 (see Table 7.9 for genotype). Indicator strains were always grown O/N in LB (without antibiotics) and HB59 and AI244 lysogens (see Table 7.9 for genotype) were always grown O/N in 1mM glucose minimal media (M9MM-1). The next day, the indicator was diluted to OD_{600} 0.05 in LB and incubated with aeration at 37°C until log phase growth (OD_{600} ~0.60). HB59 and AI244 lysogens were diluted to OD_{600} 0.15 in 20mM glucose minimal media (M9MM-20) and incubated with aeration at 37°C until OD_{600} ~0.30. Prior to UV or CA induction, a cell count plate was made for each lysogen by preparing a 10^{-4} dilution of the untreated OD_{600} ~0.30 lysogen culture, plating 10µL (without the indicator) on a L-plate and incubating O/N at 37°C.

For UV induction, 5mL of each lysogen culture (at OD_{600} 0.30) was added to a Petri dish and supplemented with 1µL 10% TWEEN-20. The Petri dish was positioned 50cm from the UV lamp and cells were exposed to 40s UV. The equivalent UV energy (at 40s) ranged between 10 to 13 µW/cm^2, which is 6.0 to 7.8 J/m^2/min as measured using the UVX-25 Digital Radiometer (UVP, Inc. serial# 031019). Immediately after induction, each culture was transferred to a 10mL sterile centrifuge tube and incubated with aeration at 37ºC. For CA induction, each lysogen culture (at OD_{600} 0.30) was treated with 150µM CA by adding 7.5µL of 100mM CA stock to 5mL of culture and incubated with aeration at 37ºC. 10mins after UV and/or CA induction, lysogen cultures were diluted 10^{-4} in pre-warmed M9MM-20 and for the remainder of the timecourse incubated at 37ºC with aeration. Induction plates were prepared at 10min intervals for AI244 and HB59 lysogens, where at each time point; the appropriate dilution was prepared in M9MM-20 (see Table 7.7) and 10µL mixed with 200µL indicator and 3mL molten 0.5% top agar (48°C) with 10mM $MgSO_4$ in a glass test tube. The mix was poured over a fresh L-plate, left to set at RT for ~30mins and incubated O/N at 37°C. Induction was assayed the next day by counting the number of plaque forming units (PFU) on each plate, which was converted to PFU/mL using formula (A) and the average PFU/mL observed for each time point plotted on a log scaled PFU/mL versus time scatter plot. Formula (B) was used to determine the average burst size for each phage.

$$(\mathbf{A})\ \text{Phage titre} = \frac{\text{Number of PFU on plate}}{(\text{Dilution factor x volume of phage culture plated})} = \frac{\text{PFU}}{\text{mL}}$$

$$(\mathbf{B})\ \text{Burst size} = \frac{\text{Average PFU/mL for first three timepoints}}{\text{Average PFU/mL for last three timepoints}} = \frac{\text{PFU}}{\text{infected cell}}$$

Table 7.7: The dilution series for the 186^{+} and 186$^{p.cym}$ phage induction assays. The count plate (#) was prepared with untreated lysogen culture without indicator, (0) is the untreated induction plate prepared with untreated lysogen culture with indicator. Each plate (excluding #) was prepared with 200µL log phase E4643 indicator, which is ~4.8x10^{7} cells/mL. *10mins after UV and/or CA induction, the entire lysogen culture was diluted 10^{-4} in pre-warmed M9MM-20. For later timepoints, ~100µL samples were taken and diluted as follows.

Time (mins)	#	0	*10	20	30	40	50	60	70	80	90	120
186^{+}	10^{-4}	10^{-2}	**10^{-4}**	10^{-0}	10^{-0}	10^{-0}	10^{-0}	10^{-0}	10^{-0}	10^{-0}	10^{-1}	10^{-1}
186$^{p.cym}$	10^{-4}	10^{-1}	**10^{-4}**	10^{-0}	10^{-0}	10^{-0}	10^{-2}	10^{-2}	10^{-2}	10^{-2}	10^{-2}	10^{-2}

7.0.3.4.2 The phage induction assay to determine virulence

To assay for virulence - the ability of phage to infect a lysogenic strain - HB59 and AI244 lysogens were plated on indicator lawns consisting of four different host strains (E4643, AI06, HB59 and AI244) (see Table 7.9 for genotypes). To prepare the indicator strains, O/N cultures of were diluted to OD_{600} 0.05 in LB and incubated with aeration at 37°C to OD_{600} ~0.60. To prepare the lysogen strains, O/N M9MM-1 cultures of HB59 and AI244 were diluted to OD_{600} 0.15 in M9MM-20 and incubated with aeration at 37°C to OD_{600} ~0.30. For UV induction, 5mL of the HB59 culture was added to a sterile Petri dish, supplemented with 1µL 10% TWEEN-20 and UV irradiated for 40s (~7.5 J/m^{2}/min) and incubated for 30mins at 37°C. For CA induction, 7.5µL of 100mM CA (150µM final conc.) was added to 5mL of the AI244 culture and incubated for 30mins at 37°C. To prepare the uninduced plates, untreated HB59 and AI244 cultures (at OD_{600} 0.30) were diluted 10^{-2} and 10^{-1} respectively. To prepare the induced plates, UV treated HB59 and CA treated AI244 cultures (at OD_{600} 0.30) were diluted 10^{-4} ~30mins after induction. 10µL of each lysogen sample was mixed with 200µL indicator strain (at OD_{600} 0.60) and 3mL molten 0.5% top agar (at 48°C) with 10mM $MgSO_4$. The mix was poured over a fresh L-plate, left to set at RT for ~30mins and then incubated O/N at 37°C. The number of PFUs per plate were counted the next day and the phage titre (PFU/mL) calculated using formula (A).

7.0.4 Induction switch plate assays

The induction switch plate assay offered a quick and easy means to assess the induction/working efficiency of the UV-inducible minimal prophage induction *pR* and *pL/pE* modules and any 186-WCB when compatibly linked to one of eight possible induction modules (IM) (Table 7.8). To prepare for these assays, frozen bacterial glycerol stocks were restreaked on L-plates with the appropriate antibiotic(s) and grown O/N at 37°C. 7mL M9MM-1 was inoculated with a single colony and grown O/N at 37°C. Cells were prepared for induction by diluting the O/N culture to OD_{600} 0.15 in 7mL M9MM-20 and incubated at 37°C with aeration until cells reached OD_{600} ~0.30.

Immediately prior to induction, an untreated switch plate was prepared, each culture was diluted 10^{-4} in M9MM-20 and 10µL (+100µL M9MM to facilitate spreading) plated on a L-plate with chloramphenicol (20µg/mL) and incubated O/N at 37°C. For UV induction, 5mL of the culture was supplemented with 1µL 10% TWEEN-20, transferred to a petri dish, positioned 50cm from the UV lamp and irradiated for 40s. For 150µM CA, VA or SA induction, 7.5µL of 100mM stocks were added to 5mL of culture and incubated at 37°C with aeration for 20/30mins, 40mins and 60mins respectively. To make the switch plates, the culture was diluted 10^{-4} in M9MM-20 from which 10µL was plated on a L-plate with the appropriate antibiotic(s) and incubated O/N at 37°C. LacZ reporter switching was assayed using L-plates with 40µg/mL X-gal, storing the plates for 2 to 3 days at 4°C (to allow for colour development) and then scoring for blue/white colonies. Fluorescent biosensor switching was examined by visualising MCherry expression on the SYPRO Ruby (Green Epi illumination with 605/50 emission filter at 1sec exposure) channel using a ChemiDoc™ MP Imaging System (BioRad). To gain some insight into the stability of a switch construct, a single induced or uninduced colony was resuspended in 10mL LB, diluted 10^{-2} in LB and 10µL plated on a L-plate ±X-gal and with the appropriate antibiotic(s). L-plates were incubated O/N at 37°C and the percentage of blue/white or red-/non-fluorescent colonies determined.

Table 7.8: The induction modules used in this thesis. Each module resides on a pIT3/4 CRIM vector, all of which harbour the R6Kγ *ori.* Any IM that encodes 186 $tum^{+/72K}$ induces expression of reporter genes, whilst any IM encoding 186 *cI* represses the expression of reporter genes.

Name	Induction	Description
$p95.tum^{+}$	40s UV (~5.2J/m^2)	pIT3-TO-$p95.tum^{+}$
$p95.tum^{72K}$	40s UV (~5.2J/m^2)	pIT3-TO-$p95.tum^{72K}$
$cymR.T5\text{-}1.tum^{+}$	20min 150µM CA	pIT4-KT-$cymR.T5\text{-}1.tum^{+}$
$cymR.T5\text{-}1.tum^{72K}$	20min 150µM CA	pIT4-KT-$cymR.T5\text{-}1.tum^{72K}$
$pVan.tum^{72K}$	40min150µM VA	pIT4-KT-$vanR.pVan^{CC}.tum^{72K}$
$pSal.tum^{72K}$	60min 150µM SA	pIT4-KT-$nahR.pSal^{TTC}.tum^{72K}$
$cymR^{AM}.pcymR^{C}.cI^{+}$ ($^1CA^{OFF}$)	20min 150µM CA	pIT4-KH-$pcymR^{C}.cI.cymR^{AM}$
$cymR.T5\text{-}6.cI^{+}$ ($^2CA^{OFF}$)	30min 150µM CA	pIT4-KH-$cymR.T5\text{-}6.cI^{+}$

7.0.5 The fluorescent-based switch stability assay for the 186-WCB

The fluorescent induction stability assay offered an easy and clear means to assess the bistability of 186-WCB strains when compatibly linked to one or more of the CA- and/or VA-IMs (see Table 7.8). Fluorescent switch stability assays were performed for 186-WCB strains AI235, AI311, AI312, AI322, AI325 and AI326 (see Table 7.9 for genotypes) to characterise ON and OFF state stability and determine bistability. To perform the assay, cells were induced with CA or VA and *mCherry* expression tracked for 3 to 5hrs each day over five days of continuous passaging of cultures in M9MM-1/20. For the VA dose-response stability assay, after VA induction (150µM for 40mins), AI311 cultures were resuspended in M9MM-20 supplemented with 0, 2, 10, 25, 50, 80, 120 and 150µM VA and *mCherry* expression tracked for three days.

For the AI311 ON state stability assays, VA-induced (150µM for 40mins) cultures were resuspended in M9MM-20 ±10µM VA and *mCherry* expression tracked for five days. For the VA dose-response induction assay, AI311 cultures were VA-induced for 40mins in M9MM-20 supplemented with 10, 15, 20, 25, 30, 35, 40, 50, 60, 70, 80 and 100µM VA and *mCherry* expression visualised the next day.

To prepare for these assays, frozen bacterial glycerol stocks were restreaked on L-plates with the appropriate antibiotic(s) and grown O/N at 37°C. 7mL M9MM-1 was inoculated with a single colony and grown O/N at 37°C. Cells were prepared for induction by diluting the O/N culture to OD_{600} 0.15 in 7mL M9MM-20 and incubated at 37°C with aeration until cells reached OD_{600} ~0.30. Immediately prior to induction, an untreated switch plate was prepared by diluting cells 10^{-4} in M9MM-20, plating 10µL (+100µL of M9MM to facilitate spreading) on a L-plate with the appropriate antibiotic(s) and incubated O/N at 37°C. At this point, a switch plate for a non-fluorescent biosensor strain was prepared to detect 'true' fluorescence from that of background. For 150µM CA or VA induction, 7.5µL of 100mM stocks were added to 5mL of culture and incubated at 37°C with aeration for 20/30mins and 40mins respectively. To make the test switch plates, cultures were diluted 10^{-4} in M9MM-20 from which 10µL (+100µL of M9MM to facilitate spreading) was plated on a L-plate with the appropriate antibiotic(s) and incubated O/N at 37°C. Immediately after preparing the switch plates, each culture was incubated at 37°C with aeration for 3 to 5hrs, with switch plates prepared every hour. To maintain log phase growth throughout the timecourse the cultures were diluted every 30mins with pre-warmed M9MM-20 to OD_{600} 0.30. To continuously track the fluorescent status of cells over multiple days, at the end of each timecourse, 7mL M9MM-1 was inoculated with 5µL of each induced culture and incubated O/N at 37°C with aeration. The next day, each O/N culture was diluted to OD_{600} 0.15 in 7mL M9MM-20 and incubated at 37°C with aeration until cells reached OD_{600} ~0.30. The timecourse was restarted with switch plates prepared every hour. At the end of the timecourse, 5µL of each culture was returned to M9MM-1 and incubated O/N at 37°C with aeration in preparation for the next day of fluorescent tracking.

7.0.6 Microtitre plate-based LacZ assays

Quantitative β-galactosidase (LacZ) assays were performed as kinetic assays in microtitre plates, as described by Dodd et al. (2001). Two versions of the assay were used to quantify LacZ expressed from reporter constructs used to investigate the *goa8* mutation and the role of CI, Apl, Tum and CII at the 186 switch during prophage induction and to characterise 186-WCB performance. The standard LB LacZ assay was used for cells harbouring non-inducible LacZ reporter constructs, whilst a modified minimal media induction LacZ assay was performed for cells harbouring an inducible reporter construct or a biosensor module. This modified assay quantifies LacZ expression over a defined timecourse following UV or chemical induction. Details of the two assay methods are given below.

7.0.6.1 The standard LB lacZ assay

Frozen bacterial glycerol stocks were restreaked on L-plates with the appropriate antibiotic(s) and grown O/N at 37°C. To prepare the O/N growth plate, 100µL LB media was added to the wells of a 96-well flat-bottomed microtitre plate (Corning Costar 3599) and inoculated with a single bacterial colony picked with a sterile wire. To prevent evaporation, the plate was sealed with a microtitre lid fitted with a sterile rubber insert and the lid taped to the plate with cellotape. The plate was incubated O/N at 37°C in a microplate shaker incubator (Grant-bio PHMP-4) with orbital shaking at 500rpm.

To prepare cells for the LacZ assay, O/N cultures were resuspended with a 15s shake and 20µL diluted into 80µL LB dispensed into the wells of a new microtitre plate. Cell density for each culture was determined by measuring the absorbance at 620nm (A_{620}) using a Multiskan Ascent V1.22 plate reader (Labsystems) and converting the A_{620s} back to OD_{600s} values using an empirically determined relationship (Dodd et al., 2001). Cultures were normalised to OD_{620} ~0.15 by adding various volumes of fresh LB to each well. The LacZ growth plate was prepared by dispensing 98µL LB into the wells of a new microtitre plate and inoculating each well with 2µL of each normalised culture to achieve a starting OD_{620} ~0.003. The plate was sealed with a sterile lid and incubated at 37°C in the microplate shaker incubator (at 500rpm) until cells reached OD_{620} 0.10 to 0.20.

Once the cultures had reached log phase growth, 50µL of culture was added to the wells of a new microtitre plate containing 190µL TZ8+ lysis and assay buffer pre-warmed to 37°C. Each well contains 150µL TZ8 (100mM Tris pH 8.0, 1mM MgSO4, 10mM KCl), 40µL ONPG (ortho-nitrophenyl-β-galactoside in 4mg/mL in TZ8), 1.9µL 2-mercaptoethanol (Sigma Aldrich) and 0.95µL polymyxin B (20mg/mL MQ H_2O, Sigma Aldrich). The plate was shaken (10s at 960rpm) in a Multiskan Ascent V1.22 plate reader (Labsystems) pre-warmed to 28°C and readings of A_{414} were measured every 30s for 30mins. The final A_{620} of the cultures and A_{414} vs time was used to calculate the LacZ units using formula (C).

$$(\mathbf{C})\ \text{LacZ units} = \frac{200{,}000 \times \text{slope}}{\text{OD}_{600} \times \text{culutre volume (µL)}}$$

7.0.6.2 The M9MM induction LacZ assay

Frozen bacterial glycerol stocks were restreaked on L-plates with the appropriate antibiotic(s) and grown O/N at 37°C. O/N stationary cultures were prepared by inoculating 7mL of M9MM-1 with a single colony and grown O/N at 37°C with aeration. To prepare cells for the LacZ assay, O/N cultures were diluted to OD_{600} 0.15 in 7mL M9MM-20 and incubated at 37°C with aeration until cells reached OD_{600} ~0.30 (ready for induction). Immediately prior to induction, a 500µL uninduced sample was taken and placed on ice.

For UV induction, 5mL of the culture was supplemented with 1µL 10% TWEEN-20, transferred to a petri dish and UV irradiated for 40s (~7.5 J/m^2/min). Immediately after induction, a 500µL 'zero' time point sample was taken and placed on ice and the remaining culture transferred to a 10mL screw cap centrifuge tube and incubated at 37°C with aeration for 3 to 5hrs. For 150µM CA, VA or SA induction, 7.5µL of 100mM stocks were added to 5mL of culture and incubated at 37°C with aeration for 20, 40 and 60mins respectively (a 500µL 'zero' time point sample was also taken and placed on ice). Following induction, the inducer was removed from each culture by pelleting the cells (3096rcf for 5mins), removing all the S/N and resuspending the cells in 5mL fresh pre-warmed M9MM-20. The cultures were incubated at 37°C for the remainder of the 3 to 5hr timecourse, taking 500µL samples every 30mins and storing them on ice. To maintain log phase growth throughout the timecourse and ensure each final sample for LacZ analysis had an OD_{600} ~0.4, the cultures were diluted every 30mins with pre-warmed M9MM-20 to OD_{600} 0.30. To perform the LacZ assay, 100uL of each sample was pipetted into the wells of a 96-well flat-bottomed microtitre plate and the final A_{620} for each culture measured using a Multiskan Ascent V1.22 plate reader (Labsystems). 50µL of each culture was then added to the wells of a new microtitre plate containing 190µL TZ8+ lysis and assay buffer pre-warmed to 37°C and the assay performed as per the standard LB LacZ assay protocol (Section 7.0.6.1).

For bacterial cultures being passaged (and their LacZ production assayed) over multiple days, at the end of each timecourse, 7mL M9MM-1 was inoculated with 5µL of each induced culture and incubated O/N at 37°C with aeration. The next day, each O/N culture was diluted to OD_{600} 0.15 in 7mL M9MM-20 and incubated at 37°C with aeration until cells reached OD_{600} ~0.30. The 3 to 5hr timecourse was restarted by taking 500µL samples every 30mins and storing them on ice, making sure to maintain log phase growth throughout the timecourse by periodically diluting the cultures with pre-warmed M9MM-20 to OD_{600} 0.30. At the end of the timecourse, 5µL of each culture was switched back to M9MM-1 and incubated O/N at 37°C with aeration in preparation for the next day of LacZ tracking.

7.0.7 Western blotting

Quantification of 186CI for the CI expression strains (AI19, AI25, AI31, AI37, AI43, AI55, AI61, AI67) and the C600(186$^+$) and C600(186^{goa8}) lysogens (E0573 and E2564) (see Table 7.9 for genotypes) was done via fluorescent Western blotting of whole-cell extracts using a polyclonal rabbit primary antibody raised against 186CI and a Cy5-labelled donkey-anti-rabbit secondary antibody. CI concentration [CI] was measured in lysogenic units, where 0 lysogenic units represents no-CI and 1 lysogenic unit represents the CI level observed in a 186$^+$ lysogen. For the CI expression strains, the negative control strain expressing no-CI (AI111) contained the empty vector pIT3-CL at λ *attB* and the positive control strain expressing a lysogenic level of CI (AI120) contained the empty λ integrated pIT3-CL vector and 186$^+$ prophage at the 186 *attB1* site.

For the C600(186^{+}) and C600(186^{goa8}) lysogens, the empty-C600 (non-lysogen) strain was used as the negative control. CI levels for each CI expression strain were quantified using a standard curve prepared for a lysogen; generated by adding various volumes of the AI120 (lysogen) whole-cell extract to the AI111 (non-lysogen) cell extract. To accurately interpolate [CI] for the high CI expression modules (M1, M2 and M9), these cell extracts were diluted to ensure their signal fell within range of the standard curve. The lysogenic unit of [CI] for the C600(186^{goa8}) lysogen was quantified by comparing the 186^{+} whole-cell extract against a *goa8* CI standard curve, generated by adding various volumes of the E2564 (*goa8*) whole-cell extract to the empty-C600 cell extract.

7.0.7.1 Preparation of cellular extracts for Western blotting

Whole-cell extracts used to generate a standard curve and for 186CI quantification were prepared by diluting (1/200) a fresh O/N stationary culture in LB with the appropriate antibiotic(s) and grown to log phase (OD_{600} ~0.60) at 37°C with aeration. C600, E0573 and E2564 were always cultured in LB without antibiotics and AI111, AI120 and AI103-AI110 strains cultured in LB with chloramphenicol (20µg/mL). Cells were chilled on ice for ~15mins and a final OD_{600} reading was taken. 1mL aliquots of each standard OD_{600} 0.60 culture was dispensed into chilled 1.5mL Eppendorf tubes (volume adjusted according to final OD_{600}), centrifuged to a pellet at 1306rcf for 10mins at 4°C and the S/N thoroughly removed. To aid cell lysis, a free/thaw step was performed (10mins at -80°C) before resuspending each pellet in 40µL lysis solution (1mL B-PER + 1µL Benzonase (25U/µL) and incubating on ice for 30mins to allow for digestion of chromosomal DNA, thus reducing the viscosity of the samples. 40uL of 2X SDS PAGE loading buffer (2X LaemmLi SDS-PAGE sample buffer (BioRad)) and 2X β-Mercaptoethanol (Sigma Aldrich) made up fresh in MQ H_2O) was added to each extract, heated at 70°C for 10mins (for protein denaturation), pulse spun to recover any condensation and stored at -20°C.

To reduce the generation of background bands, the polyclonal rabbit anti-186CI primary antibody (made in-house) was pre-absorbed against a no-CI cell extract. The pre-absorption no-CI cell extract was prepared by diluting (1/200) fresh O/N stationary C600 and AI111 cultures in 500mL LB ±chloramphenicol (20µg/mL) respectively and grown to log phase (OD_{600} ~0.60) at 37°C with aeration. 500mL cultures were centrifuged to a pellet (at 3095rcf for 10mins) and resuspended in 5mL of 10mM Tris pH 8.5 1mM $MgCl_2$ and sonicated with x2 to 4 10s pulses. 5µL Benzonase (25U/µL) (Novagen) was added to the sonicated cells and incubated on ice for 30mins. The cell extracts were dispensed into 1.5mL Eppendorf tubes and stored at -20°C. For pre-absorption, 150µL of thawed no-CI pre-absorption cell extract was mixed with 10mL PBS-T containing the primary antibody (diluted 1/500) and incubated for 30mins at 37°C.

7.0.7.2 Polyacrylamide gel electrophoresis of proteins and Western blotting

The protein content of cellular extracts was quantified by first separating the protein on the basis of molecular weight using SDS-PAGE and then transferring to a membrane and probing for 186CI by antibody detection. For SDS-PAGE, 20µL cellular extract samples were loaded onto 18-well 4-15% Criterion™ Tris-glycine precast gels (BioRad). Gels were run according to the manufacture's specifications at 200V for ~40mins with 1X Tris/Glycine/SDS Running Buffer (BioRad). Proteins were transferred from gel to a PVDF membrane with a 0.2µM pore size using the Trans-Blot Turbo™ Midi Format pack (BioRad) and the manufacture's seven-minute transfer protocol for the Turboblotter (BioRad).

Freshly transferred membranes were blocked O/N in 5% BSA prepared in PBS-T (1X PBS with 0.1% TWEEN-20) at 4°C with gentle shaking and then washed twice in 1X TBS-T (1X TBS with 0.1% TWEEN-20). To perform a wash, simply add ~20mL TBS-T, swirl the membrane and pour off the liquid. The membrane was incubated with 10mL of pre-absorbed polyclonal rabbit anti-186CI primary antibody for 1h at RT with gentle shaking. Following primary antibody incubation, the membrane was washed x4 in TBS-T with the final wash having a 5min shake and exposed to the Cy5-labelled ECL Plex donkey-anti-rabbit secondary antibody (Amersham) diluted 1/5000 in 20mL TBS-T at RT for 30mins in the dark, with gentle shaking. The membrane was washed x4 in TBS-T to remove the secondary antibody followed by two washes in TBS with the final wash having a 5min shake to remove the TWEEN-20 and any remaining antibody. The membrane was dabbed dry on blotting paper and then dried completely, sandwiched between blotting paper for 1hr at 37°C in the dark. Dried membranes were imaged on the Western blot Cy5 channel (Red Epi illumination with 695/55 filter) linked to the ChemiDoc™ MP Imaging System (BioRad). Western blot images were analysed using the BioRad Image Lab software (Version 5.2.1 build 11, 2014).

7.1 Materials

7.1.1 Bacterial strains

Table 7.9 lists the details of the *E. coli* strains used and manipulated during the course of this thesis. Refer to OpenWetWare (2020) for further descriptions of genotypes.

Table 7.9: *E. coli* strains used in this thesis. Chromosomally integrated modules are encased with squared brackets, with the ending subscript indicating the site of integration. Unless stated otherwise, all integrated modules exist as single-copy constructs at one of four possible phage integration sites (186.1, λ, φ21 or HK022). Non-standard strains have been categorised according to their area of study.

Glycerol	Name	Genotype	Description
Standard bacterial strains			
E4640	MG1655	*K-12 F⁻ λ⁻ ilvG⁻ rfb-50 rph-1*	Wildtype *E. coli* K-12 strain used routinely in molecular biology as a research tool and model organism (BW30270 (CGSC 7925)).

Glycerol	Name	Genotype	Description
E4644	EC100D *pir+*	F- *mcr*A Δ(mrr-hsdRMS-mcrBC) φ80d(*lacZ*ΔM15) Δ*lacX*74 *rec*A1 *end*A1 araD139 Δ(*ara, leu*)7697 *gal*U *gal*K λ⁻ *rps*L *str*^{R} *nup*G pir⁺ (DHFR)	Base strain used for routine cloning and low-copy number propagation of integration pIT3/4 *pir*-dependent plasmids. Obtained from Epicentre.
E4645	EC100D *pir-116*	F- *mcr*A Δ(mrr-hsdRMS-mcrBC) φ80d(*lacZ*ΔM15) Δ*lacX*74 *rec*A1 *end*A1 araD139 Δ(*ara, leu*)7697 *gal*U *gal*K λ⁻ *rps*L *str*^{R} *nup*G pir-116 (DHFR)	Strain used for routine cloning and high-copy number propagation of integration pIT3/4 *pir*-dependent plasmids. Obtained from Epicentre.
E4643	E4643	MG1655 Δ*lac*IZYA	Base strain used for chromosomal integration of pIT3/4 plasmids.
E508	C600	F- tonA21 *thi*-1 *thr*-1 *leu*B6 *lac*Y1 *gln*V44 *rfb*C1 *fhu*A1 λ⁻	Strain commonly lysogenised with 186. Used to prepare the no-CI protein whole-cell extract for Western blot analysis of the C600(186^{goa8}) lysogen.
E4704	DB3.1	F- gyrA462 endA1 glnV44 Δ(sr1-recA) mcrB mrr hsdS20(rB-, mB-) ara14 galK2 lacY1 proA2 rpsL20(Smr) xyl5 Δleu mtl1	A *ccdB* tolerant strain used for routine cloning and propagation of integration pIT3/4 *pir*-dependent plasmids harbouring the I52002 biobrick (*ccdB* gene encodes lethal DNA gyrase toxin).
E4648	E4648	E2829 + pIT3-CL	Strain used to propagate the blank pIT3-CL integration plasmid.
E2878	E2878	**BW23473:** Δ*(lacIZYA argF)U169 rph-1 rpoS396(Am) robA1 creC510 hsdR514 ΔendA9 recAI uidA (ΔMluI)::pir(wt)*	A *pir*⁺ strain used for propagating and cloning CRIM helper plasmids at medium-copy number (Haldimann and Wanner, 2001).
E2879	E2879	**BW23474:** Δ*(lacIZYA argF)U169 rph-1 rpoS396(Am) robA1 creC510 hsdR514 ΔendA9 recAI uidA (ΔMluI)::pir-116*	A *pir-116* strain used for propagating and cloning CRIM helper plasmids at high-copy number (Haldimann and Wanner, 2001).
E4781	sAJM.1506 (Marionette. Wild)	MG1655 + [sAJM.1506]	Strain contains the Marionette wildtype cluster integrated between 3,860,010 and 3,861,627 in *E. coli* MG1655 (Addgene #108254) (Meyer et al., 2019).
AI97	AI97	E4643 + pINT-ts	Strain harbours λ CRIM helper plasmid (Haldimann and Wanner, 2001).
AI99	AI99	E4643 + pAH121	Strain harbours φ21 CRIM helper plasmid (Haldimann and Wanner, 2001).
AI293	AI293	E4643 + pλ*int*-186*clts*	Strain harbours λ integration helper plasmid. Encodes 186*clts,* which controls λ*int* expression from 186*pR*.
AI122	AI122	E4643 + [pIT3-CL]$_{\lambda}$ + pAH121	Strain harbours blank pIT3-CL and φ21 CRIM helper plasmid.
CL984	DH5α + *pE-Flp*	F⁻ *endA1 glnV44 thi-1 recA1 relA1 gyrA96 deoR nupG purB20* φ80d*lacZ*ΔM15 Δ(*lacZYA-argF*)U169, hsdR17 ($r_K^- m_K^+$), λ⁻ + pKD46-*pE-Flp*	Propagation strain for the *pE-Flp* plasmid, that harbours the FLP(*frt)* recombineering system. Strain made by Cui Lun (Shearwin laboratory).
AH6044	DH5α + *pE-Cre*	F⁻ *endA1 glnV44 thi-1 recA1 relA1 gyrA96 deoR nupG purB20* φ80d*lacZ*ΔM15 Δ(*lacZYA-argF*)U169, hsdR17 ($r_K^- m_K^+$), λ⁻ + pKD46-*pE-Cre*	Propagation strain for the *pE-Cre* plasmid that harbours the Cre-*loxP* recombineering system. Strain made by Andrew Hao (Shearwin laboratory).

Glycerol	Name	Genotype	Description
E0573	E0573	C600 + $[186^{+}]_{186.1}$	*E. coli* lysogen harbouring 186^{+} prophage.
DL47	DL47	E4643 + $[$pIT3-TO-*p95.tum*$^{+}]_{186.1}$ + pINT-ts	Strain contains an integrated *p95.tum*$^{+}$ UV-IM and a λ CRIM helper plasmid. Strain made by Danna Lee (Shearwin laboratory).
DL14	DL245-I	E4643 + $[$pIT3-CL-186*cI*$^{+}$.***pR***$^{+}$.*pL*$^{+}$.*apl*$^{+}$.*cII::lacZ*$]_{\lambda}$ + $[$pIT3-TO-*p95. tum*$^{+}]_{186.1}$	Strain contains an integrated minimal ***pR***.*apl*$^{+}$ LacZ reporter and a *p95.tum*$^{+}$ UV-IM. Strain made by Danna Lee (Shearwin laboratory).
Bacterial strains used in the goa8, CI and Apl study (Chapter 2)			
IM554	IM554	E4644 + pET3α186*cI* + pIT3-CL-186*cI*$^{+}$.***pR***$^{+}$.*pL*$^{+}$.*apl*$^{+}$.*cII*$^{+}$.*fil::lacZ*	Strain harbours two plasmids. Plasmid harbouring the ***pR***.*apl*$^{+}$.*cII*$^{+}$ LacZ reporter was extracted and λ integrated into DL47. Strain made by Ian Murchland (Shearwin laboratory).
IM557	IM557	E4644 + pET3α186*cI* + pIT3-CL-186*cI*$^{+}$.***pR***$^{+}$.*pL*$^{+}$.*apl*$^{+}$.*cII*$^{-}$.*fil::lacZ*	Strain harbours two plasmids. Plasmid harbouring the ***pR***.*apl*$^{+}$.*cII*$^{-}$ LacZ reporter was extracted and λ integrated into DL47. Strain made by Ian Murchland (Shearwin laboratory).
AI111	AI111	E4643 + $[$pIT3-CL$]_{\lambda}$	Strain contains an integrated pIT3-CL plasmid. Used to generate the 186CI minus and lysogenic reporter library.
AI122	AI122	E4643 + $[$pIT3-CL$]_{\lambda}$ + pAH121	Strain contains an integrated pIT3-CL plasmid and a φ21 CRIM helper plasmid. Used to generate the 186CI minus reporter library.
AI120	AI120	E4643 + $[186^{+}]_{186.1}$ + $[$pIT3-CL$]_{\lambda}$	*E. coli* lysogen harbours 186^{+} prophage and an integrated pIT3-CL plasmid.
E2564	E2564	C600 + $[186^{goa8}]_{186.1}$	*E. coli* C600 lysogen harbouring 186^{goa8} prophage.
AI06	AI06 (WT, M1 to M11)	E4643 + $[$pIT3-CL-186*cI*$^{+}$.*pR*$^{-}$.***pL***^{WT,M1,2,3,4,5,6,7,8,9,10,11}.*apl*$^{-}$.*int::lacZ*$]_{\lambda}$	**The 186CI *pL* LacZ reporters**. Each strain harbours an integrated wildtype or mutant ***pL*** LacZ reporter.
AI100-R1	AI100-R1	E4643 + [Reporter 1: pIT3-KT-186*cI*$^{-}$.*pR*$^{+}$.***pL***$^{+}$.*apl*$^{-}$.*int::lacZ*$]_{\varphi 21}$ + pINT-ts	**The wildtype and *goa8 pL* and *pR* LacZ reporter library**. Each strain harbours an integrated reporter 1, 2, 3, 4, 5 or 6 and a λ CRIM helper plasmid.
AI100-R2	AI100-R2	E4643 + [Reporter 2: pIT3-KT-186*cI*$^{-}$.*pR*$^{+}$.*goa8*.***pL***$^{+}$.*apl*$^{-}$.*int::lacZ*$]_{\varphi 21}$ + pINT-ts	
AI100-R3	AI100-R3	E4643 + [Reporter 3: pIT3-KT-186*cI*$^{-}$.***pR***$^{+}$.*pL*$^{+}$.*apl*$^{-}$.*cII::lacZ*$]_{\varphi 21}$ + pINT-ts	
AI100-R4	AI100-R4	E4643 + [Reporter 4: pIT3-KT-186*cI*$^{-}$.***pR***$^{+}$.*goa8.pL*$^{+}$.*apl*$^{-}$.*cII::lacZ*$]_{\varphi 21}$ + pINT-ts	
AI100-R5	AI100-R5	E4643 + [Reporter 5: pIT3-KT-186*cI*$^{-}$.*pR*$^{-}$.***pL***$^{+}$.*apl*$^{-}$.*int::lacZ*$]_{\varphi 21}$ + pINT-ts	
AI100-R6	AI100-R6	E4643 + [Reporter 6: pIT3-KT-186*cI*$^{-}$.*pR*$^{-}$.*goa8*.***pL***$^{+}$.*apl*$^{-}$.*int::lacZ*$]_{\varphi 21}$ + pINT-ts	

Glycerol	Name	Genotype	Description
AI19	AI19	E4643 + [Reporter 1]$_{\varphi 21}$ + [pIT3-CL]$_{\lambda}$	**The 186CI minus library**. Each strain harbours an integrated ***pR*** or ***pL*** *goa8*$^{+/-}$ LacZ reporter and a blank pIT3-CL plasmid. AI19 was used to prepare the no-CI whole-cell extract for Western blot analysis of the 186CI expression modules.
AI20	AI20	E4643 + [Reporter 2]$_{\varphi 21}$ + [pIT3-CL]$_{\lambda}$	
AI21	AI21	E4643 + [Reporter 3]$_{\varphi 21}$ + [pIT3-CL]$_{\lambda}$	
AI22	AI22	E4643 + [Reporter 4]$_{\varphi 21}$ + [pIT3-CL]$_{\lambda}$	
AI23	AI23	E4643 + [Reporter 5]$_{\varphi 21}$ + [pIT3-CL]$_{\lambda}$	
AI24	AI24	E4643 + [Reporter 6]$_{\varphi 21}$ + [pIT3-CL]$_{\lambda}$	
AI25	AI25	E4643 + [Reporter 1]$_{\varphi 21}$ + [pIT3-CL]$_{\lambda}$ + [186^{+}]$_{186.1}$	**The 186CI lysogen library**. A lysogenic level of CI is supplied from a 186^{+} prophage. Each strain harbours an integrated ***pR*** or ***pL*** *goa8*$^{+/-}$ LacZ reporter, a blank pIT3-CL plasmid and a 186^{+} prophage. AI25 was used to prepare the lysogenic 186CI whole-cell extract for Western blot analysis of the 186CI expression modules.
AI26	AI26	E4643 + [Reporter 2]$_{\varphi 21}$ + [pIT3-CL]$_{\lambda}$ + [186^{+}]$_{186.1}$	
AI27	AI27	E4643 + [Reporter 3]$_{\varphi 21}$ + [pIT3-CL]$_{\lambda}$ + [186^{+}]$_{186.1}$	
AI28	AI28	E4643 + [Reporter 4]$_{\varphi 21}$ + [pIT3-CL]$_{\lambda}$ + [186^{+}]$_{186.1}$	
AI29	AI29	E4643 + [Reporter 5]$_{\varphi 21}$ + [pIT3-CL]$_{\lambda}$ + [186^{+}]$_{186.1}$	
AI30	AI30	E4643 + [Reporter 6]$_{\varphi 21}$ + [pIT3-CL]$_{\lambda}$ + [186^{+}]$_{186.1}$	
AI31	AI31	E4643 + [Reporter 1]$_{\varphi 21}$ + [pIT3-CL-186*cI*$^{+}$.*pR*$^{-}$.*pL*^{WT}.*apl*$^{-}$]$_{\lambda}$	**The 186CI wildtype library**. A wildtype level of CI is supplied from wildtype *pL* -35 TTGCGA, -10 CATGAT. Each strain harbours an integrated ***pR*** or ***pL*** *goa8*$^{+/-}$ LacZ reporter and a 186CI^{WT} expression module. AI31 was used to prepare the 186CI^{WT} whole-cell extract for Western blot analysis of the 186CI expression modules.
AI32	AI32	E4643 + [Reporter 2]$_{\varphi 21}$ + [pIT3-CL-186*cI*$^{+}$.*pR*$^{-}$.*pL*^{WT}.*apl*$^{-}$]$_{\lambda}$	
AI33	AI33	E4643 + [Reporter 3]$_{\varphi 21}$ + [pIT3-CL-186*cI*$^{+}$.*pR*$^{-}$.*pL*^{WT}.*apl*$^{-}$]$_{\lambda}$	
AI34	AI34	E4643 + [Reporter 4]$_{\varphi 21}$ + [pIT3-CL-186*cI*$^{+}$.*pR*$^{-}$.*pL*^{WT}.*apl*$^{-}$]$_{\lambda}$	
AI35	AI35	E4643 + [Reporter 5]$_{\varphi 21}$ + [pIT3-CL-186*cI*$^{+}$.*pR*$^{-}$.*pL*^{WT}.*apl*$^{-}$]$_{\lambda}$	
AI36	AI36	E4643 + [Reporter 6]$_{\varphi 21}$ + [pIT3-CL-186*cI*$^{+}$.*pR*$^{-}$.*pL*^{M1}.*apl*$^{-}$]$_{\lambda}$	
AI37	AI37	E4643 + [Reporter 1]$_{\varphi 21}$ + [pIT3-CL-186*cI*.*pR*$^{-}$.*pL*^{M1}.*apl*$^{-}$]$_{\lambda}$	**The 186CI M1 library**. A high level of CI is supplied from *pL* -35 TTGCGA, -10 TATAAT. Each strain harbours an integrated ***pR*** or ***pL*** *goa8*$^{+/-}$ LacZ reporter and a 186CI^{M1} expression module. AI37 was used to prepare the 186CI^{M1} whole-cell extract for Western blot analysis of the 186CI expression modules.
AI38	AI38	E4643 + [Reporter 2]$_{\varphi 21}$ + [pIT3-CL-186*cI*$^{+}$.*pR*$^{-}$.*pL*^{M1}.*apl*$^{-}$]$_{\lambda}$	
AI39	AI39	E4643 + [Reporter 3]$_{\varphi 21}$ + [pIT3-CL-186*cI*$^{+}$.*pR*$^{-}$.*pL*^{M1}.*apl*$^{-}$]$_{\lambda}$	
AI40	AI40	E4643 + [Reporter 4]$_{\varphi 21}$ + [pIT3-CL-186*cI*$^{+}$.*pR*$^{-}$.*pL*^{M1}.*apl*$^{-}$]$_{\lambda}$	
AI41	AI41	E4643 + [Reporter 5]$_{\varphi 21}$ + [pIT3-CL-186*cI*$^{+}$.*pR*$^{-}$.*pL*^{M1}.*apl*$^{-}$]$_{\lambda}$	
AI42	AI42	E4643 + [Reporter 6]$_{\varphi 21}$ + [pIT3-CL-186*cI*$^{+}$.*pR*$^{-}$.*pL*^{M1}.*apl*$^{-}$]$_{\lambda}$	
AI43	AI43	E4643 + [Reporter 1]$_{\varphi 21}$ + [pIT3-CL-186*cI*$^{+}$.*pR*$^{-}$.*pL*^{M2}.*apl*$^{-}$]$_{\lambda}$	**The 186CI M2 library**. A very high level of CI is supplied from *pL* -35 TTGCGA, -10 TATCAT. Each strain harbours an integrated ***pR*** or ***pL*** *goa8*$^{+/-}$ LacZ reporter and a 186CI^{M2} expression module. AI43 was used to prepare the 186CI^{M2} whole-cell extract for Western blot analysis of the 186CI expression modules.
AI44	AI44	E4643 + [Reporter 2]$_{\varphi 21}$ + [pIT3-CL-186*cI*$^{+}$.*pR*$^{-}$.*pL*^{M2}.*apl*$^{-}$]$_{\lambda}$	
AI45	AI45	E4643 + [Reporter 3]$_{\varphi 21}$ + [pIT3-CL-186*cI*$^{+}$.*pR*$^{-}$.*pL*^{M2}.*apl*$^{-}$]$_{\lambda}$	
AI46	AI46	E4643 + [Reporter 4]$_{\varphi 21}$ + [pIT3-CL-186*cI*$^{+}$.*pR*$^{-}$.*pL*^{M2}.*apl*$^{-}$]$_{\lambda}$	
AI47	AI47	E4643 + [Reporter 5]$_{\varphi 21}$ + [pIT3-CL-186*cI*$^{+}$.*pR*$^{-}$.*pL*^{M2}.*apl*$^{-}$]$_{\lambda}$	
AI48	AI48	E4643 + [Reporter 6]$_{\varphi 21}$ + [pIT3-CL-186*cI*$^{+}$.*pR*$^{-}$.*pL*^{M2}.*apl*$^{-}$]$_{\lambda}$	

Glycerol	Name	Genotype	Description
AI55	AI55	E4643 + [Reporter 1]$_{\varphi 21}$ + [pIT3-CL-186*cI*$^{+}$.*pR*$^{-}$.*pL*^{M7}.*apI*$^{-}$]$_{\lambda}$	**The 186CI M7 library**. A moderate level of CI is supplied from *pL* -35 TTGCGA, -10 AATAAT. Each strain harbours an integrated ***pR*** or ***pL*** *goa8*$^{+/-}$ LacZ reporter and a 186CI^{M3} expression module. AI55 was used to prepare the 186CI^{M3} whole-cell extract for Western blot analysis of the 186CI expression modules.
AI56	AI56	E4643 + [Reporter 2]$_{\varphi 21}$ + [pIT3-CL-186*cI*$^{+}$.*pR*$^{-}$.*pL*^{M7}.*apI*$^{-}$]$_{\lambda}$	
AI57	AI57	E4643 + [Reporter 3]$_{\varphi 21}$ + [pIT3-CL-186*cI*$^{+}$.*pR*$^{-}$.*pL*^{M7}.*apI*$^{-}$]$_{\lambda}$	
AI58	AI58	E4643 + [Reporter 4]$_{\varphi 21}$ + [pIT3-CL-186*cI*$^{+}$.*pR*$^{-}$.*pL*^{M7}.*apI*$^{-}$]$_{\lambda}$	
AI59	AI59	E4643 + [Reporter 5]$_{\varphi 21}$ + [pIT3-CL-186*cI*$^{+}$.*pR*$^{-}$.*pL*^{M7}.*apI*$^{-}$]$_{\lambda}$	
AI60	AI60	E4643 + [Reporter 6]$_{\varphi 21}$ + [pIT3-CL-186*cI*$^{+}$.*pR*$^{-}$.*pL*^{M7}.*apI*$^{-}$]$_{\lambda}$	
AI61	AI61	E4643 + [Reporter 1]$_{\varphi 21}$ + [pIT3-CL-186*cI*$^{+}$.*pR*$^{-}$.*pL*^{M8}.*apI*$^{-}$]$_{\lambda}$	**The 186CI M8 library**. A low level of CI is supplied from *pL* -35 TTGCGA, -10 GTACAT. Each strain harbours an integrated ***pR*** or ***pL*** *goa8*$^{+/-}$ LacZ reporter and a 186CI^{M8} expression module. AI61 was used to prepare the 186CI^{M8} whole-cell extract for Western blot analysis of the 186CI expression modules.
AI62	AI62	E4643 + [Reporter 2]$_{\varphi 21}$ + [pIT3-CL-186*cI*$^{+}$.*pR*$^{-}$.*pL*^{M8}.*apI*$^{-}$]$_{\lambda}$	
AI63	AI63	E4643 + [Reporter 3]$_{\varphi 21}$+ [pIT3-CL-186*cI*$^{+}$.*pR*$^{-}$.*pL*^{M8}.*apI*$^{-}$]$_{\lambda}$	
AI64	AI64	E4643 + [Reporter 4]$_{\varphi 21}$+ [pIT3-CL-186*cI*$^{+}$.*pR*$^{-}$.*pL*^{M8}.*apI*$^{-}$]$_{\lambda}$	
AI65	AI65	E4643 + [Reporter 5]$_{\varphi 21}$+ [pIT3-CL-186*cI*$^{+}$.*pR*$^{-}$.*pL*^{M8}.*apI*$^{-}$]$_{\lambda}$	
AI66	AI66	E4643 + [Reporter 6]$_{\varphi 21}$ + [pIT3-CL-186*cI*$^{+}$.*pR*$^{-}$.*pL*^{M8}.*apI*$^{-}$]$_{\lambda}$	
AI67	AI67	E4643 + [Reporter 1]$_{\varphi 21}$ + [pIT3-CL-186*cI*$^{+}$.*pR*$^{-}$.*pL*^{M9}.*apI*$^{-}$]$_{\lambda}$	**The 186CI M9 library**. A very high level of CI is supplied from *pL* -35 TTGACA pL-10 CATGAT. Each strain harbours an integrated ***pR*** or ***pL*** *goa8*$^{+/-}$ LacZ reporter and a 186CI^{M9} expression module. AI67 was used to prepare the 186CI^{M9} whole-cell extract for Western blot analysis of the 186CI expression modules.
AI68	AI68	E4643 + [Reporter 2]$_{\varphi 21}$ + [pIT3-CL-186*cI*$^{+}$.*pR*$^{-}$.*pL*^{M9}.*apI*$^{-}$]$_{\lambda}$	
AI69	AI69	E4643 + [Reporter 3]$_{\varphi 21}$ + [pIT3-CL-186*cI*$^{+}$.*pR*$^{-}$.*pL*^{M9}.*apI*$^{-}$]$_{\lambda}$	
AI70	AI70	E4643 + [Reporter 4]$_{\varphi 21}$ + [pIT3-CL-186*cI*$^{+}$.*pR*$^{-}$.*pL*^{M9}.*apI*$^{-}$]$_{\lambda}$	
AI71	AI71	E4643 + [Reporter 5]$_{\varphi 21}$ + [pIT3-CL-186*cI*$^{+}$.*pR*$^{-}$.*pL*^{M9}.*apI*$^{-}$]$_{\lambda}$	
AI72	AI72	E4643 + [Reporter 6]$_{\varphi 21}$+ [pIT3-CL-186*cI*$^{+}$.*pR*$^{-}$.*pL*^{M9}.*apI*$^{-}$]$_{\lambda}$	
AI85	AI85	E4643 + [pIT3-TO-*p95.tum*$^{+}$]$_{186.1}$ + [pIT3-CL-186*cI*$^{+}$.***pR***$^{+}$.*pL*$^{+}$.*apI*$^{+}$.*cII*$^{+}$.*fil::lacZ*]$_{\lambda}$	**The wildtype minimal prophage induction *pR* modules**. Each strain harbours an integrated *p95.tum*$^{+}$ UV-IM and a ***pR***.*apI*$^{+/-}$.*cII*$^{+/-}$ LacZ reporter.
AI86	AI86	E4643 + [pIT3-TO-*p95.tum*$^{+}$]$_{186.1}$ + [pIT3-CL-186*cI*$^{+}$.***pR***$^{+}$.*pL*$^{+}$.*apI*$^{+}$.*cII*$^{-}$.*fil::lacZ*]$_{\lambda}$	
AI87	AI87	E4643 + [pIT3-TO-*p95.tum*$^{+}$]$_{186.1}$ + [pIT3-CL-186*cI*$^{+}$.***pR***$^{+}$.*pL*$^{+}$.*apI*$^{-}$.*cII*$^{+}$.*fil::lacZ*]$_{\lambda}$	
AI88	AI88	E4643 + [pIT3-TO-*p95.tum*$^{+}$]$_{186.1}$ + [pIT3-CL-186*cI*$^{+}$.***pR***$^{+}$.*pL*$^{+}$.*apI*$^{-}$.*cII*$^{-}$.*fil::lacZ*]$_{\lambda}$	
AI116	AI116	E4643 + [pIT3-TO-*p95.tum*$^{+}$]$_{186.1}$ + [pIT3-CL-186*cI*$^{+}$.***pR***$^{+}$.*goa8.pL*$^{+}$.*apI*$^{+}$.*cII*$^{+}$.*fil::lacZ*]$_{\lambda}$	**The *goa8* minimal prophage induction *pR* modules**. Each strain harbours an integrated *p95.tum*$^{+}$ UV-IM and a *goa8* ***pR***.*apI*$^{+/-}$.*cII*$^{+/-}$ LacZ reporter.
AI117	AI117	E4643 + [pIT3-TO-*p95.tum*$^{+}$]$_{186.1}$ + [pIT3-CL-186*cI*$^{+}$.***pR***$^{+}$.*goa8.pL*$^{+}$.*apI*$^{+}$.*cII*$^{-}$.*fil::lacZ*]$_{\lambda}$	
AI118	AI118	E4643 + [pIT3-TO-*p95.tum*$^{+}$]$_{186.1}$ + [pIT3-CL-186*cI*$^{+}$.***pR***$^{+}$.*goa8.pL*$^{+}$.*apI*$^{-}$.*cII*$^{+}$.*fil::lacZ*]$_{\lambda}$	
AI119	AI119	E4643 + [pIT3-TO-*p95.tum*$^{+}$]$_{186.1}$ + [pIT3-CL-186*cI*$^{+}$.***pR***$^{+}$.*goa8.pL*$^{+}$.*apI.cII*$^{-}$.*fil::lacZ*]$_{\lambda}$	

Glycerol	Name	Genotype	Description
AI184	AI184	E4643 + [pIT3-TO-*p95.tum*$^{+}$]$_{186.1}$ + [pIT3-CL-186*cI*$^{+}$.*pR*$^{+}$.***pL***$^{+}$.*apl*$^{+}$.*cII*$^{+}$.***pE***$^{+}$.*int::lacZ*]$_{\lambda}$	**The minimal prophage induction *pL/pE* modules**. Each strain harbours an integrated *p95.tum*$^{+}$ UV-IM and a ***pL/pE***.*apl*$^{+/-}$.*cII*$^{+/-/145}$ LacZ reporter. Strains AI184, AI185 and AI224 were used in the CII study (Chapter 4).
AI185	AI185	E4643 + [pIT3-TO-*p95.tum*$^{+}$] $_{186.1}$ + [pIT3-CL-186*cI*$^{+}$.*pR*$^{+}$.***pL***$^{+}$.*apl*$^{+}$.*cII*$^{-}$.***pE***$^{+}$.*int::lacZ*]$_{\lambda}$	
AI186	AI186	E4643 + [pIT3-TO-*p95.tum*$^{+}$]$_{186.1}$ + [pIT3-CL-186*cI*$^{+}$.*pR*$^{+}$.***pL***$^{+}$.*apl*$^{-}$.*cII*$^{+}$.***pE***$^{+}$.*int::lacZ*]$_{\lambda}$	
AI187	AI187	E4643 + [pIT3-TO-*p95.tum*$^{+}$]$_{186.1}$ + [pIT3-CL-186*cI*$^{+}$.*pR*$^{+}$.***pL***$^{+}$.*apl*$^{-}$.*cII*$^{-}$.***pE***$^{+}$.*int::lacZ*]$_{\lambda}$	
AI224	AI224	E4643 + [pIT3-TO-*p95.tum*$^{+}$]$_{186.1}$ + [pIT3-CL-186*cI*$^{+}$.*pR*$^{+}$.***pL***$^{+}$.*apl*$^{+}$.*cII*^{145}.***pE***$^{+}$.*int::lacZ*]$_{\lambda}$	
AI225	AI225	E4643 + [pIT3-TO-*p95.tum*$^{+}$]$_{186.1}$ + [pIT3-CL-186*cI*$^{+}$.*pR*$^{+}$.***pL***$^{+}$.*apl*$^{-}$.*cII*^{145}.***pE***$^{+}$.*int::lacZ*]$_{\lambda}$	
Bacterial strains used in the Tum study (Chapter 3)			
DL241	DL241	E4643 + [pIT3-CL-186*cI*$^{+}$.***pR***$^{+}$.*pL*$^{+}$.*apl*$^{+}$.*cII::lacZ*]$_{\lambda}$ + pλ*int*-186*cIts*	Strains contain an integrated *cI*$^{+}$ or *cIts*.***pR***$^{+}$.*apl*$^{+}$ LacZ reporter and a 186 integration helper plasmid. Strains made by Danna Lee (Shearwin laboratory).
DL242	DL242	E4643 + [pIT3-CL-186*cIts*.***pR***$^{+}$.*pL*$^{+}$.*apl*$^{+}$.*cII::lacZ*]$_{\lambda}$ + pλ*int*-186*cIts*	
AI188	AI188	E4643 + [pIT3-CL-186*cI*$^{+}$.***pR***$^{+}$.*pL*$^{+}$.*apl*$^{+}$.*cII::lacZ*]$_{\lambda}$ + pAH121	Strain contains an integrated *cI*$^{+}$.***pR***$^{+}$.*apl*$^{+}$ LacZ reporter and a φ21 CRIM helper plasmid. Strain made by Danna Lee (Shearwin laboratory).
AI194	AI194	E4643 + [pIT3-CL-186*cI*$^{+}$.***pR***$^{+}$.*pL*$^{+}$.*apl*$^{+}$.*cII::lacZ*]$_{\lambda}$ + [pIT4-KT.*cymR.T5-1.tum*$^{+}$]$_{\varphi 21}$	Strain contains an integrated *cI*$^{+}$.***pR***$^{+}$.*apl*$^{+}$ LacZ reporter and a *cymR.T5-1.tum*$^{+}$ CA-IM.
DL243	DL243	E4643 + [pIT3-CL-186*cI*$^{+}$.***pR***$^{+}$.*pL*$^{+}$.*apl*$^{+}$.*cII::lacZ*]$_{\lambda}$ + [pIT3-TO]$_{186.1}$	Strain contains an integrated *cI*$^{+}$.***pR***$^{+}$.*apl*$^{+}$ LacZ reporter and a blank pIT3-TO plasmid. Strain made by Danna Lee (Shearwin laboratory).
DL244	DL244	E4643 + [pIT3-CL-186*cI*$^{+}$.***pR***$^{+}$.*pL*$^{+}$.*apl*$^{+}$.*cII::lacZ*]$_{\lambda}$ + [pIT3-TO-*p95.tum*^{44G*}]$_{186.1}$	Strain contains an integrated *cI*$^{+}$.***pR***$^{+}$.*apl*$^{+}$ LacZ reporter and a *p95.tum*^{44G*} UV-IM. Strain made by Danna Lee (Shearwin laboratory).
DL245-II	DL245-II	E4643 + [pIT3-CL-186*cI*$^{+}$.***pR***$^{+}$.*pL*$^{+}$.*apl*$^{+}$.*cII::lacZ*]$_{\lambda}$ + [pIT3-TO-*p95. tum*$^{+}$]$_{186.1}$ + [pIT3-TO-*p95. tum*$^{+}$]$_{186.2}$	Strain contains an integrated *cI*$^{+}$.***pR***$^{+}$.*apl*$^{+}$ LacZ reporter and two copies of the *p95.tum*$^{+}$ UV-IM. Strain made by Danna Lee (Shearwin laboratory).
DL249	DL249	E4643 + [pIT3-CL-186*cIts*.***pR***$^{+}$.*pL*$^{+}$.*apl*$^{+}$.*cII::lacZ*]$_{\lambda}$ + [pIT3-TO]$_{186.1}$	Strain contains an integrated *cIts*.***pR***$^{+}$.*apl*$^{+}$ LacZ reporter and a blank pIT3-TO plasmid. Strain made by Danna Lee (Shearwin laboratory).
DL254	DL254	E4643 + [pIT3-CL-186*cI*$^{+}$.***pR***$^{+}$.*pL*$^{+}$.*apl*$^{+}$.*cII::lacZ*]$_{\lambda}$ + [pIT3-TO-*p95.tum*$^{4-5-}$]$_{186.1}$	Strain contains an integrated *cI*$^{+}$.***pR***$^{+}$.*apl*$^{+}$ LacZ reporter and a *p95.tum*$^{4-5-}$ UV-IM. Strain made by Danna Lee (Shearwin laboratory).
DL255	DL255	E4643 + [pIT3-CL-186*cI*$^{+}$.***pR***$^{+}$.*pL*$^{+}$.*apl*$^{+}$.*cII::lacZ*]$_{\lambda}$ + [pIT3-TO-*p95. tum*^{72K*}]$_{186.1}$	Strain contains an integrated *cI*$^{+}$.***pR***$^{+}$.*apl*$^{+}$ LacZ reporter and a *p95.tum*^{72K*} UV-IM. Strain made by Danna Lee (Shearwin laboratory).
DL257	DL257	E4643 + [pIT3-CL-186*cI*$^{+}$.***pR***$^{+}$.*pL*$^{+}$.*apl*$^{+}$.*cII::lacZ*]$_{\lambda}$ + [pIT3-TO-*P*$_{LlacO-1}$.*tum*$^{+}$]$_{186.1}$ + [pIT3-SH-*PlacI*^{q}.*lacI*]$_{HK022}$	Strain contains an integrated *cI*$^{+}$.***pR***$^{+}$.*apl*$^{+}$ LacZ reporter, the *P*$_{LlacO-1}$.*tum*$^{+}$ IM and the *PlacI*^{q}.*lacI* module. Strain made by Danna Lee (Shearwin laboratory).

Glycerol	Name	Genotype	Description
DL258	DL258	E4643 + [pIT3-CL]$_{\lambda}$ + [pIT3-TO-*p95.tum^{+}.lacZ*]$_{186.1}$ + [pIT3-SH-*PlacI^{q}.lacI*]$_{HK022}$	Strain contains an integrated blank pIT3-CL plasmid, the *p95.tum^{+}* LacZ reporter and the *PlacI^{q}.lacI* module. Strain made by Danna Lee (Shearwin laboratory).
AI194	AI194	E4643 + [pIT3-CL-186*cI^{+}.**pR**$^{+}$.pL^{+}.apl^{+}.cII::lacZ*]$_{\lambda}$ + [pIT4-KT-*cymR.T5-1.tum^{+}*]$_{\varphi21}$	Strain contains an integrated minimal *cI^{+}.**pR**.apl^{+}* LacZ reporter and a *cymR.T5-1.tum* CA-IM.
AI292	AI292	E4643 + [pIT4-KT-*cymR.T5-1.tum^{+}*]$_{\varphi21}$	Strain expresses CymR from an integrated *cymR.T5-1.tum^{+}* CA-IM.
HB59	HB59	E4643 + [186^{+}]$_{186.1}$	*E. coli* lysogen harbouring 186^{+} prophage. Strain made by Hannah Bonham (Shearwin laboratory).
AI238	AI238	E4643 + [186^{+}]$_{186.1}$ + pAH121	*E. coli* lysogen harbouring 186^{+} prophage and a φ21 CRIM helper plasmid.
AI239	AI239	E4643 + [186^{+}]$_{186.1}$ + [pIT4-KT-*cymR.T5-1*]$_{\varphi21}$	*E. coli* lysogen harbouring 186^{+} prophage and an integrated *cymR.T5-1* CA-IM.
AI241	AI241	E4643 + [186^{+}]$_{186.1}$ + [pIT4-KT-*cymR.T5-1*]$_{\varphi21}$ + pSIM6	*E. coli* lysogen harbouring 186^{+} prophage, an integrated *cymR.T5-1* CA-IM and the pSIM6 plasmid.
AI243	AI243	E4643 + [186$^{loxP.chlorR.loxP.T5\text{-}1.tum+}$]$_{186.1}$ + [pIT4-KT-*cymR.T5-1*]$_{\varphi21}$	*E. coli* lysogen harbouring 186$^{loxP.chlorR.loxP.T5\text{-}1.tum+}$ prophage and an integrated *cymR.T5-1* CA-IM.
AI244	AI244	E4643 + [186$^{loxP.T5\text{-}1.tum+}$]$_{186.1}$ + [pIT4-KT-*cymR.T5-1*]$_{\varphi21}$	*E. coli* lysogen harbouring 186$^{loxP.T5\text{-}1.tum+}$ prophage and an integrated *cymR.T5-1* CA-IM.
Bacterial strains used in the E. coli 186-WCB study (Chapter 5)			
TC015	NEB Turbo + pAccessory-*SF(gfp)-mCherry-dCas9(SG)*	*glnV44 thi-1 Δ(lac-proAB) galE15 galK16 R(zgb-210*::Tn*10*)Tet^{S} *endA1 fhuA2 Δ(mcrB-hsdSM)5*, ($r_{K}^{-}m_{K}^{-}$) F'[*traD36 proAB^{+} lacI^{q} lacZΔM15*] + pAccessory-*SF(gfp)-mCherry-dCas9* scrambled guide	A chemically competent K12 *E. coli* (NEB) strain used to propagate pAccessory-*SF(gfp)-mCherry-dCas9* scrambled guide (SG) plasmid. Strain made by Tristrom Cooke (Shearwin laboratory).
AI220	AI220	E4643 + [pIT4-KT-*cymR.T5-1.tum^{+}*]$_{\varphi21}$ + pINT-ts	Strain contains an integrated *cymR.T5-1.tum^{+}* CA-IM and a λ CRIM helper plasmid.
AI221	AI221	E4643 + [pIT4-KT-*cymR.T5-1.tum^{72K}*]$_{\varphi21}$ + pINT-ts	Strain contains an integrated *cymR.T5-1.tum^{72K}* CA-IM and a λ CRIM helper plasmid.
AI266	AI266	E4643 + [pIT4-KT-*vanR.pVan^{CC}.tum^{72K}*]$_{\varphi21}$ + pINT-ts	Strain contains an integrated *pVan.tum^{72K}* VA-IM and a λ CRIM helper plasmid.
AI267	AI267	E4643 + [pIT4-KT-*nahR.pSal^{TTC}.tum^{72K}*]$_{\varphi21}$ + pINT-ts	Strain contains an integrated *pSal.tum^{72K}* SA-IM and a λ CRIM helper plasmid.
AI194	AI194	E4643 + [pIT4-KT-*cymR.T5-1.tum^{+}*]$_{\varphi21}$ + [pIT3-CL-186*cI^{+}.**pR**$^{+}$.pL^{+}.apl^{+}. cII::lacZ*]$_{\lambda}$	Strain contains an integrated *cymR.T5-1.tum^{+}* CA-IM and a *cI^{+}.**pR**$^{+}$.apl^{+}* LacZ reporter.
AI195	AI195	E4643 + [pIT4-KT-*cymR.T5-1.tum^{72K}*]$_{\varphi21}$ + [pIT3-CL-186*cI^{+}.**pR**$^{+}$.pL^{+}.apl^{+}.cII::lacZ*]$_{\lambda}$	Strain contains an integrated *cymR.T5-1.tum^{72K}* CA-IM and a *cI^{+}.**pR**$^{+}$.apl^{+}* LacZ reporter.
AI199	AI199	E4643 + [pIT3-TO-*p95.tum^{72K}*]$_{186.1}$ + [pIT3-CL-186*cI^{+}.**pR**$^{+}$.pL^{+}.apl^{+}. cII::lacZ*]$_{\lambda}$	Strain contains an integrated *p95.tum^{72K}* UV-IM and a *cI^{+}.**pR**$^{+}$.apl^{+}* LacZ reporter. Strain made by Danna Lee (Shearwin laboratory).

Glycerol	Name	Genotype	Description
AI168	AI168	E4643 + [pIT3-TO-*p95.tum*$^{+}$]$_{186.1}$ + [pIT3-CL-186*cI*$^{+}$.***pR***$^{+}$.*pL*$^{+}$.*apI*$^{+}$. *tum*^{72K}. *fil::lacZ*]$_{\lambda}$	Strains contain an integrated *p95.tum*$^{+}$ UV-IM and a ***pR***$^{+}$.*apI*$^{+/-}$.*tum*$^{72K/-}$ LacZ reporter.
AI169	AI169	E4643 + [pIT3-TO-*p95.tum*$^{+}$]$_{186.1}$ + [pIT3-CL-186*cI*$^{+}$.***pR***$^{+}$.*pL*$^{+}$.*apI*$^{+}$. *tum*$^{-}$. *fil::lacZ*]$_{\lambda}$	
AI170	AI170	E4643 + [pIT3-TO-*p95.tum*$^{+}$]$_{186.1}$ + [pIT3-CL-186*cI*$^{+}$.***pR***$^{+}$.*pL*$^{+}$.*apI*$^{-}$.*tum*^{72K}. *fil::lacZ*]$_{\lambda}$	
AI171	AI171	E4643 + [pIT3-TO-*p95.tum*$^{+}$]$_{186.1}$ + [pIT3-CL-186*cI*$^{+}$.***pR***$^{+}$.*pL*$^{+}$.*apI*$^{-}$.*tum*$^{-}$. *fil::lacZ*]$_{\lambda}$	
AI172	AI172	E4643 + [pIT3-TO-*p95.tum*^{72K}]$_{186.1}$ + [pIT3-CL-186*cI*$^{+}$.***pR***$^{+}$.*pL*$^{+}$.*apI*$^{+}$. *tum*^{72K}.*fil::lacZ*]$_{\lambda}$	Strains contain an integrated *p95.tum*^{72K} UV-IM and a ***pR***$^{+}$.*apI*$^{+/-}$.*tum*$^{72K/-}$ LacZ reporter.
AI173	AI173	E4643 + [pIT3-TO-*p95.tum*^{72K}]$_{186.1}$ + [pIT3-CL-186*cI*$^{+}$.***pR***$^{+}$.*pL*$^{+}$.*apI*$^{+}$. *tum*$^{-}$.*fil::lacZ*]$_{\lambda}$	
AI174	AI174	E4643 + [pIT3-TO-*p95.tum*^{72K}]$_{186.1}$ + [pIT3-CL-186*cI*$^{+}$.***pR***$^{+}$.*pL*$^{+}$.*apI*$^{-}$. *tum*^{72K}.*fil::lacZ*]$_{\lambda}$	
AI175	AI175	E4643 + [pIT3-TO-*p95.tum*^{72K}]$_{186.1}$ + [pIT3-CL-186*cI*$^{+}$.***pR***$^{+}$.*pL*$^{+}$.*apI*$^{-}$. *tum*$^{-}$.*fil::lacZ*]$_{\lambda}$	
AI160	AI160	E4643 + [pIT3-TO-*p95.tum*^{72K}]$_{186.1}$ +pINT-ts	Strain contains an integrated *p95.tum*^{72K} UV-IM and a λ CRIM helper plasmid. Strain made by Danna Lee (Shearwin laboratory).
AI208	AI208	E4643 + [pIT3-TO-*p95.tum*$^{+}$]$_{186.1}$ + [pIT3-CL-186*cI*$^{+}$.***pR***$^{+}$.*pL*$^{+}$.*apI*$^{+}$. *tum*^{*72K}.*fil::lacZ*]$_{\lambda}$	Strain contains an integrated *p95.tum*$^{+}$ UV-IM and a ***pR***$^{+}$.*apI*$^{+}$. *tum*^{*72K} LacZ reporter.
AI209	AI209	E4643 + [pIT3-TO-*p95.tum*$^{+}$]$_{186.1}$ + [pIT3-CL-186*cI*$^{+}$.***pR***$^{+}$.*pL*$^{+}$.*apI*$^{-}$. *tum*^{*72K}.*fil::lacZ*]$_{\lambda}$	Strain contains an integrated *p95.tum*$^{+}$ UV-IM and a ***pR***$^{+}$.*apI*$^{-}$. *tum*^{*72K} LacZ reporter.
AI210	AI210	E4643 + [pIT3-TO-*p95.tum*^{72K}]$_{186.1}$ + [pIT3-CL-186*cI*$^{+}$.***pR***$^{+}$.*pL*$^{+}$.*apI*$^{+}$. *tum*^{*72K}.*fil::lacZ*]$_{\lambda}$	Strain contains an integrated *p95.tum*^{72K} UV-IM and a ***pR***$^{+}$.*apI*$^{+}$. *tum*^{*72K} LacZ reporter.
AI211	AI211	E4643 + [pIT3-TO-*p95.tum*^{72K}]$_{186.1}$ + [pIT3-CL-186*cI*$^{+}$.***pR***$^{+}$.*pL*$^{+}$.*apI*$^{-}$. *tum*^{*72K}.*fil::lacZ*]$_{\lambda}$	Strain contains an integrated ***pR***$^{+}$.*apI*$^{-}$.*tum*^{*72K} LacZ reporter and a *p95.tum*^{72K} UV-IM.
AI215	AI215	E4643 + [pIT4-KT-*cymR.T5-1. tum*$^{+}$]$_{\varphi 21}$ + [pIT3-CL-186*cI*$^{+}$.***pR***$^{+}$. *pL*$^{+}$. *apI*$^{-}$.*tum*^{*72K}.*fil::lacZ*]$_{\lambda}$	Strain contains an integrated *cymR.T5-1.tum*$^{+}$ CA-IM and a ***pR***$^{+}$. *apI*$^{-}$.*tum*^{*72K} LacZ reporter.
AI219	AI219	E4643 + [pIT4-KT-*cymR.T5-1. tum*^{72K}]$_{\varphi 21}$ + [pIT3-CL-186*cI*$^{+}$.***pR***$^{+}$. *pL*$^{+}$.*apI*$^{-}$.*tum*^{*72K}.*fil::lacZ*]$_{\lambda}$	Strain contains an integrated *cymR.T5-1.tum*^{72K} CA-IM and a ***pR***$^{+}$. *apI*$^{-}$.*tum*^{*72K} LacZ reporter.
AI226	AI226	E4643 + [pIT4-KT-*cymR.T5-1. tum*^{72K}]$_{\varphi 21}$ + [pIT3-CL-186*cI*$^{+}$.***pR***$^{+}$. *pL*$^{+}$.*apI*$^{-}$.*tum*$^{-}$.*fil::lacZ*]$_{\lambda}$	Strain contains an integrated *cymR.T5-1.tum*^{72K} CA-IM and a ***pR***$^{+}$. *apI*$^{-}$.*tum*$^{-}$ LacZ reporter.
AI233	AI233	E4643 + [pIT3-TO-*p95.tum*^{72K}]$_{186.1}$ + [pIT3-CL-186*cI*$^{+}$.***pR***$^{+}$.*pL*$^{+}$.*apI*$^{+}$. *tum*^{*72K}.*mCherry*]$_{\lambda}$	Strain contains an integrated *p95.tum*^{72K} UV-IM and a ***pR***$^{+}$.*apI*$^{+}$.*tum*^{*72K} MCherry reporter.
AI234	AI234	E4643 + [pIT3-TO-*p95.tum*^{72K}]$_{186.1}$ + [pIT3-CL-186*cI*$^{+}$.***pR***$^{+}$.*pL*$^{+}$.*apI*$^{-}$. *tum*$^{-}$.*mCherry*]$_{\lambda}$	Strain contains an integrated *p95.tum*^{72K} UV-IM and a ***pR***$^{+}$.*apI*$^{-}$.*tum*$^{-}$ MCherry reporter.
AI235	AI235	E4643 + [pIT4-KT-*cymR.T5-1. tum*^{72K}]$_{\varphi 21}$ + [pIT3-CL-186*cI*$^{+}$.***pR***$^{+}$. *pL*$^{+}$.*apI*$^{-}$.*tum*^{*72K}.*mCherry*]$_{\lambda}$	Strain contains an integrated *cymR.T5-1.tum*^{72K} CA-IM and a ***pR***$^{+}$. *apI*$^{-}$.*tum*^{*72K} MCherry reporter.
AI236	AI236	E4643 + [pIT4-KT-*cymR.T5-1. tum*^{72K}]$_{\varphi 21}$ + [pIT3-CL-186*cI*$^{+}$.***pR***$^{+}$. *pL*$^{+}$.*apI*$^{-}$.*tum*$^{-}$.*mCherry*]$_{\lambda}$	Strain contains an integrated *cymR.T5-1.tum*^{72K} CA-IM and a ***pR***$^{+}$.*apI*$^{-}$.*tum*$^{-}$ MCherry reporter.

Glycerol	Name	Genotype	Description
AI256	AI256	E4643 + [pIT4-KT-*vanR.pVan^{CC}.tum^{72K}*]$_{\varphi 21}$ + [pIT3-CL-186*cI*$^{+}$.***pR***$^{+}$.*pL*$^{+}$.*apl*$^{-}$.*tum*^{*72K}.*fil::lacZ*]$_{\lambda}$	Strain contains an integrated *pVan.tum^{72K}* VA-IM and a ***pR***$^{+}$*.apl*$^{-}$*.tum*^{*72K} LacZ reporter.
AI257	AI257	E4643 + [pIT4-KT-*vanR.pVan^{CC}.tum^{72K}*]$_{\varphi 21}$ + [pIT3-CL-186*cI*$^{+}$.***pR***$^{+}$.*pL*$^{+}$.*apl*$^{-}$.*tum*$^{-}$.*fil::lacZ*]$_{\lambda}$	Strain contains an integrated *pVan.tum^{72K}* VA-IM and a ***pR***$^{+}$*.apl*$^{-}$*.tum*$^{-}$ LacZ reporter.
AI258	AI258	E4643 + [pIT4-KT-*vanR.pVan^{CC}.tum^{72K}*]$_{\varphi 21}$ + [pIT3-CL-186*cI*$^{+}$.***pR***$^{+}$.*pL*$^{+}$.*apl*$^{-}$.*tum*^{*72K}.*mCherry*]$_{\lambda}$	Strain contains an integrated *pVan.tum^{72K}* VA-IM and a ***pR***$^{+}$*.apl*$^{-}$*.tum*^{*72K} MCherry reporter.
AI259	AI259	E4643 + [pIT4-KT-*vanR.pVan^{CC}.tum^{72K}*]$_{\varphi 21}$ + [pIT3-CL-186*cI*$^{+}$.***pR***$^{+}$.*pL*$^{+}$.*apl*$^{-}$.*tum*$^{-}$.*mCherry*]$_{\lambda}$	Strain contains an integrated *pVan.tum^{72K}* VA-IM and a ***pR***$^{+}$*.apl*$^{-}$*.tum*$^{-}$ MCherry reporter.
AI260	AI260	E4643 + [pIT4-KT-*nahR.pSal^{TTC}.tum^{72K}*]$_{\varphi 21}$ + [pIT3-CL-186*cI*$^{+}$.***pR***$^{+}$.*pL*$^{+}$.*apl*$^{-}$.*tum*^{*72K}.*fil::lacZ*]$_{\lambda}$	Strain contains an integrated *pSal.tum^{72K}* SA-IM and a ***pR***$^{+}$*.apl*$^{-}$*.tum*^{*72K} LacZ reporter.
AI261	AI261	E4643 + [pIT4-KT-*nahR.pSal^{TTC}.tum^{72K}*]$_{\varphi 21}$ + [pIT3-CL-186*cI*$^{+}$.***pR***$^{+}$.*pL*$^{+}$.*apl*$^{-}$.*tum*$^{-}$.*fil::lacZ*]$_{\lambda}$	Strain contains an integrated *pSal.tum^{72K}* SA-IM and a ***pR***$^{+}$*.apl*$^{-}$*.tum*$^{-}$ LacZ reporter.
AI262	AI262	E4643 + [pIT4-KT-*nahR.pSal^{TTC}.tum^{72K}*]$_{\varphi 21}$ + [pIT3-CL-186*cI*$^{+}$.***pR***$^{+}$.*pL*$^{+}$.*apl*$^{-}$.*tum*^{*72K}. *mCherry*]$_{\lambda}$	Strain contains an integrated *pSal.tum^{72K}* SA-IM and a ***pR***$^{+}$*.apl*$^{-}$*.tum*^{*72K} MCherry reporter.
AI263	AI263	E4643 + [pIT4-KT-*nahR.pSal^{TTC}.tum^{72K}*]$_{\varphi 21}$ + [pIT3-CL-186*cI*$^{+}$.***pR***$^{+}$.*pL*$^{+}$.*apl*$^{-}$.*tum*$^{-}$.*mCherry*]$_{\lambda}$	Strain contains an integrated *pSal.tum^{72K}* SA-IM and a ***pR***$^{+}$*.apl*$^{-}$*.tum*$^{-}$ MCherry reporter.
AI278	AI278	E4643 + [pIT3-CL-186*cI*$^{+}$.***pR***$^{+}$.*pL*$^{+}$.*cI-CTD.tum*^{*72K}.*mCherry*]$_{\lambda}$	Strain contains an integrated ***pR***$^{+}$*. cI-CTD.tum*^{*72K} MCherry reporter.
AI279	AI279	E4643 + [pIT3-CL-186*cI*$^{+}$.***pR***$^{+}$.*pL*$^{+}$.*cI-CTD.tum*$^{-}$.*mCherry*]$_{\lambda}$	Strain contains an integrated ***pR***$^{+}$*.cI-CTD.tum*$^{-}$ MCherry reporter.
AI286	AI286	E4643 + [pIT3-CL-186*cI*$^{+}$.***pR***$^{+}$.*pL*$^{+}$.*cI-CTD.tum*^{*72K}.*mCherry*]$_{\lambda}$ + pAH121	Strain contains an integrated ***pR***$^{+}$*.cI-CTD.tum*^{*72K} MCherry reporter and a φ21 CRIM helper plasmid.
AI287	AI287	E4643 + [pIT3-CL-186*cI*$^{+}$.***pR***$^{+}$.*pL*$^{+}$.*cI-CTD.tum*$^{-}$.*mCherry*]$_{\lambda}$ + pAH121	Strain contains an integrated ***pR***$^{+}$*.cI-CTD.tum*$^{-}$ MCherry reporter and a φ21 CRIM helper plasmid.
AI314	AI314	E4643 + [pIT3-CL-186*cI*$^{+}$.***pR***$^{+}$.*pL*$^{+}$.*cI-CTD.tum*^{*72K}.*mCherry*]$_{\lambda}$ + pAH69	Strain contains an integrated ***pR***$^{+}$*.cI-CTD.tum*^{*72K} MCherry reporter and a HK022 CRIM helper plasmid.
AI315	AI315	E4643 + [pIT3-CL-186*cI*$^{+}$.***pR***$^{+}$.*pL*$^{+}$.*cI-CTD.tum*$^{-}$.*mCherry*]$_{\lambda}$ + pAH69	Strain contains an integrated ***pR***$^{+}$*.cI-CTD.tum*$^{-}$ MCherry reporter and a HK022 CRIM helper plasmid.
AI316	AI316	E4643 + [pIT3-CL-186*cI*$^{+}$.***pR***$^{+}$.*pL*$^{+}$.*cI-CTD.tum*^{*72K}.*mCherry*]$_{\lambda}$ + [pIT4-*loxP*.KH.*pcymR^{C}.cI*$^{+}$.*PlacI^{q}.cymR^{AM}*]$_{HK022}$	Strain contains an integrated ***pR***$^{+}$*.cI-CTD.tum*^{*72K} MCherry reporter and the ^{1}CA^{OFF}-IM.
AI317	AI317	E4643 + [pIT3-CL-186*cI*$^{+}$.***pR***$^{+}$.*pL*$^{+}$.*cI-CTD.tum*$^{-}$.*mCherry*]$_{\lambda}$ + [pIT4-*loxP*.KH.*pcymR^{C}.cI*$^{+}$.*PlacI^{q}.cymR^{AM}*]$_{HK022}$	Strain contains an integrated ***pR***$^{+}$*.cI-CTD.tum*$^{-}$ MCherry reporter and the ^{1}CA^{OFF}-IM.
AI307	AI307	E4643 + [pIT3-CL-186*cI*$^{+}$.***pR***$^{+}$.*pL*$^{+}$.*cI-CTD.tum*^{*72K}.*mCherry*]$_{\lambda}$ + [pIT4-T-*vanR.pVan^{CC}.tum^{72K}*]$_{\varphi 21}$ + pAH69	Strain contains an integrated ***pR***$^{+}$*.cI-CTD.tum*^{*72K} MCherry reporter, a *pVan.tum^{72K}* VA-IM and a HK022 CRIM helper plasmid.
AI308	AI308	E4643 + [pIT3-CL-186*cI*$^{+}$.***pR***$^{+}$.*pL*$^{+}$.*cI-CTD.tum*$^{-}$.*mCherry*]$_{\lambda}$ + [pIT4-T-*vanR.pVan^{CC}.tum^{72K}*]$_{\varphi 21}$ + pAH69	Strain contains an integrated ***pR***$^{+}$*.cI-CTD.tum*$^{-}$ MCherry reporter, a *pVan.tum^{72K}* VA-IM and a HK022 CRIM helper plasmid.

Glycerol	Name	Genotype	Description
AI310	AI310	E4643 + [pIT3-CL-186*cI*$^{+}$.***pR***$^{+}$. *pL*$^{+}$*.cI-CTD.tum*$^{-}$*.fil::lacZ*]$_{\lambda}$ + [pIT4-*vanR. pVan*^{CC}*.tum*^{72K}]$_{\varphi21}$ + [pIT4-*loxP*.KH. *pcymR*^{C}*.cI*$^{+}$*. PlacI*^{q}*.cymR*^{AM}]$_{HK022}$	Strain contains an integrated ***pR***$^{+}$*.cI-CTD.tum*$^{-}$ LacZ reporter, a *pVan.tum*^{72K} VA-IM and the ^{1}CA^{OFF}-IM.
AI316	AI316	E4643 + [pIT3-CL-186*cI*$^{+}$.***pR***$^{+}$. *pL*$^{+}$*.cI-CTD.tum*^{*72K}*. mCherry*]$_{\lambda}$ + [pIT4-*loxP*.KH.*pcymR*^{C}.186*cI*$^{+}$*. PlacI*^{q}*.cymR*^{AM}]$_{HK022}$	Strain contains an integrated ***pR***$^{+}$*.cI-CTD.tum*^{*72K} MCherry reporter and the ^{1}CA^{OFF}-IM.
AI317	AI317	E4643 + [pIT3-CL-186*cI*$^{+}$.***pR***$^{+}$. *pL*$^{+}$*.cI-CTD.tum*$^{-}$*. mCherry*]$_{\lambda}$ + [pIT4-*loxP*.KH.*pcymR*^{C}.186*cI*$^{+}$*. PlacI*^{q}*.cymR*^{AM}]$_{HK022}$	Strain contains an integrated ***pR***$^{+}$*.cI-CTD.tum*$^{-}$ MCherry reporter and the ^{1}CA^{OFF}-IM.
AI311	AI311	E4643 + [pIT4-T-*vanR.pVan*^{CC}*. tum*^{72K}]$_{\varphi21}$ + [pIT4-KH-*pcymR*^{C}*.* 186*cI*$^{+}$*.PlacI*^{q}*.cymR*^{AM}]$_{HK022}$ + [pIT3-CL-186*cI*$^{+}$*.* ***pR***$^{+}$*.pL*$^{+}$*.cI-CTD. tum*^{*72K}*.mCherry*]$_{\lambda}$	Strain contains an integrated *pVan.tum*^{72K} VA-IM, the ^{1}CA^{OFF}-IM and a ***pR***$^{+}$*.cI-CTD.tum*^{*72K} MCherry reporter.
AI312	AI312	E4643 + [pIT4-T-*vanR.pVan*^{CC}*. tum*^{72K}]$_{\varphi21}$ + [pIT4-KH-*pcymR*^{C}*.* 186*cI*$^{+}$*.PlacI*^{q}*.cymR*^{AM}]$_{HK022}$ + [pIT3-CL-186*cI*$^{+}$*.* ***pR***$^{+}$*.pL*$^{+}$*.cI-CTD. tum*$^{-}$*.mCherry*]$_{\lambda}$	Strain contains an integrated *pVan.tum*^{72K} VA-IM, the ^{1}CA^{OFF}-IM and a ***pR***$^{+}$*.cI-CTD.tum*$^{-}$ MCherry reporter.
AI322	AI322	E4643 + [pIT4-T-*vanR.pVan*^{CC}*. tum*^{72K}]$_{\varphi21}$ + [pIT4-KH-*cymR.T5-6.* 186*cI*$^{+}$]$_{HK022}$ + [pIT3-CL-186*cI*$^{+}$*.* ***pR***$^{+}$*.pL*$^{+}$*.cI-CTD.tum*^{*72K}*.mCherry*]$_{\lambda}$	Strain contains an integrated *pVan.tum*^{72K} VA-IM, the ^{2}CA^{OFF}-IM and a ***pR***$^{+}$*.cI-CTD.tum*^{*72K} MCherry reporter.
AI323	AI323	E4643 + [pIT4-T-*vanR.pVan*^{CC}*. tum*^{72K}]$_{\varphi21}$ + [pIT4-KH-*cymR.T5-6.* 186*cI*$^{+}$]$_{HK022}$ + [pIT3-CL-186*cI*$^{+}$*.* ***pR***$^{+}$*.pL*$^{+}$*.cI-CTD.tum*$^{-}$*.mCherry*]$_{\lambda}$	Strain contains an integrated *pVan.tum*^{72K} VA-IM, the ^{2}CA^{OFF}-IM and a ***pR***$^{+}$*.cI-CTD.tum*$^{-}$ MCherry reporter.
AI326	AI326	E4643 + [pIT3-CL-186*cI*$^{+}$.***pR***$^{+}$. *pL*$^{+}$*. apI*$^{-}$*.tum*^{*72K}*.mCherry*]$_{\lambda}$ + [pIT4-T-*vanR. pVan*^{CC}*.tum*^{72K}]$_{\varphi21}$ + [pIT4-KH-*cymR.T5-6.* 186*cI*$^{+}$]$_{HK022}$	Strain harbours an integrated ***pR***$^{+}$*. apI*$^{-}$*.tum*^{*72K} MCherry reporter, a *pVan.tum*^{72K} VA-IM and the ^{2}CA^{OFF}-IM.

7.1.2 186 bacteriophage strains

186^{+}: wildtype 186 bacteriophage

186$^{p.cym}$: cumic acid (CA) inducible 186 bacteriophage

7.1.3 Plasmids

Table 7.10 lists the plasmids previously made and constructed during the course of this thesis. Unless otherwise specified, *pR*$^{-}$ denotes a -35 inactive 186 *pR* lytic promoter (site changed from TTTACT to CTCGAG) and *apI*$^{-}$ and *cII*$^{-}$ genes encode inactive helix-turn-helix (HTH) minus proteins, where the *apI* HTH was changed from TGAACGCACCGCCTA to CGCGAAACCGCCTACCAG and the *cII* HTH was changed from TGTTCAAA to TGAATCAA. These changes are designed to eliminate DNA binding activity by altering key DNA binding residues within the HTH. The *cII*^{145} gene encodes a stabilised, active CII145 mutant, truncated to its first 145 residues, removing its protease sensitive CTD. *tum*^{72K} encodes the hyperactive Tum^{72K} mutant, truncated to its first 72 residues, removing most of its DinI-like CTD. The *tum*$^{-}$ gene encodes an inactive Tum^{72K-} mutant, due to the presence of the inactivating ΔD30G mutation.

In respect to pSIM6 and the CRIM helper plasmids, λ*cI857* encodes a temperature sensitive λCIts immunity repressor (permissive temperature 30°C). When referring to a mutant 186CI expression module (*lacZ*$^{+/*}$), *cI* expression has been altered by mutating the *pL* -10 or -35 site to enhance or reduce *cI* expression. All 186CI expression modules and LacZ reporters (wildtype and mutant) encode an intact 186CI immunity repressor. Lastly, when integrating into the 186 *att* sites, single integration at the primary 186 *attB1* site was the preferred and consequently the selected outcome.

Table 7.10: Plasmids previously made and constructed throughout the course of this thesis.

Name	Origin	Resist.	Description
pINT-ts	R101-ts	Amp	CRIM helper plasmid for integration at λ *attB* site (Haldimann and Wanner, 2001). Plasmid encodes λ*int* driven by λ*pR* repressed by λ*cI857* (also borne by this plasmid) at 30°C. Strains with plasmid are cultured at 30°C due to *ori*R101-ts.
pλ*int*-186*cIts*	R101-ts	Amp	Integration helper plasmid for integration at λ *attB* site. Plasmid encodes λ*int* driven by 186*pR* repressed by 186*cIts* (also borne by this plasmid) at 30°C. Strains with plasmid are cultured at 30°C due to *ori*R101-ts. Plasmid constructed by Ian Dodd (Shearwin laboratory).
pAH121	R101-ts	Amp	CRIM helper plasmid for integration at φ21 *attB* site (Haldimann and Wanner, 2001). Plasmid encodes φ21*int* driven by λ*pR* repressed by λ*cI857* (also borne by this plasmid) at 30°C. Strains with plasmid are cultured at 30°C due to *ori*R101-ts.
p186*int*-λ*cIts*	R101-ts	Amp	Integration helper plasmid for integration at 186 *attB*1 and *attB*2. Plasmid encodes 186*int* driven by λ*pR* repressed by λ*cI857* (also borne by this plasmid) at 30°C. Strains with plasmid are cultured at 30°C due to *ori*R101-ts. Plasmid constructed by Ian Dodd (Shearwin laboratory).
pAH69	R101-ts	Amp	CRIM helper plasmid for integration at HK022 *attB* site (Haldimann and Wanner, 2001). Plasmid encodes HK022*int* driven by λ*pR* repressed by λ*cI857* (also borne by this plasmid) at 30°C. Strains with plasmid are cultured at 30°C due to *ori*R101-ts.
pUCIDT-186*cI*$^{+}$.*pR*$^{-}$.*pL*$^{+}$.*apl*$^{-}$	pMB1	Amp	Original source of the wildtype 186CI expression module synthesised by Integrated DNA Technologies (IDT) and cloned into pUCIDT vector.
pIT3-CL-*lac*Ztrimfuse	*R6Kγ*	Chlor	Integrating vector for protein expression constructs and LacZ reporters. This vector has a truncated *lacZ* gene enabling the fusion of a foreign gene to the ninth codon of *lacZ*.
pIT3-CL	*R6Kγ*	Chlor	Blank integrating vector for protein expression constructs and genetic switches.
pIT3-CL-186*cI*$^{+}$.*pR*$^{-}$.***pL***$^{WT,\ M1,2,3,4,5,6,7,8,9,10,11}$.*apl*$^{-}$.*int::lacZ*	*R6Kγ*	Chlor	The wildtype and 11 mutant 186CI *pL* LacZ reporters propagated in E4644 and λ integrated into E4643 using the CRIM system (Haldimann and Wanner, 2001).
pIT3-CL-186*cI*$^{+}$.*pR*$^{-}$.***pL***$^{WT,\ M1,2,3,7,8,9}$.*apl*$^{-}$	*R6Kγ*	Chlor	The wildtype and seven selected mutant 186CI expression modules propagated in E4644 and λ integrated into E4643 using the CRIM system (Haldimann and Wanner, 2001).

Name	Origin	Resist.	Description
pIT3-KT-I52002	*R6Kγ*	Kan	Digested with *Nhe*I and *Psp*OMI to generate the *kan*^{R}*.oriR6Kγ.attP*^{φ21} fragment to assemble the pIT3-KT-*lacZ*trimfuse integration plasmid. Propagated in *ccdB* tolerant strain DB3.1.
pIT3-KT-*lacZ*trimfuse	*R6Kγ*	Kan	Integrating vector for LacZ reporters. Harbours a truncated *lacZ* gene enabling the fusion of a foreign gene to the ninth codon of *lacZ*.
Reporter 1: pIT3-KT-186*cI*$^{-}$*. pR*$^{+}$***.pL***$^{+}$*.apI*$^{-}$*.int::lacZ*	*R6Kγ*	Kan	The six 186 *pL* and *pR goa8*$^{+/-}$ LacZ reporters propagated in E4644 and φ21 integrated into E4643 using the CRIM system (Haldimann and Wanner, 2001). *pR* reporters have a *cII::lacZ* fusion reporter, *pL* reporters have an *int::lacZ* fusion reporter.
Reporter 2: pIT3-KT-186*cI*$^{-}$*. pR*$^{+}$*.goa8.***pL***$^{+}$*.apI*$^{-}$*.int::lacZ*			
Reporter 3: pIT3-KT-186*cI*$^{-}$*.* ***pR***$^{+}$*.pL*$^{+}$*.apI*$^{-}$*.cII::lacZ*			
Reporter 4: pIT3-KT-186*cI*$^{-}$*.* ***pR***$^{+}$*.goa8.pL*$^{+}$*.apI*$^{-}$*.cII::lacZ*			
Reporter 5: pIT3-KT-186*cI*$^{-}$*. pR*$^{-}$*. **pL***$^{+}$*.apI*$^{-}$*.int::lacZ*			
Reporter 6: pIT3-KT-186*cI*$^{-}$*. pR*$^{-}$*. goa8.***pL***$^{+}$*.apI*$^{-}$*.int::lacZ*			
pIT3-TO-*p95.tum*$^{+}$	R6Kγ	Tet	Contains the wildtype *p95.tum*$^{+}$ UV-IM. Propagated in E4644 and integrated into E4643 186 *attB1* site using the CRIM system (Haldimann and Wanner, 2001). Plasmid constructed by Danna Lee (Shearwin laboratory).
pIT3-TO-*p95.tum*^{72K}	R6Kγ	Tet	Contains the modified *p95.tum*^{72K} UV-IM. Propagated in E4644 and integrated into E4643 186 *attB1* site using the CRIM system (Haldimann and Wanner, 2001). Plasmid constructed by Danna Lee (Shearwin laboratory).
pIT3-CL-186*cI*$^{+}$***.pR***$^{+}$*.pL*$^{+}$*.apI*$^{+}$*. cII::lacZ*	R6Kγ	Chlor	Contains the *cI*$^{+}$ or *cIts* ***pR***$^{+}$*.apI*$^{+}$ LacZ reporter. Plasmids constructed by Danna Lee (Shearwin laboratory).
pIT3-CL-186*cIts.***pR***$^{+}$*.pL*$^{+}$*.apI*$^{+}$*. cII::lacZ*			
pIT3-CL-186*cI*$^{+}$***.pR***$^{+}$*.pL*$^{+}$*.apI*$^{-}$*. cII::lacZ*	R6Kγ	Chlor	Contains the *cI*$^{+}$***.pR***$^{+}$*.apI*$^{-}$*.* LacZ reporter. Plasmid constructed by Danna Lee (Shearwin laboratory).
pIT3-CL-186*cI*$^{+}$***.pR***$^{+}$*.pL*$^{+}$*.apI*$^{+}$*. cII*$^{+}$*. fiI::lacZ*	R6Kγ	Chlor	**The wildtype minimal prophage induction *pR* modules**. Propagated in E4644 and λ integrated into E4643 DL47 using the CRIM system (Haldimann and Wanner, 2001). The ***pR***$^{+}$*.apI*$^{+}$*.cII*$^{+/-}$ LacZ reporters were originally constructed by Ian Murchland (Shearwin laboratory) and used as PCR template to generate the *cII*$^{+}$ and *cII*$^{-}$ gene fragments for assembly of the ***pR***$^{+}$*.apI*$^{-}$*.cII*$^{+/-}$ LacZ reporters.
pIT3-CL-186*cI*$^{+}$***.pR***$^{+}$*.pL*$^{+}$*.apI*$^{+}$*. cII*$^{-}$*.fiI::lacZ*			
pIT3-CL-186*cI*$^{+}$***.pR***$^{+}$*.pL*$^{+}$*.apI*$^{-}$*. cII*$^{+}$*.fiI::lacZ*			
pIT3-CL-186*cI*$^{+}$***.pR***$^{+}$*.pL*$^{+}$*.apI*$^{-}$*. cII*$^{-}$*.fiI::lacZ*			
pIT3-CL-186*cI*$^{+}$***.pR***$^{+}$*.goa8.pL*$^{+}$*. apI*$^{+}$*.cII*$^{+}$*.fiI::lacZ*	R6Kγ	Chlor	**The *goa8* minimal prophage induction *pR* modules.** Propagated in E4644 and λ integrated into E4643 DL47 using the CRIM system (Haldimann and Wanner, 2001).
pIT3-CL-186*cI*$^{+}$***.pR***$^{+}$*.goa8.pL*$^{+}$*. apI*$^{+}$*.cII*$^{-}$*.fiI::lacZ*			
pIT3-CL-186*cI*$^{+}$***.pR***$^{+}$*.goa8.pL*$^{+}$*. apI*$^{-}$*.cII*$^{+}$*.fiI::lacZ*			
pIT3-CL-186*cI*$^{+}$***.pR***$^{+}$*.goa8.pL*$^{+}$*. apI*$^{-}$*.cII*$^{-}$*.fiI::lacZ*			
pIT3-CL-186*cI*$^{+}$*.pR*$^{+}$***.pL***$^{+}$*.apI*$^{+}$*. int::lacZ*	R6Kγ	Chlor	**The preliminary wildtype minimal prophage induction *pL/pE* modules**. Used as PCR template to generate *apI*$^{+/-}$ gene fragments for assembly of the ***pL***$^{+}$***/pE***$^{+}$*.apI*$^{+/-}$*.cII*$^{+/-}$ LacZ reporters. Propagated in E4644 and λ integrated into E4643 DL47 using the CRIM system (Haldimann and Wanner, 2001).
pIT3-CL-186*cI*$^{+}$*.pR*$^{+}$***.pL***$^{+}$*.apI*$^{-}$*.int::lacZ*			

Name	Origin	Resist.	Description
pIT3-CL-186*cI*$^{+}$*.pR*$^{+}$***.pL***$^{+}$*.apl*$^{+}$*. cII*$^{+}$***.pE***$^{+}$*.int::lacZ* pIT3-CL-186*cI*$^{+}$*.pR*$^{+}$***.pL***$^{+}$*.apl*$^{+}$*. cII*$^{-}$***.pE***$^{+}$*.int::lacZ* pIT3-CL-186*cI*$^{+}$*.pR*$^{+}$***.pL***$^{+}$*.apl*$^{-}$*.cII*$^{+}$***.pE***$^{+}$*.int::lacZ* pIT3-CL-186*cI*$^{+}$*.pR*$^{+}$***.pL***$^{+}$*.apl*$^{-}$*.cII*$^{-}$***.pE***$^{+}$*.int::lacZ* pIT3-CL-186*cI*$^{+}$*.pR*$^{+}$***.pL***$^{+}$*.apl*$^{+}$*. cII*^{145}***.pE***$^{+}$*.int::lacZ* pIT3-CL-186*cI*$^{+}$*.pR*$^{+}$***.pL***$^{+}$*.apl*$^{-}$*. cII*^{145} ***pE***$^{+}$*.int::lacZ*	R6Kγ	Chlor	**The minimal prophage induction *pL/pE* modules**. The ***pL***$^{+}$***/pE***$^{+}$*.apl*$^{+/-}$*.cII*$^{+}$ LacZ reporters were digested with *Sap*I and *Bam*HI-HF to assemble the ***pL***$^{+}$***/pE***$^{+}$*.apl*$^{+/-}$*.cII*^{145} LacZ reporters. The *cII*^{145} gene fragment was generated via PCR of the ***pL***$^{+}$***/pE***$^{+}$*.apl*$^{+}$*.cII*$^{+}$ LacZ reporter using primers 2619 and 2620. Reporters propagated in E4644 and λ integrated into E4643 DL47 using the CRIM system (Haldimann and Wanner, 2001).
pIT3-CL-186*cI*$^{+}$***.pR***$^{+}$*.pL*$^{+}$*.apl*$^{+}$*. tum*^{72K}*.fil::lacZ* pIT3-CL-186*cI*$^{+}$***.pR***$^{+}$*.pL*$^{+}$*.apl*$^{+}$*. tum*$^{-}$*.fil::lacZ* pIT3-CL-186*cI*$^{+}$***.pR***$^{+}$*.pL*$^{+}$*.apl*$^{-}$*.tum*^{72K}*. fil::lacZ* pIT3-CL-186*cI*$^{+}$***.pR***$^{+}$*.pL*$^{+}$*.apl*$^{-}$*.tum*$^{-}$*. fil::lacZ*	R6Kγ	Chlor	**The initial 186-WCB *pR*.*apl*$^{+/-}$*.tum*$^{72K/-}$ LacZ reporters**. Propagated in E4644 and λ integrated into E4643 DL47 and AI160 using the CRIM system (Haldimann and Wanner, 2001).
pIT3-CL-186*cI*$^{+}$***.pR***$^{+}$*.pL*$^{+}$*.apl*$^{+}$*. tum*^{72K}.fil::lacZ* pIT3-CL-186*cI*$^{+}$***.pR***$^{+}$*.pL*$^{+}$*.apl*$^{-}$*.tum*^{72K}. fil::lacZ*	R6Kγ	Chlor	**The optimised 186-WCB *pR*.*apl*$^{+/-}$*.tum*^{72K}*.LacZ reporters**. Each reporter features an enhanced *tum*^{72K} RBS. Propagated in E4644 and λ integrated into E4643 DL47 and A160 using the CRIM system (Haldimann and Wanner, 2001).
pSB1A2-BBa_I746908-*SF(gfp)*	ColE1	Amp	Harbours the *superfolder(gfp)* gene driven by *pBAD* promoter controlled by AraC (also borne by this plasmid). Used as PCR template to generate the *SF(gfp)* gene fragment for assembly of the fluorescent 186-WCB reporter. Propagated in *E. coli* DH5α-Z1.
pAccessory-*SF(gfp)-mCherry-dCas9* scrambled guide	pSC101	Spec	Harbours the *mCherry* gene driven by *pAH2841* promoter. Used as PCR template to generate the *mCherry* gene fragment for assembly of the fluorescent 186-WCB reporter. Propagated in *E. coli* NEB Turbo. Plasmid constructed by Tristrom Cooke (Shearwin laboratory).
pIT3-CL-186*cI*$^{+}$***.pR***$^{+}$*.pL*$^{+}$*.apl*$^{-}$*.tum*^{72K}. mCherry* pIT3-CL-186*cI*$^{+}$***.pR***$^{+}$*.pL*$^{+}$*.apl*$^{-}$*. tum*$^{-}$*. mCherry*	R6Kγ	Chlor	**The fluorescent 186-WCB *pR*.*apl*$^{-}$*.tum*$^{72K/-}$ reporters**. The *lacZ* gene was replaced with *mCherry* and the *superfolder-gfp* cloned 28bp downstream of 186 *cI*. Propagated in E4644 and λ integrated into E4643 using the CRIM system (Haldimann and Wanner, 2001).
pIT3-CL-186*cI*$^{+}$***.pR***$^{+}$*.pL*$^{+}$*. cI-CTD.tum*^{72K}.fil::lacZ* pIT3-CL-186*cI*$^{+}$***.pR***$^{+}$*.pL*$^{+}$*. cI-CTD.tum*$^{-}$*.fil::lacZ* pIT3-CL-186*cI*$^{+}$***.pR***$^{+}$*.pL*$^{+}$*. cI-CTD.tum*^{72K}.mCherry* pIT3-CL-186*cI*$^{+}$***.pR***$^{+}$*.pL*$^{+}$*. cI-CTD.tum*$^{-}$*.mCherry*	R6Kγ	Chlor	**The 186-WCB *pR*.*cI-CTD.tum*$^{72K/-}$ reporters**. Optimised for improved stability by replacing *apl* with the *cI-CTD*. Propagated in E4644 and λ integrated into E4643 using the CRIM system (Haldimann and Wanner, 2001).
pIT4-KT-*cymR.T5-1*	R6Kγ	Kan	Contains the blank *cymR.T5-1* CA-IM. Propagated in E4644 and λ integrated into E4643 using the CRIM system (Haldimann and Wanner, 2001). Digested with *Spe*I to assemble the pIT4-KT-*cymR.T5-1.tum*$^{+/72K}$ IMs. Plasmid constructed by Ian Dodd (Shearwin laboratory).

Name	Origin	Resist.	Description
pIT4-KT-*cymR.T5-6.φK02CB*	R6Kγ	Kan	Contains the *cymR.T5-6.φK02CB* CA-IM. Propagated in E4644 and digested with *Spe*I and *Nar*I to assemble the ^{2}CA^{OFF}-IM. Plasmid constructed by Ian Dodd (Shearwin laboratory).
pIT4-KT-*cymR.T5-1.* 186*cI*$^{+}$	R6Kγ	Kan	Contains the c*ymR.T5-1.cI*$^{+}$ CA-IM, with *T5-1* promoter, -10 site mutated from TATAAT to AATAAT to reduce leaky expression of 186 *cI*. Propagated in E4644 and φ21 integrated into E4643 using the CRIM system (Haldimann and Wanner, 2001). Used as PCR template to generate the *cI*$^{+}$ gene fragment for assembly of the *pcymR^{C}.cI*$^{+}$*.cymR^{AM}* CA-IM. Plasmid constructed by Ian Dodd (Shearwin laboratory).
pIT4-KT-*cymR.T5-1.tum*$^{+}$	R6Kγ	Kan	Contains the c*ymR.T5-1.tum*$^{+}$ CA-IM. Propagated in E4644 and φ21integrated into E4643 using the CRIM system (Haldimann and Wanner, 2001).
pIT4-KT-*cymR.T5-1.tum^{72K}*	R6Kγ	Kan	Contains the c*ymR.T5-1.tum^{72K}* CA-IM. Digested with *Kpn*I and *Xma*I to assemble the *vanR.pVan^{CC}.tum^{72K}* and *nahR.pSal^{TTC}.tum^{72K}* IMs. Propagated in E4644 and φ21 integrated into E4643 using the CRIM system (Haldimann and Wanner, 2001).
pIT4-KT-*vanR.pVan^{CC}.tum^{72K}*	R6Kγ	Kan	Contains the *pVan.tum^{72K}* VA-IM. Propagated in E4644 and φ21 integrated into E4643 using the CRIM system (Haldimann and Wanner, 2001).
IT4-KT-*nahR.pSal^{TTC}.tum^{72K}*	R6Kγ	Kan	Contains the *pSal.tum^{72K}* SA-IM. Propagated in E4644 and φ21 integrated into E4643 using the CRIM system (Haldimann and Wanner, 2001).
pIT4-*loxP*-KH-*pcymR^{C}.* 186*cI*$^{+}$*.PlacI^{q}.cymR^{AM}*	R6Kγ	Kan	Contains the ^{1}CA^{OFF}-IM. Propagated in E4644 and HK022 integrated into E4643 using the CRIM system (Haldimann and Wanner, 2001).
pIT4-KH-*cymR.T5-6.* 186*cI*$^{+}$	R6Kγ	Kan	Contains the ^{2}CA^{OFF}-IM with *T5-6* promoter, -10 site mutated from TATAAT to GATAAT to prevent leaky expression of 186 *cI*. Propagated in E4644 and HK022 integrated into E4643 using the CRIM system (Haldimann and Wanner, 2001).
pIT4-*frt*-KT	R6Kγ	Kan	Standard cloning vector for the CA, VA and SA *tum^{72K}* IMs. The *kan^{R}* selective marker is *cis* flanked with two *frt* sites allowing for its deletion via the FLP(*frt*) recombineering system.
pIT4-*loxP*-KH-*pcymR^{C}.PlacI^{q}.cymR^{AM}*	R6Kγ	Kan	Standard cloning vector for the ^{1}CA^{OFF}-IM.The *kan^{R}* selective marker is *cis* flanked with two *loxP* sites allowing for its deletion via the Cre-*loxP* recombineering system.
pSIM6	pSC101 *re*pA-ts	Amp	Source of the λ Red phage recombineering system, where λ*red gam, exo, beta* genes are driven by native λ*pL* promoter, which is induced by heat-shock using λ*cI857* (Sharan et al., 2009). Plasmid used for recombineering AI239 to AI243 lysogen
pE-Flp	R6Kγ-ts	Amp	Source of the *Saccharomyces cerevisiae* flippase recombinase constitutively expressed from P2 phage *pE* promoter. Propagated in *E. coli* DH5α P2 lysogen (St-Pierre et al., 2013).
pE-Cre	R6Kγ-ts	Amp	Source of the P1 bacteriophage cyclization recombination (Cre) recombinase constitutively expressed from P2 phage *pE* promoter. Propagated in *E. coli* DH5α P2 lysogen. Plasmid constructed by Andrew Hao (Shearwin laboratory).

7.1.4 Oligonucleotides and gBlock gene fragments

Table 7.11 and Table 7.12 list the primers and gBlock gene fragments used throughout the course of this thesis respectively. Primers were prepared by dissolving the dried-down DNA to 100mM in sterile H_2O and stored at -20°C. gBlock gene fragments were reconstituted to 25-50ng/µL in Tris-EDTA buffer, heated at 50°C for 20mins and stored at -20°C. All primers and gBlocks were synthesised by Integrated DNA Technologies (IDT).

Table 7.11: Primers used during the course of this thesis. Sequences are written 5' to 3', capitalisation indicates the intended priming region and lowercase indicates the 'tail' region required for Gibson isothermal assembly or overlapping PCR. Primers have been categorised according to their application or area of study.

Name	Sequence	Description
Standard primers used for screening and Sanger sequencing		
148	ggaattcCATGGGGTCGATGGTTGC	Used for screening and sequencing clones harbouring a CA-IM. Primes 14bp downstream of 186*tum* gene.
281	TGAAAATCAAACATGTTGCATCCT	Used for screening and sequencing clones. Primes across RBS and start of 186*cII.*
301	CGCCAGGGTTTTCCCAGTCACGAC	Used for screening and sequencing clones harbouring pIT3 vectors.
326	CCAGCGCCCGTTGCACCACAG	Used for screening and sequencing clones harbouring pIT3-*lacZ*trimfuse vectors. Primes within *lacZ*.
329	TAAACTGCCAGGAATTGGGGATC	Used for screening and sequencing clones.
441	GGATCGGAATTCGAGCTCG	Used for screening and sequencing clones.
789	CTCAAAAAATACGCCCGGTAGTG	Used for screening and sequencing clones, primes 33bp upstream of *chlor*^{R} ATG.
837	GCCTGTCAGTTTAGGTTAGGCG	Used for screening and sequencing clones, primes across rrnBTR terminator in pIT3/4 vectors.
948	GCAGACAGTTTTATTGTTC	Used for screening and sequencing clones.
1001	GACGCCCGCCATAAACTGCCAGGAA TTGGGGATCGGAATT	Used for screening and sequencing clones, primes across rrnBT1 terminator in pIT3/4 vectors.
1202	GATGGGCGCATCGTAACCG	Used for screening and sequencing the E4643 (186$^{p.cym}$) lysogen. Primes within *lacZ*.
1350	CGGACCATCTCATCTGTAAC	Used for screening and sequencing the E4643 (186$^{p.cym}$) lysogen. Primes within *kan*^{R}.
1535	TACGAGCCTTATGCATGCCC	Used for screening and sequencing the E4643 (186$^{p.cym}$) lysogen. Primes within *proA* promoter.
1963	AAGCGATCCACCGATACTCG	Used for screening and sequencing the E4643 (186$^{p.cym}$) lysogen. Primes within 186 *A* gene.
2037	CATGATCACCATAGATCCTTTCTCC	Used for screening and sequencing clones harbouring a CA-IM. Primes at start of *cymR* gene.
Primers used to verify chromosomal integration		
Underlined primers were designed to create an optimised primer set that clearly differentiates between single, multiple and no integration events.		
465	GGGAATTAATTCTTGAAGACG	P3 primer combined with primers 467, 871, 872 or 2404 to screen for single integration at the φ21 *attB* site.
466	GGCATCACGGCAATATAC	P1 Haldimann and Wanner (2001) CRIM primer combined with primers 467, 468 and 469 to screen for single integration at the λ *attB* site.
467	ACTTAACGGCTGACATGG	P2 Haldimann and Wanner (2001) CRIM primer used to screen for single integration at the 186, λ, φ21 and HK022 *attB* sites.
468	ACGAGTATCGAGATGGCA	P3 Haldimann and Wanner (2001) CRIM primer used to screen for single integration at the 186, λ and HK022 *attB* sites.

Name	Sequence	Description
469	TCTGGTCTGGTAGCAATG	P4 Haldimann and Wanner (2001) CRIM primer used to screen for single integration at the λ *attB* site.
871	ATCGCCTGTATGAACCTG	P1 Haldimann and Wanner (2001) CRIM primer combined with primers 465, 467, 872 or 2404 to screen for single integration at the φ21 *attB* site.
872	TAGAACTACCACCTGACC	P4 Haldimann and Wanner (2001) CRIM primer combined with primers 465, 467, 871 to screen for single integration at the φ21 *attB* site.
2404	GCAGCCTAACAAAAAACAACG	Alternate P4 primer combined with primers 465, 467, 871 to screen for single integration at the φ21 *attB* site.
585	GGAATCAATGCCTGAGTG	P1 Haldimann and Wanner (2001) CRIM primer combined with primers 467, 468 and 586 to screen for single integration at the HK022 *attB* site.
586	GGCATCAACAGCACATTC	P4 Haldimann and Wanner (2001) CRIM primer combined with primers 467, 468 and 585 to screen for single integration at the HK022 *attB* site.
597	GCTCAGCTAGCTATGCACTCCTCAG GAAAGTGG	P3 186 internal primer used to screen for single integration at both 186 *attB1* and *attB2* sites.
598	GCTCATCCATGGGCGATGGTTCTGA GTAACAGATAATAGAATGG	P2 186 internal primer used to screen for single integration at both 186 *attB1* and *attB2* sites.
610	CTCATTCGAAACCACCCACCG	P1 St-Pierre et al. (2013) primer combined with primers 597, 598 and 611 to screen for single integration at the primary 186 *attB1* site.
611	GATCATCATGTTTATTGCGTGG	P4 St-Pierre et al. (2013) primer combined with primers 597, 598 and 610 to screen for single integration at the primary 186 *attB1* site.
1103	CCCTGGAGCCAAAATATCC	P4 St-Pierre et al. (2013) primer combined with primers 597, 598 and 1104 to screen for single integration at the secondary 186 *attB2* site.
1104	TCCGGAATGCCTGCATTG	P1 St-Pierre et al. (2013) primer combined with primers 597, 598 and 1103 to screen for single integration at the secondary 186 *attB2* site.
Primers used in the goa8, CI and Apl study (Chapter 2)		
The 186CI *pL* LacZ reporters: The wildtype CI *pL* LacZ reporter was 2-fragment assembled using the (1) *Bam*HI and *Acc*65I digested pIT3-CL-*lacZ*trimfuse vector and the (2) $cI^{+}.pR^{-}.pL^{+}.apl^{-}$ PCR amplicon sourced from pUCIDT-$cI^{+}.pR^{-}.pL^{+}.apl^{-}$ using primers 1372 and 1606. Mutations at *pL* were introduced by performing site-specific mutagenesis with mutagenic primers designed to introduce mutations at the *pL* -10 or -35 site. The mutant CI *pL* LacZ reporters were 3-fragment assembled with the following fragments: **1**. The *Nru*I and *Xho*I digested pIT3-CL-$cI^{+}.cI^{+}.pR^{-}.\mathbf{pL}^{WT}.apl^{-}.int::lacZ$ reporter. **2**. For the *pL* -10 mutant reporters, the 164bp $cI^{+}.pR^{-}$ PCR amplicon from pIT3-CL-$cI^{+}.cI^{+}.pR^{-}.\mathbf{pL}^{WT}.apl^{-}.int::lacZ$ using primers 1730 and 1731. For the *pL* -35 mutant reporters, the 189bp $cI^{+}.pR^{-}$ PCR amplicon from pIT3-CL-$cI^{+}.cI^{+}.pR^{-}.\mathbf{pL}^{WT}.apl^{-}.int::lacZ$ using primers 1730 and 1740. **3**. For the *pL* -10 mutant reporters, one of eight 208bp $pL^{M1\text{-}8}.apl^{-}$ PCR amplicons from pIT3-CL-$cI^{+}.cI^{+}.pR^{-}.\mathbf{pL}^{WT}.apl^{-}.int::lacZ$ using reverse primer 1739 with a *pL* -10 mutagenic primer (1733-38, 1830-31). For the *pL* -35 mutant reporters, one of three 183bp $pL^{M9\text{-}11}.apl^{-}$ PCR amplicons from pIT3-CL-$cI^{+}.cI^{+}.pR^{-}.\mathbf{pL}^{WT}.apl^{-}.int::lacZ$ using reverse primer 1739 with a *pL-35* mutagenic primer (1832-34). Red text denotes mutations made to *pL* -10 *or* -35 site.		
1372	TGCCAGGAATTGGGGATCG	Used to generate the $cI^{+}.pR^{-}.pL^{+}.apl^{-}$ amplicon to assemble the wildtype CI *pL* LacZ reporter. Used routinely for screening and Sanger sequencing.
1606	GGTAACGCCAGGGTTTTCCCAGTC	
1730	CGGTCAAGTACATCCACGTTGCTCC	Used to generate the $cI^{+}.pR^{-}$ amplicon to assemble the *pL* -10 and *pL* -35 mutant CI *pL* LacZ reporters. Primes CTD of *cI*.
1731	CCTATTAGCCAAAGTTTGCAATTGA TTTGACTCTGTTTGC	Paired with 1730 to generate the $cI^{+}.pR^{-}$ amplicon to assemble the *pL* -10 mutant CI *pL* LacZ reporters. Primes across *pL*.

Name	Sequence	Description
1740	TTTCAGAAGCCATATTGCATGATTC CCTATTAG	Paired with 1730 to generate the *cI*$^{+}$.*pR*$^{-}$ amplicon to assemble the *pL* -35 mutant CI *pL* LacZ reporters. Primes across *pL*.
1739	GCTTTCTTGCAGCCTTTACGGATTG TG	Used to generate the mutant *pL*$^{M1\text{-}11}$.*apl*$^{-}$ amplicons to assemble the mutant CI *pL* LacZ reporters. Primes within *apl*$^{-}$.
1733	CAAATCAATTGCAAACTTTGGCTAA TAGGGAATTATACAATATGGCTTCT GAAATC	M1 *pL* -10 mutagenic primer paired with 1739 to generate the *pL*^{M1}.*apl*$^{-}$ amplicon.
1734	CAAATCAATTGCAAACTTTGGCTAA TAGGGAATGATACAATATGGCTTCT GAAATC	M2 *pL* -10 mutagenic primer paired with 1739 to generate the *pL*^{M2}.*apl*$^{-}$ amplicon.
1735	CAAATCAATTGCAAACTTTGGCTAA TAGGGAATTTAGCAATATGGCTTCT GAAATC	M3 *pL* -10 mutagenic primer paired with 1739 to generate the *pL*^{M3}.*apl*$^{-}$ amplicon.
1736	CAAATCAATTGCAAACTTTGGCTAA TAGGGAATGACCCAATATGGCTTCT GAAATC	M4 *pL* -10 mutagenic primer paired with 1739 to generate the *pL*^{M4}.*apl*$^{-}$ amplicon.
1737	CAAATCAATTGCAAACTTTGGCTAA TAGGGAATTAACCAATATGGCTTCT GAAATC	M5 *pL* -10 mutagenic primer paired with 1739 to generate the *pL*^{M5}.*apl*$^{-}$ amplicon.
1738	CAAATCAATTGCAAACTTTGGCTAA TAGGGAATGGGCCAATATGGCTTCT GAAATC	M6 *pL*-10 mutagenic primer paired with 1739 to generate the *pL*^{M6}.*apl*$^{-}$ amplicon.
1830	CAAATCAATTGCAAACTTTGGCTAA TAGGGAATTATTCAATATGGCTTCT GAAATC	M7 *pL* -10 mutagenic primer paired with 1739 to generate the *pL*^{M7}.*apl*$^{-}$ amplicon.
1831	CAAATCAATTGCAAACTTTGGCTAA TAGGGAATGTACCAATATGGCTTCT GAAATC	M8 *pL* -10 mutagenic primer paired with 1739 to generate the *pL*^{M8}.*apl*$^{-}$ amplicon.
1832	TAGGGAATCATGCAATATGGCTTCT GAAATGTCAATCATCAAAGTGCCTG CAC	M9 *pL*-35 mutagenic primer paired with 1739 to generate the *pL*^{M9}.*apl*$^{-}$ amplicon.
1833	TAGGGAATCATGCAATATGGCTTCT GAAATGACATTCATCAAAGTGCCTG CAC	M10 *pL* -35 mutagenic primer paired *with* 1739 to generate the *pL*^{M10}.*apl*$^{-}$ amplicon.
1834	TAGGGAATCATGCAATATGGCTTCT GAAAACGTCCTCATCAAAGTGCCTG CAC	M11 *pL* -35 mutagenic primer paired with 1739 to generate the *pL*^{M11}.*apl*$^{-}$ amplicon.

The wildtype minimal prophage induction *pR* modules: The ***pR***$^{+}$.*apl*$^{+}$.*cII*$^{+}$ and ***pR***$^{+}$.*apl*$^{+}$.*cII*$^{-}$ LacZ reporter modules were previously made by Ian Murchland (Shearwin laboratory). The ***pR***$^{+}$.*apl*$^{-}$.*cII*$^{+}$ and ***pR***$^{+}$.*apl*$^{-}$.*cII*$^{-}$ LacZ reporter modules were 3-fragment assembled with the following fragments:

1. The *Bsa*BI and *SmlI* digested pIT3-CL-*cI*$^{+}$.***pR***$^{+}$.*pL*$^{+}$.*apl*$^{+}$.*cII*$^{+}$.*fil::lacZ* reporter

2. The 682bp *cI*$^{+}$.*apl*$^{-}$ PCR amplicon from pIT3-CL-*cI*$^{+}$.***pR***$^{+}$.*pL*$^{+}$.*apl*$^{-}$.*cII::lacZ* using primers 1890 and 1891.

3. For the *cII*$^{+}$ reporter, the 679bp *apl.cII*$^{+}$ PCR amplicon from pIT3-CL-*cI*$^{+}$.***pR***$^{+}$.*pL*$^{+}$.*apl*$^{+}$.*cII*$^{+}$.*fil::lacZ* using primers 1892 and 1893.
For the *cII*$^{-}$ reporter, the 679bp *apl.cII*$^{-}$ PCR amplicon from pIT3-CL-*cI*$^{+}$.***pR***$^{+}$.*pL*$^{+}$.*apl*$^{+}$.*cII*$^{-}$.*fil::lacZ* using primers 1892 and 1893.

1890	GCTTGTCCACAAAATAAATTTTCCC CTCGG	Used to generate the *cI*$^{+}$.*apl*$^{-}$ amplicon from pIT3-CL-pIT3-CL-*cI*$^{+}$.***pR***$^{+}$.*pL*$^{+}$.*apl*$^{-}$.*cII::lacZ*. 1890 primes immediately upstream of *cI*$^{+}$ *Bsa*BI site, 1891 primes 27bp downstream of the *apl* HTH mutation. 1890 also used as routine sequencing primer.
1891	GCCTTTACGGATTGTGCGGGGTTCG ATTGG	
1892	CCAATCGAACCCCGCACAATCCGTA AAGGC	Used to generate the *apl.cII*$^{+/-}$ amplicons from pIT3-CL-*cI*$^{+}$.***pR***$^{+}$.*pL*$^{+}$.*apl*$^{+}$.*cII*$^{+/-}$.*fil::lacZ*. 1892 primes within *apl* and 1893 primes at the end of *cII*.
1893	CTCAAATCAGACCAAACGATGCGCC AATAC	

Name	Sequence	Description
The minimal prophage induction *pL/pE* modules: The preliminary minimal ***pL/pE***.*apl*$^{+/-}$ LacZ reporters were assembled with the (1) *Bsa*BI and *Sap*I digested pIT3-CL-*cI*$^{+}$.*cI*$^{+}$.*pR*$^{-}$.***pL***^{WT}.*apl*$^{-}$.*int::lacZ* and the (2) 781bp *cI*$^{+}$.*apl*$^{+/-}$ PCR amplicon from pIT3-CL-*cI*$^{+}$.***pR***$^{+}$.*pL*$^{+}$.*apl*$^{+/-}$.*cII*$^{+}$.*fil::lacZ* using primers 1890 and 2477. The ***pL/pE***.*apl*$^{+/-}$.*cII*$^{+/-}$ LacZ reporters were 3-fragment assembled with the with the following fragments: **1.** *Bam*HI and *Acc*65I digested pIT3-CL-*lacZ*timfuse vector **2.** The 933bp *cI*$^{+}$.*apl*$^{+/-}$ PCR amplicon from pIT3-CL-*cI*$^{+}$.*pR*$^{+}$.***pL***$^{+}$.*apl*$^{+/-}$.*int::lacZ* using primers 301 and 1891. **3.** The 701bp *apl.cII*$^{+/-}$ PCR amplicon sourced from pIT3-CL-*cI*$^{+}$.***pR***$^{+}$.*pL*$^{+}$.*apl*$^{+}$.*cII*$^{+/-}$.*fil::lacZ* using primers 1892 and 2530. The ***pL/pE***.*apl*$^{+/-}$.*cII*^{145} LacZ reporters were assembled with the (1) *Sap*I and *Bam*HI-HF digested pIT3-CL-*cI*$^{+}$.*pR*$^{+}$.***pL***$^{+}$.*apl*$^{+/-}$.*cII*$^{+}$.***pE***$^{+}$.*int::lacZ* and the (2) 607bp *apl.cII*^{145} PCR amplicon from pIT3-CL-*cI*$^{+}$.*pR*$^{+}$.***pL***$^{+}$.*apl*$^{+}$.*cII*$^{+}$.***pE***$^{+}$.*int::lacZ* using primers 2619 and 2620.		
2477	GATGACGAGTTGAAAACGGGAATGTCCCAAC	Paired with 1890 to generate the *cI*$^{+}$.*apl*$^{+/-}$ amplicon from pIT3-CL-*cI*$^{+}$.***pR***$^{+}$.*pL*$^{+}$.*apl*$^{+/-}$.*cII*$^{+}$.*fil::lacZ*. 2477 primes at the end of *apl* and 1890 primes immediately upstream of the *cI*$^{+}$ *Bsa*BI site.
301	CGCCAGGGTTTTCCCAGTCACGAC	Paired with 1891 to generate the *cI*$^{+}$.*apl*$^{+/-}$ amplicon from pIT3-CL-*cI*$^{+}$.*pR*$^{+}$.***pL***$^{+}$.*apl*$^{+/-}$.*int::lacZ*. 301 primes within plasmid vector 43bp downstream of *int* ATG and 1891 primes 27bp downstream of the *apl* HTH mutation and overlaps with 1892.
2530	caggaattggggatcggaattcgagctcCGGGATCCTTCAGCATACGCACC	Paired with 1892 to generate the *apl.cII*$^{+/-}$ amplicon from pIT3-CL-*cI*$^{+}$.***pR***$^{+}$.*pL*$^{+}$.*apl*$^{+}$.*cII*$^{+/-}$.*fil::lacZ*. 2530 primes end of *cII,* with 28bp homology tail to pIT3-CL-*lacZ*timfuse vector and 1892 primes 27bp downstream of the *apl* HTH mutation and overlaps with 1891.
2619	GAAAGCAGGTGGCCCGATTCGCATTTATTACGC	Primer pair used to generate the *apl.cII*^{145} amplicon from pIT3-CL-*cI*$^{+}$.*pR*$^{+}$.***pL***$^{+}$.*apl*$^{+}$.*cII*$^{+}$.***pE***$^{+}$.*int::lacZ.* 2620 designed to incorporate a stop codon immediately after the 145th residue of *cII* gene and has 28bp homology tail to pIT3-CL-*lacZ*timfuse vector. 2619 primes 62bp downstream of the *apl* HTH mutation.
2620	caggaattggggatcggaattcgagctccgggatccttaACGTGCATGCAGCGCCAGAGC	
Primers used in the Tum study (Chapter 3)		
The E4643(186$^{p.cym}$) lysogen: Recombineering methods were used to generate the CA-inducible 186$^{p.cym}$ phage. Cassette 17-*loxP.chlor*^{R}.*loxP.T5-1* was designed to replace the natural UV-inducible *p95.tum*$^{+}$ locus with the CA-inducible *T5-1.tum*$^{+}$ cassette. Due to synthesis issues, cassette 17 was subdivided into gBlock 17B-*loxP.chlor*^{R} and gBlock 17C-*loxP.T5-1.tum* (see Table 7.12 for sequences), which were combined via overlapping PCR using primers 2797 and 2798.		
2797	CCGCTAATATTCATCCATATCATGTACATACAG	Used in overlapping PCR to generate cassette 17-*loxP.chlor*^{R}.*loxP.T5-1* using gBlocks 17B and 17C. 2797 primes immediately upstream of gene *A* terminator of gBlock 17B and 2798 primes within *tum* of gBlock 17C.
2798	CCCGCTCAATCATAACGTGCTCATTTAG	
Primers used in the 186-WCB study (Chapter 5)		
The CA-inducible *cymR.T5-1.tum*$^{+/72K}$ IM: Each IM was 2-fragment assembled with the (1) *Spe*I digested pIT4-KT-*cymR.T5-1* module and a (2) *tum*$^{+/72K}$ gene PCR fragment from pIT3-TO-*p95.tum*$^{+/72K}$ IMs using primers 2460, 2461 and 2462. **The ^{1}CA^{OFF} inducible *pcymR*^{C}.*cI*$^{+}$.*cymR*^{AM} IM:** 2-fragment assembled with the (1) *Xba*I digested pIT4-*loxP*-KH-*pcymR*^{C}.*PlacI*^{q}.*cymR*^{AM} plasmid made by Andrew Hao (Shearwin laboratory) (4377bp) and the (2) 705bp *cI* gene PCR fragment from pIT4-KT-*cymR.T5-1.cI*$^{+}$ using primers 2883 and 2884. **The ^{2}CA^{OFF} inducible *cymR.T5-6.cI*$^{+}$ IM:** Assembled in two stages. Stage 1 required replacement of the φ21 *attP* site with the HK022 *attP* site, modifying the cloning vector from pIT4-KT-*cymR.T5-6.φK02CB* to pIT4-KH-*cymR.T5-6.φK02CB.* The vector was assembled by ligation of the (1) 3014bp pIT4-*cymR.T5-6.φK02CB* fragment (sourced from *Nhe*I and *Psp*OMI digested pIT4-KT-*cymR.T5-6.φK02CB*) and (2) the 1886bp KH fragment (sourced from *Nhe*I and *Psp*OMI digested pIT4-*loxP*-KH-*pcymR*^{C}.*cI*$^{+}$.*PlacI*^{q}.*cymR*^{AM}). Stage 2 required replacement of *φK02CB* gene with 186*cI*$^{+}$ gene. The IM was assembled with the (1) *Spe*I-HF and *Nar*I digested pIT4-KH-*cymR.T5-6.φK02CB* and (2) the 705bp *cI*$^{+}$ gene PCR fragment from pIT4-KT-*cymR.T5-1.cI*$^{+}$ using primers 3115 and 3116.		

Name	Sequence	Description
5460	gtctgtttgtattatgaattccagcacactggcggccgttaCTCGTAGTGGAGGTTGTGTGGATAGAGAGC	Paired with 2461 or 2462 to generate the *tum*$^{+/72K}$ amplicon from pIT3-TO-*p95.tum*$^{+/72K}$. Primes at the start of *tum* with 41bp homology tail with pIT4-KT-*cymR.T5-1* vector.
5461	gttaggcgcctccggacttaagcagctgcccgggtgcactagTTAACGCCAGCTCTCATCTTCCCACAC	Paired with 2461 to generate the *tum*$^{+}$ amplicon from pIT3-TO-*p95.tum*$^{+}$. Primes at the end of *tum*$^{+}$ with 42bp homology tail with pIT4-KT-*cymR.T5-1* vector.
5462	gttaggcgcctccggacttaagcagctgcccgggtgcactagTCATTTCACTTTGCCCTCCTTTGCAAATG	Paired with 2462 to generate the *tum*^{72K} amplicon from pIT3-TO-*p95.tum*^{72K}. Primes at the end of *tum*^{72K} with 42bp homology tail with pIT4-KT-*cymR.T5-1* vector.
2883	gtgaggacgaaacagcctctacaaataattttgtttaatACTAGTGCACACTAGAAATAATTTTGTGTAAATAG	Used to generate the *cI*$^{+}$ gene fragment from pIT4-KT-*cymR.T5-1.cI*$^{+}$. 2883 primes across the *cI* RBS and 2884 primes at the end of *cI*.
2884	cttttctggaatttggtaccgagactagtctcgagtctagTTAGTTAACCTCGCTGTATACACCC	
3092	GGATACTGTATGGCACTGAATCTG	Used to verify successful ligation of pIT4-KH-*cymR.T5-6.φK02CB* plasmid. 3092 primes within *φK02CB* gene and 3093 primes within HK022 *attP* site.
3093	GATTCATAGTGACTGGATATGTTGCG	
3115	GTTTGTATTATGAATTCCAGCACACTGGCGGC	Used to generate the *cI*$^{+}$ gene fragment from pIT4-KT-*cymR.T5-1.cI*$^{+}$ for pIT4-KH-*cymR.T5-6.cI*$^{+}$ assembly. 3115 primes 5bp upstream of *cI* ATG and 3116 primes 10bp downstream *cI* TAA.
3116	GGCCTTCTGCTTAATTTGATGCCTGTCAGTTTAG	
2037	CATGATCACCATAGATCCTTTCTCC	Used to verify successful assembly of pIT4-KH-*cymR.T5-6.cI*$^{+}$ plasmid. 2037 primes at the start of *cymR* gene and 1350 primes within *kan*^{R} gene.
1350	CGGACCATCTCATCTGTAAC	
The 186-WCB *pR.apI*$^{-}$.*tum*^{*72K} MCherry reporter: 4-fragment assembled with the following fragments: **1**. For the *apI*$^{-}$.*tum*^{*72K} reporter, the 1226bp *cI*$^{+}$.*apI*$^{-}$.*tum*^{*72K} PCR amplicon from pIT3-CL- *cI*$^{+}$.***pR***$^{+}$.*pL*$^{+}$.*apI*$^{-}$.*tum*^{*72K}.*fil::lacZ* using primers 2650 and 2651. For the *cI*$^{+}$.*apI*$^{-}$.*tum*$^{-}$ control reporter, the 1226bp *cI*$^{+}$.*apI*$^{-}$.*tum*$^{-}$ PCR from pIT3-CL-*cI*$^{+}$.***pR***$^{+}$.*pL*$^{+}$.*apI*$^{-}$.*tum*$^{-}$.*fil::lacZ* using primers 2650 and 2651. **2**. The 940bp *SF(gfp)* gene PCR fragment from pSB1A2-BBa_I746908-*SF(gfp)* using primers 2652 and 2653. **3**. The 786bp *mCherry* gene PCR fragment from pAccessory-*SF(gfp)-mCherry-dCas9* scrambled guide using primers 2654 and 2655. **4**. The *Bam*HI and *Acc*65I digested pIT3-CL integration vector.		
2650	TCCTTAGTTAACCTCGCTGTATACACCCAC	Used to generate the *cI*$^{+}$.*pR*$^{+}$.*pL*$^{+}$.*apI*$^{-}$.*tum*$^{72K/-}$ amplicons from pIT3-CL-*cI*$^{+}$.***pR***$^{+}$.*pL*$^{+}$.*apI*$^{-}$.*tum*$^{*72K/-}$.*fil::lacZ*. 2650 primes at the end of *cI* and 2651 primers at the end of *tum*$^{72K/-}$.
2651	CCTCATTTCACTTTGCCCTCCTTTGCAAATG	
2652	ccaggaattggggatcggaattcgagctcgTATAAACGCAGAAAGGCCCACCCG	Used to generate the *SF(gfp)* gene fragment from pSB1A2-BBa_I746908-*SF(gfp)*. 2653 primes across the RBS and start of *SF(gfp)* and 2652 primes at the end of *SF(gfp)*.
2653	ggtgtatacagcgaggttaactaaggaTACTAGAGAAAGAGGAGAAATACTAGATGCG	
2654	ttgcaaaggagggcaaagtgaaatgaggAAGAAGGAGATATACATATGGTGAGCAAGGGC	Used to generate the *mCherry* gene fragment from pAccessory-*SF(gfp)-mCherry-dCas9* scrambled guide. 2654 primes across *pET* RBS and start of *mCherry* and 2655 primes at the end of *mCherry*.
2655	gcatgcctgcaggtcgactctagaggatcCTTACTTGTACAGCTCGTCCATGCCG	

Table 7.12: gBlock gene fragments used during this thesis. Sequences are written 5' to 3'. Each gBlock has been categorised according to its area of study.

gBlock	Sequence
gBlocks used in the goa8, CI and ApI study (Chapter 2)	
The *pL and pR goa8*$^{+/-}$ LacZ reporters 1-6: 2-fragment assembled using gBlocks 1 to 6 and the *Acc*65I and *Bam*HI digested pIT3-KT-*lacZ*trimfuse vector. The pIT3-KT-*lacZ*trimfuse vector was initially assembled via DNA ligation of the 2113bp *kan*^{R}.*oriR6Kγ.attP*$^{\varphi 21}$ fragment and 4564bp pIT3-*lacZ*trimfuse fragment from *Nhe*I and *Psp*OMI digested pIT3-KT and pIT3-CL-*lacZ*trimfuse respectively. *apI*$^{-}$ gene (pink), *cI*$^{-}$ gene (green), mutations (bold), site of *goa8* mutation (bold red Δ), *FL* and *FR* sites (underlined).	
gBlock 1 (*int.cI*$^{-}$*.pR*$^{+}$***.pL***$^{+}$*.apI*$^{-}$) Used to generate reporter 1.	GCCATAAACTGCCAGGAATTGGGGATCGGAATTCGAGCTCGGTACCATCCTTACAATTCACATAAAGTGAATTATTAAGCACCGATGACGAGTTGAAAACGGGAATGTCCCAACGCCTTACGCAACTGCTCTTCTTTCCAGCGTGCGTAATAAATGCGAATCGGGCCACCTGCTTTCTTGCAGCCTTTACGGATTGTGCGGGGTTCGATTGGTACACAAGGGTTGTCGCCGGTTGTCCA**CTGGTAGGCGGTTTCGCG**AGAAACACCCTCAAGCTCTGCGAATTGTTGCAGAGTAACGATAGGTGCAGGCACTTTGATGATTGCGATTTCAGAAGCCATATTGCATGATTCCCTATTAGCCAAAGTTTGCAATTGATTTGACTCTGTTTGCCAACACTTGCCATCAATTGCGTGGGTTTAGCCAAAATATATCTCCCAATTGAGAGATAGTAAATAGGTTTTATCGAAATGAGAATAGATTCTTTAGGATGGAGCAACGTGGATGTACTTGACCGCATCTGCGAGGCGTACGGATTTTCGCAGAAAATTCAATTAGCTAACCACTTCGATATCGCG**CGCGAG**TCATTGTCAAACAGGTACACCCGAGGCGCTATCTCCTATGACTTTGCGGCTCACTGTGCCCTTGAAACAGGTGCTAATCTCCAGTGGTTACTTACCGGAGAAGGAGAAGCATTTGTAAATAACAGAGAATCGAGCGACGCAAAAAGGATTGAGGGATTCACATTAAGTGAAGAAATCCTCAAATTACAGCGAGGTTAACTAATGACCGTCCGTAAAAATCCGGCTGGCGGATCCGTCGTTTTACAACGTCGTGACTGGGAAAACCCTGGCGTTACC
gBlock 1 (*int.cI*$^{-}$*.pR*$^{+}$*.goa8.****pL***$^{+}$*.apI*$^{-}$) Used to generate reporter 2.	GCCATAAACTGCCAGGAATTGGGGATCGGAATTCGAGCTCGGTACCATCCTTACAATTCACATAAAGTGAATTATTAAGCACCGATGACGAGTTGAAAACGGGAATGTCCCAACGCCTTACGCAACTGCTCTTCTTTCCAGCGTGCGTAATAAATGCGAATCGGGCCACCTGCTTTCTTGCAGCCTTTACGGATTGTGCGGGGTTCGATTGGTACACAAGGGTTGTCGCCGGTTGTCCA**CTGGTAGGCGGTTTCGCG**AGAAACACCCTCAAGCTCTGCGAATTGTTGCAGAGTAACGATAGGTGCAGGCACTTTGATGATTGCGATTTCAGAAGCCATATTGCATGATTCCCTATTAGCCAAAGTTTGCAATTGATTTGACTCTGΔCAACACTTGCCATCAATTGCGTGGGTTTAGCCAAAATATATCTCCCAATTGAGAGATAGTAAATAGGTTTTATCGAAATGAGAATAGATTCTTTAGGATGGAGCAACGTGGATGTACTTGACCGCATCTGCGAGGCGTACGGATTTTCGCAGAAAATTCAATTAGCTAACCACTTCGATATCGCG**CGCGAG**TCATTGTCAAACAGGTACACCCGAGGCGCTATCTCCTATGACTTTGCGGCTCACTGTGCCCTTGAAACAGGTGCTAATCTCCAGTGGTTACTTACCGGAGAAGGAGAAGCATTTGTAAATAACAGAGAATCGAGCGACGCAAAAAGGATTGAGGGATTCACATTAAGTGAAGAAATCCTCAAATTACAGCGAGGTTAACTAATGACCGTCCGTAAAAATCCGGCTGGCGGATCCGTCGTTTTACAACGTCGTGACTGGGAAAACCCTGGCGTTACC
gBlock 3 (*cI*$^{-}$***.pR***$^{+}$*.pL*$^{+}$*.apI*$^{-}$*.cII*) Used to generate reporter 3.	GGTAACGCCAGGGTTTTCCCAGTCACGACGTTGTAAAACGACGGGATCCATGTTGCATCCTTACAATTCACATAAAGTGAATTATTAAGCACCGATGACGAGTTGAAAACGGGAATGTCCCAACGCCTTACGCAACTGCTCTTCTTTCCAGCGTGCGTAATAAATGCGAATCGGGCCACCTGCTTTCTTGCAGCCTTTACGGATTGTGCGGGGTTCGATTGGTACACAAGGGTTGTCGCCGGTTGTCCA**CTGGTAGGCGGTTTCGCG**AGAAACACCCTCAAGCTCTGCGAATTGTTGCAGAGTAACGATAGGTGCAGGCACTTTGATGATTGCGATTTCAGAAGCCATATTGCATGATTCCCTATTAGCCAAAGTTTGCAATTGATTTGACTCTGTTTGCCAACACTTGCCATCAATTGCGTGGGTTTAGCCAAAATATATCTCCCAATTGAGAGATAGTAAATAGGTTTTATCGAAATGAGAATAGATTCTTTAGGATGGAGCAACGTGGATGTACTTGACCGCATCTGCGAGGCGTACGGATTTTCGCAGAAAATTCAATTAGCTAACCACTTCGATATCGCG**CGCGAG**TCATTGTCAAACAGGTACACCCGAGGCGCTATCTCCTATGACTTTGCGGCTCACTGTGCCCTTGAAACAGGTGCTAATCTCCAGTGGTTACTTACCGGAGAAGGAGAAGCATTTGTAAATAACAGAGAATCGAGCGACGCAAAAAGGATTGAGGGATTCACATTAAGTGAAGAAATCCTCAAATTACAGCGAGGTTAAGAGCTCGAATTCCGATCCCCAATTCCTGGCAGTTTATGGC

gBlock	Sequence
gBlock 4 (*cI⁻.**pR⁺**.goa8.pL⁺.apI⁻ .cII*) Used to generate reporter 4.	GGTAACGCCAGGGTTTTCCCAGTCACGACGTTGTAAAACGACGGGATCCATGTTGCA TCCTTACAATTCACATAAAGTGAATTATTAAGCACCGATGACGAGTTGAAAACGGGA ATGTCCCAACGCCTTACGCAACTGCTCTTCTTTCCAGCGTGCGTAATAAATGCGAAT CGGGCCACCTGCTTTCTTGCAGCCTTTACGGATTGTGCGGGGTTCGATTGGTACACA AGGGTTGTCGCCGGTTGTCCA**CTGGTAGGCGGTTTCGCG**AGAAACACCCTCAAGCTC TGCGAATTGTTGCAGAGTAACGATAGGTGCAGGCACTTTGATGATTGCGATTTCAGA AGCCATATTGCATGATTCCCTATTAGCCAAAGTTTGCAATTGATTTGACTCTGΔCAA CACTTGCCATCAATTGCGTGGGTTTAGCCAAAATATATCTCCCAATTGAGAGATAGT AAATAGGTTTTATCGAAATGAGAATAGATTCTTTAGGATGGAGCAACGTGGATGTAC TTGACCGCATCTGCGAGGCGTACGGATTTTCGCAGAAAATTCAATTAGCTAACCACT TCGATATCGCG**CGCGAG**TCATTGTCAAACAGGTACACCCGAGGCGCTATCTCCTATG ACTTTGCGGCTCACTGTGCCCTTGAAACAGGTGCTAATCTCCAGTGGTTACTTACCG GAGAAGGAGAAGCATTTGTAAATAACAGAGAATCGAGCGACGCAAAAAGGATTGAGG GATTCACATTAAGTGAAGAAATCCTCAAATTACAGCGAGGTTAAGAGCTCGAATTCC GATCCCCAATTCCTGGCAGTTTATGGC
gBlock 5 (*int.cI⁻.pR⁻.**pL⁺**. apI⁻*) Used to generate reporter 5.	GCCATAAACTGCCAGGAATTGGGGATCGGAATTCGAGCTCGGTACCATCCTTACAAT TCACATAAAGTGAATTATTAAGCACCGATGACGAGTTGAAAACGGGAATGTCCCAAC GCCTTACGCAACTGCTCTTCTTTCCAGCGTGCGTAATAAATGCGAATCGGGCCACCT GCTTTCTTGCAGCCTTTACGGATTGTGCGGGGTTCGATTGGTACACAAGGGTTGTCG CCGGTTGTCCA**CTGGTAGGCGGTTTCGCG**AGAAACACCCTCAAGCTCTGCGAATTGT TGCAGAGTAACGATAGGTGCAGGCACTTTGATGATTGCGATTTCAGAAGCCATATTG CATGATTCCCTATTAGCCAAAGTTTGCAATTGATTTGACTCTGTTTGCCAACACTTG CCATCAATTGCGTGGGTTTAGCCAAAATATATCTCCCAATTGAGAGAT**CTCGAG**TAG GTTTTATCGAAATGAGAATAGATTCTTTAGGATGGAGCAACGTGGATGTACTTGACC GCATCTGCGAGGCGTACGGATTTTCGCAGAAAATTCAATTAGCTAACCACTTCGATA TCGCG**CGCGAG**TCATTGTCAAACAGGTACACCCGAGGCGCTATCTCCTATGACTTTG CGGCTCACTGTGCCCTTGAAACAGGTGCTAATCTCCAGTGGTTACTTACCGGAGAAG GAGAAGCATTTGTAAATAACAGAGAATCGAGCGACGCAAAAAGGATTGAGGGATTCA CATTAAGTGAAGAAATCCTCAAATTACAGCGAGGTTAACTAATGACCGTCCGTAAAA ATCCGGCTGGCGGATCCGTCGTTTTACAACGTCGTGACTGGGAAAACCCTGGCGTTA CC
gBlock 6 (*int.cI⁻.pR⁻.goa8.**pL⁺**. apI⁻*) Used to generate reporter 6.	GCCATAAACTGCCAGGAATTGGGGATCGGAATTCGAGCTCGGTACCATCCTTACAAT TCACATAAAGTGAATTATTAAGCACCGATGACGAGTTGAAAACGGGAATGTCCCAAC GCCTTACGCAACTGCTCTTCTTTCCAGCGTGCGTAATAAATGCGAATCGGGCCACCT GCTTTCTTGCAGCCTTTACGGATTGTGCGGGGTTCGATTGGTACACAAGGGTTGTCG CCGGTTGTCCA**CTGGTAGGCGGTTTCGCG**AGAAACACCCTCAAGCTCTGCGAATTGT TGCAGAGTAACGATAGGTGCAGGCACTTTGATGATTGCGATTTCAGAAGCCATATTG CATGATTCCCTATTAGCCAAAGTTTGCAATTGATTTGACTCTGΔCAACACTTGCCAT CAATTGCGTGGGTTTAGCCAAAATATATCTCCCAATTGAGAGAT**CTCGAG**TAGGTTT TATCGAAATGAGAATAGATTCTTTAGGATGGAGCAACGTGGATGTACTTGACCGCAT CTGCGAGGCGTACGGATTTTCGCAGAAAATTCAATTAGCTAACCACTTCGATATCGC G**CGCGAG**TCATTGTCAAACAGGTACACCCGAGGCGCTATCTCCTATGACTTTGCGGC TCACTGTGCCCTTGAAACAGGTGCTAATCTCCAGTGGTTACTTACCGGAGAAGGAGA AGCATTTGTAAATAACAGAGAATCGAGCGACGCAAAAAGGATTGAGGGATTCACATT AAGTGAAGAAATCCTCAAATTACAGCGAGGTTAACTAATGACCGTCCGTAAAAATCC GGCTGGCGGATCCGTCGTTTTACAACGTCGTGACTGGGAAAACCCTGGCGTTACC

gBlock	Sequence

The *goa8* minimal prophage induction *pR* modules: For the ***pR***$^{+}$*.apl*$^{+}$*.cII*$^{+/-}$*.goa8* reporters, *Bsa*BI and *Sml*I digested pIT3-CL-*cI*$^{+}$.***pR***$^{+}$*.pL*$^{+}$*.apl*$^{+}$*.cII*$^{+/-}$*.fil::lacZ* was assembled with gBlock 9-*cI*$^{+}$*.pR*$^{+}$*.goa8.pL*$^{+}$*.apl*$^{+}$. For the ***pR***$^{+}$*.apl*$^{-}$*.cII*$^{+/-}$*.goa8* reporter, *Bsa*BI and *Sml*I digested pIT3-CL-*cI*$^{+}$.***pR***$^{+}$*.pL*$^{+}$*.apl*$^{-}$*.cII*$^{+/-}$*.fil::lacZ* was assembled with gBlock 10-*cI*$^{+}$*.pR*$^{+}$*.goa8.pL*$^{+}$*.apl*$^{-}$. *apl* gene (pink), *cI* gene (green), *apl* HTH mutation (black bold), site of *goa8* mutation (bold red Δ).

gBlock 9
(*cI*$^{+}$*.pR*$^{+}$*.goa8.pL*$^{+}$*.apl*$^{+}$)

GATGCTTGCTTGTCCACAAAATAAATTTTCCCCTCGGAACGGATAGCCATCCCATCT
GTGAGCGGTTTTGTGAAAAATTGGGCATCAACACTCAATTGTTTATCGGATTTGAGG
ATTTCTTCACTTAATGTGAATCCCTCAATCCTTTTTGCGTCGCTCGATTCTCTGTTA
TTTACAAATGCTTCTCCTTCTCCGGTAAGTAACCACTGGAGATTAGCACCTGTTTCA
AGGGCACAGTGAGCCGCAAAGTCATAGGAGATAGCGCCTCGGGTGTACCTGTTTGAC
AATGAGCTGGACGCGATATCGAAGTGGTTAGCTAATTGAATTTTCTGCGAAAATCCG
TACGCCTCGCAGATGCGGTCAAGTACATCCACGTTGCTCCATCCTAAAGAATCTATT
CTCATTTCGATAAAACCTATTTACTATCTCTCAATTGGGAGATATATTTTGGCTAAA
CCCACGCAATTGATGGCAAGTGTTGΔCAGAGTCAAATCAATTGCAAACTTTGGCTAA
TAGGGAATCATGCAATATGGCTTCTGAAATCGCAATCATCAAAGTGCCTGCACCTAT
CGTTACTCTGCAACAATTCGCAGAGCTTGAGGGTGTTTCTGAACGCACCGCCTACCG
CTGGACAACCGGCG

gBlock 10
(*cI*$^{+}$*.pR*$^{+}$*.goa8.pL*$^{+}$*.apl*$^{-}$)

GATGCTTGCTTGTCCACAAAATAAATTTTCCCCTCGGAACGGATAGCCATCCCATCT
GTGAGCGGTTTTGTGAAAAATTGGGCATCAACACTCAATTGTTTATCGGATTTGAGG
ATTTCTTCACTTAATGTGAATCCCTCAATCCTTTTTGCGTCGCTCGATTCTCTGTTA
TTTACAAATGCTTCTCCTTCTCCGGTAAGTAACCACTGGAGATTAGCACCTGTTTCA
AGGGCACAGTGAGCCGCAAAGTCATAGGAGATAGCGCCTCGGGTGTACCTGTTTGAC
AATGAGCTGGACGCGATATCGAAGTGGTTAGCTAATTGAATTTTCTGCGAAAATCCG
TACGCCTCGCAGATGCGGTCAAGTACATCCACGTTGCTCCATCCTAAAGAATCTATT
CTCATTTCGATAAAACCTATTTACTATCTCTCAATTGGGAGATATATTTTGGCTAAA
CCCACGCAATTGATGGCAAGTGTTGΔCAGAGTCAAATCAATTGCAAACTTTGGCTAA
TAGGGAATCATGCAATATGGCTTCTGAAATCGCAATCATCAAAGTGCCTGCACCTAT
CGTTACTCTGCAACAATTCGCAGAGCTTGAGGGTGTTTCT**CGCGAAACCGCCTACCA**
GTGGACAACCGGCG

gBlocks used in the Tum study (Chapter 3)

The E4643(186$^{p.cym}$) lysogen: gBlock 17B-*loxP.chlor*^{R} and gBlock 17C-*loxP.T5-1.tum* were combined via overlapping PCR using primers 2797 and 2798 to generate cassette 17-*loxP.chlor*^{R}*.loxP.T5-1.tum. gene A* terminator (bold), *loxP* site (pink), *chlor*^{R} gene (green), *tum*$^{+}$ (blue), *T5-1*.cymR^{OPERATOR} (underlined).

Cassette 17
(*loxP.chlor*^{R}*.loxP.T5-1.tum*)

CCGCTAATATTCATCCATATCATGTACA**TACAGTGTATTTAACTGTGATTTTTTT**CT
ACCGTTCGTATAATGTATGCTATACGAAGTTATGATATCTGGCGAAAATGAGACGTT
GATCGGCACGTAAGAGGTTCCAACTTTCACCATAATGAAATAAGATCACTACCGGGC
GTATTTTTTGAGTTATCGAGATTTTCAGGAGCTAAGGAAGCTAAAATGGAGAAAAAA
ATTACTGGGTATACAACCGTAGACATTTCGCAGTGGCACCGCAAGGAACATTTTGAA
GCGTTCCAGTCGGTGGCGCAATGCACATATAACCAAACTGTCCAATTGGACATTACT
GCGTTTTTGAAGACTGTCAAGAAAAATAAACACAAGTTCTACCCTGCGTTTATTCAT
ATCCTGGCTCGTCTGATGAATGCACACCCTGAGTTCCGCATGGCCATGAAGGACGGC
GAATTGGTTATCTGGGACAGCGTTCATCCCTGCTACACTGTGTTTCACGAGCAGACT
GAAACATTCTCCTCACTTTGGTCAGAGTACCATGACGACTTTCGCCAATTCTTACAT
ATTTATTCGCAGGACGTAGCCTGTTATGGAGAGAATCTTGCGTATTTTCCGAAGGGG
TTCATCGAGAACATGTTTTTTGTGAGTGCGAACCCTTGGGTGTCATTTACGTCGTTT
GATCTGAACGTGGCCAATATGGATAACTTCTTTGCCCCTGTGTTCACTATGGGCAAG
TACTACACTCAAGGAGACAAAGTTCTGATGCCTCTTGCTATCCAAGTACACCACGCA
GTCTGTGATGGCTTCCACGTTGGGCGTATGTTGAATGAACTGCAACAGTACTGCGAT
GAATGGCAGGGCGGGGCTTAATAAGAATTAGGAAGATAACTTCGTATAATGTATGCT
ATACGAACGGTAACGCGTAAATCATAAAAAATTTATTTGCTTTGTGCCTAATAATGA
CTAATAATAGATTCAACAAACAGACAATCTGGTCTGTTTGTATTATGAATTCCAGCA
TATAGGGATCGTCGTCTCGTAGTGGAGGTTGTGTGGATAGAGAGCTAAATGAGCACG
TTATGATTGAGCGGG

gBlock	Sequence
gBlock 17B (*loxP.chlor*^{R})	CCGCTAATATTCATCCATATCATGTACA**TACAGTGTATTTAACTGTGATTTTTTT**CTAC CGTTCGTATAATGTATGCTATACGAAGTTATGATATCTGGCGAAAATGAGACGTTGATC GGCACGTAAGAGGTTCCAACTTTCACCATAATGAAATAAGATCACTACCGGGCGTATTT TTTGAGTTATCGAGATTTTCAGGAGCTAAGGAAGCTAAAATGGAGAAAAAAATTACTGG GTATACAACCGTAGACATTTCGCAGTGGCACCGCAAGGAACATTTTGAAGCGTTCCAGT CGGTGGCGCAATGCACATATAACCAAACTGTCCAATTGGACATTACTGCGTTTTTGAAG ACTGTCAAGAAAAATAAACACAAGTTCTACCCTGCGTTTATTCATATCCTGGCTCGTCT GATGAATGCACACCCTGAGTTCCGCATGGCCATGAAGGACGGCGAATTGGTTATCTGGG ACAGCGTTCATCCCTGCTACACTGTGTTTCACGAGCAGACTGAAACATTCTCCTCACTT TGGTCAGAGTACCATGACGACTTTCGCCAATTCTTACATATTTATTCGCAGGACGTAGC CTGTTATGGAGAGAATCTTGCGTATTTTCCGAAGGGGTTCATCGAGAACATGTTTTTTG TGAGTGCGAACCCTTGGGTGTCATTTACGTCGTTTGATCTGAACGTGGCCAATATGGAT AACTTCTTTGCCCCTGTGTTCACTATGGGCAAGTACTACACTCAAGGAGACAAAGTTCT GATGCCTCTTGCTATCCAAGTACACCACGCAGTCTGTGATGGCTTCCACGTTGGGCGTA TGTTGAATGAACTGCAACAGTACTGCGATGAATGGCAGGGCGGGGCTTAATAAGAATTA GGAAG
gBlock 17C (*loxP.T5-1.tum*)	CAACAGTACTGCGATGAATGGCAGGGCGGGGCTTAATAAGAATTAGGAAGATAACTTCGT ATAATGTATGCTATACGAACGGTAACGCGTAAATCATAAAAAATTTATTTGCTTTGTGCC TAATAATGACTAATAATAGATTCAACAAACAGACAATCTGGTCTGTTTGTATTATGAATT CCAGCATATAGGGATCGTCGTCTCGTAGTGGAGGTTGTGTGGATAGAGAGCTAAATGAGC ACGTTATGATTGAGCGGG
gBlocks used in the 186-WCB study (Chapter 5)	
The VA and SA *tum*^{72K} IMs: The VA (*vanR.pVan.tum*^{72K}) and SA (*nahR.pSal.tum*^{72K}) IMs were assembled with the (1) *Kpn*I and *Xma*I digested pIT4-KT-*cymR.T5-1.tum*^{72K} IM and (2) gBlock 15 or gBlock 16 respectively. Repressor gene (pink), *tum*^{72K} gene (green), *pVanCC* or *pSalTTC* promoter (black bold), *proA* promoter (underlined).	
gBlock 15 (*vanR*^{AM}*.pVan*^{CC}*. tum*^{72K})	TAAACTGCCAGGAATTGGGGATCGGAATTCGAGCTCGGTACCTTATCAATCTGCACGAA TTGACCATGCTGCACCCAGCGGTGCGCCTGCGCTTGCTGCTGCTTCAAAAACTTTTGCA TTACGAATTGCTGCCAGTGCATGATCACGCATAATACGTTCTGCACCTTCGGCATCACC ACAGCTAACTGCATCCAGAACTGCCTGATGCTGACGATGTGCTGCCAGCAGATGTTCAT ATTCGGCAGACAGGTCCATCAGATCCAGGGCCAGTGCACCGGCTGCTGCAAACGGTTCA AAACCATTACGTGCCAGTGCGCTTTCAACTGCACCATTACCTGCTGCGCTAACCAGGGT ATCATGAAATGCCTGATTATATGCGGCATAACGATCCAGATCTTCACCATTCAGGCGAC CGGCTGCAAACAGTGCTTCACCTTCTGCAATCAGTACAACAAAACGTGCATGGGTTTCT GCGGTCATACCACGTTCTGCCAGACGACGTGCTGCAAAACCTTCCAGAACACCACGAAC TTCAATTGCATCACGAATCTGATCGCTGCTAACACCACGGGCTGCATAACCACGTGCAC CCAGACGAACAACCAGACCTTCTTGTTCCAGTGAACGCAGTGCGATACGAACCGGCATA CGGCTAACACCCAGTGCTGCTGCGGTCGGAATTTCTGCAATACGTTCACCACTTTTGAT TTCACCGCTTGCAATCATTTTACGCAGTGCCATCATAACACGCTGACCCGGTTTAATAC GAGGCATGTCCATAGATCCTTTCTCCTCTTTAGATCTCTCTAGTAAAAGTTAAACAAAA TTATTTGTAGAGGGAAACCGTTGTGGTCTCCCTGAATATAGCCTACGAGCCTTATGCAT GCCCGTAAAGTTATCCAGCAACCACTCATAGACCTACGCGT**ATTGGATCCAATTGACAG** **CTAGCTCAGTCCTAGGTACCATTGGATCCAAT**GAATTCCAGCACACTGGCGGCCGTTAC TCGTAGTGGAGGTTGTGTGGATAGAGAGCTAAATGAGCACGTTATGATTGAGCGGGTCG AAATGATTGCGCGTCTGACTGCTGAAGGTACTTGTCAGGAAAGAGACCGTGAAATCGCA TTGAATCTAATTGCGGAAATAGCAAGAGGCAACCTAATGAAAAATAATAATTTTTCTGT TGTTTTTTCCGCACCGCCTGTTGGTGAAACATTTGCAAAGGAGGGCAAAGTGAAATGAC TAGTGCACCCGGGCAGCTGCTTAAGTCCGGAGGCGCCTAACCTAAACTGACAG

gBlock	Sequence
gBlock 16 (*nahR*^{AM}.*pSal*^{TTC}.*tum*^{72K})	TAAACTGCCAGGAATTGGGGATCGGAATTCGAGCTCGGTACCTTATCAATCCGTAAACA GGTCAAACATCAGTTGCCGCAACCAAATATTGGCTAGGTCCTTGTGGTACTTCGCATGC CAGAACATGTTGATGGCTATTTCAGGCAAGACGACTGGGTGCGGCAAGGCGCTTAGGCC GAAGGGCTCTACGCAGCAGTCGGCTAAACATATCGGCACAGTGGCGAGCAGATCGGTGC GCTGGAGGATGTGGCCAACGGCGGCGAAGTGCGGCACTTCCAGACGGATGTCGCGCCGG ATGCCGACCCGTGTCATGTACGTGTCCACCTCGCCGTGGCCGGTGCCAGCGGCGATGAC ACGCACGTGGCCGTAGGAACAGAAGCGCTCCAGAGTCAGGGGTTCGCGGGTGACTGGAT GGTCCTTGCGACATAGGCACACGTAGTGATTCTGGAGCAGCCGGCGCTGAAAGAAGCCA GTTTGCAGATTGGGAAGCAGGCCCACGGCCAAGTCCACGGTTCCGTTCTGCAAGGCCTG CATCAGGCTCATCGAACTGTCGCGCACCGTACTGATCACGCAATTGGGGGCCTGGTGAG CCAGCGCATCCATCAGCCGCGGCATGAAGTAGATCTCGCCAATGTCGGTCATGGCCAGG GTGAAGGTACGCTCGCTGGTCAGCGGATCGAAGCTTTCATGGTGCTGTAGGGCGTTGCG CAGTGCGTGCATGGCCGAAGTGACGTGCTCGGCCAGATGCGCGGCATAGGGTGTGGGTT CCATTCCCTGATGTGTGCGCACGAAGAGTGGGTCCTGTAGCGAGGTGCGCAGGCGTTTC AGCGCATTGCTCACGGCAGGCTGGGTCAGGCCCAGGTTCTCCGCAGTGACAGAGACGCG TCTGTCGACCAGCAACTGGTTGAACACCACCAGCAGGTTTAAATCCAGGTCACGCAGTT CCATAGATCCTTTCTCCTCTTTAGATCTCTCTAGTAAAAGTTAAACAAAATTATTTGTA GAGGGAAACCGTTGTGGTCTCCCTGAATATAGCCTACGAGCCTTATGCATGCCCGTAAA GTTATCCAGCAACCACTCATAGACCTACGCGT**GGGGCCTCGCTTGGGTTATTGCTGGTG** **CCCGGCCGGGCGCAATATTCATGTTGATGATTTATTATATATCGAGTGGTGTATTTATT** **TATATTGTTTGCTCCGTTACCGTTATTAAC**GAATTCCAGCACACTGGCGGCCGTTACTC GTAGTGGAGGTTGTGTGGATAGAGAGCTAAATGAGCACGTTATGATTGAGCGGGTCGAA ATGATTGCGCGTCTGACTGCTGAAGGTACTTGTCAGGAAAGAGACCGTGAAATCGCATT GAATCTAATTGCGGAAATAGCAAGAGGCAACCTAATGAAAAATAATAATTTTTCTGTTG TTTTTTCCGCACCGCCTGTTGGTGAAACATTTGCAAAGGAGGGCAAAGTGAAATGACTA GTGCACCCGGGCAGCTGCTTAAGTCCGGAGGCGCCTAACCTAAACTGACAG
gBlock 11 (*apl.tum*^{72K})	AGAAAGCAGGTGGCCCGATTCGCATTTATTACGCACGCTGGAAAGAAGAGCAGTTGCGT AAGGCGTTGGGACATTCTAGATTTCAACTCGTCATCGGTGCTTAATTCACTTTATGTGA ATTGTAAGGATGCAACATGGATAGAGAGCTAAATGAGCACGTGATGATTGAGCGGGTCG AAATGATTGCGCGTCTGACTGCTGAAGGTACTTGTCAGGAAAGAGACCGTGAAATCGCA TTGAATCTAATTGCGGAAATAGCAAGAGGCAACCTAATGAAAAATAATAATTTTTCTGT TGTTTTTTCCGCACCGCCTGTTGGTGAAACATTTGCAAAGGAGGGCAAAGTGAAATGAG GTGCGTATGCTGAAGGATCCCGTCGTTTTACAACGTCGTGACTGGGAAAACCCTGGCGT TACCCAACTTAATCGCCTTGCAGCACATCCCCCTTTCGCCAGCTGGCGTAATAGCGAAG AGGCCCGCACCGATCGCCCTTCCCAACAGTTGCGCAGCCTGAATGGCGAATGGCGCTTT GCCTGGTTTCCGGCACCAGAAGCGGTGCCGGAAAGCTGGCTGGAGTGCGATCTTCCTGA GGCCGATACTGTCGTCGTCCCCTCAAACTGGCAGATG
gBlock 12 (*apl.tum*$^{-}$)	AGAAAGCAGGTGGCCCGATTCGCATTTATTACGCACGCTGGAAAGAAGAGCAGTTGCGT AAGGCGTTGGGACATTCTAGATTTCAACTCGTCATCGGTGCTTAATTCACTTTATGTGA ATTGTAAGGATGCAACATGGATAGAGAGCTAAATGAGCACGTGATGATTGAGCGGGTCG AAATGATTGCGCGTCTGACTGCTGAAGGTACTTGTCAGGAAAGA**GGA**CGTGAAATCGCA TTGAATCTAATTGCGGAAATAGCAAGAGGCAACCTAATGAAAAATAATAATTTTTCTGT TGTTTTTTCCGCACCGCCTGTTGGTGAAACATTTGCAAAGGAGGGCAAAGTGAAATGAG GTGCGTATGCTGAAGGATCCCGTCGTTTTACAACGTCGTGACTGGGAAAACCCTGGCGT TACCCAACTTAATCGCCTTGCAGCACATCCCCCTTTCGCCAGCTGGCGTAATAGCGAAG AGGCCCGCACCGATCGCCCTTCCCAACAGTTGCGCAGCCTGAATGGCGAATGGCGCTTT GCCTGGTTTCCGGCACCAGAAGCGGTGCCGGAAAGCTGGCTGGAGTGCGATCTTCCTGA GGCCGATACTGTCGTCGTCCCCTCAAACTGGCAGATG

The initial 186-WCB *pR*$^{+}$.*apl*$^{+/-}$.*tum*$^{72K/-}$ LacZ reporters: 2-fragment assembled with the (1) *Bsu*36I and *Sap*I digested pIT3-CL-*cI*$^{+}$.***pR***$^{+}$.*pL*$^{+}$.*apl*$^{+/-}$.*cII*$^{+}$.*fil::lacZ* reporters and (2) gBlock 11 or gBlock 12.

The 186-WCB *tum* RBS optimised *pR*$^{+}$.*apl*$^{+/-}$.*tum*$^{*72K/-}$ LacZ reporters: 2-fragment assembled with the (1) *Xba*I and *Pml*I digested CL-*cI*$^{+}$.***pR***$^{+}$.*pL*$^{+}$.*apl*$^{+/-}$.*tum*^{72K}.*fil::lacZ* reporters and (2) gBlock 14.

The 186-WCB *pR*$^{+}$.*cI-CTD*.*tum*$^{*72K/-}$ reporters: gBlock 18 assembled with one of four *Bsa*BI and *Pml*I digested 186-WCB reporters:

1. pIT3-CL-*cI*$^{+}$.***pR***$^{+}$.*pL*$^{+}$.*apl*$^{-}$.*tum*$^{-}$.*fil::lacZ*
2. pIT3-CL-*cI*$^{+}$.***pR***$^{+}$.*pL*$^{+}$.*apl*$^{-}$.*tum*^{*72K}.*fil::lacZ*
3. pIT3-CL-*cI*$^{+}$.***pR***$^{+}$.*pL*$^{+}$.*apl*$^{-}$.*tum*$^{-}$.*mCherry*
4. pIT3-CL-*cI*$^{+}$.***pR***$^{+}$.*pL*$^{+}$.*apl*$^{-}$.*tum*^{*72K}.*mCherry*

apl gene (pink), *tum*$^{72K/-}$ gene (green), *tum*^{72K} *ΔD30G* (bold green), *tum*^{*72K} (underlined), *cI-CTD* (blue), *cI*$^{+}$ (orange).

gBlock	Sequence
gBlock 14 (*apl.tum*72K*)	GAAGAGCAGTTGCGTAAGGCGTTGGGACATTCTAGATTTCAACTCGTCATCGGTGCTTA ATTCACTTTATGTGAATTGTAAGGATGCAACGATAAGCAACAGAAATAAGGACTATAGT AATGGATAGAGAGCTAAATGAGCACGTGATGATTGAGCGGGTCGAAATGATTGCGCGT
gBlock 18 (*cI⁺.cI-CTD.tum*72K*)	GCTTGTCCACAAAATAAATTTTCCCCTCGGAACGGATAGCCATCCCATCTGTGAGCGGT TTTGTGAAAAATTGGGCATCAACACTCAATTGTTTATCGGATTTGAGGATTTCTTCACT TAATGTGAATCCCTCAATCCTTTTTGCGTCGCTCGATTCTCTGTTATTTACAAATGCTT CTCCTTCTCCGGTAAGTAACCACTGGAGATTAGCACCTGTTTCAAGGGCACAGTGAGCC GCAAAGTCATAGGAGATAGCGCCTCGGGTGTACCTGTTTGACAATGAGCTGGACGCGAT ATCGAAGTGGTTAGCTAATTGAATTTTCTGCGAAAATCCGTACGCCTCGCAGATGCGGT CAAGTACATCCACGTTGCTCCATCCTAAAGAATCTATTCTCATTTCGATAAAACCTATT TACTATCTCTCAATTGGGAGATATATTTTGGCTAAACCCACGCAATTGATGGCAAGTGT TGGCAAACAGAGTCAAATCAATTGCAAACTTTGGCTAATAGGGAATCATGCAATTTGGC TTCTGAAATCGCAATCATCAAAAAGAAGGAGATATACATATGAGCGATGCTAAACGTAT TGAGGGGTTCACCCTTTCCGAAGAAATTCTGAAGAGTGACAAGCAGCTTTCCGTGGATG CCCAGTTTTTCACAAAGCCCCTTACCGACGGCATGGCTATTCGCTCAGAGGGCAAAATT TATTTCGTGGATAAACAGGCAAGTCTTTCCGATGGCTTGTGGTTGGTTGACATTGAGGG TGCTATTTCGATCCGCGAGCTGACGAAGTTACCAGGGCGTAAGCTGCATGTAGCTGGAG GAAAAGTGCCCTTTGAGTGTGGTATCGACGACATCAAGACTCTTGGTCGCGTCGTTGGG GTGTATAGCGAGGTCAACTAATTCACTTTATGTGAATTGTAAGGATGCAACGATAAGCA ACAGAAATAAGGACTATAGTAATGGATAGAGAGCTAAATGAGCACGTGATGATTGAGCG GGTCGAAATGATTGCGCGTCTGACTG

7.1.5 Standard chemicals and reagents

All chemicals and reagents used in this thesis were of analytical grade or the highest purity available. Tables 7.13, 7.14 and 7.15 list the standard chemicals and reagents, enzymes and DNA purification kits used in this thesis respectively. Unless specified otherwise, all kits were used in accordance with the manufacturer's directions

Table 7.13: Standard reagents used in this thesis.

Name	Abbrev.	Company	Notes
General salts, acids and bases			
Calcium Chloride	$CaCl_2$	Sigma Aldrich	1M stock solution, filter sterilised.
Hydrochloric Acid	HCl	B.D.H. (B.D.H. Labs, Aus)	1M stock solution.
Magnesium Chloride	$MgCl_2$	Ajax	1M stock solution.
Magnesium Sulphate	$MgSO_4$	Ajax	1M stock solution.
Milli-Q Water	H_2O		Purified using Millipore Corporation filters.
Potassium Chloride	KCl	B.D.H	
Sodium Chloride	NaCl	B.D.H	
Sodium Hydroxide	NaOH	Ajax	
Tris Acetate	Tris	B.D.H	
Chloroform		Sigma Aldrich	
Biochemicals			
2-Log DNA Molecular Markers	2-Log ladder	New England Biolabs (NEB)	
Gold Standard DNA Ladder	Gold ladder	Alchemy Biosciences	
Agarose		Sigma Aldrich	
Bovine Serum Albumin	BSA		
Deoxyribonucleoside Triphosphates	dNTPs	NEB	
Glucose	Glu	B.D.H Labs	20% stock solution.
Glycerol	Gly	Boehringer Mannheim	80% stock solution.

Name	Abbrev.	Company	Notes
6X DNA Loading Buffer		NEB	
10,000X SYBR® Safe DNA Gel Stain	SYBR	Invitrogen	
Big Dye Terminator v3.1		Applied Biosystems	
EZ-Vision 6. DNA Loading Dye	EZ-V6	Amresco	
6xBlue Vision DNA Dye		NEB	
10X Tris/Glycine/SDS		BioRad	1X formulation has 25mM Tris, 192mM glycine, 0.1% SDS, pH 8.3.
Antibiotics			
Ampicillin	Amp	Sigma Aldrich	Stock solutions (100mg/mL in H_2O) Millipore filtered and stored at -20ºC.
Chloramphenicol	Chlor	Sigma Aldrich	Stock solutions (30mg/mL in 100% ethanol) stored at -20ºC.
Kanamycin	Kan	Sigma Aldrich	Stock solutions (50mg/mL in H_2O) Millipore filtered and stored at -20ºC.
Spectinomycin	Spec	Sigma Aldrich	Stock solutions (50mg/mL in H_2O) Millipore filtered and stored at -20ºC.
Tetracyclin	Tet	Upjohn Pty. Ltd.	Stock solutions (20mg/mL in 100% ethanol) and stored at -20ºC.
Other chemicals and solvents			
B-PER® Reagent	B-PER	Thermo Fisher Scientific Inc.	
Ethanol	EtOH	Crown Scientific	RNase-free.
Ethylenediaminetetraacetic Acid (disodium salt)	EDTA	Sigma Aldrich	0.4M stock solution.
Isopropanol		Merck	75% stock solution.
5-bromo-4-chloro-indolyl-β-D-galactopyranoside	X-gal	Sigma Aldrich	Stock solutions (30mg/mL in dimethyl formamide) stored at -20ºC.
2-mercaptoethanol	β-ME	Sigma Aldrich	Stored at -20ºC.
ortho-nitrophenyl-β-galactoside	ONPG	Diagnostic Chemicals Ltd.	Powder and stock solutions (4mg/mL in TZ8 buffer) stored at -20°C.
Polymyxin B Sulphate	PMB	Sigma Aldrich	Stock solutions (20mg/mL in H_2O) stored at -20ºC.
Dimethyl Sulfoxide	DMSO	Sigma Aldrich	
Potassium Chloride	KCl	B.D.H. Labs	1M stock solution.
Sodium Dodecyl Sulphate	SDS	Sigma Aldrich	
Sodium Hydroxide	NaOH	Ajax	2M stock.
Tris-EDTA Buffer	TE		0.1 EDTA, 1M Tris-Ultrapure, 100X stock in MQ H_2O.
2X LaemmLi Sample Buffer		BioRad	
TWEEN® 20		Sigma Aldrich	
4-isopropylbenzoic Acid	CA	Sigma Aldrich	100mM stock solution in EtOH.
Vanillic acid	VA	Sigma Aldrich	100mM stock solution in EtOH.
Salicylic acid	SA	Sigma Aldrich	100mM stock solution in H_2O.
Cumic acid	CA	Sigma Aldrich	

Table 7.14: Enzymes used in this thesis

Name	Company	Notes
Benzonase	Novagen	Stock concentration is 25U/µL.
BigDye Version 3.1 Ready Mix	Life Technologies	
T4 DNA Ligase	NEB (Catalog #: M0202S)	Stock concentration is 400U/µL.
Taq DNA Polymerase	NEB (Catalog #: M0273S)	Stock concentration 5U/µL.
Restriction Endonucleases	NEB	Stock concentration 5 to 100U/µL.
KAPA2G HiFi DNA Polymerase	Kapa Biosystems	Stock concentration 1U/µL.
KAPA2G Robust DNA Polymerase	Kapa Biosystems	Stock concentration 5U/µL.
Phusion® High-Fidelity DNA Polymerase	NEB (Catalog #: M0530S)	Stock concentration 2U/µL.

Table 7.15: Standard kits used in this thesis.

Name	Company	Notes
QIAprep® Spin Miniprep Kit	QIAGEN	Designed for isolation of up to 20µg high-purity plasmid DNA.
Zymoclean™ Gel DNA Recovery Kit	ZYMO Research	Used for rapid purification of high quality *DNA* from TAE buffered agarose gels.
DNA Clean and Concentrator™-5	ZYMO Research	Provides purification of up to 5µg DNA from PCR, endonuclease digestions, DNA modification reactions etc.
ZymoPURE™ Plasmid Midiprep Kit	ZYMO research	Fast spin column based procedure for purifying up to 300µg of ultrapure plasmid DNA.
NucleoSpin® Gel and PCR Clean-up Kit	Macherey-Nagel	A two-in-one kit with optimised recovery and elution volume used for purification of PCR products and extraction of DNA from agarose gels.
Monarch® PCR and DNA Clean-up Kit	NEB	Provides purification of up to 5µg DNA from PCR and other enzymatic reactions.
GenElute™ HP Plasmid Miniprep Kit	Sigma Aldrich-Aldrich	Used to purify and isolate up to 350ug of plasmid DNA.
KAPA2G Robust PCR Kit	KAPA Biosystems	Recommended for amplification of crude samples (colony PCR), DNA templates with high GC or AT content, templates containing common PCR inhibitors and to improve product yield when template quality or primer design is problematic.
KAPA HiFi™ PCR Kit	KAPA Biosystems	Recommended for the amplification of long DNA fragments for conventional sequencing, short AT- and GC-rich DNA fragments for next-generation sequencing, to generate DNA fragments for cloning and perform site-directed mutagenesis from genomic, plasmid and phage DNA templates.
Phusion® High-Fidelity PCR Kit	NEB	Ideal for high speed and high-performance PCR. The Phusion DNA polymerase offers robust performance, low error rate, short protocol times and generates higher yields with lower enzyme amounts than other DNA polymerases.

7.1.6 Standard buffers and growth media

Standard buffers and growth media were prepared in H_2O unless specified otherwise.

Table 7.16: Standard buffers and growth media used in this thesis.

Name	Formulation
Standard buffers	
Agarose Gel	1.5%(w/v) gels used for the examination and quantification of plasmid preparations and PCR/DNA digests. 1.5% gels prepared by mixing 1.5g agarose in 100mL 1X TAE, heating until dissolved, pouring and allowing to set.
Big Dye Dilution Buffer	200mM Tris-HCl pH 9.0 and 5mM $MgCl_2$ dissolved in MQ water.
LacZ Lysis-Assay Buffer	Per microtitre plate well, 150µL TZ8, 40µL ONPG (4mg/mL TZ8), 1.9µL 2-mercaptoethanol and 0.95µL polymyxin B (20mg/mL MQ H_2O) for assaying 50µL of culture (e.g. culture + media per well = 50µL).
Phage Storage Buffer (PSB)	0.4M Tris-HCL pH 7.4, 10mM $MgCl_2$, 100mM NaCl, 0.05% gelatin.
SYBR Safe (Invitrogen) 1	10,000X stock in DMSO, used with 1 in 10,000 dilution in 1XTAE.

Name	Formulation
TAE	10X stock solution, 0.4 Tris-acetate, 0.2M NaAc, 10mM EDTA, pH 8.2.
TZ8	100mM Tris pH 8.0, 1mM $MgSO_4$, 10mM KCl.
TZ8+	50µg/mL polymyxin B (PMB) and 0.27% (v/v) 2-mercaptoethanol (β-ME) made up fresh in TZ8.
Transformation and Storage Solution (TSS)	2mL 1M $MgSO_4$, 2mL 1M $MgCl_2$, 10g PEG 8000 ~10%(w/v) pH 6.5, 5mL DMSO, dissolved in LB to a total volume of 100mL.
Gibson Assembly Super Mix	1x IOS buffer, 10U/µL T5 exonuclease, 2U/µL Phusion DNA polymerase, 40U/µL T4 ligase in MQ H_2O. 15µL aliquots stored in PCR tubes at -20°C.
5X IOS Buffer	1mL 1M Tris-HCl pH 7.5, 50µL 2M $MgCl_2$, 200µL 10mM Deoxynucleotide Solution Mix (NEB), 100µL 1M DTT, 0.5g PEG-8000 (Sigma Aldrich-Aldrich), 200µL 50mM NAD (NEB) in MQ H_2O to a total volume of 2mL, stored at -20°C.
M9 Salts	10x stock solution, 67.8g NaH_2PO_4, 30.0g KH_2PO_4, 10g NH_4Cl and 5g NaCl/L of MQ H_2O.
TM Buffer	50mM TRIS pH 7.5 + 10mM $MgSO_4$, stored at RT.
1X Phosphate Buffered Saline (*PBS*)	137mM NaCl, 2.7mM KCl, 10mM Na_2HPO_4, 1.8mM KH_2PO_4, pH 7.4.
Standard growth media	
Luria Broth	1% (w/v) Bactotryptone, 1%NaCl, 0.5% (w/v) yeast extract. pH 7.0, sterilised by autoclaving.
Minimal Media 20mM Glucose	Per 100mL, 10mL 10x M9 salts, 1.8mL 20% glucose (20mM), 100µL 1M $MgSO_4$ (1mM), 25µL 0.4M $CaCl_2$ (0.1mM), 10µL 0.1M $(NH_4)_2Fe(SO_4)_2$ $6H_2O$ (0.01mM), to 100mL with MQ H_2O.
Minimal Media 1mM Glucose	Per 100mL, 10mL 10x M9 salts, 180µL 20% glucose (1mM), 100µL 1M $MgSO_4$ (1mM), 25µL 0.4M $CaCl_2$ (0.1mM), 10µL 0.1M $(NH_4)_2Fe(SO_4)_2 \bullet 6H_2O$ (0.01mM), to 100mL with MQ H_2O.
L-plates	1.5% (w/v) bacteriological agar added to Luria Broth base, autoclaved and kept molten at 45°C. Antibiotics added as required. Plates poured with ~ 20mL of L-agar, set at RT, dried at 37°C for ~1hr and stored at 4°C.
TB plates	1.2% (w/v) bacteriological agar, 1% (w/v) tryptone and 0.5% NaCl added to MQ H_2O and autoclaved. Plates poured with ~20mL of TB-agar, set at RT, dried at 37°C for ~1hr and stored at 4°C.
0.5% - 0.7% top agar	5%-7% bacteriological agar added to MQ H_2O and autoclaved. Luria Broth 1% (w/v) Bacto-tryptone, 1%NaCl, 0.5% (w/v) yeast extract. pH7.0, sterilised by autoclaving.
Super Optimal Broth with Catabolite Repression (SOC) Media	2% tryptone, 0.5% yeast extract, 10 mM NaCl, 2.5 mM KCl, 10 mM $MgCl_2$, 10 mM $MgSO_4$, and 20 mM glucose. pH 7.0, sterilised by autoclaving.

References

Ackermann, H.W., 2005. Bacteriophage Classification, in: Kutter, E., Sulakvelidze, A. (Eds.), Bacteriophages: Biology and Applications. CRC Press, Boca Raton, pp. 67-89.

AGDH: Australian Government Department of Health, 2019. Prostate cancer screening. Australian Government Department of Health. URL http://www.cancerscreening.gov.au/internet/screening/publishing.nsf/Content/prostate-cancer-screening (accessed 11.14.19).

AGRF, 2014. Sanger Sequencing Sample Submission Guide (GSEQDOC00166) v1.8.

Ahmed, A., Rushworth, J.V., Hirst, N.A., Millner, P.A., 2014. Biosensors for Whole-Cell Bacterial Detection. *Clinical Microbiology Reviews* **27**, 631–646.

Akiyama, Y., Ito, K., 2003. Reconstitution of Membrane Proteolysis by FtsH. *Journal of Biological Chemistry* **278**, 18146–18153.

Akiyama, Y., Kanehara, K., Ito, K., 2004. RseP (YaeL), an *Escherichia coli* RIP protease, cleaves transmembrane sequences. *The EMBO Journal* **23**, 4434–4442.

Akiyama, Y., Ogura, T., Ito, K., 1994. Involvement of FtsH in protein assembly into and through the membrane. I. Mutations that reduce retention efficiency of a cytoplasmic reporter. *The Journal of Biological Chemistry* **269**, 5218–5224.

Anderson, J.C., Voigt, C.A., Arkin, A.P., 2007. Environmental signal integration by a modular AND gate. *Molecular Systems Biology* **3**, 133.

Anderson, L.M., Yang, H., 2008. DNA looping can enhance lysogenic CI transcription in phage lambda. *PNAS* **105**, 5827–5832.

Andrianantoandro, E., Basu, S., Karig, D.K., Weiss, R., 2006. Synthetic biology: new engineering rules for an emerging discipline. *Molecular Systems Biology* **2**, 2006.0028.

Arber, W., Linn, S., 1969. DNA Modification and Restriction. *Annual Review of Biochemistry* **38**, 467–500.

Avlund, M., Krishna, S., Semsey, S., Dodd, I.B., Sneppen, K., 2010. Minimal Gene Regulatory Circuits for a Lysis-Lysogeny Choice in the Presence of Noise. *PLoS ONE* **5**, 1–7.

Baba, T., Ara, T., Hasegawa, M., Takai, Y., Okumura, Y., Baba, M., Datsenko, K.A., Tomita, M., Wanner, B.L., Mori, H., 2006. Construction of Escherichia coli K-12 in-frame, single-gene knockout mutants: The Keio collection. *Molecular Systems Biology* **2**.

Balázsi, G., van Oudenaarden, A., Collins, J.J., 2011. Cellular Decision Making and Biological Noise: From Microbes to Mammals. *Cell* **144**, 910–925.

Banuett, F., Hoyt, M.A, McFarlane, L., Echols, H., Herskowitz, I., 1986. hflB, a new *Escherichia coli* locus regulating lysogeny and the level of bacteriophage lambda cII protein. *Journal of Molecular Biology* **187**, 213–224.

Barbu, E.M., Cady, K.C., Hubby, B., 2016. Phage Therapy in the Era of Synthetic Biology. *Cold Spring Harbor Perspectives in Biology* **8**, a023879.

Barrangou, R., Fremaux, C., Deveau, H., Richards, M., Boyaval, P., Moineau, S., Romero, D., Horvath, P., 2007. CRISPR provides acquired resistance against viruses in prokaryotes. *Science* **315**, 1709–1712.

Bashor, C.J., Helman, N.C., Yan, S., Lim, W.A., 2008. Using engineered scaffold interactions to reshape MAP kinase pathway signaling dynamics. *Science* **319**, 1539–1543.

Bauman, A., 1990. The epidemiology of clinical tests. *Australian Prescriber* **13**, 62–64.

Bayer, T.S., Smolke, C.D., 2005. Programmable ligand-controlled riboregulators of eukaryotic gene expression. *Nature Biotechnology* **23**, 337–343.

Bednarz, M., Halliday, J.A., Herman, C., Golding, I., 2014. Revisiting Bistability in the Lysis/Lysogeny Circuit of Bacteriophage Lambda. *PLoS ONE* **9**.

Bernstein, J.A., Khodursky, A.B., Lin, P., Lin-chao, S., Cohen, S.N., 2002. Global analysis of mRNA decay and abundance in *Escherichia coli* at single-gene resolution using two-color fluorescent DNA microarrays. *PNAS U.S.A.* **99**, 9697–9702.

Bertani, G., 2004. Lysogeny at Mid-Twentieth Century: P1, P2, and Other Experimental Systems. *Journal of Bacteriology* **186**, 595–600.

Bhalla, N., Jolly, P., Formisano, N., Estrela, P., 2016. Introduction to biosensors. *Essays in Biochemistry* **60**, 1–8.

Bohunicky, B., Mousa, S.A., 2010. Biosensors: the new wave in cancer diagnosis. *Nanotechnology, Science and Applications* **4**, 1–10.

Bondy-Denomy, J., Pawluk, A., Maxwell, K.L., Davidson, A.R., 2013. Bacteriophage genes that inactivate the CRISPR/Cas bacterial immune system. *Nature* **493**, 429–432.

Bonnet, J., Yin, P., Ortiz, M.E., Subsoontorn, P., Endy, D., 2013. Amplifying Genetic Logic Gates. *Science* **340**, 599–603.

Bosch, 2019. 40 Years of Bosch Lambda Sensor. Bosch History Blog. URL https://www.bosch.com/stories/40-years-of-bosch-lambda-sensor/ (accessed 11.12.19).

Brenner, S., Jacob, F., Meselson, M., 1961. An Unstable Intermediate Carrying Information from Genes to Ribosomes for Protein Synthesis. *Nature* **190**, 576–581.

Brumby, A.M., Lamont, I., Dodd, I.B., Egan, J.B., 1996. Defining the SOS Operon of Coliphage 186. *Virology* **219**, 105–114.

Burney, I.A., Al-Moundhri, M.S., 2008. Major Advances in the Treatment of Cancer. *Sultan Qaboos University Medical Journal* **8**, 137–148.

Burrill, D.R., Silver, P.A., 2010. Making cellular memories. *Cell* **140**, 13–18.

Callen, B.P., Shearwin, K.E., Egan, J.B., 2004. Transcriptional interference between convergent promoters caused by elongation over the promoter. *Molecular Cell* **14**, 647–656.

Campanale, C., Massarelli, C., Savino, I., Locaputo, V., Uricchio, V., 2020. A Detailed Review Study on Potential Effects of Microplastics and Additives of Concern on Human Health. *IJERPH* **17**, 1212.

Cancer Council Australia, 2019a. Prostate cancer. Cancer Council. URL https://www.cancer.org.au/about-cancer/early-detection/early-detection-factsheets/prostate-cancer.html (accessed 11.14.19).

Cancer Council Australia, 2019b. Understanding your Pap Smear/Cervical Screening Test Results. Cancer Council. URL https://www.cancer.org.au/about-cancer/early-detection/early-detection-factsheets/understanding-your-pap-smear-results.html (accessed 11.14.19).

Cancer Council Australia, 2019c. Understanding your FOBT. Cancer Council. URL https://cancer.org.au/about-cancer/early-detection/early-detection-factsheets/understanding-your-fobt.html (accessed 11.14.19).

Casjens, S.R., Hendrix, R.W., 2015. Bacteriophage lambda: Early pioneer and still relevant. *Virology* **479–480**, 310–330.

Chang, H.J., Voyvodic, P.L., Zúñiga, A., Bonnet, J., 2017. Microbially derived biosensors for diagnosis, monitoring and epidemiology. *Microbial Biotechnology* **10**, 1031–1035.

Chiang, Y.N., Penadés, J.R., Chen, J., 2019. Genetic transduction by phages and chromosomal islands: The new and noncanonical. *PLoS Pathogens* **15**, 1–7.

Choi, Y.J., Morel, L., Le Francois, T., Bourque, D., Bourget, L., Groleau, D., Massie, B., Miguez, C.B., 2010. Novel, Versatile, and Tightly Regulated Expression System for *Escherichia coli* Strains. *Applied and Environmental Microbiology* **76**, 5058–5066.

Christie, G.E, Calendar, R., 2016. Bacteriophage P2. *Bacteriophage* **7081**, e1145782.

Christie, G.E., Dokland, T., 2012. Pirates of the Caudovirales. *Virology* **434**, 210–221.

Chung, C.T., Niemela, S.L., Miller, R.H., 1989. One-step preparation of competent Escherichia coli : Transformation and storage of bacterial cells in the same solution. *PNAS U.S.A.* **86**, 2172–2175.

Citorik, R.J, Mimee, M., Lu, T.K., 2014a. Bacteriophage-based synthetic biology for the study of infectious diseases. *Current Opinion in Microbiology* **19**, 59–69.

Citorik, R.J., Mimee, M., Lu, T.K., 2014b. Sequence-specific antimicrobials using efficiently delivered RNA-guided nucleases. *Nature Biotechnology*. **32**, 1141–1145.

Courbet, A., Endy, D., Renard, E., Molina, F., Bonnet, J., 2015. Detection of pathological biomarkers in human clinical samples via amplifying genetic switches and logic gates. *Science Translational Medicine* **7**, 289ra83-289ra83.

Cozzarelli, N., Melechen, N., Jovin, T., Kornberg, A., 1967. Polynucleotide cellulose as a substrate for a polynucleotide ligase induced by phage T4. *Biochemical and Biophysical Research Communications* **28**, 578–586.

Crick, F.H.C., Barnett, L., Brenner, S., Watts-Tobin, R.J., 1961. General Nature of the Genetic Code for Proteins. *Nature* **192**, 1227–1232.

Cui, L., Murchland, I., Shearwin, K.E., Dodd, I.B., 2013. Enhancer-like long-range transcriptional activation by CI-mediated DNA looping. *PNAS* **110**, 2922–2927.

Curtin, J.J., Donlan, R.M., 2006. Using bacteriophages to reduce formation of catheter-associated biofilms by Staphylococcus epidermidis. *Antimicrobial Agents and Chemotherapy* **50**, 1268–1275.

Cutts, E.E., Barry Egan, J., Dodd, I.B., Shearwin, K.E., 2020. A quantitative binding model for the Apl protein, the dual purpose recombination-directionality factor and lysis-lysogeny regulator of bacteriophage 186. *Nucleic Acids Research* **48**, 8914–8926.

d'Herelle, F., 1917. Sur un microbe invisible antagoniste des bacilles dysentériques. *Comptes Rendus Academie des Sciences Paris* **165**, 373–375.

Danino, T., Prindle, A., Kwong, G.A., Skalak, M., Li, H., Allen, K., Hasty, J., Bhatia, S.N., 2015. Programmable probiotics for detection of cancer in urine. *Science Translational Medicine* **7**, 289ra84

Datsenko, K.A., Wanner, B.L., 2000. One-step inactivation of chromosomal genes in Escherichia coli K-12 using PCR products. *PNAS* **97**, 6640–6645.

Datsenko, K.A., Wanner, B.L., 2002. One-step inactivation of chromosomal genes in Escherichia coli K-12 using PCR products. *PNAS* **97**, 6640–6645.

Datta, S., Costantino, N., Court, D.L., 2006. A set of recombineering plasmids for gram-negative bacteria. *Gene* **379**, 109–115.

Davis, M.W., 2018. ApE - A plamid Editor. URL http://jorgensen.biology.utah.edu/wayned/ape/ (accessed 2.2.19).

De Paepe, M., Leclerc, M., Tinsley, C.R., Petit, M.A., 2014. Bacteriophages: an underestimated role in human and animal health? *Frontiers in Cellular and Infection Microbiology* **4**, 11.

De Sordi, L., Lourenço, M., Debarbieux, L., 2018. “I will survive”: A tale of bacteriophage-bacteria coevolution in the gut. *Gut Microbes* **10**, 92–99.

Deltcheva, E., Chylinski, K., Sharma, C., Gonzales, K., Chao, Y., Pirzada, Z., Eckert, M., Vogel, J., Charpentier, E., 2011. CRISPR RNA maturation by trans-encoded small RNA and host factor RNase III. *Nature* **471**, 602–607.

Deveau, H., Barrangou, R., Garneau, J.E., Labonté, J., Fremaux, C., Boyaval, P., Romero, D.A., Horvath, P., Moineau, S., 2008. Phage Response to CRISPR-Encoded Resistance in *Streptococcus thermophilus*. *Journal of Bacteriology* **190**, 1390–1400.

Dodd, I.B., Egan, J.B, 1996. DNA binding by the Coliphage 186 Repressor Protein CI. *Journal of Biological Chemistry* **271**, 11532–11540.

Dodd, I.B., Egan, J.B., 1999. P2, 186 and related phages (Myoviridae), in: Webster, R., Granoff, A. (Eds.), Encyclopaedia of Virology. Academic Press, London, United Kingdom, pp. 1087–1094.

Dodd, I.B., Egan, J.B., 2002. Action at a distance in CI repressor regulation of the bacteriophage 186 genetic switch. *Molecular Microbiology* **45**, 697–710.

Dodd, I.B., Kalionis, B., Egan, J.B., 1990. Control of gene expression in the temperate coliphage 186: VIII. Control of lysis and lysogeny by a transcriptional switch involving face-to-face promoters. *Journal of Molecular Biology* **214**, 27–37.

Dodd, I.B., Shearwin, K.E., Perkins, A.J., Burr, T., Hochschild, A. and Egan, J.B., 2004. Cooperativity in long-range gene regulation by the lambda CI repressor. *Genes & Development* **18**, 344–354.

Dodd, I.B., Perkins, A.J., Tsemitsidis, D., Egan, J.B., 2001. Octamerization of λ CI repressor is needed for effective repression of PRM and efficient switching from lysogeny. *Genes & Development* **15**, 3013–3022.

Dodd, I.B., Reed, M.R., Egan, J.B., 1993. The Cro-like Apl repressor of coliphage 186 is required for prophage excision and binds near the phage attachment site. *Molecular Microbiology* **10**, 1139–1150.

Dodd, I.B., Shearwin, K.E., Sneppen, K., 2007. Modelling transcriptional Interference and DNA Looping in gene regulation. *Journal of Molecular Biology* **369**, 1200–1213.

Eliava Institute, 2018. About Us - Eliava Institute. Eliava Institute. URL http://eliava-institute.org/about-us/ (accessed 11.4.19).

Elowitz, M.B., Leibler, S., 2000. A synthetic oscillatory network of transcriptional regulators. *Nature* **403**, 335–338.

Espah Borujeni, A., Channarasappa, A.S., Salis, H.M., 2014. Translation rate is controlled by coupled trade-offs between site accessibility, selective RNA unfolding and sliding at upstream standby sites. *Nucleic Acids Research* **42**, 2646–2659.

Espinosa-Urgel, M., Serrano, L., Ramos, J.L., Fernández-Escamilla, A.M., 2015. Engineering Biological Approaches for Detection of Toxic Compounds: A New Microbial Biosensor Based on the Pseudomonas putida TtgR Repressor. *Molecular Biotechnology* **57**, 558–564.

Ferrell, J.E., 2002. Self-perpetuating states in signal transduction: positive feedback, double-negative feedback and bistability. *Current Opinion in Cell Biology* **14**, 140–148.

Fleming, A., 1929. On the antibacterial action of cultures of a penicillium, with special reference to their use in the isolation of B. influenzae. *The British Journal of Experimental Pathology* **10**, 226–236.

Fornelos, N., Bamford, J.K.H., Mahillon, J., 2011. Phage-Borne Factors and Host LexA Regulate the Lytic Switch in Phage GIL01. *Journal of Bacteriology* **193**, 6008–6019.

François, P., Hakim, V., 2005. Core genetic module: The mixed feedback loop. *Physical Reviews E* **72**, 031908.

Friedland, A.E., Lu, T.K., Wang, X., Shi, D., Church, G., Collins, J.J., 2009. Synthetic gene networks that count. *Science* **324**, 1199–1202.

Galkin, V.E., Yu, X., Bielnicki, J., Ndjonka, D., Bell, C.E., Egelman, E.H., 2009. Cleavage of Bacteriophage λ cI Repressor Involves the RecA C-terminal Domain. *Journal of Molecular Biology* **385**, 779–787.

Gardner, T.S., Cantor, C.R., Collins, J.J., 2000. Construction of a genetic toggle switch in *Escherichia coli*. *Nature* **403**, 339–342.

Gefter, M., Becker, A., Hurwitz, J., 1967. The enzymatic repair of DNA. I. Formation of circular lambda-DNA. *PNAS* **58**, 240–247.

Gellert, M., 1967. Formation of covalent circles of lambda DNA by *E. coli* extracts. *PNAS* **57**, 148–155.

Gibson, D.G., Benders, G.A., Andrews-Pfannkoch, C., Denisova, E.A., Baden-Tillson, H., Zaveri, J., Stockwell, T.B., Brownley, A., Thomas, D.W., Algire, M.A., Merryman, C., Young, L., Noskov, V.N., Glass, J.I., Venter, J.C., Hutchison, C.A., Smith, H.O., 2008. Complete chemical synthesis, assembly, and cloning of a Mycoplasma genitalium genome. *Science* **319**, 1215–1220.

Gibson, D.G., Glass, J.I., Lartigue, C., Noskov, V.N., Chuang, R.Y., Algire, M.A., Benders, G.A., Montague, M.G., Ma, L., Moodie, M.M., Merryman, C., Vashee, S., Krishnakumar, R., Assad-Garcia, N., Andrews-Pfannkoch, C., Denisova, E.A., Young, L., Qi, Z.Q., Segall-Shapiro, T.H., Calvey, C.H., Parmar, P.P., Hutchison, C.A., Smith, H.O., Venter, J.C., 2010. Creation of a bacterial cell controlled by a chemically synthesized genome. *Science* **329**, 52–56.

Gibson, D.G., Young, L., Chuang, R.Y., Venter, J.C., Hutchison, C.A., Smith, H.O., 2009. Enzymatic assembly of DNA molecules up to several hundred kilobases. *Nature Methods* **6**, 343–345.

Gladskin, 2019. Gladskin - The targeted approach for people with skin problems. Gladskin EU. URL https://www.gladskin.com/ (accessed 11.4.19).

Golding, I., 2016. Single-Cell Studies of Phage λ: Hidden Treasures Under Occam's Rug. *Annual Review of Virology* **3**, 7.1-7.20.

Goryshin, I.Y., Jendrisak, J., Les, M., Meis, R., Reznikoff, W.S., 2000. Insertional transposon mutagenesis by electroporation of released Tn5 transposition complexes. *Nature Biotechnology* **18**, 97–100.

Gui, Q., Lawson, T., Shan, S., Yan, L., Liu, Y., 2017. The Application of Whole Cell-Based Biosensors for Use in Environmental Analysis and in Medical Diagnostics. *Sensors (Basel)* **17**, 1623.

Guttman, B., Raya, R., Kutter, E., 2004. Basic Phage Biology, in: Kutter, E., Sulakvelidze, A. (Eds.), Bacteriophages Biology and Applications. Taylor and Francis Group, LLC, Boca Raton.

Haldimann, A., Wanner, B.L., 2001. Conditional-Replication, Integration, Excision, and Retrieval Plasmid-Host Systems for Gene Structure-Function Studies of Bacteria. *Journal of Bacteriology* **183**, 6384–6393.

Han, T., Chen, Q., Liu, H., 2017. Engineered Photoactivatable Genetic Switches Based on the Bacterium Phage T7 RNA Polymerase. *ACS Synthetic Biology* **6**, 357–366.

Hankin, M.E., 1896. The bactericidal action of the waters of the Jamuna and Ganges rivers on Cholera microbes. Annales de l'Institut Pasteur **10**, 511–523.

Hao, N., Crooks, M.T., Palmer, A.C., Dodd, I.B., Shearwin, K.E., 2019. RNA polymerase pausing at a protein roadblock can enhance transcriptional interference by promoter occlusion. *FEBS Letters* **593**, 903–917.

Haq, I.U., Chaudhry, W.N., Akhtar, M.N., Andleeb, S., Qadri, I., 2012. Bacteriophages and their implications on future biotechnology: a review. *Virology Journal* **9**, 9.

Harada, L.K., Silva, E.C., Campos, W.F., Del Fiol, F.S., Vila, M., Dąbrowska, K., Krylov, V.N., Balcão, V.M., 2018. Biotechnological applications of bacteriophages: State of the art. *Microbiological Research* **212–213**, 38–58.

Harper, D.R., McConville, M., Anderson, F.J., Enright, M.C., 2015. Chapter 31: Antimicrobial Phages, in: Academic Press, Molecular Medical Microbiology. Elsevier Science Ltd., pp. 567–581.

Herman, C., 2006. What Makes a Screening Exam "Good"? *Ethics Journal of the American Medical Association* **8**, 34–37.

Herman, C., Ogura, T., Tomoyasu, T., Hiraga, S., U.S.A., Y., Ito, K., Thomas, R., D'Ari, R., Bouloc, P., 1993. Cell growth and lambda phage development controlled by the same essential Escherichia coli gene, ftsH/hflB. *PNAS U.S.A.* **90**, 10861–10865.
Herman, C., Thévenet, D., D'Ari, R., Bouloc, P., 1995. Degradation of sigma 32, the heat shock regulator in Escherichia coli, is governed by HflB. *PNAS U.S.A.* **92**, 3516–3520.

Hershey, A.D., Chase, M., 1952. Independent functions of viral protein and nucleic acid in growth of bacteriophage. The *Journal of General Physiology* **36**, 39–56.

Herskowitz, I., Hagen, D., 1980. The Lysis-Lysogeny Decision of Phage lambda: Explicit Programming and Responsiveness. An*nual Review of Genetics* **14**, 399–445.

Holmes, R.K., 2000. Biology and Molecular Epidemiology of Diphtheria Toxin and the tox Gene. *The Journal of Infectious Diseases* **181**, 156–167.

Hooper, I., Woods, W.H., Egan, B., 1981. Coliphage 186 Replication is delayed when the host cell is UV irradiated before infection. *Journal of Virology* **40**, 341–349.

Howard-Varona, C., Hargreaves, K.R., Abedon, S.T., Sullivan, M.B., 2017. Lysogeny in nature: mechanisms, impact and ecology of temperate phages. *The ISME Journal* **11**, 1511–1520.

Hoyt, M.A, Knight, D.M., Das, A., Miller, H.I., Echols, H., 1982. Control of phage lambda development by stability and synthesis of cII protein: role of the viral cIII and host hflA, himA and himD genes. *Cell* **31**, 565–573.

Hwang, J., Choi, D., Han, S., Jung, S.Y., Choi, J., Hong, J., 2020. Potential toxicity of polystyrene microplastic particles. *Scientific Reports* **10**, 7391.

ICTV: International Committee on Taxonomy of Viruses, 2019. Taxonomy. International Committee on Taxonomy of Viruses (ICTV). URL https://talk.ictvonline.org/taxonomy/ (accessed 11.4.19).

Ike, K., Arasawa, Y., Koizumi, S., Mihashi, S., Kawai-Noma, S., Saito, K., Umeno, D., 2015. Evolutionary Design of Choline-Inducible and -Repressible T7-Based Induction Systems. *ACS Synthetic Biology* **4**, 1352–1360.

Inniss, M.C., Silver, P.A., 2013. Building synthetic memory. *Current Biology* **23**, R812-R816.

Integrated DNA Technologies, 2019. Codon Optimization Tool. SciTools Web Tools. URL https://sg.idtdna.com/pages/tools?utm_source=google&utm_medium=cpc&utm_campaign=ga_codon_opt_us&utm_content=ad_group_codon_opt&gclid=EAIaIQobChMI2rrZ2tzI5gIVg42PCh22VgzCEAAYASAAEgIeHPD_BwE (accessed 12.22.19).

IOM: Institute of Medicine, 2011. The Science and Applications of Synthetic and Systems Biology. The National Academies Press, Washington DC.

Jacob, F., Monod, J., 1961. Genetic regulatory mechanisms in the synthesis of proteins. *Journal of Molecular Biology* **3**, 318–356.

Jinek, M., Chylinski, K., Fonfara, I., Hauer, M., Doudna, J.A., Charpentier, E., 2012. A Programmable Dual-RNA-Guided DNA Endonuclease in Adaptive Bacterial Immunity. *Science* **337**, 816–821.

Kanehara, K., Ito, K., Akiyama, Y., 2002. YaeL (EcfE) activates the sigma E pathway of stress response through a site-2 cleavage of anti-sigma E, RseA. *Genes & Development* **16**, 2147–2155.

Kasmna, L., Porter, L., 2019. Bacteriophage, in: StatPearls [Internet]. StatPearls Publishing, Treasure Island (FL).

Keen, E.C., 2015. A century of phage research: Bacteriophages and the shaping of modern biology: Cause to reflect. *Bioessays* **37**, 6–9.

Khalil, A.S., Collins, J.J., 2010. Synthetic biology: applications come of age. *Nature Reviews Genetics* **11**, 367–379.

Kiehl, T.R., Mattheyses, R.M., Simmons, M.K., 2004. Hybrid simulation of cellular behavior. *Bioinformatics* **20**, 316–322.

Kim, E.J., Yu, H.J., Lee, J.H., Kim, J.O., Han, S.H., Yun, C.H., Chun, J., Nair, G.B., Kim, D.W., 2017. Replication of Vibrio cholerae classical CTX phage. *PNAS* **114**, 2343–2348.

Knight, T., 2003. Idempotent Vector Design for Standard Assembly of Biobricks, in: MIT Synthetic Biology Working Group0. MIT Artificial Intelligence Laboratory; MIT Synthetic Biology Working Group.

Kobiler, O., Rokney, A., Friedman, N., Court, D.L., Stavans, J., Oppenheim, A.B., 2005. Quantitative kinetic analysis of the bacteriophage λ genetic network. *PNAS* **102**, 4470–4475.

Kobiler, O., Rokney, A., Oppenheim, A.B., 2007. Phage Lambda CIII: A Protease Inhibitor Regulating the Lysis-Lysogeny Decision. *PLoS ONE* **2**, e363.

Koskella, B., Brockhurst, M.A., 2014. Bacteria–phage coevolution as a driver of ecological and evolutionary processes in microbial communities. *FEMS Microbiology Review* **38**, 916–931.

Kotula, J.W., Kerns, S.J., Shaket, L.A., Siraj, L., Collins, J.J., Way, J.C., Silver, P.A., 2014. Programmable bacteria detect and record an environmental signal in the mammalian gut. *PNAS U.S.A.* **111**, 4838–4843.

Krüger, D.H., Bickle, T.A., 1983. Bacteriophage survival: multiple mechanisms for avoiding the deoxyribonucleic acid restriction systems of their hosts. *Microbiology Review* **47**, 345–360.

Kruger, S., Ilmer, M., Kobold, S., Cadilha, B.L., Endres, S., Ormanns, S., Schuebbe, G., Renz, B.W., D'Haese, J.G., Schloesser, H., Heinemann, V., Subklewe, M., Boeck, S., Werner, J., von Bergwelt-Baildon, M., 2019. Advances in cancer immunotherapy 2019 – latest trends. Journ*al of Experimental & Clinical Cancer Research* **38**, 268.

Kutter, E., 2001. Bacteriophages, in: Brenner, S., Miller, J.H. (Eds.), Encyclopedia of Genetics. Elsevier Science Ltd., pp. 179–186.

Kwok, R., 2010. Five hard truths for synthetic biology. *Nature* **463**, 288–290.

Lamont, I., Brumby, A.M., Egan, J.B., 1989. UV induction of coliphage 186: prophage induction as an SOS function. *PNAS U.S.A.* **86**, 5492–5496.

Lamont, I., Richardson, H., Carter, D.R., Egan, J.B., 1993. Genes for the establishment and maintenance of lysogeny by the temperate coliphage 186. *Journal of Bacteriology* **175**, 5286–5288.

Landsmann, J., Kröger, M., Hobom, G., 1982. The rex region of bacteriophage lambda: two genes under three-way control. *Gene* **20**, 11–24.

Leduc, S., 1912. La biologie synthétique, in: Études de biophysique II. A. Poinat, Paris.

Lee, S.K., Chou, H.H., Pfleger, B.F., Newman, J.D., Yoshikuni, Y., Keasling, J.D., 2007. Directed evolution of AraC for improved compatibility of arabinose- and lactose-inducible promoters. *Applied Environmental Microbiology* **73**, 5711–5715.

Lemire, S., Figueroa-Bossi, N., Bossi, L., 2011. Bacteriophage Crosstalk: Coordination of Prophage Induction by Trans-Acting Antirepressors. PLoS Genetics **7**, e1002149.

Lewis, D., Le, P., Zurla, C., Finzi, L., Adhya, S., 2011. Multilevel autoregulation of λ repressor protein CI by DNA looping in vitro. *PNAS U.S.A.* **108**, 14807–14812.

Lewis, L.K., Harlow, G.R., Gregg-Jolly, L.A., Mount, D.W., 1994. Identification of high affinity binding sites for LexA which define new DNA damage-inducible genes in Escherichia coli. *Journal of Molecular Biology* **241**, 507–523.

Li, M., Moyle, H., Susskind, M.M., 1994. Target of the transcriptional activation function of phage lambda cI protein. *Science* **263**, 75–77.

Lin, D.M., Koskella, B., Lin, H.C., 2017. Phage therapy: An alternative to antibiotics in the age of multi-drug resistance. *World Journal of Gastrointestinal Pharmacology and Therapeutics* **8**, 162–173.

Linn, T., St Pierre, R., 1990. Improved vector system for constructing transcriptional fusions that ensures independent translation of lacZ. *Journal of Bacteriology* **172**, 1077–1084.

Little, J.W., Edmiston, S.H., Pacelli, L.Z., Mount, D.W., 1980. Cleavage of the Escherichia coli lexA protein by the recA protease. *PNAS* **77**, 3225–3229.

Little, J.W., Mount, D.W., 1982. The SOS regulatory system of Escherichia coli. *Cell* **29**, 11–22.

Liu, C., Sun, D., Zhu, J., Liu, W., 2019. Two-Component Signal Transduction Systems: A Major Strategy for Connecting Input Stimuli to Biofilm Formation. *Frontiers in Microbiology* **9**, 3279.

Liu, T., Renberg, S.K., Haggård-Ljungquist, E., 1997. Derepression of prophage P2 by satellite phage P4: cloning of the P4 epsilon gene and identification of its product. *Journal of Virology* **71**, 4502–4508.

Ljungquist, E., Bukhari, A.I., 1977. State of prophage Mu DNA upon induction. *PNAS U.S.A.* **74**, 3143–3147.

Lobocka, M.B., Rose, D.J., Plunkett, G., Rusin, M., Samojedny, A., Lehnherr, H., Yarmolinsky, M.B., Blattner, F.R., 2004. Genome of Bacteriophage P1. Jo*urnal of Bacteriology* **186**, 7032–7068.

Looger, L.L., Dwyer, M.A., Smith, J.J., Hellinga, H.W., 2003. Computational design of receptor and sensor proteins with novel functions. *Nature* **423**, 185–190.

Lopez, D., Vlamakis, H., Kolter, R., 2010. Biofilms. *Cold Spring Harbor Perspectives in Biology* **2**, a000398.

Lu, T.K., Collins, J.J., 2007. Dispersing biofilms with engineered enzymatic bacteriophage. *PNAS* **104**, 11197–11202.

Luria, S., Delbrück, M., 1943. Mutations of bacteria from virus sensitivity to virus resistance. *Genetics* **28**, 491–511.

Lutz, R., Bujard, H., 1997. Independent and tight regulation of transcriptional units in Escherichia coli via the LacR/O, the TetR/O and AraC/I1-I2 regulatory elements. *Nucleic Acids Research* **25**, 1203–1210.

Maniloff, J., Ackermann, H.W., 1998. Taxonomy of bacterial viruses: establishment of tailed virus genera and the order Caudovirales. *Virology Division News* **143**, 2051–2063.

Mardanov, A.V., Ravin, N.V., 2007. The Antirepressor Needed for Induction of Linear Plasmid-Prophage N15 Belongs to the SOS Regulon. *Journal of Bacteriology* **189**, 6333–6338.

Markham, M.J., Wachter, K., Agarwal, N., Bertagnolli, M.M., Chang, S.M., Dale, W., Diefenbach, C.S.M., Rodriguez-Galindo, C., George, D.J., Gilligan, T.D., Harvey, R.D., Johnson, M.L., Kimple, R.J., Knoll, M.A., LoConte, N., Maki, R.G., Meisel, J.L., Meyerhardt, J.A., Pennell, N.A., Rocque, G.B., Sabel, M.S., Schilsky, R.L., Schneider, B.J., Tap, W.D., Uzzo, R.G., Westin, S.N., 2020. Clinical Cancer Advances 2020: Annual Report on Progress Against Cancer From the American Society of Clinical Oncology. *Journal of Clinical Oncology* **38**, 1081–1101

Maxim, L.D., Niebo, R., Utell, M.J., 2014. Screening tests: a review with examples. *Inhalation Toxicology* **26**, 811–828.

Mehrotra, P., 2016. Biosensors and their applications – A review. *Journal of Oral Biology and Craniofacial Research* **6**, 153–159.

Merrick, C.A., Zhao, J., Rosser, S.J., 2018. Serine Integrases: Advancing Synthetic Biology. *ACS Synthetic Biology* **7**, 299–310.

Meselson, M., Weigle, J., 1961. Chromosome breakage accompanying genetic recombination in bacteriophage. *PNAS* **47**, 857–868.

Meyer, A.J., Segall-Shapiro, T.H., Glassey, E., Zhang, J., Voigt, C.A., 2019. Escherichia coli "Marionette" strains with 12 highly optimized small-molecule sensors. *Nature Chemical Biology* **15**, 196–204.

Meyer, B.J., Maurer, R., Ptashne, M., 1980. Gene regulation at the right operator (OR) of bacteriophage λ: II. OR1, OR2, and OR3: Their roles in mediating the effects of repressor and cro. *Journal of Molecular Biology* **139**, 163–194.

Meyer, J.R., Dobias, D.T., Weitz, J.S., Barrick, J.E., Quick, R.T., Lenski, R.E., 2012. Repeatability and contingency in the evolution of a key innovation in phage lambda. *Science* **335**, 428–432.

Michel, A., Clermont, O., Denamur, E., Tenaillon, O., 2010. Bacteriophage PhiX174's Ecological Niche and the Flexibility of Its Escherichia coli Lipopolysaccharide Receptor. *Applied and Environmental Microbiology* **76**, 7310–7313.

Micreos, 2019. Phage Guard - Micreos Food Safety. URL https://www.micreos.com/content/food-safety.aspx (accessed 11.4.19).

Mitrophanov, A.Y., Groisman, E.A., 2008. Signal integration in bacterial two-component regulatory systems. *Genes & Development* **22**, 2601–2611.

Monteiro, R., Pires, D.P., Costa, A.R., Azeredo, J., 2019. Phage Therapy: Going Temperate? *Trends in Microbiology* **27**, 368–378.

Morris, K.A., 2011. What is Hysteresis? *Applied Mechanics Reviews* **64**, 050801.

Moye, Z., Woolston, J., Sulakvelidze, A., 2018. Bacteriophage Applications for Food Production and Processing. *Viruses* **10**, 205.

Müller, J., Oehler, S., Müller-Hill, B., 1996. Repression of lac promoter as a function of distance, phase and quality of an auxiliary lac operator. *Journal of Molecular Biology* **257**, 21–29.

Muller-Hill, B., 1996. The lac Operon: A Short History of a Genetic Paradigm. Walter de Gruyter, Berlin, Germany.

Murchland, I., Ahlgren-Berg, A., Priest, D.G., Dodd, I.B., Shearwin, K.E., 2014. Promoter Activation by CII, a Potent Transcriptional Activator from Bacteriophage 186. J*ournal of Biological Chemistry* **289**, 32094–32108.

National Bowel Cancer Screening Program, 2019. Bowel Screening. Australian Government Department of Health. URL http://www.cancerscreening.gov.au/internet/screening/publishing.nsf/Content/bowel-screening-2 (accessed 11.14.19).

National Cancer Institute, 2019. Tumor Markers - National Cancer Institute. Tumour Markers. URL https://www.cancer.gov/about-cancer/diagnosis-staging/diagnosis/tumor-markers-fact-sheet (accessed 6.27.20).

National Cervical Screening Program, 2019. Cervical Screening. URL http://www.cancerscreening.gov.au/internet/screening/publishing.nsf/Content/cervical-screening-1 (accessed 11.14.19).

Nelson, D., 2004. Phage Taxonomy: We Agree To Disagree. *Journal of Bacteriology* **186**, 7029–7031.
Neufing, P.J., Shearwin, K.E., Camerotto, J., Egan, J.B., 1996. The CII protein of bacteriophage 186 establishes lysogeny by activating a promoter upstream of the lysogenic promoter. *Molecular Microbiology* **21**, 751–61.

Neufing, P.J., Shearwin, K.E., Egan, J.B., 2001. Establishing Lysogenic Transcription in the Temperate Coliphage 186. *Journal of Bacteriology* **183**, 2376–2379.

NIH: National Library of Medicine Profiles in Science, 1959. Creating Life in the Test Tube. Arthur Kornberg Papers. URL https://profiles.nlm.nih.gov/spotlight/wh/feature/creating-life-in-the-test-tube-1959-1970 (accessed 11.4.19).

Nilsson, A., Haggård-Ljungquist, E., 2005. The P2-like bacteriophages, in: Calendar, R.L. (Eds.), The Bacteriophages. Oxford University Press Incorporated, Oxford, United States.

Nilsson, H., Cardoso-Palacios, C., Haggård-Ljungquist, E., Nilsson, A.S., 2011. Phylogenetic structure and evolution of regulatory genes and integrases of P2-like phages. *Bacteriophage* **1**, 207–218.

Noman, N., Inniss, M., Iba, H., Way, J.C., 2016. Pulse Detecting Genetic Circuit - A New Design Approach. *PLoS ONE* **11**, e0167162.

Novak, B., Tyson, J.J., 1993. Numerical analysis of a comprehensive model of M-phase control in Xenopus oocyte extracts and intact embryos. *Journal of Cell Science* **106**,1153–1168.

Novik, G., Ladutska, A., Rakhuba, D., 2017. Bacteriophage taxonomy and classification, in: Antimicrobial Research: Novel Bioknowledge and Educational Programs, Microbiology Book Series 6. Formatex, Badjoz, Spain, pp. 251–259.

O'Brien, A., Newland, J., Miller, S., Holmes, R., Smith, H., Formal, S., 1984. Shiga-like toxin-converting phages from Escherichia coli strains that cause hemorrhagic colitis or infantile diarrhea. *Science* **226**, 694–696.

Ogura, T., Inoue, K., Tatsuta, T., Suzaki, T., Karata, K., Young, K., Su, L.-H., Fierke, C.A., Jackman, J.E., Raetz, C.R.H., Coleman, J., Tomoyasu, T., Matsuzawa, H., 1999. Balanced biosynthesis of major membrane components through regulated degradation of the committed enzyme of lipid A biosynthesis by the AAA protease FtsH (HflB) in Escherichia coli. *Molecular Microbiology* **31**, 833–844.

Olivera, B., Lehman, I., 1967. Linkage of polynucleotides through phosphodiester bonds by an enzyme from Escherichia coli. *PNAS* **57**, 1426–1433.

OpenWetWare, 2020. E. coli genotypes. URL https://openwetware.org/wiki/E._coli_genotypes (accessed 2.9.20).

Oppenheim, A.B., Kobiler, O., Stavans, J., Court, D.L., Adhya, S., 2005. Switches in Bacteriophage Lambda Development. *Annual Review of Genetics* **39**, 409–429.

Orlova, E.V., 2012. Chapter 2: Bacteriophages and Their Structural Organisation, in: Kurtboke, I. (Eds.), Bacteriophages [Internet]. In Tech. pp. 5–30.

Ortiz, M.E., Endy, D., 2012. Engineered cell-cell communication via DNA messaging. *Journal of Biological Engineering* **6**, 16.

Palmer, A.C., Ahlgren-Berg, A., Egan, J.B., Dodd, I.B., Shearwin, K.E., 2009. Potent Transcriptional Interference by Pausing of RNA Polymerases over a Downstream Promoter. *Molecular Cell* **34**, 545–555.

Pande, J., Szewczyk, M., Grover, A., 2010. Phage display: Concept, innovations, applications and future. *Biology Advances* **28**, 849–858.

Patel, S., Nanda, R., Sahoo, S., Mohapatra, E., 2016. Biosensors in Health Care: The Milestones Achieved in Their Development Towards Lab-on-Chip-Analysis. *Biochemistry Research International* **2016**, 1–12.

Paul, J.H., 2008. Prophages in marine bacteria: dangerous molecular time bombs or the key to survival in the seas? *The ISME Journal* **2**, 579–589.

Pepin, K.M., Domsic, J., McKenna, R., 2008. Genomic evolution in a virus under specific selection for host recognition. *Infection, Genetics and Evolution* **8**, 825–834.

Phage Therapy Center, 2018. Welcome to Phage Therapy Center. Phage Therapy Center. URL http://www.phagetherapycenter.com/pii/PatientServlet?command=static_home (accessed 11.4.19).

Pietsch, J.M.J., 2015. The Design, Synthesis and Quantitative Analysis of a Bistable Mixed Feedback Loop Gene Network. The University of Adelaide.

Piñero-Lambea, C., Bodelón, G., Fernández-Periáñez, R., Cuesta, A.M., Álvarez-Vallina, L., Fernández, L.Á., 2015. Programming Controlled Adhesion of E. coli to Target Surfaces, Cells, and Tumors with Synthetic Adhesins. *ACS Synthetic Biology* **4**, 463–473.

Pinkett, H.W., Shearwin, K.E., Stayrook, S., Dodd, I.B., Burr, T., Hochschild, A., Egan, J.B., Lewis, M., 2006. The structural basis of cooperative regulation at an alternate genetic switch. *Molecular Cell* **21**, 605–615.

Porcar, M., Danchin, A., de Lorenzo, V., dos Santos, V.A., Krasnogor, N., Rasmussen, S., Moya, A., 2011. The ten grand challenges of synthetic life. *Systems and Synthetic Biology* **5**, 1–9.

Portelli, R., Dodd, I.B., Xue, Q., Egan, J.B., 1998. The Late-Expressed Region of the Temperate Coliphage 186 Genome. *Virology* **248**, 117–130.

Priest, D.G., Cui, L., Kumar, S., Dunlap, D.D., Dodd, I.B., Shearwin, K.E., 2014. Quantitation of the DNA tethering effect in long-range DNA looping in vivo and in vitro using the Lac and λ repressors. *PNAS U.S.A.* **111**, 349–54.

Ptashne, M., 2006. Lambda's Switch: Lessons from a Module Swap. *Current Biology* **16**, R459–R462.

Ptashne, M., 2004. A Genetic Switch Phage Lambda Revisited (Third Edition), in: Weisberg, R.A. (Eds.), *The Quarterly Review of Biology* **79**, 427-428. https://doi.org/10.1086/428187.

Quinones, M., Kimsey, H.H., Waldor, M.K., 2005. LexA cleavage is required for CTX prophage induction. *Molecular Cell* **17**, 291–300.

Reed, M.R., 1994. Apl: a multifunctional repressor and excisionase essential for prophage induction of temperate coliphage 186. The University of Adelaide.

Reed, M.R., Shearwin, K.E., Pell, L.M., Egan, J.B., 1997. The dual role of Apl in prophage induction of coliphage 186. *Molecular Microbiology* **23**, 669–81.

Roberts, J.W., Roberts, C.W., Craig, N.L., 1978. Escherichia coli recA gene product inactivates phage lambda repressor. *PNAS* **75**, 4717–4718.

Rokney, A., Kobiler, O., Amir, A., Court, D.L., Stavans, J., Adhya, S., Oppenheim, A.B., 2008. Host responses influence on the induction of lambda prophage. *Molecular Microbiology* **68**, 29–36.

Rozanov, D.V., D'Ari, R., Sineoky, S.P., 1998. RecA-Independent Pathways of Lambdoid Prophage Induction in Escherichia coli. *Journal of Bacteriology* **180**, 6306–6315.

Runyen-Janecky, L.J., Hong, M., Payne, S.M., 1999. The Virulence Plasmid-Encoded impCAB Operon Enhances Survival and Induced Mutagenesis in Shigella flexneri after Exposure to UV Radiation. *Infection and Immunity* **67**, 1415–1423.

Salmond, G.P.C., Fineran, P.C., 2015. A century of the phage: past, present and future. *Nature Reviews Microbiology* **13**, 777–786.

Sanger, F., Air, G.M., Barrell, B.G., Brownt, N.L., Coulson, A.R., Fiddes, C., Hutchison, C.A., 1977. Nucleotide sequence of bacteriophage φX174 DNA. *Nature* **265**, 687–695.

Sassanfar, M., Roberts, J.W., 1990. Nature of the SOS-inducing signal in Escherichia coli. The involvement of DNA replication. *Journal of Molecular Biology* **212**, 79–96.

Sauer, B., 1987. Functional expression of the cre-lox site-specific recombination system in the yeast Saccharomyces cerevisiae. *Molecular Cell Biology* **7**, 2087–2096.

Schaerli, Y., Gili, M., Isalan, M., 2014. A split intein T7 RNA polymerase for transcriptional AND-logic. *Nucleic Acids Research* **42**, 12322–12328.

Schmidt, H., Hensel, M., 2004. Pathogenicity Islands in Bacterial Pathogenesis. *Clinical Microbiology Reviews* **17**, 14–56.

Schubert, R.A., Dodd, I.B., Egan, J.B., Shearwin, K.E., 2007. Cro's role in the CI–Cro bistable switch is critical for λ's transition from lysogeny to lytic development. *Genes & Development* **21**, 2461–2472.

Schyfter, P., Frow, E., Calvert, J., 2013. Guest Editorial: Synthetic biology: making biology into an engineering discipline. *Engineering Studies* **5**, 1–5.

Shams, M., Alam, I., Chowdhury, I., 2020. Aggregation and stability of nanoscale plastics in aquatic environment. *Water Research* **171**, 115401.

Shaner, N.C., Campbell, R.E., Steinbach, P.A., Giepmans, B.N.G., Palmer, A.E., Tsien, R.Y., 2004. Improved monomeric red, orange and yellow fluorescent proteins derived from Discosoma sp. red fluorescent protein. *Nature Biotechnology* **22**, 1567–1572.

Sharan, S.K., Thomason, L.C., Kuznetsov, S.G., Court, D.L., 2009. Recombineering: A Homologous Recombination-Based Method of Genetic Engineering. *Nature Protocols* **4**, 206–223.

Shearwin, K.E., Brumby, A.M., Egan, J.B., 1998. The Tum protein of coliphage 186 is an antirepressor. *Journal of Biological Chemistry* **273**, 5708–5715.

Shearwin, K.E., Callen, B.P., Egan, J.B., 2005. Transcriptional interference - A crash course. *Trends in Genetics* **21**, 339–345.

Shearwin, K.E., Dodd, I.B., Egan, J.B., 2002. The Helix-Turn-Helix Motif of the Coliphage 186 Immunity Repressor Binds to Two Distinct Recognition Sequences. *Journal of Biological Chemistry* **277**, 3186–3194.

Shearwin, K.E., Egan, J.B., 2000. Establishment of lysogeny in bacteriophage 186 DNA binding and transcriptional activation by the CII protein. *Journal of Biological Chemistry* **275**, 29113–29122.

Shearwin, K.E., Egan, J.B., 1996. Purification and Self-association Equilibria of the Lysis-Lysogeny Switch Proteins of Coliphage 186. *Journal of Biological Chemistry* **271**, 11525–11531.

Shis, D.L., Bennett, M.R., 2013. Library of synthetic transcriptional AND gates built with split T7 RNA polymerase mutants. *PNAS U.S.A.* **110**, 5028–5033.

Sillankorva, S., Oliveira, R., Vieira, M.J., Sutherland, I.W., Azeredo, J., 2004. Bacteriophage Phi S1 infection of Pseudomonas fluorescens planktonic cells versus biofilms. *Biofouling* **20**, 133–138.

Siuti, P., Yazbek, J., Lu, T.K., 2013. Synthetic circuits integrating logic and memory in living cells. *Nature Biotechnology* **31**, 448–452.

Sivaprasad, A.V., Jarvinen, R., Puspurs, A., Egan, J.B., 1990. DNA Replication Studies with Coliphage 186. A Single Phage Gene is Required for Phage 186 Replication. *Journal of Molecular Biology* **213**, 449–463.

Smith, D., 2012. FDA 510(k) Summary K120563 - The KeyPathTM MRSA/MSSA Blood Culture Test-BT.

Smith, G., 1985. Filamentous fusion phage: novel expression vectors that display cloned antigens on the virion surface. *Science* **228**, 1315–1317.

Smith, M., Love, D.C., Rochman, C.M., Neff, R.A., 2018. Microplastics in Seafood and the Implications for Human Health. *Current Environmental Health Reports* **5**, 375–386.

Sneppen, K., Dodd, I.B., Shearwin, K.E., Palmer, A.C., Schubert, R.A., Callen, B.P., Egan, J.B., 2005. A mathematical model for transcriptional interference by RNA polymerase traffic in Escherichia coli. *Journal of Molecular Biology* **346**, 399–409.

Stirling, F., Bitzan, L., O'Keefe, S., Redfield, E., Oliver, J.W.K., Way, J., Silver, P.A., 2017. Rational Design of Evolutionarily Stable Microbial Kill Switches. *Molecular Cell* **68**, 686-697.e3.

Stone, E., Campbell, K., Grant, I., McAuliffe, O., 2019. Understanding and Exploiting Phage-Host Interactions. *Viruses* **11**, 567.

St-Pierre, F., Cui, L., Priest, D.G., Endy, D., Dodd, I.B., Shearwin, K.E., 2013. One-Step Cloning and Chromosomal Integration of DNA. *ACS Synthetic Biology* **2**, 537–541.

St-Pierre, F., Endy, D., 2008. Determination of cell fate selection during phage lambda infection. *PNAS U.S.A.* **105**, 20705–20710.

Sturino, J.M., Klaenhammer, T.R., 2006. Engineered bacteriophage-defence systems in bioprocessing. *Nature Reviews Microbi*ology **4**, 395–404.

Sulakvelidze, A., 2013. Using lytic bacteriophages to eliminate or significantly reduce contamination of food by foodborne bacterial pathogens: Bacteriophages and food safety. *Journal of the Science of Food and Agriculture* **93**, 3137–3146.

Suttle, C., Chan, A., 1993. Marine cyanophages infecting oceanic and coastal strains of Synechococcus: abundance, morphology, cross-infectivity and growth characteristics. *Marine Ecology Progress Series* **92**, 99–109.

Svenningsen, S.L., Costantino, N., Court, D.L., Adhya, S., 2005. On the role of Cro in prophage induction. *PNAS* **102**, 4465–4469.

Svenningsen, S.L., Semsey, S., 2014. Commitment to Lysogeny Is Preceded by a Prolonged Period of Sensitivity to the Late Lytic Regulator Q in Bacteriophage λ. *Journal of Bacteriology* **196**, 3582–3588.

Tabor, J.J., Salis, H.M., Simpson, Z.B., Chevalier, A.A., Levskaya, A., Marcotte, E.M., Voigt, C.A., Ellington, A.D., 2009. A synthetic genetic edge detection program. *Cell* **137**, 1272–1281.

Takeda, Y., Sarai, A., Rivera, V.M., 1989. Analysis of the sequence-specific interactions between Cro repressor and operator DNA by systematic base substitution experiments. *PNAS* **86**, 439–443.

The International Genetically Engineered Machine Foundation (iGEM), 2019. Registry of Standard Biological Parts. URL http://parts.igem.org/Main_Page (accessed 11.11.19).

Thron, C.D., 1996. A model for a bistable biochemical trigger of mitosis. *Biophysical Chemistry* **57**, 239–251.

Twort, F.W., 1915. An investigation on the nature of ultra-microscopic viruses. *The Lancet* **186**, 1241–1243.

Voelker, R., 2019. FDA Approves Bacteriophage Trial. *JAMA* **321**, 638–638.

Voloshin, O.N., Ramirez, B.E., Bax, A., Camerini-Otero, R.D., 2001. A model for the abrogation of the SOS response by an SOS protein: a negatively charged helix in DinI mimics DNA in its interaction with RecA. *Genes & Development* **15**, 415–427.

Waldor, M.K., Mekalanos, J.J., 1996. Lysogenic Conversion by a Filamentous Phage Encoding Cholera Toxin. *Science* **272**, 1910–1914.

Walkinshaw, M.D., Taylor, P., Sturrock, S.S., Atanasiu, C., Berge, T., Henderson, R.M., Edwardson, J.M., Dryden, D.T.F., 2002. Structure of Ocr from bacteriophage T7, a protein that mimics B-form DNA. *Molecular Cell* **9**, 187–194.

Wang, H., Dodd, I.B., Dunlap, D.D., Shearwin, K.E., Finzi, L., 2013. Single molecule analysis of DNA wrapping and looping by a circular 14mer wheel of the bacteriophage 186 CI repressor. *Nucleic Acids Research* **41**, 5746–5756.

Weiss, B., Richardson, C., 1967. Enzymatic breakage and joining of deoxyribonucleic acid, I. Repair of single-strand breaks in DNA by an enzyme system from Escherichia coli infected with T4 bacteriophage. *PNAS* **57**, 1021–1028.

Werts, C., Michel, V., Hofnung, M., Charbit, A., 1994. Adsorption of bacteriophage lambda on the LamB protein of Escherichia coli K-12: point mutations in gene J of lambda responsible for extended host range. *Journal of Bacteriology* **176**, 941–947.

Winkler, W.C., Nahvi, A., Roth, A., Collins, J.A., Breaker, R.R., 2004. Control of gene expression by a natural metabolite-responsive ribozyme. *Nature* **428**, 281–286.

Woods, W.H., Egan, J.B., 1974. Prophage Induction of Noninducible Coliphage 186. *Journal of Virology* **14**, 1349–1356.

Yang, L., Nielsen, A.A.K., Fernandez-Rodriguez, J., McClune, C.J., Laub, M.T., Lu, T.K., Voigt, C.A., 2014. Permanent genetic memory with >1 byte capacity. *Nature Methods* **11**, 1261–1266.

Yasuda, T., Morimatsu, K., Horii, T., Nagata, T., Ohmori, H., 1998. Inhibition of Escherichia coli RecA coprotease activities by DinI. *The EMBO Journal* **17**, 3207–3216.

Yoo, E.H., Lee, S.Y., 2010. Glucose Biosensors: An Overview of Use in Clinical Practice. *Sensors (Basel)* **10**, 4558–4576.

Yosef, I., Manor, M., Kiro, R., Qimron, U., 2015. Temperate and lytic bacteriophages programmed to sensitize and kill antibiotic-resistant bacteria. *PNAS U.S.A.* **112**, 7267–7272.

Zeng, L., Skinner, S.O., Zong, C., Sippy, J., Feiss, M., Golding, I., 2010. Decision Making at a Subcellular Level Determines the Outcome of Bacteriophage Infection. *Cell* **141**, 682–691.

Ziermann, R., Calendar, R., 1990. Characterization of the cos sites of bacteriophages P2 and P4. *Gene* **96**, 9–15.

Zinder, N.D., Lederberg, J., 1952. Genetic exchange in Salmonella. *Journal of Bacteriology* **64**, 679–699.

Zschiedrich, C.P., Keidel, V., Szurmant, H., 2016. Molecular mechanisms of two-component signal transduction. *Journal of Molecular Biology* **428**, 3752–3775.